



**HITACHI**

**GE Hitachi Nuclear Energy**

NEDO-33866

Revision 6

April 2020

*Non-Proprietary Information*

# **Model 2000 Radioactive Material Transport Package Safety Analysis Report**

*Copyright 2016 - 2020 GE-Hitachi Nuclear Energy Americas LLC  
All Rights Reserved*

## **PROPRIETARY INFORMATION NOTICE**

This is a non-proprietary version of the document NEDE-33866P Revision 6, which has the proprietary information removed. Portions of the document that have been removed are indicated by an open and closed bracket as shown here [[        ]].

## **IMPORTANT NOTICE REGARDING CONTENTS OF THIS REPORT**

### **Please Read Carefully**

The information contained in this document is furnished for the purpose of licensing the Model 2000 Radioactive Material Transport Package. The use of this information by anyone other than that for which it is intended is not authorized; and with respect to any unauthorized use, GE-Hitachi Nuclear Energy Americas, LLC (GEH) makes no representation or warranty, and assumes no liability as to the completeness, accuracy, or usefulness of the information contained in this document.



## TABLE OF CONTENTS

<b>TABLE OF CONTENTS .....</b>	<b>III</b>
<b>LIST OF TABLES .....</b>	<b>VIII</b>
<b>LIST OF FIGURES .....</b>	<b>XIV</b>
<b>REVISION SUMMARY .....</b>	<b>XX</b>
<b>ACRONYMS .....</b>	<b>XLVI</b>
<b>1 GENERAL INFORMATION .....</b>	<b>1-1</b>
<b>1.1 Introduction .....</b>	<b>1-1</b>
<b>1.2 Package Description .....</b>	<b>1-1</b>
1.2.1. Packaging.....	1-2
1.2.2. Contents .....	1-4
1.2.3. Special Requirements for Plutonium .....	1-5
1.2.4. Operational Features .....	1-5
<b>1.3 Appendix .....</b>	<b>1-12</b>
1.3.1. Drawings.....	1-12
1.3.2. Material Specifications .....	1-37
<b>1.4 References.....</b>	<b>1-38</b>
<b>2 STRUCTURAL EVALUATION .....</b>	<b>2-1</b>
<b>2.1 Description of Structural Design .....</b>	<b>2-1</b>
2.1.1. Discussion.....	2-1
2.1.2. Design Criteria.....	2-3
2.1.3. Weights and Centers of Gravity.....	2-4
2.1.4. Identification of Codes and Standards for Package Design .....	2-6
<b>2.2 Materials.....</b>	<b>2-7</b>
2.2.1. Material Properties and Specifications .....	2-7
2.2.2. Chemical, Galvanic, or Other Reactions.....	2-13
2.2.3. Effects of Radiation on Materials .....	2-13
<b>2.3 Fabrication and Examination .....</b>	<b>2-14</b>
2.3.1. Fabrication .....	2-14
2.3.2. Examination.....	2-14
<b>2.4 General Requirements for All Packages.....</b>	<b>2-14</b>
2.4.1. Minimum Package Size .....	2-14
2.4.2. Tamper-Indicating Feature .....	2-14
2.4.3. Positive Closure .....	2-14

NEDO-33866 Revision 6  
Non-Proprietary Information

<b>2.5</b>	<b>Lifting and Tie-Down Standards for All Packages .....</b>	<b>2-15</b>
2.5.1.	Lifting Devices .....	2-15
2.5.2.	Tie-Down Devices .....	2-18
<b>2.6</b>	<b>Normal Conditions of Transport.....</b>	<b>2-20</b>
2.6.1.	Heat.....	2-20
2.6.2.	Cold .....	2-26
2.6.3.	Reduced External Pressure .....	2-26
2.6.4.	Increased External Pressure .....	2-26
2.6.5.	Vibration.....	2-26
2.6.6.	Water Spray .....	2-27
2.6.7.	Free Drop .....	2-27
2.6.8.	Corner Drop .....	2-72
2.6.9.	Compression .....	2-72
2.6.10.	Penetration .....	2-72
<b>2.7</b>	<b>Hypothetical Accident Conditions.....</b>	<b>2-72</b>
2.7.1.	Free Drop .....	2-72
2.7.2.	Crush.....	2-98
2.7.3.	Puncture .....	2-98
2.7.4.	Thermal.....	2-99
2.7.5.	Immersion - Fissile Material.....	2-101
2.7.6.	Immersion - All Packages.....	2-101
2.7.7.	Deep Water Immersion Test (for Type B Packages Containing More than $10^5$ A <sub>2</sub> ).....	2-101
2.7.8.	Summary of Damage .....	2-101
<b>2.8</b>	<b>Accident Conditions for Air Transport of Plutonium .....</b>	<b>2-101</b>
<b>2.9</b>	<b>Accident Conditions for Fissile Material Packages for Air Transport .....</b>	<b>2-101</b>
<b>2.10</b>	<b>Special Form .....</b>	<b>2-102</b>
<b>2.11</b>	<b>Fuel Rods.....</b>	<b>2-102</b>
<b>2.12</b>	<b>Appendix .....</b>	<b>2-102</b>
2.12.1.	LS-DYNA Evaluation of the Model 2000 Transport Package .....	2-102
2.12.2.	Lead Slump Calculation.....	2-154
2.12.3.	Lifting and Tie-Down Analysis .....	2-160
2.12.4.	Cask Closure Bolt Evaluation .....	2-199
2.12.5.	Model 2000 Scale Model Drop Test Report .....	2-215
2.12.6.	Fabrication Stresses .....	2-264
<b>2.13</b>	<b>References.....</b>	<b>2-276</b>
<b>3</b>	<b>THERMAL EVALUATION .....</b>	<b>3-1</b>
<b>3.1</b>	<b>Description of Thermal Design .....</b>	<b>3-4</b>
3.1.1.	Design Features .....	3-4
3.1.2.	Content's Decay Heat .....	3-4
3.1.3.	Summary Tables of Temperatures .....	3-4
3.1.4.	Summary Tables of Maximum Pressures .....	3-7
<b>3.2</b>	<b>Material Properties and Component Specifications .....</b>	<b>3-8</b>
3.2.1.	Material Properties.....	3-8

NEDO-33866 Revision 6  
Non-Proprietary Information

3.2.2.	Component Specifications .....	3-11
<b>3.3</b>	<b>Thermal Evaluation under Normal Conditions of Transport .....</b>	<b>3-11</b>
3.3.1.	Heat and Cold .....	3-34
3.3.2.	Maximum Normal Operating Pressure .....	3-42
<b>3.4</b>	<b>Thermal Evaluation under Hypothetical Accident Conditions .....</b>	<b>3-42</b>
3.4.1.	Initial Conditions .....	3-43
3.4.2.	Fire Test Conditions .....	3-47
3.4.3.	Maximum Temperatures and Pressure.....	3-48
3.4.4.	Maximum Thermal Stresses .....	3-56
3.4.5.	Accident Conditions for Fissile Material Packages for Air Transport.....	3-56
<b>3.5</b>	<b>Appendix .....</b>	<b>3-57</b>
3.5.1.	Model 2000 Transport Package with HPI and No Material Basket.....	3-57
<b>3.6</b>	<b>References.....</b>	<b>3-67</b>
<b>4</b>	<b>CONTAINMENT .....</b>	<b>4-1</b>
<b>4.1</b>	<b>Description of Containment System.....</b>	<b>4-1</b>
4.1.1.	Containment Vessel .....	4-1
4.1.2.	Closure.....	4-1
4.1.3.	Containment Penetrations .....	4-1
<b>4.2</b>	<b>Containment Under Normal Conditions of Transport.....</b>	<b>4-5</b>
<b>4.3</b>	<b>Containment Under Hypothetical Accident Conditions.....</b>	<b>4-6</b>
<b>4.4</b>	<b>Leakage Rate Tests for Type B Packages .....</b>	<b>4-6</b>
<b>4.5</b>	<b>References.....</b>	<b>4-7</b>
<b>5</b>	<b>SHIELDING EVALUATION .....</b>	<b>5-1</b>
<b>5.1</b>	<b>Description of Shielding Design.....</b>	<b>5-1</b>
5.1.1.	Design Features .....	5-1
5.1.2.	Summary Table of Maximum Radiation Levels.....	5-2
<b>5.2</b>	<b>Source Specification.....</b>	<b>5-3</b>
5.2.1.	Gamma Source.....	5-4
5.2.2.	Neutron Source .....	5-7
<b>5.3</b>	<b>Shielding Model .....</b>	<b>5-7</b>
5.3.1.	Configuration of Source and Shielding.....	5-7
5.3.2.	Material Properties.....	5-15
<b>5.4</b>	<b>Shielding Evaluation.....</b>	<b>5-17</b>
5.4.1.	Methods .....	5-17
5.4.2.	Input and Output Data.....	5-19
5.4.3.	Flux-to-Dose-Rate Conversion .....	5-20
5.4.4.	External Radiation Levels.....	5-21

NEDO-33866 Revision 6  
Non-Proprietary Information

<b>5.5</b>	<b>Appendices .....</b>	<b>5-29</b>
5.5.1.	ORIGEN-S Irradiated Fuel Source Term Calculation .....	5-29
5.5.2.	ORIGEN-S Irradiated Hardware and Byproduct Source Term Calculation .....	5-32
5.5.3.	Cobalt-60 Isotope Rod Activity Distribution .....	5-41
5.5.4.	Radionuclide Decay Heat Conversion Factors .....	5-47
5.5.5.	Irradiated Fuel Loading Table .....	5-49
5.5.6.	Irradiated Hardware and Byproduct Loading Table .....	5-53
5.5.7.	Combined Content Shipments .....	5-55
<b>5.6</b>	<b>References.....</b>	<b>5-57</b>
<b>6</b>	<b>CRITICALITY EVALUATION.....</b>	<b>6-1</b>
<b>6.1</b>	<b>Description of Criticality Design .....</b>	<b>6-1</b>
6.1.1.	Design Features .....	6-1
6.1.2.	Summary Table of Criticality Evaluation .....	6-1
6.1.3.	Criticality Safety Index.....	6-3
<b>6.2</b>	<b>Fissile Material Contents.....</b>	<b>6-3</b>
6.2.1.	Fuel Rods .....	6-3
<b>6.3</b>	<b>General Considerations .....</b>	<b>6-3</b>
6.3.1.	Model Configuration .....	6-3
6.3.2.	Material Properties.....	6-11
6.3.3.	Computer Codes and Cross Section Libraries .....	6-14
6.3.4.	Demonstration of Maximum Reactivity .....	6-15
<b>6.4</b>	<b>Single Package Evaluation .....</b>	<b>6-16</b>
6.4.1.	Configuration.....	6-16
6.4.2.	Results .....	6-16
<b>6.5</b>	<b>Evaluation of Package Arrays Under Normal Conditions of Transport .....</b>	<b>6-18</b>
6.5.1.	Configuration.....	6-18
6.5.2.	Results .....	6-18
<b>6.6</b>	<b>Package Arrays under Hypothetical Accident Conditions.....</b>	<b>6-20</b>
6.6.1.	Configuration.....	6-20
6.6.2.	Results .....	6-20
<b>6.7</b>	<b>Fissile Material Packages for Air Transport.....</b>	<b>6-21</b>
<b>6.8</b>	<b>Benchmark Evaluations .....</b>	<b>6-21</b>
6.8.1.	Applicability of Benchmark Experiments.....	6-22
6.8.2.	Bias Determination .....	6-22
<b>6.9</b>	<b>Appendices .....</b>	<b>6-27</b>
6.9.1.	Comparison of Modeled Fuel Rod Pitch.....	6-27
6.9.2.	Benchmark Critical Experiments .....	6-29
6.9.3.	MCNP Results .....	6-35
6.9.4.	Bounding Fuel Rod Parameters for Approved Content .....	6-43
<b>6.10</b>	<b>References.....</b>	<b>6-48</b>

<b>7</b>	<b>OPERATING PROCEDURES .....</b>	<b>7-1</b>
<b>7.1</b>	<b>Package Loading.....</b>	<b>7-1</b>
7.1.1.	Preparation for Loading.....	7-1
7.1.2.	Loading of Contents .....	7-1
<b>7.1.3.</b>	<b>Closing the Cask and Performing Leakage Tests .....</b>	<b>7-2</b>
7.1.4.	Preparation for Transport.....	7-2
<b>7.2</b>	<b>Package Unloading .....</b>	<b>7-2</b>
7.2.1.	Receipt of Package from Carrier.....	7-2
7.2.2.	Removal of Contents .....	7-3
<b>7.3</b>	<b>Preparation of Empty Packaging for Transport.....</b>	<b>7-3</b>
7.3.1.	Cask Cavity Inspection .....	7-3
7.3.2.	Installation of the Cask Closure Lid .....	7-3
7.3.3.	Assembly Verification Leakage Testing.....	7-3
7.3.4.	Preparing the Empty Cask for Transport .....	7-3
<b>7.4</b>	<b>Other Operations.....</b>	<b>7-3</b>
<b>7.5</b>	<b>Appendix .....</b>	<b>7-4</b>
7.5.1.	Irradiated Hardware and Byproduct Loading Table .....	7-4
7.5.2.	Verification of Compliance for Cobalt-60 Isotope Rods .....	7-8
7.5.3.	Irradiated Fuel.....	7-10
7.5.4.	Combined Contents .....	7-16
<b>7.6</b>	<b>References.....</b>	<b>7-18</b>
<b>8</b>	<b>ACCEPTANCE TESTS AND MAINTENANCE PROGRAM .....</b>	<b>8-1</b>
<b>8.1</b>	<b>Acceptance Test .....</b>	<b>8-1</b>
8.1.1.	Visual Inspections and Measurements.....	8-1
8.1.2.	Weld Examinations.....	8-1
8.1.3.	Structural and Pressure Tests .....	8-2
8.1.4.	Fabrication Leakage Tests .....	8-2
8.1.5.	Component and Material Tests .....	8-3
8.1.6.	Shielding Tests.....	8-4
8.1.7.	Thermal Tests .....	8-4
8.1.8.	Miscellaneous Tests.....	8-5
<b>8.2</b>	<b>Maintenance Program.....</b>	<b>8-7</b>
8.2.1.	Structural and Pressure Tests .....	8-7
8.2.2.	Leak Tests.....	8-8
8.2.3.	Component and Material Tests .....	8-8
8.2.4.	Thermal Tests .....	8-9
8.2.5.	Miscellaneous Tests.....	8-9
<b>8.3</b>	<b>Appendix .....</b>	<b>8-9</b>
<b>8.4</b>	<b>References.....</b>	<b>8-9</b>

## LIST OF TABLES

Table 1.3-1. Model 2000 Packaging Licensing Drawings.....	1-12
Table 2.1-1. Structural Design Criteria for Model 2000 Cask.....	2-4
Table 2.1-2. Structural Design Criteria for HPI and Material Basket .....	2-4
Table 2.1-3. Summary of Maximum Weights .....	2-5
Table 2.1-4. Overpack Base Weight.....	2-5
Table 2.2-1. Structural Properties of Type 304 Stainless Steel .....	2-7
Table 2.2-2. Structural Properties of ASME Type [[	2-8
Table 2.2-3. Structural Properties of ASME Type [[	2-9
Table 2.2-4. Structural Properties of Depleted Uranium Metal.....	2-9
Table 2.2-5. Structural Properties of Lead.....	2-10
Table 2.2-6. Bolt – ASTM A-540 Grade B21 Class 3.....	2-10
Table 2.2-7. Internal Thread – ASME SA-182 F304.....	2-11
Table 2.2-8. ASTM A-193 B6 Bolt Properties.....	2-12
Table 2.2-9. ASTM A-540 Grade B22 Class 3 Bolt Properties.....	2-12
Table 2.5.1-1. Summary of Cask Lifting Device Stresses.....	2-17
Table 2.5.2-1. Tie-Down System Stress Analysis Results.....	2-18
Table 2.6.1-1. Temperature Results, NCT (in Shade and with Insolation) .....	2-23
Table 2.6.1-2. Radial Thermal Expansion Evaluation for HPI and Material Basket.....	2-24
Table 2.6.1-3. Axial Thermal Expansion Evaluation for HPI and Material Basket .....	2-24
Table 2.6.1-4. NCT Thermal Stress Results (psi).....	2-24
Table 2.6.1-5. Model 2000 Cask NCT Stress Analysis Summary (psi) .....	2-25
Table 2.6.7-1. LS-DYNA Results.....	2-28
Table 2.6.7-2. NCT End Drop Section 1 Stress Results (psi).....	2-40
Table 2.6.7-3. NCT End Drop Section 1 Stress Results (psi).....	2-40
Table 2.6.7-4. NCT End Drop Section 2 Stress Results (psi).....	2-43
Table 2.6.7-5. NCT End Drop Section 2 Stress Results (psi).....	2-43
Table 2.6.7-6. NCT Side Drop Section 3 Stress Results (psi) .....	2-46
Table 2.6.7-7. NCT Side Drop Section 3 Stress Results (psi) .....	2-46
Table 2.6.7-8. NCT Side Drop Section 4 Stress Results (psi) .....	2-48
Table 2.6.7-9. NCT Side Drop Section 4 Stress Results (psi) .....	2-48
Table 2.6.7-10. NCT Side Drop Section 5 Stress Results (psi) .....	2-50
Table 2.6.7-11. NCT Side Drop Section 5 Stress Results (psi) .....	2-50
Table 2.6.7-12. LS-DYNA NCT Impact Results Summary .....	2-58
Table 2.6.7-13. NCT Case 1 HPI Body Top 30 Results.....	2-63
Table 2.6.7-14. NCT Support Disk Case 1 Results .....	2-64
Table 2.6.7-15. NCT Case 2 HPI Body Top 30 Results.....	2-66
Table 2.6.7-16. NCT Support Disk Case 2 Results .....	2-67

NEDO-33866 Revision 6  
Non-Proprietary Information

Table 2.6.7-17. NCT End Drop Stress Summary .....	2-68
Table 2.6.7-18. Moment of Inertia Calculation .....	2-71
Table 2.7.1-1. LS-DYNA Results.....	2-73
Table 2.7.1-2. HAC End Drop Section 6 Stress Results (psi) .....	2-76
Table 2.7.1-3. HAC End Drop Section 6 Stress Results (psi) .....	2-76
Table 2.7.1-4. HAC End Drop Section 7 Stress Results (psi) .....	2-78
Table 2.7.1-5. HAC End Drop Section 7 Stress Results (psi) .....	2-78
Table 2.7.1-6. HAC Side Drop Section 8 Stress Results (psi).....	2-80
Table 2.7.1-7. HAC Side Drop Section 8 Stress Results (psi).....	2-81
Table 2.7.1-8. HAC Side Drop Section 9 Stress Results (psi).....	2-83
Table 2.7.1-9. HAC Side Drop Section 9 Stress Results (psi).....	2-83
Table 2.7.1-10. HAC End Drop Stress Summary .....	2-86
Table 2.7.1-11. HAC Case 1 HPI Body Top 30 Results.....	2-87
Table 2.7.1-12. HAC Support Disk Case 1 Results.....	2-88
Table 2.7.1-13. HAC Case 2 HPI Body Top 30 Results.....	2-89
Table 2.7.1-14. HAC Support Disk Case 2 Results .....	2-90
Table 2.7.1-15. Moment of Inertia Calculation .....	2-96
Table 2.7.1-16. Summary Temperatures for HAC .....	2-99
Table 2.7.4-1. Summary of HAC Stress Results .....	2-100
Table 2.12.1-1. Summary of Drop Cases and Results .....	2-104
Table 2.12.1-2. Benchmark Runs and the Drop Parameters.....	2-106
Table 2.12.1-3. Normal Condition of Transport Runs and the Drop Parameters .....	2-107
Table 2.12.1-4. Hypothetical Accident Condition of Transport Runs and the Drop Parameters.....	2-108
Table 2.12.1-5. Shallow Angle Drop Runs and the Drop Parameters .....	2-109
Table 2.12.1-6. HAC Drop Cases with Pin Puncture .....	2-109
Table 2.12.1-7. Mechanical Properties of SS304 at Temperature of Interest.....	2-110
Table 2.12.1-8. Stress Strain Curve of SS304 at -40°F .....	2-110
Table 2.12.1-9. Stress Strain Curve of SS304 at Ambient Temperature .....	2-111
Table 2.12.1-10. Stress Strain Curve of SS304 at 300°F.....	2-112
Table 2.12.1-11. Lead Temperature Dependent Properties .....	2-115
Table 2.12.1-12. Strain-Rate Factors that elevated the Stress-Strain Curves of SS304 .....	2-116
Table 2.12.1-13. Component Temperature Range and Justification .....	2-117
Table 2.12.1-14. Comparison of Benchmark Simulations and Drop Tests Acceleration.....	2-153
Table 2.12.1-15. Comparison of Benchmark Simulations and Drop Tests Deformations .....	2-153
Table 2.12.1-16. Comparison of Shallow Angle Drop Analyses .....	2-154
Table 2.12.2-1. Compressive Stress in Lead Shield .....	2-157
Table 2.12.3-1. Bolt Loading Per Ear Design and Load Case.....	2-173
Table 2.12.3-2. Lifting Ear Bolt Percent Proof Load .....	2-175
Table 2.12.3-3. Summary of Ear Analysis for Model 2000.....	2-179

NEDO-33866 Revision 6  
Non-Proprietary Information

Table 2.12.3-4. Tie-Down Ropes Tension Forces .....	2-192
Table 2.12.3-5. Tie-Down System Stress Analysis Results.....	2-199
Table 2.12.4-1. Input Parameters .....	2-201
Table 2.12.4-2. Lid Bolt Evaluation Input Parameters .....	2-202
Table 2.12.4-3. Calculation of Required Length of Engagement at 150°F .....	2-204
Table 2.12.4-4. Model 2000 Stress Analysis Design Input Parameter .....	2-205
Table 2.12.4-5. Forces/Moments Results (NCT).....	2-211
Table 2.12.4-6. Forces/Moments Results (HAC) .....	2-212
Table 2.12.4-7. Total Loads/Bolt Stresses (NCT) .....	2-212
Table 2.12.4-8. Total Loads/Bolt Stresses (HAC).....	2-213
Table 2.12.4-9. Fatigue Analysis Results .....	2-215
Table 2.12.6-1. Dimensions of Stainless Steel Shells.....	2-264
Table 2.12.6-2. Dimensions of Inner and Outer Shell at 620°F .....	2-268
Table 2.12.6-3. Dimensions of Shells at 70°F .....	2-270
Table 2.12.6-4. Summary of Stresses Due to Lead Pouring, Solidification, and Shrinkage ...	2-275
Table 3.1.3-1. Temperature Limits .....	3-5
Table 3.1.3-2. NCT Temperature Summary and Comparison with Allowable Temperatures.....	3-5
Table 3.1.3-3. HAC Maximum Temperature Summary and Comparison with Allowable Temperatures.....	3-7
Table 3.1.4-1. Maximum Pressures .....	3-7
Table 3.2.1-1. Thermal Properties of Solid Regions in the Model 2000 Finite Element Thermal Model.....	3-9
Table 3.2.1-2. Thermal Properties of Gaseous Regions in the Finite Element Thermal Model .....	3-10
Table 3.3-1. Typical Thermal Contact Conductance Values from Open Literature.....	3-19
Table 3.3-2. TCC Values Used in the Thermal Analyses.....	3-20
Table 3.3-3. Thermal Contact Resistance Levels Assigned to the Modeled Contact Elements .....	3-21
Table 3.3-4. Thermophysical Properties of Dry Air (from Reference 3-3) .....	3-27
Table 3.3-5. Constants 'C' and 'm' for the Nusselt Number Calculation of a Cylinder in Cross Flow (from Reference 3-3, Table 7.2) .....	3-29
Table 3.3.1-1. Temperature Results, NCT (in Shade and with Insolation) .....	3-37
Table 3.3.1-2. Comparison of Mixed and Perfect Thermal Contact for NCT with Insolation.....	3-40
Table 3.3.1-3. Model 2000 Transport Package Temperatures for Exposure to -40°F in Shade.....	3-41
Table 3.4.3-1. Temperature Results, Hypothetical Accident Conditions .....	3-49
Table 3.4.3-2. Comparison of Mixed and Perfect Thermal Contact for HAC.....	3-55
Table 3.5.1-1. Model 2000 Transport Package with HPI (No Material Basket) Temperature Results, NCT (100°F Ambient Temperature in Shade and with Insolation) .....	3-59



NEDO-33866 Revision 6  
Non-Proprietary Information

Table 3.5.1-2. Model 2000 Transport Package with HPI (No Material Basket) Temperature Results, -40°F & -20°F Ambient Temperatures in Shade .....	3-60
Table 3.5.1-3. NCT Temperature Summary and Comparison with Allowable Temperatures.....	3-61
Table 3.5.1-4. Model 2000 Transport Package with HPI (No Material Basket) Temperature Results, HAC .....	3-63
Table 3.5.1-5. HAC Temperature Summary and Comparison with Allowable Temperatures.....	3-63
Table 3.5.1-6. Model 2000 Transport Package with HPI (No Material Basket) Temperature Results, 100°F Ambient Temperature with Insolation, NCT, Thermal Contact Resistance Study.....	3-65
Table 3.5.1-7. Model 2000 Transport Package with HPI (No Material Basket) Temperature Results, 100°F Ambient with Insolation During Pre- and Post-Fire, HAC, Thermal Contact Resistance Study .....	3-66
Table 5.1-1. Model 2000 Transport Package Shielding Design Features.....	5-1
Table 5.1-2. Maximum NCT Dose Rates .....	5-2
Table 5.1-3. Maximum HAC Dose Rates .....	5-3
Table 5.2-1. Irradiated Hardware and Byproduct Radionuclides Significant to External Dose Rates .....	5-6
Table 5.2-2. Isotope Rod Source Term (97,250 Ci Cobalt-60) .....	5-7
Table 5.3-1. Relevant Shielding Model Dimensions .....	5-11
Table 5.3-2. Type 304 Stainless Steel Material Composition .....	5-16
Table 5.3-3. [[ ]] Material Composition.....	5-16
Table 5.3-4. Lead Material Composition.....	5-16
Table 5.3-5. Depleted Uranium Material Composition .....	5-16
Table 5.4-1. Gamma Flux-to-Dose-Rate Conversion Factors (ANSI/ANS-6.1.1 1977).....	5-20
Table 5.4-2. Neutron Flux-to-Dose-Rate Conversion Factors (ANSI/ANS-6.1.1 1977) .....	5-21
Table 5.4-3. NCT Top Surface Dose Rates per g U-235 by Burnup-Enrichment Pairing .....	5-22
Table 5.4-4. NCT Side Surface Dose Rates per g U-235 by Burnup-Enrichment Pairing.....	5-22
Table 5.4-5. NCT Bottom Surface Dose Rates per g U-235 by Burnup-Enrichment Pairing.....	5-22
Table 5.4-6. NCT 2-meter Dose Rates per g U-235 by Burnup-Enrichment Pairing.....	5-23
Table 5.4-7. NCT Cab Dose Rates per g U-235 by Burnup-Enrichment Pairing.....	5-23
Table 5.4-8. HAC Top 1-meter Dose Rates per g U-235 by Burnup-Enrichment Pairing.....	5-23
Table 5.4-9. HAC Side 1-meter Dose Rates per g U-235 by Burnup-Enrichment Pairing .....	5-24
Table 5.4-10. HAC Bottom 1-meter Dose Rates per g U-235 by Burnup-Enrichment Pairing .....	5-24
Table 5.4-11. Maximum External Dose Rates - Irradiated Fuel.....	5-25
Table 5.4-12. Irradiated Hardware and Byproduct Dose Rate per Curie Results - NCT .....	5-26
Table 5.4-13. Irradiated Hardware and Byproduct Dose Rate per Curie Results - HAC .....	5-26
Table 5.4-14. Maximum Activities for Irradiated Hardware and Byproduct Individual	

NEDO-33866 Revision 6  
Non-Proprietary Information

Radionuclides .....	5-27
Table 5.4-15. Maximum External Dose Rates - Irradiated Hardware and Byproducts .....	5-28
Table 5.4-16. Cobalt-60 Isotope Rod Dose Rate per Curie Results – NCT .....	5-28
Table 5.4-17. Cobalt-60 Isotope Rod Dose Rate per Curie Results - HAC.....	5-28
Table 5.4-18. Maximum External Dose Rates – Cobalt-60 Isotope Rods.....	5-28
Table 5.5-1. Burnup Bands and Analyzed Values .....	5-30
Table 5.5-2. Initial Enrichment Bands and Analyzed Values.....	5-30
Table 5.5-3. Secondary Source Term Calculation Parameters .....	5-30
Table 5.5-4. Example Source [[ ..... ]]	5-31
Table 5.5-5. Irradiated Fuel Total Radionuclide Decay Heat (W/gU235) .....	5-32
Table 5.5-6. Irradiated Hardware and Byproduct Irradiation Materials .....	5-34
Table 5.5-7. Irradiated Hardware and Byproduct Radionuclides .....	5-35
Table 5.5-8. Sc-46 Gamma Emission Energy Spectrum .....	5-35
Table 5.5-9. Cr-51 Gamma Emission Energy Spectrum .....	5-36
Table 5.5-10. Mn-54 Gamma Emission Energy Spectrum.....	5-36
Table 5.5-11. Co-58 Gamma Emission Energy Spectrum.....	5-36
Table 5.5-12. Fe-59 Gamma Emission Energy Spectrum .....	5-36
Table 5.5-13. Co-60 Gamma Emission Energy Spectrum.....	5-36
Table 5.5-14. Zn-65 Gamma Emission Energy Spectrum.....	5-37
Table 5.5-15. Nb-92m Gamma Emission Energy Spectrum .....	5-37
Table 5.5-16. Nb-94 Gamma Emission Energy Spectrum .....	5-37
Table 5.5-17. Zr/Nb-95 Gamma Emission Energy Spectrum.....	5-37
Table 5.5-18. Sb-124 Gamma Emission Energy Spectrum .....	5-38
Table 5.5-19. Sb-125 Gamma Emission Energy Spectrum .....	5-38
Table 5.5-20. Sb-126 Gamma Emission Energy Spectrum .....	5-39
Table 5.5-21. Cs-134 Gamma Emission Energy Spectrum .....	5-39
Table 5.5-22. Cs-137 (Ba-137m) Gamma Emission Energy Spectrum.....	5-39
Table 5.5-23. Hf-175 Gamma Emission Energy Spectrum .....	5-40
Table 5.5-24. Hf-181 Gamma Emission Energy Spectrum .....	5-40
Table 5.5-25. Ta-182 Gamma Emission Energy Spectrum .....	5-40
Table 5.5-26. Cobalt-60 Isotope Rod Shielding Analysis Case Summary .....	5-42
Table 5.5-27. Cobalt-60 Isotope Rod Shielding Analysis NCT Dose Rate Results .....	5-46
Table 5.5-28. Cobalt-60 Isotope Rod Shielding Analysis Maximum NCT Dose Rates.....	5-46
Table 5.5-29. Isotope Decay Heat Data .....	5-48
Table 5.5-30. Hypothetical Irradiated Fuel Rod Shipment Information.....	5-49
Table 5.5-31. Irradiated Fuel NCT Side Surface Dose Rate Calculation .....	5-50
Table 5.5-32. Hypothetical Irradiated Fuel Rod Shipment Irradiated Fuel Loading Table.....	5-51
Table 5.5-33. Maximum Allowable Mass (g) of U-235 Based on NCT Side Surface Dose Rate.....	5-52
Table 5.5-34. Maximum Allowable Mass (g) of U-235 Based on Thermal Limit.....	5-52

NEDO-33866 Revision 6  
Non-Proprietary Information

Table 5.5-35. Overall Maximum Allowable Mass (g) of U-235 Based on All Cask Limits.....	5-53
Table 5.5-36. Example Irradiated SS304 Radionuclide Inventory .....	5-54
Table 5.5-37. Example Zr-95 Radionuclide Inventory .....	5-54
Table 5.5-38. Example Hf Poison Rod Radionuclide Inventory .....	5-54
Table 5.5-39. Example SS304 Irradiated Hardware and Byproduct Loading Table .....	5-55
Table 5.5-40. Example Zr-95 Irradiated Hardware and Byproduct Loading Table .....	5-55
Table 5.5-41. Example Hf Poison Rod Irradiated Hardware and Byproduct Loading Table....	5-55
Table 5.5-42. Example Combined Contents Loading Table.....	5-56
Table 6.1.2-1. Most Reactive Fuel Rod Content Summary at 5 wt.% U-235 .....	6-2
Table 6.1.2-2. Most Limiting Fuel Rod Content Summary using the Administrative U-235 Mass Limit .....	6-2
Table 6.3.1-1. Initial Fuel Rod Content Model Parameters .....	6-5
Table 6.3.1-2. Relevant MCNP Model Dimensions .....	6-7
Table 6.3.2-1. Nuclear Properties of Type 304 Stainless Steel .....	6-12
Table 6.3.2-2. Nuclear Properties of [[ ..... ]]	6-13
Table 6.3.2-3. Nuclear Properties of Lead.....	6-14
Table 6.3.2-4. Nuclear Properties of Depleted Uranium .....	6-14
Table 6.3.2-5. Nuclear Properties of Fissile Content.....	6-14
Table 6.4.2-1. Fuel Rod Content, Single Package, Maximum Cases .....	6-16
Table 6.4.2-2. Nominal vs. Analyzed Fuel Parameters for the GE2000 Criticality Analysis.....	6-17
Table 6.5.2-1. Fuel Rod Content, NCT 5N, Maximum Cases.....	6-19
Table 6.6.2-1. Fuel Rod Content, HAC 2N, Maximum Cases .....	6-20
Table 6.8.2-1. Model 2000 Transport Package Criticality Safety USL Functions .....	6-23
Table 6.8.2-2. Shapiro-Wilk $a_i$ Coefficients for the $W$ Test (Reference 6-12) .....	6-26
Table 6.8.2-3. Shapiro-Wilk Percentage Points of the $W$ Test (Reference 6-12) .....	6-26
Table 6.9.1-1. Fissile Mass Content, HAC 2N, Maximum Cases .....	6-28
Table 6.9.2-1. USLSTATS Input from Critical Benchmark Lattice Experiments .....	6-30
Table 6.9.2-2. Fuel Rod Content, HAC 2N, Moderator Variation Study .....	6-34
Table 6.9.3-1. Fuel Rod Content.....	6-35
Table 6.9.3-2. FRLSmh MCNP Results (Section 6.4.2).....	6-36
Table 6.9.3-3. FRLANmh MCNP Results (Section 6.5.2) .....	6-37
Table 6.9.3-4. FRLAHmh MCNP Results (Section 6.6.2) .....	6-38
Table 6.9.3-5. FRLAHm MCNP Results (Section 6.9.1) .....	6-39
Table 6.9.3-6. Limiting Fuel Pellet Radius MCNP Results (Section 6.9.4.2) .....	6-40
Table 6.9.3-7. Optimal Fuel Rod Pitch MCNP Results (Section 6.9.4.3) .....	6-41
Table 7.5.3-1. Irradiated Fuel Loading Table Column 3 Labels .....	7-12
Table 7.5.3-2. Irradiated Fuel Loading Table Column 4 Labels .....	7-12
Table 7.5.3-3. Irradiated Fuel Loading Table Dose Rate Multipliers.....	7-13

## LIST OF FIGURES

Figure 1.2-1. Model 2000 Packaging with High Performance Insert.....	1-6
Figure 1.2-2. Model 2000 Cask .....	1-7
Figure 1.2-3. Model 2000 Overpack.....	1-8
Figure 1.2-4. Model 2000 High Performance Insert with Material Basket .....	1-9
Figure 1.2-5. Material Basket and Rod [[                 ]] Holder .....	1-10
Figure 1.2-6. Material Basket Details .....	1-11
Figure 2.5.1-1. Lifting Ear Details.....	2-16
Figure 2.5.1-2. Magnitude and Direction of Loading in Ear Analysis .....	2-16
Figure 2.5.2-1. Tie-Down of Transport Package to Vehicle.....	2-19
Figure 2.6.1-1. HPI Support Disk Details.....	2-22
Figure 2.6.1-2. Material Basket Detail.....	2-22
Figure 2.6.1-3. HPI Inside Diameter.....	2-23
Figure 2.6.7-1. ANSYS Finite Element Model of the Cask Body.....	2-32
Figure 2.6.7-2. Applied Boundary Conditions for End Drop Model.....	2-33
Figure 2.6.7-3. Cosine Distribution to Simulate Contents Loading During Side Drop.....	2-34
Figure 2.6.7-4. Applied Boundary Conditions for Side Drop Model .....	2-35
Figure 2.6.7-5. Temperature Profile for Thermal Stress Evaluation .....	2-36
Figure 2.6.7-6. NCT End Drop Cask Body Stress Intensity (total stress psi).....	2-38
Figure 2.6.7-7. NCT End Drop Linearized Stress Location (Section 1).....	2-39
Figure 2.6.7-8. NCT End Drop Lid Stress Intensity (total stress psi).....	2-41
Figure 2.6.7-9. NCT End Drop Linearized Stress Location (Section 2).....	2-42
Figure 2.6.7-10. NCT Side Drop Cask Inner Shell Stress Intensity (total stress psi).....	2-45
Figure 2.6.7-11. NCT Side Drop Linearized Stress Location (Section 3).....	2-45
Figure 2.6.7-12. NCT Side Drop Cask Flange Stress Intensity (total stress psi).....	2-47
Figure 2.6.7-13. NCT Side Drop Linearized Stress Location (Section 4).....	2-47
Figure 2.6.7-14. NCT Side Drop Cask Lid Stress Intensity (total stress psi).....	2-49
Figure 2.6.7-15. NCT Side Drop Linearized Stress Location (Section 5).....	2-49
Figure 2.6.7-16. NCT Side Drop Normal Stress Distribution (psi).....	2-51
Figure 2.6.7-17. HPI Solid Model .....	2-54
Figure 2.6.7-18. HPI Side Drop Finite Element Model.....	2-55
Figure 2.6.7-19. Contact Elements Between HPI and Cask Inner Shell.....	2-55
Figure 2.6.7-20. Solid Model of HPI Bottom Plug.....	2-56
Figure 2.6.7-21. Finite Element Model of HPI Bottom Plug.....	2-56
Figure 2.6.7-22. Cosine Pressure Distribution Simulating Material Basket [[ ]].....	2-59
Figure 2.6.7-23. Cosine Pressure Distribution Assuming Uniform Contact .....	2-59
Figure 2.6.7-24. Linearized Section Locations for the HPI Body Evaluation.....	2-61
Figure 2.6.7-25. Linearized Section Locations for the Support Disk Evaluation.....	2-62

NEDO-33866 Revision 6  
Non-Proprietary Information

Figure 2.6.7-26. Case 1, NCT, Stress Intensity Result (psi).....	2-64
Figure 2.6.7-27. Case 2, NCT, Stress Intensity Result (psi).....	2-67
Figure 2.6.7-28. HPI NCT End Drop Results – Peak Stress Intensity (psi) and Displacement (inches) .....	2-69
Figure 2.7.1-1. HAC End Drop Cask Body Stress Intensity (total stress psi) .....	2-75
Figure 2.7.1-2. HAC End Drop Linearized Stress Location (Section 6) .....	2-75
Figure 2.7.1-3. HAC End Drop Lid Stress Intensity (total stress psi) .....	2-77
Figure 2.7.1-4. HAC End Drop Linearized Stress Location (Section 7) .....	2-77
Figure 2.7.1-5. HAC Side Drop Cask Body Stress Intensity (total stress psi) .....	2-79
Figure 2.7.1-6. HAC Side Drop Linearized Stress Location (Section 8) .....	2-80
Figure 2.7.1-7. HAC Side Drop Lid Stress Intensity (total stress psi).....	2-81
Figure 2.7.1-8. HAC Side Drop Linearized Stress Location (Section 9) .....	2-82
Figure 2.7.1-9. HPI HAC End Drop Results – Peak Stress Intensity (psi) and Displacement (in) .....	2-85
Figure 2.7.1-10. Case 1, HAC, Stress Intensity Result (psi) .....	2-88
Figure 2.7.1-11. Case 2, HAC, Stress Intensity Result (psi) .....	2-90
Figure 2.7.1-12. Overpack Loading, HAC Side Drop .....	2-92
Figure 2.7.1-13. Free Body Diagram of Overpack Top.....	2-93
Figure 2.7.1-14. Overpack Junction.....	2-94
Figure 2.12.1-1. Model 2000 Solid Model .....	2-105
Figure 2.12.1-2. Drop Orientations.....	2-106
Figure 2.12.1.5-1. Shallow Angle Drops .....	2-108
Figure 2.12.1.7-1. Stress-Strain Curve of SS304 at -40°F.....	2-113
Figure 2.12.1.7-2. Stress-Strain Curve of SS304 at Ambient Temperature .....	2-114
Figure 2.12.1.7-3. Stress-Strain Curve of SS304 at 300°F .....	2-115
Figure 2.12.1.7-4. Temperature Effect of Honeycomb Material .....	2-116
Figure 2.12.1.8-1. Model 2000 Overpack and Cask Finite Element Model.....	2-118
Figure 2.12.1.8-2. Rigid Plane and Pin Model for the End Drop Configuration.....	2-119
Figure 2.12.1.8-3. Rigid Plane and Pin Model for the Side Drop Configuration .....	2-119
Figure 2.12.1.8-4. Deformed Geometry of the Overpack after a 30 foot End Drop.....	2-120
Figure 2.12.1.8-5. Deformed Geometry of the Overpack after a 30 foot Side Drop .....	2-121
Figure 2.12.1.11-1. Case 1 Deformed Overpack Shape (Effective Plastic Strain).....	2-124
Figure 2.12.1.11-2. Case 1 Payload Acceleration Time History .....	2-124
Figure 2.12.1.11-3. Case 1 Impact Energy Plot.....	2-125
Figure 2.12.1.11-4. Case 1 Interface Sliding Energy Time History .....	2-125
Figure 2.12.1.11-5. Case 2 Deformed Overpack Shape (Effective Plastic Strain).....	2-126
Figure 2.12.1.11-6. Case 2 Payload Acceleration Time History .....	2-126
Figure 2.12.1.11-7. Case 2 Impact Energy Plot.....	2-127
Figure 2.12.1.11-8. Case 2 Interface Sliding Energy Time History .....	2-127
Figure 2.12.1.11-9. Case 3 Deformed Overpack Shape (Effective Plastic Strain).....	2-128

NEDO-33866 Revision 6  
Non-Proprietary Information

Figure 2.12.1.11-10. Case 3 Payload Acceleration Time History .....	2-128
Figure 2.12.1.11-11. Case 3 Impact Energy Plot.....	2-129
Figure 2.12.1.11-12. Case 3 Interface Sliding Energy Time History .....	2-129
Figure 2.12.1.11-13. Case 4 Deformed Overpack Shape (Effective Plastic Strain).....	2-130
Figure 2.12.1.11-14. Case 4 Payload Acceleration Time History .....	2-130
Figure 2.12.1.11-15. Case 4 Impact Energy Plot.....	2-131
Figure 2.12.1.11-16. Case 4 Interface Sliding Energy Time History .....	2-131
Figure 2.12.1.11-17. Case 5 Deformed Overpack Shape (Effective Plastic Strain).....	2-132
Figure 2.12.1.11-18. Case 5 Payload Acceleration Time History .....	2-132
Figure 2.12.1.11-19. Case 5 Impact Energy Plot.....	2-133
Figure 2.12.1.11-20. Case 5 Interface Sliding Energy Time History .....	2-133
Figure 2.12.1.11-21. Case 6 Deformed Overpack Shape (Effective Plastic Strain).....	2-134
Figure 2.12.1.11-22. Case 6 Payload Acceleration Time History .....	2-134
Figure 2.12.1.11-23. Case 6 Impact Energy Plot.....	2-135
Figure 2.12.1.11-24. Case 6 Interface Sliding Energy Time History .....	2-135
Figure 2.12.1.11-25. Case 7 Deformed Overpack Shape (Effective Plastic Strain).....	2-136
Figure 2.12.1.11-26. Case 7 Payload Acceleration Time History .....	2-136
Figure 2.12.1.11-27. Case 7 Impact Energy Plot.....	2-137
Figure 2.12.1.11-28. Case 7 Interface Sliding Energy Time History .....	2-137
Figure 2.12.1.11-29. Case 8 Deformed Overpack Shape (Effective Plastic Strain).....	2-138
Figure 2.12.1.11-30. Case 8 Payload Acceleration Time History .....	2-138
Figure 2.12.1.11-31. Case 8 Impact Energy Plot.....	2-139
Figure 2.12.1.11-32. Case 8 Interface Sliding Energy Time History .....	2-139
Figure 2.12.1.11-33. Case 9 Deformed Overpack Shape (Effective Plastic Strain).....	2-140
Figure 2.12.1.11-34. Case 9 Payload Acceleration Time History .....	2-140
Figure 2.12.1.11-35. Case 9 Impact Energy Plot.....	2-141
Figure 2.12.1.11-36. Case 9 Interface Sliding Energy Time History .....	2-141
Figure 2.12.1.11-37. Case 10 Deformed Overpack Shape (Effective Plastic Strain).....	2-142
Figure 2.12.1.11-38. Case 10 Payload Acceleration Time History .....	2-142
Figure 2.12.1.11-39. Case 10 Impact Energy Plot.....	2-143
Figure 2.12.1.11-40. Case 10 Interface Sliding Energy Time History .....	2-143
Figure 2.12.1.11-41. Case 11 Deformed Overpack Shape (Effective Plastic Strain).....	2-144
Figure 2.12.1.11-42. Case 11 Payload Acceleration Time History .....	2-144
Figure 2.12.1.11-43. Case 11 Impact Energy Plot.....	2-145
Figure 2.12.1.11-44. Case 11 Interface Sliding Energy Time History .....	2-145
Figure 2.12.1.11-45. Case 12 Deformed Overpack Shape (Effective Plastic Strain).....	2-146
Figure 2.12.1.11-46. Case 12 Payload Acceleration Time History .....	2-146
Figure 2.12.1.11-47. Case 12 Impact Energy Plot.....	2-147
Figure 2.12.1.11-48. Case 12 Interface Sliding Energy Time History .....	2-147
Figure 2.12.1.11-49. Case 13 Deformed Overpack Shape (Effective Plastic Strain).....	2-148

NEDO-33866 Revision 6  
Non-Proprietary Information

Figure 2.12.1.11-50. Case 13 Payload Acceleration Time History .....	2-148
Figure 2.12.1.11-51. Case 13 Impact Energy Plot.....	2-149
Figure 2.12.1.11-52. Case 13 Interface Sliding Energy Time History .....	2-149
Figure 2.12.1.11-53. Case 14 Deformed Overpack Shape (Effective Plastic Strain).....	2-150
Figure 2.12.1.11-54. Case 14 Payload Acceleration Time History .....	2-150
Figure 2.12.1.11-55. Case 14 Impact Energy Plot.....	2-151
Figure 2.12.1.11-56. Case 14 Interface Sliding Energy Time History .....	2-151
Figure 2.12.1.11-57. Strain Contour of Package after 30 ft End Drop and Pin Puncture Sequence.....	2-152
Figure 2.12.1.11-58. Strain Contour of Package after 30 ft Side Drop and Pin Puncture Sequence.....	2-152
Figure 2.12.3-1. Structural Locations for Ear Analysis .....	2-160
Figure 2.12.3-2. Magnitude and Direction of Loading in Model 2000 Cask .....	2-161
Figure 2.12.3-3. Ear Hole Cross Section .....	2-163
Figure 2.12.3-4. Standard Ear Load Case I or III .....	2-165
Figure 2.12.3-5. Auxiliary Ear, Case I and Case II Weld Stresses .....	2-167
Figure 2.12.3-6. Standard Ear, Case I and Case II Weld Stresses .....	2-170
Figure 2.12.3-7. Lifting Ear Contact Bearing Stresses .....	2-176
Figure 2.12.3-8. Design Fatigue Curves For High Strength Steel Bolting Above 700°F .....	2-178
Figure 2.12.3-9. Analytical Model of Lifting Lug.....	2-181
Figure 2.12.3-10. Loading on the Weld Area .....	2-182
Figure 2.12.3-11. Stresses Acting on the Weld .....	2-183
Figure 2.12.3-12. Tie-Down of Transport Package to Vehicle.....	2-185
Figure 2.12.3-13. Tie-Down Wire Ropes .....	2-187
Figure 2.12.3-14. Wire Rope Extension at Small Angle ( $\theta$ ) Rotation .....	2-187
Figure 2.12.3-15. Final Length of Rope 5 .....	2-188
Figure 2.12.3-16. Final to Initial Rope Length Ratio per Small Angle Rotation .....	2-190
Figure 2.12.3-17. Tie-Down Rib Hole Loading .....	2-194
Figure 2.12.3-18. Weld Pattern of Top Tie Down Rib .....	2-195
Figure 2.12.3-19. Weld Geometry of Tie-Down Rib and Gusset to Overpack .....	2-197
Figure 2.12.4-1. Seal with Contact Width Dimension.....	2-201
Figure 3-1. Model 2000 Transport Package (High Performance Insert and Material Basket Not Shown).....	3-3
Figure 3.3-1. Finite Element Model of the Model 2000 Transport Package .....	3-14
Figure 3.3-2. Finite Element Model of the Model 2000 Transport Package - Air and Helium Not Shown.....	3-15
Figure 3.3-3. Finite Element Model of the Model 2000 Transport Package - Exploded View .....	3-16
Figure 3.3-4. Heat Transfer Through the Contact Plane Between Two Solid Surfaces .....	3-17
Figure 3.3-5. Thermal Contact Pair Locations in the Finite Element Model .....	3-24
Figure 3.3-6. Natural Convection Boundary Conditions for NCT .....	3-31

NEDO-33866 Revision 6  
Non-Proprietary Information

Figure 3.3-7. Natural Convection and Thermal Radiation Coefficients for NCT .....	3-32
Figure 3.3-8. Contents Heat Flux Applied to Material Basket [[            ]] .....	3-34
Figure 3.3.1-1. Solar Heat Flux Boundary Conditions for NCT .....	3-36
Figure 3.3.1-2. Steady-State Temperature Distribution—NCT.....	3-38
Figure 3.3.1-3. Overpack Steady-State Temperatures, 100°F Ambient Temperature.....	3-39
Figure 3.4.1-1. Three-Dimensional Finite Element Model of the Model 2000 (Half Symmetry) .....	3-44
Figure 3.4.1-2. LINK34 Incorporated to Simulate HAC Side Contact and Puncture Damage.....	3-45
Figure 3.4.1-3. Natural Convection Boundary Conditions for HAC.....	3-46
Figure 3.4.1-4. Natural/Forced Convection and Thermal Radiation Coefficients for HAC.....	3-47
Figure 3.4.2-1. Solar Heat Flux Boundary Conditions for HAC (Post-Fire Cool-Down).....	3-48
Figure 3.4.3-1. Temperature-History of the Material Basket and Overpack for HAC.....	3-50
Figure 3.4.3-2. Temperature-History of the HPI and Cask for HAC .....	3-51
Figure 3.4.3-3. Temperature-History of the Cask Ports for HAC .....	3-52
Figure 3.4.3-4. Temperature-History of the HPI and Cask Fill Gases .....	3-53
Figure 3.4.3-5. Temperature Contours During HAC 30-Minute Fire and Cool-Down.....	3-54
Figure 3.4.3-6. Gap Between HPI Bottom Plug and Cask Cavity Bottom (INCH) .....	3-56
Figure 3.5.1-1. 3D FEA Model of the Model 2000 Transport Package with HPI and No Material Basket (Half Symmetry) - Elements Representing Air and Helium Not Shown for Clarity .....	3-58
Figure 3.5.1-2. Package Temperature Contours for NCT with 100°F Ambient Temperature in Shade and with Insolation.....	3-61
Figure 3.5.1-3. Package Exterior Surface Temperature Contours for NCT with 100°F Ambient Temperature in Shade.....	3-62
Figure 4.1.3-1. Cask Containment Boundary .....	4-3
Figure 4.1.3-2. Cask Port Configuration (Assembled View).....	4-4
Figure 4.1.3-3. Cask Lid Seal Design.....	4-4
Figure 4.1.3-4. Cask Port Configuration (Exploded View).....	4-5
Figure 5.3-1. Point / Line Source Locations .....	5-9
Figure 5.3-2. NCT Shielding Models .....	5-12
Figure 5.3-3. HAC Shielding Models.....	5-13
Figure 5.3-4. NCT MCNP6 Tallies with 10% Margin to the Regulatory Limit.....	5-14
Figure 5.3-5. HAC MCNP6 Tallies with 10% Margin to the Regulatory Limit .....	5-15
Figure 5.5-1. HPI Material Basket with ‘Realistic’ Source Geometry Locations .....	5-41
Figure 5.5-2. ‘Realistic’ Source Arrangement for Bottom Dose Rates .....	5-42
Figure 5.5-3. ‘Bounding’ Source Arrangement for Bottom Dose Rates .....	5-43
Figure 5.5-4. ‘Realistic’ Source Arrangement for Top Dose Rates.....	5-43
Figure 5.5-5. ‘Bounding’ Source Arrangement for Top Dose Rates.....	5-44
Figure 5.5-6. ‘Realistic’ Source Arrangement for Side Dose Rates .....	5-44
Figure 5.5-7. ‘Bounding’ Source Arrangement for Side Dose Rates – Case 1 .....	5-45



NEDO-33866 Revision 6  
Non-Proprietary Information

Figure 5.5-8. ‘Bounding’ Source Arrangement for Side Dose Rates – Case 2 .....	5-45
Figure 6.3.1-1. Fuel Rod Content Model Geometry .....	6-5
Figure 6.3.1-2. Fuel Rod Content Boundary Model Geometry (Not to Scale).....	6-5
Figure 6.3.1-3. Package Model Geometry .....	6-8
Figure 6.3.1-4. Package Array NCT, 5N Model Geometry .....	6-9
Figure 6.3.1-5. Package Array NCT, 5N Model Geometry, Content Positioning .....	6-10
Figure 6.3.1-6. Package Array HAC, 2N Model Geometry .....	6-11
Figure 6.3.1-7. Package Array HAC, 2N Model Geometry, Content Positioning .....	6-11
Figure 6.4.2-1. Fuel Rod Content, Single Package, Results .....	6-17
Figure 6.5.2-1. Fuel Rod Content, NCT 5N, Results.....	6-19
Figure 6.6.2-1. Fuel Rod Content, HAC 2N, Results .....	6-21
Figure 6.8.2-1. USLSTATS Trend Plot of H/U-235 versus $k_{\text{norm}}$ – Lattice Systems .....	6-24
Figure 6.9.1-1. Fuel Rod Content Pitch Modeling Comparison (Not to Scale).....	6-27
Figure 6.9.1-2. HAC, Fuel Rod Pitch Comparison.....	6-28
Figure 6.9.2-1. Fuel Rod Content, HAC 2N, Moderator Variation Study.....	6-33
Figure 6.9.4-1. Fuel Column Evaluation at same H/U-235 Ratio (6 wt% U-235) .....	6-44
Figure 6.9.4-2. Fuel Column Height/Radius Evaluation at 5 wt% U-235 .....	6-45
Figure 6.9.4-3. Optimal Fuel Rod Pitch Evaluation at 5 wt% U-235 .....	6-46
Figure 7.5.1-1. Irradiated Hardware and Byproduct Loading Table .....	7-5
Figure 7.5.3-1. Irradiated Fuel Loading Table.....	7-11
Figure 8-1. Cask Shielding Inspection Points.....	8-5
Figure 8-2. Thermocouple Locations.....	8-6

## REVISION SUMMARY

Changes from Revision 0 to Revision 1 are listed in the following table. No revision bars are used for these changes. Changes for Revisions 2, 3, 4, 5, and 6 are listed in separate tables immediately following this one. Those changes from Revision 5 to Revision 6 are indicated with revision bars as appropriate.

Location	Description of Change (Rev. 0 to Rev. 1)	Reason for Change
<b>Chapter 1</b>		
Section 1.1	Deleted “fissile materials” from the first paragraph.	Responses to RAIs 5.1, 5.2, and 5.6.
Section 1.1	Deleted Reference 1-1, as 10 CFR 71 does not need to be a chapter reference. Adjusted all other reference numbers accordingly in Chapter 1. Added pointer to Section 5.1.2 for discussion of exclusive use shipment.	Administrative change.
Section 1.1	Reworded last sentence of first paragraph – CSI not applicable due to removal of fissile content from SAR, as stated in the responses to RAIs 5.1, 5.2, and 5.6.	Responses to RAIs 5.1, 5.2, and 5.6.
Section 1.2	Modified third bullet under “Contents” consistent with removal of fissile material from SAR.	Responses to RAIs 5.1, 5.2, and 5.6.
Section 1.2.1.1	Second paragraph – regarding the cask lid seal, deleted the information associated with Configuration 2.	Removing reference to decay heat configurations and Configuration 2 seal material per response to RAI 4.1.
Section 1.2.1.1	Fourth paragraph – regarding the cask lid seal, deleted the information associated with Configuration 2.	Removing reference to decay heat configurations and Configuration 2 seal material per response to RAI 4.1.
Section 1.2.2.1	Added “nominally” for the HPI dimensions, as the supporting drawing lists the dimensions as nominal.	Change made for clarity.
Section 1.2.2.3	Removed “and fissile materials” from the first sentence. Removed irradiated fuel rods and special nuclear material from the second sentence.	Responses to RAIs 5.1, 5.2, and 5.6.
Section 1.2.2.3	Item d rewritten to remove reference to Configuration 1 and 2 and clarify the decay heat basis for the SAR.	Removing reference to decay heat configurations consistent with the response to RAI 4.1.

NEDO-33866 Revision 6  
Non-Proprietary Information

Location	Description of Change (Rev. 0 to Rev. 1)	Reason for Change
Table 1.2-1	Deleted due to the changes to Section 1.2.2.3 Item d.	Removing reference to decay heat configurations consistent with the response to RAI 4.1.
Section 1.2.2.3	Removed Irradiated Cut or Segmented Fuel Rods and Special Nuclear Material as contents for shipment. Also, updated the Cobalt-60 Isotope Rods Item c. to reflect consistency with Section 5.5.2.	Responses to RAIs 1.1, 5.1, 5.2, and 5.6.
Section 1.2.3	Reworded to clarify that fissile material is not an approved content.	Responses to RAIs 5.1, 5.2, and 5.6.
Section 1.2.4	Administratively updated wording related to the additional shoring. Deleted last part of last sentence in fourth paragraph, as there are no longer multiple decay heat configuration designs.	Removing reference to decay heat configurations consistent with the response to RAI 4.1.
Section 1.2.4	Updated the reference to the Chapter 3 section that discussed the protective personnel barrier.	Administrative change.
Table 1.3-1	Updated revision numbers for licensing drawings.	Update made because drawings have been revised since SAR Revision 0 was issued.
Section 1.3.1	Provided revised licensing drawings and associated parts lists in accordance with Table 1.3-1.	Update made because drawings have been revised since SAR Revision 0 was issued.
Section 1.3.2.1	Rewritten to only address the one seal material (originally associated with Configuration 1). References 1-3 and 1-5 deleted, as they are specific to the Former Configuration 2 seal material. Reference 1-4 revised to only provide information for the one seal material (and the reference renumbered due to the other reference deletions).	Responses to RAIs 4.1, 4.2, and 4.3.
Section 1.4	Deleted Reference 1-1 as discussed above. Deleted References 1-3 and 1-5 per the changes to Section 1.3.2.1.	Response to RAIs 4.1, 4.2, and 4.3.
<b>Chapter 2</b>		
Chapter 2	Changed the title of Chapter 2 from “Structural Analysis” to “Structural Evaluation”.	For strict adherence to Regulatory Guide 7.9.
Section 2	Created paragraph 2 explaining the licensing basis (1500 W) and the Chapter 2 analysis basis (3000 W).	Elimination of Configuration 2.

NEDO-33866 Revision 6  
Non-Proprietary Information

Location	Description of Change (Rev. 0 to Rev. 1)	Reason for Change
Section 2	Removed bullet 5 concerning support of criticality analysis assumptions.	Criticality analysis has been removed from Chapter 6. Fissile material is no longer in content scope.
Section 2.1.1	Removed Configuration 2 seal materials.	Elimination of Configuration 2.
Table 2.1-3	Removed HPI component weights.	Consistent with GEH licensing drawings 001N8425, 001N8427 and 001N8428
Table 2.1-4	Added for overpack base weight.	Response to RAI 7.2.
Section 2.4.3	Changed closure bolt torque from 500 ft-lb to 720±30 ft pound.	Response to RAI 7.2.
Table 2.5.1-1	Updated lifting device bolt stresses and margins of safety.	Response to RAI 7.2.
Section 2.5.1.2	Changed lifting ear bolt expected life from 12.5 to 11 years.	Response to RAI 7.2.
Section 2.5.2.1	Added missing word “shows”.	Editorial correction.
Section 2.6.1	Removed “maximum” from description of internal power generation.	1500 W is maximum, 3000 W bounding for structural analysis.
Section 2.6.1.1	Removed references to Configuration 2 and Configuration 1, replaced with 3000W and 1500W.	GE2000 with HPI is licensed for 1500W with 3000W bounding for structural evaluation.
Section 2.6.1.2	Subsection Radial Thermal Expansion, added “worst case” and changed difference in diameters from 0.19” to 0.020”.	Worst case dimensions used consistent with GEH licensing drawings 001N8424R2, 001N8425R2, 101E8718R17 and 105E9520R9; difference in diameters consistent with revised Table 2.6.1-2.
Section 2.6.1.2	Subsection Axial Thermal Expansion, added “worst case” and changed difference in lengths from 0.23” to 0.13”.	Worst case dimensions used consistent with GEH licensing drawings 001N8424R2, 001N8425R2, 101E8718R17 and 105E9520R9; difference in diameters consistent with revised Table 2.6.1-3.
Figure 2.6.1-1	Updated to reflect HPI support disk diameter as built condition.	Consistent with GEH licensing drawing 001N8425 R2.
Figure 2.6.1-2	Updated to reflect material basket as built condition.	Consistent with GEH licensing drawing 001N8424 R2.
Figure 2.6.1-3	Updated to reflect HPI inside diameter as built condition.	Consistent with GEH licensing drawing 001N8425 R2.

NEDO-33866 Revision 6  
Non-Proprietary Information

Location	Description of Change (Rev. 0 to Rev. 1)	Reason for Change
Table 2.6.1-2	Updated for worst case as built dimensions and corrected maximum component temperatures consistent with supporting calculations.	Consistent with as built condition per GEH licensing drawing 001N8425R2 and temperature error correction.
Table 2.6.1-3	Updated for worst case as built dimensions for MB height and corrected maximum component temperatures consistent with supporting calculations.	Consistent with as built condition per GEH licensing drawings 001N1824R2, 001N8425R2, 101E8718 and 105E9520 and temperature error correction.
Table 2.6.1-5	Updated stress component $P_m + P_b + Q$ values and margins of safety as appropriate, deleted stress component Q for all cases because there is no acceptance criteria secondary stress.	Response to RAI 7.2; additional analysis for cask body stresses due to increase in cask lid bolt preload.
Section 2.6.7.1.1	Under subsection "Closure Lid Bolt Preload", replace 32,000 lb preload with 48,000 lb preload consistent with a maximum torque of 750 ft-lb.	Response to RAI 7.2.
Figure 2.6.7-2	Updated for 48,000 lb cask closure bolt preload.	Response to RAI 7.2; additional analysis for cask body stresses due to increase in cask lid bolt preload.
Figure 2.6.7-4	Updated for 48,000 lb cask closure bolt preload.	Response to RAI 7.2; additional analysis for cask body stresses due to increase in cask lid bolt preload.
Section 2.6.7.1.2	Updated paragraph 2 & 3 margin of safety for $P_m + P_b + Q$ consistent with changes to Table 2.6.1-5.	Response to RAI 7.2; additional analysis for cask body stresses due to increase in cask lid bolt preload.
Figure 2.6.7-6	Updated consistent with 48,000 lb cask closure bolt preload.	Response to RAI 7.2; additional analysis for cask body stresses due to increase in cask lid bolt preload.
Table 2.6.7-3	Updated consistent with 48,000 lb cask closure bolt preload.	Response to RAI 7.2; additional analysis for cask body stresses due to increase in cask lid bolt preload.
Figure 2.6.7-8	Updated consistent with 48,000 lb cask closure bolt preload.	Response to RAI 7.2; additional analysis for cask body stresses due to increase in cask lid bolt preload.
Table 2.6.7-5	Updated consistent with 48,000 lb cask closure bolt preload.	Response to RAI 7.2; additional analysis for cask body stresses due to increase in cask lid bolt preload.
Section 2.6.7.1.3	Updated paragraph 3 and 4 margin of safety for $P_m + P_b + Q$ consistent with changes to Tables 2.6.7-9 and Table 2.6.7-10.	Response to RAI 7.2; additional analysis for cask body stresses due to increase in cask lid bolt preload.

NEDO-33866 Revision 6  
Non-Proprietary Information

Location	Description of Change (Rev. 0 to Rev. 1)	Reason for Change
Figure 2.6.7-10	Updated consistent with 48,000 lb cask closure bolt preload.	Response to RAI 7.2; additional analysis for cask body stresses due to increase in cask lid bolt preload.
Table 2.6.7-7	Updated consistent with 48,000 lb cask closure bolt preload.	Response to RAI 7.2; additional analysis for cask body stresses due to increase in cask lid bolt preload.
Figure 2.6.7-12	Updated consistent with 48,000 lb cask closure bolt preload.	Response to RAI 7.2; additional analysis for cask body stresses due to increase in cask lid bolt preload.
Table 2.6.7-9	Updated consistent with 48,000 lb cask closure bolt preload.	Response to RAI 7.2; additional analysis for cask body stresses due to increase in cask lid bolt preload.
Figure 2.6.7-14	Updated consistent with 48,000 lb cask closure bolt preload.	Response to RAI 7.2; additional analysis for cask body stresses due to increase in cask lid bolt preload.
Table 2.6.7-11	Updated consistent with 48,000 lb cask closure bolt preload.	Response to RAI 7.2; additional analysis for cask body stresses due to increase in cask lid bolt preload.
Section 2.6.7.1.6	Added new section for cask overpack NCT end drop bolt evaluation.	Response to RAI 7.2.
Section 2.6.7.3	Deleted 2 <sup>nd</sup> sentence in paragraph 1, added NCT end drop case to material basket evaluation.	Response to RAI 2.1.
Section 2.7.1.2.5	Added new section for cask overpack HAC end drop bolt evaluation.	Response to RAI 7.2.
Section 2.7.1.3	Added material basket HAC end drop evaluation.	Response to RAI 2.2.
Section 2.7.1.3	Added subsection title “HAC Side Drop”.	Editorial change.
Section 2.7.1.3	Corrected “NCT side drop. . .” to “HAC side drop. . .” in G definition.	Editorial correction.
Section 2.7.5	Changed paragraph to state that the Model 2000 Transport Package is not licensed to transport fissile material.	Criticality analysis has been removed from Chapter 6. Fissile material is no longer in content scope.
Section 2.12.3.1	Subsection “Bolt Preload”, updated for 600±20 ft-lb lifting ear bolt torque.	Response to RAI 7.2.
Figure 2.12.3-7	Label added to figure showing lifting ear contact bearing stresses.	Editorial change.
Table 2.12.3-2	Added new table for summarizing lifting ear bolt percent preload.	Response to RAI 7.2.

NEDO-33866 Revision 6  
Non-Proprietary Information

Location	Description of Change (Rev. 0 to Rev. 1)	Reason for Change
Section 2.12.3.1	Subsection “Bolt Fatigue Analysis”, updated for 600±20 ft-lb lifting ear bolt torque.	Response to RAI 7.2.
Table 2.12.2-3	Updated bolt and thread stresses and margins of safety.	Response to RAI 7.2.
Section 2.12.4.1	Updated based on a cask lid closure bolt torque of 720±30 ft-lbs.	Response to RAI 7.2.
Section 2.12.4.1	Removed soft steel and stainless steel gasket retainer options.	Elimination of Configuration 2.
Table 2.12.4-1	Updated removing carbon steel and stainless steel parameters.	Elimination of Configuration 2.
Table 2.12.4-2	Deleted – Bolt torque sizing analysis removed.	Response to RAI 7.2 and elimination of Configuration 2.
Table 2.12.4-3	Deleted – Cask lid bolt torque sizing analysis removed.	Response to RAI 7.2 and elimination of Configuration 2.
Table 2.12.4-4	Deleted– Cask lid bolt torque sizing analysis removed.	Response to RAI 7.2 and elimination of Configuration 2.
Table 2.12.4-7 (now Table 2.12.4-4)	Updated existing parameters consistent with cask lid bolt torque and low temperature aluminum cask seal, added additional parameters from deleted Table 2.12.4-2 required for the bolt load and stress evaluation.	Response to RAI 7.2 and elimination of Configuration 2.
Table 2.12.4-8 (now Table 2.12.4-5)	Updated consistent with revised cask closure bolt load analysis.	Response to RAI 7.2 and elimination of Configuration 2.
Table 2.12.4-9 (now Table 2.12.4-6)	Updated consistent with revised cask closure bolt load analysis.	Response to RAI 7.2 and elimination of Configuration 2.
Table 2.12.4-10 (now Table 2.12.4-7)	Updated consistent with revised cask closure bolt load analysis.	Response to RAI 7.2 and elimination of Configuration 2.
Table 2.12.4-11 (now Table 2.12.4-8)	Updated consistent with revised cask closure bolt load analysis.	Response to RAI 7.2 and elimination of Configuration 2.
Section 2.12.4.2.16	Updated results consistent with revised cask closure bolt load analysis.	Response to RAI 7.2 and elimination of Configuration 2.
Section 2.12.4.2.17	Updated results consistent with revised with cask closure bolt load analysis.	Response to RAI 7.2 and elimination of Configuration 2.
Table 2.12.4-12 (now Table 2.12.4-9)	Updated consistent with revised cask closure bolt load analysis.	Response to RAI 7.2 and elimination of Configuration 2.

NEDO-33866 Revision 6  
Non-Proprietary Information

Location	Description of Change (Rev. 0 to Rev. 1)	Reason for Change
<b>Chapter 3</b>		
Section 3	Removed Configurations 1 and 2, added 2 <sup>nd</sup> paragraph explaining the licensing basis (1500W) and the Chapter 3 analysis basis (3000W).	Elimination of Configuration 2.
Section 3.1.1	Updated 3 <sup>rd</sup> paragraph, cask lid seal discussion.	Elimination of Configuration 2.
Section 3.1.2	Removed “configurations” from first sentence, removed irradiated fuel as a content, deleted last sentence.	Elimination of Configuration 2 and revised content scope.
Section 3.1.3	Removed Configuration 2.	Elimination of Configuration 2.
Table 3.1.3-1	Changed note c to “See Chapter 4 for additional discussion”.	Chapter 4 provides the 1500 W decay heat licensing basis temperatures for the seal locations.
Section 3.1.3.1	Removed Configuration 2.	Elimination of Configuration 2.
Table 3.1.3-2	Added note c callouts to lid seal and O-ring allowable temperatures and added note c “See Chapter 4 for additional discussion”.	Chapter 4 provides the 1500 W decay heat licensing basis temperatures for the seal locations.
Section 3.1.3.2	Removed Configuration 2.	Elimination of Configuration 2.
Table 3.1.3-3	Added note b callouts to lid seal and O-ring allowable temperatures and added note b “See Chapter 4 for additional discussion”.	Chapter 4 provides the 1500 W decay heat licensing basis temperatures for the seal locations.
Section 3.2.2	Removed Configuration 2, updated description of seal, O-ring and retainer materials.	Elimination of Configuration 2.
Section 3.3	Removed Configuration 2.	Elimination of Configuration 2.
Figure 3.3-1	Removed Configuration 2 from title.	Elimination of Configuration 2.
Figure 3.3-2	Removed Configuration 2 from title.	Elimination of Configuration 2.
Figure 3.3-3	Removed Configuration 2 from title.	Elimination of Configuration 2.
Section 3.3.1.1.2	Removed Configuration 2.	Elimination of Configuration 2.
Figure 3.3.1-2	Removed Configuration from title.	Elimination of Configuration 2.
Section 3.3.1.1.3	Removed Configuration 2.	Elimination of Configuration 2.
Figure 3.3.1-3	Removed Configuration from title.	Elimination of Configuration 2.
Section 3.4	Removed Configuration 2.	Elimination of Configuration 2.
Section 3.4.3	Removed Configuration 2.	Elimination of Configuration 2.
Table 3.4.3-1	Removed Configuration 2 from title.	Elimination of Configuration 2.
Figure 3.4.3-1	Removed Configuration 2 from title.	Elimination of Configuration 2.



NEDO-33866 Revision 6  
Non-Proprietary Information

Location	Description of Change (Rev. 0 to Rev. 1)	Reason for Change
Figure 3.4.3-2	Removed Configuration 2 from title.	Elimination of Configuration 2.
Figure 3.4.3-3	Removed Configuration 2 from title.	Elimination of Configuration 2.
Figure 3.4.3-4	Removed Configuration 2 from title.	Elimination of Configuration 2.
Figure 3.4.3-5	Removed Configuration 2 from title.	Elimination of Configuration 2.
Table 3.4.3-2	Removed Configuration 2 from title.	Elimination of Configuration 2.
Figure 3.4.3-6	Removed Configuration 2 from title.	Elimination of Configuration 2.
Section 3.5.1	Removed Configuration 1 and Configuration 2 from section title and text.	Elimination of Configuration 2.
Figure 3.5.1-1	Removed Configuration 1 from title.	Elimination of Configuration 2.
Table 3.5.1-1	Removed Configuration 1 from title.	Elimination of Configuration 2.
Table 3.5.1-2	Removed Configuration 1 from title.	Elimination of Configuration 2.
Table 3.5.1-3	Removed Configuration 1 from title.	Elimination of Configuration 2.
Figure 3.5.1-2	Removed Configuration 1 from title.	Elimination of Configuration 2.
Figure 3.5.1-3	Removed Configuration 1 from title.	Elimination of Configuration 2.
Table 3.5.1-4	Removed Configuration 1 from title.	Elimination of Configuration 2.
Table 3.5.1-5	Removed Configuration 1 from title, updated note a, deleted note b.	Elimination of Configuration 2.
Table 3.5.1-6	Removed Configuration 1 from title.	Elimination of Configuration 2.
Table 3.5.1-7	Removed Configuration 1 from title.	Elimination of Configuration 2.
References	Updated References 3-4 and 3-7.	Response to RAI 3.1.
<b>Chapter 4</b>		
Section 4	Removed “primary” from 4 <sup>th</sup> sentence in response to RAI 8.2. Reference 4-1 has been deleted – see basis in description of change for Section 4.6.	Response to RAI 8.2.
Section 4.1	Reworded section to clarify thermal decay heat basis for Chapter 4.	Removes reference to decay heat configurations and establishes the basis for Chapter 4.
Section 4.1.2	Revised the cask lid closure torque, consistent with the response to RAI 7.2.	Response to RAI 7.2.
Section 4.1.3	Deleted Reference 4-2 – see basis in description of change for Section 4.6.	Administrative change.
Section 4.1.3.2	Eliminated reference to the configuration numbers, as well as the lid seal for the 3000 W case, as the 1500 W decay heat case forms the basis for Chapter 4 as stated in Section 4.1.	Removes reference to decay heat configurations and establishes the basis for Chapter 4. Changes are consistent with the responses to RAIs 4.2 and 4.3.

NEDO-33866 Revision 6  
Non-Proprietary Information

Location	Description of Change (Rev. 0 to Rev. 1)	Reason for Change
Figure 4.1.3-3	Replaced the figure by removing the material options for the lid gasket.	Removes Configuration 2 seal material.
Section 4.1.3.3	<p>Added wording to note that the cask port O-rings and covers are outside the containment boundary, consistent with the response to RAI 4.1.</p> <p>Eliminated reference to the configuration numbers, as well as the O-ring material for the 3000 W case, as the 1500 W decay heat case forms the basis for Chapter 4 as stated in Section 4.1.</p>	Removes reference to decay heat configurations and establishes the basis for Chapter 4. Changes are consistent with the responses to RAIs 4.2 and 4.3.
Section 4.2.1	<p>Section heading has been deleted, and the text has been moved to Section 4.2.</p> <p>Maximum pressure during NCT has been updated in the second paragraph to reflect the 1500 W case.</p>	Removes reference to decay heat configurations and establishing the basis for Chapter 4.
Section 4.2.2	Section has been deleted in its entirety.	The 1500 W case forms the basis for Chapter 4 as stated in Section 4.1, and Configuration 2 has been removed per the response to RAI 4.2.
Section 4.3.1	<p>Section heading 4.3.1 has been deleted.</p> <p>Maximum pressure during HAC has been updated to reflect the 1500 W case.</p> <p>Clarification has been added for the cask drain and test ports exceeding the 400°F seal material design temperature consistent with the response in RAI 4.1.</p>	Response to RAI 4.1.
Section 4.3.2	Section has been deleted in its entirety.	The 1500 W case forms the basis for Chapter 4 as stated in Section 4.1, and Configuration 2 has been removed per the response to RAI 4.2.
Section 4.4	Eliminated reference to the configuration numbers and stated the values for the 1500 W decay heat thermal basis. Clarified the conditions used in the acceptance testing.	Removes reference to decay heat configurations and establishes the basis for Chapter 4.
Section 4.5	Section in its entirety has been deleted, as it refers to Configuration 2 results.	Removes reference to decay heat configurations and establishes the basis for Chapter 4.

NEDO-33866 Revision 6  
Non-Proprietary Information

Location	Description of Change (Rev. 0 to Rev. 1)	Reason for Change
Section 4.6	Renumbered to Section 4.5 based on the change above. References 4-1 and 4-2 have been deleted. Reference 4-1 points to 10 CFR 71, which does not need a reference, and Reference 4-2 is redundant to the licensing drawings listed in Section 1.3.1. Remaining references have been renumbered.	Administrative change.
<b>Chapter 5</b>		
Section 5.1.1	Removed “and solid fissile materials”.	Fissile material is no longer an approved shipping content per responses to RAI 5.1, RAI 5.2 and RAI 5.6.
Section 5.1.2	Changed from three content types to two content types.	Fissile material is no longer an approved shipping content per responses to RAI 5.1, RAI 5.2 and RAI 5.6.
Table 5.1-2	Removed row of Content 1 and updated dose rates; changed note from 1 and 2 to a and b.	Fissile material is no longer an approved shipping content per responses to RAI 5.1, RAI 5.2 and RAI 5.6. Update the dose rates due to the elimination of Configuration 2 (3000W) per response to RAI 5.5.
Table 5.1-3	Removed row of Content 1 and updated dose rates; changed note from 1 and 2 to a and b.	Fissile material is no longer an approved shipping content per responses to RAI 5.1, RAI 5.2 and RAI 5.6. Updated the dose rates due to the elimination of Configuration 2 (3000W) per response to RAI 5.5.
Section 5.2	In first paragraph, removed the content regarding irradiated fuel and special nuclear material.	Fissile material is no longer an approved shipping content per responses to RAI 5.1, RAI 5.2 and RAI 5.6.
Section 5.2	Removed description of Irradiated Fuel.	Fissile material is no longer an approved shipping content per responses to RAI 5.1, RAI 5.2 and RAI 5.6.
Section 5.2	Removed description of Special Nuclear Material.	Fissile material is no longer an approved shipping content per responses to RAI 5.1, RAI 5.2 and RAI 5.6.

NEDO-33866 Revision 6  
Non-Proprietary Information

Location	Description of Change (Rev. 0 to Rev. 1)	Reason for Change
Section 5.2.1.1	Deleted Section 5.2.1.1.	Fissile material is no longer an approved shipping content per responses to RAI 5.1, RAI 5.2 and RAI 5.6.
Section 5.2.1.2 (now 5.2.1.1)	Added ORIGIN-S description.	Carry over from deleted Section 5.2.1.1.
Section 5.2.1.3 (now 5.2.1.2)	Changed from 3000W to 1500W and from 194,500 Ci to 97,250 Ci.	Configuration 2 (3000W) is no longer an approved configuration per response to RAI 5.5.
Table 5.2-4 (now 5.2-2)	Changed from 194,500 Ci to 97,250 Ci and reduce source strength to half.	Configuration 2 (3000W) is no longer an approved configuration per response to RAI 5.5.
Section 5.2.2.1	Deleted Section 5.2.2.1.	Fissile material is no longer an approved shipping content per responses to RAI 5.1, RAI 5.2 and RAI 5.6.
Section 5.3.1.1	Removed description of Irradiated Fuel.	Fissile material is no longer an approved shipping content per responses to RAI 5.1, RAI 5.2 and RAI 5.6.
Section 5.3.1.1	Editorial modification under Irradiated Hardware and Byproducts and Cobalt-60 Isotope Rods.	For consistency and match shielding model.
Section 5.3.1.3	Added “(except cavity radius which is nominal)” to the third sentence of Section 5.3.1.3.	Drawing 001N8425 Revision 2 includes a tolerance.
Table 5.3-1	Added Note d.	Drawing 001N8425 Revision 2 includes a tolerance.
Section 5.3.1.3	Editorial modification due to removal of neutron shielding model because it is not applicable to irradiated hardware and byproduct and Co-60 isotope rod.	Fissile material is no longer an approved shipping content per responses to RAI 5.1, RAI 5.2 and RAI 5.6.
Table 5.3-1	Changed from MCNP to MCNP6, delete MCNP Surface column, change Dimension column to Parameter column, change value columns to Dimension columns, change note from 1-3 to a-c, add description in Parameter column.	For consistency.
Figure 5.3-2	Removed neutron shielding model because it is not applicable to irradiated hardware and byproduct and Co-60 isotope rod.	Fissile material is no longer an approved shipping content per responses to RAI 5.1, RAI 5.2 and RAI 5.6.

NEDO-33866 Revision 6  
Non-Proprietary Information

Location	Description of Change (Rev. 0 to Rev. 1)	Reason for Change
Section 5.3.1.4	Editorial modification due to removal of neutron shielding model because it is not applicable to irradiated hardware and byproduct and Co-60 isotope rod.	Fissile material is no longer an approved shipping content per responses to RAI 5.1, RAI 5.2 and RAI 5.6.
Figure 5.3-3	Removed neutron shielding model because it is not applicable to irradiated hardware and byproduct and Co-60 isotope rod.	Fissile material is no longer an approved shipping content per responses to RAI 5.1, RAI 5.2 and RAI 5.6.
Section 5.3.1.5	Changed from MNCP to MCNP6 and delete tally description.	Tally description is not needed because it is consistent with 10 CFR 71.47 and 10 CFR 71.51.
Tables 5.3-2	Deleted Table 5.3-2.	Tally description is not needed because it is consistent with 10 CFR 71.47 and 10 CFR 71.51.
Tables 5.3-3	Deleted Table 5.3-3.	Tally description is not needed because it is consistent with 10 CFR 71.47 and 10 CFR 71.51.
Section 5.3.2	Removed description of neutron shielding model because it is not applicable to irradiated hardware and byproduct and Co-60 isotope rod.	Fissile material is no longer an approved shipping content per responses to RAI 5.1, RAI 5.2 and RAI 5.6.
Section 5.4.1.1	Editorial modification due to removal of neutron shielding model because it is not applicable to irradiated hardware and byproduct and Co-60 isotope rod.	Fissile material is no longer an approved shipping content per responses to RAI 5.1, RAI 5.2 and RAI 5.6.
Section 5.4.1.2	Editorial modification due to removal of neutron shielding model because it is not applicable to irradiated hardware and byproduct and Co-60 isotope rod.	Fissile material is no longer an approved shipping content per responses to RAI 5.1, RAI 5.2 and RAI 5.6.
Section 5.4.1.3	Deleted Section 5.4.1.3.	Fissile material is no longer an approved shipping content per responses to RAI 5.1, RAI 5.2 and RAI 5.6.
Section 5.4.3	Deleted description of neutron conversion factor.	The neutron conversion factor is not applicable to irradiated hardware and byproduct and Co-60 isotope rod.
Table 5.4-2	Deleted Table 5.4-2.	The neutron conversion factor is not applicable to irradiated hardware and byproduct and Co-60 isotope rod.

NEDO-33866 Revision 6  
Non-Proprietary Information

Location	Description of Change (Rev. 0 to Rev. 1)	Reason for Change
Section 5.4.4	Changed from three content types to two content types.	Fissile material is no longer an approved shipping content per responses to RAI 5.1, RAI 5.2 and RAI 5.6.
Section 5.4.4.1	Deleted previous Section 5.4.4.1.	Fissile material is no longer an approved shipping content per responses to RAI 5.1, RAI 5.2 and RAI 5.6.
Section 5.4.4.2 (now 5.4.4.1)	Changed from 3000 W to 1500 W.	Configuration 2 (3000W) is no longer an approved configuration per response to RAI 5.5.
Table 5.4-15 (now 5.4-4)	Updated activity limit in Table 5.4-15 (now 5.4-4) due to 1500W. thermal limit	Configuration 2 (3000W) is no longer an approved configuration per response to RAI 5.5.
Table 5.4-16 (now 5.4-5)	Updated dose rate in Table 5.4-16 (now 5.4-5) due to 1500W thermal limit.	Configuration 2 (3000W) is no longer an approved configuration per response to RAI 5.5.
Section 5.4.4.3 (now 5.4.4.2)	Changed from 3000 W to 1500 W.	Configuration 2 (3000W) is no longer an approved configuration per response to RAI 5.5.
Table 5.4-19 (now 5.4-8)	Updated dose rate in Table 5.4-19 (now 5.4-8) due to 1500W thermal limit.	Configuration 2 (3000W) is no longer an approved configuration per response to RAI 5.5.
Section 5.4.4.4 (now 5.4.4.3)	Removed irradiated fuel related text.	Fissile material is no longer an approved shipping content per responses to RAI 5.1, RAI 5.2 and RAI 5.6.
Section 5.5.1	Deleted Section 5.5.1.	Fissile material is no longer an approved shipping content per responses to RAI 5.1, RAI 5.2 and RAI 5.6.
Section 5.5.2 (now 5.5.1)	Added a sentence to the end of the first paragraph.	Updated per responses to RAI 5.3 and RAI 7.3.
Table 5.5-7 (now 5.5-2)	Changed note from 1 to a.	For consistency.
Section 5.5.3 (now 5.5.2)	Removed Configuration 2 from the sentence before Table 5.5-28 (now 5.5-23).	Configuration 2 (3000W) is no longer an approved configuration per response to RAI 5.5.
Table 5.5-28 (now 5.5-23)	Changed note from 1 to a.	For consistency.
Section 5.5.3 (now 5.5.2)	Deleted the last 5 paragraphs.	Paragraphs are not needed per response to RAI 5.4.

NEDO-33866 Revision 6  
Non-Proprietary Information

Location	Description of Change (Rev. 0 to Rev. 1)	Reason for Change
Table 5.5-29	Deleted Table 5.5-29.	Table is not needed per response to RAI 5.4.
Section 5.5.4 (now 5.5.3)	Removed Configuration 1 and Configuration 2 from the first sentence.	Configuration 2 (3000W) is no longer an approved configuration per response to RAI 5.5.
Table 5.5-30 (now 5.5-24)	Changed note from 1 and 2 to a and b; removed isotopes Sn-117 and Sn-119.	Consistent with Table 5.5-7 (now 5.5-2).
Section 5.5.5	Deleted Section 5.5.5.	Fissile material is no longer an approved shipping content per responses to RAI 5.1, RAI 5.2 and RAI 5.6.
Section 5.5.6 (now 5.5.4)	Removed the sentence (related to Configuration 2) before Table 5.5-40 (now 5.5-28).	Configuration 2 (3000W) is no longer an approved configuration per response to RAI 5.5.
Table 5.5-39 (now 5.5-27)	Updated the total activity.	Configuration 2 (3000W) is no longer an approved configuration per response to RAI 5.5.
Table 5.5-40 (now 5.5-28)	Changed the decay heat limit from 3000 W to 1500 W.	Configuration 2 (3000W) is no longer an approved configuration per response to RAI 5.5.
Table 5.5-41 (now 5.5-29)	Changed the decay heat limit from 3000 W to 1500 W.	Configuration 2 (3000W) is no longer an approved configuration per response to RAI 5.5.
Table 5.5-42 (now 5.5-30)	Changed the decay heat limit from 3000 W to 1500 W and update values.	Configuration 2 (3000W) is no longer an approved configuration per response to RAI 5.5.
Section 5.5.7 (now 5.5.5)	Removed irradiated fuel related text.	Fissile material is no longer an approved shipping content per responses to RAI 5.1, RAI 5.2 and RAI 5.6.
Table 5.5-43	Deleted Table 5.5-4.	Fissile material is no longer an approved shipping content per responses to RAI 5.1, RAI 5.2 and RAI 5.6.
References	Deleted References 5-3 and 5-10.	Fissile material is no longer an approved shipping content per responses to RAI 5.1, RAI 5.2 and RAI 5.6.
<b>Chapter 6</b>		
Chapter 6	Replaced Chapter 6 content with a paragraph.	Fissile material is no longer an approved shipping content per responses to RAI 6.1 and RAI 6.2.

NEDO-33866 Revision 6  
Non-Proprietary Information

Location	Description of Change (Rev. 0 to Rev. 1)	Reason for Change
<b>Chapter 7</b>		
Chapter 7 has been modified to reflect the global removal of the 3000W configuration and text associated with irradiated fuel rods and special nuclear material. In addition to the changes listed below to address the RAIs provided, Chapter 7 has been modified to incorporate operational experiences and current lessons learned.		
Section 7.1.1.3:b	Inserted “± 20”.	In response to RAI 7.2.
Section 7.1.2.2	Deleted.	Removal of Irradiated Fuel Rods from the Cask scope and in response to RAI 7.5.
Section 7.1.2.2.c (Previously Section 7.1.2.3.c)	Deleted second sentence. Inserted “The HPI material basket may be used as shoring, but is not required.”	Clarification in response to RAI 7.1.
Section 7.1.2.4	Deleted.	Removal of Special Nuclear Material from the Cask scope and in response to RAI 7.5.
Section 7.1.3.2.a	Inserted “500” deleted, “720±30”.	Correction to the required torque bolt and in response to RAI 7.2.
Section 7.1.4.1.e	Inserted “±5”.	Addition of tolerance in response to RAI 7.2.
Section 7.2.1.3.c	Inserted “±20”.	Addition of tolerance in response to RAI 7.2.
Section 7.2.2.1	Removed reference to irradiated fuel.	Removal of Irradiated Fuel Rods from the Cask scope.
Section 7.2.2.2	Deleted “/ 500 grams U-235 Equivalent Mass of SNM”.	Removal of Special Nuclear Material from the Cask scope and in response to RAI 7.5.
Section 7.2.2.2	Deleted “either” and “or 500 grams U-235 equivalent mass of SNM”.	Removal of Special Nuclear Material from the Cask scope.
Section 7.2.2.3.b	Inserted “Install the spacer, if one came with the packaging” deleted, “If spacer was provided, confirm it is secured to the HPI top plug”.	Clarification on spacer use and in response to RAI 7.2.
Section 7.3.2.b	Inserted “500” deleted, “720±30”.	In response to RAI 7.2.
Section 7.5.1 (Previously Section 7.5.2)	Inserted second to last bullet “criticality” deleted, “activity.”	In response to RAI 8.3.
Section 7.5.1 – 2.	Inserted “(alpha and beta emitters)”; inserted “A list of radionuclides for consideration to include in the loading plan is provided in, but not limited to, Table 5.5-24.”	In response to RAI 7.3.



NEDO-33866 Revision 6  
Non-Proprietary Information

Location	Description of Change (Rev. 0 to Rev. 1)	Reason for Change
Section 7.5.2 – 1.	Changed to “Verify that the peak activity in any axial 1-inch increment in the HPI cavity is in accordance with Section 5.5.2.”	In response to RAI 7.4.
Section 7.5.2 – 1.	All bullets deleted.	Clarification in response to RAI 7.4.
Section 7.5.4 – 1.	Deleted.	Removal of Irradiated Fuel Rods from the Cask scope.
Section 7.5.5	Deleted.	Removal of Special Nuclear Material from the Cask scope and in response to RAI 7.5.
<b>Chapter 8</b>		
Section 8	Removed Reference 8-1, which points to 10 CFR 71, which does not need a reference. Other references have been renumbered.	Administrative change.
Section 8.1.5.2	Eliminated reference to the configuration numbers, as well as the lid seal material for the 3000 W case, as the 1500 W decay heat case forms the basis for containment as stated in Section 4.1. Clarified the lid seal test conditions.	The lid seal material is based on the 1500 W decay heat case, as stated in Section 4.1.
Section 8.1.7	Added clarification at the end of the section denoting the decay heat basis.	Because the thermal testing is designed for 2000 W, it was necessary to clarify that the thermal basis for the cask is 3000 W, even though the allowable decay heat for shipping is 1500 W.
Section 8.2	Clarified the end of the second.	In response to RAI 8.1.
Section 8.2.1.2	Clarified the first sentence.	In response to RAI 8.1.
Section 8.2.2.2	Clarified the end of the second.	In response to RAI 8.1.
Section 8.2.3.1	Eliminated reference to Configuration 2.	There is no Configuration 1/ Configuration 2 designation for contents as seen in Section 1.2.2.3.
Section 8.4	Along with the deletion of Reference 8-1, as stated previously, References 8-8, 8-9, 8-10, 8-12, and 8-13 have been deleted (and citations in the text removed). These are internal GEH specifications and reports that normally are not cited in a SAR.	Administrative change.

NEDO-33866 Revision 6  
Non-Proprietary Information

Changes from Revision 1 to Revision 2 are listed in the following table. No revision bars are used for these changes.

Location	Description of Change (Rev. 1 to Rev. 2)	Reason for Change
Revision Summaries	Clarified that the Revision Summary for Revision 0 to Revision 1 is maintained, while this Revision Summary for Revision 1 to Revision 2 is added. Revision bars are used only for Revision 2 changes.	Clarification.
Section 1.2	Moved bulleted information for the high performance insert and the HPI material basket from “Contents” to “Packaging”.	The HPI and material basket are packaging, not contents.
Former Section 1.2.2.1  New Section 1.2.1.3	Moved former Section 1.2.2.1, High Performance Insert, from Section 1.2.2, Contents, to Section 1.2.1, Packaging. It is now Section 1.2.1.3.	The HPI is packaging, not a content.
Former Section 1.2.2.2  New Section 1.2.1.4	Moved former Section 1.2.2.2, HPI Material Basket, from Section 1.2.2, Contents, to Section 1.2.1, Packaging. It is now Section 1.2.1.4.	The material basket is packaging, not a content.
Former Section 1.2.2.3  Now Section 1.2.2.1	Renumbered this section due to relocating Sections 1.2.2.1 and 1.2.2.2. Also, in Item a), defined “payload” as all cask internals and contents. This is consistent with existing information in Revision 1 (e.g., as stated in Section 2.12.1.2).	Administrative and clarification change.
Section 1.2.3	In the second sentence in the section, changed the pointer for package content from Section 1.2.2.3 to Section 1.2.2.1.	Administrative change.
Chapter 2	In the chapter lead-in discussion, second paragraph, first bullet, changed: “Ensure the maximum content weight does not exceed 5,450 pounds.” To: “Ensure the maximum payload weight does not exceed 5,450 pounds.”	Clarification change.

NEDO-33866 Revision 6  
Non-Proprietary Information

Location	Description of Change (Rev. 1 to Rev. 2)	Reason for Change
Table 2.1-3	<p>In the first data row, first column, changed “Total Packaging Weight” to “Total Overpack plus Cask Weight”.</p> <p>In the fifth data row, first column, changed “Allowed Contents Weight” to “Payload Weight”.</p> <p>Changed footnotes “*” and “**” to “1” and “3”, respectively. In footnote 3, changed “If material basket is not included in contents...” to “If material basket is not used...”.</p> <p>Added footnote 2: “The HPI plus material basket plus radioactive contents (with shoring) is defined as payload for purposes of this report”.</p>	The HPI and material basket are packaging, not contents.
Section 2.6.7.1.1	<p>In the second sentence under subheading “Cask Contents Loading – End Drop” (below Table 2.6.7-1), changed “one half the contents weight of 5,450 lb” to “one half the payload weight of 5,450 lb (see Table 2.1-3)”.</p> <p>Also, in the second sentence under subheading “Cask Contents Loading – Side Drop”, changed “produced by the 5,450 lb contents weight” to “produced by the 5,450 lb payload weight”.</p>	Clarification change.
Tale 2.12.4-4	Changed the data entry cell “Weight of Cask Contents” to “Weight of Cask Payload”.	Clarification change.
Section 3.1.1	In the last sentence of the section, changed the pointer for information on the high performance insert from Section 1.2.2.1 to Section 1.2.1.3.	Administrative change.
Section 3.3	In the first sentence of the second paragraph under subheading “Heat Generation by Contents,” (below Figure 3.3-7), changed the pointer for information on the material basket from Section 1.2.2.2 to Section 1.2.1.4.	Administrative change.
Section 4.1	In the first sentence of the section, changed the pointer for package content from Section 1.2.2.3 to Section 1.2.2.1.	Administrative change.
Section 5.5.5	In the last sentence of the section, changed the pointer for package content from Section 1.2.2.3 to Section 1.2.2.1.	Administrative change.
Chapter 6	In the first sentence of the chapter, changed the pointer for package content from Section 1.2.2.3 to Section 1.2.2.1.	Administrative change.

NEDO-33866 Revision 6  
Non-Proprietary Information

Location	Description of Change (Rev. 1 to Rev. 2)	Reason for Change
Section 7.5.1	In procedure step 2, first bullet, changed the parenthetical “alpha and beta emitters” to “alpha, beta, and gamma emitters”.	Clarification change.
Section 7.5.2	Modified the procedure steps by explicitly stating the allowable per inch activity level and clarifying use of the Combined Contents Loading Table.	Clarification change.
Section 7.5.3	Added a new procedure sub-step 2.1 to address the allowable per inch activity level to include point source values.  Also, corrected the pointer to the previous steps from “Steps 1 through 3” to “Steps 1 and 2”.	Clarification change.
Section 8.1.7	In the fourth sentence of the section, changed the pointer for package content from Section 1.2.2.3 to Section 1.2.2.1.	Administrative change.

NEDO-33866 Revision 6  
Non-Proprietary Information

Changes from Revision 2 to Revision 3 are listed in the following table. No revision bars are used for these changes.

Location	Description of Change (Rev. 2 to Rev. 3)	Reason for Change
Revision Summaries	<p>Clarified that the Revision Summary for Revision 0 to Revision 1 and from Revision 1 to Revision 2 is maintained, while this revision summary for Revision 2 to Revision 3 is added.</p> <p>The only revision made to Revision 3 was to unredact instances of “bottom plug”. However, since this document does not have specific instances of GEH proprietary information marked, there are no revisions to Revision 3 other than the addition of this table.</p>	Clarification.

NEDO-33866 Revision 6  
Non-Proprietary Information

Changes from Revision 3 to Revision 4 are listed in the following table. No revision bars are used for these changes.

Location	Description of Change (Rev. 3 to Rev. 4)	Reason for Change
<b>Chapter 1</b>		
Section 1.1	Updated the Criticality Safety Index value with the changes to Chapter 6.	Adding irradiated fuel to the cask scope.
	Capitalized “Docket Number”	Administrative change.
Section 1.2.2.1	Added “irradiated fuel” as contents in the first paragraph and as new item 3 in second to last paragraph.	Adding irradiated fuel to the cask scope.
	Changed “Table 2.1.3” to “Table 2.1-3.”	Administrative change.
	Changed “Section 7.5.2” to “Section 7.5.1.” Changed “Section 5.5.2” to “Section 7.5.2.”	
Section 1.2.3	Updated text to discuss plutonium requirements.	Adding irradiated fuel to the cask scope.
<b>Chapter 2</b>		
Section 2.6.7.3	Corrected 316 stainless steel yield strength value from 16900 psi to 17700 psi and reference from Table 2.2-1 to Table 2.2-2. Updated minimum margin of safety with revised yield strength.	Editorial correction.
Section 2.7.1.2.5	Corrected drawing number from 1018719 to 101E8719.	Administrative change.
Section 2.7.5	Revised wording to address fissile content.	Adding irradiated fuel to the cask scope.
Section 2.7.8	Added “and shielding” for completeness.	Administrative change.
Section 2.12.3.2	Changed “to 2.12.3-11” to “Figure 2.12.3-13”.	Administrative change.
<b>Chapter 3</b>		
Section 3	Deleted text from regulations and Table 3-1, as the regulation section numbers are cited and the wording is unnecessary.	Administrative change.
Section 3.1.2	Added “irradiated fuel” as contents.	Adding irradiated fuel to the cask scope.
Section 3.1.3.1	Changed reference to deleted Table 3-1 to reference to 10 CFR 71.71.	Administrative change.

NEDO-33866 Revision 6  
Non-Proprietary Information

Location	Description of Change (Rev. 3 to Rev. 4)	Reason for Change
Section 3.2.1	Deleted “HPI and” as the thermal properties of the HPI are discussed in the first sentence of this section.	Administrative change.
Section 3.3	Changed reference to deleted Table 3-1 to reference to 10 CFR 71.71.	Administrative change.
Section 3.3.1.1.1	Changed reference to deleted Table 3-1 to reference to 10 CFR 71.71 (two locations).	Administrative change.
<b>Chapter 5</b>		
Revised to include irradiated fuel as part of the approved content. The text, tables, and figures pertaining to irradiated hardware and byproducts, and to cobalt-60 isotope rods are unchanged. The majority of information pertaining to irradiated fuel was restored from Rev. 0, but with changes to reflect the current methodology. Minor administrative changes.		
<b>Chapter 6</b>		
Criticality evaluations reintroduced into Chapter 6 to add GE BWR 10x10 irradiated fuel as part of the approved contents. The majority of information pertaining to irradiated fuel was restored from Rev. 0, but with changes to reflect the current methodology.		
<b>Chapter 7</b>		
Chapter 7 content has been reduced to include only operating and regulatory requirements, since site specific procedures contain the detailed loading and unloading operations. Key parameters such as bolt torque values and decontamination requirements were not removed.		
Section 7.5	Updated to cite new last subsection of Chapter 7.	Administrative change.
Section 7.5.1	Updated references to Chapter 5 table and equation numbers. Changed “Reference 7-2” to “Reference 7-1.” Updated Loading Table to include the 1500 W thermal limit.	Administrative change.
Section 7.5.2	Updated references to Chapter 5 table numbers. Updated to cite new last subsection of Chapter 7. Updated Loading Table to include the 1500 W thermal limit.	Administrative change.
Section 7.5.3	Section added to include irradiated fuel as contents.	Adding irradiated fuel to the cask scope.
Section 7.5.4	Section updated to include irradiated fuel as contents.	Adding irradiated fuel to the cask scope.

NEDO-33866 Revision 6  
Non-Proprietary Information

Changes from Revision 4 to Revision 5 are listed in the following table. No revision bars are used for these changes. As indicated below, some of these changes were included to address NRC RAIs (U.S. NRC ADAMS Accession Number ML19296C273).

Location	Description of Change (Rev. 4 to Rev. 5)	Reason for Change
<b>Chapter 1</b>		
Section 1.2.2.1	Changed Item 3.e from “6 wt%” to “5 wt%.”	In response to RAIs 6.1 and 6.2.
<b>Chapter 5</b>		
Section 5.2	Irradiated Fuel Item 4 changed from “6 wt%” to “5 wt%.”	In response to RAIs 6.1 and 6.2.
Section 5.3.1.1	Included additional clarification for modeling the irradiated fuel source distribution.	In response to RAI 5.1.
Section 5.4.1.1	Removed the word “since.”	Administrative change.
Section 5.4.1.3	Removed the word “since.”	Administrative change.
Section 5.4.4.1	Removed enrichment ranges “ $5.0 \leq E < 5.5$ ” and “ $5.5 \leq E < 6.0$ ” from Tables 5.4-3, 5.4-4, 5.4-5, 5.4-6, 5.4-7, 5.4-8, 5.4-9, and 5.4-10.	In response to RAIs 6.1 and 6.2.
Section 5.5.1	Removed enrichment ranges “ $5.0 \leq E < 5.5$ ” and “ $5.5 \leq E < 6.0$ ” from Tables 5.5-2 and 5.5-5. Updated Table 5.5-4 naming convention.	In response to RAIs 6.1, 6.2, and clarification.
Section 5.5.5	Removed enrichment ranges “ $5.0 \leq E < 5.5$ ” and “ $5.5 \leq E < 6.0$ ” from Tables 5.5-33, 5.5-34, and 5.5-35.	In response to RAIs 6.1 and 6.2.
<b>Chapter 6</b>		
Section 6.9.4 was added to address RAI 6.1, which resulted in reducing the allowed content U-235 enrichment to 5 wt% and increasing the minimum pellet outer diameter. The initial baseline analyses and general conclusions presented in Section 6.3 through 6.6 remain applicable and were used as the starting point for the Section 6.9.4 analyses. The USL is based on the H/U-235 ratio of the most limiting evaluation; therefore, the USL decreased from 0.9387 to 0.9370. Additional discussions and administrative changes were included in several locations throughout Chapter 6 for the Section 6.9.4 analyses and the changes to the USL.		
Section 6.1.2	Table 6.1.2-1 updated to include the most limiting results from Section 6.9.4. Added Table 6.1.2-2 for justification of maintaining the 1750 g U-235 mass limit.	In response to RAI 6.1.
Section 6.3.2	Updated Table 6.3.2-5 to a U-235 enrichment of 5 wt%.	In response to RAIs 6.1 and 6.2.



NEDO-33866 Revision 6  
Non-Proprietary Information

Location	Description of Change (Rev. 4 to Rev. 5)	Reason for Change
Section 6.3.2	Removed Notes 2 and 3 below Table 6.3.2-5 for fissile materials that are not applicable to the approved content.	Administrative change.
Section 6.3.4	Updated USL based on a more conservative H/U-235 ratio from Section 6.9.4 analyses. Corrected the equation H/U-235 ratio calculation equation.	In response to RAI 6.1 and clarification.
Section 6.4.2	Removed statements about the final maximum $k_{eff}$ values; these values are determined by Section 6.9.4. Figure 6.4.2-1 updated with new USL value on plot. Updated Table 6.4.2-2 with the parameters for the cases modeled for fuel rod transport.	In response to RAI 6.1.
Section 6.5.2	Removed statements about the final maximum $k_{eff}$ values; these values are determined by Section 6.9.4. Figure 6.5.2-1 updated with new USL value on plot.	In response to RAI 6.1.
Section 6.6.2	Removed statements about the final maximum $k_{eff}$ values; these values are determined by Section 6.9.4. Figure 6.6.2-1 updated with new USL value on plot.	In response to RAI 6.1.
Section 6.8	Included a statement to justify the use and applicability of using MCNP6 Version 2.0 for the assessments in Section 6.9.4.	In response to RAI 6.1 and 6.5.
Section 6.8.1	Corrected the number of critical experiments from “69” to “36” and the enrichment from “4.92” to “4.306” weight percent.	In response to RAI 6.3.
Section 6.8.2.2.1	Added Section 6.8.2.2.1 to demonstrate that the benchmark data passes the normality tests.	In response to RAI 6.4.
Section 6.9.1	Clarification on the fuel rod pitch uncertainty. Figure 6.9.1-2 updated with new USL value on plot.	Clarification and in response to RAI 6.1.
Section 6.9.2.1.2	Figure 6.9.2-1 updated with new USL value on plot.	In response to RAI 6.1.
Section 6.9.3	Updated Table 6.9.3-1 to include descriptions for additional MCNP input files. Added Tables 6.9.3-6 and 6.9.3-7 for the MCNP results presented in Section 6.9.4.	In response to RAI 6.1.
Section 6.9.4	Included additional sensitivity studies to assess the criticality effects of changing fuel rod height.	In response to RAI 6.1.

NEDO-33866 Revision 6  
Non-Proprietary Information

Location	Description of Change (Rev. 4 to Rev. 5)	Reason for Change
Section 6.10	Added References 6-6, 6-10, 6-11, and 6-12.	In response to RAI 6.1 and 6.4.
<b>Chapter 7</b>		
Section 7.5.3	Removed enrichment ranges “ $5.0 \leq E < 5.5$ ” and “ $5.5 \leq E < 6.0$ ” from Table 7.5.3-1.	In response to RAIs 6.1 and 6.2.

NEDO-33866 Revision 6  
Non-Proprietary Information

Changes from Revision 5 to Revision 6 are listed in the following table. Revision bars are used for these changes.

Location	Description of Change (Rev. 5 to Rev. 6)	Reason for Change
<b>Chapter 1</b>		
Section 1.1	Updated reference to most recent NRC approved GEH Quality Assurance Program.	Administrative change.
Section 1.2.2.1	<p>Changed Item 1.a description:</p> <p>From: “Irradiated hardware components composed of stainless steels, carbon steels, nickel alloys, and zirconium alloys”</p> <p>To: “Irradiated hardware components composed of metallic alloys (e.g., stainless steels, carbon steels, Iron Chromium Aluminum (FeCrAl), nickel alloys, and zirconium alloys).”</p>	Clarification change.
Section 1.4	Updated Reference 1-1 to most recent NRC approved GEH Quality Assurance Program.	Administrative change.
<b>Chapter 5</b>		
Section 5.2	<p>Irradiated Hardware and Byproducts Item 1 description changed:</p> <p>From: “Hardware: Irradiated metals composed of materials such as SS, carbon steels, nickel alloys, and zirconium alloys.”</p> <p>To: “Hardware: Irradiated components composed of metallic alloys (e.g., SS, carbon steels, FeCrAl, nickel alloys, and zirconium alloys).”</p>	Clarification change.
<b>Chapter 8</b>		
Section 8.1	Updated references to most recent NRC approved GEH Quality Assurance Program.	Administrative change.
Section 8.1.1	Updated reference to most recent NRC approved GEH Quality Assurance Program.	Administrative change.
Section 8.4	Updated References 8-1 and 8-2 to most recent NRC approved GEH Quality Assurance Program.	Administrative change.

## ACRONYMS

Term	Definition
3D	Three-Dimensional
AEG	Average Energy Group
Amb.	Ambient
ANSI	American National Standards Institute
APDL	ANSYS Parametric Design Language
ASM	American Society for Metals
ASME	American Society of Mechanical Engineers
ASNT	American Society for Nondestructive Testing
ASTM	American Society for Testing and Materials
Aux.	Auxiliary
B&PVC	Boiler and Pressure Vessel Code
CFR	Code of Federal Regulations
C.G.	Center of Gravity
CSI	Criticality Safety Index
DOF	Degree-of-Freedom
DR	Total Dose Rate
DU	Depleted Uranium
EALF	Energy of Average Lethargy Causing Fission
[[	]]
FEA	Finite Element Analysis
FeCrAl	Iron Chromium Aluminum
GE	General Electric
GEH	GE-Hitachi Nuclear Energy Americas LLC
HAC	Hypothetical Accident (Transport) Conditions
HEPA	High Efficiency Particulate Air
HPI	High Performance Insert
H/U-235 Ratio	Hydrogen-to-U-235 Ratio

NEDO-33866 Revision 6  
Non-Proprietary Information

Term	Definition
IAEA	International Atomic Energy Agency
ID	Inner Diameter
MCNP	Monte Carlo N-Particle
MS	Margin of Safety
MSLD	Mass Spectrometer Leak Detector
NBS	National Bureau of Standards
NCT	Normal Conditions of Transport
NDE	Nondestructive Examination
Nom.	Nominal
NPT	National Pipe Taper (Thread)
NRC	Nuclear Regulatory Commission
OD	Outer Diameter
OR	Outer Radius
PNNL	Pacific Northwest National Lab
QAP	GEH Quality Assurance Program
S/N	Serial Number
SS	Stainless Steel
Std.	Standard
TCC	Thermal Contact Conductance
UNC	Unified Coarse
U-235	Uranium-235
UO <sub>2</sub>	Uranium Dioxide
U.S.	United States
USL	Upper Subcritical Limit
wt%	Weight Percent

## **1 GENERAL INFORMATION**

### **1.1 Introduction**

The Model 2000 Radioactive Material Transport Package was developed at Vallecitos Nuclear Center. The primary use of the packaging is to provide containment, shielding, impact resistance, criticality safety, and thermal resistance for its contents during normal and hypothetical accident conditions. The packaging is designed to transport Type B quantities of radioactive materials. It complies with the Nuclear Regulatory Commission (NRC) regulations contained in the Code of Federal Regulations, Title 10, Part 71 (10 CFR 71). The package is to be shipped in all modes of transportation, except air. The Model 2000 Transport Package may only be shipped exclusive use, as discussed in Section 5.1.2. The Criticality Safety Index (CSI) is determined to be 50, as discussed in Section 6.1.3.

Calculations, engineering logic, and all related documents that demonstrate compliance with regulations are presented in subsequent sections of this report.

The GEH Quality Assurance Program (QAP) (Reference 1-1) controls design, purchase, fabrication, handling, shipping, storing, cleaning, assembly, inspection, testing, operation, maintenance, repair and modification of the packages. The NRC has approved the GEH QAP under Docket Number 71-0254 upon demonstration that the quality assurance plan meets the requirements of Subpart H of 10 CFR 71.

### **1.2 Package Description**

The Model 2000 Transport Package, shown in Figure 1.2-1, is transported exclusive use, in the upright position. The approximate overall packaging dimensions are 131.5 inches in height and 72 inches in diameter. The approximate total weight of the package (packaging plus the contents) is 33,550 lb. Table 2.1-3 shows the breakdown of the component weights for the Model 2000 Transport Package.

The Model 2000 Transport Package and contents are described below:

#### **Packaging**

- Cask
- Overpack
- High performance insert (HPI)
- HPI material basket

#### **Contents**

- Solid radioactive materials

## 1.2.1. Packaging

### 1.2.1.1. Cask

The cask body (the containment vessel), shown in Figure 1.2-2, is constructed of two concentric, 1-inch thick stainless steel (SS) SS304 cylindrical shells (ASTM A240 / ASME SA 240). The shells are joined at the bottom end by a type SS304 forging (ASTM A182 / ASME SA 182). A SS304 forging connects the cask shell and cavity shell at the top end of the cask. This flange is part of the cask lid sealing joint and has an electropolished finish on the sealing surface. The annulus between the two shells is approximately 4 inches thick and filled with lead. The cask body height is approximately 71 inches and the outer diameter (OD) is approximately 38.5 inches. The cavity is approximately 26.5 inches in diameter and 54 inches deep.

The cask lid is made of SS304 and lead. It has a stepped design and is fully recessed into the cask top flange. The lid sealing surface is on the underside of the top flange and has an electropolish finish. The cask lid seal is composed of four rings of contoured [[ ]] material (two on the top and two on the bottom) bonded to a [[ ]] thick metal retainer with an OD of 34 inches. The area between the inner and outer seal is designed to permit flow for a seal test port to verify leak-tightness of the package by evaluating the performance of the inner seal. The cask lid [[ ]] and metal retainer material design is evaluated to support 1500 W decay heat. The cask lid seal is a [[ ]] retainer with four Parker Compound No. [[ ]] rings. The material specifications are included in Section 1.3.2.1. The cask lid is secured to the cask body by fifteen (15) 1¼-inch diameter socket head screws.

The cask has three penetrations. Only two of the three penetrations are within the cask containment boundary. They include: the drain and vent ports for the cask cavity. The drain port hole leads from the center of the cavity bottom out the side of the outer shell. The vent port line spirals through the cask lid near the cask centerline. The third penetration, that is not within the containment boundary, is the test port, which is used to test the adequacy of the seal joint after the cask body and lid are assembled. The test port path leads from the side of the top forging to the region between the inner and outer seals and is sealed in the same manner as the other penetrations.

All of the cask port seals are composed of ½ National Pipe Taper (NPT) thread socket head pipe plugs, followed by an exterior plug cover with O-ring to seal the port. The plug cover and O-ring provide a backup seal to the pipe plug, and they are not considered part of the containment boundary. The O-ring [[ ]] compound.

The cask body utilizes attachment plates for lifting devices that are detached during transport and rendered inoperable. There are three types of lifting devices use in the Model 2000 cask: (1) standard ears used for crane and fork truck handling; (2) auxiliary ears used for crane only handling; and (3) optional ears that function as a trunnion. Except for these devices, there are no other devices or features of the cask that could be used for lifting the package, once the cask is within the overpack.

### 1.2.1.2. Overpack

The cask is positioned inside a protective overpack, shown in Figure 1.2-3, for transport. The overpack is constructed of two 0.5-inch thick SS304 concentric cylindrical shells (ASTM A240/ASME SA 240), which are separated radially by eight equally spaced tubes along the length of the shells, and by two tube sections around the perimeter of the shells. A toroidal shell impact limiter made of SS304 is attached to each end of the overpack shells. The overpack opens just above the lower impact limiter for access to the cask. The top section of the overpack is joined to the base by fifteen (15) 1<sup>3</sup>/<sub>8</sub>-inch diameter shoulder screws. Gussets on the top and bottom impact limiters provide tie-down points for the package.

Additional impact protection is provided by aluminum honeycomb impact absorbers permanently positioned on the inside of the overpack at the top and bottom ends of the cask.

The cask sits on a 0.5-inch thick, 42-inch diameter plate called the cask support plate. It features eight square cross-section prongs welded to the plate perimeter to ensure cask concentricity within the overpack. The cask support plate material of construction is SS304; however, there are two cask support plate options. One option is solid SS304, while the other option includes a tungsten insert.

### 1.2.1.3. High Performance Insert

The Model 2000 Transport Package is equipped with an HPI, shown in Figure 1.2-4, to increase the shielding capability of the package. The HPI is nominally [[

]] The HPI body consists of [[ ]] SS concentric cylindrical shells. The annulus between the two shells is filled with [[ ]] thick depleted uranium. The HPI body is positioned in the cask cavity by five [[ ]] support disks [[ ]] to provide uniform support. The support disks are joined together by [[ ]] arms that function as the primary lifting fixture. The HPI body assembly is completed with the addition of ASME [[ ]] at each end of the cylindrical sub-assembly.

Closure of the HPI is provided by top and bottom plugs [[ ]] The bottom plug is a stepped design comprised of a [[ ]] thick depleted uranium cylinder encapsulated by a [[ ]] shell. Holes are machined in the [[ ]] on the HPI body. The bottom plug [[

]] The top plug is a stepped design comprised of a [[ ]] depleted uranium cylinder encapsulated by a [[ ]] shell. To facilitate lifting of the top plug, [[ ]] circular plate. The top plug is held in position by [[ ]] Attachment of the top and bottom plugs does not produce a pressure boundary. Grooves are cut into the surface of the plugs to allow moisture to escape during the vacuum drying process.



#### 1.2.1.4. HPI Material Basket

The material basket is shown in Figure 1.2-5 with an example of supplemental dunnage. The material basket is constructed of [[

]] pattern and are identified as Item 1 on Drawing 001N8424. See Figure 1.2-6 for material basket details. The outer [[ ]]] of the material basket form a composite section with the addition of [[

]] The center location of the material basket is a developed cell, which is created by the surrounding [[ ]]] To allow for the proper insertion of supplemental dunnage and facilitate fabrication, [[ ]]] are inserted at the top and bottom of the developed cell and are identified as Item 2 on Drawing 001N8424. Therefore, the exterior view of the material basket shows [[

]] facilitate loading and positioning of the material basket within the HPI cavity. Parts List 001N8424G001 is provided in Section 1.3.

### 1.2.2. Contents

#### 1.2.2.1. Radioactive Material Contents

The Model 2000 Transport Package is designed to transport Type B quantities of radioactive materials. This may include irradiated hardware and byproducts, Co-60 isotope rods, or irradiated fuel. The following are requirements for all shipments:

- a) The maximum quantity of material per package shall not exceed 5,450 lb, including all cask internals and contents (defined as “payload” for purposes of this report – see Table 2.1-3).
- b) All contents shipped shall be in solid form.
- c) All configurations require the use of the HPI.
- d) The decay heat for shipping all contents shall be limited to no more than 1500 W. However, a decay heat of 3000 W is conservatively used as the design basis for the Model 2000 Transport Package, where applicable. There are a few exceptions as noted within this SAR where 1500 W forms the basis; while a 1500 W decay heat is used in these sections, it is demonstrated that the 3000 W design basis is bounding.

The specific radioactive contents transported in the Model 2000 cask are:

1. Irradiated Hardware and Byproducts
  - a. Irradiated hardware components composed of metallic alloys (e.g., stainless steels, carbon steels, Iron Chromium Aluminum (FeCrAl), nickel alloys, and zirconium alloys).
  - b. Irradiated byproducts such as control rods and/or blades composed of hafnium and boron carbide.
  - c. Minimum decay time shall be at least 30 days prior to shipment.
  - d. Refer to loading table provided in Section 7.5.1
2. Cobalt-60 Isotope Rods
  - a. Must be shipped with the HPI material basket in the upright position and confined per 2.b and demonstrated to meet NCT.

NEDO-33866 Revision 6  
Non-Proprietary Information

- b. Content shall be in the form of pellets or cylindrical solid rods with the source(s) evenly distributed and encapsulated in normal or special form.
  - c. Total activity in any axial 1-inch increment in the HPI cavity must be  $\leq 17,000$  Ci (see Section 7.5.2).
3. Irradiated fuel
- a. Fuel type is GNF BWR 10x10 fuel.
  - b. Minimum cooling time of 120 days.
  - c. The active fuel length of any segment must be at least 5.3 inches.
  - d. Must be shipped with the HPI material basket in the upright position.
  - e. Maximum initial U-235 enrichment of 5 wt%.
  - f. Maximum U-235 mass of 1750 g.
  - g. Maximum burnup of 72 GWd/MTU.
  - h. Refer to loading table provided in Section 7.5.3.

Shipment of combined contents is allowed.

### 1.2.3. Special Requirements for Plutonium

All contents in the Model 2000 Transport Package are in solid form. Thus, any plutonium in excess of 0.74 TBq (20 Ci) per package shall be in solid form.

### 1.2.4. Operational Features

The Model 2000 Transport Package description in Section 1.2.1 shows that the packaging is not a complex system. There are no valves or items that require specialized knowledge for proper operation, and cooling is provided through natural convection and radiation. [[ ]] during installation, and only normal practices for seal handling (e.g., cleanliness) are required.

The Model 2000 Transport Package operation is described in Chapter 7. The loading operation is a dry or wet-loaded operation. If wet-loaded, the cask and cask internals contain features to allow easy drainage of water for underwater loading. To vacuum dry the cask, its cavity pressure is reduced below the vapor pressure of water and maintained at or below this pressure level for a period of time.

Content shoring may include components such as the rod [[ ]] holders shown in Figure 1.2-5. This example shoring is designed to fit into the HPI material basket (Drawing 001N8424), but other shoring components may be placed directly into the HPI cavity (Drawing 001N8423). The HPI material basket is loaded into the HPI cavity (Figure 1.2-4) if required for a specific content.

When the HPI top plug is installed (Drawing 001N8427), additional shoring may be added, as necessary, to ensure the [[ ]] between the bottom of the cask lid and the top of the HPI does not exceed 0.25 inches. However, no credit for shoring is given in the Normal Conditions of Transport (NCT) and Hypothetical Accident Conditions (HAC) evaluations. The required evaluations are included in this application to demonstrate safe transport of the Model 2000 Transport Package for the included contents with specified required internals.

NEDO-33866 Revision 6  
Non-Proprietary Information

Once the package is loaded onto the transport vehicle, external temperature measurements are taken of the loaded overpack. If any temperature exceeds 185°F, a protective personnel barrier is installed around the package to block access as discussed in Section 3.3.1.1.3. The cask containment boundary is illustrated in Figure 4.1.3-1.

[[

]]

**Figure 1.2-1. Model 2000 Packaging with High Performance Insert**

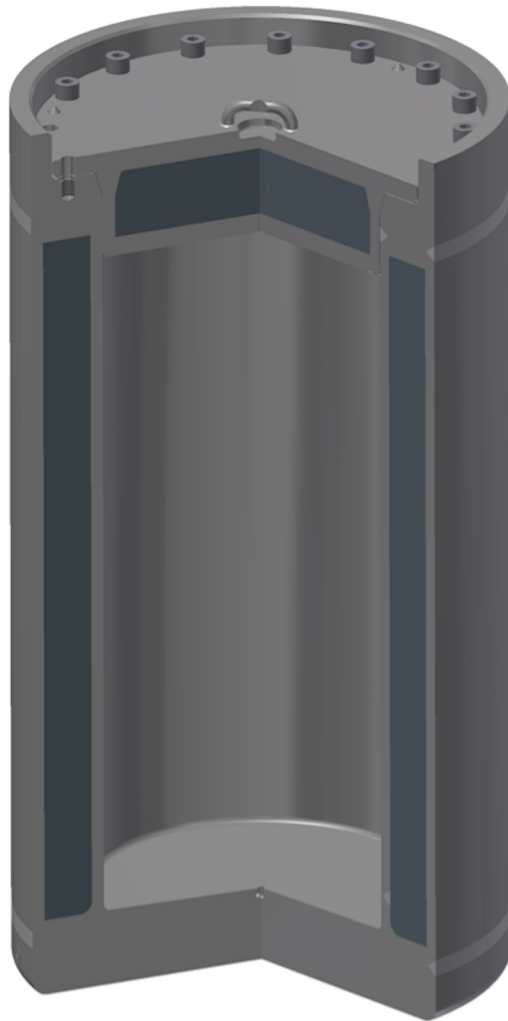


**Figure 1.2-2. Model 2000 Cask**

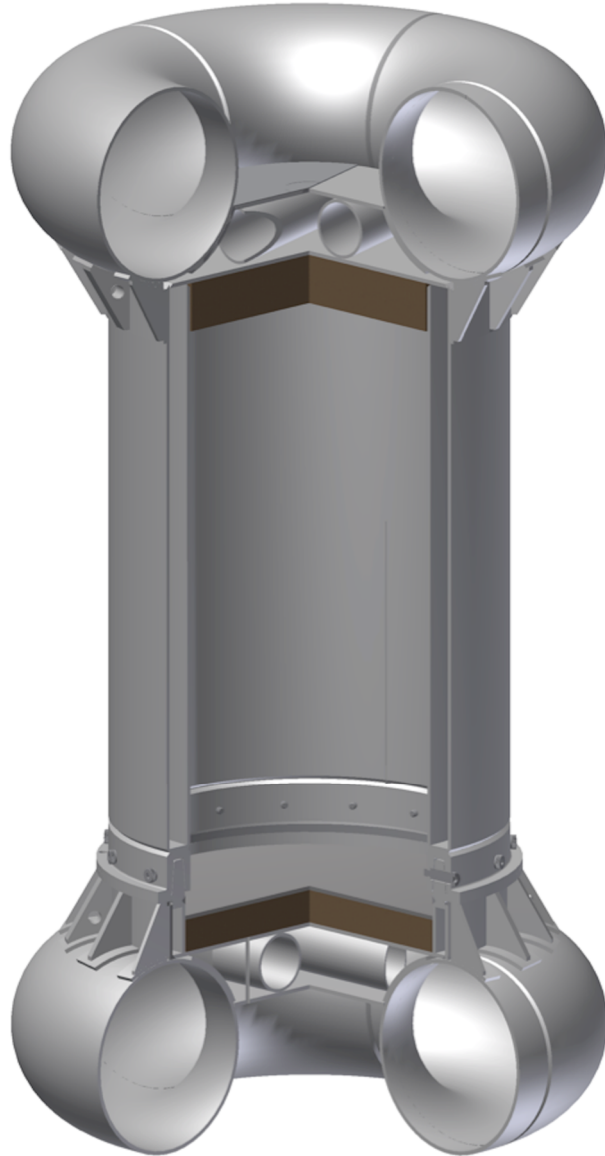


**Figure 1.2-3. Model 2000 Overpack**

[[

]]

**Figure 1.2-4. Model 2000 High Performance Insert with Material Basket**

[[

]]

**Figure 1.2-5. Material Basket and Rod [[ ]]** **Holder**

[[

]]

**Figure 1.2-6. Material Basket Details**



## 1.3 Appendix

### 1.3.1. Drawings

This section contains the Model 2000 Transport Package licensing drawings and bill of materials. Table 1.3-1 provides a list of current licensing drawings, which follow, and current revision level.

**Table 1.3-1. Model 2000 Packaging Licensing Drawings**

Drawing Number	Title	Revision
001N8422	GE 2000 HPI and Material Basket Licensing Drawing	3
001N8423	GE 2000 HPI Licensing Drawing	2
001N8424	GE 2000 HPI Material Basket Assembly Licensing Drawing	2
001N8425	GE 2000 HPI Body Licensing Drawing	2
001N8427	GE 2000 HPI Top Plug Assembly Licensing Drawing	2
001N8428	GE 2000 HPI Bottom Plug Assembly Licensing Drawing	2
101E8718	Model 2000 Shipping Cask S/N 2001	17
105E9520	Model 2000 Shipping Cask all S/N's Except S/N 2001	9
129D4946	Model 2000 Transport Container Assembly	12
101E8719	Model 2000 Shipping Cask Overpack S/N 2001	14
105E9521	Model 2000 Shipping Cask Overpack all S/N's Except S/N 2001	7

PARTS LIST 001N8422G001

[[						
						]]

NEDO-33866 Revision 6  
Non-Proprietary Information

DWG 001N8422 DRAWING

Proprietary in its Entirety

[[

]]

PARTS LIST 001N8423G001

[[						
						]]

NEDO-33866 Revision 6  
Non-Proprietary Information

**DWG 001N8423 DRAWING**

**Proprietary in its Entirety**

II

II

PARTS LIST 001N8424G001

[[						

]]

NEDO-33866 Revision 6  
Non-Proprietary Information

**DWG 001N8424 DRAWING**

**Proprietary in its Entirety**

II

II

PARTS LIST 001N8425G001

[[						

]]



NEDO-33866 Revision 6  
Non-Proprietary Information

**DWG 001N8425 DRAWING**

**Proprietary in its Entirety**

II

II

PARTS LIST 001N8427G001

[[						

]]

NEDO-33866 Revision 6  
Non-Proprietary Information

**DWG 001N8427 DRAWING**

**Proprietary in its Entirety**

II

II

PARTS LIST 001N8428G001

[[						

]]

NEDO-33866 Revision 6  
Non-Proprietary Information

**DWG 001N8428 DRAWING**

**Proprietary in its Entirety**

II

II

NEDO-33866 Revision 6  
Non-Proprietary Information

## PARTS LIST 101E8718

[illegible]

]]

NEDO-33866 Revision 6  
Non-Proprietary Information

**DWG 101E8718 DRAWING**

**Proprietary in its Entirety**

II

II

NEDO-33866 Revision 6  
Non-Proprietary Information

**DWG 101E8718 DRAWING**

**Proprietary in its Entirety**

II

II



NEDO-33866 Revision 6  
Non-Proprietary Information

## PARTS LIST 105E9520

[illegible]

]]

NEDO-33866 Revision 6  
Non-Proprietary Information

**DWG 105E9520 DRAWING**

**Proprietary in its Entirety**

II

II

NEDO-33866 Revision 6  
Non-Proprietary Information

DWG 105E9520 DRAWING

Proprietary in its Entirety

[[

]]

PARTS LIST 129D4946

[[							

]]

NEDO-33866 Revision 6  
Non-Proprietary Information

DWG 129D4946 DRAWING

Proprietary in its Entirety

[[

]]

NEDO-33866 Revision 6  
Non-Proprietary Information

## PARTS LIST 101E8719

[illegible]

]]

[[

]]

NEDO-33866 Revision 6  
Non-Proprietary Information

## PARTS LIST 105E9521

[illegible]

]]



NEDO-33866 Revision 6  
Non-Proprietary Information

**DWG 105E9521 DRAWING**

**Proprietary in its Entirety**

II

II

### **1.3.2. Material Specifications**

#### **1.3.2.1. Seal Specifications**

The Parker [[ ]] material specification for Parker Compound [[ ]] for the cask lid seal and port "O" rings is provided below.

[[

]]

#### **1.4 References**

- 1-1 GE-Hitachi Nuclear Energy, "Quality Assurance Program Description," NEDO-11209-A, Latest NRC Approved Revision.
- 1-2 Parker Hannifin Corporation, "Gask-O-Seal and Integral Seal Design Handbook," CSS 5124, 2010.

## **2 STRUCTURAL EVALUATION**

This chapter presents the structural evaluation of the Model 2000 Transport Package, and demonstrates that the design meets all applicable structural criteria. All components that comprise the Model 2000 Transport Package are evaluated to the applicable regulatory requirements that includes the NCT and HAC, in accordance with 10 CFR 71 (Reference 2-1). Detailed description of each package component is provided in in Section 2.1.1.

The decay heat limit for shipping all contents shall be conservatively limited to 1500 W. However, a decay heat of 3000 W is conservatively used as the basis for the Model 2000 Transport Package structural evaluation (analysis) in this chapter. Analyses comply with the methodology and criteria presented in Section 2.1.2. The structural design of the Model 2000 Transport Package is based on the following critical characteristics:

- Ensure the maximum payload weight does not exceed 5,450 pounds.
- Maintain structural integrity when subjected to the thermal conditions (3000 W maximum) associated with NCT and HAC in Chapter 3. This section demonstrates packaging integrity at extreme thermal conditions during NCT and HAC.
- Maintain containment integrity to remain leaktight during NCT and HAC as documented in Chapter 4. This section demonstrates cask containment integrity during NCT and HAC.
- Maintain integrity of lead and depleted uranium (DU) shielding boundaries during NCT and HAC to support Chapter 5. This section demonstrates that the shielding integrity is maintained during NCT and HAC to support the shielding analysis assumptions.

### **2.1 Description of Structural Design**

#### **2.1.1. Discussion**

The Model 2000 Transport Package consists of a welded overpack structure containing a steel-encased, lead cask structure. The cask structure is a lead-filled SS304 weldment, cylindrical in shape, and measuring approximately 38.5 inches OD by 71 inches high. The inner cavity is 26.5 inches ID by 54 inches high. The lead shielding provided is approximately 4 inches of lead on the sides.

The cask body shell is made of 1 inch thick SS304 plate. At the bottom, the shells are welded to a 6-inch thick SS304 forging. At the upper section, the containment shell joins a 9-inch thick SS304 forging. This forging provides support and sealing surface to the cask seal. Also, it contains 15 equally spaced, internally threaded holes on a 32.25-inch diameter bolt circle. Fifteen 1¼-inch diameter ASTM A540 socket head screws attach the lid to the cask body during operation. The cask lid is SS304 encasing a lead cylinder. The lid has a lifting lug for handling.

There are three penetrations into the cask cavity. One serves as a drain for the cask cavity and another one as a vent. The drain hole goes from the center of the cavity bottom to the side of the outer surface. The vent line spirals through the cask lid around the center. These penetrations provide means to eliminate water from the cask cavity collected during underwater operations.

A ½ NPT socket head pipe plug followed by a 1¾ - 12 UN-2A cap closes both penetrations. The cap O-ring provides backup sealant to the pipe plug. The third penetration is used as a testing port for the cask seal joint. It is located in the upper forging on the side surface of the cask.

The cask lid seal and O-rings use Parker Compound No. [ ] material retainer. The cask lid seal retainer has a 34 inch OD and 28 inch ID. The cask lid seal and O-rings are designed for a 1500 W maximum content heat load.

The welded SS304 overpack structure is composed of two concentric cylinders, separated vertically by eight equally spaced [ ] sections. The external cylinder has a 48.5-inch OD. The internal cylindrical shell is 40.5-inch ID. A 24-inch [ ] diameter toroidal shell is attached at both ends of the external cylinder, and a circular plate is welded across the inner region of the torus. The internal cylinder is closed at each end by circular plates. All materials are 0.5 inches thick with the exception of the space [ ] and toroidal shells. The vertical [ ]

]]

The toroidal shells may be fabricated using four 90° elbows (or two 180° returns). However, the Model 2000 toroidal shell wall thickness range is limited to 0.5 inches minimum to 0.76 inches maximum. The overpack structure separates near the bottom end to allow access to the lead cask. A collar 0.75 inches thick is attached in this area to provide bearing surface for the connecting bolts. A total of fifteen (15) 1-⅜ inches diameter ASTM A540 shoulder screws join both portions of the overpack structure. The toroidal shell of the overpack structure acts as an energy-absorbing device during the postulated drop conditions. In addition, the overpack structure provides thermal shielding for the lead cask in the event of a fire.

A total of 20 reinforcing ribs cradle the toroidal shell to the vertical cylinder. Four of the ribs provide tie-down points for the package during transport. These ribs also provide a means for lifting and removing the overpack top section using a spreader bar. The spreader bar is not part of the transport packaging.

There is a 6-inch thick aluminum honeycomb pad attached to the top inner surface of the overpack structure. A 4-inch thick aluminum honeycomb pad covered by a ½ inch thick circular plate provides a surface base for the lead cask structure. These honeycomb pads are included in the overpack structure design to assure a uniform loading distribution on the cask surface during the postulated free-drop events.

The Model 2000 Transport Package is equipped with a high performance insert (HPI) to increase the shielding capability of the package. The HPI is [ ]

[ ] The cavity is approximately [ ] The HPI body consists [ ] inch stainless steel concentric cylindrical shells. The annulus between the [ ] shells is filled with [ ] thick depleted uranium. The HPI body is positioned in the cask cavity by five [ ] (Table 2.2-3) support disks arranged axially to provide uniform support. The support disks are joined together by four [ ] vertical lifting arms that function as the primary lifting fixture. The HPI body assembly is completed with the addition of ASME [ ] at each end of the cylindrical sub-assembly.

Top and bottom plugs joined to the ASME [[ ]] provide closure of the HPI. The bottom plug [[ ]] and a [[ ]] thick depleted uranium cylinder encapsulated by a [[ ]] shell. Holes are machined in the [[ ]] on the HPI body. The bottom plug is attached to the bottom [[ ]] with eight (8) 7/8-inch socket head cap screws and four [[ ]] The top plug is a stepped design comprised of [[ ]] depleted uranium cylinder encapsulated by a [[ ]] shell. To facilitate lifting of the top plug, four hoist rings are recessed into the [[ ]] circular plate. The top plug is held in position by [[ ]] Attachment of the top and bottom plugs does not produce a pressure boundary. Grooves are cut into the surface of the plugs to allow moisture to escape during the vacuum drying process.

The material basket is a shoring device, which may be used for carrying various contents. The material basket is constructed of 18 full-length [[ ]], which form a [[ ]] pattern and are identified as Item 1 on drawing 001N8424. See for material basket details. The outer [[ ]] of the material basket form a composite section with the addition of stiffener plates welded to adjacent [[ ]] The center location of the basket is a developed cell, which is created by the surrounding [[ ]] To allow for the proper insertion of additional content shoring and facilitate fabrication, two partial length [[ ]] are inserted at the top and bottom of the developed cell and are identified as Item 2 on drawing 001N8424. Therefore, the exterior view of the basket shows [[ ]] Four circular [[ ]] evenly spaced in the axial direction facilitate loading and positioning of the material basket within the HPI cavity. In addition, dunnage (for example [[ ]] holders) may be used as a cask loading mechanism and to shore the contents during transport.

### **2.1.2. Design Criteria**

This section defines the stress allowables for all the stresses resulting from the regulatory load combinations given in NRC Regulatory Guide 7.8 (Reference 2-2).

The cask is evaluated per ASME Service Levels A and D, normal and accident conditions, respectively. The analyses methods and stress criterion allowed by the ASME Code, Section III-Subsection NB is employed. Stress intensities caused by mechanical loads are combined before comparing to ASME code stress allowables, which are listed in Table 2.1-1.

**Table 2.1-1. Structural Design Criteria for Model 2000 Cask**

ASME CLASS 1 DESIGN	STRESS LIMITS
Normal conditions: Service Level A	$P_m \leq S$ $P_m + P_b \leq 1.5 S_m$ $P_m + P_b + Q \leq 3 S_m$ Bearing Stress $\leq S_y$ at temperature
Accident conditions: Service Level D	$P_m \leq 2.4 S_m$ or $0.7 S_u$ (whichever is less) $P_m + P_b \leq 3.6 S_m$ or $1.0 S_u$ (whichever is less)

Note:  $P_m$  = primary membrane stress intensity,  $P_b$  = primary bending stress intensity,  $S_m$  = design stress intensity,  $S_y$  = yield strength,  $S_u$  = ultimate strength,  $Q$  = secondary stress associated with thermal expansion.

The HPI is evaluated per ASME Service Levels A and D, normal and accident conditions, respectively. The analyses methods and stress criterion allowed by the ASME Code, Section III-Subsection NF is employed. Allowable stresses are based on section NF-3200. For normal conditions (Service Level A), design limits are defined in paragraph NF-3221.1. For accident conditions (Service Level D), design limits are defined in Appendix F of ASME Code, Section III (Reference 2-3). Note the evaluation of thermal stresses is not required per ASME Code III-NF (NF-3121.11). Stress intensities caused by mechanical loads are combined before comparing to ASME code stress allowables, which are listed in Table 2.1-2.

**Table 2.1-2. Structural Design Criteria for HPI and Material Basket**

ASME CLASS 1 DESIGN	STRESS LIMITS
Normal Conditions: Service Level A (NF-3221.1)	$P_m \leq S_m$ $P_m + P_b \leq 1.5 S_m$
Bearing Loads: Service Level A (NF-3223.1)	$S_y$ at temperature
Pure Shear: Service Level A (NF-3223.2)	$0.6 S_m$
Bearing Loads: Service Level D (Appendix F, F-1332.3)	Except for pinned and bolted joints, bearing stresses need not be evaluated for loads for which Level D Service Limits are specified.
Pure Shear: Service Level D (Appendix F, F-1332.4)	$0.42 S_u$
Accident Conditions: Service Level D (Appendix F, F-1332)	$P_m > 1.2 S_y$ and $1.5 S_m < 0.7 S_u$ $P_m + P_b < 150\%$ of the limit for general primary stress intensity $P_m$

Note:  $P_m$  = primary membrane stress intensity,  $P_b$  = primary bending stress intensity,  $S_m$  = design stress intensity,  $S_y$  = yield strength,  $S_u$  = ultimate strength.

### 2.1.3. Weights and Centers of Gravity

The weights and center of gravity of the Model 2000 Transport Package and detailed contents are presented in Table 2.1-3. Refer to Section 1.3.1 for component dimensions.

NEDO-33866 Revision 6  
Non-Proprietary Information

**Table 2.1-3. Summary of Maximum Weights**

DESCRIPTION	DRAWING NUMBER	WEIGHT (LB)	C.G. (IN) <sup>1</sup>
<b>Total Overpack plus Cask Weight</b>	—	<b>28,100</b>	<b>63.9</b>
Cask Overpack	101E8719/ 105E9521	10,200	—
Cask Body	101E8718/ 105E9520	16,000	—
Closure Lid	101E8718/ 105E9520	1,900	—
<b>Payload Weight<sup>2</sup></b>	—	<b>5,450</b>	<b>62.3</b>
HPI Assembly	001N8423	[[	—
Material Basket	001N8424		—
Contents plus Shoring	—	]] <sup>3</sup>	—
<b>Total Package Weight</b>	—	<b>33,550</b>	<b>63.6</b>

- Notes:
1. Center of Gravity (C.G.) measured from component base.
  2. The HPI plus material basket plus radioactive contents (with shoring) is defined as payload for purposes of this report.
  3. If material basket is not used, contents plus shoring maximum weight is [[ ]] lb.

**Table 2.1-4. Overpack Base Weight**

Assembly ID	Component Description	Weight (lb)
2	[[	
4		
5		
6		
7		
8		
12		
13		
14		
15		
16		
19		
25		
26		
27		]]
	Total Overpack Base Weight =	3,633.15



#### **2.1.4. Identification of Codes and Standards for Package Design**

This section identifies the established codes and standards proposed for use in the Model 2000 Transport Package design, fabrication, assembly, testing, maintenance, and use.

The Model 2000 cask with HPI and material basket is allowed to ship a maximum of 1500 W of various radioactive contents. Per Regulatory Guide 7.11 (Reference 2-4), the package is considered Category I—Greater than 3,000 A2 or greater than 30,000 Ci. From NUREG/CR-3854 (Reference 2-5), the fabrication code and standard is:

- The criteria for fabricating metal components of shipping containers used for transporting radioactive materials are based on the ASME Code Section III (Reference 2-3). ASME Code Section III is used for the design and fabrication of the HPI and material basket.

##### **2.1.4.1. Category I Requirements**

Acceptable criteria for the fabrication of metal components of shipping containers are contained in the ASME Code Section III, Subsection NB for containment components; Subsection NG for criticality components and Section VIII, Division I or Section III, Subsection NF for other safety components.

- The Model 2000 cask provides containment. Therefore, the cask shall be fabricated to Section III, Subsection NB.
- The HPI and material basket are relied upon for shielding, which falls under Component Safety Group "Other Safety". Therefore, the insert shall be fabricated to Section VIII, Division 1 or Section III, Subsection NF.

##### **2.1.4.2. Component Classification According to Importance to Safety**

The parts lists in Section 1.3.1 identify the Category A, B and C items for the Model 2000 cask, overpack, HPI, and material basket. The safety classification of all components is based on importance to safety criteria per NUREG/CR-6407 (Reference 2-6).

- For the Model 2000 cask, the components that comprise the cask inner shell, top forging, cask seals and lid are considered part of the containment boundary. Therefore, these items are Category A. Components such as the lead shielding, lifting and tie-down devices meet the definition of Category B items. See the parts lists in Section 1.3.1 for Drawing 101E8718 and 105E9520 for the Model 2000 cask assembly parts classification.
- See the parts list, Section 1.3.1, Drawing 001N8424, for the material basket assembly parts classification.
- The material basket is considered dunnage, and is not required to reduce impact loading on the containment boundary. However, it is required to maintain geometry during NCT to support the shielding analysis assumptions. Therefore, it is considered a Category B item. In addition, for fabrication, [[ ]] welds are Safety Category B. See the parts list in Section 1.3.1 for Drawing 001N8424 for the material basket assembly parts classification.

## 2.2 Materials

This section presents the mechanical properties of materials used to evaluate the performance of the Model 2000 cask, overpack, HPI, and material basket. Materials of construction for each component are found in Section 1.3.1, in the parts lists that accompany drawings.

### 2.2.1. Material Properties and Specifications

The material properties used in the structural analysis of the Model 2000 cask, HPI and material basket are presented in Tables 2.2-1 through 2.2-9. Material properties specific to the impact analysis are presented in Section 2.12.1.

**Table 2.2-1. Structural Properties of Type 304 Stainless Steel**

Temperature (°F)	-20	70	200	300	400	500	600	700	800	900	1000
Ultimate Tensile Strength $S_u$ (ksi)	75.0	75.0	71.0	66.2	64.0	63.4	63.4	63.4	62.8	60.8	57.4
Yield Strength $S_y$ (ksi)	30.0	30.0	25.0	22.4	20.7	19.4	18.4	17.6	16.9	16.2	15.5
Design Stress Intensity $S_m$ (ksi)	20.0	20.0	20.0	20.0	18.6	17.5	16.6	15.8	15.2	—	—
Modulus of Elasticity (E+3, ksi)	28.8 <sup>a</sup>	28.3	27.5	27.0	26.4	25.9	25.3	24.8	24.1	23.5	22.8
Mean Coefficient of Thermal Expansion $\alpha$ (E-6, in/in/°F)	—	8.5	8.9	9.2	9.5	9.7	9.9	10.0	10.1	10.2	10.3
Poisson's Ratio	← 0.31 →										
Density (lb/in <sup>3</sup> )	← 0.290 →										

References:

Reference 2-7 Ultimate Tensile Strength: Table U, Page 493, Line 22.

Reference 2-7 Yield Strength: Table Y-1, Page 610 & 611, Line 26.

Reference 2-7 Design Stress Intensity: Table 2A, Page 306, Line 19.

Reference 2-7 Modulus of Elasticity: Table TM-1, Material Group G, Page 738.

Reference 2-7 Mean Coefficients of Thermal Expansion: Table TE-1, Group 3, Coefficient B, Page 711.

Reference 2-7 Poisson's Ratio: Table PRD, High Alloy Steels (300 series), Page 744.

Reference 2-7 Density: Table PRD, High Alloy Steels (300 series), Page 744.

Note:

<sup>a</sup> This value was interpolated.

Table 2.2-2. Structural Properties of ASME Type [[

[[											

Note:  
<sup>a</sup> Interpolated.

]]

**Table 2.2-3. Structural Properties of ASME Type [[**

[[											

]]

Note:

<sup>a</sup> Interpolated.

**Table 2.2-4. Structural Properties of Depleted Uranium Metal**

Temperature (°F)	-20	70	200	300	400	500	600	700	800	900	1000
Yield Strength S <sub>y</sub> (ksi)	—	47.2	43.8	40.2	36.3	33.3	30.5	23.9	15.3	9.3	5.8
Modulus of Elasticity (E+3, ksi)	—	23.6	—	—	—	—	—	—	—	—	—
Poisson's Ratio	← 0.335 →										
Density (lbm/in <sup>3</sup> )	← 0.674 – 0.689 →										

References:

Reference 2-8 Yield Strength: Figure 1, Page 671.

Reference 2-8 Density: Page 670.

Reference 2-9 Modulus of Elasticity: Table 7, Page 19.

Reference 2-9 Poisson's Ratio: Table 7, Page 19.

**Table 2.2-5. Structural Properties of Lead**

Temperature (°F)	-40	-20	70	200	300	400	600
Modulus of Elasticity (E+3, ksi)	2.58	2.55 <sup>a</sup>	2.42	2.21	2.04	1.77	1.49
Yield Strength (psi)	795	763 <sup>a</sup>	620	500	400	—	—
Mean Coefficient of Thermal Expansion $\alpha$ (E-6, in/in/°F)	15.6 <sup>a</sup>	15.7 <sup>a</sup>	16.1 <sup>a</sup>	16.7 <sup>a</sup>	17.3 <sup>a</sup>	18.5 <sup>b</sup>	—
Poisson's Ratio	← 0.4 →						
Density (lb/in <sup>3</sup> )	← 0.4097 →						

References:

Reference 2-10 Modulus of Elasticity: Figure B-8.

Reference 2-11 Yield Strength at (-40°F – 70°F ).

Reference 2-12 Yield Strength: (200°F – 300°F ): Figure 12.

Reference 2-10 Mean Coefficient of Thermal Expansion: Figure A-3.

Reference 2-13 Poisson's Ratio: Table 6.1.9, Page 6-10.

Reference 2-13 Density: Table 6.4.1, Page 6-47.

Notes:

<sup>a</sup> Interpolated

<sup>b</sup> Value for 440.33°F (500 K) used.

**Table 2.2-6. Bolt – ASTM A-540 Grade B21 Class 3**

Temperature (°F)	150	455
Ultimate Tensile Strength $S_u$ (ksi)	145	
Yield Strength $S_y$ (ksi)	127.9 <sup>a</sup>	117.2 <sup>a</sup>
Design Stress Intensity $S_m$ (ksi)	42.6 <sup>a</sup>	39.1 <sup>a</sup>
Modulus of Elasticity (E+3, ksi)	29.2 <sup>a</sup>	27.7 <sup>a</sup>
Mean Coefficient of Thermal Expansion $\alpha$ (E-6, in/in/°F)	6.6	7.2
Poisson's Ratio	← 0.30 →	
Density (lb/in <sup>3</sup> )	← 0.280 →	

References:

Reference 2-7 Tensile Strength: Table U, Page 473, Line 11

Reference 2-7 Yield Strength: Table Y-1, Page 562, Line 36

Reference 2-7 Design Stress Intensity: Table 4, Page 366, Line 20

Reference 2-7 Modulus of Elasticity: Table TM-1, Material Group C, Page 738

Reference 2-7 Mean Coefficient of Thermal Expansion: Table TE-1, Group 1, Coefficient B, Page 708

Reference 2-7 Poisson's Ratio: Table PRD, Low alloy steels: ½Cr to 1-¼Cr steels, Page 744

Reference 2-7 Density: Table PRD, Low alloy steels: ½Cr to 1-¼Cr steels, Page 744

Note:

<sup>a</sup> Interpolated

**Table 2.2-7. Internal Thread – ASME SA-182 F304**

Temperature (°F)	150	455
Ultimate Tensile Strength $S_u$ (ksi)	73 <sup>a</sup>	63.7 <sup>a</sup>
Yield Strength $S_y$ (ksi)	26.7	20 <sup>a</sup>
Design Stress Intensity $S_m$ (ksi)	20.0	17.9 <sup>a</sup>
Modulus of Elasticity (E+3, ksi)	27.8 <sup>a</sup>	26.1 <sup>a</sup>
Mean Coefficient of Thermal Expansion $\alpha$ (E-6, in/in/°F)	8.8	9.7 <sup>a</sup>
Poisson's Ratio	← 0.31 →	
Density (lb/in <sup>3</sup> )	← 0.290 →	

References:

Reference 2-7 Tensile Strength: Table U, Page 493, Line 16

Reference 2-7 Yield Strength: Table Y-1, Page 610, Line 11

Reference 2-7 Design Stress Intensity: Table 5A, Page 410, Line 25

Reference 2-7 Modulus of Elasticity: Table TM-1, Material Group G, Page 738

Reference 2-7 Mean Coefficient of Thermal Expansion: Table TE-1, Group 3, Coefficient B, Page 711

Reference 2-7 Poisson's Ratio: Table PRD, High Alloy Steels (300 series), Page 744

Reference 2-7 Density: Table PRD, High Alloy Steels (300 series), Page 744

Note:

<sup>a</sup> Interpolated

**Table 2.2-8. ASTM A-193 B6 Bolt Properties**

Minimum Ultimate Tensile Strength $S_u$ (ksi)	110
Minimum Yield Strength $S_y$ (ksi)	85
Design Stress Intensity $S_m$ (ksi)	26.5 <sup>ab</sup>
Modulus of Elasticity (E+3, ksi)	28.1 <sup>ab</sup>
Mean Coefficient of Thermal Expansion $\alpha$ (E-6, in/in/°F)	6.2 <sup>b</sup>
Poisson's Ratio	0.31
Density (lb/in <sup>3</sup> )	0.280

References:

Reference 2-7 Minimum Ultimate Tensile Strength: Table 3, Page 339, Line 17

Reference 2-7 Minimum Yield Strength: Table 3, Page 339, Line 17

Reference 2-7 Stress Intensity: Table 4, Page 366, Line 25

Reference 2-7 Modulus of Elasticity: Table TM-1, Material Group F, Page 738

Reference 2-7 Mean Coefficient of Thermal Expansion: Table TE-1; Coefficients for 12Cr, 12Cr-1Al, 13Cr, and 13Cr-4Ni Steels; Page 710.

Reference 2-7 Poisson's Ratio: Table PRD, High alloy steels (400 series), Page 744

Reference 2-7 Density: Table PRD, High alloy steels (400 series), Page 744

Notes:

<sup>a</sup> Interpolated

<sup>b</sup> Evaluated at 250°F

**Table 2.2-9. ASTM A-540 Grade B22 Class 3 Bolt Properties**

Minimum Ultimate Tensile Strength $S_u$ (ksi)	145
Minimum Yield Strength $S_y$ (ksi)	115.7
Design Stress Intensity $S_m$ (ksi)	37.6 <sup>a1</sup>
Modulus of Elasticity (E+3, ksi)	27.4 <sup>a1</sup>
Mean Coefficient of Thermal Expansion $\alpha$ (E-6, in/in/°F)	7.3 <sup>a</sup>
Poisson's Ratio	0.30
Density (lb/in <sup>3</sup> )	0.280

References:

Reference 2-7 Minimum Ultimate Tensile Strength: Table 3, Page 335, Line 25

Reference 2-7 Minimum Yield Strength: Table 3, Page 335, Line 25

Reference 2-7 Design Stress Intensity: Table 4, Page 366, Line 4

Reference 2-7 Modulus of Elasticity: Table TM-1, Group C, Page 738

Reference 2-7 Mean Coefficient of Thermal Expansion: Table TE-1, Group 1, Column B, Page 708

Reference 2-7 Density: Table PRD, Low alloy steels: ½-Cr to 1-¼Cr steels, Page 744

Notes:

<sup>a</sup> Evaluated at 500°F

<sup>1</sup> B21 Bolt properties used because data for B22 Bolts could not be found

### 2.2.2. Chemical, Galvanic, or Other Reactions

The Model 2000 cask is fabricated from SS304, SS316, and lead. The lead is completely encased in the SS. This construction excludes moisture at the stainless boundary, thus assuring no galvanic or deleterious reactions could occur. The cask contents contact the stainless cavity surface. The radioactive material contents are in solid form and typically are placed in supplemental shoring. GEH's experiences in operating other transport packages with similar arrangements show that chemical, galvanic or other reactions between the cask cavity surface and the radioactive material shoring, or between the shoring and their solid contents, do not occur.

The structural components of the HPI and material basket are fabricated from SS304, [[ ]] steels, which are chemically compatible. These materials are selected because of their strength, ductility, and high resistance to corrosion and brittle fracture over a broad temperature range and high levels of radiation. Therefore, no chemical or galvanic reaction is anticipated. The primary function of the HPI body, including top and bottom plugs, is to encapsulate the depleted uranium shield. Depleted uranium is cast and machined to precise tolerance to form the required shield geometry. To prevent potential oxidation, assembly of the shield is performed in an inert atmosphere. Once encapsulated, oxidation and galvanic reactions with stainless steel does not occur.

The cask containment features have no indication of chemical or galvanic reactions between [[ ]] compounds and stainless interfaces of the cask. This has been confirmed in the qualification of the cask containment.

### 2.2.3. Effects of Radiation on Materials

Gamma radiation has no significant effect on metal and therefore, the radiation produced by the contents does not cause any measurable damage to the packaging metallic components (stainless steel, aluminum, depleted uranium, and lead). Seals are inspected prior to each use. The Parker O-ring Handbook (Reference 2-14) states that when experiencing radiation levels  $1 \times 10^6$  rads the effects on all compounds are minor. The maximum absorbed dose rates that these [[ ]]

seals could be exposed to through a year of continuous use, with the cask loaded and maximum cobalt-60 activity, are on the order of  $10^2$  to  $10^4$  rad. As the Model 2000 is not a storage cask, overall exposure time for the seals is significantly shorter than an entire year. With a 1-year replacement period on the [[ ]] seals and O-rings, there is no significant degradation of the seals due to irradiation.



## **2.3 Fabrication and Examination**

### **2.3.1. Fabrication**

Fabrication and examination of the Model 2000 Transport Package (i.e., overpack and cask) conform to the requirements of ASME Section, III, Subsection NB for Category A and B components. Components of the HPI assembly and material basket assembly that are Category B items are fabricated in accordance with ASME Section III, Subsection NF. Fabrication of package components follows the guidelines presented in NUREG/CR-3854, Fabrication Criteria for Shipping Containers (Reference 2-5). All package components are fabricated in accordance with an NRC approved quality assurance program.

### **2.3.2. Examination**

Examination of the Model 2000 Transport Package (i.e., overpack and cask) conforms to the requirements of ASME Section, III, Subsection NB for Category A and B components. Components of the HPI assembly and material basket assembly that are Category B items are examined in accordance with ASME Section III, Subsection NF. All package components are examined in accordance with an NRC approved quality assurance program.

## **2.4 General Requirements for All Packages**

This section addresses the requirements of 10 CFR 71.43, “General Standards for All Packages.”

### **2.4.1. Minimum Package Size**

The smallest overall dimension of the Model 2000 Transport Package is 131.5 inches. The cask overall dimensions are 71.0 inches high and 38.5 inches OD.

### **2.4.2. Tamper-Indicating Feature**

A lock wire and seal of the type that must be broken is installed across the overpack joint section. This seal while intact, would be evidence that unauthorized persons have not opened the package.

### **2.4.3. Positive Closure**

The Model 2000 Transport Package is an assembly of components for shipping radioactive material contents inside of a cask with a design pressure of 30 psia. The cask is sealed using a gasket and fifteen 1¼-inch socket head screws. In turn, the cask is contained by the overpack structure, which is bolted closed during transport by 15 shoulder bolts. With this double closure, overpack and cask, inadvertent opening of the cask cannot occur. The vent and drain ports on the cask each are plugged and sealed by pipe plugs and straight thread caps with O-rings.

The evaluation of the closure bolts is presented in Section 2.12.4. Review of the closure bolt evaluation at 3000 W shows that the bolt preload does not change as a result of the increase in thermal load. The closure bolt calculation shows that the controlling loads for the bolt preload are the internal pressure and the pin puncture loads. Further review of the temperatures presented in Chapter 3 show that because of the thermal modeling methodology, the heat load is concentrated

in the HPI and material basket. As a result, the temperature distribution in the closure bolt and flange are more uniform resulting in a smaller temperature delta and lower thermal stresses. To maintain positive closure during normal and hypothetical accident conditions, the closure bolts are torqued to  $720 \pm 30$  ft-lb.

## **2.5 Lifting and Tie-Down Standards for All Packages**

The regulations require that lifting devices which are a structural part of the package shall be capable of supporting three times the weight of the loaded package without generating stress in any material of the package in excess of its yield stress. The following sections provide a summary of the lifting and tie-down evaluation, which is presented in Section 2.12.3.

### **2.5.1. Lifting Devices**

The Model 2000 Transport Package lifting components are evaluated structurally in the following sections. The lifting and tie-down requirements are as specified in 10 CFR 71.45(a).

#### **2.5.1.1. Lifting Ear Evaluation**

As shown in Figure 2.5.1-1, there are two types of lifting ear designs employed during the handling of the Model 2000 cask, standard and auxiliary. The ears are removed from the cask during transport and are shipped separately. The ear design identified as Standard is used for crane and fork truck lifting, and only one pair is required for these operations. The Auxiliary ear is used in crane lifting only, and 2 pairs or 4 ears are required. The user may combine the different types of ears as necessary including, 2 Standard/2 Auxiliary, 4 Auxiliary or 2 Standard.

Both ear designs are attached to the cask outer shell by means of four ASTM A193-B6 1-8 UNC-2-1/2 bolts. For this evaluation, the following loading conditions are considered:

- Load rating of  $W = 23,630$  pounds, which includes the dead weight of the cask, lifting ears and the cask maximum payload.
- The two pairs of auxiliary ears are to support  $3W$  such that the lifting cable does not make an angle of more than  $+30^\circ$  measured from the vertical.
- The pair of standard ears is to support  $3W$ .

Three load cases are considered for this evaluation: Case I – vertical lift by crane; Case II – angular lift  $30^\circ$  from vertical by crane; and Case III – fork truck lift at two different points on the standard ears only. Figure 2.5.1-1 provides a free-body diagram for Cases I and II. Case III is similar to Case I and is not shown.

The magnitude and direction of loading in the ear analysis is shown in Figure 2.5.1-2. The analysis of each type of ear is presented in Section 2.12.3.

Material properties are based upon  $250^\circ\text{F}$  for the outer cask. The  $249^\circ\text{F}$  temperature is the maximum temperature under normal conditions for the cask outer surface (Section 3.3.1). Both standard and auxiliary ears and the cask outer shell are ASTM A240, Type 304 stainless steel. The attaching bolt material is ASTM A193-B6.

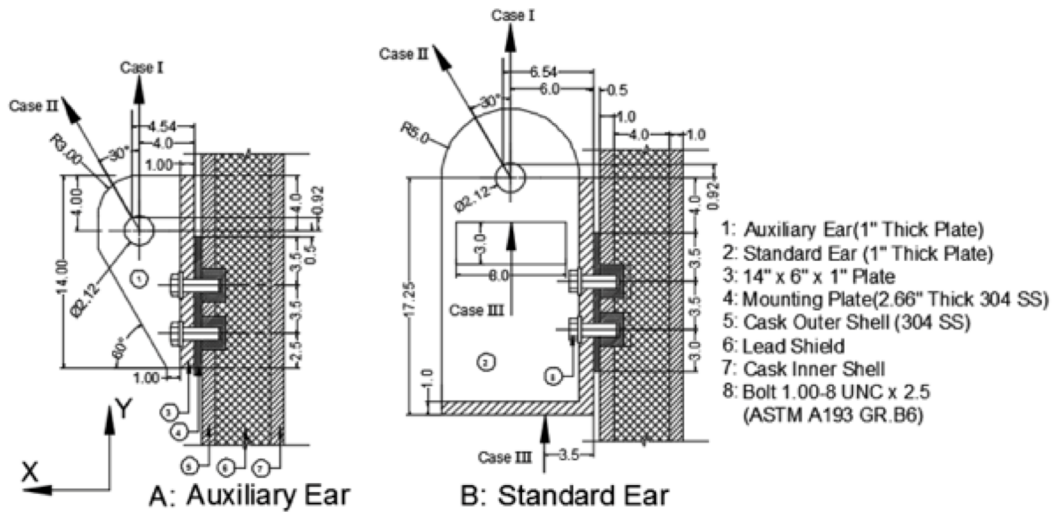


Figure 2.5.1-1. Lifting Ear Details

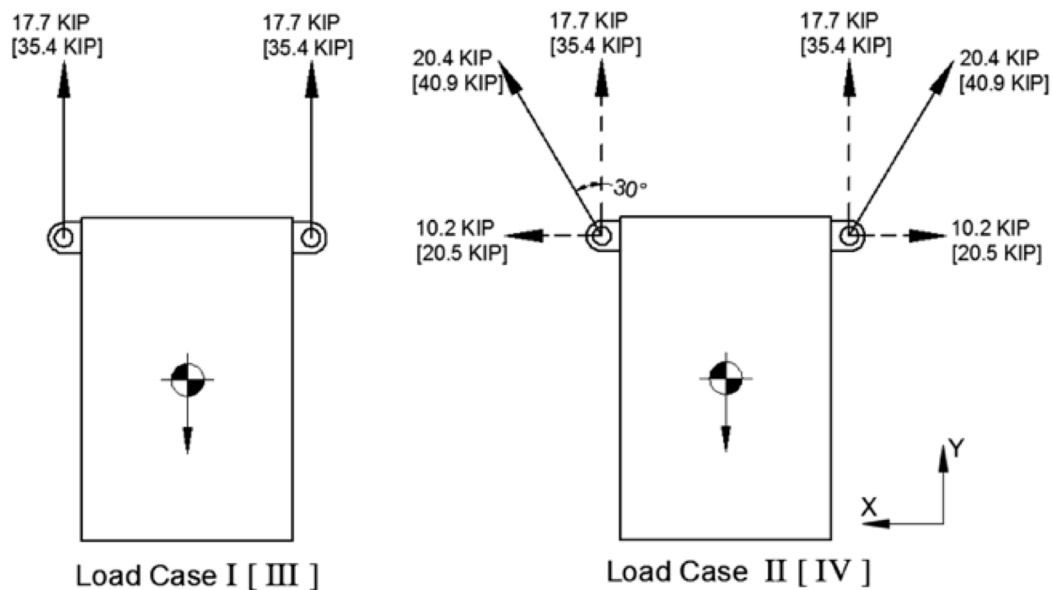


Figure 2.5.1-2. Magnitude and Direction of Loading in Ear Analysis

Table 2.5.1-1 provides a summary of the stress evaluation presented in Section 2.12.3. As the table shows, the margin of safety for all components and cases are positive. Therefore, the cask lifting device meets the requirements of 10 CFR 71.45.

**Table 2.5.1-1. Summary of Cask Lifting Device Stresses**

Condition	Allowable Yield (ksi)	Allowable Ultimate (ksi)	Case I			Case II			Case III		
			Stress (ksi)	*MS (y)	*MS (U)	Stress (ksi)	MS (y)	MS (U)	Stress (ksi)	MS (y)	MS (U)
Shear tearout of lifting hole - Auxiliary	14.00	26.18	6.02	1.33	3.35	---	---	---	---	---	---
Shear tearout of lifting hole - Standard	14.00	26.18	8.98	0.56	1.92	---	---	---	---	---	---
Tensile failure of lifting ear plate - Auxiliary	23.70	68.60	4.82	3.92	13.23	---	---	---	---	---	---
Tensile failure of lifting ear plate - Standard	23.70	68.60	17.70	0.34	2.88	---	---	---	---	---	---
Bearing of shackle pin on ear - Auxiliary	23.70	68.60	10.20	1.32	5.73	---	---	---	---	---	---
Bearing of shackle pin on ear - Standard	23.70	68.60	17.70	0.34	2.88	---	---	---	4.72	4.02	13.53
Tensile stress on weld joint - Auxiliary	23.70	68.60	6.50	2.65	9.55	---	---	---	---	---	---
Tensile stress on base metal - Auxiliary	23.70	68.60	9.19	1.58	6.46	9.20	1.58	6.46	---	---	---
Tensile stress on weld joint - Standard	23.70	68.60	8.16	1.90	7.41	---	---	---	---	---	---
Tensile stress on base metal - Standard	23.70	68.60	5.77	3.11	10.89	4.85	3.89	13.14	---	---	---
Tensile stress on mounting bolt-Standard	85.00	110.00	61.42	0.38	0.79	---	---	---	---	---	---
Shearing of bolt - Standard	51.00	---	14.60	2.49	---	---	---	---	---	---	---
Shearing of bolt threads-Standard	51.00	---	11.76	3.34	---	---	---	---	---	---	---
Shearing of tapered threads - Standard	14.00	26.18	9.18	0.53	1.85	---	---	---	---	---	---
Tensile stress on cask outer shell - Standard	23.70	68.60	10.95	1.16	5.26	---	---	---	---	---	---

\*Note:

MS(y): Margin of safety based on yield strength.

MS(U): Margin of safety based on ultimate strength.

### 2.5.1.2. Cask Lifting Ear Mounting Bolt Fatigue Evaluation

The fatigue evaluation of the lifting ear mounting bolts per ASME Section III NB indicates that the bolts have an expected life of 11 years based on 12 usages per year. Bolts are inspected during the installation of the lifting ears. Damaged or defective bolts are replaced as needed.

### 2.5.1.3. Excessive Load Failure

The lifting devices must be designed such that their failure under excessive load would not impair the ability of the package to meet other requirements of 10 CFR 71.45(a). A review of the above margin of safety from Table 2.5.1-1 indicates that, under excessive loading, the ear attaching bolts will fail before the ear plates, ear welds or cask shell. Failure of the bolts assures that the ability of the package to meet any other regulatory requirements is not impaired.

#### 2.5.1.4. Model 2000 Lid Lifting Lug Analysis

The lid is lifted by a single lifting lug that is composed of a 1-inch diameter stainless steel rod located at the center of the lid top. It is shown by analysis that this lifting device complies with requirements of 10 CFR 71.45(a). The lifting lug is able to support three times the weight of the lid without yielding.

The weakest part of the lifting lug is determined to have a factor of safety of 1.76 when analyzed for lifting three times the weight of the lid. Details of the analysis are documented in Section 2.12.3.

Because the lid lifting lug is covered by the cask overpack during transport the device is rendered inoperable. Therefore, no further evaluation is required.

#### 2.5.2. Tie-Down Devices

The Model 2000 Transport Package tie-down components are evaluated structurally in the following sections. The lifting and tie-down requirements are as specified in 10 CFR 71.45(b).

##### 2.5.2.1. Tie-Down Evaluation

The Model 2000 Transport Package is normally shipped by truck. Figure 2.5.2-1 shows the overall plan for tying the package to the vehicle. Eight wire ropes or chains tie the package to the vehicle: four connect to the upper [[ ]] tie-down ribs of the overpack, and the other four connect to the overpack base [[ ]] tie-down ribs. In addition, the base of the package is wedged to the truck bed to prevent sliding. Evaluation of the tie-down stresses is presented in Table 2.5.2-1. As the table shows all components exhibit a positive margin of safety.

**Table 2.5.2-1. Tie-Down System Stress Analysis Results**

Condition	Stress (ksi)	Allowable based on Yield (ksi)	MS	Allowable Based on Ultimate Strength (ksi)	MS
Shear tear-out of rib hole	20.99	$0.6 \times 45.2 = 27.12$	0.29	$96.8/(2 \times 1.31) = 36.95$	0.76
Bearing of shackle pin	42.46	45.2	0.06	96.8	1.28
Shear stress in weld joints	20.99	$0.6 \times 45.2 = 27.12$	0.29	$96.8/(2 \times 1.31) = 36.95$	0.76

##### 2.5.2.2. Excessive Load Failure

Tie-down devices must be designed such that their failure under excessive load would not impair the ability of the package to meet other requirements of 10 CFR 71.45(b)(3). A review of the above margin of safety from Table 2.5.2-1 indicates that, under excessive loading, either the rib hole will tear out or the connecting weld will fail in shear. Failure of the rib or connecting weld does not impair the ability of the overpack or other package components from meeting other regulatory requirements.

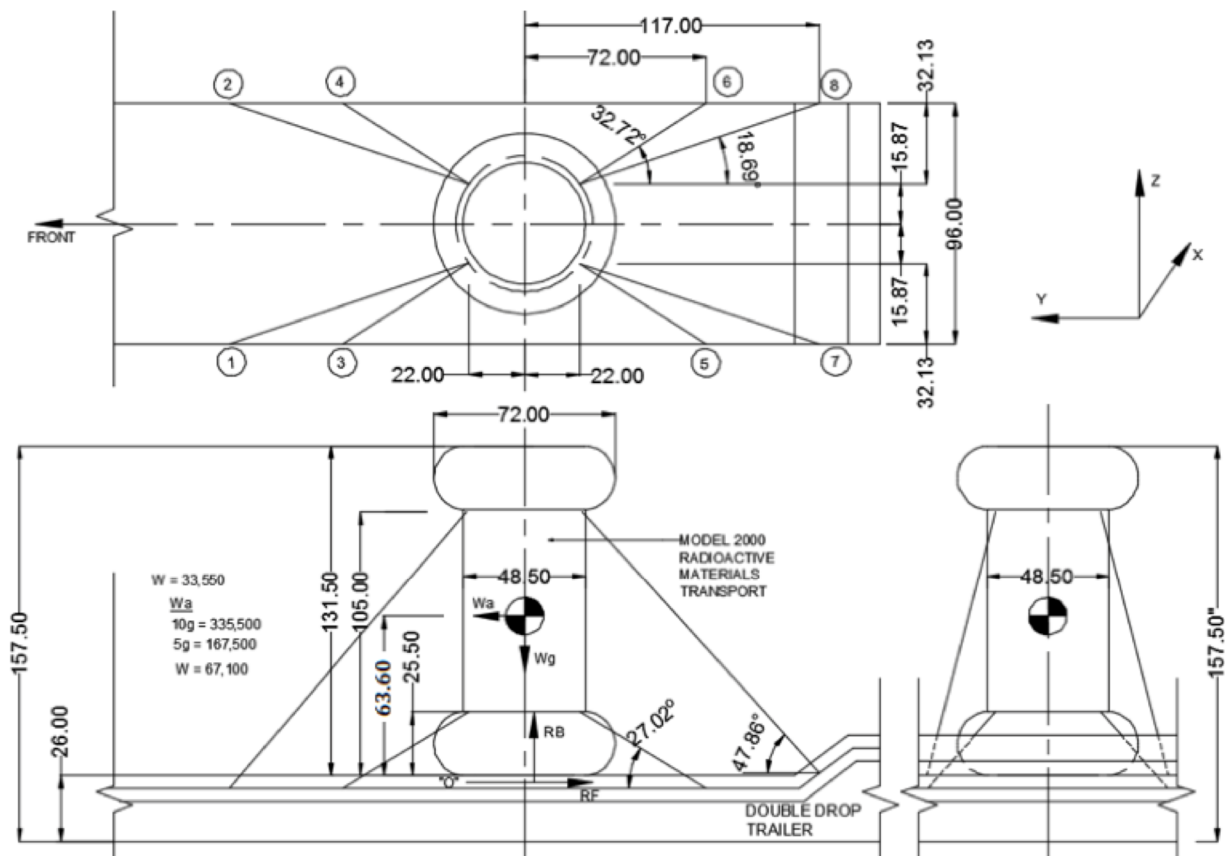


Figure 2.5.2-1. Tie-Down of Transport Package to Vehicle

## 2.6 Normal Conditions of Transport

This section provides the evaluation that shows the Model 2000 Transport Package, with HPI and material basket, meets the standards specified in 10 CFR 71.43 and 71.51, when subjected to the tests and conditions specified in 10 CFR 71.71 (Normal Conditions of Transport). The package is evaluated against each condition individually.

### 2.6.1. Heat

The thermal evaluation for the NCT heat conditions is presented in Section 3.3. The NCT heat condition consists of exposing the cask to direct sunlight and 100°F still air. For routine conditions, solar insolation is neglected. For NCT, solar insolation is applied to the package surface. For both cases, an initial temperature of 100°F and an internal power generation of 3000 W are used for the evaluation.

#### 2.6.1.1. Summary of Pressures and Temperatures

Table 2.6.1-1 provides a summary of temperatures for the 3000 W thermal evaluation which thermally bounds 1500 W presented in Chapter 3 of this application. Additionally, internal gases in the cask and HPI are explicitly modeled in Chapter 3. Evaluation of the maximum pressure at the calculated average gas temperatures, presented in Section 3.1.4, shows that the 3000 W heat decay does not exceed the design pressure of 30 psia.

#### 2.6.1.2. Differential Thermal Expansion

The differential thermal expansion of the Model 2000 cask is evaluated as part of the ASME Section III NB stress analysis included in Section 2.6.7 of this application to show compliance with the design criteria presented in Section 2.1.2. Review of the NCT heat conditions shows that a bounding thermal expansion model is possible by applying a 300°F temperature differential from the outside surface to the inside surface of the cask. To maximize thermal expansion, a temperature of 300°F is applied to the outer surface of the cask and 600°F to the inside surface of the cask. For the HPI and material basket thermal expansion and fit during worst-case thermal conditions assuming an initial temperature of 70°F.

#### Radial Thermal Expansion

Figure 2.6.1-1 through Figure 2.6.1-3 shows the HPI support disk, material basket, and HPI [ ] and cask inner shell diameters. Using the bounding temperature for each component, the change in diameter is calculated as:

$$d_{\text{final}} = d_0 (1 + \alpha \Delta T)$$

Where, the initial diameter,  $d_0$ , is multiplied by the product of the coefficient of thermal expansion,  $\alpha$ , and change in temperature,  $\Delta T$ , plus one. Table 2.6.1-2 shows the results of the evaluation. The minimum worst case difference in diameters is calculated to be [ ] between the HPI [ ], which results in no radial interference. Therefore, the HPI and material basket can be removed from the cask following shipment.

### **Axial Thermal Expansion**

Axial thermal expansion occurs when the material basket is heated by the source material from ambient conditions to NCT steady-state temperatures. Axial thermal expansion also occurs as the HPI heat reaches steady state and the inner shell of the cask expands. Using the bounding temperature for each component, the change in length is calculated as:

$$L_{\text{final}} = L_0 (1 + \alpha \Delta T)$$

Where, the initial length,  $L_0$ , is multiplied by the product of the coefficient of thermal expansion,  $\alpha$ , and change in temperature,  $\Delta T$ . Table 2.6.1-3 shows the results of the evaluation. The minimum worst case difference in lengths is calculated to be 0.13 inches between the material basket and HPI inner cavity, which results in no axial interference.

#### **2.6.1.3. Stress Calculations**

Regulatory Guide 7.8 stress combination results are presented in Section 2.6.7. Individual thermal stresses are summarized in Table 2.6.1-4. For the HPI and material basket, the evaluation of thermal stresses is not required per ASME Code III-NF (NF-3121.11).

#### **2.6.1.4. Comparison with Allowable Stresses**

This section presents the stress combinations based upon the design criteria presented in Section 2.1.2 for NCT. The cask stresses resulting from NCT are presented in Table 2.6.1-5. Comparison of the calculated stresses to the allowable stresses presented in Section 2.1.2 demonstrates that the Model 2000 cask meets the performance requirements. In addition, the condition of the overpack during NCT is evaluated in Section 2.12.1, Cases 4, 5, and 6.

Evaluation of the HPI for end and side drop orientations calculated stresses in key components including the inner and outer [[ ]] and support disks. The results show that in all cases the calculated margin of safety is greater than +1. Therefore, the HPI meets the performance requirements specified in Section 2.1.2. The material basket was also evaluated for NCT drop conditions using classic methods. The results of the analysis show that the margin of safety is greater than +1. Therefore, the material basket meets the performance requirements specified in Section 2.1.2.

The NCT analysis results show that the overpack, cask, HPI and material basket meet all performance requirements, which include maintaining containment and geometry.



[[

]]

**Figure 2.6.1-1. HPI Support Disk Details**

[[

]]

**Figure 2.6.1-2. Material Basket Detail**

[[

]]

**Figure 2.6.1-3. HPI Inside Diameter**

**Table 2.6.1-1. Temperature Results, NCT (in Shade and with Insolation)**

Component	100°F Ambient Temperature, in Shade			100°F Ambient Temperature, with Insolation		
	Max	Min	Avg	Max	Min	Avg
Material Basket	989	465	801	1,001	490	815
HPI	581	360	---	604	388	---
HPI Shielding (top)	517	506	513	539	529	535
HPI Shielding (sides)	581	435	544	601	460	565
HPI Shielding (bottom)	477	427	451	501	452	475
Cask (bottom, shells, top, lid)	430	309	---	455	338	---
Cask Shielding (lid)	424	408	414	449	433	440
Cask Shielding (sides)	405	341	385	431	370	412
Cask Lid Seal	406	383	---	432	409	---
Cask Drain Port (bottom)	342	309	---	370	338	---
Cask Test Port (top)	400	383	---	426	409	---
Cask Vent Port (lid)	416	410	---	442	435	---
Overpack Base	335	159	---	364	184	---
Overpack Cover	272	108	---	308	174	---
Overpack Toroidal Shell (top)	159	110	125	207	165	179
Overpack Toroidal Shell (bottom)	215	114	139	249	136	176
Overpack Honeycomb Impact Limiter (top)	220	205	215	263	249	258
Overpack Honeycomb Impact Limiter (bottom)	330	275	304	359	305	334
HPI Fill Gas	971	460	672	983	485	689
Cask Fill Gas	574	346	462	594	374	486
HPI and Cask Fill Gas, Combined	971	346	481	983	374	505

Note: Data taken from Table 3.3.1-1

**Table 2.6.1-2. Radial Thermal Expansion Evaluation for HPI and Material Basket**

[[						
						]]

**Table 2.6.1-3. Axial Thermal Expansion Evaluation for HPI and Material Basket**

[[						
						]]

**Table 2.6.1-4. NCT Thermal Stress Results (psi)**

Case	Section Number	Thermal Stress (psi)
NCT End Drop	1	15110
NCT End Drop	2	6404
NCT Side Drop	3	9649
NCT Side Drop	4	15110
NCT Side Drop	5	7039

**Table 2.6.1-5. Model 2000 Cask NCT Stress Analysis Summary (psi)**

Case	Stress Component	Stress Combination	Stress Intensity	Allowable	Margin of Safety
1	$P_m$	5411	20000	20000	2.7
	$P_m + P_b$	17510	20000	30000	0.7
	$P_m + P_b + Q$	40690	20000	60000	0.5
2	$P_m$	14500	20000	20000	0.4
	$P_m + P_b$	25000	20000	30000	0.2
	$P_m + P_b + Q$	42864	20000	60000	0.4
3	$P_m$	2906	19300	19300	5.6
	$P_m + P_b$	9699	19300	28950	2.0
	$P_m + P_b + Q$	19355	19300	57900	2.0
4	$P_m$	6023	19300	19300	2.2
	$P_m + P_b$	17910	19300	28950	0.6
	$P_m + P_b + Q$	41280	19300	57900	0.4
5	$P_m$	16090	19300	19300	0.2
	$P_m + P_b$	25950	19300	28950	0.1
	$P_m + P_b + Q$	44469	19300	57900	0.3

### **2.6.2. Cold**

The Model 2000 Transport Package is analyzed for structural adequacy in accordance with the thermal evaluation of the Model 2000 Transport Package for the temperatures specified in 10 CFR 71.71(c)(2) is presented in Chapter 3. The thermal evaluation demonstrates that the Model 2000 Transport Package component temperatures are maintained within their safe operating ranges for all normal conditions of transport. The bounding methodology for evaluating the thermal stress in the Model 2000 Transport Package is presented in Section 2.6.1 and individual thermal stresses are summarized in Table 2.6.1-4. Thermal stresses are combined with mechanical stresses in Section 2.6.7 and compared to the appropriate ASME Code allowables.

### **2.6.3. Reduced External Pressure**

The drop in atmospheric pressure to 24 kPa (3.5 psia) is specified in 10 CFR 71.71(c)(3). This additional differential pressure has a negligible effect on the Model 2000 cask because, in Section 2.6.7, the cask is analyzed for a normal transport conditions internal pressure of 15.3 psig (30 psia). Maximum internal pressure is included in combination with internal loads. Because the margins of safety are all positive, this satisfies the requirements of 10 CFR 71.71(c)(3) for reduced external pressure.

### **2.6.4. Increased External Pressure**

An increased external pressure of 20 psia (5.3 psig external pressure), as specified in 10 CFR 71.71(c)(4), has a negligible effect on the Model 2000 cask because of the thick outer shell and end closures. Section 2.6.7 addresses many different loading cases, which exceed these prescribed external pressure requirements. Therefore, the requirements of 10 CFR 71.71(c)(4) are satisfied.

### **2.6.5. Vibration**

The Model 2000 Transport Package is evaluated for effects of vibrations that are normally incident to transport, as specified in 10 CFR 71.71(c)(5). The effects of shock and vibration loads associated with this road on transportation on the Model 2000 are negligible as determined in this section. For this evaluation, rather than determining the frequency of vibration of the package to establish the maximum acceleration, the cask has been structurally analyzed using the accelerations associated with NCT. Table 2.6.7-1 provides a summary of the accelerations used to evaluate the cask. The accelerations are applied statically to the ANSYS model described in detail in Section 2.6.7 to produce the maximum stress intensity in the package components. The results of the cask body, HPI and material basket analyses show that the package is capable of experiencing continuous NCT accelerations without degrading the ability of the package to meet the other parts of the regulations. Additionally, the closure system is designed in accordance with NUREG/CR-6007, which determines the bolt preload based on the impact loads experienced during HAC, which bounds the loads experienced during transport (Reference 2-15). Further, a fatigue analysis is performed in accordance with ASME Code, Section III, NB-3232.3, which concluded that after 190 transports, all bolts shall be replaced. Therefore, the requirements of 10 CFR 71.71(c)(5) are satisfied.

#### **2.6.6. Water Spray**

Water causes negligible corrosion of the stainless shell of the Model 2000 Transport Package. The cask housed in the overpack and the contents are protected in the sealed cask cavity. A water spray as specified in 10 CFR 71.71(c)(6) has no adverse effect on the package. Therefore, the requirements of 10 CFR 71.71(c)(6) are satisfied.

#### **2.6.7. Free Drop**

The free drop scenario outlined by 10 CFR 71.71(c)(7) requires a demonstration of the structural adequacy of the Model 2000 cask for a 1-ft drop onto a flat, essentially unyielding horizontal surface in the orientation that inflicts the maximum damage to the cask. The Model 2000 Transport Package is shown to meet the free drop requirements through a combination of classic calculations, impact analyses, and static finite element. The evaluations include the qualification of the Model 2000 cask lid bolt design for the combined effects of free drop impact force, internal pressures, thermal stress, O-ring compression force, and bolt preload following the methodology of NUREG/CR-6007 (Reference 2-15) (Section 2.12.4). The combined effects of inertial loads, internal pressures, and thermal stress are considered for packaging components. The impact analysis of the package is presented in Section 2.12.1. Section 2.6.7.1 presents the evaluation of the cask body and Section 2.6.7.2 presents the structural evaluation of the HPI and material basket during free drop conditions. The cask body and HPI structural analyses are performed using the finite element program ANSYS (Reference 2-16) and the material basket is analyzed using classic methods.

##### **2.6.7.1. Cask Body Stress Analysis**

This section evaluates the structural performances of the Model 2000 cask body analyses and shows that the design meets the requirements of 10 CFR 71.71. Specifically, the evaluation addresses the loads associated with the NCT. The results of the analyses for various load cases are presented pictorially in stress intensity contour plots as well as in table form, with the corresponding safety factors in critical components of the cask body.

###### **2.6.7.1.1. Model Description**

Finite element analysis methods are used to perform the stress evaluation of the Model 2000 cask for normal free drop conditions. Each drop condition is analyzed using a three-dimensional finite element model using the computational modeling software ANSYS that were developed in accordance with the certification drawings. Figure 2.6.7-1 shows the major components of the cask represented in the model including the inner and outer shells, flange, top and bottom forgings, lid, and closure bolts.

As shown in Figure 2.6.7-1, the finite element model, which corresponds to half (180°) of the cask body, is generated by de-featuring the AutoDesk Inventor solid model and exporting the model to a .STEP file format. The .STEP file is imported directly into ANSYS where the finite element model is developed. The solid portion of the model is constructed using ANSYS solid (SOLID185) elements. Surface-to-surface contact elements are used to simulate the interaction between adjacent components. Specifically, contact between the cask shells and lead shielding is

modeled using CONTAC174/TARGE170 surface-to-surface contact elements with zero friction, which allows the lead to float between the inner and outer shells. Contact elements are also used to bond dissimilarly meshed components. Nodal displacements are used to simulate the interaction between the cask and overpack. Weak springs elements (COMBIN14) are inserted automatically during the solution to help stabilize the model. ANSYS assigns low spring stiffness so their presence will not adversely affect the accuracy of the solution.

Boundary conditions are applied to the model simulating the loading conditions the Model 2000 cask experiences during NCT. The categories of cask loading considered in the free drop event are closure lid bolt preload, internal pressure load, thermal load, inertial body load and displacement. ANSYS input files are used to apply boundary conditions and loads to the cask model.

#### ***Closure Lid Bolt Preload***

The closure lid bolt preload for 750 ft-lb maximum torque is 48,000 lb (Section 2.12.4). To apply the bolt preload ANSYS pre-tension elements (PRETS179) are used to define the 3D pre-tension section within the meshed bolt. The PRETS179 element uses a single translation degree of freedom to define pretension direction. The pretension section is modeled by a set of pretension elements defined by the bolt shaft. Figure 2.6.7-2 shows the bolt pretension values and locations. As the figure shows, the bolt divided by the symmetry plane of the model is half of the other values presented.

#### ***Internal Pressure Loading***

A pressure of 30 psia is used to envelope the maximum design pressure for all NCT impact loadings considered.

#### ***Inertial Loads***

To evaluate the impact performance of the cask, an LS-DYNA analysis was performed (Section 2.12.1) to determine the maximum acceleration during hot/cold and heavy/light environmental conditions and varying impact limiter shell thicknesses. Table 2.6.7-1 provides a summary of the maximum accelerations that occur during cold/light conditions.

**Table 2.6.7-1. LS-DYNA Results**

DESCRIPTION	DROP ANGLE (DEGREE)	APPLICABLE BOUNDARY CONDITION						ACCELERATION (g)
		Temperature			Payload			
		*Amb.	Hot	Cold	*Nom.	Heavy	Light	
NCT, End Drop, Cold	90	—	—	✓	—	—	✓	15.5
NCT, Side Drop, Cold	0	—	—	✓	—	—	✓	55.1
NCT, C.G.-Over-Corner Drop, Cold	22	—	—	✓	—	—	✓	14.6

\*Note: Amb. = Ambient; Nom. = Nominal.

### ***Cask Contents Loading - End Drop***

For the end drop analyses, the contents weight is assumed to be uniformly distributed on the cask top end, over an area determined by the inside diameter of the cask lid. Therefore, one half the payload weight of 5,450 lb (see Table 2.1-3) is applied to the cask inner shell bottom plate as nodal forces. The contents load is multiplied by the appropriate g-load to accurately represent the 1-foot and 30-foot end drop.

### ***Cask Contents Loading - Side Drop***

For side drop conditions, the contact area between the contents and the cask cavity is approximately 120° (60° on each side of the drop centerline). The inertial load produced by the 5,450 lb payload weight is represented as nodal forces applied on the interior surface of the cask. The force is applied at the HPI [[ ]] and is varied in the circumferential direction as a cosine distribution. The maximum pressure occurs at the impact centerline; the load decreases to zero at locations that are approximately 60° either side of the impact centerline, as illustrated in Figure 2.6.7-3. The actual location is dependent on the actual nodal position. The following formula is used to determine the contents forces for the side drop analyses. This method uses a summation scheme to approximate the integration of the cosine-shaped pressure distribution:

$$F_{\text{total}} = \sum_{i=1}^4 F_{\text{max}} \cos(\theta_i) \cos(\theta'_i)$$

$$F_{\text{total}} = 5,450/2 \text{ lb} \times G$$

where

$$F_{\text{max}} = \text{maximum pressure (at impact centerline)}$$

$$\theta_i = \text{average angle of subtended arc of } i^{\text{th}} \text{ element measured from centerline at point of impact, to obtain vertical component of pressure}$$

$$i = i^{\text{th}} \text{ circumferential sector}$$

$$\theta'_i = \text{normalized angle to peak at } 0^\circ \text{ and to be zero at } 61.2^\circ$$

$$G = \text{impact acceleration}$$

Figure 2.6.7-4 shows the applied nodal forces in the four regions for HAC based on the cosine distribution.

### ***Nodal Displacement***

With the absence of the overpack, nodal displacements are used to simulate the interaction between the overpack and cask body, which treats the cask body as a beam. For the side the nodes are constrained radially at the location where the cask body contacts the overpack. For the end drop, the nodal locations are visible in Figure 2.6.7-2 as a radial band at the top end of the cask. For the side drop, an additional smaller band of nodes located at the bottom end of the cask is used to represent the bottom impact limiter. Nodal displacements are also applied at the center plane of the cask to simulate symmetry. This is accomplished by fixing the out of plane displacement (Y) and the rotations about the other axes (X and Z).



***Thermal***

According to Regulatory Guide 7.8 (Reference 2-2), four credible thermal conditions must be considered.

*Condition 1 – Hot Case 1:*

- a. Ambient temperature, 100°F
- b. Initial temperature, 100°F
- c. Heat transfer to ambient by natural convection, still air
- d. Heat transfer to ambient by radiation
- e. Solar insolation as a periodic heat flux applied as 12-hr on and 12-hr off
- f. Internal heat load of 3000 W

*Condition 2 – Hot Case 2:*

- a. Ambient temperature, 100°F
- b. Initial temperature, 100°F
- c. Heat transfer to ambient by natural convection, still air
- d. Heat transfer to ambient by radiation
- e. No solar insolation, in shade
- f. Internal heat load of 3000 W

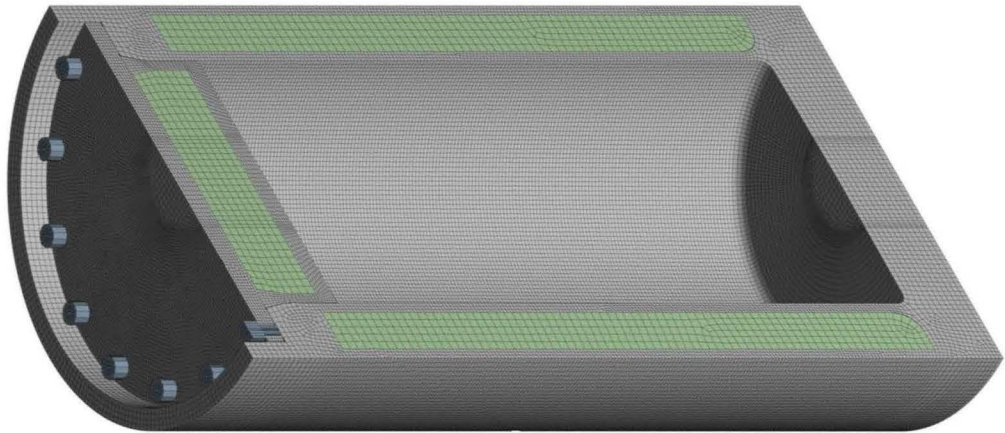
*Condition 3 – Cold Case 1:*

- a. Ambient temperature, -40°F
- b. Initial temperature, -40°F
- c. Heat transfer to ambient by natural convection, still air
- d. Heat transfer to ambient by radiation
- e. No solar insolation, in shade
- f. Internal heat load of 500 W (minimum payload case)

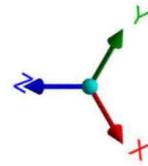
*Condition 4 – Cold Case 2:*

- a. Ambient temperature, -20°F
- b. Initial temperature, -20°F
- c. Heat transfer to ambient by natural convection, still air
- d. Heat transfer to ambient by radiation
- e. No solar insolation
- f. Internal heat load of 3000 W

Review of the four heat conditions shows that a bounding thermal expansion model is possible by applying a 300°F temperature differential from the outside surface to the inside surface of the cask. For the thermal stress evaluation, a temperature of 300°F is applied to the outer surface of the cask and 600°F to the inside surface of the cask. Using the higher temperatures maximizes the thermal expansion of the materials. The temperatures for the structural analysis are obtained from the results file and database file of the thermal analysis by writing the results to an ASCII file using the ANSYS BFINT command. Nodes for the structural model are transferred to the same coordinate system as used by the thermal run and the thermal results are interpolated for each thermal condition. The temperatures are applied as a boundary condition static structural model using the ANSYS BF command. Figure 2.6.7-5 shows the temperature distribution that is imported into the static structural model to solve for the thermal stresses. The resulting thermal stresses (Q) are combined with the inertial and pressure stresses ( $P_m + P_b$ ) to meet the stress requirements presented in Section 2.1.2.



**Figure 2.6.7-1. ANSYS Finite Element Model of the Cask Body**



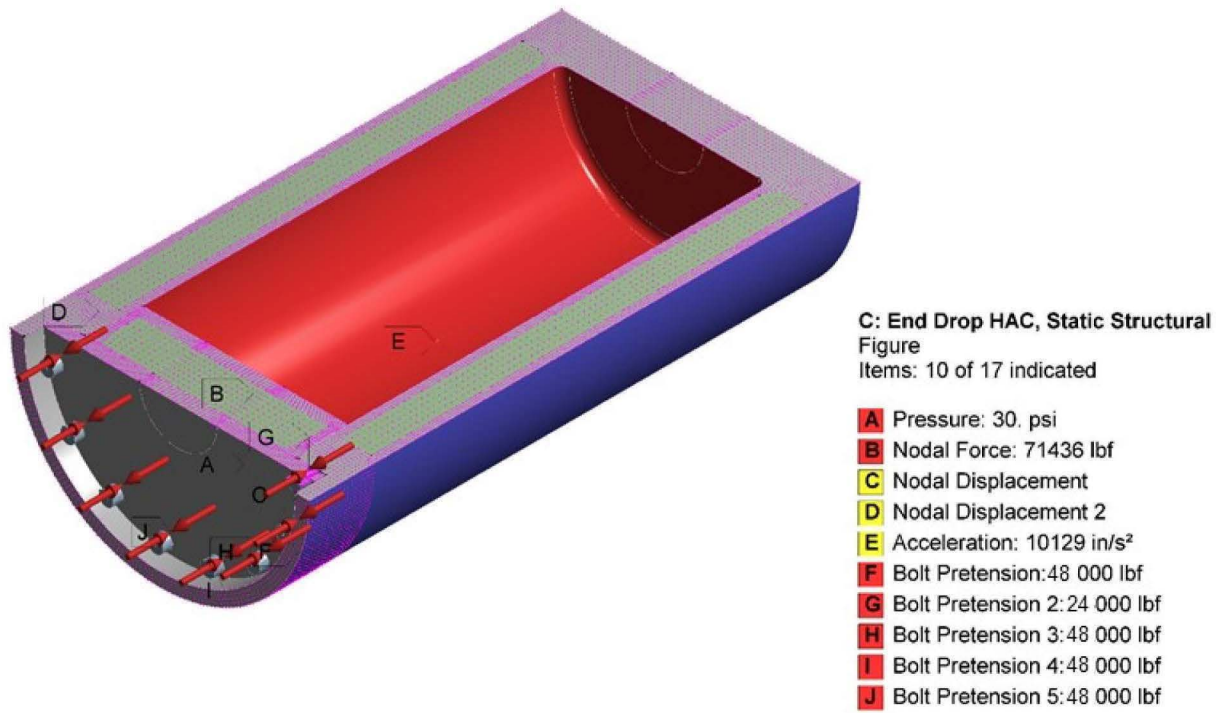


**Figure 2.6.7-2. Applied Boundary Conditions for End Drop Model**

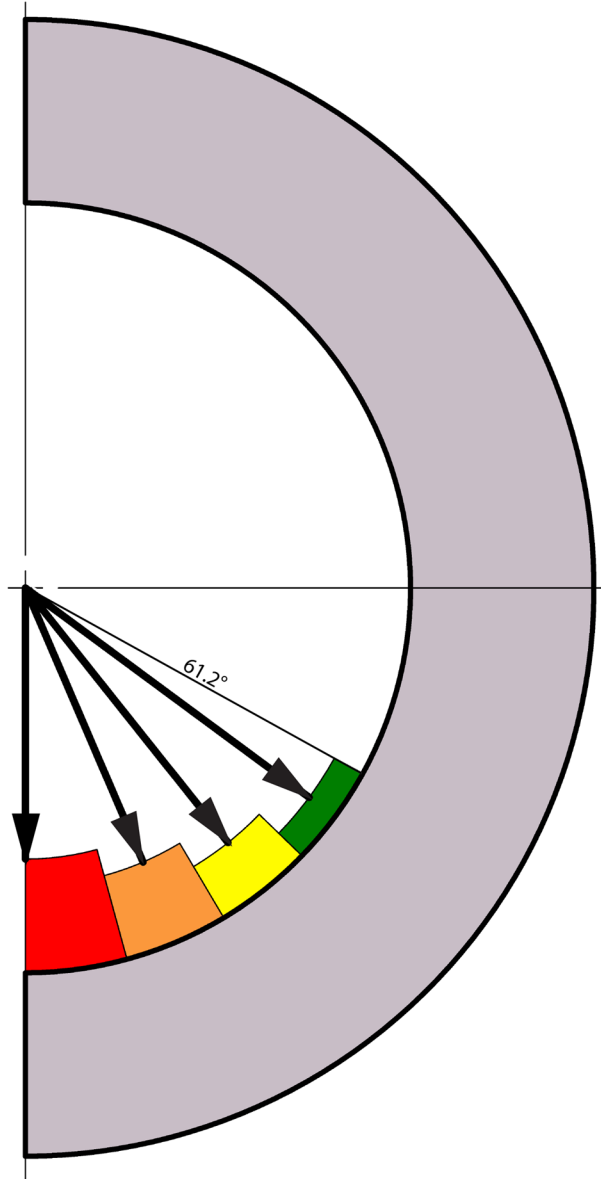
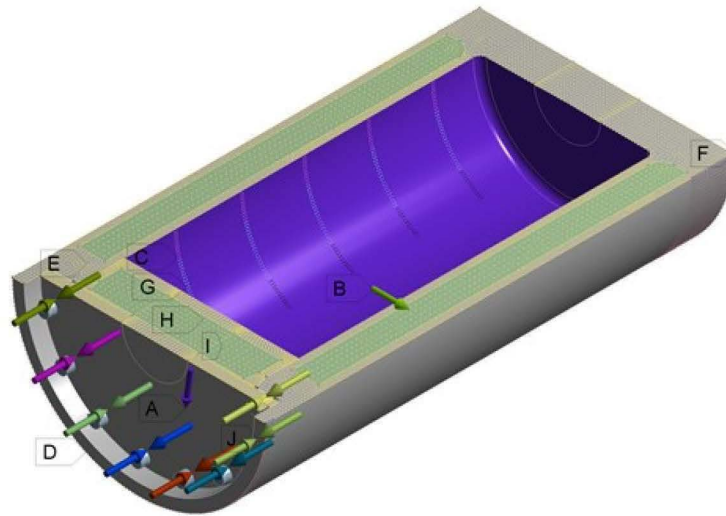


**Figure 2.6.7-3. Cosine Distribution to Simulate Contents Loading During Side Drop**



**A: Side Drop HAC, Static Structural**  
Figure 2  
Items: 10 of 17 indicated  
2/4/2016 4:17 PM

- A** Pressure: 30. psi
- B** Acceleration: 5877.9 in/s<sup>2</sup>
- C** Nodal Force: 23587 lbf
- D** Nodal Displacement
- E** Nodal Displacement 2
- F** Nodal Displacement 3
- G** Nodal Force 2: 21048 lbf
- H** Nodal Force 3: 17017 lbf
- I** Nodal Force 4: 11780 lbf
- J** Bolt Pretension: 48 000 lbf

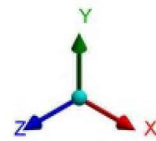


**Figure 2.6.7-4. Applied Boundary Conditions for Side Drop Model**

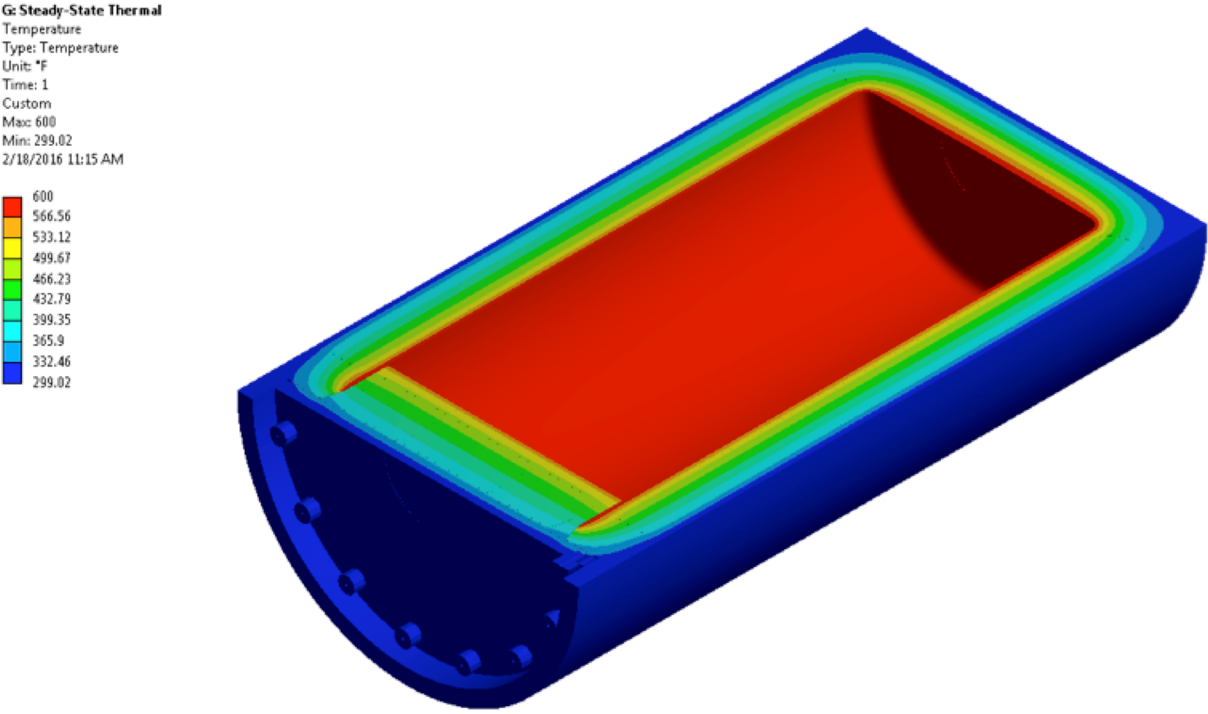


Figure 2.6.7-5. Temperature Profile for Thermal Stress Evaluation

#### 2.6.7.1.2. NCT End Drop

In accordance with the requirements of 10 CFR 71.71, the Model 2000 cask is structurally evaluated for the normal condition of transport 1-foot end-drop. In this event, the cask (equipped with an impact limiter over each end) falls a distance of 1-foot onto a flat, unyielding, horizontal surface. The cask strikes the surface in a vertical position; consequently, an end impact on the bottom end or top end of the cask occurs. Because the cask bottom is fabricated from a solid stainless steel forging, the top drop orientation was chosen to maximize damage to the cask containment boundary. Closure bolts are evaluated separately (Section 2.12.4).

The most critically stressed component in the system is the cask flange region, which is due to bending of the flange from the inertial load imposed by the cask lid. The second region of interest is in the cask lid in the closure bolt contact region. To evaluate the stresses in these regions linearized stress is calculated across the thickness of the plate. For the top flange, Figure 2.6.7-6 shows the location of the maximum total stress intensity and Figure 2.6.7-7 indicates the path (Section 1) location where the stresses are calculated. Table 2.6.7-2 is a listing of the Section 1 stresses. Table 2.6.7-3 documents the primary membrane ( $P_m$ ), primary membrane plus primary bending ( $P_m+P_b$ ), primary membrane plus primary bending plus secondary stress ( $P_m+P_b+Q$ ) in accordance with the criteria presented in Regulatory Guide 7.6 (Reference 2-17). Stresses are compared to the allowable at a bounding temperature of 300°F. The minimum margin of safety is found to be +2.7 for primary membrane, +0.7 for primary membrane plus bending and +0.5 for primary membrane plus bending plus secondary stress intensity.

Figure 2.6.7-8 shows the location of the maximum total stress intensity in the lid and Figure 2.6.7-9 indicates the path (Section 2). Table 2.6.7-4 presents a listing of the Section 2 stresses and Table 2.6.7-5 provides the stress combinations in accordance with the Regulatory Guide 7.6 criteria. The minimum margin of safety is found to be +0.4 for primary membrane, +0.2 for primary membrane plus bending and 0.4 for primary membrane plus bending plus secondary stress intensity. Because all of the margins of safety are positive, the Model 2000 cask meets the end drop requirement of 10 CFR 71.71(c)(7).



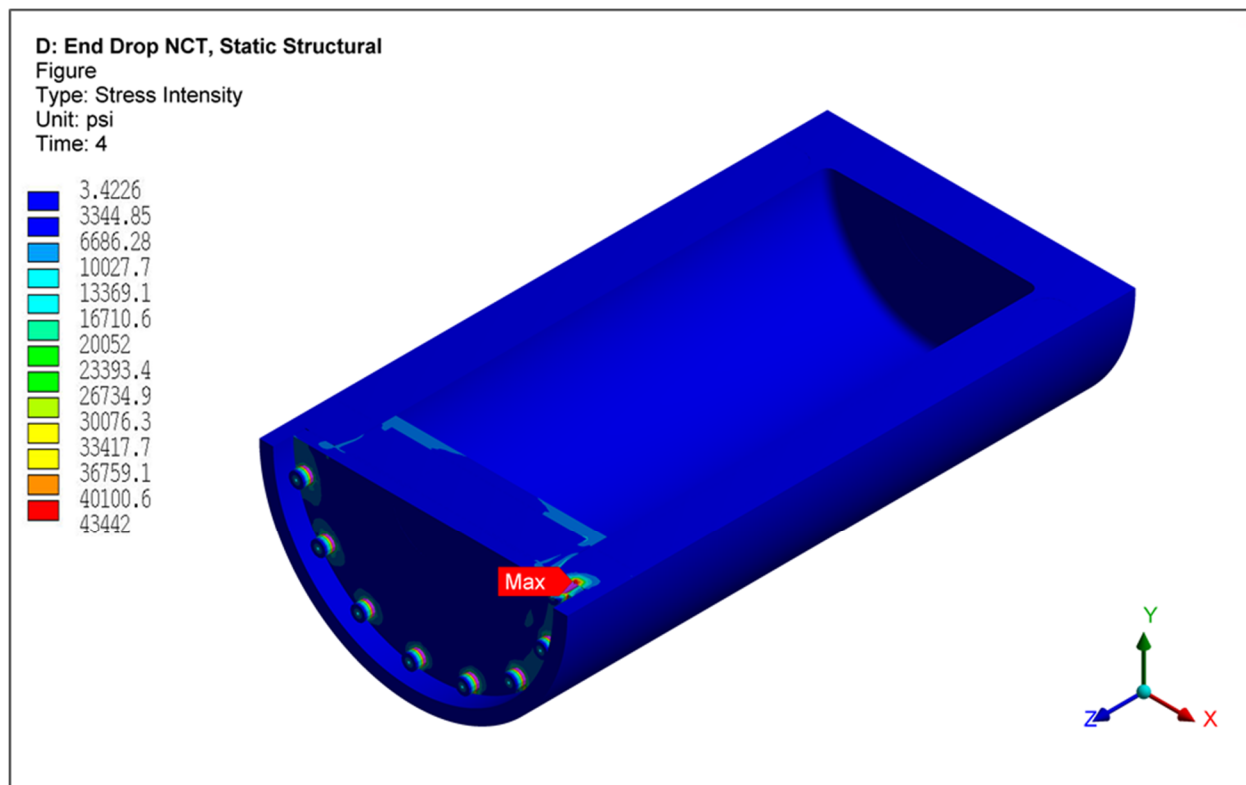
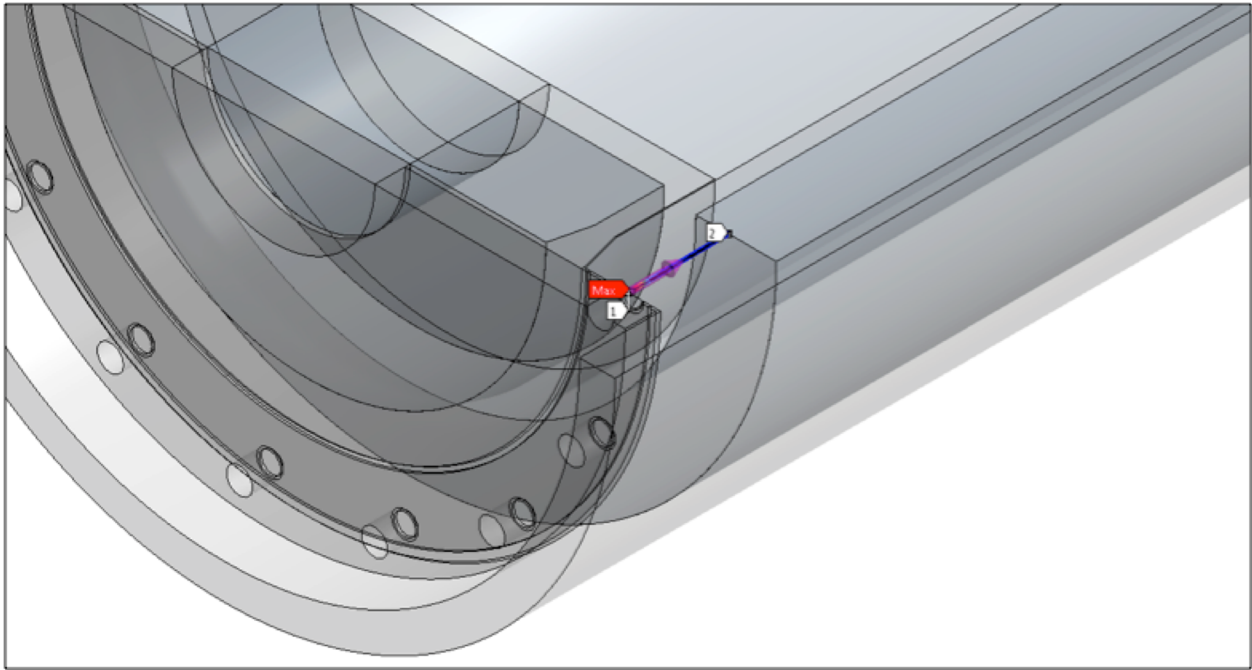


Figure 2.6.7-6. NCT End Drop Cask Body Stress Intensity (total stress psi)



**Figure 2.6.7-7. NCT End Drop Linearized Stress Location (Section 1)**

NEDO-33866 Revision 6  
Non-Proprietary Information

**Table 2.6.7-2. NCT End Drop Section 1 Stress Results (psi)**

Stress State	Location	S1	S2	S3	SINT
MEMBRANE ( $P_m$ )	—	5846	902	435	5411
BENDING ( $P_b$ )	Inside	14100	2053	1685	12420
	Center	0	0	0	0
	Outside	-1685	-2053	-14100	12420
MEMBRANE + BENDING	Inside	19920	2688	2411	17510
	Center	5846	902	435	5411
	Outside	-748	-1599	-8309	7561
PEAK	Inside	23120	13060	9779	13340
	Center	-626	-827	-5431	4805
	Outside	7948	1290	966	6982
TOTAL	Inside	42540	15680	12760	29781
	Center	962	-224	-438	1401
	Outside	366	-369	-449	815

**Table 2.6.7-3. NCT End Drop Section 1 Stress Results (psi)**

Stress Component	Stress Combination	Stress Intensity	Allowable	Margin of Safety
$P_m$	5411	20000	20000	2.7
$P_m + P_b$	17510	20000	30000	0.7
$P_m + P_b + Q$	40690	20000	60000	0.5

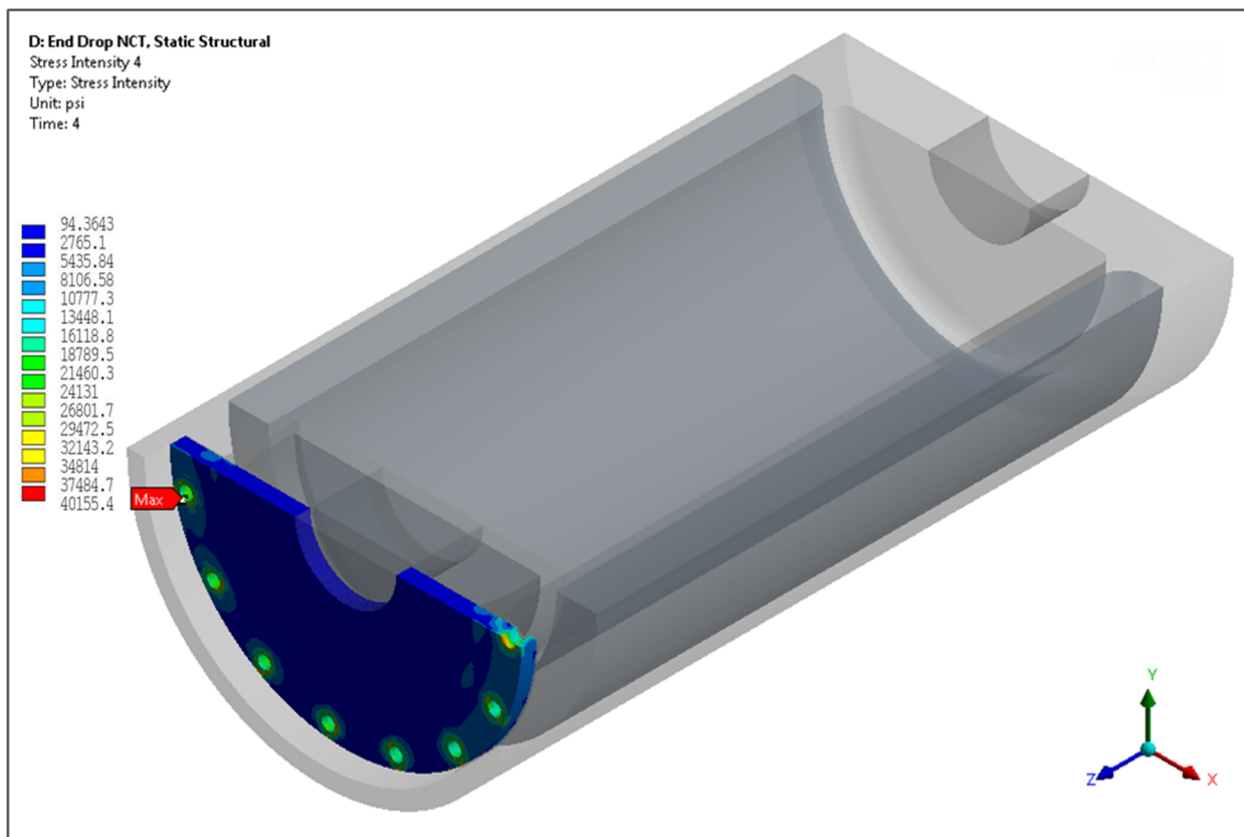
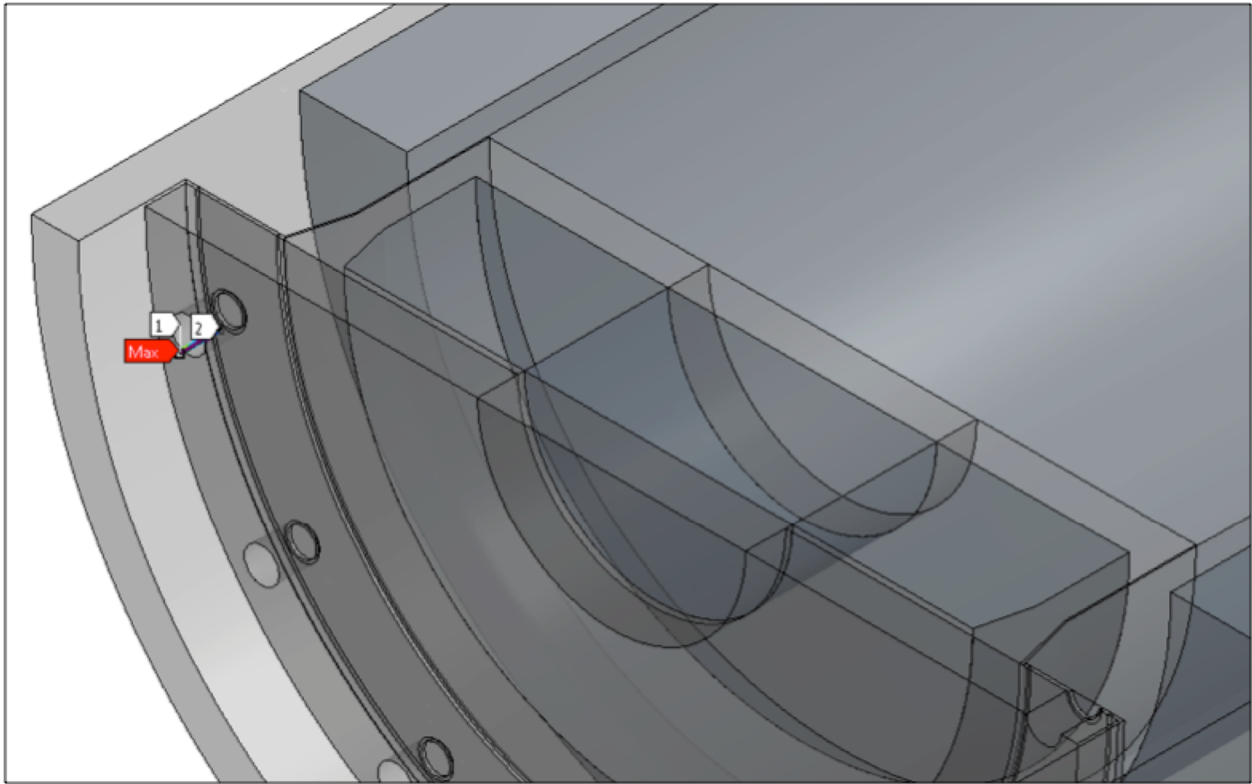


Figure 2.6.7-8. NCT End Drop Lid Stress Intensity (total stress psi)



**Figure 2.6.7-9. NCT End Drop Linearized Stress Location (Section 2)**

**Table 2.6.7-4. NCT End Drop Section 2 Stress Results (psi)**

Stress State	Location	S1	S2	S3	SINT
MEMBRANE ( $P_m$ )	—	285	-189	-14210	14500
BENDING ( $P_b$ )	Inside	-2024	-5455	-13050	11030
	Center	0	0	0	0
	Outside	13050	5455	2024	11030
MEMBRANE + BENDING	Inside	-2239	-5170	-27240	25000
	Center	285	-189	-14210	14500
	Outside	5740	2036	-1360	7100
PEAK	Inside	-9130	-10750	-14340	5215
	Center	4992	2307	395	4597
	Outside	235	-3380	-6623	6858
TOTAL	Inside	-13380	-14350	-41140	27760
	Center	2592	294	-9308	11900
	Outside	2789	1800	-7942	10730

**Table 2.6.7-5. NCT End Drop Section 2 Stress Results (psi)**

Stress Component	Stress Combination	Stress Intensity	Allowable	Margin of Safety
$P_m$	14500	20000	20000	0.4
$P_m + P_b$	25000	20000	30000	0.2
$P_m + P_b + Q$	42864	20000	60000	0.4

### 2.6.7.1.3. NCT Side Drop

In accordance with the requirements of 10 CFR 71.71, the Model 2000 cask is structurally evaluated for the normal condition of transport 1-foot side-drop. In this event, the cask (equipped with an impact limiter over each end) falls a distance of 1-foot onto a flat, unyielding, horizontal surface. The cask strikes the surface in a horizontal position. Closure bolts are evaluated separately Section 2.12.4.

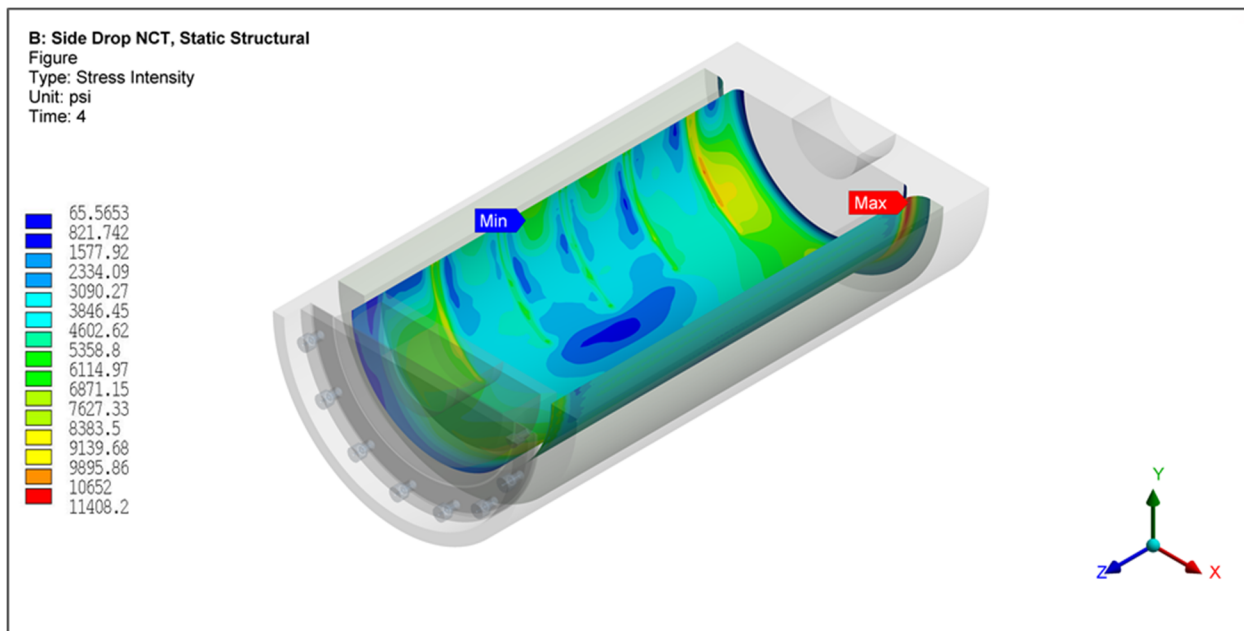
The most critically stressed component in the system is the cask inner shell at the interface with the bottom forging, the cask flange region, and the cask lid. To evaluate the stresses in these

regions linearized stress are calculated across the thickness of the plate. For the cask inner shell, Figure 2.6.7-10 shows the location of the maximum total stress intensity and Figure 2.6.7-11 indicates the path (Section 3) location where the stresses are calculated. Table 2.6.7-6 is a listing of the Section 3 stresses. Table 2.6.7-7 documents the primary membrane ( $P_m$ ), primary membrane plus primary bending ( $P_m+P_b$ ), primary membrane plus primary bending plus secondary stress ( $P_m+P_b+Q$ ) in accordance with the criteria presented in Regulatory Guide 7.6. Stresses are compared to the allowable at a bounding temperature of 350°F. The minimum margin of safety is found to be +5.6 for primary membrane, +2.0 for primary membrane plus bending and +2.0 for primary membrane plus bending plus secondary stress intensity.

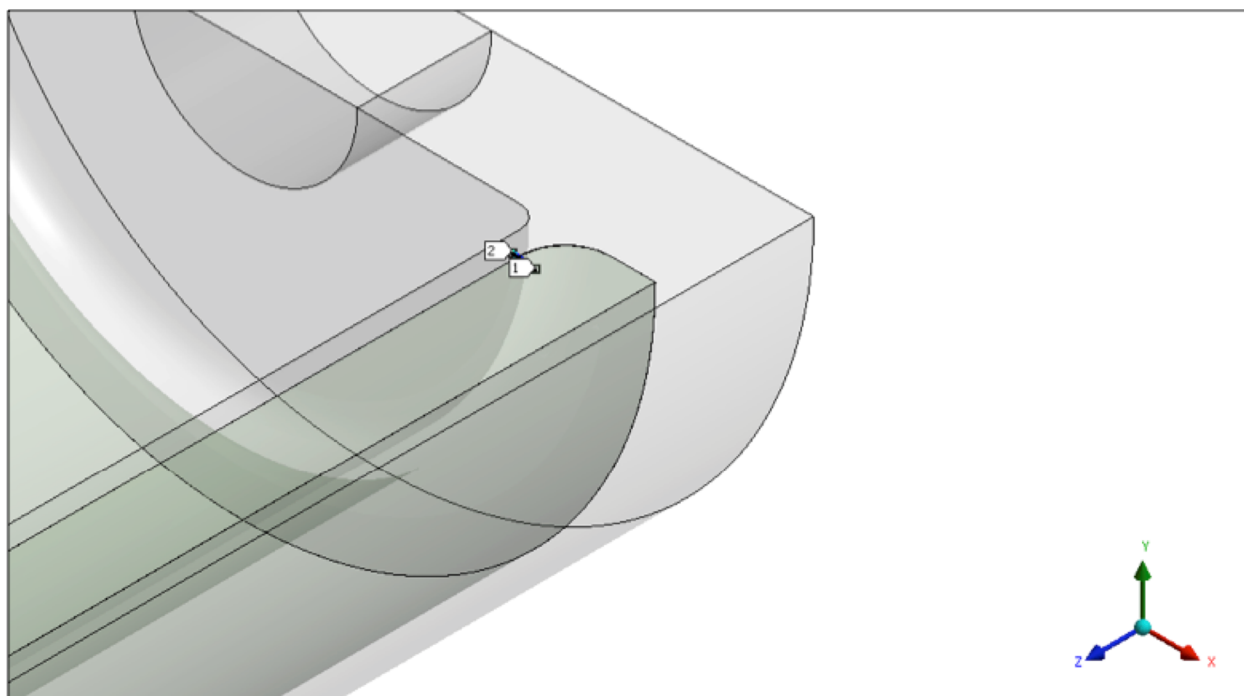
For the top flange, Figure 2.6.7-12 shows the location of the maximum total stress intensity and Figure 2.6.7-13 indicates the path (Section 4) location where the stresses are calculated. Table 2.6.7-8 is a listing of the Section 4 stresses. Table 2.6.7-9 documents the primary membrane ( $P_m$ ), primary membrane plus primary bending ( $P_m+P_b$ ), primary membrane plus primary bending plus secondary stress ( $P_m+P_b+Q$ ) in accordance with the criteria presented in Regulatory Guide 7.6. The minimum margin of safety is found to be +2.2 for primary membrane, +0.6 for primary membrane plus bending and +0.4 for primary membrane plus bending plus secondary stress intensity.

Figure 2.6.7-14 shows the location of the maximum total stress intensity in the lid and Figure 2.6.7-15 indicates the path (Section 5). Table 2.6.7-10 presents a listing of the Section 5 stresses and Table 2.6.7-11 provides the stress combinations in accordance with the Regulatory Guide 7.6 criteria. The minimum margin of safety is found to be +0.2 for primary membrane, +0.1 for primary membrane plus bending and +0.3 for primary membrane plus bending plus secondary stress intensity. Because all of the margins of safety are positive, the Model 2000 cask meets the end drop requirement of 10 CFR 71.71.

For NCT bearing stresses are also considered in the region where the HPI contacts the cask inner shell. Bearing stress is the total applied load divided by the contact area. Because contact with the HPI is explicitly modeled by applying nodal force at the location of the HPI support disk, the bearing stress can be represented as the normal stress in ANSYS. Figure 2.6.7-16 presents the normal stress distribution. As predicted the compressive stress with the largest magnitude, -10,009 psi, occurs at the centerline of the cask. Comparing the absolute value of the compressive stress to the yield strength of the 304 stainless steel at 600°F, 18,400 psi, the margin of safety is +0.84. Therefore, the bearing stress meets the stress criteria presented in Section 2.1.2.



**Figure 2.6.7-10. NCT Side Drop Cask Inner Shell Stress Intensity (total stress psi)**



**Figure 2.6.7-11. NCT Side Drop Linearized Stress Location (Section 3)**



NEDO-33866 Revision 6  
Non-Proprietary Information

**Table 2.6.7-6. NCT Side Drop Section 3 Stress Results (psi)**

Stress State	Location	S1	S2	S3	SINT
MEMBRANE ( $P_m$ )	—	2685	1199	-221	2906
BENDING ( $P_b$ )	Inside	7757	2447	384	7373
	Center	0	0	0	0
	Outside	-384	-2447	-7757	7373
MEMBRANE + BENDING	Inside	10150	3660	447	9699
	Center	2685	1199	-221	2906
	Outside	-50	-1218	-5656	5606
PEAK	Inside	1466	320	-257	1723
	Center	118	-40	-328	446
	Outside	379	-33	-363	742
TOTAL	Inside	11600	3980	200	11401
	Center	2363	1155	-104	2468
	Outside	41	-1251	-5731	5772

**Table 2.6.7-7. NCT Side Drop Section 3 Stress Results (psi)**

Stress Component	Stress Combination	Stress Intensity	Allowable	Margin of Safety
$P_m$	2906	19300	19300	5.6
$P_m + P_b$	9699	19300	28950	2.0
$P_m + P_b + Q$	19355	19300	57900	2.0

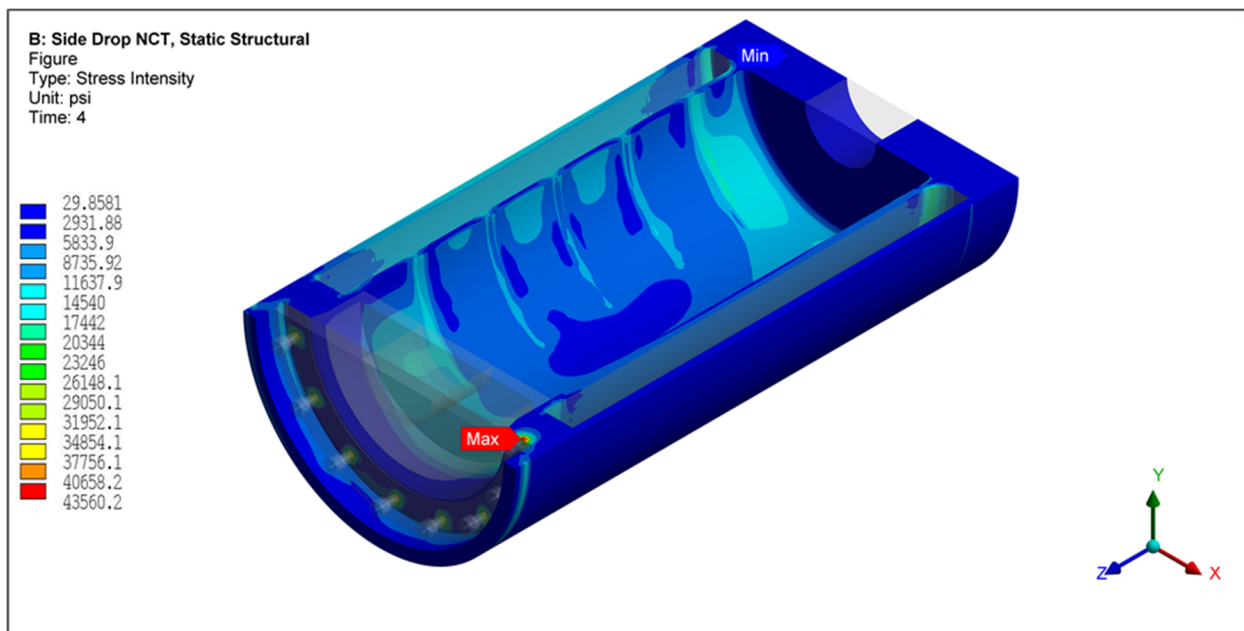


Figure 2.6.7-12. NCT Side Drop Cask Flange Stress Intensity (total stress psi)

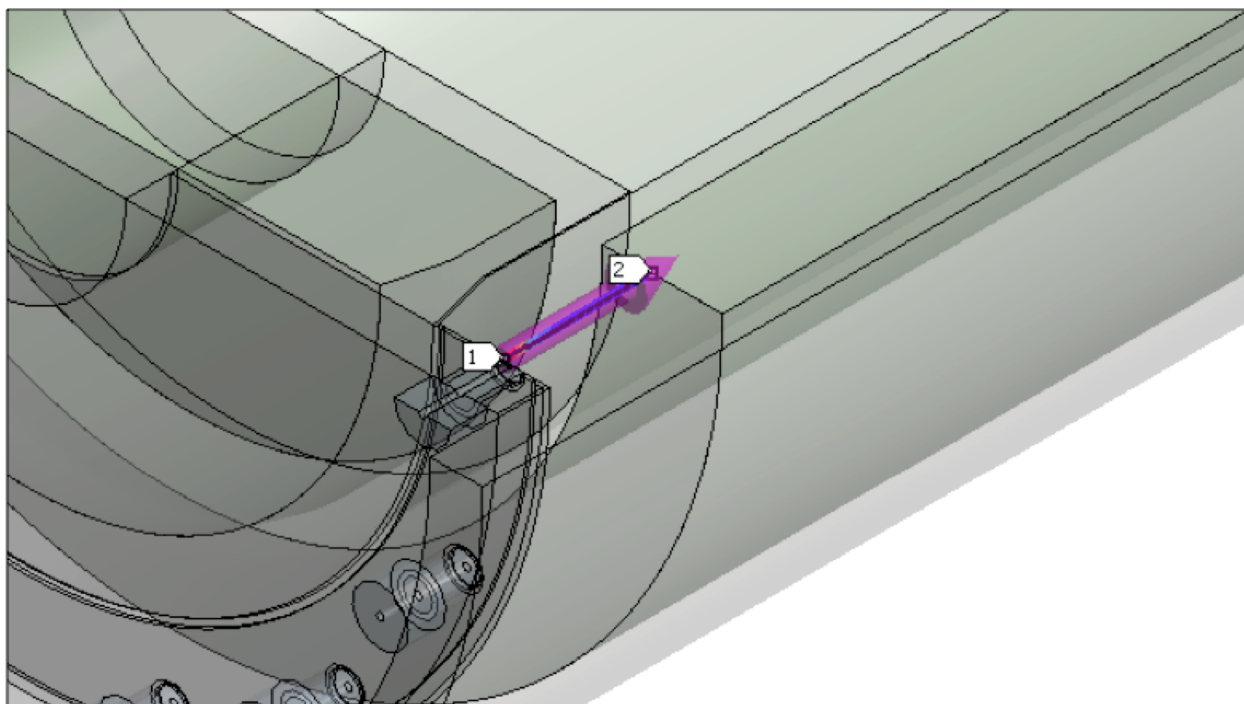


Figure 2.6.7-13. NCT Side Drop Linearized Stress Location (Section 4)

NEDO-33866 Revision 6  
Non-Proprietary Information

**Table 2.6.7-8. NCT Side Drop Section 4 Stress Results (psi)**

Stress State	Location	S1	S2	S3	SINT
MEMBRANE ( $P_m$ )	—	6412	939	389	6023
BENDING ( $P_b$ )	Inside	13800	2527	1895	11900
	Center	0	0	0	0
	Outside	-1895	-2527	-13800	11900
MEMBRANE + BENDING	Inside	20200	3478	2287	17910
	Center	6412	939	389	6023
	Outside	-1476	-1576	-7429	5952
PEAK	Inside	22380	12760	10030	12350
	Center	-681	-1027	-5044	4363
	Outside	7436	1432	1107	6329
TOTAL	Inside	42240	16060	12840	29400
	Center	1480	-190	-302	1782
	Outside	45	-120	-431	477

**Table 2.6.7-9. NCT Side Drop Section 4 Stress Results (psi)**

Stress Component	Stress Combination	Stress Intensity	Allowable	Margin of Safety
$P_m$	6023	19300	19300	2.2
$P_m + P_b$	17910	19300	28950	0.6
$P_m + P_b + Q$	41280	19300	57900	0.4

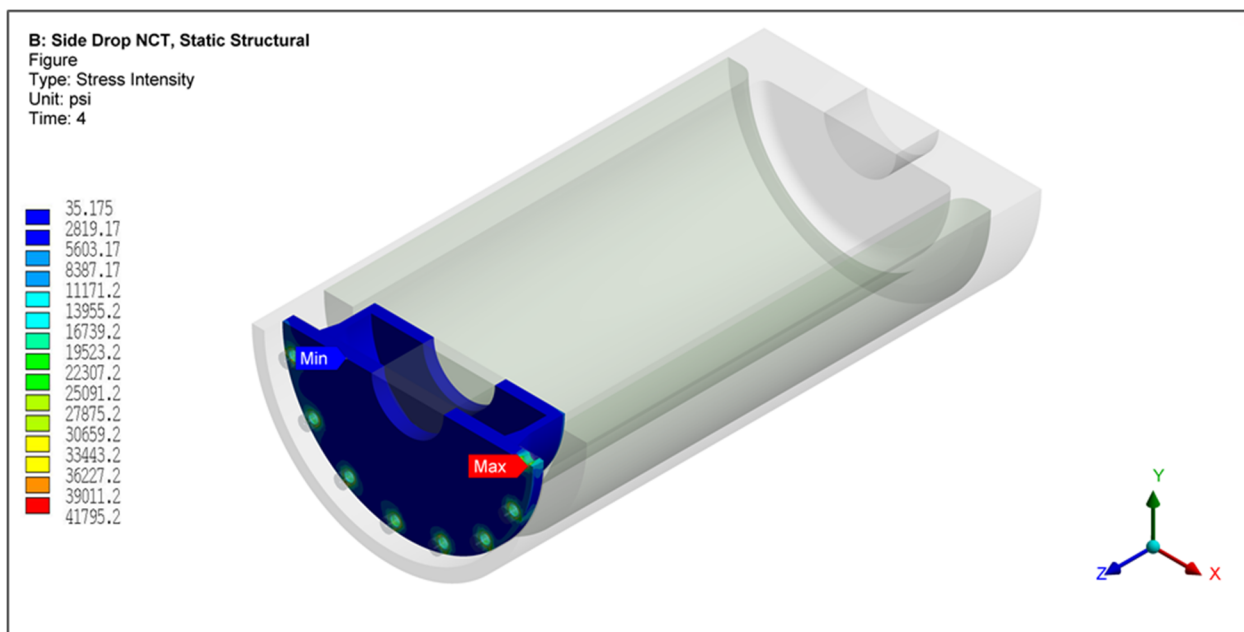


**Figure 2.6.7-14. NCT Side Drop Cask Lid Stress Intensity (total stress psi)**

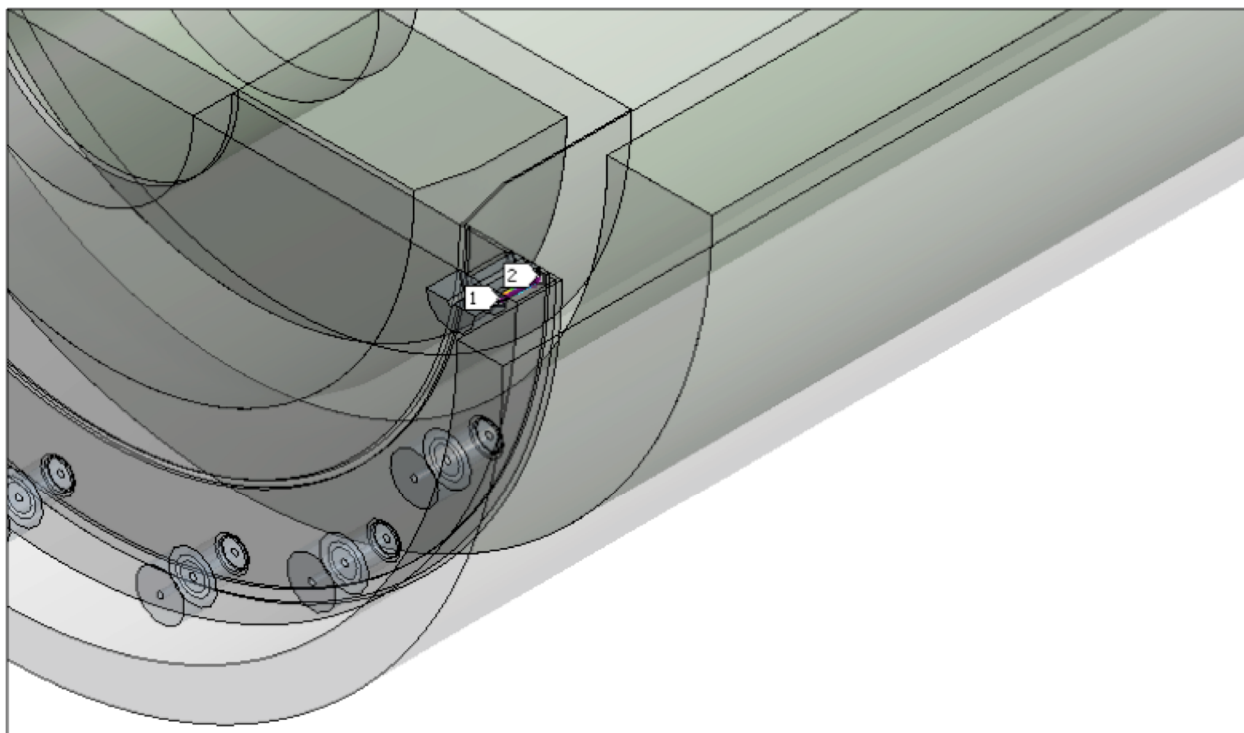


**Figure 2.6.7-15. NCT Side Drop Linearized Stress Location (Section 5)**

NEDO-33866 Revision 6  
Non-Proprietary Information

**Table 2.6.7-10. NCT Side Drop Section 5 Stress Results (psi)**

Stress State	Location	S1	S2	S3	SINT
MEMBRANE ( $P_m$ )	—	-684	-4079	-16770	16090
BENDING ( $P_b$ )	Inside	-343	-5757	-10400	10060
	Center	0	0	0	0
	Outside	10400	5757	343	10060
MEMBRANE + BENDING	Inside	-1106	-9877	-27050	25950
	Center	-684	-4079	-16770	16090
	Outside	1773	-30	-6771	8544
PEAK	Inside	117	-4066	-6171	6288
	Center	3818	2746	408	3410
	Outside	640	-4755	-5971	6611
TOTAL	Inside	-1541	-15960	-30660	29120
	Center	10	-1488	-13080	13090
	Outside	726	-3232	-12610	13330

**Table 2.6.7-11. NCT Side Drop Section 5 Stress Results (psi)**

Stress Component	Stress Combination	Stress Intensity	Allowable	Margin of Safety
$P_m$	16090	19300	19300	0.2
$P_m + P_b$	25950	19300	28950	0.1
$P_m + P_b + Q$	44469	19300	57900	0.3

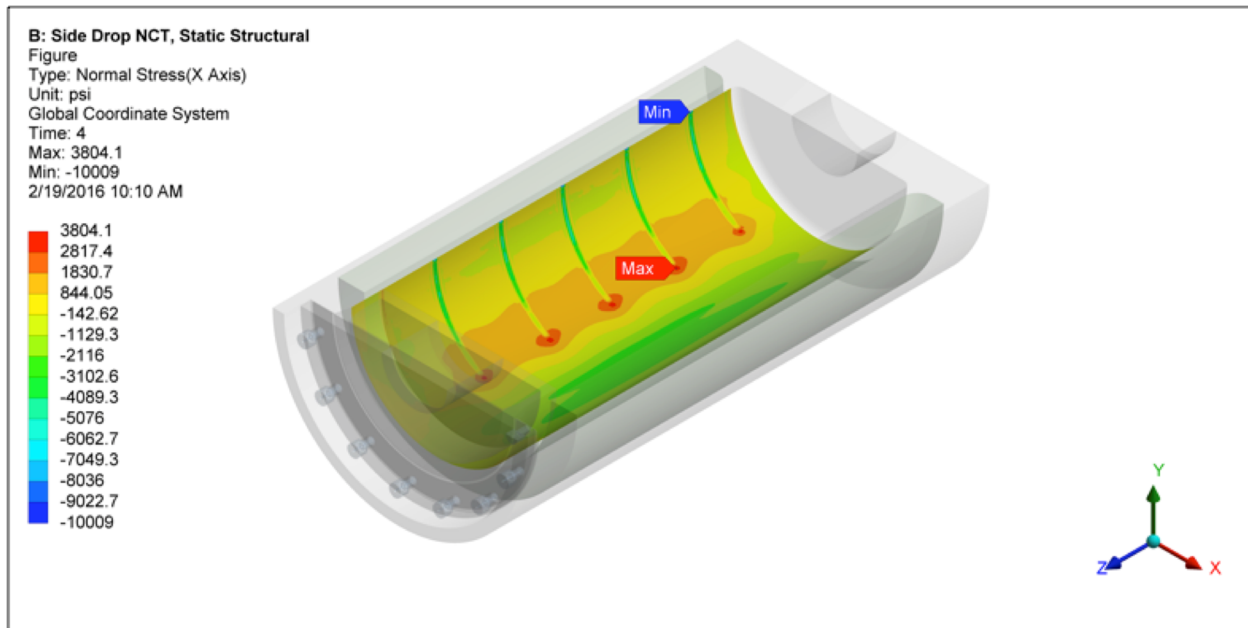


**Figure 2.6.7-16. NCT Side Drop Normal Stress Distribution (psi)**

#### **2.6.7.1.4. NCT Corner Drop**

The Model 2000 cask is composed of materials other than fiberboard or wood. Also, the weight of the Model 2000 cask exceeds 220 lb. According to 10 CFR 71.71(c)(8), the corner drop test is not applicable to the Model 2000 cask.

#### **2.6.7.1.5. Penetration**

According to 10 CFR 71.71(c)(10), a penetration test involving a 13-lb penetration cylinder dropped from a height of 40 inches is required for evaluation of packages during normal conditions of transport. However, Regulatory Guide 7.8 states “the penetration test of 10 CFR 71.71 is not considered by the NRC staff to have structural significance for large shipping casks (except for unprotected valves and rupture disks) and is not considered as a general requirement.” A penetration evaluation is not performed because the Model 2000 cask has no unprotected valves or rupture disks that could be affected by normal conditions of transport.

#### **2.6.7.1.6. Cask Overpack Bolt Evaluation**

During normal use, the overpack bolt is subjected to two stresses. One is the stress due to preload and acts on the reduced cross sectional area between the threaded region and the shoulder. The other stress is due to the shear from lifting the package by the top part of the overpack. Fatigue life for each stress case is evaluated to determine the limiting value.

##### Preload Stress:

Because the bolt is loaded in shear, preloading is only required to prevent its loosening during transport. To further ensure that the bolt will not come loose during transport, an adhesive/sealant compound is applied to the bolt threads prior to installation. The required torque for the overpack bolts is 100±5 ft-lb dry per 101E8719 and 105E9521.

The cask overpack uses 15 equally spaced 7/8-9 UNC-2A, ASTM A540 Grade B22, Class 3 bolts:

Proof Strength = Minimum Yield Strength x 85% = 115700 (0.85) = 98345 psi (Table 2.2-9)

Temperature = 192°F (Figure 3.5.1-2(b), Average of 175.0°F and 209.8°F)

The maximum preload on the bolt is:

$$P = 5T_{\text{Max}} / D_{\text{Nom}} = 7200 \text{ lb}$$

where:

$$T_{\text{Max}} = 100 + 5 = 105 \text{ ft-lb} = 1260 \text{ in-lb}$$

$$D_{\text{Nom}} = \text{Nominal thread size} = 7/8 \text{ in} = 0.875 \text{ in}$$

The area of the reduced cross section between the threads and the shoulder is

$$A = 0.25 \pi (0.726)^2 = 0.414 \text{ in}^2 \text{ The tensile stress in this region is:}$$

$$\sigma_T = P/A = 7200/0.414 = 17391 \text{ psi} \ll \text{Proof Strength} = 98345 \text{ psi}$$

From ASME NB 3232.3 (Reference 2-18), the fatigue strength reduction factor is 4.0. The modulus of elasticity at 192°F is  $29.04(10)^6$  psi (Reference 2-7, Table TM-1, Material Group C, Page 785). Because the fatigue curve (ASME Section III, Figure I-9.4, Page 12) is based on a modulus of elasticity of  $30(10)^6$  psi, the stress range is given by:

$$S_r = 17391 (4.0) [30(10)^6/29.04(10)^6] = 71864 \text{ psi}$$

The alternating component is one-half of the range:

$$S_a = S_r/2 = 71864/2 = 35932 \text{ psi}$$

The number of cycles to fatigue failure is determined from Reference 2-18, Table I-9.0, Figure I-9.4:  $MNS \leq 2.7S_m$ . The number of cycles to failure is calculated using the procedure defined in Table I-9.0, general note (b):

$$\text{Fatigue Limit} = 5000 (10,000/5,000)^{\text{Log}(45/35.9)/\text{Log}(45/34)} = 5000 (2)^{0.806} \text{ cycles}$$

$$\text{Fatigue Limit} \approx 8700 \text{ cycles}$$

Assuming an average of 2 cycles/usage and 12 usages per year, the expected life of the bolts is:

$$\text{Bolt life} = 8700/[2(12)] = 362 \text{ years}$$

Lifting Shear Stress:

The weight transferred through the bolts during lifting of the assembled package is equal to the combined weight of the cask, HPI, material basket, contents, and overpack base. This total combined weight is:

$$\begin{aligned} W_T &= (W_{\text{cask body}} + W_{\text{cask lid}}) + W_{\text{HPI}} + (W_{\text{material basket}} + W_{\text{contents}}) + W_{\text{overpack base}} \\ &= (16000 + 1900) + 5,133 + (114 + 203) + 3633 = 26983 \text{ lb} \end{aligned}$$

The above component weights are obtained from Table 2.1-3 and Table 2.1-4.

The area of the 15 bolts loaded in double shear is:

$$A_T = \text{Total area of bolt shoulders} = (2)(15)(0.25)\pi(1.375)^2 = 44.55 \text{ in}^2$$

The bolt shearing stress associated with a vertical lift of the package and contents is:

$$\tau = W_T / A_T = 26983 / 44.55 = 606 \text{ psi}$$

Correcting for fatigue strength and modulus of elasticity gives a stress range of:

$$\tau_r = 606 (4.0) [30(10)^6 / 29.04(10)^6] = 2504 \text{ psi}$$

The alternating component is:

$$\tau_a = \tau_r / 2 = 2,504 / 2 = 1,252 \text{ psi}$$

The fatigue limit is  $> 10^6$  cycles (ASME Section III, Figure I-9.4, Page 12)

#### **2.6.7.2. HPI Stress Analysis**

The purpose of this section is to document the Model 2000 HPI and material basket analyses that shows the design meets the requirements of 10 CFR 71. Specifically, the evaluation addresses the mechanical loads associated with the NCT.

The results of the analyses for various load cases are presented pictorially as stress intensity contour plots as well as in table form, with the corresponding margin of safety in each component of the cask body.

##### **2.6.7.2.1. HPI Model Description**

The HPI design was developed using Autodesk Inventor. To generate the ANSYS compatible solid model, the Inventor model of the HPI is divided in half ( $180^\circ$ ) along the center plane. The final solid model is exported as a .STEP file and is imported directly into ANSYS where the finite element model is meshed. The solid model of the HPI is shown in Figure 2.6.7-17.

The solid portion of the model is constructed using ANSYS solid (SOLID185) elements. Surface-to-surface contact elements are used to simulate the interaction between adjacent components. Specifically, contact between the HPI shells and depleted uranium shielding is modeled using CONTAC174/TARGE170 surface-to-surface contact elements with zero friction, which allows the DU to float between the inner and outer shells. Contact elements are also used to bond dissimilarly meshed components. Spring elements (COMBIN14) are inserted automatically during the solution to help stabilize the model. ANSYS assigns low spring stiffness so their presence will not adversely affect the accuracy of the solution. Welds are modeled using ANSYS contact elements.



#### **2.6.7.2.2. HPI Side Drop Model**

The HPI side drop model evaluates the stresses in the support disks and HPI assembly to ensure the HPI maintains structural integrity during NCT. Using the base model, refinements are made in the support disk mesh to ensure accurate results. Figure 2.6.7-18 shows the finite element model of the HPI.

To simulate contact with the cask, the interaction between the HPI and cask inner shell is modeled using CONTAC52 gap elements, which acts as a compression only element. The size of the CONTAC52 gaps is determined from nominal dimensions between the impact limiter and cask body. Figure 2.6.7-19 shows the distribution of the contact elements used to simulate contact between the HPI and cask inner shell.

#### **2.6.7.2.3. HPI End Drop Model**

Of primary concern during a top or bottom end impact event is the inertial loading of the depleted uranium filled plug. For this case, a top impact is assumed because the HPI bottom plug [[  
]] of depleted uranium. To evaluate the bottom plug, the plug subassembly is treated as a separate component. Figure 2.6.7-20 shows the solid model of the bottom plug assembly. The bottom plug is bolted to the HPI as a means of lifting the HPI from the cask without the need to remove the material basket. However, no credit is taken for the bolt. Therefore, only the lid assembly is evaluated using a highly-refined mesh to accurately predict stresses at the weld seam. Figure 2.6.7-21 shows the finite element model of the bottom plug.

[[

]]

**Figure 2.6.7-17. HPI Solid Model**

[[

]]

**Figure 2.6.7-18. HPI Side Drop Finite Element Model**

[[

]]

**Figure 2.6.7-19. Contact Elements Between HPI and Cask Inner Shell**

[[

]]

**Figure 2.6.7-20. Solid Model of HPI Bottom Plug**

[[

]]

**Figure 2.6.7-21. Finite Element Model of HPI Bottom Plug**

#### **2.6.7.2.4. Boundary Conditions**

Boundary conditions are applied to the model simulating the loading conditions the HPI will experience during NCT. The five categories of cask loading considered in the free drop event are pressure loaded to simulate side drop contents, discrete mass to simulate end drop, thermal conditions, inertial body load and displacement. ANSYS input files are used to apply boundary conditions and loads to the cask model.

### **Inertial Load**

To evaluate the impact performance of the HPI, an LS-DYNA analysis was performed (Section 2.12.1) to determine the maximum acceleration during hot/cold and heavy/light environmental conditions and varying impact limiter shell thicknesses. Table 2.6.7-12 provides a summary of the maximum accelerations that occur during cold conditions. With the exception of corner drop case, the accelerations listed in Table 2.6.7-12 are applied to the HPI model using the ANSYS ACEL command equivalent to NCT accelerations corresponding to the 0.3-meter drop case. Equivalent static forces, in accordance with D'Alembert's principle, represent the applied accelerations.

### **Pressure Loading Contents - Side Drop**

Two cases are presented to evaluate the performance of the HPI during the side drop. Case 1 is a concentrated pressure distribution at the four [[ ]] Case 2 is a uniform pressure distribution ("area load"). The contact area between the material basket and the HPI inner shell is approximately 180° (90° on each side of the drop centerline). The inertial load produced by the 317-lb. content weight is represented as an equivalent static pressure applied on the interior surface of the cask. The pressure is uniformly distributed along the cavity length and is varied in the circumferential direction as a cosine distribution. The maximum pressure occurs at the impact centerline; the pressure decreases to zero at locations that are 90° from either side of the impact centerline. The pressure loading simulating the Case 1 (line load) is illustrated in Figure 2.6.7-22 and Figure 2.6.7-23 shows the pressure loading for Case 2 (area load). The following formula is used to determine the contents pressures for the side drop analyses, which vary around the circumference. This method uses a summation scheme to approximate the integration of the cosine-shaped pressure distribution:

$$F_{\text{total}} = \sum_{i=1}^{180} P_{\text{max}} A_i \cos(\theta_i) \cos(\theta'_i)$$

$$F_{\text{total}} = 317/2 \text{ kg} \times G$$

where

- $P_{\text{max}}$  = maximum pressure (at impact centerline)
- $\theta_i$  = average angle of subtended arc of  $i^{\text{th}}$  element measured from centerline at point of impact, to obtain vertical component of pressure
- $i$  =  $i^{\text{th}}$  circumferential sector
- $\theta'_i$  = normalized angle to peak at 0° and to be zero at 90°
- $A_i$  =  $i^{\text{th}}$  circumferential area over which the pressure is applied
- $G$  = side acceleration

Gap elements are defined at both ends of the cask to simulate the pressure applied by the cask inner shell during side drop conditions (see Figure 2.6.7-19). This is accomplished by defining the gap stiffness as a cosine function from a maximum value  $1 \times 10^6$  lb/in at the centerline to 87,156 lb/in at 85° from the centerline of impact, and a value 50,000 lb/in from 90° to 180°.

**Table 2.6.7-12. LS-DYNA NCT Impact Results Summary**

DESCRIPTION	DROP ANGLE (DEGREE)	APPLICABLE BOUNDARY CONDITION						ACCELERATION (g)
		Temperature			Payload			
		Amb.	Hot	Cold	Nom.	Heavy	Light	
NCT, Cold, End Drop	90	—	—	X	—	—	X	15.5
NCT, Cold, Side Drop	0	—	—	X	—	—	X	55.1
NCT, Cold, Corner Drop	68 (=90-22)	—	—	X	—	—	X	14.6

[[

]]

**Figure 2.6.7-22. Cosine Pressure Distribution Simulating Material Basket** [[  
]]

[[

]]

**Figure 2.6.7-23. Cosine Pressure Distribution Assuming Uniform Contact**

#### **2.6.7.2.5. HPI NCT Side Drop Results**

To evaluate the stresses in the HPI body, with a concentrated pressure load at the material basket [[ ]], linearized section stresses are evaluated at the intersection of plates, weld joints and anywhere a stress riser is observed. Stresses are evaluated using the ANSYS Parametric Design Language (APDL) macro language to cycle through each location of interest. To provide a thorough understanding of the stress profile, 684 individual sections are evaluated at axial and radial increments. At each section location, the primary membrane ( $P_m$ ) and primary membrane plus primary bending ( $P_m+P_b$ ) are calculated and compared to the stress criteria in accordance with the criteria presented in ASME Section III-NF (Reference 2-3). Figure 2.6.7-24 provides a visual representation of the section stress locations. Because of the total number of sections and close proximity, the section numbers are not legible. Separately, an additional seven sections are evaluated in the worst-case support disk. Figure 2.6.7-25 provides a visual representation of the section stress locations for the support disk.

#### **2.6.7.2.6. NCT Case 1 Stress Results**

The top 30 stress results for the Case 1 NCT HPI body results are presented in Table 2.6.7-13. Figure 2.6.7-26 and Table 2.6.7-14 present the Case 1 NCT support disk stress results. As shown in the tables, the margins of safety when compared to the stress intensity for each category are greater than one.

Bearing loads, per ASME III-NF-3223.1 for Service Level A (NCT) events, are compared to the yield stress at temperature. From the ANSYS output, the maximum bearing stress that results from the total force applied by the material basket [[ ]] to the HPI inner shell is 1690.2 psi. Assuming a maximum temperature of 1000°F the yield stress is 17,000 psi. Therefore, the margin of safety is 9.1.

[[

]]

**Figure 2.6.7-24. Linearized Section Locations for the HPI Body Evaluation**



[[

]]

**Figure 2.6.7-25. Linearized Section Locations for the Support Disk Evaluation**

**Table 2.6.7-13. NCT Case 1 HPI Body Top 30 Results**

[illegible]

Table Key:

- M = Membrane stress intensity (psi)
- M+B = Membrane + Bending stress intensity (psi)
- In = stress at the inside surface of the element (psi)
- Cen = stress at the center of the element (psi)
- Out = stress at the outer surface of the element (psi)
- Max = maximum of in, cen, and out, which is compared to the allowable stress (psi)
- Allowable = Allowable stress at temperature (psi)
- MS = Margin of safety

[[

]]

Figure 2.6.7-26. Case 1, NCT, Stress Intensity Result (psi)

Table 2.6.7-14. NCT Support Disk Case 1 Results

[[										
										]]

#### **2.6.7.2.7. NCT Case 2 Stress Results**

The top 30 stress results for the Case 2 NCT HPI body results are presented in Table 2.6.7-15. Figure 2.6.7-27 and Table 2.6.7-16 present the Case 2 NCT support disk stress results. Review of the stress results shows that there is sufficient positive margin of safety of all cases.

Bearing loads per ASME III-NF-3223.1 for Service Level A (NCT) events are compared to the yield stress at temperature. From the ANSYS output the maximum bearing stress that results from the total force applied by the material basket to the HPI inner shell is 60.0 psi. Assuming a maximum temperature of 1000°F the yield stress is 17,000 psi. Therefore, the margin of safety is +Large.

**Table 2.6.7-15. NCT Case 2 HPI Body Top 30 Results**

[illegible]

Table Key:

- M = Membrane stress intensity (psi)
- M+B = Membrane + Bending stress intensity (psi)
- In = stress at the inside surface of the element (psi)
- Cen = stress at the center of the element (psi)
- Out = stress at the outer surface of the element (psi)
- Max = maximum of in, cen, and out, which is compared to the allowable stress (psi)
- Allowable = Allowable stress at temperature (psi)
- MS = Margin of safety

[[

]]

Figure 2.6.7-27. Case 2, NCT, Stress Intensity Result (psi)

Table 2.6.7-16. NCT Support Disk Case 2 Results

[[										
										]]

#### 2.6.7.2.8. HPI NCT End Drop Results

Stress results for the NCT end drop discussed previously are documented in Table 2.6.7-17. The table presents the primary membrane ( $P_m$ ) and primary membrane plus primary bending ( $P_m+P_b$ ) in accordance with the criteria presented in ASME Section III-NF (Reference 2-3).

As shown in the table, the margins of safety when compared to the stress intensity for each category are positive. The most critically stressed component in the system is the [[

]] The minimum margin of safety is found to be large. The locations of the critical sections corresponding to the maximum stress location and axial displacement are shown in Figure 2.6.7-28.

**Table 2.6.7-17. NCT End Drop Stress Summary**

[[							
							]]

[[

]]

**Figure 2.6.7-28. HPI NCT End Drop Results – Peak Stress Intensity (psi) and Displacement (inches)**



### 2.6.7.3. Material Basket Evaluation

This section evaluates the material basket for NCT. Factors of safety for the basket are calculated based on the criteria for Service Level 'A' limits from ASME Section III-NF (NF-3221).

#### End Drop Case

During the end drop the material basket is loaded by inertia loads acting on the end of the [[ ]]. Depending on the orientation of the outer cask when dropped, the basket contents will either load the material basket or the lid of the high performance insert (HPI). There is a washer welded to the bottom of the basket [[ ]] that holds the rod holders. Nothing prevents the rod holders from exiting the top of the material basket. If the outer cask is dropped while in the upright position, the material basket will be loaded by the contents. The worst-case condition of upright end drop is evaluated. The inertial loading will load the [[ ]] bundle in compression. There is no bending or shear stress present. For this evaluation, all 18 full length [[ ]] are loaded.

Stresses at bottom of [[ ]]:

$$\sigma_{\text{membrane}} = \frac{P}{A} = 837 \text{ psi compression}$$

$$\sigma_{\text{bending}} = 0 \text{ psi}$$

$$\tau_{\text{shear}} = 0 \text{ psi}$$

where  $P = W \times G = 4913.5 \text{ lbs}$  inertial load on 18 [[ ]] bundle

$W = [[ ]] \text{ lbs}$  basket plus contents weight

$G = 15.5$  NCT end drop acceleration

$A = [[ ]] \text{ in}^2$  Cross section area of [[ ]], Table 2.6.7-18)

$S_y = 17700 \text{ psi}$  Yield Strength, 316 stainless steel, 800°F (Table 2.2-2)

Minimum Margin of Safety:

The minimum margin of safety for the NCT end drop case is:

$$MS = \frac{S_y}{\sigma_m} - 1 = \frac{17700}{837} - 1 = +20.1$$

#### Side Drop Case

During the side drop the steel [[ ]] provides a close fit with the high performance insert inner shell, which distributes the inertial load as three beam segments along the length of the basket assembly. The basket is assembled using short [[ ]] at each end of the basket starting at the center location. To provide strength to the basket assembly, [[ ]] are added between the [[ ]] at the outside of the assembly forming a [[ ]] shape. For this evaluation it is assumed that only the outer [[ ]] carry the load. Additionally, no credit is taken for the [[ ]], which is significantly stiffer than the individual [[ ]]. The basket is analyzed using classical hand calculations for a 55.1 g side drop inertia load and a bounding weight of [[ ]] pounds. Assuming one-third of the inertial load is carried by one of the equivalent beam segments, the bending stress in the basket is:

NEDO-33866 Revision 6  
Non-Proprietary Information

$$\sigma_b = \frac{Mc}{I_{cc}} = 688.4 \text{ psi}$$

where

$$P = W \times G = \text{[[ ]]} \text{ lb}$$

Bounding basket weight

$$W = \text{[[ ]]} \text{ lb}$$

NCT side drop acceleration

$$G = 55.1 \text{ g}$$

$$M = \frac{Waxl^2}{12} = 7,224.4 \text{ lb-in}$$

Bending moment

$$l = \text{[[ ]]} \text{ in}$$

Length of beam section

$$W_a = 391.02 \text{ lb/in}$$

Uniformly distributed load

$$c = 3.73 \text{ in}$$

Neutral axis to outer fiber

$$I_{cc} = 39.09 \text{ in}^4$$

Moment of inertia (12 [[ ]])

The moment of inertia calculation is shown in Table 2.6.7-18.

**Table 2.6.7-18. Moment of Inertia Calculation**

[[ ]]

]]

The pure shear stress, ASME III NF-3223.2, which develops across the composite [[ ]] section during the side drop is:

$$\tau = \frac{P}{2A} \approx 744.8 \text{ psi} < 0.6S_m = 0.6 \times 15,900 = 9,540 \text{ psi}$$

where

$$P = 5822.2 \text{ lb}$$

$$A = 3.91 \text{ in}^2$$

Cross-sectional area (12 [[ ]])

$$d_o = \text{[[ ]]} \text{ in}$$

Outside diameter of [[ ]]

$$d_i = \text{[[ ]]} \text{ in}$$

Inside diameter of [[ ]]

The stress intensity in the basket that results from the combination of the bending and shear stresses is

$$\sigma = \sqrt{\sigma_b^2 + 4\tau^2} = 1641.0 \text{ psi}$$

The margin of safety is

$$MS = \frac{1.5S_m}{\sigma} - 1 = \frac{23850}{1641.0} - 1 = +\text{Large}$$

[[ ] hold the basket together using [[ ] (ASME III-NF, Class 1). The [[ ] and welds are equivalent in thickness and strength to the adjoining [[ ]]. Therefore, the previous analysis bounds the stresses generated in the welds.

### 2.6.8. Corner Drop

The Model 2000 cask is composed of materials other than fiberboard or wood. Also, the weight of the Model 2000 cask exceeds 220 lb. According to 10 CFR 71.71(c)(8), the corner drop test is not applicable to the Model 2000 cask. Additionally, as can be seen in Table 2.6.7-12, the end drop and side drop NCT accelerations bound the corner drop. Therefore, a stress analysis of the corner drop scenario is not required.

### 2.6.9. Compression

This test does not apply to the Model 2000 Transport Package, because the package weight is in excess of 11,000 lb (5,000 kg).

### 2.6.10. Penetration

According to 10 CFR 71.71(c)(10), a penetration test involving a 13-lb penetration cylinder dropped from a height of 40 inches is required for evaluation of packages during NCT. However, Regulatory Guide 7.8 states “the penetration test of 10 CFR 71.71 is not considered by the NRC staff to have structural significance for large shipping casks (except for unprotected valves and rupture disks) and is not considered as a general requirement.” A penetration evaluation is not performed because the Model 2000 cask has no unprotected valves or rupture disks that could be affected by normal conditions of transport.

## 2.7 Hypothetical Accident Conditions

The Model 2000 Transport Package has been demonstrated to meet the performance requirements specified in Subpart E of 10 CFR 71, when subjected to hypothetical accident conditions as specified in 10 CFR 71.73. According to the Regulatory Guide 7.6 (Reference 2-17), for the hypothetical accident conditions the stress intensities resulting from primary membrane and primary bending stresses are to be investigated. The stress intensities from the thermal stresses are presented in this section.

### 2.7.1. Free Drop

The free drop scenario outlined by 10 CFR 71.73(c)(1) requires a demonstration of the structural adequacy of the Model 2000 cask for a 30-ft drop onto a flat, essentially unyielding horizontal surface in the orientation that inflicts the maximum damage to the cask. The Model 2000 Transport Package is shown to meet the free drop requirements through a combination of classic calculations,

impact analyses, and static finite element. The evaluations include the qualification of the Model 2000 cask lid bolt design for the combined effects of free drop impact force, internal pressures, thermal stress, O-ring compression force, and bolt preload following the methodology of NUREG/CR-6007 (Reference 2-15) (Section 2.12.4). The combined effects of inertial loads, and internal pressures are considered for packaging components. The impact analysis of the package is presented in Section 2.12.1. Section 2.7.1.1 presents the evaluation of the cask body and Section 2.7.1.2 presents the structural evaluation of the HPI and material basket during free drop conditions. The cask body and HPI structural analyses are performed using the finite element program ANSYS (Reference 2-16) and the material basket is analyzed using classic methods. Table 2.7.1-1 provides a summary of the HAC accelerations predicted by the LS-DYNA analysis presented in Section 2.12.1. A lead slump analysis is provided in Section 2.12.2.

**Table 2.7.1-1. LS-DYNA Results**

DESCRIPTION	DROP ANGLE (DEGREE)	APPLICABLE BOUNDARY CONDITION						ACCELERATION (g)
		Temperature			Payload			
		Amb.	Hot	Cold	Nom.	Heavy	Light	
HAC, End Drop, Hot	90	—	✓	—	—	✓	—	157.5
HAC, Side Drop, Cold	0	—	—	✓	—	—	✓	161.9
HAC, Corner Drop, Cold	68 (90-22)	—	—	✓	—	—	✓	80.3
HAC, Slap Down	5	✓	—	—	✓	—	—	114.4
HAC, Slap Down	10	✓	—	—	✓	—	—	118.0

### 2.7.1.1. Cask Body Stress Analysis

This section evaluates the structural results of the Model 2000 cask body analyses and shows that the design meets the requirements of 10 CFR 71.71. Specifically, the evaluation addresses the loads associated with the HAC. The results of the analyses for various load cases are presented pictorially in stress intensity contour plots as well as in table form, with the corresponding safety factors in critical components of the cask body.

#### 2.7.1.1.1. End Drop

In accordance with the requirements of 10 CFR 71.73(c)(1), the Model 2000 Transport Package is structurally evaluated for the 30-foot end-drop condition. In this hypothetical accident, the cask including the payload and the impact limiters falls 30 feet onto a flat, unyielding, horizontal surface. The cask strikes the surface in a vertical upright position. For the Model 2000 cask, the bottom end drop is bounding. In the bottom down position, the prying load on the closure bolts is maximized. Closure bolts are evaluated separately in Section 2.12.4.

The most critically stressed component in the system is the cask flange region, which is due to bending of the flange from the inertial load imposed by the cask lid. The second region of interest is in the cask lid in the closure bolt contact region. To evaluate the stresses in these regions

linearized stress are calculated across the thickness of the plate. For the top flange, Figure 2.7.1-1 shows the location of the maximum total stress intensity and Figure 2.7.1-2 indicates the path (Section 6) location where the stresses are calculated. Table 2.7.1-2 is a listing of the Section 6 stresses. Table 2.7.1-3 documents the primary membrane ( $P_m$ ) and primary membrane plus primary bending ( $P_m + P_b$ ) in accordance with the criteria presented in Regulatory Guide 7.6. Stresses are compared to the allowable at a bounding temperature of 300°F. The minimum margin of safety is found to be +3.7 for primary membrane, and +1.8 for primary membrane plus bending.

Figure 2.7.1-3 shows the location of the maximum total stress intensity in the lid and Figure 2.7.1-4 indicates the path (Section 7). Table 2.7.1-4 presents a listing of the Section 2 stresses and Table 2.7.1-5 provides the stress combinations in accordance with the Regulatory Guide 7.6 criteria. The minimum margin of safety is found to be +1.4 for primary membrane and +0.8 for primary membrane plus bending. Because all of the margins of safety are positive, the Model 2000 cask meets the end drop requirement of 10 CFR 71.73.

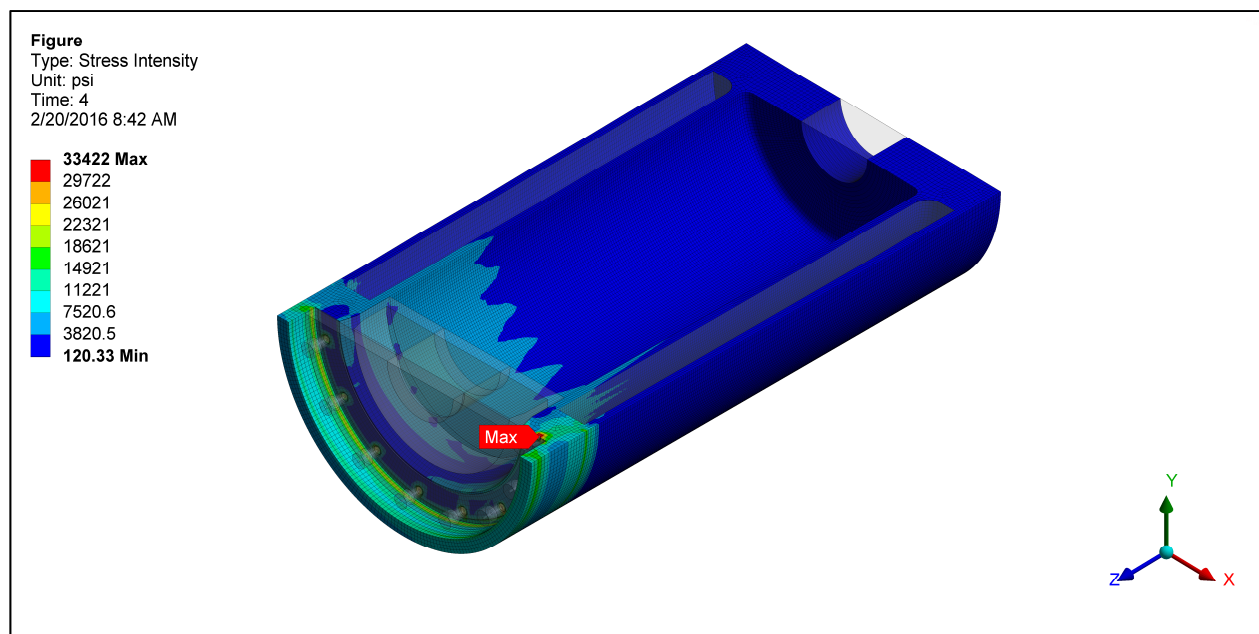


**Figure 2.7.1-1. HAC End Drop Cask Body Stress Intensity (total stress psi)**

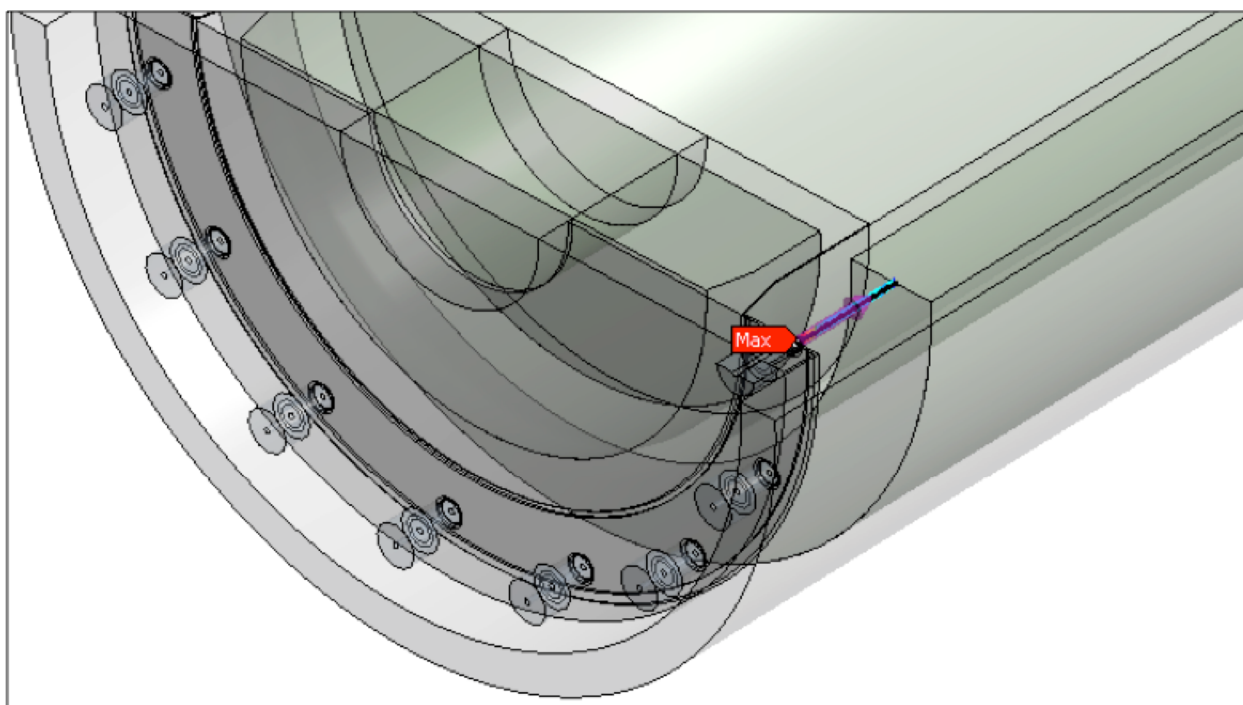


**Figure 2.7.1-2. HAC End Drop Linearized Stress Location (Section 6)**

NEDO-33866 Revision 6  
Non-Proprietary Information

**Table 2.7.1-2. HAC End Drop Section 6 Stress Results (psi)**

Stress State	Location	S1	S2	S3	SINT
MEMBRANE ( $P_m$ )	—	6581	-895	-3558	10140
BENDING ( $P_b$ )	Inside	14700	1514	-5075	19770
	Center	0	0	0	0
	Outside	5075	-1514	-14700	19770
MEMBRANE + BENDING	Inside	19290	500	-6531	25830
	Center	6581	-895	-3558	10140
	Outside	5773	-2708	-12070	17840
PEAK	Inside	23680	14560	11820	11860
	Center	-301	-939	-5909	5608
	Outside	7995	1326	524	7471
TOTAL	Inside	41600	13550	8174	33422
	Center	4518	-1942	-7597	12120
	Outside	6665	-1547	-4280	10940

**Table 2.7.1-3. HAC End Drop Section 6 Stress Results (psi)**

Stress Component	Stress Combination	Stress Intensity	Allowable	Margin of Safety
$P_m$	10140	20000	48000	3.7
$P_m + P_b$	25830	20000	72000	1.8

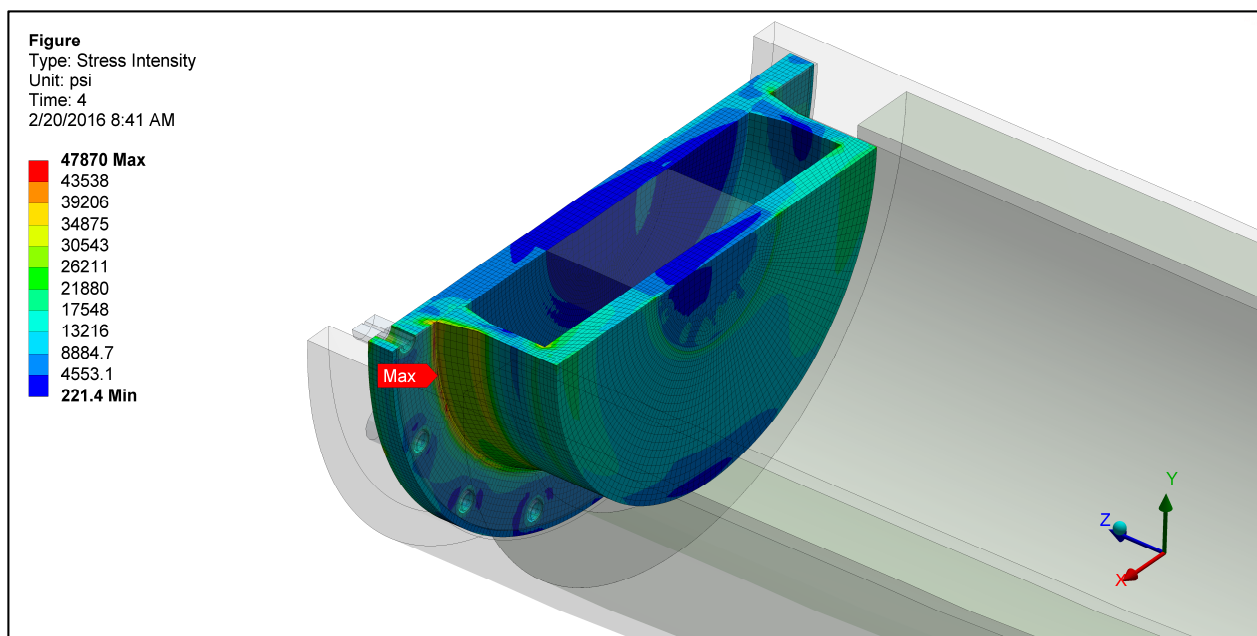


**Figure 2.7.1-3. HAC End Drop Lid Stress Intensity (total stress psi)**

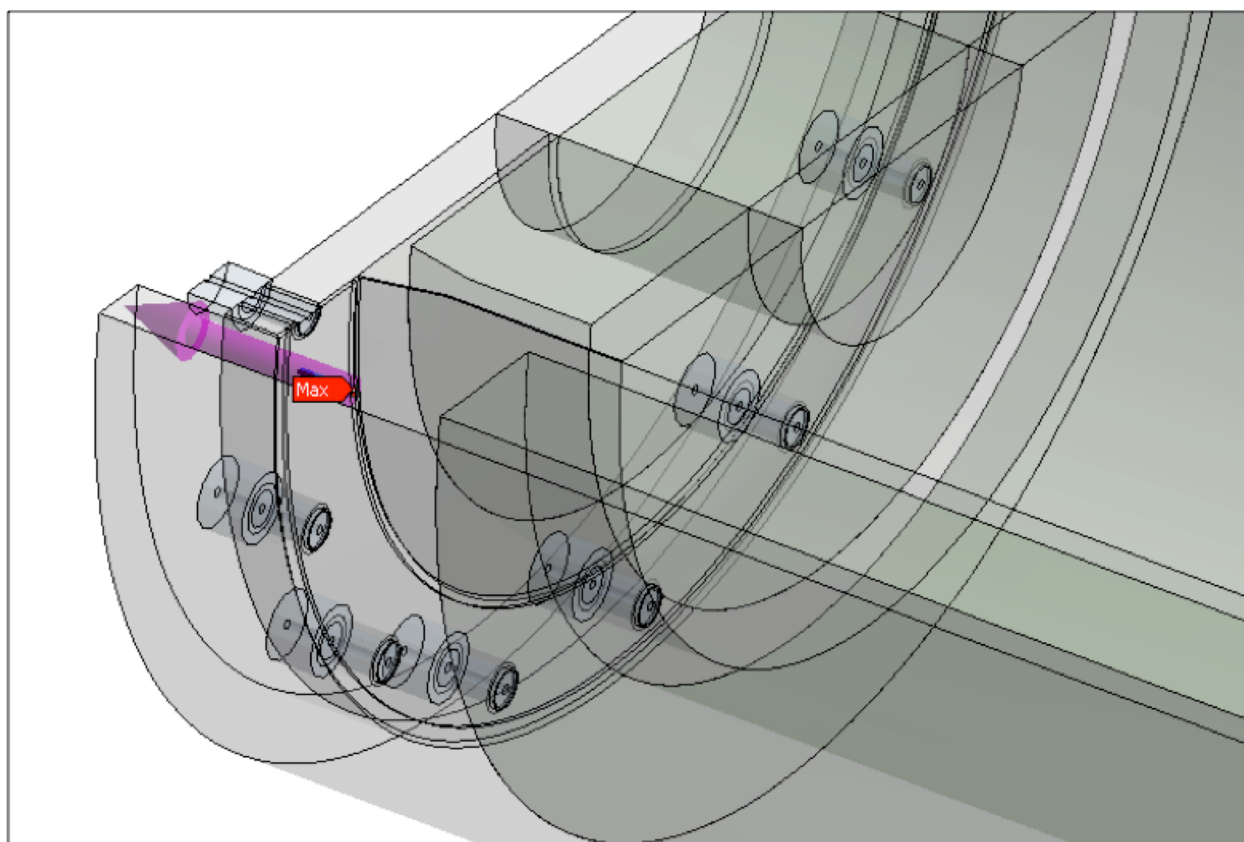


**Figure 2.7.1-4. HAC End Drop Linearized Stress Location (Section 7)**



**Table 2.7.1-4. HAC End Drop Section 7 Stress Results (psi)**

Stress State	Location	S1	S2	S3	SINT
MEMBRANE ( $P_m$ )	—	4664	-9598	-15170	19830
BENDING ( $P_b$ )	Inside	6095	-5767	-15640	21730
	Center	0	0	0	0
	Outside	15640	5767	-6095	21730
MEMBRANE + BENDING	Inside	10350	-15400	-30370	40720
	Center	4664	-9598	-15170	19830
	Outside	3790	-4026	-4558	8348
PEAK	Inside	6105	805	-4285	10390
	Center	1161	-449	-3088	4249
	Outside	3340	607	-925	4265
TOTAL	Inside	14800	-14510	-33070	47870
	Center	3087	-10080	-15480	18570
	Outside	3323	-1612	-3483	6806

**Table 2.7.1-5. HAC End Drop Section 7 Stress Results (psi)**

Stress Component	Stress Combination	Stress Intensity	Allowable	Margin of Safety
$P_m$	19830	20000	48000	1.4
$P_m + P_b$	40720	20000	72000	0.8

#### 2.7.1.1.2. Side Drop

In accordance with the requirements of 10 CFR 71.73(c)(1), the Model 2000 cask is structurally evaluated for the hypothetical accident 30-foot side drop condition. In this event, the cask including the payload and impact limiters falls 30 feet onto a flat, unyielding, horizontal surface. The package strikes the surface in a horizontal position resulting in a side impact. The types of loading involved in a side drop accident are closure lid bolt preload, internal pressure, and inertial body load. Closure bolts are evaluated separately in Section 2.12.4.

The most critically stressed component in the system is the cask inner shell at the interface with the bottom forging, the cask flange region, and the cask lid. To evaluate the stresses in these regions linearized stress are calculated across the thickness of the plate. For the cask inner shell, Figure 2.7.1-5 shows the location of the maximum total stress intensity and Figure 2.7.1-6 indicates the path (Section 8) location where the stresses are calculated. Table 2.7.1-6 is a listing of the Section 8 stresses. Table 2.7.1-7 documents the primary membrane ( $P_m$ ) and primary membrane plus primary bending ( $P_m+P_b$ ) in accordance with the criteria presented in Regulatory Guide 7.6. Stresses are compared to the allowable at a bounding temperature of 350°F. The minimum margin of safety is found to be +4.5 for primary membrane and +1.5 for primary membrane plus.

Figure 2.7.1-7 shows the location of the maximum total stress intensity in the lid and Figure 2.7.1-8 indicates the path (Section 9). Table 2.7.1-8 presents a listing of the Section 9 stresses and Table 2.7.1-9 provides the stress combinations in accordance with the Regulatory Guide 7.6 criteria. The minimum margin of safety is found to be +1.6 for primary membrane and +1.2 for primary membrane plus bending. Because all of the margins of safety are positive, the Model 2000 cask meets the end drop requirement of 10 CFR 71.71.

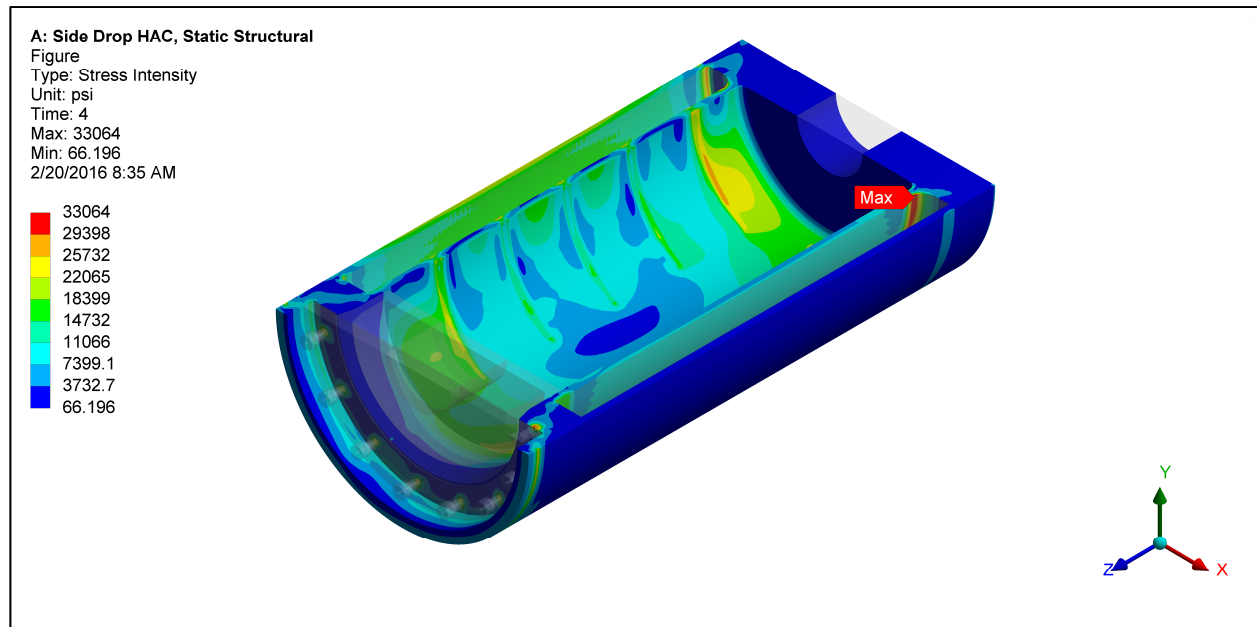


**Figure 2.7.1-5. HAC Side Drop Cask Body Stress Intensity (total stress psi)**

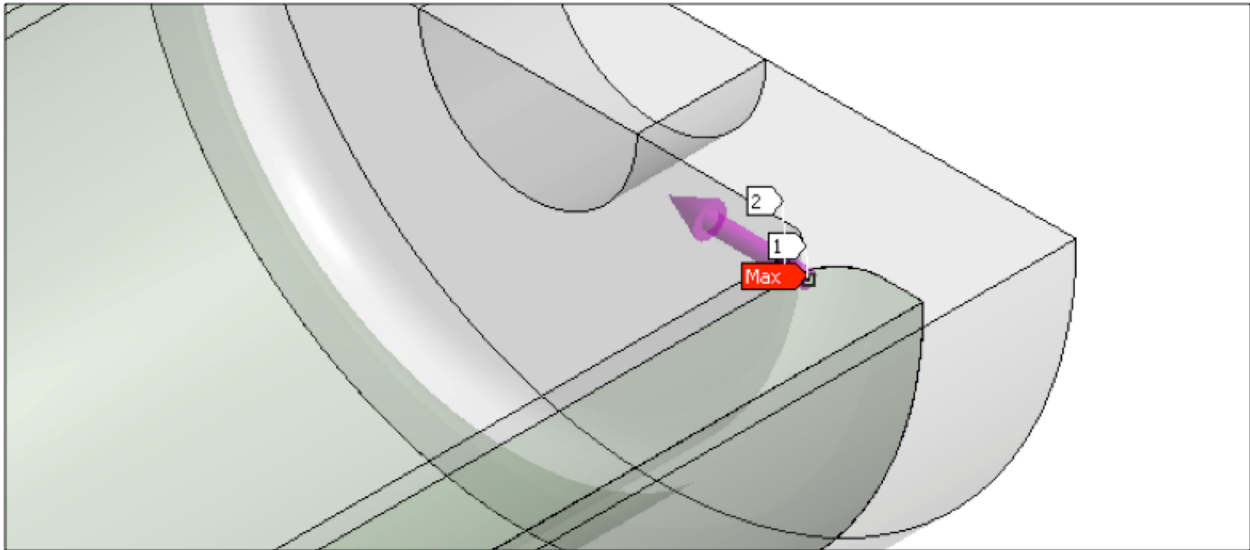


**Figure 2.7.1-6. HAC Side Drop Linearized Stress Location (Section 8)**

**Table 2.7.1-6. HAC Side Drop Section 8 Stress Results (psi)**

Stress State	Location	S1	S2	S3	SINT
MEMBRANE ( $P_m$ )	—	7919	3810	-536	8455
BENDING ( $P_b$ )	Inside	22400	7025	1106	21300
	Center	0	0	0	0
	Outside	-1106	-7025	-22400	21300
MEMBRANE + BENDING	Inside	29540	10850	1339	28200
	Center	7919	3810	-536	8455
	Outside	-98	-3191	-16050	15950
PEAK	Inside	4194	930	-743	4937
	Center	335	-133	-962	1297
	Outside	1120	-76	-1042	2162
TOTAL	Inside	33700	11780	633	33060
	Center	6962	3673	-204	7167
	Outside	175	-3267	-16250	16420

**Table 2.7.1-7. HAC Side Drop Section 8 Stress Results (psi)**

Stress Component	Stress Combination	Stress Intensity	Allowable	Margin of Safety
$P_m$	8455	19300	46320	4.5
$P_m + P_b$	28200	19300	69480	1.5

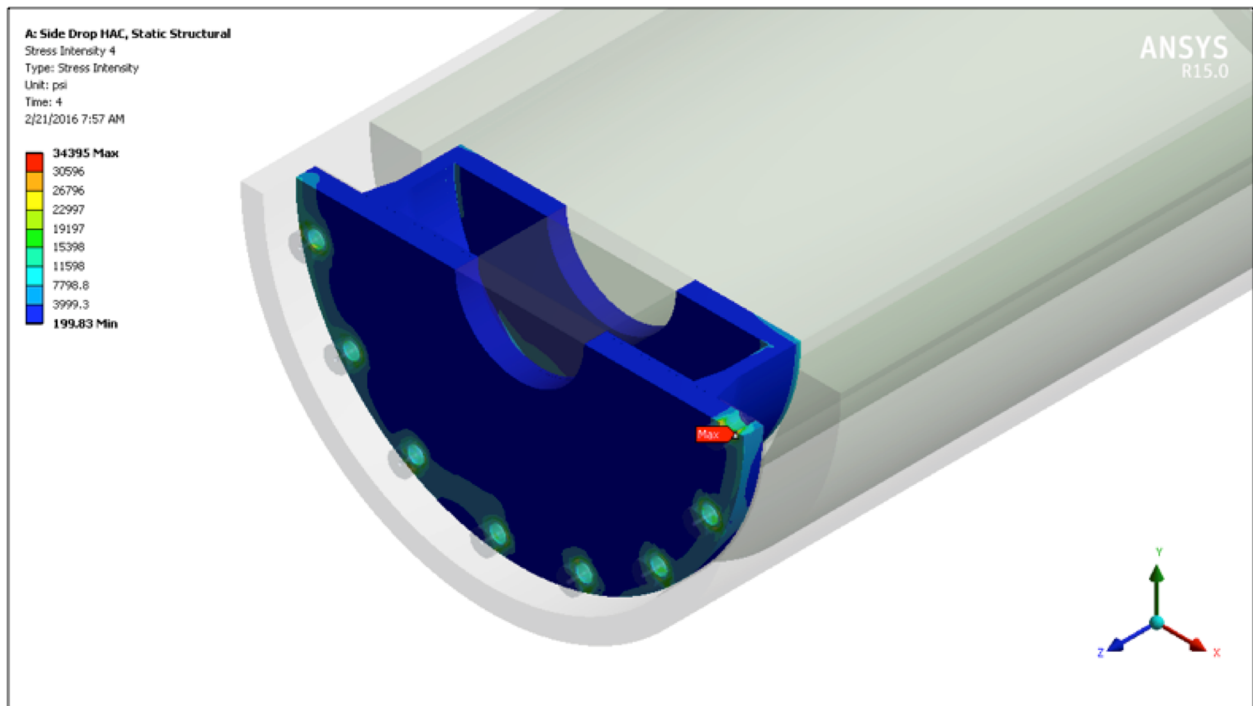


**Figure 2.7.1-7. HAC Side Drop Lid Stress Intensity (total stress psi)**

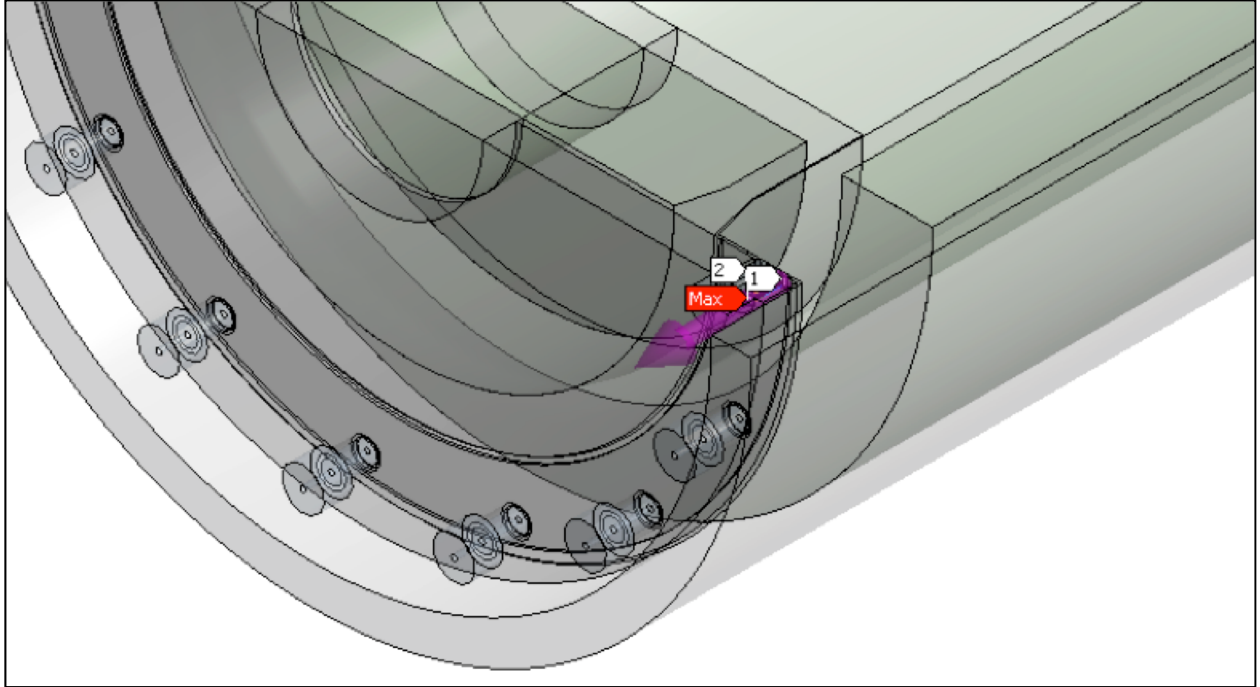


**Figure 2.7.1-8. HAC Side Drop Linearized Stress Location (Section 9)**

**Table 2.7.1-8. HAC Side Drop Section 9 Stress Results (psi)**

Stress State	Location	S1	S2	S3	SINT
MEMBRANE ( $P_m$ )	—	191	-4176	-17400	17590
BENDING ( $P_b$ )	Inside	13120	4683	-811	13930
	Center	0	0	0	0
	Outside	811	-4683	-13120	13930
MEMBRANE + BENDING	Inside	1165	-624	-4936	6102
	Center	191	-4176	-17400	17590
	Outside	993	-9012	-30360	31350
PEAK	Inside	945	-4458	-6602	7547
	Center	4003	2423	215	3787
	Outside	1120	-3506	-6124	7244
TOTAL	Inside	379	-4426	-10460	10840
	Center	1337	-1978	-14100	15440
	Outside	1005	-14500	-33390	34400

**Table 2.7.1-9. HAC Side Drop Section 9 Stress Results (psi)**

Stress Component	Stress Combination	Stress Intensity	Allowable	Margin of Safety
$P_m$	17590	19300	46320	1.6
$P_m + P_b$	31350	19300	69480	1.2

#### 2.7.1.1.3. Corner Drop

In accordance with the requirements of 10 CFR 71.73(c)(1), the Model 2000 cask is structurally evaluated for the hypothetical accident 30-foot corner drop condition. The impact analysis presented in Section 2.12.1 and the summary of accelerations provided in Table 2.7.1-1 shows that the end and side drop accelerations bound the C.G. over corner drop acceleration. Therefore, the corner drop requirement is satisfied.

#### **2.7.1.1.4. Oblique Drops**

In accordance with the requirements of 10 CFR 71.73(c)(1), the Model 2000 cask is structurally evaluated for the hypothetical accident 30-foot oblique drop condition. The impact analysis presented in Section 2.12.1 and the summary of accelerations provided in Table 2.7.1-1 shows that the end and side drop accelerations bound the slap-down/oblique angle drops. Therefore, the oblique drop requirement is satisfied.

#### **2.7.1.2. HPI Stress Analysis**

The purpose of this section is to document the Model 2000 HPI and material basket analyses that shows the design meets the requirements of 10 CFR 71. Specifically, the evaluation addresses the mechanical loads associated with the HAC.

The results of the analyses for various load cases are presented pictorially as stress intensity contour plots as well as in table form, with the corresponding margin of safety in each component of the cask body.

##### **2.7.1.2.1. End Drop**

The HPI is evaluated using the ANSYS finite element model presented in Section 2.6.7. Stress results for the HAC end drop discussed previously are documented in Table 2.7.1-10. The table presents the primary membrane ( $P_m$ ) and primary membrane plus primary bending ( $P_m+P_b$ ) in accordance with the criteria presented in ASME Section III, Appendix F (Reference 2-18).

As shown in Table 2.7.1-10, the margins of safety when compared to the stress intensity for each category are positive. The most critically stressed component in the system is the interface between the [[ ]] that surrounds and supports the depleted uranium shield. The minimum margin of safety is +8.0 for primary membrane stress intensity. The locations of the critical sections correspond to the maximum stress location and axial displacement is shown in Figure 2.7.1-9.

[[

]]

**Figure 2.7.1-9. HPI HAC End Drop Results – Peak Stress Intensity (psi) and Displacement (in)**



**Table 2.7.1-10. HAC End Drop Stress Summary**

[[							
							]]

#### 2.7.1.2.2. Side Drop

The HPI is evaluated using the ANSYS finite element model presented in Section 2.6.7. Table 2.7.1-1 provides a summary of the HAC accelerations predicted by the LS-DYNA analysis presented in Section 2.12.1. As with the NCT evaluation, two cases are presented to evaluate the performance of the HPI during the side drop. Case 1 is concentrated pressure distribution at the four [[ ]] locations (“line load”). Case 2 is a uniform pressure distribution (“area load”).

Stress results for Case 1 are presented in Tables 2.7.1-11 and 2.7.1-12. Stress results for Case 2 are presented in Table 2.7.1-13 and 2.7.1-14. Figures 2.7.1-10 and 2.7.1-11 illustrate the stresses in the support disk for Case 1 and Case 2, respectively. The tables present the primary membrane ( $P_m$ ) and primary membrane plus primary bending ( $P_m+P_b$ ) in accordance with the criteria presented in ASME Section III, Appendix F (Reference 2-18).

As Tables 2.7.1-11 through 2.1.7-14 show, the margins of safety for the HPI body and support disk when compared to the stress intensity for each category are positive. The minimum margin of safety in the HPI body is found to be +0.8 for primary membrane plus bending stress intensity for both Cases 1 and 2.

**Table 2.7.1-11. HAC Case 1 HPI Body Top 30 Results**

[illegible]

[[

]]

Figure 2.7.1-10. Case 1, HAC, Stress Intensity Result (psi)

Table 2.7.1-12. HAC Support Disk Case 1 Results

[[										
										]]

**Table 2.7.1-13. HAC Case 2 HPI Body Top 30 Results**

[illegible]

[[

]]

Figure 2.7.1-11. Case 2, HAC, Stress Intensity Result (psi)

Table 2.7.1-14. HAC Support Disk Case 2 Results

[[										
										]]

#### **2.7.1.2.3. Corner Drop**

Results of the LS-DYNA analysis presented in Section 2.12.1 shows that the side drop accelerations bound the corner drop.

#### **2.7.1.2.4. Oblique Drops**

Results of the LS-DYNA analysis presented in Section 2.12.1 shows that the side drop accelerations bound the oblique drop angles.

#### **2.7.1.2.5. Cask Overpack Bolt Evaluation**

##### Bolt Torque

Per Model 2000 cask overpack drawings 101E8719 and 105E9521 (Table 1.3-1), the overpack bolt torque is 100±5 lb-ft dry. The following overpack evaluation assumes a maximum torque of 105 lb-ft.

##### Bolt Evaluation Procedure

This analysis is based on the procedure outlined in NEDE-31581, Subsection 2.10.7, which was developed to account for the overpack fastener failure during the quarter-scale model side drop test. Once the procedure was satisfactorily developed to explain the fastener failure, it was used to redesign the fastening system. This section presents the steps and results of this analysis as applied to the Model 2000 with the HPI.

##### Bolt Stresses – HAC Side Drop

The Model 2000 transport package overpack is fastened together with 15 equally spaced ASTM A-540 Grade B22, Class 3 or equivalent 7/8-9 UNC socket head shoulder bolts. The adequacy of these fasteners is determined by comparing the service loads (from the HAC) to the allowable loads, using the criteria given in the ASME Code, Section III, Division 1, Appendix F.

Bolts: 7/8-9 UNC-2A, ASTM A540 Grade B22, Class 3, 15 equally spaced

Tensile area of threaded portion = 0.462 in<sup>2</sup>

Proof Strength = Minimum Yield Strength x 85% = 115700 (0.85) = 98345 psi

Loading: The highest stresses for the overpack fasteners occur during the HAC side drop accident condition. The maximum load is calculated for an impact acceleration of 161.9 g's.

For the side drop case, the load is applied to the overpack junction as shown in Figure 2.7.1-12. The overpack is modeled as a simple beam with the force of the cask and contents as a distributed load and the neutral axis at the side of the overpack opposite the side of impact.

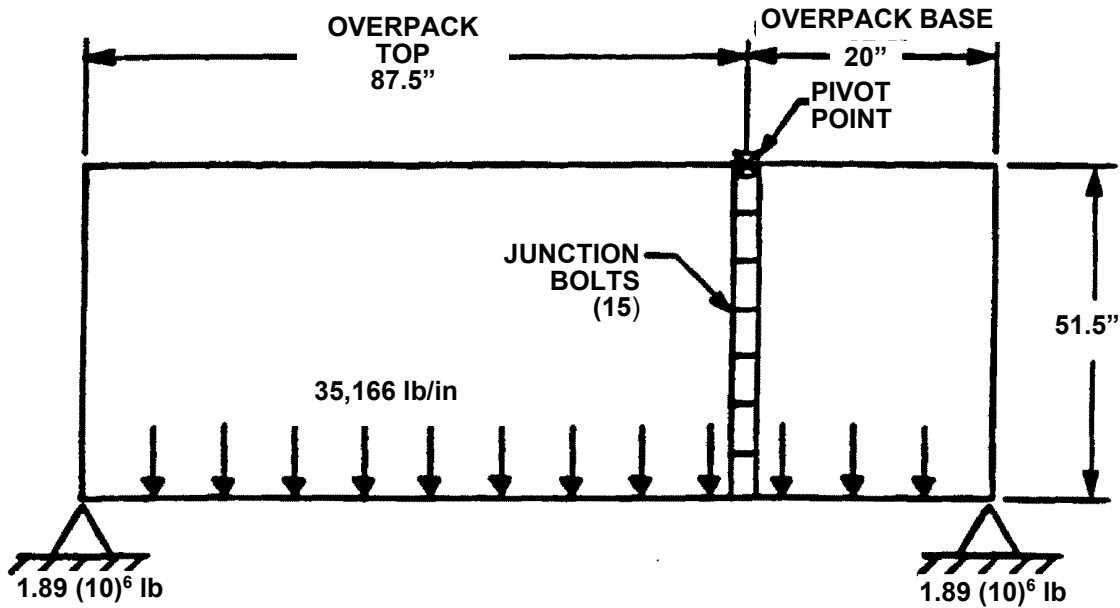


**Figure 2.7.1-12. Overpack Loading, HAC Side Drop**

The distributed load equals the weight of the cask (cask body and closure lid) and contents (HPI assembly + material basket + content) times the acceleration, divided by the length between toroidal reaction points:

$$\text{Distributed Load} = WG/L = 35,166 \text{ lb/in}$$

Where:

$$W = (16,000 + 1,900) + [ ] = 23,350 \text{ lb}$$

$$G = 161.9 \text{ g} \quad \text{HAC Side Drop Cold}$$

$$\begin{aligned} L &= \text{Overpack vertical length} - \text{toroid diameter} \\ &= 131.50 - 24 = 107.5 \text{ in} \end{aligned}$$

The total load to be reacted is:

$$F_T = WG = 3.780(10)^6 \text{ lb}$$

The force at each reaction point is:

$$F_R = 0.5F_T = 1.890(10)^6 \text{ lb}$$

Figure 2.7.1-13 shows a free body diagram of the overpack top. The distributed load from the cask is applied as a point load so that the moments can be calculated and the bolt loads determined.

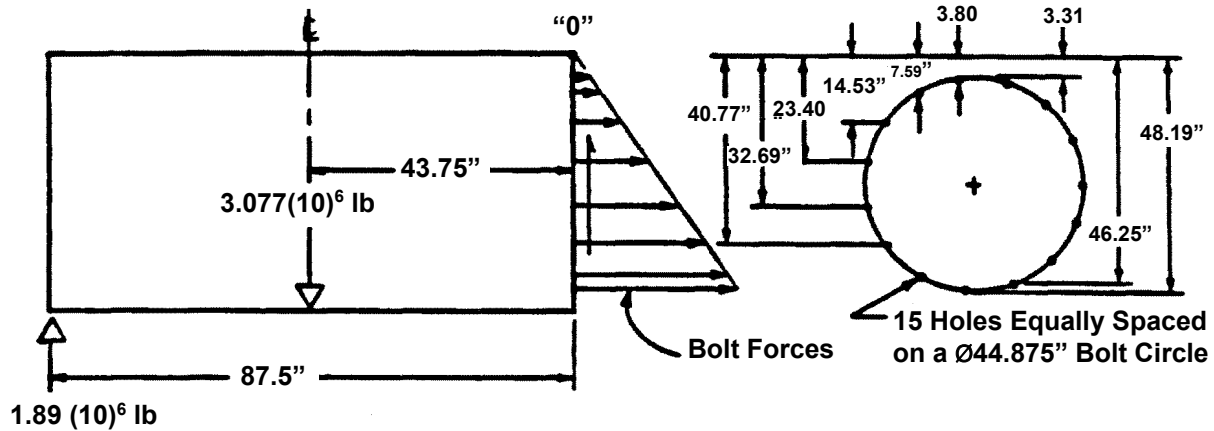


**Figure 2.7.1-13. Free Body Diagram of Overpack Top**

Summing the moments about the pivot point "0" yields the following equation:

$$\begin{aligned}\Sigma M_0 = 0 = & -1.89(10)^6 (87.5) + 3.077(10)^6 (43.75) + k (48.19)^2 + \\ & 2k (46.25)^2 + 2k (40.77)^2 + 2k (32.69)^2 + 2k (23.40)^2 + \\ & 2k (14.53)^2 + 2k (7.59)^2 + 2k (3.80)^2\end{aligned}$$

Solving for k yields:

$$\begin{aligned}k &= 3.0756(10)^7 / [48.19^2 + 2(46.25^2 + 40.77^2 + 32.69^2 + 23.40^2 + 14.53^2 + 7.59^2 + 3.80^2)] \\ k &= 2,241 \text{ lb/in}\end{aligned}$$

The maximum shear force on a bolt occurs at the point farthest from the pivot point, so the maximum bolt load is:

$$F_{S \text{ Max}} = (2,241) 48.19 = 10,7994 \text{ lb}$$

Because the bolts are loaded in double shear on the shoulder (see Figure 2.7.1-14), the maximum shear stress in the bolt material is:

$$\tau_{\text{Max}} = F_{S \text{ Max}} / (2A_s) = 36,362 \text{ psi}$$

where:

$$A_s = \text{Area of bolt shoulder} = 0.25\pi D_s^2 = 1.485 \text{ in}^2$$

$$D_s = \text{Diameter of bolt shoulder} = 1.375 \text{ in}$$

The allowable shear stress in the bolt for HAC conditions is  $0.42S_U$ .

where:

$$S_U = \text{Ultimate strength for the bolts} = 14,5000 \text{ psi}$$

$$\tau_{\text{All}} = 0.42S_U = 60900 \text{ psi} > \tau_{\text{Max}} = 36,362 \text{ psi}$$

$$MS = (.42S_U / \tau_{\text{Max}}) - 1 = 0.67$$

The results indicate that the cask overpack bolts are sufficient for HAC side drop loading.



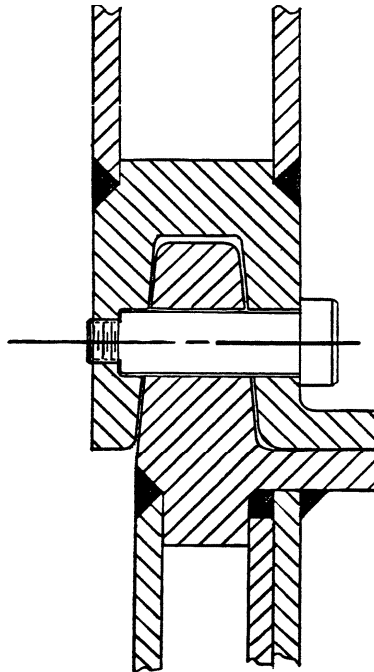


Figure 2.7.1-14. Overpack Junction

### 2.7.1.3. Material Basket Evaluation

This section evaluates the material basket for HAC. Factors of safety for the basket are calculated based on the criteria for Service Level ‘D’ limits from ASME Section III, Appendix F (F-1332).

#### HAC End Drop

The worst-case condition of upright end drop is evaluated. The inertial loading will load the [[ ]] in compression. There is no bending or shear stress present. For this evaluation, all 18 [[ ]] are loaded. The compression stress on the bottom of the [[ ]] is:

$$\sigma_{\text{membrane}} = \frac{P}{A} = 8,505.5 \text{ psi compression}$$

$$\sigma_{\text{bending}} = 0 \text{ psi}$$

$$\tau_{\text{shear}} = 0 \text{ psi}$$

where  $P = W \times G = [[ ]] \text{ lbs}$  Inertial load on 18 [[ ]] sections

$W = [[ ]] \text{ lbs}$  Basket plus contents weight

$G = 157.5 \text{ G}$  HAC end drop acceleration (Table 2.7.1-1)

$A = [[ ]]$  Cross section area of [[ ]] x 1.5)

Per Table 2.1-2, except for pinned and bolted joints, the bearing stress margin of safety need not be evaluated for which Level D service limits are specified.

The basket elastic stability is evaluated at HAC end drop conditions. The basket [[ ]] are modeled as a column with pinned ends. The bottom third of the 18 [[ ]] bundle is located between the HPI bottom and the material package center of gravity and is therefore evaluated using the Euler equation for buckling of a column with pinned ends:

$$P_{cr} = \frac{\pi^2 EI_{cc}}{L^2} = 5.553 \times 10^7 \text{ lbs}$$

where  $E = 24.1 \times 10^6$  psi

Modulus of 316 stainless steel, 800°F  
(Table 2.2-2)

$L = [[ ]]$

Length of lower 3<sup>rd</sup> of basket between [[ ]]  
(Drawing 001N1824)

$I_{cc} = 51.76 \text{ in}^4$

Moment of inertia (18 [[ ]])

For the HAC end drop elastic stability evaluation, the moment of inertia for the 18 [[ ]] is determined from Table 2.6.7-18, as follows:

[[ ]]		
		]]

Comparing the critical load to the load applied to the 18-[[ ]] basket during the HAC end drop, the factor of safety is:

$$FS = \frac{P_{cr}}{P} = \frac{5.553 \times 10^7}{49927.5} = +1112.2$$

### HAC Side Drop

Assuming one-third of the inertial load is carried by one of the segments, the bending stress in the basket is:

$$\sigma_b = \frac{Mc}{I_{cc}} = 2022.7 \text{ psi}$$

where	$P = W \times G = [ ] \text{ lb}$	Load on [ ] section
	$W = [ ] \text{ lb}$	Bounding basket weight
	$G = 161.9 \text{ g}$	HAC side drop acceleration
	$M = \frac{W_a \times l^2}{12} = 21227.5 \text{ lb-in}$	Bending moment
	$l = [ ] \text{ in}$	Length of beam section
	$W_a = 1148.92 \text{ lb/in}$	Uniformly distributed load
	$c = 3.73 \text{ in}$	Neutral axis to outer fiber
	$I_{cc} = 39.09 \text{ in}^4$	Moment of inertia [ ]

The moment of inertia calculation is shown in Table 2.7.1-15.

**Table 2.7.1-15. Moment of Inertia Calculation**

[

]

The pure shear stress, ASME Appendix F (F-1332.4), which develops across the section during the side drop is

$$\tau = \frac{P}{2A} \approx 2188.5 \text{ psi} < 0.42S_u = 0.42 \times 70800 = 29736 \text{ psi}$$

where

P	=	17107.4 lb	
A	=	3.91 in <sup>2</sup>	Cross-sectional area (12 [[ ]])
d <sub>o</sub>	=	[[ ]]	Outside diameter of [[ ]]
d <sub>i</sub>	=	[[ ]]	Inside diameter of [[ ]]

The stress intensity in the basket that results from the combination of the bending and shear stresses is

$$\sigma = \sqrt{\sigma_b^2 + 4\tau^2} = 4821.8 \text{ psi}$$

The margin of safety is per ASME Appendix F (F-1332) is

$$MS = \frac{1.5 \times (1.5S_m)}{\sigma} - 1 = \frac{35775}{4821.8} - 1 = +6.4$$

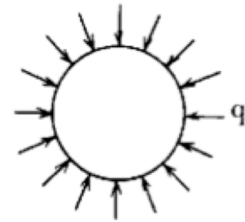
[[ ]] hold the basket together using [[ ]] (ASME III-NF, Class 1). The [[ ]] are equivalent in thickness and strength to the adjoining [[ ]]. Therefore, the previous analysis bounds the stresses generated in the [[ ]].

Because the [[ ]] form a composite section with the addition of [[ ]] is distributed along the face of the disk. Therefore, [[ ]] wall permanent deformation is unlikely to occur. However, assuming the basket [[ ]] are unsupported and uniformly loaded, a lateral external pressure load may be applied along the length of the [[ ]]. Treating the [[ ]] as a thin shell, the elastic stability can be evaluated during HAC side drop event. From Roark's, Table 15.2, Case 19 (Reference 2-19), the elastic stability of a single basket [[ ]] is evaluated by applying the total payload weight times the side drop acceleration that is then applied as an exterior pressure load, q. The critical external pressure, q', is:

$$q' = \frac{1}{4} \frac{E}{1-\nu^2} \frac{t^3}{r^3} = 3180 \text{ psi}$$

E	=	24.1 × 10 <sup>6</sup> psi
ν	=	0.3
t	=	[[ ]]
r	=	[[ ]]

Modulus at 800°F
Poisson's ratio
Wall thickness
[[ ]] outside radius



Applying the total contents weight during the HAC side drop to a single [[ ]], the external pressure is:

$$q = \frac{P}{A} = 208.5 \text{ psi}$$

G	= 161.9 g	Side drop acceleration
W	= [[ ]] lb	Bounding loaded basket weight
P	= W × G = 51322.3 lb	Total load
l	= [[ ]] in	Basket length
A	= 2πrl = 246.1 in <sup>2</sup>	Surface area of single [[ ]]

Comparing the critical external pressure to the external pressure applied to a single [[ ]] during the HAC side drop event, the factor of safety is:

$$FS = \frac{q'}{q} = 15.2$$

Therefore, unsupported basket [[ ]] sections will not collapse during HAC side drop conditions and the Subsection NF, Level A stress acceptance criteria still applies.

#### 2.7.1.4. Summary of Results

Structural analyses are performed for the Model 2000 cask, HPI and material basket for hypothetical accident conditions free drop conditions. To evaluate the Model 2000 Transport Package, ANSYS finite element models and classic calculations are used to analyze the governing drop cases. All structural members have a positive margin of safety under worst case loading conditions. It is concluded that the Model 2000 Transport Package is structurally adequate for the HAC free drop conditions. Therefore, the requirements of 10 CFR 71.73(c)(1) have been satisfied.

#### 2.7.2. Crush

In accordance with the requirements of 10 CFR 71.73(c)(2), the Model 2000 Transport Package is to be subjected to a dynamic crush test by evaluating the package on essentially unyielding horizontal surface so as to suffer maximum damage by the drop of an 1,100 pound mass from 30 feet onto the package. The mass must consist of a solid mild steel plate 40 inches × 40 inches and must fall in a horizontal attitude. The crush test is required only when the specimen has a mass not greater than 1,100 pounds, and overall density not greater than 1000 kg/m<sup>3</sup> (62.4 lb/ft<sup>3</sup>) based on external dimension. The crush condition is not applicable because the Model 2000 Transport Package weighs more than 500 kg (1,100 lb.) and overall density is greater than 62.4 lb/ft<sup>3</sup>.

#### 2.7.3. Puncture

This section addresses the second event in the accident design sequence outlined in 10 CFR 71.73(c)(3), the 40-inch drop of the Model 2000 Transport Package onto a mild steel cylindrical punch. The evaluation of this condition is conducted for the package structure and the containment vessel. The demonstration of the puncture capability of the package is presented in Section 2.12.1 to predict the accumulated damage in support of the thermal analysis. The

maximum strain in the outer shell of the cask is 31% and limited to the puncture area. Therefore, no gross deformations of the cask are predicted.

#### 2.7.4. Thermal

The fire condition is analyzed in Section 3.4. In this section, maximum values of temperatures and pressures are provided.

##### 2.7.4.1. Summary of Pressures and Temperatures

Table 2.7.1-16 provides summary temperatures for the Model 2000 Transport Package for HAC. During HAC, the average temperature of the cask fill gas (including the gas within the HPI) peaks at 585°F 11 hours after the end of the 30-minute fire. Using the ideal gas law, the cask internal pressure from gas expansion is 29.0 psia, which is less than the design pressure of 30 psia.

**Table 2.7.1-16. Summary Temperatures for HAC**

Item	Peak Temperature (°F)
Material basket	1,045
HPI shielding (side)	670
HPI shielding (top)	599
HPI shielding (bottom)	618
Cask lid seal	508
Cask shielding (side)	570
Cask shielding (top)	529
Cask shell, puncture location	782
Cask shell, opposite side to puncture location	512
Overpack outer shell, puncture location	1,103
Overpack outer shell, opposite side to puncture location	1,337
Cask drain port (bottom)	612
Cask test port (top)	608
Cask vent port (lid)	520
HPI fill gas (average)	740
Cask fill gas (average)	571
HPI and cask fill gas, combined (average)	585

(Note: Data taken from Table 3.4.3-1)

#### 2.7.4.2. Differential Thermal Expansion

Differential thermal expansion resulting from the fire transient has minimal consequence to the Model 2000 Transport Package. All stresses are classified ASME Section III Subsection NB as secondary displacement-limited stresses. Heat conditions that bound both NCT and HAC are presented in Section 2.6.7, which evaluates the thermal expansion of the Model 2000 cask by applying a temperature differential 300°F from the outside surface to the inside surface of the cask. Thermal expansion of the closure bolts is evaluated using the temperatures associated with the HAC fire in Section 2.12.4.

#### 2.7.4.3. Stress Calculations

In accordance with the requirements of 10 CFR 71.73(c)(4), the Model 2000 Transport Package is structurally evaluated when subjected to the design pressure of 30 psia. The design pressure is applied in combination with the mechanical loads defined in Section 2.7.1. To obtain stress results, a uniform internal pressure of 30 psia is applied to the ANSYS finite element in combination with the mechanical loading conditions of Section 2.7.1.

#### 2.7.4.4. Comparison with Allowable Stresses

The combined HAC pressure and mechanical stresses are presented in Table 2.7.4-1, which documents the primary membrane ( $P_m$ ), primary membrane and plus primary bending ( $P_m + P_b$ ) stresses in accordance with the criteria presented in Regulatory Guide 7.6. As Table 2.7.4-1 shows, the margins of safety are positive when the allowable is compared to the stress intensity for each category. Therefore, the requirement of 10 CFR 71.73(c)(4) is satisfied.

**Table 2.7.4-1. Summary of HAC Stress Results**

Case	Component	Stress Component	Stress Combination	Stress Intensity	Allowable	Margin of Safety
End Drop	Cask body	$P_m$	10140	20000	48000	+3.7
		$P_m + P_b$	25830	20000	72000	+1.8
	Cask Lid	$P_m$	19830	20000	48000	+1.4
		$P_m + P_b$	40720	20000	72000	+0.8
Side Drop	Cask body	$P_m$	8455	19300	46320	+4.5
		$P_m + P_b$	28200	19300	69480	+1.5
	Cask Lid	$P_m$	17590	19300	46320	+1.6
		$P_m + P_b$	31350	19300	69480	+1.2

#### **2.7.5. Immersion - Fissile Material**

Subpart F of 10 CFR 71 requires performing an immersion test for fissile material packages in accordance with the requirements of 10 CFR 71.73(c)(5). The criticality evaluation presented in Chapter 6.0 assumes optimum hydrogenous moderation of the contents, thereby conservatively addressing the effects and consequences of water in-leakage.

#### **2.7.6. Immersion - All Packages**

According to the requirements of 10 CFR 71.73(c)(6), a package must be subjected to water pressure equivalent to immersion under a head of water of at least 15 meters (50 feet) for a period of 8 hours, which is equivalent to 21.7 psig. The cask closure including the lid and bolts are designed to survive puncture loads, which exceed the load experienced during immersion (Sections 2.12.1 and 2.12.4). From ASME Section III-NB, A-2221, when subjected to 21.7 psig the 1.0-inch thick outer shell of the cask with a mean radius of 18.75 inches, produces a primary membrane stress intensity 418 psi that is much less than the material yield strength. Therefore, the Model 2000 Transport Package satisfies all of the immersion requirements for a package that is used for the international shipment of radioactive materials.

#### **2.7.7. Deep Water Immersion Test (for Type B Packages Containing More than $10^5$ A<sub>2</sub>)**

The contents specified in this application is less than  $10^5$  A<sub>2</sub>. Therefore, this is not applicable for the Model 2000 Transport Package with HPI and material basket.

#### **2.7.8. Summary of Damage**

The analytical results reported in Sections 2.7.1 through 2.7.7 indicate that the damage incurred by the Model 2000 Transport Package during the hypothetical accident is minimal, and such damage does not diminish the cask ability to maintain the containment boundary. A 30-foot side drop followed by the 40-inch pin puncture accident may damage the overpack and inflict local damage on the outer shell of the cask. However, the shielding remains intact and satisfies the accident shielding criteria. Additionally, the HPI and material baskets maintain structural integrity during all postulated HAC events, which supports the criticality and shielding analysis assumptions. Based on the analyses of Sections 2.7.1 through 2.7.7, the Model 2000 Transport Package fulfills the structural and shielding requirements of 10 CFR 71.73 for all of the hypothetical accident conditions.

### **2.8 Accident Conditions for Air Transport of Plutonium**

This section does not apply for the Model 2000 Transport Package with HPI and material basket.

### **2.9 Accident Conditions for Fissile Material Packages for Air Transport**

This section does not apply for the Model 2000 Transport Package with HPI and material basket.



## **2.10 Special Form**

Special form capsules specifically designed for carrying isotope source materials are permitted in the Model 2000 Transport Package. Each special form capsule shall show compliance with the requirements of 10 CFR 71.75 when subjected to the applicable test conditions of 10 CFR 71.77 and independently certified. Special form capsules are not a requirement of this application, because containment is provided by the cask.

## **2.11 Fuel Rods**

This section does not apply for the Model 2000 Transport Package, because containment is provided by the cask.

## **2.12 Appendix**

### **2.12.1. LS-DYNA Evaluation of the Model 2000 Transport Package**

This section summarizes the results of impact evaluation of the Model 2000 Transport Package during NCT of 10 CFR 71.71 and HAC of 10 CFR 71.73 (Reference 2-1) and supplements the test data documented in Section 2.12.5. The primary purpose of this section is to report accelerations for the HPI cask contents and provide realistic damage predictions for the thermal evaluation presented in Chapter 3.

#### **2.12.1.1. Introduction**

The NCT and HAC impact analyses presented in this section evaluate the performance of the Model 2000 Transport Package using LS-DYNA Version 971 finite element code (Reference 2-20). Benchmarks of the analysis methodology are first performed using 3-drop orientations to compare with the actual drop tests of a quarter-scale model (see Section 2.12.5). The benchmark results are presented in detail in Section 2.12.1.11.1 through Section 2.12.1.11.3 as Drop Cases 1 through 3, respectively. The benchmark performed confirmed that the LS-DYNA program and dynamic analysis methodology are conservative and bounding.

The accident conditions are conservatively simulated using material properties corresponding to temperatures ranging from -40°F to 300°F for stainless steel and 400°F for aluminum honeycomb. Also considered are variations of the payload weight that is up to 10% of the maximum weight. The overpack toroidal shell thickness is also varied between two thicknesses of 0.50 inches and 0.76 inches. The overall variations include the following configurations,

1. NCT and HAC (2 variations of initial velocities)
2. Hot and cold temperature conditions. (2 variations of material properties)
3. Payload weight of  $\pm 10\%$  of the maximum weight. (3 variations of payload weights)
4. Two different toroidal shell thicknesses of 0.50 inches and 0.76 inches. (2 variations of shell thicknesses)
5. Four-drop orientations including two end drops, side drop, and C.G. over corner drops. (4 variations of drop geometries)

There are 96 ( $=2 \times 2 \times 3 \times 2 \times 4$ ) possible drop configurations. Evaluating the bounding cases reduces the total number of drop configurations. This simplification resulted in performing nine (9) bounding drop configurations. The bounding drop configurations are designated as Drop Cases 4 through 12. The summary of results for the 9 bounding drop cases is presented in Table 2.12.1-1. The worst-case HAC accelerations occur during the cold/thick/light side drop and the hot/thin/heavy bottom end drop. For the bottom end drop, the acceleration trend showed that the accelerations dropped until the honeycomb temperature was increased to 400°F and the honeycomb fully compresses. Because the average temperature of the honeycomb is less than 350°F, the honeycomb has sufficient capacity to protect the package during hot conditions.

Two shallow angle drop simulations are also performed. The drop configurations include nominal payload at ambient temperature with thick toroidal shell thickness ( $t=0.76$  inches) to compare with the side-drop test performed for the benchmarking test. The results for the two shallow angle drop cases are presented in Table 2.12.1-1. The two shallow angles are 5° and 10° slapdown drops that are designated as Drop Case 13 and 14. The results of shallow angle drops for the 0° (Drop Case 2, side drop), 5° (Drop Case 13) and 10° (Drop Case 14) conclude that the side drop bounds the shallow angle cases with an acceleration of 157 g.

Besides the 30-foot drop configurations, two HAC drop configurations (side drop and end drop) are selected to perform the code-required pin puncture test, where the cask is dropped 30 feet and then followed by a drop height of 40 inches onto a rigid pin 6 inches in diameter. The maximum strain in the cask outer shell is 31% and limited to the puncture location. No gross deformations of the cask are predicted and the structural integrity of the containment boundary is maintained. Additionally, results for the combined 30-foot impact and pin puncture are used as input for the HAC thermal evaluation.

NEDO-33866 Revision 6  
Non-Proprietary Information

**Table 2.12.1-1. Summary of Drop Cases and Results**

Case No.	Description	Drop Angle degree	Drop Height (ft)	Shell thickness	Applicable Boundary Condition						Acceleration Results (g)
					Temperature			Payload			
					Amb	Hot	Cold	Normal	Heavy	light	
1	Benchmark HAC End Drop	90	30	Thick	X			X			130.0
2	Benchmark HAC Side Drop	0	30	Thick	X			X			157.0
3	Benchmark HAC Corner Drop	68 (=90-22)	30	Thick	X			X			73.8
4	NCT, Cold, End Drop	90	1	Thick			X			X	15.5
5	NCT, Cold, Side Drop	0	1	Thick			X			X	55.1
6	NCT, Cold, Corner Drop	68 (=90-22)	1	Thick			X			X	14.6
7	HAC, Cold, End Drop	90	30	Thick			X			X	129.8
8	HAC, Hot, End Drop	90	30	Thin		X			X		157.5
9	HAC, Cold, Side Drop	0	30	Thick			X			X	161.9
10	HAC, Hot, Side Drop	0	30	Thin		X			X		110.7
11	HAC, Cold, Corner Drop	68 (=90-22)	30	Thick			X			X	80.3
12	HAC, Hot, Corner Drop,	68 (=90-22)	30	Thin		X			X		52.8
13	HAC, Ambient, Slap down	5	30	Thick	X			X			114.4
14	HAC, Ambient, Slap down	10	30	Thick	X			X			118.0
15	HAC, Hot, End Drop + Puncture	90	30 ft + 40 in.	Thin		X			X		Same as Case No. 8
16	HAC, Hot, Side Drop + Puncture	0	30 ft + 40 in	Thin		X			X		Same as Case No. 10

Multiple LS-DYNA dynamic finite element analyses are performed to determine the structural response of the Model 2000 cask during the impacts onto unyielding surface following NCT and HAC accident events. For each drop case the acceleration of the payload and inner containment enclosure is calculated. Three full 3D half-symmetry models are used to account for the asymmetry of the cask configuration. The three finite element models consist of the same node numbers, elements, material properties and control cards. The only differences are the nodal geometry and the direction of initial velocity. A representative finite element solid model is shown in Figure 2.12.1-1.

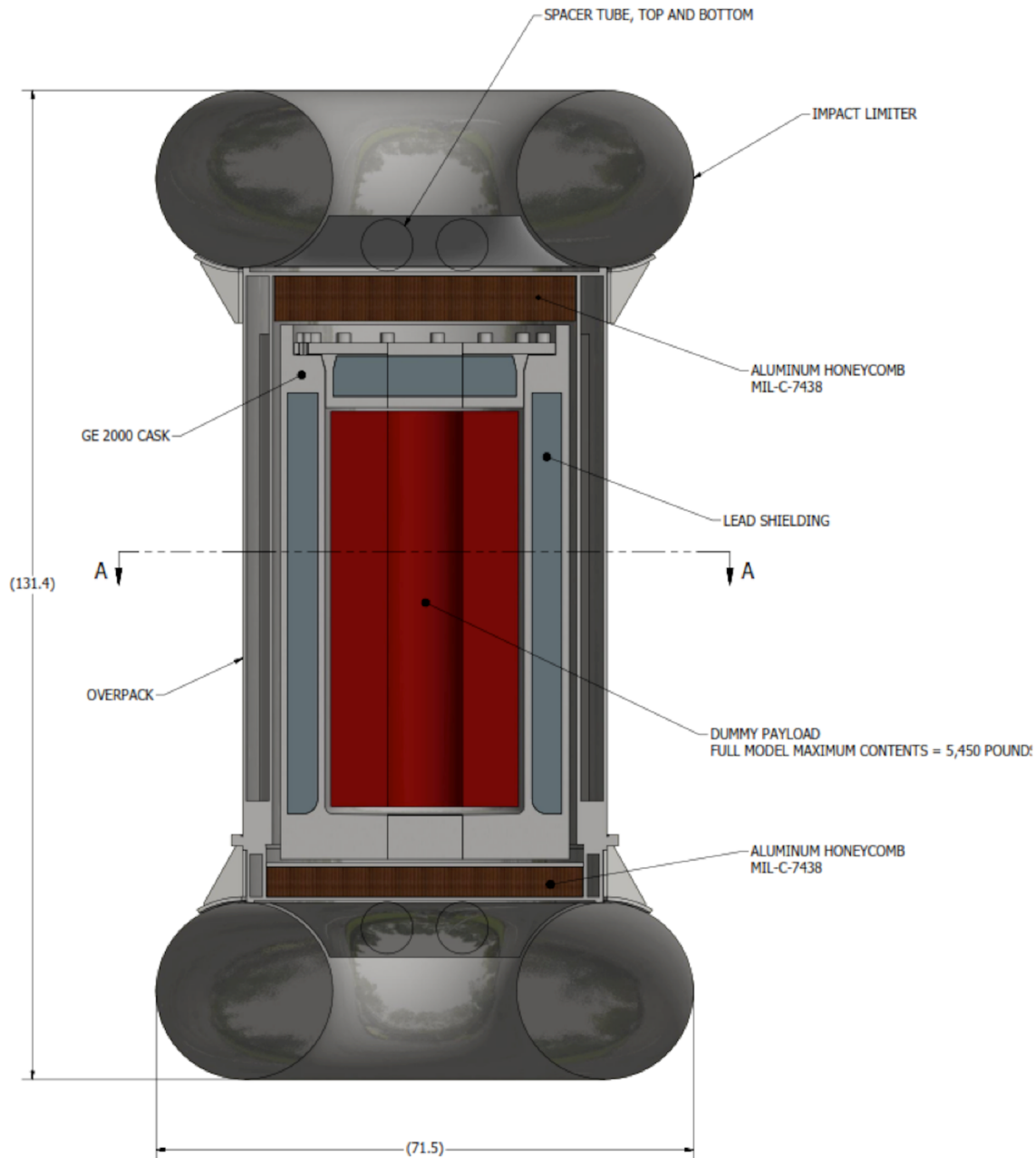


**Figure 2.12.1-1. Model 2000 Solid Model**

The three drop orientations are shown in Figure 2.12.1-2.

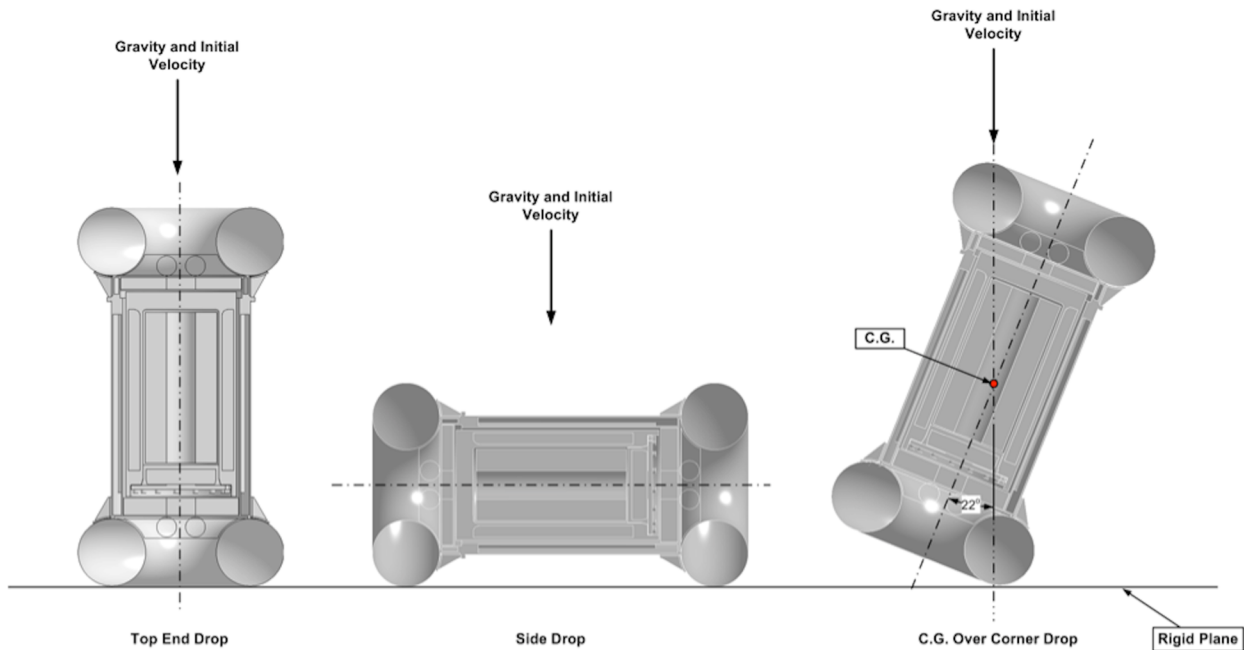


**Figure 2.12.1-2. Drop Orientations**

#### 2.12.1.2. Benchmarking Runs

The selection of the drop cases is described in this section. Section 2.12.1.2.1 contains the benchmark results. Benchmarks of the analysis methodology are performed using the 3-drop orientations shown in Figure 2.12.1-2 to compare with the actual drop tests performed on a quarter-scale model. The benchmark runs are designated as Drop Cases 1 through 3. The actual drop tests were performed under at ambient temperature. The nominal payload weight is 5,450 pounds. The thickness in the toroidal shell is 0.76 inches. The drop height is 30 feet. The parameters of the benchmarking runs are listed in Table 2.12.1-2.

**Table 2.12.1-2. Benchmark Runs and the Drop Parameters**

Case No.	Description	Drop Angle degree	Drop Height, (ft)	Toroid Thickness (in)	Applicable Boundary Condition					
					Temperature			Payload		
					Amb.	Hot	Cold	Normal	Heavy	light
1	End Drop	90	30	0.76	X	—	—	X	—	—
2	Side Drop	0	30	0.76	X	—	—	X	—	—
3	C.G. Over Corner Drop	22	30	0.76	X	—	—	X	—	—

#### 2.12.1.3. Normal Condition of Transport

The purpose of the drop simulation is to determine the peak acceleration of the payload and contents during the drop. The bounding acceleration occurs when the toroidal shell is thick so a stiffer response will result. At cold temperature, the material properties have greater elasticity and

yield strength, therefore results in a stiffer response. Finally, a lighter payload will result in lower total cask weight, which in turn causes greater acceleration during impact. The bounding three drops are simulated with thick toroidal shell, reduced-weight payload, and material properties at cold temperature. The drop cases are designated as Drop Case 4 through Drop Case 6, as listed in Table 2.12.1-3.

**Table 2.12.1-3. Normal Condition of Transport Runs and the Drop Parameters**

Case No.	Description	Drop Angle degree	Drop Height, (ft)	Shell Thickness (in)	Applicable Boundary Condition					
					Temperature			Payload		
					Amb.	Hot	Cold	Normal	Heavy	light
4	NCT Cold, End Drop	90	1.0	0.76	—	—	X	—	—	X
5	NCT Cold, Side Drop	0	1.0	0.76	—	—	X	—	—	X
6	NCT Cold, Corner Drop	68 (=90-22)	1.0	0.76	—	—	X	—	—	X

#### 2.12.1.4. Hypothetical Accident Condition

The purpose of the drop simulation is to determine the peak acceleration of the payload and/or the maximum damage during the drop.

The bounding acceleration occurs when the toroidal shell is thick so a stiffer response will result. At cold temperatures, the material properties have greater elasticity and yield strength, which results in a stiffer response. Finally, a lighter payload will result in lowered total cask weight, which in turn causes greater acceleration during impact. The three drops with bounding accelerations are simulated with thick toroidal shell, reduced payload, and material properties at cold temperature. For the end drop, the maximum force on the closure lid bolts occurs when the container lid is oriented towards to the rigid plane. The drop cases are designated as Drop Cases 7, 9, and 11 for the end drop, side drop and C.G. over corner drop, respectively.

The maximum damage of the cask occurs when the toroidal shell is thin and has less structural strength. At warmer temperature, comparing with the material strength at ambient temperature, the material has lower elasticity and yield strength therefore resulted in greater damage to the cask. The heavier payload will also result in greater deformation of the toroidal shell. The drop cases with the bounding damage are designated as Drop Cases 8, 10, and 12 for the end drop, side drop and C.G. over corner drop, respectively. The six bounding drop cases for the HAC are listed in Table 2.12.1-4.

**Table 2.12.1-4. Hypothetical Accident Condition of Transport Runs and the Drop Parameters**

Case No.	Description	Drop Angle degree	Drop Height, (ft)	Shell Thickness (in)	Applicable Boundary Condition					
					Temperature			Payload		
					Amb.	Hot	Cold	Normal	Heavy	light
7	HAC, Cold, End Drop	90	30.0	0.76	—	—	X	—	—	X
8	HAC, Hot, End Drop	90	30.0	0.50	—	X	—	—	X	—
9	HAC, Cold, Side Drop	0	30.0	0.76	—	—	X	—	—	X
10	HAC, Hot, Side Drop	0	30.0	0.5	—	X	—	—	X	—
11	HAC, Cold, Corner Drop	68 (=90-22)	30.0	0.76	—	—	X	—	—	X
12	HAC, Hot, Corner Drop	68 (=90-22)	30.0	0.50	—	X	—	—	X	—

### 2.12.1.5. Shallow Angle Drops

Two shallow angle drops (5° and 10° from horizontal) with the drop configuration shown in Figure 2.12.1.5-1 are performed to compare the acceleration with the result of the side drop benchmark run. With the same material parameters as the benchmark run, the shallow angle drop parameters consist of the nominal payload weight, material properties at ambient temperature, and thick toroidal shell thickness. The drop cases are designated as Drop Cases 13 and 14 as listed in Table 2.12.1-5.

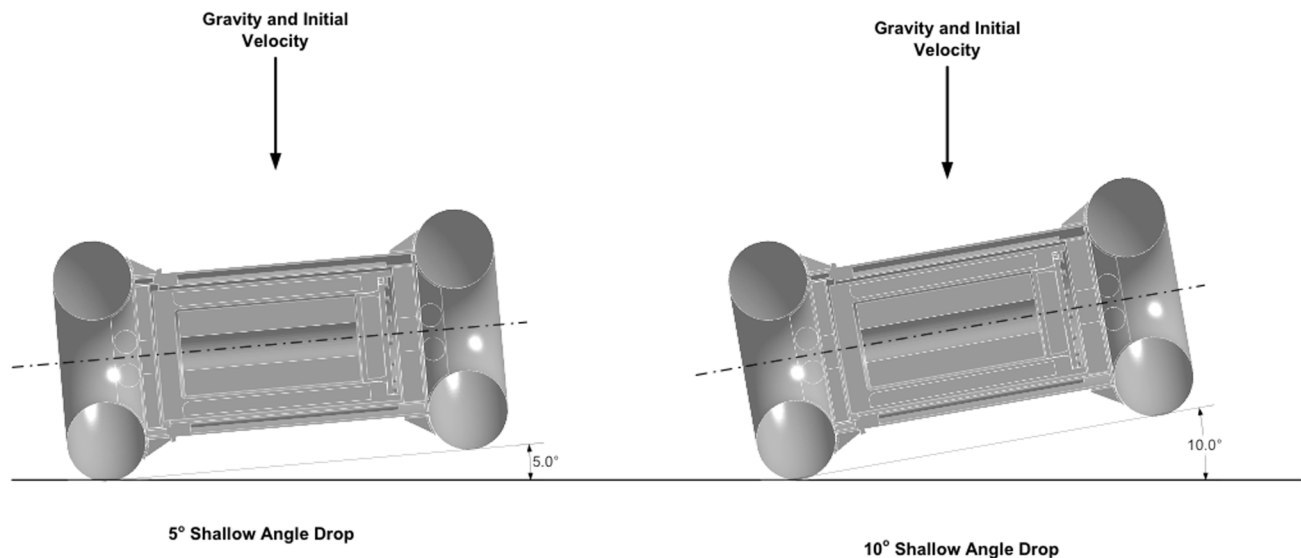


**Figure 2.12.1.5-1. Shallow Angle Drops**

**Table 2.12.1-5. Shallow Angle Drop Runs and the Drop Parameters**

Case No.	Description	Drop Angle degree	Drop Height, (ft)	Shell Thickness (in)	Applicable Boundary Condition					
					Temperature			Payload		
					Amb.	Hot	Cold	Normal	Heavy	light
13	HAC, Ambient, Slap Down	5	30.0	0.76	X	—	—	X	—	—
14	HAC, Ambient, Slap Down	10	30.0	0.76	X	—	—	X	—	—

#### 2.12.1.6. Pin Puncture

10 CFR 71.73 requires that a free drop of the specimen through a distance of 1 meter (40 inches) in a position for which maximum damage is expected, onto the upper end of a solid, vertical, cylindrical, mild steel bar mounted on an essentially unyielding, horizontal surface. The bar must be 15 cm (6 inches) in diameter, with the top horizontal and its edge rounded to a radius of not more than 6 mm (0.25 inches), and of a length as to cause maximum damage to the package, but not less than 20 cm (8 inches) long. The long axis of the bar must be vertical.

To simulate the sequential drops, a rigid plane and a rigid pin 6 inches in diameter and 8 inches long are created, for the end drop and side drop respectively. During the pin puncture, the model is allowed to pass through the rigid plane; therefore, the puncture is independent of the pin length. Two-drop configurations are selected, that will be subjected to maximum damage. The drop configurations selected for the pin puncture drop are listed in Table 2.12.1-6. The drop cases are designated as Drop Cases 15 and 16 as listed in Table 2.12.1-6.

**Table 2.12.1-6. HAC Drop Cases with Pin Puncture**

Case No.	Description	Drop Angle degree	Drop Height (ft)	Pin Puncture Height in)	Shell Thickness (in)	Applicable Boundary Condition					
						Temperature			Payload		
						Amb.	Hot	Cold	Normal	Heavy	light
15	HAC, Hot, End Drop + Pin Puncture	90	30.0	40	0.50	—	X	—	—	X	—
16	HAC, Hot, Side Drop + Pin Puncture	0	30.0	40	0.50	—	X	—	—	X	—

#### 2.12.1.7. Material Properties

##### 2.12.1.7.1. 304 Stainless Steel

This material is used in the cask inner shell, over pack outer shell, gussets, and toroidal shell (impact limiter). The mechanical properties of the 304 SS at three different temperatures of interest in this calculation are tabulated in Table 2.12.1-7.



**Table 2.12.1-7. Mechanical Properties of SS304 at Temperature of Interest**

Temperature	-40°F	70°F	300°F
Ultimate Tensile Strength, ksi	75.0	75.0	66.2
Yield Strength, ksi	30.0	30.0	22.4
Modulus of Elasticity, E (10 <sup>6</sup> psi)	28.8	28.3	27.0
Poisson's Ratio	0.31	0.31	0.31
Density, lb/in <sup>3</sup>	0.29	0.29	0.29

The stress strain curves for SS304, taken from References 2-7 and 2-21, and are presented in Tables 2.12.1-8 through 2.12.1-10. The graphical representations of the stress strain curves of the SS304 are displayed in Figures 2.12.1.7-1 through 2.12.1.7-3.

**Table 2.12.1-8. Stress Strain Curve of SS304 at -40°F**

Strain	Stress, psi
0.0020	27,000
0.0034	30,000
0.0074	34,868
0.0182	39,736
0.0395	44,604
0.0625	49,472
0.0816	54,340
0.0998	59,208
0.1189	64,076
0.1398	68,944
0.1624	73,812
0.1870	78,680
0.2134	83,548
0.2418	88,416
0.2722	93,284
0.3045	98,152
0.3389	103,020
0.3753	107,888
0.4137	112,755
0.4542	117,623
0.5542	117,623
0.6542	117,623
0.7542	117,623

NEDO-33866 Revision 6  
Non-Proprietary Information

**Table 2.12.1-9. Stress Strain Curve of SS304 at Ambient Temperature**

Strain	Stress, psi
0.0020	27,000
0.0035	30,000
0.0075	34,868
0.0183	39,736
0.0396	44,604
0.0626	49,472
0.0817	54,340
0.0999	59,208
0.1191	64,076
0.1399	68,944
0.1626	73,812
0.1871	78,680
0.2136	83,548
0.2420	88,416
0.2723	93,284
0.3047	98,152
0.3391	103,020
0.3755	107,888
0.4139	112,755
0.4544	117,623
0.5544	117,623
0.6544	117,623
0.7544	117,623

NEDO-33866 Revision 6  
Non-Proprietary Information

**Table 2.12.1-10. Stress Strain Curve of SS304 at 300°F**

Strain	Stress, psi
0.0022	22,500
0.0033	25,000
0.0076	29,477
0.0198	33,953
0.0431	38,430
0.0659	42,906
0.0849	47,383
0.1036	51,859
0.1236	56,336
0.1454	60,812
0.1691	65,289
0.1947	69,765
0.2223	74,242
0.2518	78,719
0.2832	83,195
0.3167	87,672
0.3522	92,148
0.3896	96,625
0.4291	101,101
0.4707	105,578
0.5707	105,578
0.6707	105,578

**Stress Strain curve for SS304**  
per ASME VIII, Div 2, Annex 3.D

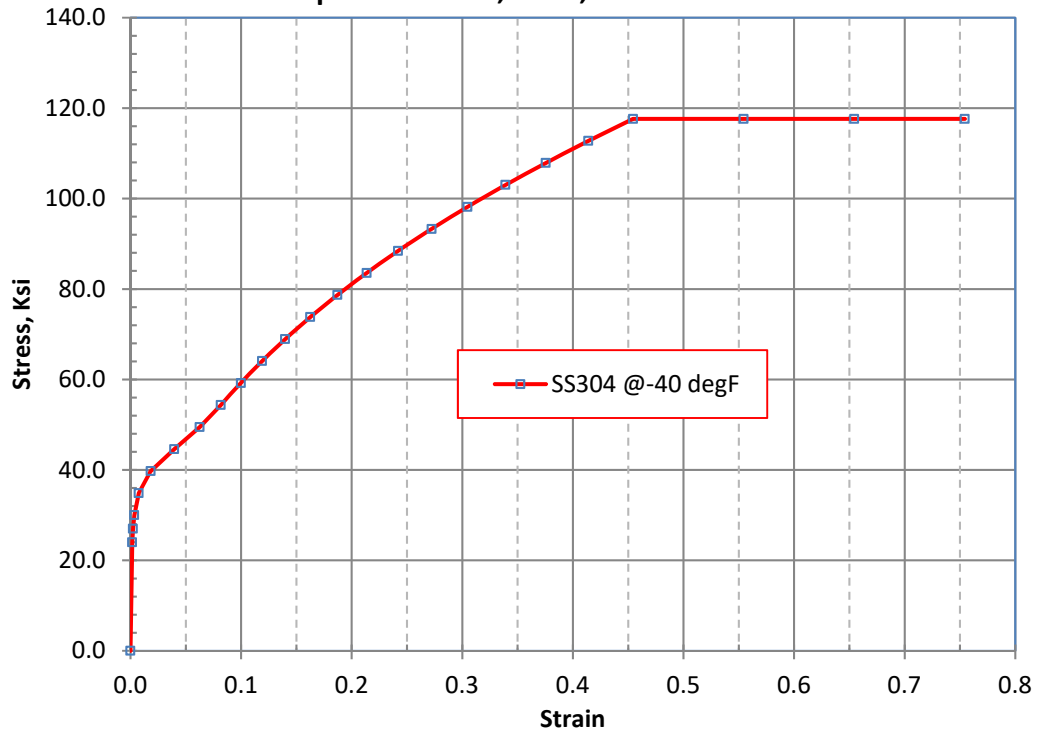


**Figure 2.12.1.7-1. Stress-Strain Curve of SS304 at -40°F**

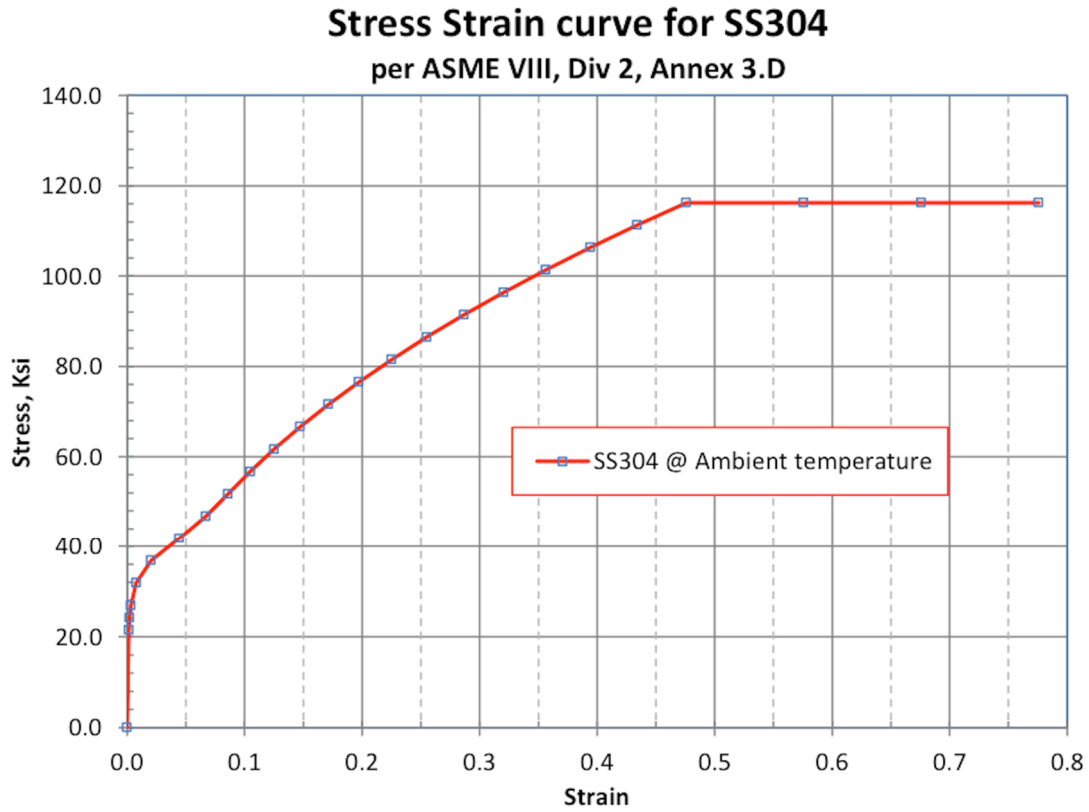


**Figure 2.12.1.7-2. Stress-Strain Curve of SS304 at Ambient Temperature**

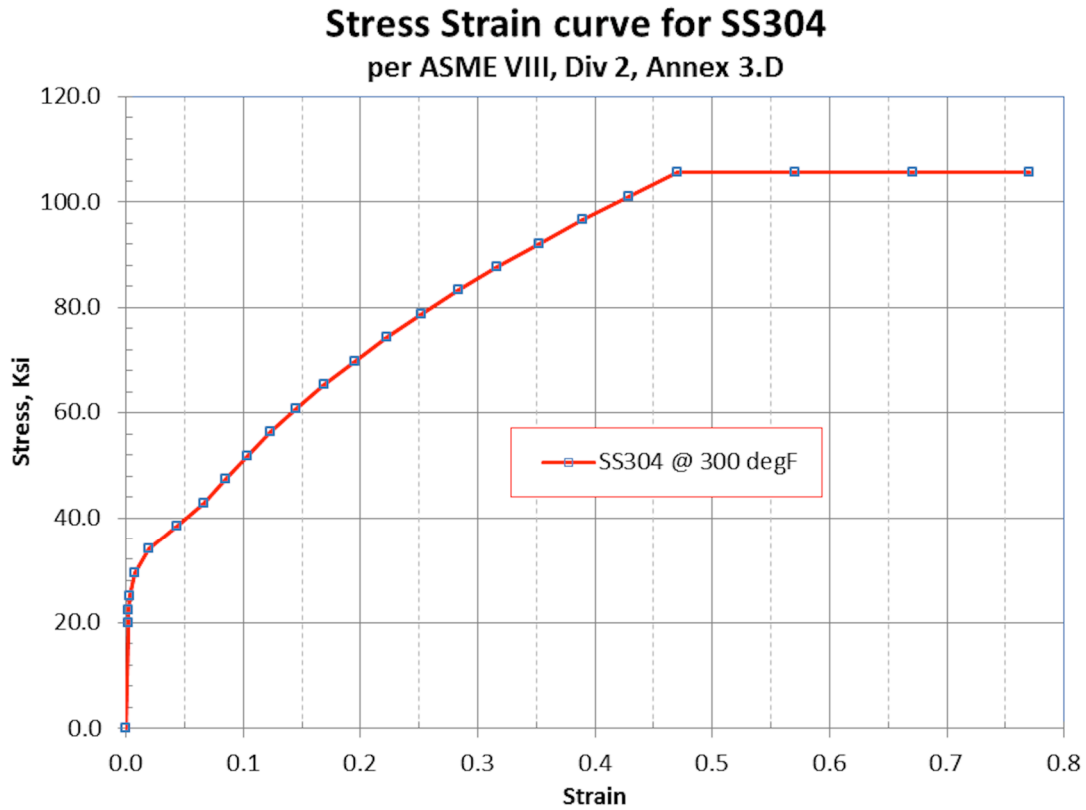


**Figure 2.12.1.7-3. Stress-Strain Curve of SS304 at 300°F**

#### 2.12.1.7.2. Lead

Chemical lead is used in the cask as shielding material. The mechanical property of the chemical lead is presented in Table 2.12.1-11.

**Table 2.12.1-11. Lead Temperature Dependent Properties**

Temperature, (°F)	Modulus of Elasticity, $\times 10^6$ (psi)	Density (lb <sub>m</sub> /in <sup>3</sup> )	Yield Strength, (psi)
-40	2.58	0.41	795
75	2.41	0.41	620
100	2.38	0.41	580
150	2.30	0.41	550
300	2.04	0.41	390

### 2.12.1.7.3. Strain-Rate Sensitive Material Properties of SS304

The factors that elevate true stress-strain curves for SS304 at various strain rates and temperatures were generated by Reference 2-22 (pp. 84-87) and reproduced in Table 2.12.1-12.

**Table 2.12.1-12. Strain-Rate Factors that elevated the Stress-Strain Curves of SS304**

Strain Rate (in/in/sec)	-20°F	70°F	300°F	600°F
5	1.333	1.235	1.166	1.043
10	1.361	1.278	1.210	1.094
22	1.428	1.381	1.316	1.217
25	1.445	1.407	1.342	1.247

The data from the above table are used to generate the strain-rate multiplication factors for the current analyses at temperatures of -40°F, ambient temperature and 300°F.

### 2.12.1.7.4. Honeycomb Material Property

The crush strength of the honeycomb material is 750 psi. The material property at temperature of -20°F is assigned a value of 10% greater to account for the increase of rigidity due to cold temperature. Based on the HPI thermal analyses presented in Section 3, the temperature of the honeycomb material is bounded by 400°F. For the crush strength of honeycomb material at 400°F, a reduction of the crush strength of 40% is conservatively assigned. This is based on the thermal tests from Reference 2-23, p. 9. The temperature test result is presented in Figure 2.12.1.7-4.

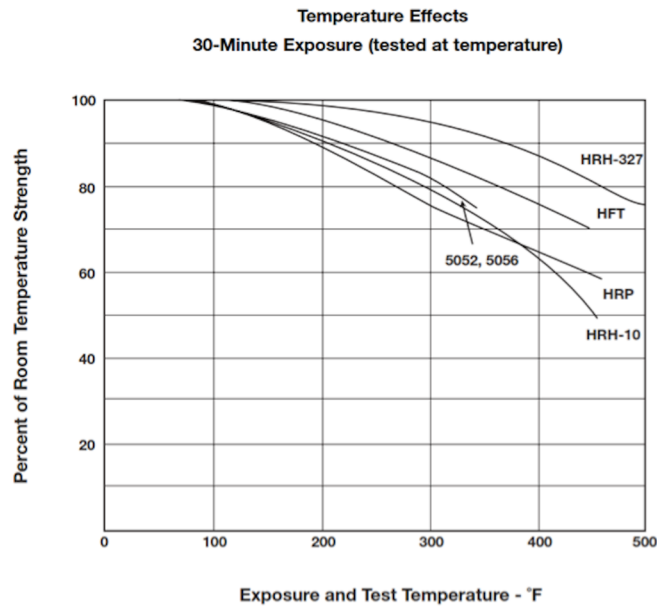


**Figure 2.12.1.7-4. Temperature Effect of Honeycomb Material**

#### 2.12.1.7.5. Temperature Range for Material Properties

The component temperature range and justification for the applied temperature is discussed in Table 2.12.1-13.

**Table 2.12.1-13. Component Temperature Range and Justification**

Component, Material	Predicted Temperature Range	Applied Temperature	Justification for Use of Non-Bounding Peak Temperature
Overpack Toroids, 304 SS	-20 to 110-250	-20 to 300	Bounding. Provides primary impact protection
Cask Shell, 304 SS	-20 to 300-460	-20 to 300	Cask does not provide primary impact protection. Temperature range selected to best represent the performance of the cask during impact.
Cask Shielding, Lead	-20 to 330-450	-20 to 300	Lead does not provide primary impact protection. Therefore, temperature range considered acceptable for analyses.
Overpack Cover and Base, 304 SS	-20 to 170-370	-20 to 300	Overpack cover not included in model. The base does not provide primary impact protection. Therefore, range considered acceptable for analyses.
Overpack Honeycomb, Aluminum	-20 to 200-360	-20 to 400	40% compressive strength reduction bounds temperature of 400F. 10% compressive strength increase bounds temperature of -20F.

#### 2.12.1.8. LS-DYNA Model Description

##### 2.12.1.8.1. Finite Element Model

In accordance with the Model 2000 licensing drawings, an LS-DYNA finite element model was generated to evaluate the structural performance of the cask when loaded with the maximum content weight. The model includes the overpack and the Model 2000 cask body with lead shield and lid. The contents of the cask are modeled as a rigid body.

The 3D (half-symmetry) solid model of the Model 2000 cask and overpack was generated using Autodesk Inventor, which was imported into ANSYS Workbench Design Modeler (Reference 2-16). The finite element mesh was generated using the ANSYS Workbench Mechanical interface. The completed FEA model was then saved as a text input file to perform the analyses. Figure 2.12.1.8-1 shows the finite element model.

The finite element model is comprised of 3D brick elements (fully integrated selective-reduced solid) that represent the main body of cask components. Contact between components is modeled as surfaces using contact pairs. Boundary conditions such as symmetry are applied to the symmetry plane of the model. The final model includes 790,526 elements and 1,355,593 nodes.



[[

]]

**Figure 2.12.1.8-1. Model 2000 Overpack and Cask Finite Element Model**

#### 2.12.1.8.2. Pin Puncture Analysis Methodology

The accident sequence presented in 10 CFR 71.73 requires that the cask, after a 30-foot drop, be dropped onto 6-inch diameter pin. To simulate the sequential drops, a rigid plane and a rigid pin with a 6-inch diameter and 8-inch length are created as shown in Figures 2.12.1.8-2 and 2.12.1.8-3 for the end drop and side drop, respectively.

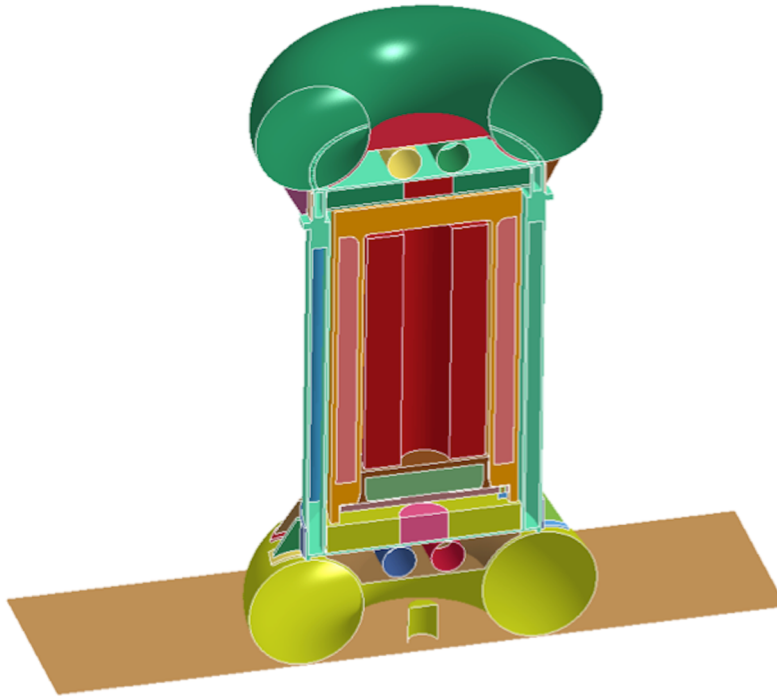


Figure 2.12.1.8-2. Rigid Plane and Pin Model for the End Drop Configuration

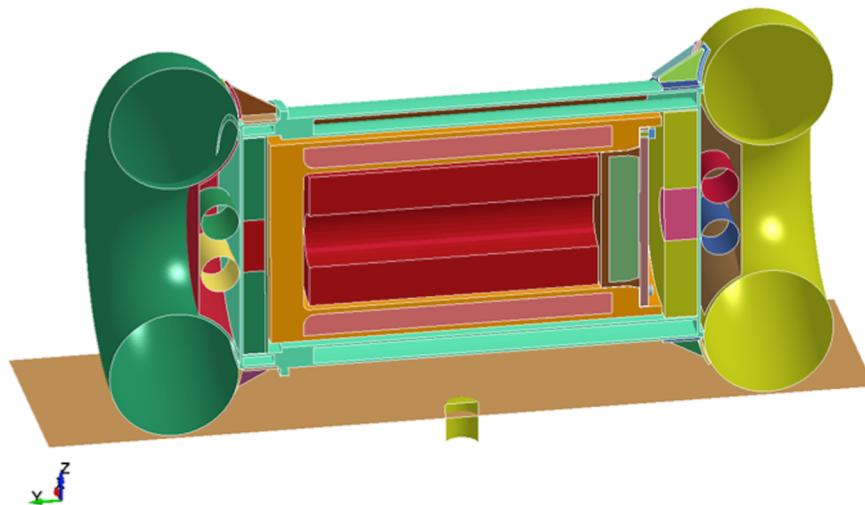
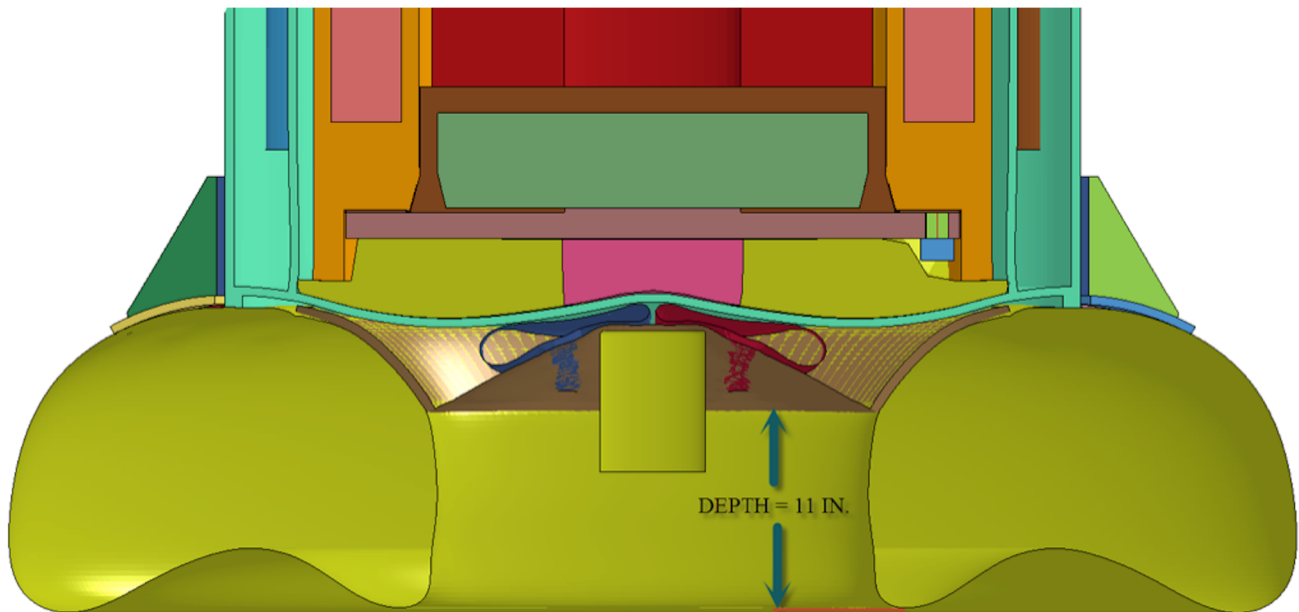


Figure 2.12.1.8-3. Rigid Plane and Pin Model for the Side Drop Configuration

The dynamic simulation for this 30-foot drop onto an unyielding surface followed by a 40-inch drop onto a pin is performed using a two steps drop sequence. For the first sequence, the impact velocity of the 30-foot drop is 527.5 in/sec. For the second sequence, the initial velocity for a 40-inch drop is 175.8 in/sec.

During the first drop sequence at the beginning of the 30-foot drop accident, the cask travels in the downward direction with an initial velocity of 703.3 in/sec ( $=527.5+175.8$ ). The rigid plane and the pin travel at an initial velocity of 175.8 in/sec and the contact interface is activated between the cask and the rigid plane while the contact interface between the cask and the pin is not activated. Therefore, the relative velocity between the cask and the rigid plane is 527.5 in/sec, which is equivalent to a drop height of 30 feet. During this sequence, the distance between the cask the pin is reduced as time progresses. The kinetic energy of the cask dissipates to zero at time = 35 milliseconds. This is the time at which the puncture impact starts.

At the beginning of the second sequence, the distance between the pin and the cask is reduced to a minimum gap but not touching. At this point, the absolute velocity of the cask and pin is 175.8 in/sec. At this time, the contact interface between the pin and the cask is activated while the contact interface between the rigid plane and the cask is deactivated, which allows the damaged impact limiters to pass through the rigid plane. Additionally, the velocity of the pin is set to zero, which results in relative velocity between the cask and the pin of 175.8 in/sec. Figure 2.12.1.8-4 shows the cumulative damage following the 30-foot top end drop and 40-inch pin puncture.



**Figure 2.12.1.8-4. Deformed Geometry of the Overpack after a 30 foot End Drop**

Figure 2.12.1.8-5 shows the cumulative damage for the side drop and pin puncture sequence. For the side drop, the depth of the unexposed cavity below the toroidal shell is less than 2.3 inches (taken from the result of Drop Case 10). Therefore, the modeled pin length of 8 inches is sufficient to sustain maximum damage.

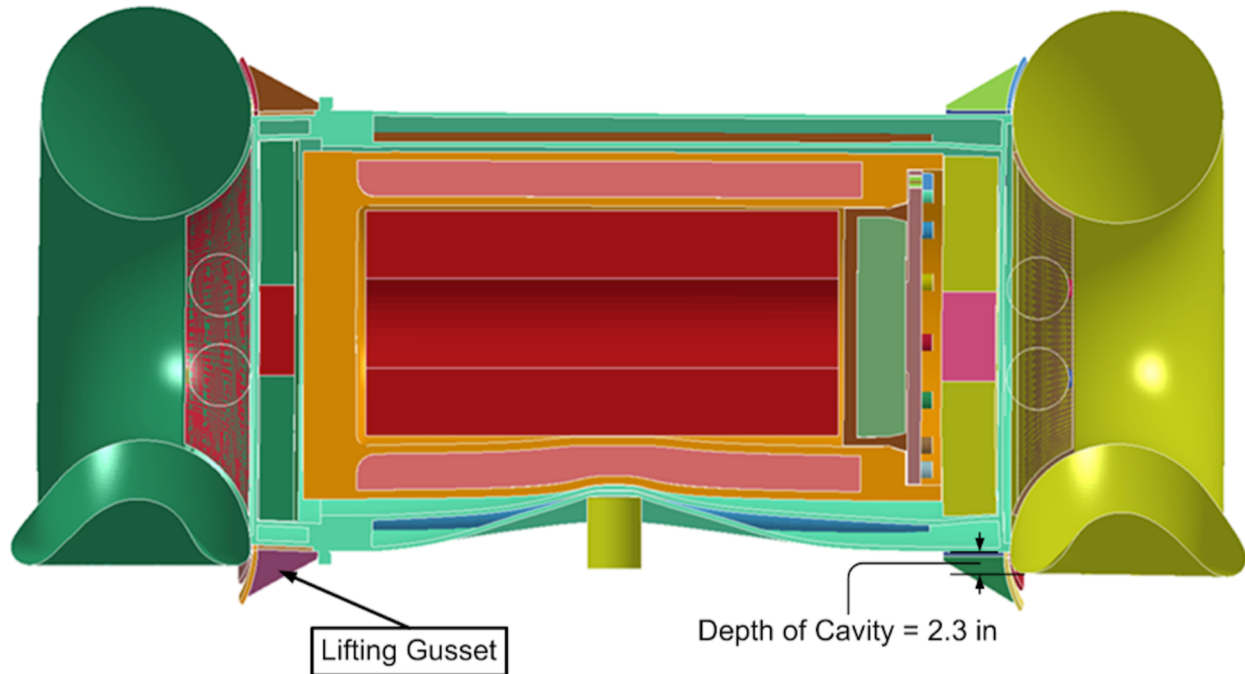


**Figure 2.12.1.8-5. Deformed Geometry of the Overpack after a 30 foot Side Drop**

#### **2.12.1.9. Weight**

The Model 2000 Transport Package components consist of the closure lid, cask body and overpack. The dimensions used in the calculations are taken from the Model 2000 Transport Package fabrication drawings. The total weight of the Model 2000 Transport Package empty is calculated to be 28,100 lb. From the finite element model, the center of gravity is located 1.5 inches below the centerline of the overpack, 64.25 inches from the bottom line. Table 2.1-3 presents the breakdown of the components weights used for the dynamic analyses.

##### **2.12.1.9.1. Material Model**

The LS-DYNA material models used in the analyses are described below:

- The stainless steel shells are modeled using \*MAT\_PIECEWISE\_LINEAR\_PLASTICITY.
- The honeycomb impact limiters are modeled using \*MAT\_CRUSHABLE\_FOAM.
- The payload is modeled as \*MAT\_RIGID.
- The closure lid bolts of the inner shell are modeled as \*MAT\_ELASTIC.

#### **2.12.1.9.2. Contact Interfaces**

The control card \*CONTACT\_TIED\_SURFACE\_TO\_SURFACE is used to fasten the welded components. For the components within the cask and the overpack, the control card \*CONTACT\_AUTOMATIC\_SINGLE\_SURFACE is used to provide global contact control. The honeycomb material has significant stiffness difference between the adjacent part, therefore the control card \*CONTACT\_AUTOMATIC\_SURFACE\_TO\_SURFACE is used to control and prevent penetration between parts.

#### **2.12.1.10. Boundary Conditions**

##### **2.12.1.10.1. Symmetry Plane**

The half-symmetry finite element model utilizes symmetry boundary conditions that are applied to the cut plane of the half-model in the Z-direction.

##### **2.12.1.10.2. Initial Velocity**

The drop height, H, is converted to kinetic energy using the formula below.

$$V = \sqrt{2 \times g \times H}$$

where

V = the initial velocity at the threshold of impact, in/s

g = gravity constant = 386.4 in/s<sup>2</sup>.

H = drop height, in

Therefore, the drop height of H=30 ft is converted to initial velocity, V360-in, as

$$V_{360\text{-in}} = \sqrt{2 \times g \times 360} = 527.45 \text{ in/s}$$

And the drop height of H=40-in is converted to initial velocity, V40-in, as

$$V_{40\text{-in}} = \sqrt{2 \times g \times 40} = 175.8 \text{ in/s}$$

##### **2.12.1.10.3. Gravity**

The gravity of 386.4 in/s is applied to all components in the global Z-direction with an initial ramp up period of 0.05 seconds.

#### **2.12.1.11. Dynamic Analysis Results HAC 30-foot Drops**

The results of the impact analyses of the Model 2000 cask model in the forms of acceleration of the payload and plastic strain of the toroid shell are presented in Sections 2.12.1.11.1 through 2.12.1.11.14. Further, each section contains four plots, which include a plot for the deformed overpack shape, the cask acceleration time history, energy time histories and interface sliding energy time history (Figures 2.12.1.11-1 through 2.12.1.11-58). Section 2.12.1.11.15 presents the results of the 30-foot drop followed by pin puncture drop. The significance of the accelerations and energy time histories (kinetic energy, internal energy, hourglass energy, and sliding energy) of the simulations are described below.

**Accelerations** – Accelerations are extracted from the LS-DYNA MATSUM file. Using the MATSUM data allows for the reporting of the maximum acceleration in any part and at any point in the model.

**Kinetic Energy** - The kinetic energy time history is used to confirm that the kinetic energy of the cask assembly is completely dissipated during the impact and the acceleration has peaked. For a normal and completed drop impact scenario, the kinetic energy must be decreasing to a minimum value as close to zero as possible and starts to increase (due to gravity loading). At the moment of minimum kinetic energy, the primary impact event is over.

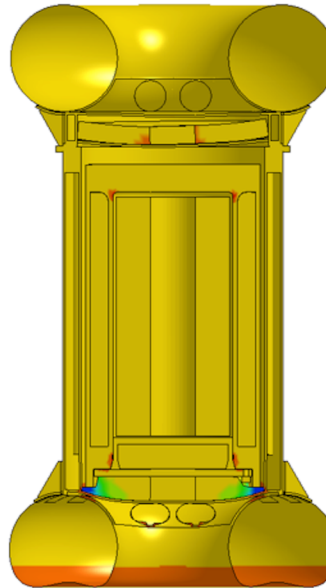
**Internal Energy** - The internal energy plot is a measure of how much of the kinetic energy is converted into strain energy, either elastic or inelastic. Most likely, the internal energy is a measure of inelastic strain energy corresponding to the permanent deformation of the energy absorber material. The accumulated internal energy is a measure of how well the impact limiter is working as designed. Internal energy that is significantly smaller than the initial kinetic energy is an indication that the impact limiter is not dissipating the impact energy.

**Hourglass Energy** - The hourglass energy and the sliding energy are numerical terms that are produced by the mathematic solver but not derived from kinetic energy. The hourglass energy is strain energy numerically produced and proportional to the energy used to control the distortion of brick finite elements (solid element). As recommended by the LS-DYNA user manual, the brick elements perform best during the solution when the hourglass energy is limited to less than 10% of the internal energy.

**Sliding Energy** - The sliding energy plots represent the efficiency of the contact interface and the level of penetration between adjacent parts. A negative sliding energy indicates that the contact interface is not working well with a high degree of part penetrations. The contact interface control parameters must be revised to allow the use of different contact algorithms to prevent parts penetrations and pass-through. A positive sliding energy indicates the contact interface is working well and no penetrations are present.

### 2.12.1.11.1. Case 1 End Drop Benchmark

GE-2000 CASK AND OVERPACK MODEL  
Time = 0.035  
Contours of Effective Plastic Strain  
min=-1.63975, at elem# 388422  
max=0.429583, at elem# 296895



Fringe Levels  
4.296e-01  
2.227e-01  
1.572e-02  
-1.912e-01  
-3.981e-01  
-6.051e-01  
-8.120e-01  
-1.019e+00  
-1.226e+00  
-1.433e+00  
-1.640e+00

Figure 2.12.1.11-1. Case 1 Deformed Overpack Shape (Effective Plastic Strain)

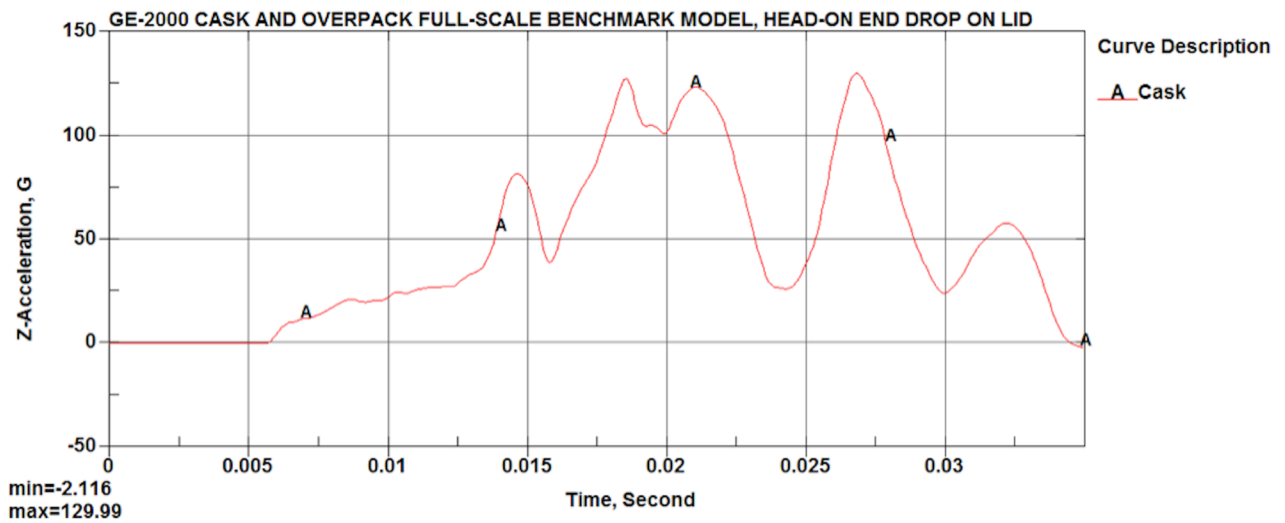
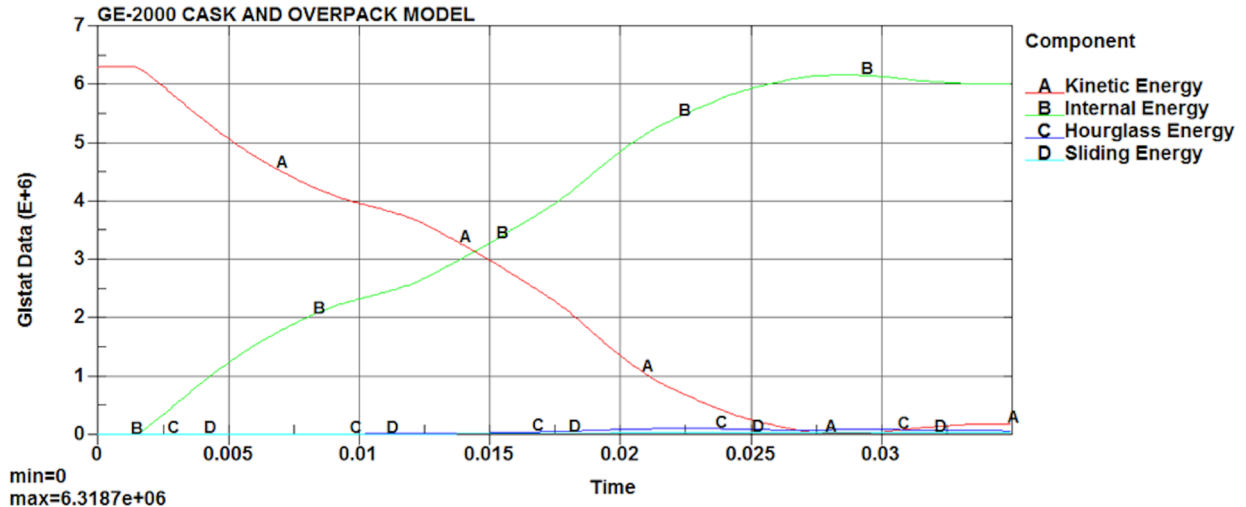


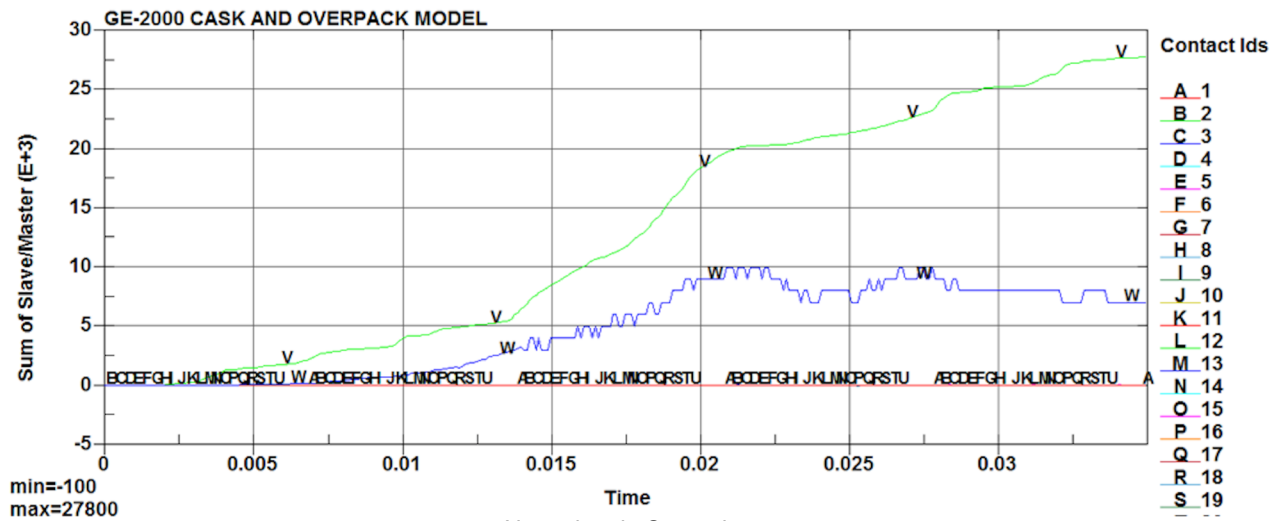
Figure 2.12.1.11-2. Case 1 Payload Acceleration Time History

NEDO-33866 Revision 6  
Non-Proprietary Information



Note: time in Seconds

Figure 2.12.1.11-3. Case 1 Impact Energy Plot



Note: time in Seconds

Figure 2.12.1.11-4. Case 1 Interface Sliding Energy Time History



## 2.12.1.11.2. Case 2 Side Drop Benchmark

GE-2000 CASK AND OVERPACK MODEL

Time = 0.025  
Contours of Effective Plastic Strain  
max IP. value  
min=-0.0581017, at elem# 388099  
max=0.442052, at elem# 420824

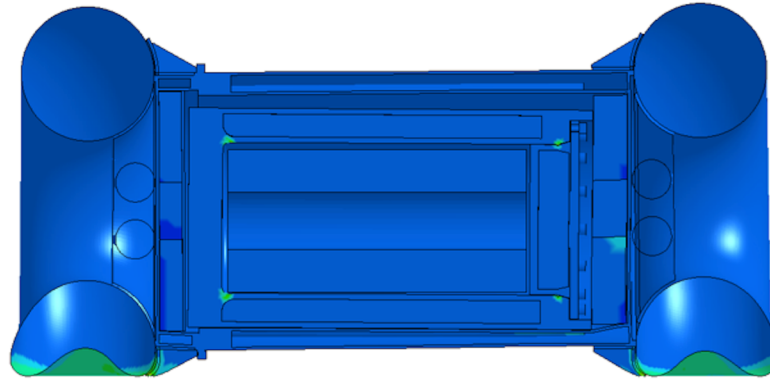


Figure 2.12.1.11-5. Case 2 Deformed Overpack Shape (Effective Plastic Strain)

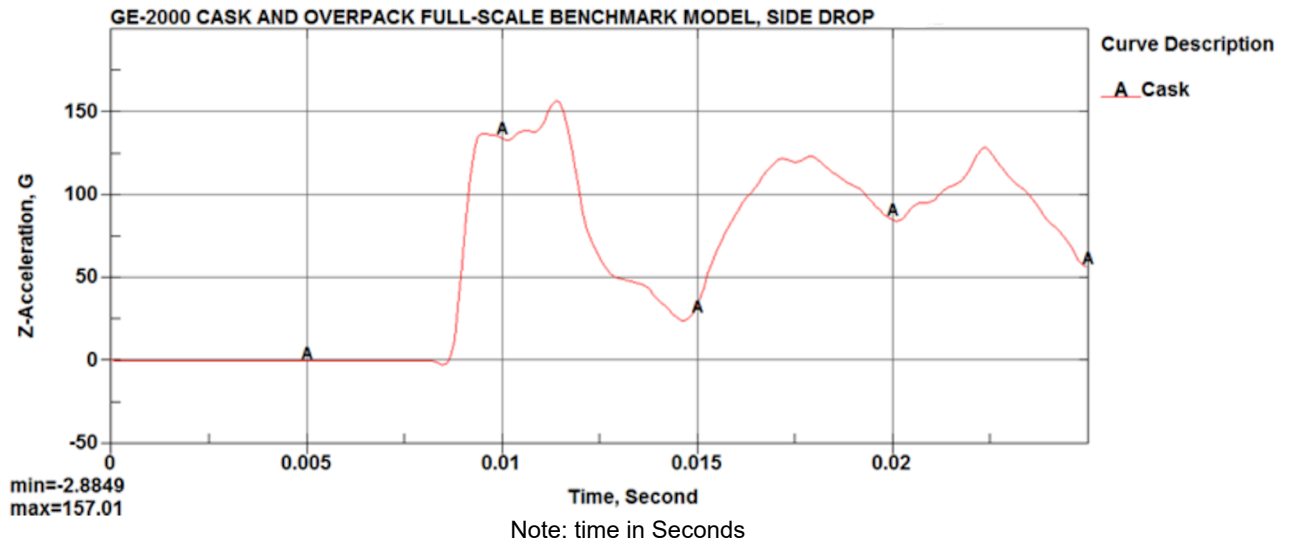


Figure 2.12.1.11-6. Case 2 Payload Acceleration Time History

NEDO-33866 Revision 6  
Non-Proprietary Information

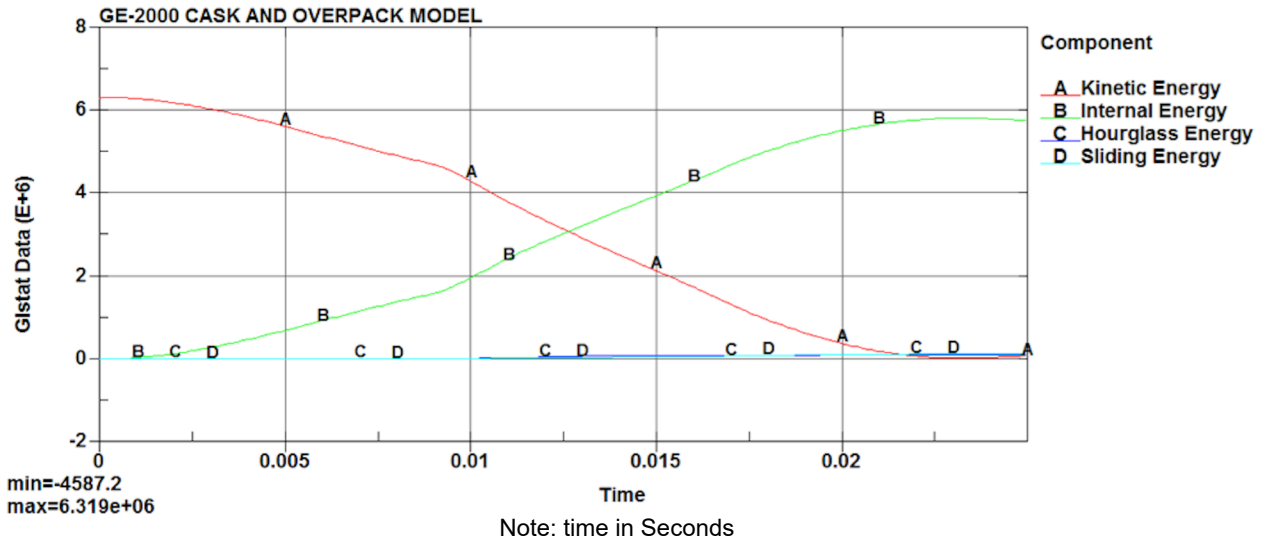


Figure 2.12.1.11-7. Case 2 Impact Energy Plot

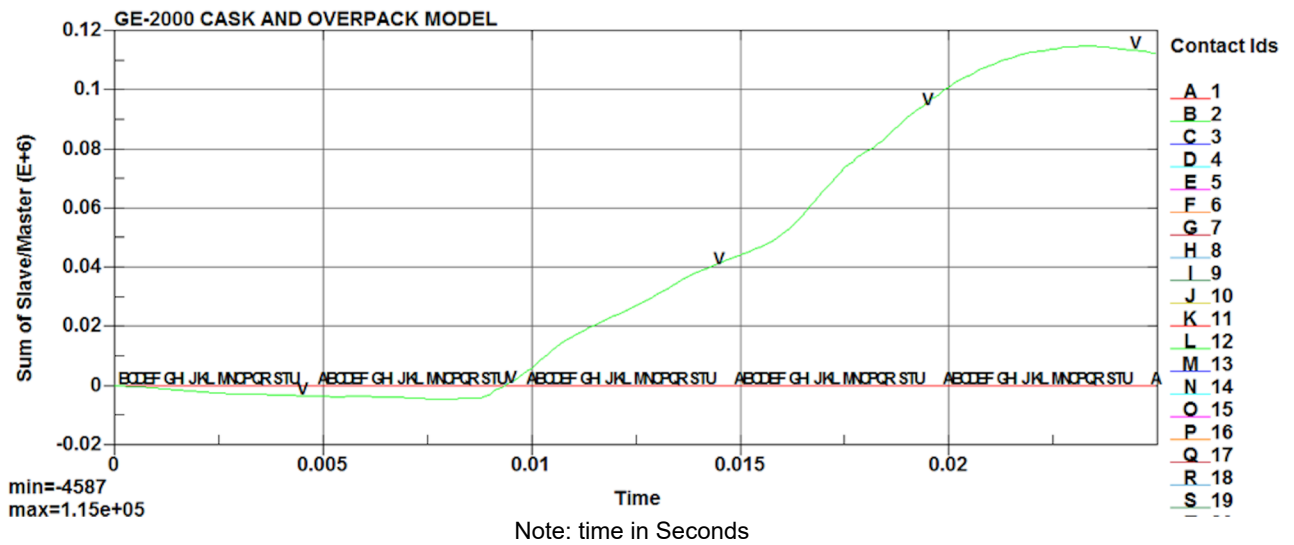


Figure 2.12.1.11-8. Case 2 Interface Sliding Energy Time History

### 2.12.1.11.3. Case 3 C.G. over Corner Drop Benchmark

GE-2000 CASK AND OVERPACK MODEL  
Time = 0.045001  
Contours of Effective Plastic Strain  
max IP. value  
min=-1.47019, at elem# 388062  
max=0.402424, at elem# 296780

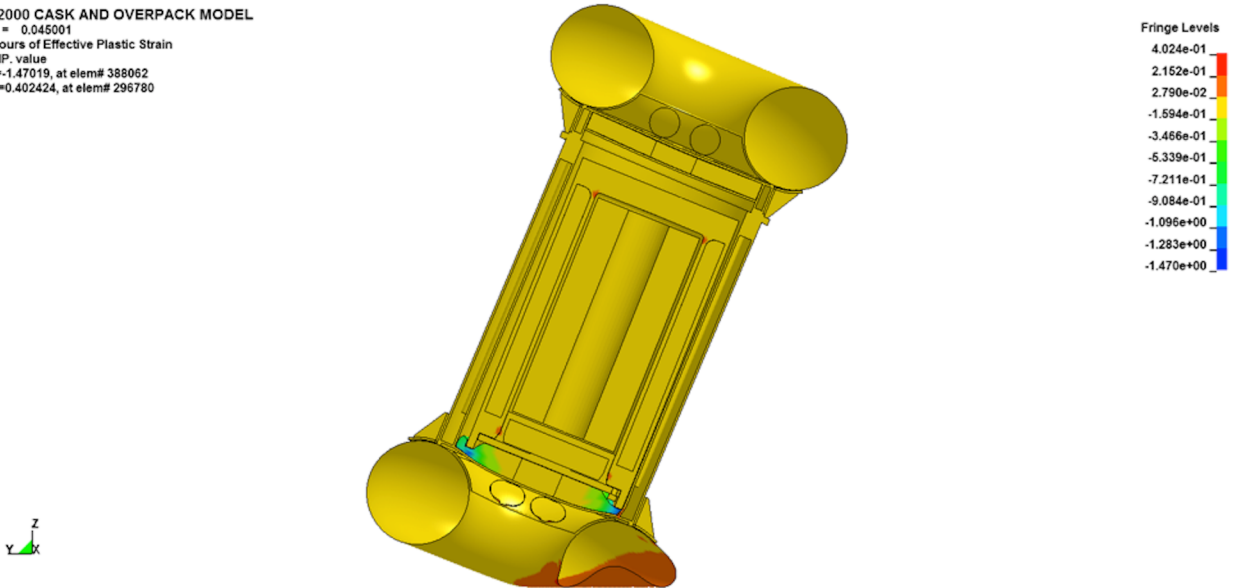
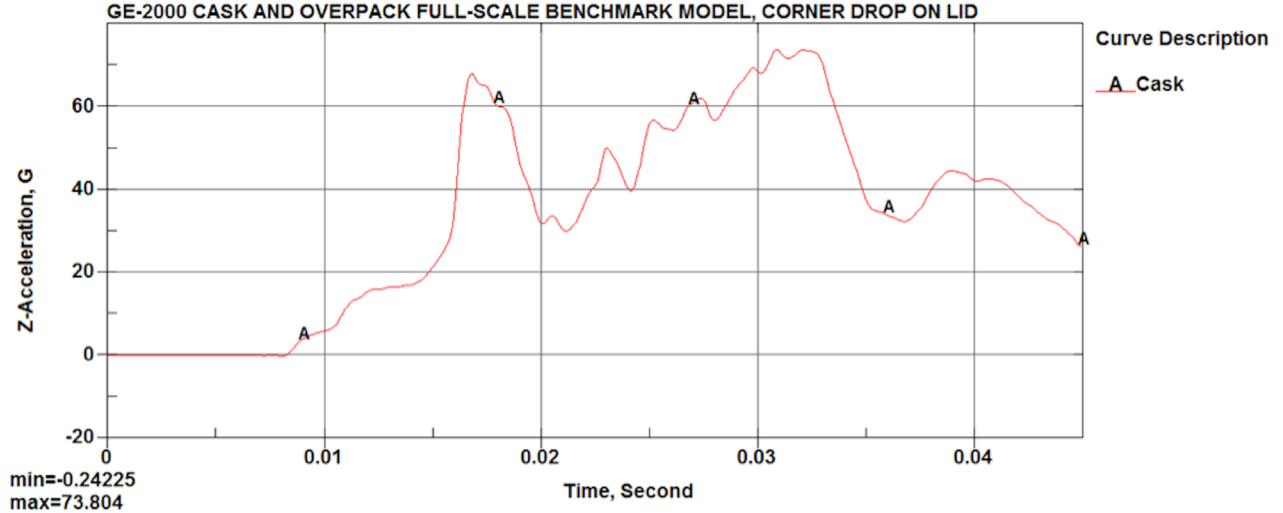


Figure 2.12.1.11-9. Case 3 Deformed Overpack Shape (Effective Plastic Strain)



Note: time in Seconds

Figure 2.12.1.11-10. Case 3 Payload Acceleration Time History

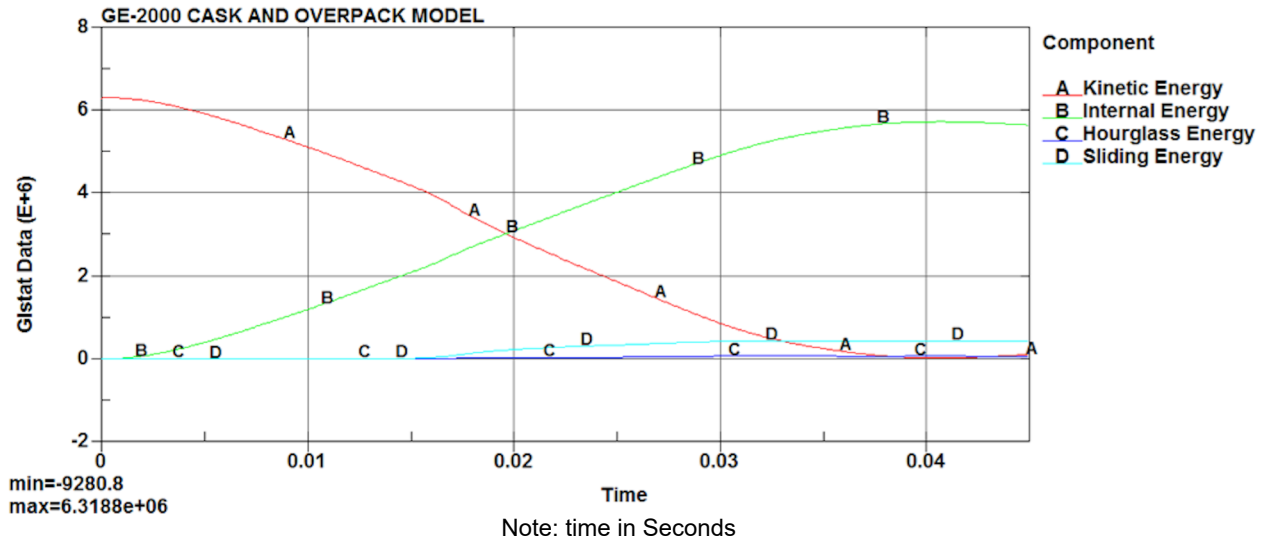


Figure 2.12.1.11-11. Case 3 Impact Energy Plot

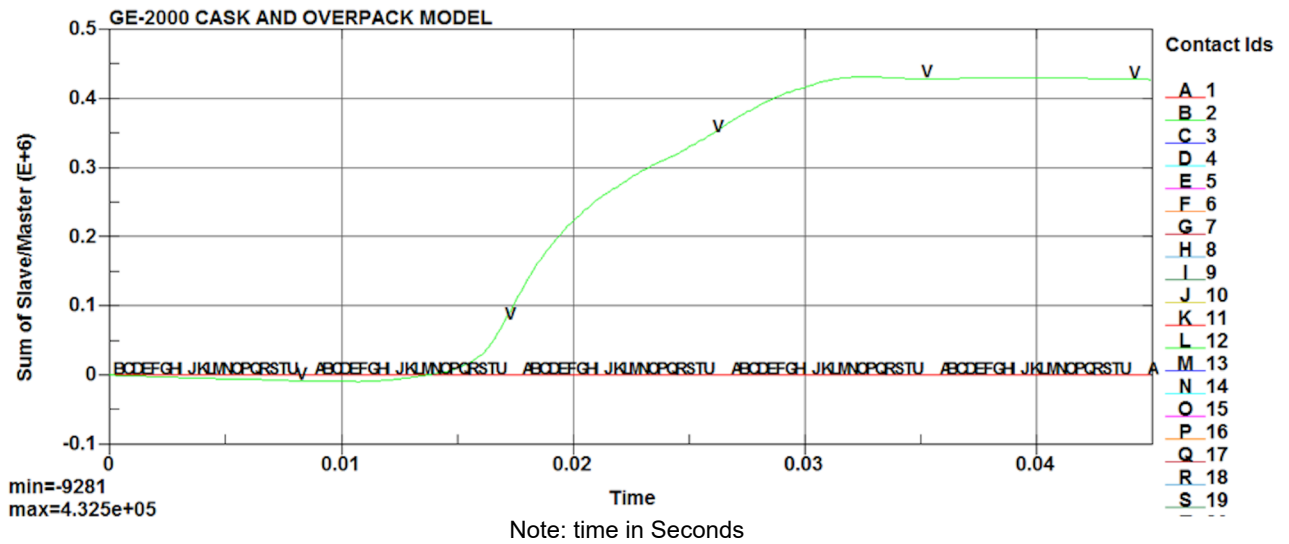
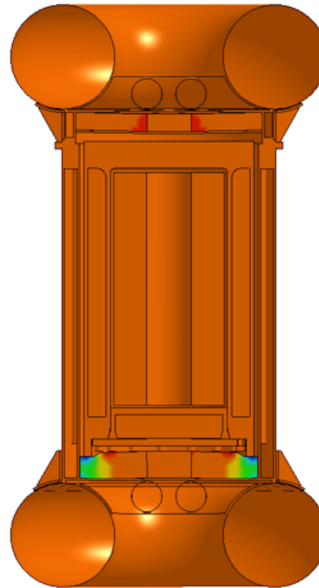


Figure 2.12.1.11-12. Case 3 Interface Sliding Energy Time History

#### 2.12.1.11.4. Case 4 NCT End Drop with Thick Shell, Cold Condition and Light Payload

Case\_4\_Thick\_Cold\_Light\_EndDrop  
Time = 0.035  
Contours of Effective Plastic Strain  
max IP. value  
min=-0.290278, at elem# 388255  
max=0.0441127, at elem# 388087



Fringe Levels  
4.411e-02  
1.067e-02  
-2.277e-02  
-5.620e-02  
-8.964e-02  
-1.231e-01  
-1.565e-01  
-1.900e-01  
-2.234e-01  
-2.568e-01  
-2.903e-01

Figure 2.12.1.11-13. Case 4 Deformed Overpack Shape (Effective Plastic Strain)

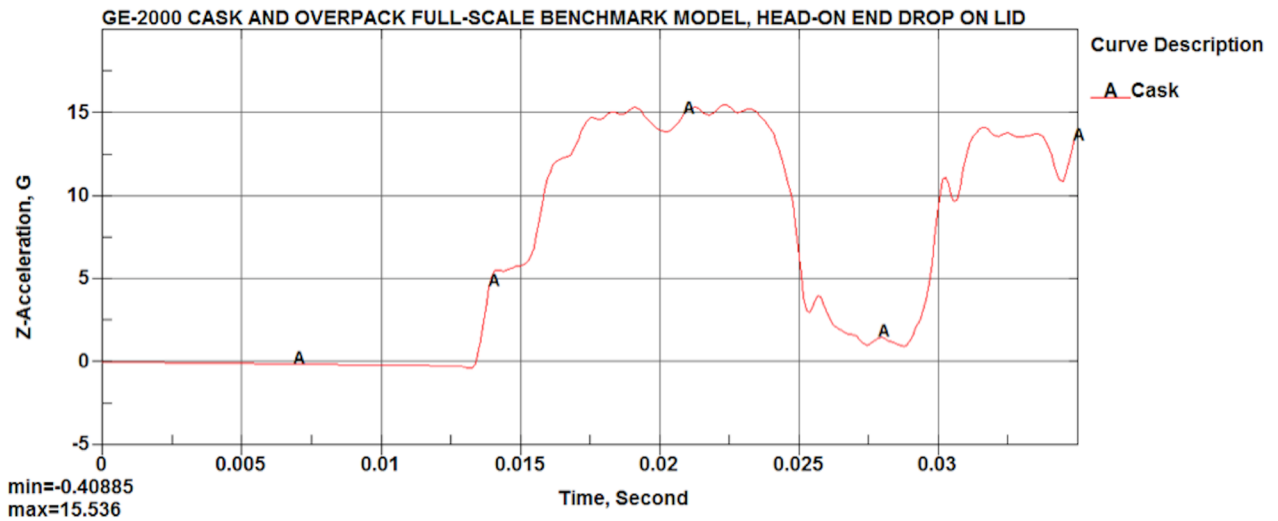


Figure 2.12.1.11-14. Case 4 Payload Acceleration Time History

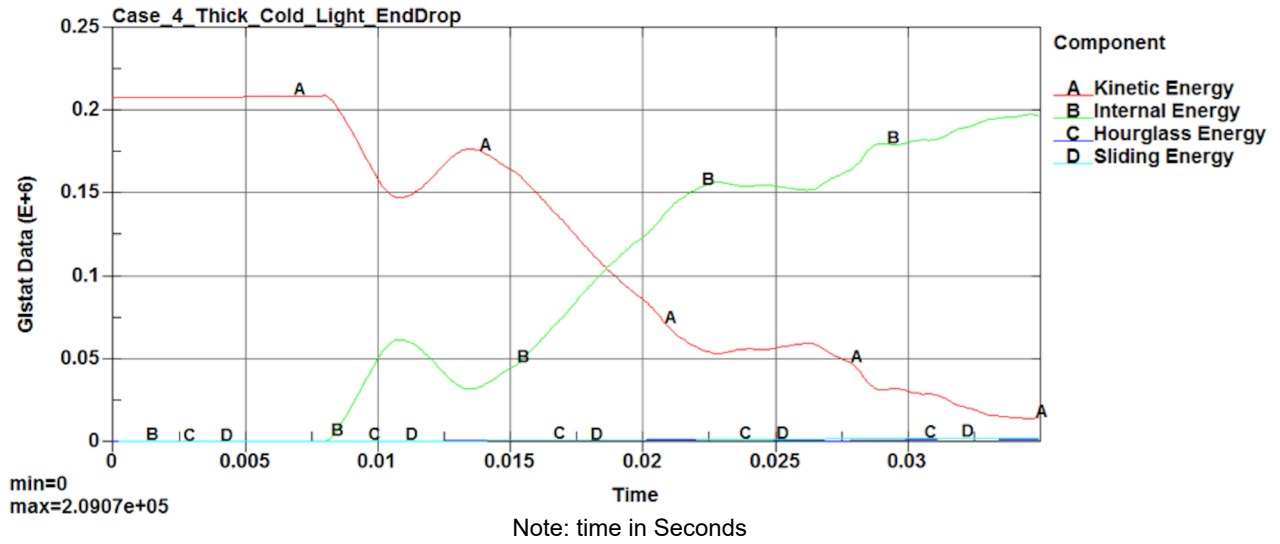


Figure 2.12.1.11-15. Case 4 Impact Energy Plot

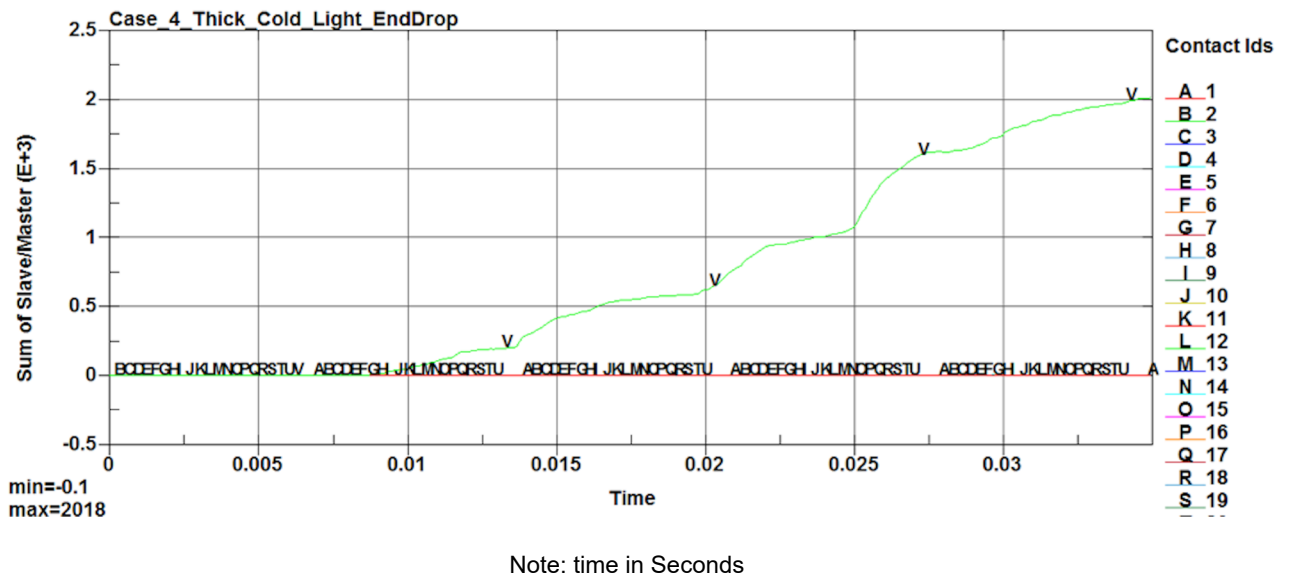
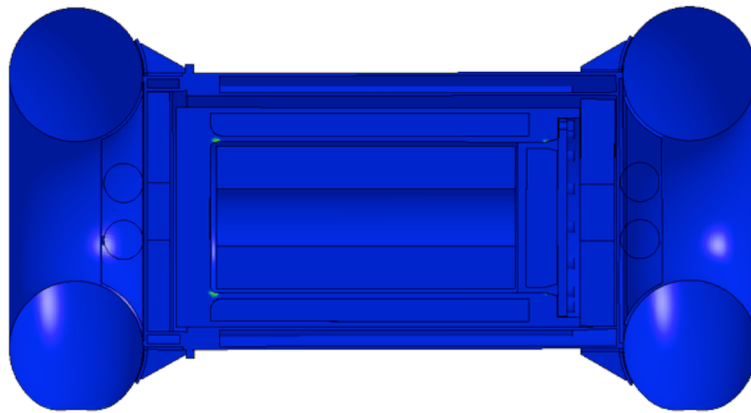


Figure 2.12.1.11-16. Case 4 Interface Sliding Energy Time History

### 2.12.1.11.5. Case 5 NCT Side Drop with Thick Shell, Cold Condition and Light Payload

Case\_5\_thick\_thick\_Cold\_Light\_SideDrop  
Time = 0.04  
Contours of Effective Plastic Strain  
max IP value  
min=-0.0123294, at elem# 387939  
max=0.368119, at elem# 296779



Fringe Levels  
3.681e-01  
3.301e-01  
2.920e-01  
2.540e-01  
2.159e-01  
1.779e-01  
1.398e-01  
1.018e-01  
6.376e-02  
2.672e-02  
-1.233e-02

Figure 2.12.1.11-17. Case 5 Deformed Overpack Shape (Effective Plastic Strain)

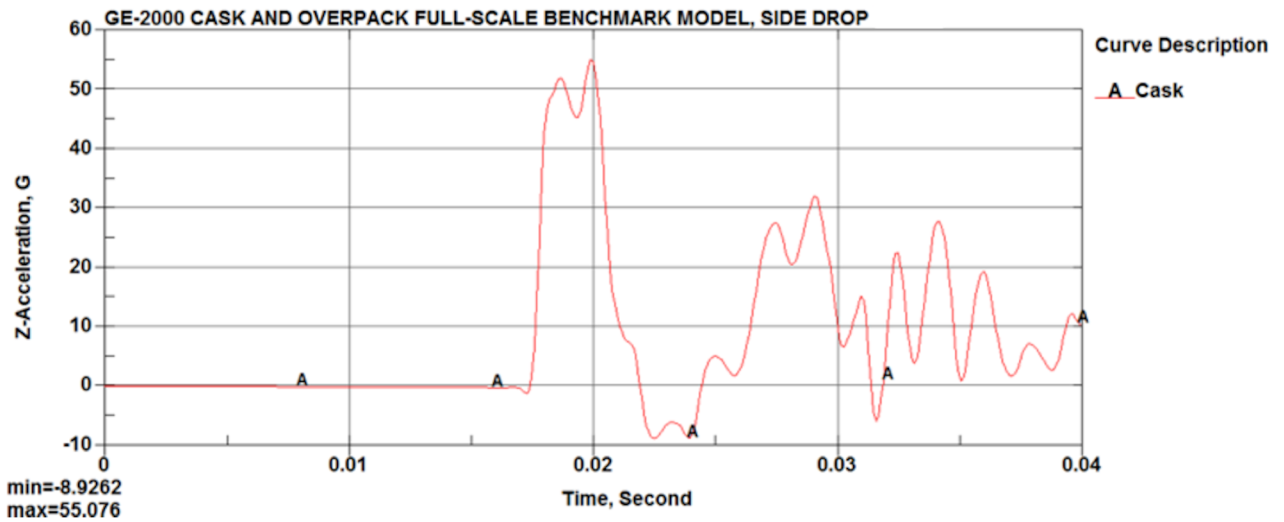


Figure 2.12.1.11-18. Case 5 Payload Acceleration Time History

NEDO-33866 Revision 6  
Non-Proprietary Information

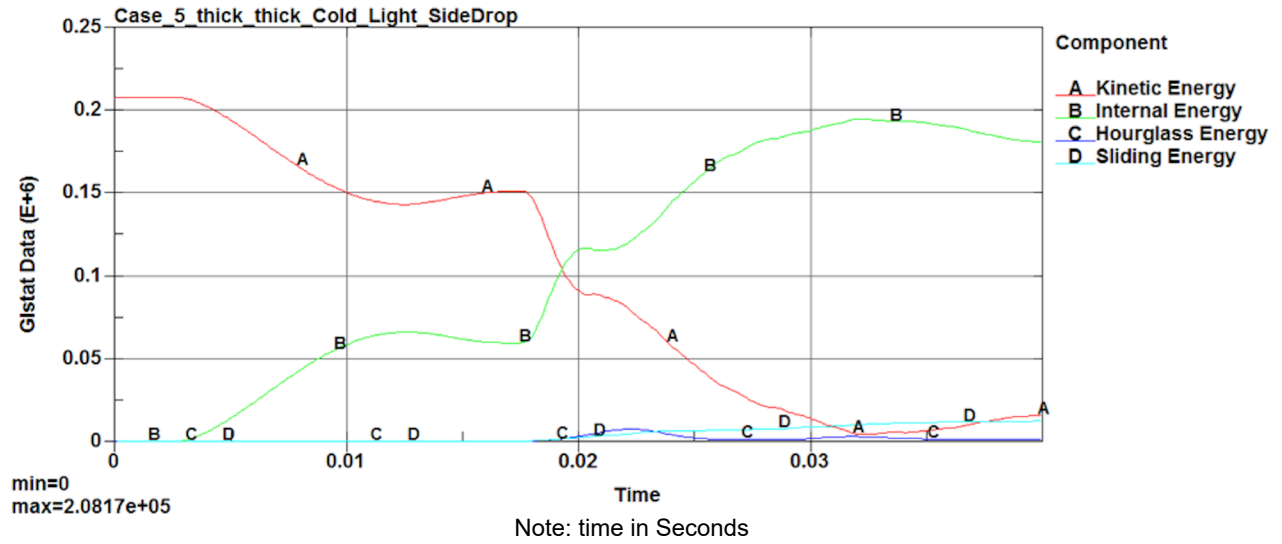


Figure 2.12.1.11-19. Case 5 Impact Energy Plot

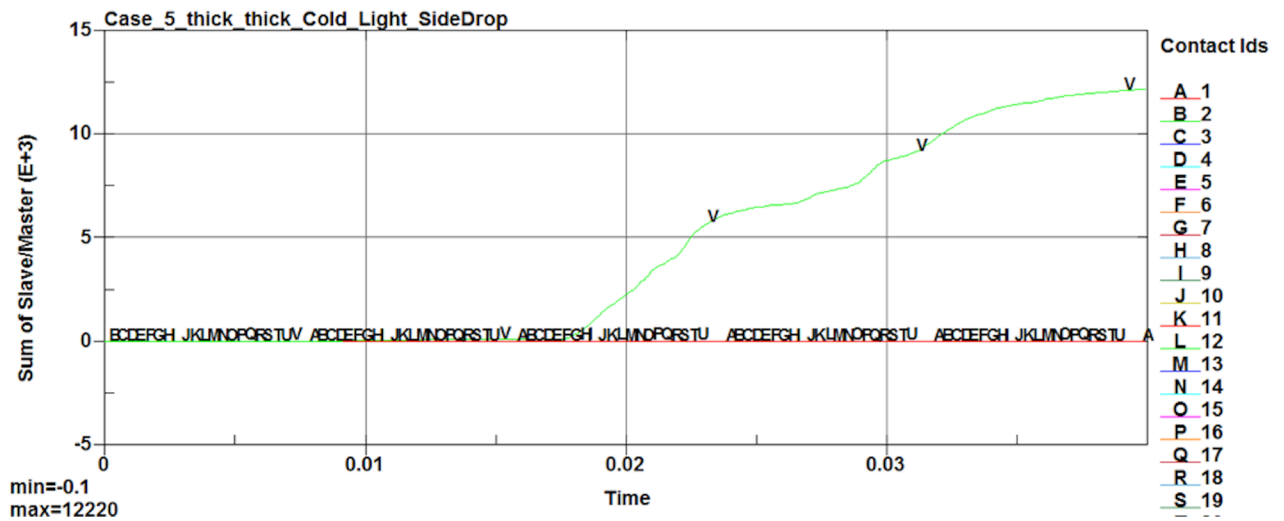


Figure 2.12.1.11-20. Case 5 Interface Sliding Energy Time History



### 2.12.1.11.6. Case 6 NCT Corner Drop with Thick Shell, Cold Condition and Light Payload

Case\_6\_Thick\_Cold\_Light\_Corner\_Drop  
Time = 0.045001  
Contours of Effective Plastic Strain  
max IP. value  
min=-0.222077, at elem# 388419  
max=0.174147, at elem# 296780

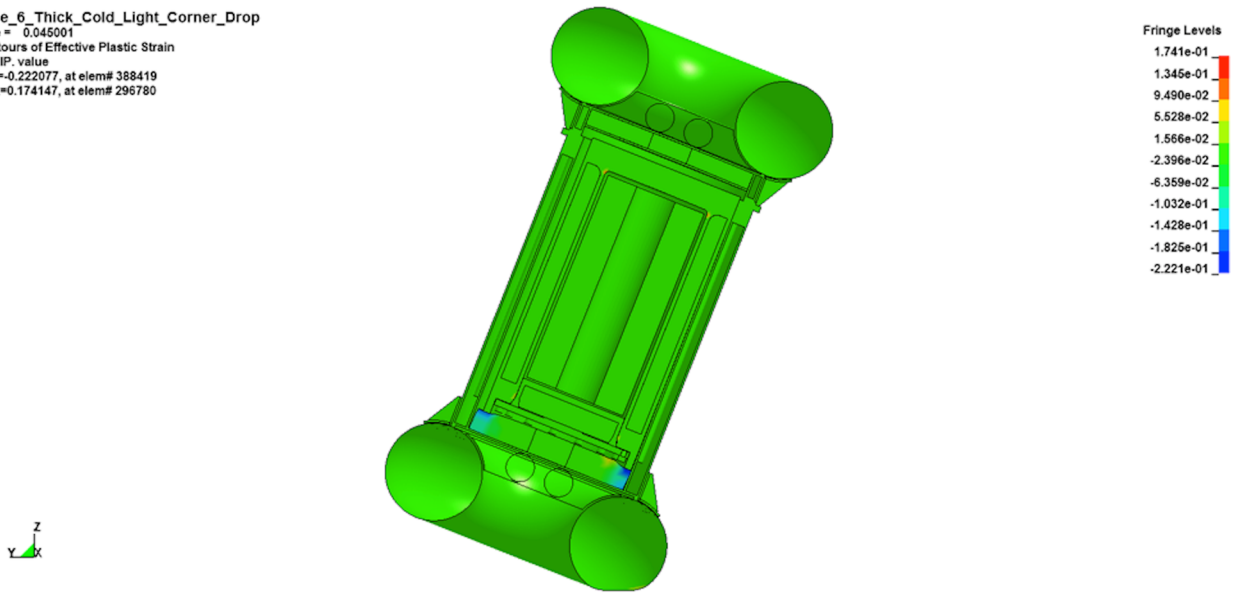


Figure 2.12.1.11-21. Case 6 Deformed Overpack Shape (Effective Plastic Strain)

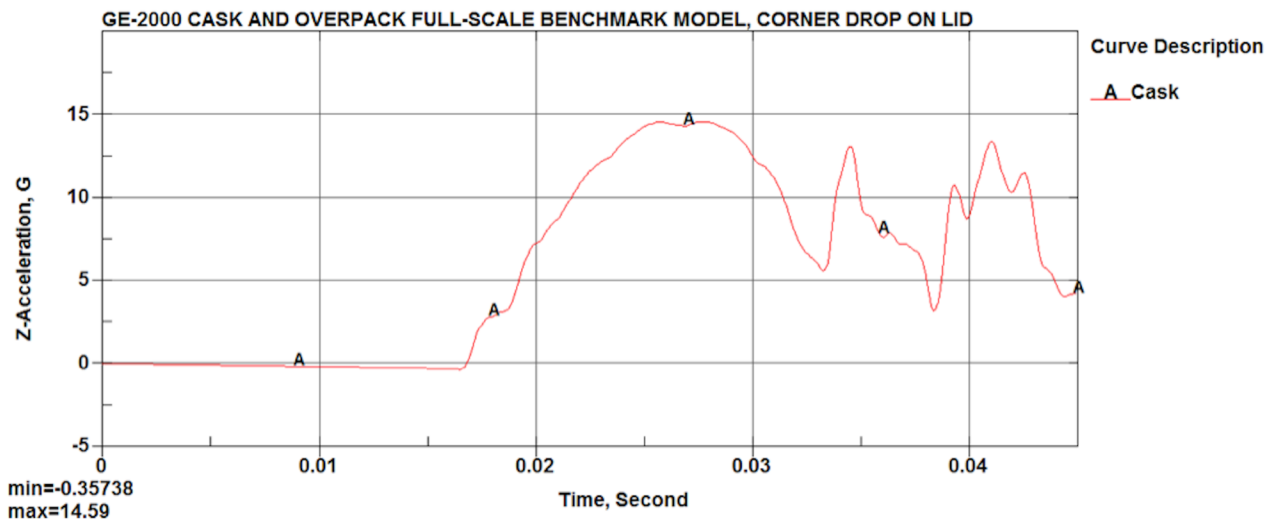


Figure 2.12.1.11-22. Case 6 Payload Acceleration Time History

NEDO-33866 Revision 6  
Non-Proprietary Information

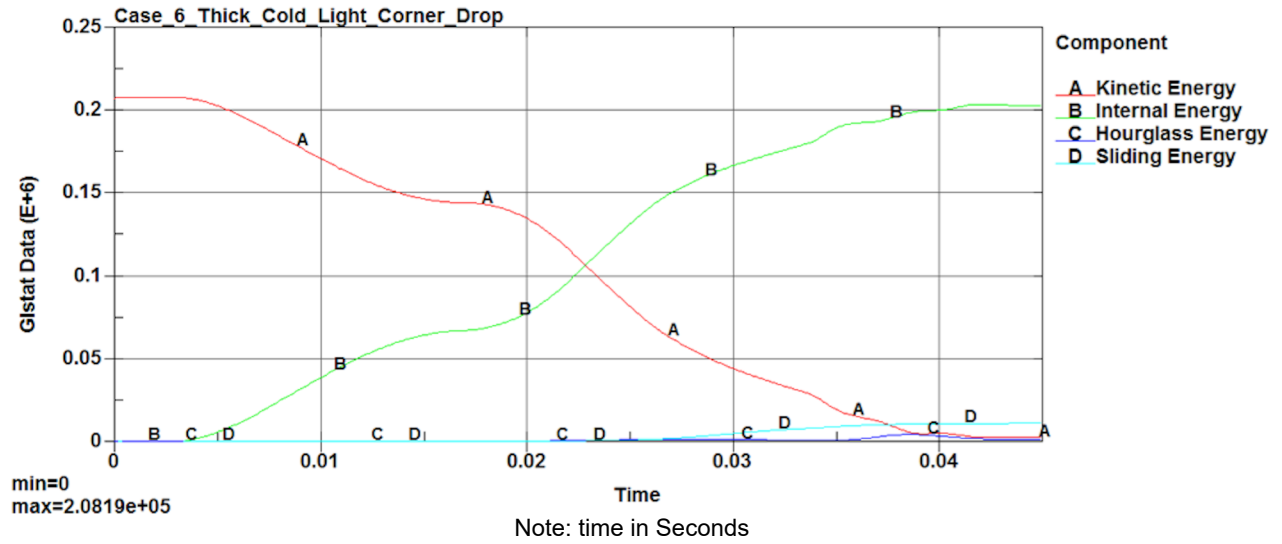


Figure 2.12.1.11-23. Case 6 Impact Energy Plot

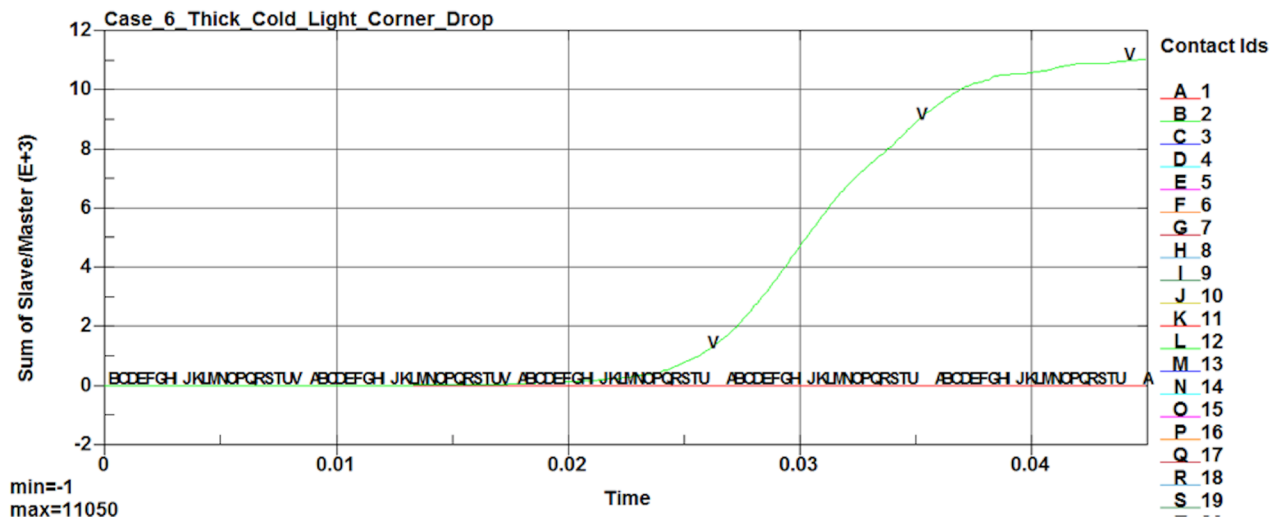


Figure 2.12.1.11-24. Case 6 Interface Sliding Energy Time History

### 2.12.1.11.7. Case 7 HAC End Drop with Thick Shell, Cold Condition and Light Payload

Case\_7A\_EndDrop\_thick\_cold\_Light  
Time = 0.035  
Contours of Effective Plastic Strain  
max IP. value  
min=-1.63149, at elem# 388422  
max=0.386009, at elem# 296895



Fringe Levels  
3.860e-01  
1.843e-01  
-1.749e-02  
-2.192e-01  
-4.210e-01  
-6.227e-01  
-8.245e-01  
-1.026e+00  
-1.228e+00  
-1.430e+00  
-1.631e+00

Figure 2.12.1.11-25. Case 7 Deformed Overpack Shape (Effective Plastic Strain)

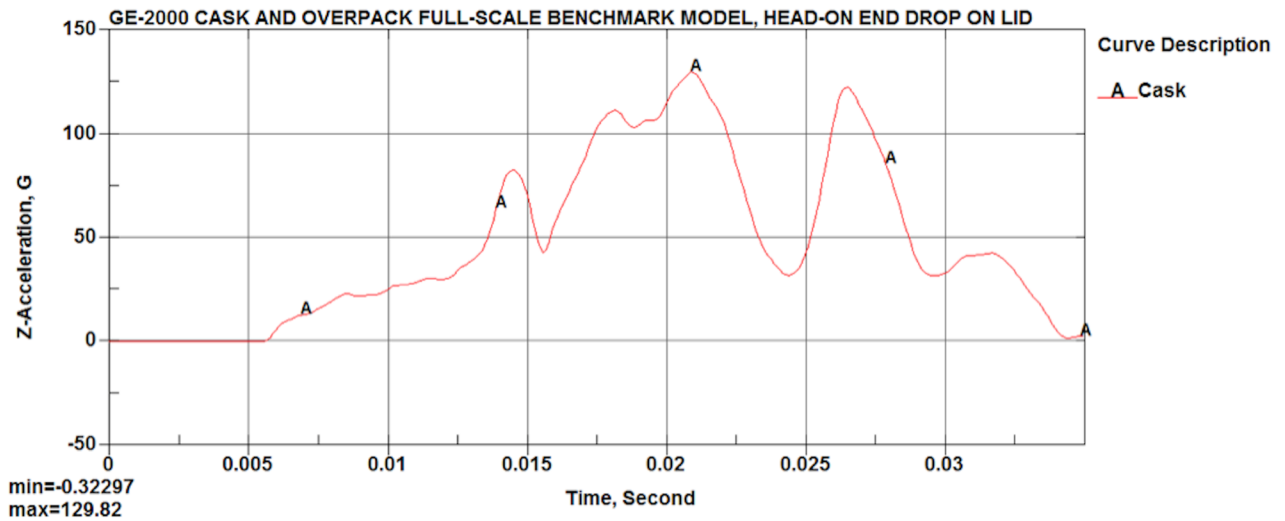


Figure 2.12.1.11-26. Case 7 Payload Acceleration Time History

NEDO-33866 Revision 6  
Non-Proprietary Information

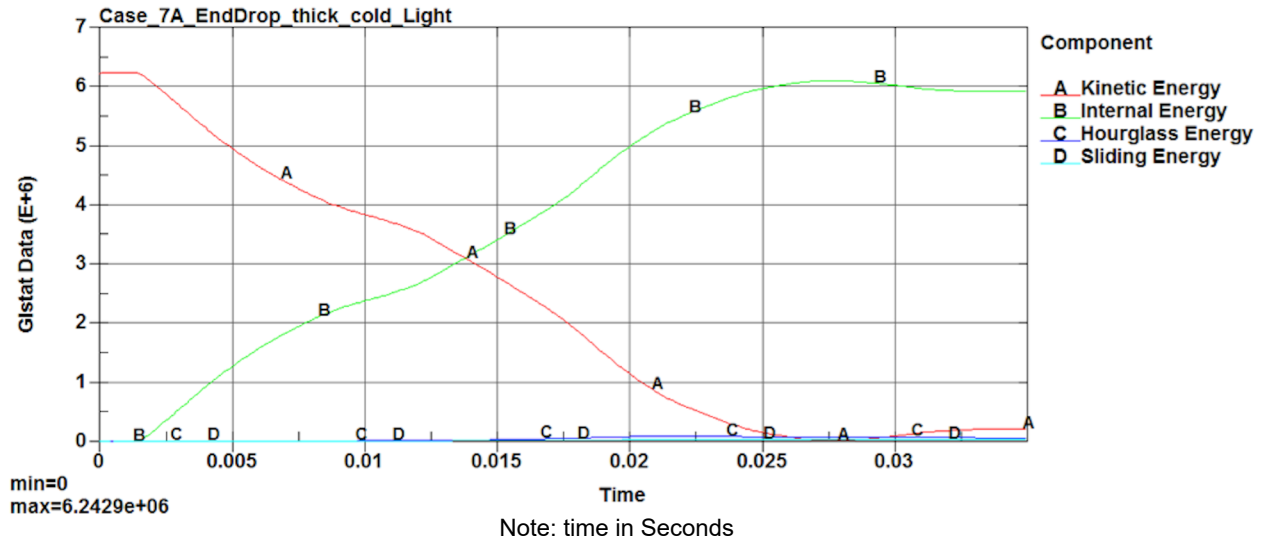


Figure 2.12.1.11-27. Case 7 Impact Energy Plot

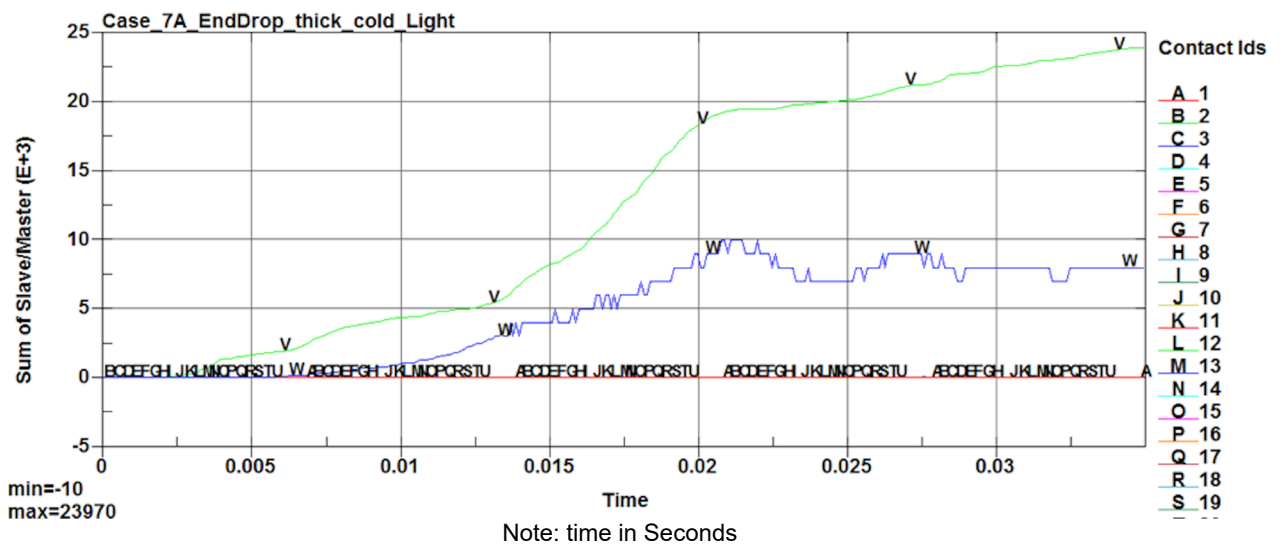
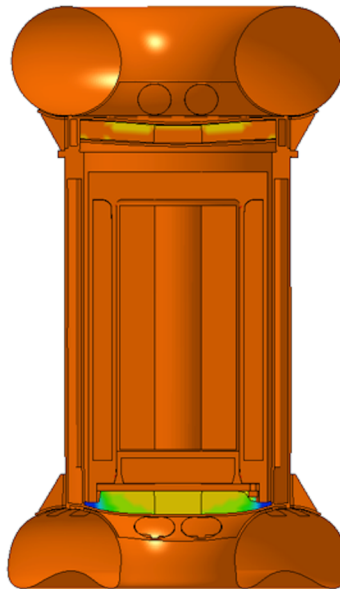


Figure 2.12.1.11-28. Case 7 Interface Sliding Energy Time History

## 2.12.1.11.8. Case 8 HAC End Drop with Thick Shell, Hot Condition and Heavy Payload

Case\_8C\_EndDrop\_thin\_hot\_heavy  
Time = 0.035  
Contours of Effective Plastic Strain  
max IP. value  
min=-1.72667, at elem# 388419  
max=0.414945, at elem# 275552



Fringe Levels  
4.149e-01  
2.008e-01  
-1.338e-02  
-2.275e-01  
-4.417e-01  
-6.569e-01  
-8.700e-01  
-1.084e+00  
-1.298e+00  
-1.513e+00  
-1.727e+00

Figure 2.12.1.11-29. Case 8 Deformed Overpack Shape (Effective Plastic Strain)

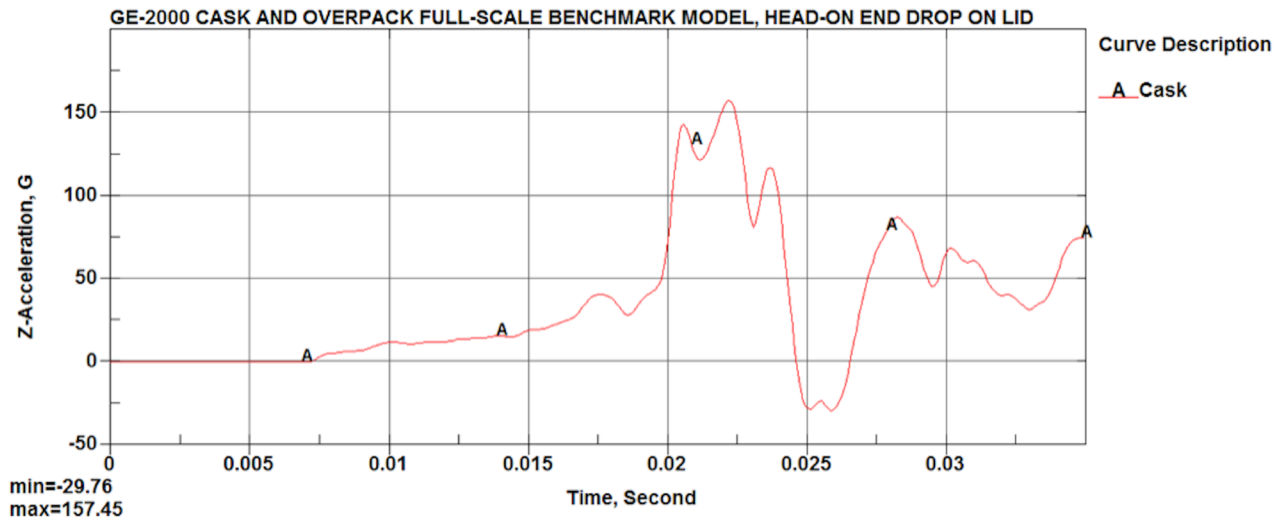


Figure 2.12.1.11-30. Case 8 Payload Acceleration Time History

NEDO-33866 Revision 6  
Non-Proprietary Information

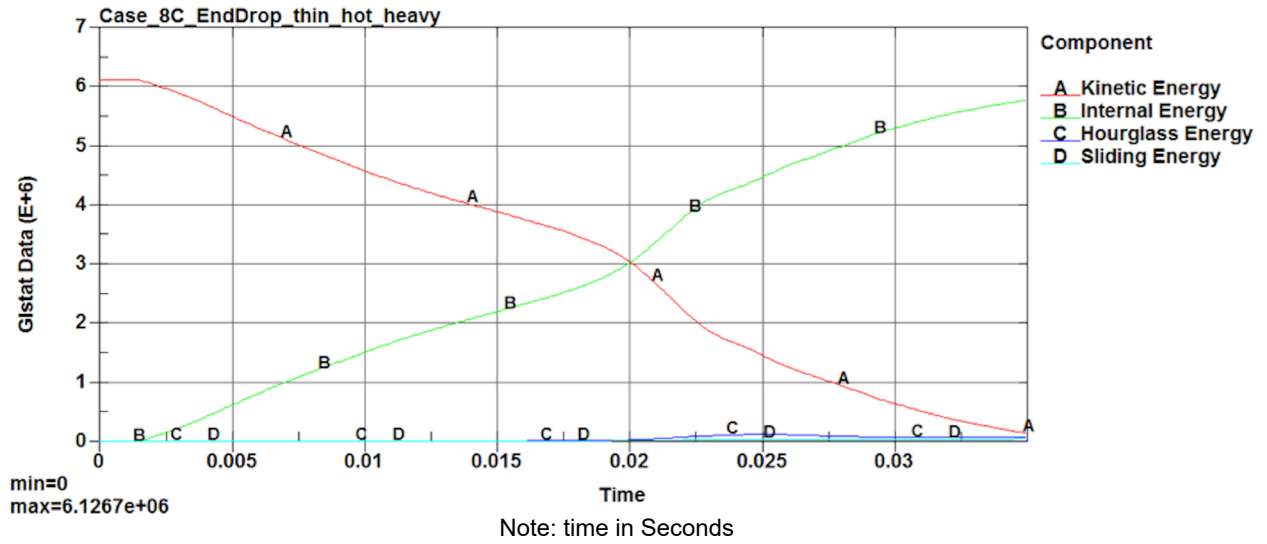


Figure 2.12.1.11-31. Case 8 Impact Energy Plot

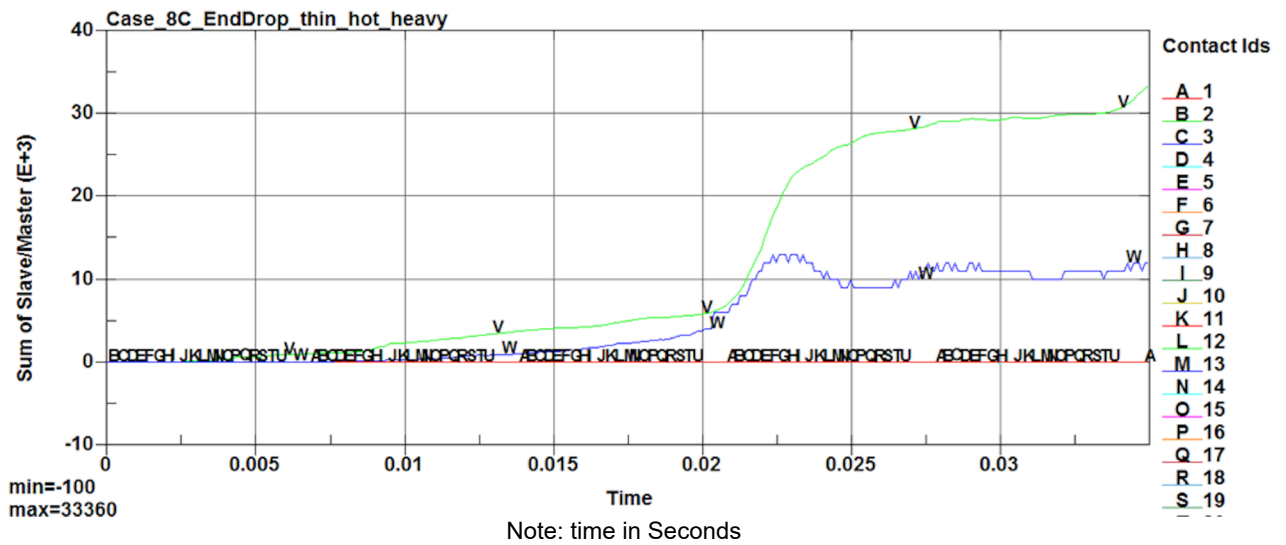


Figure 2.12.1.11-32. Case 8 Interface Sliding Energy Time History

### 2.12.1.11.9. Case 9 Side Drop with Thick Shell, Cold Condition and Light Payload

Case\_9\_SideDrop\_thick\_cold\_light  
Time = 0.025  
Contours of Effective Plastic Strain  
max IP value  
min=-0.0578508, at elem# 388099  
max=0.427268, at elem# 398569

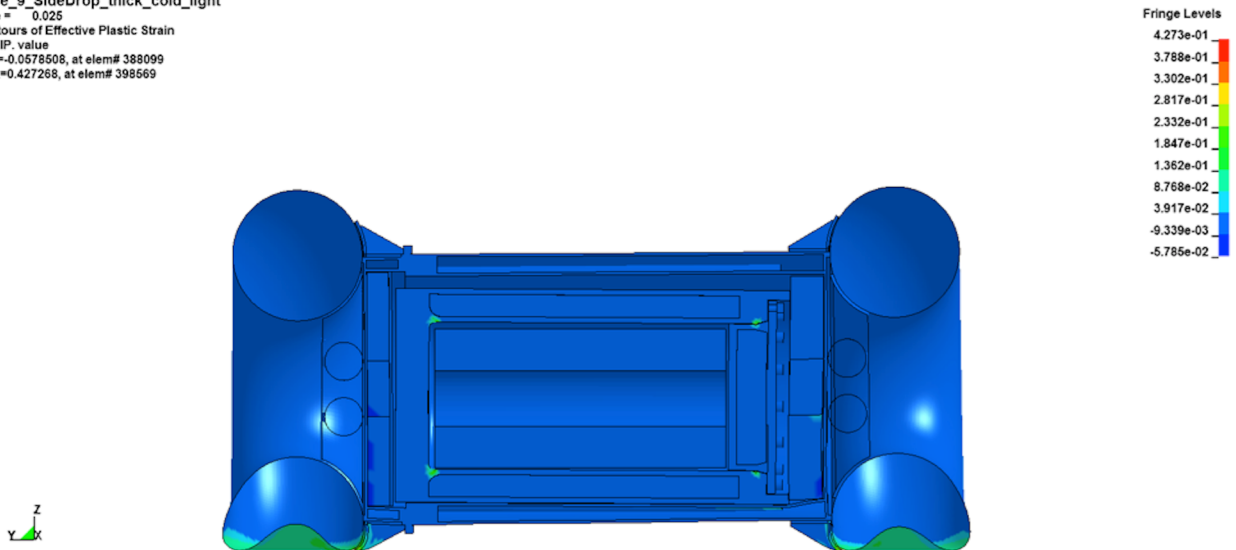


Figure 2.12.1.11-33. Case 9 Deformed Overpack Shape (Effective Plastic Strain)

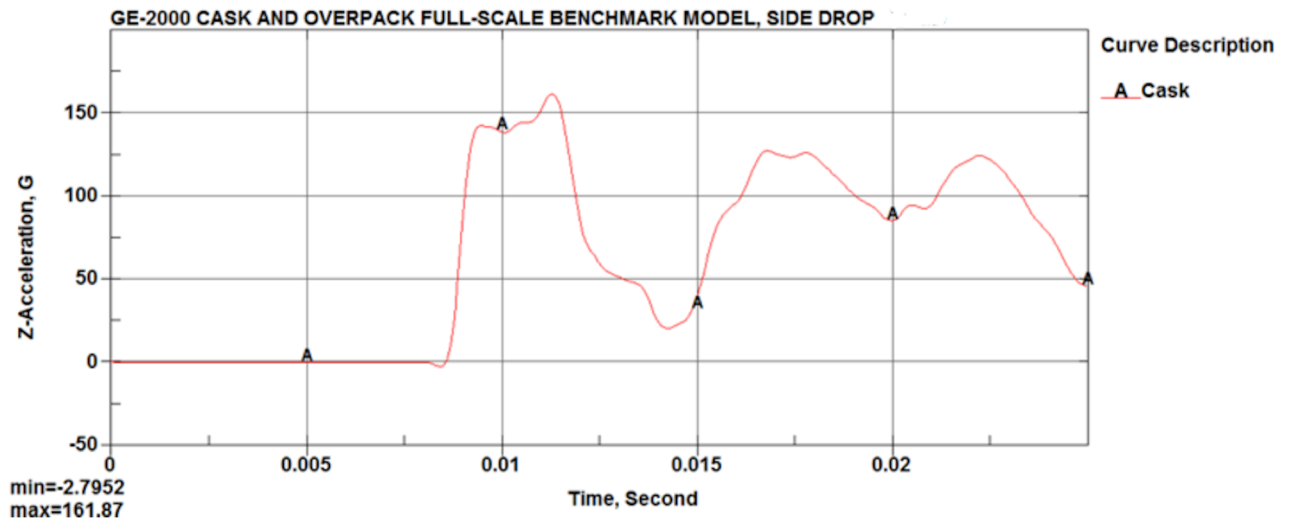


Figure 2.12.1.11-34. Case 9 Payload Acceleration Time History

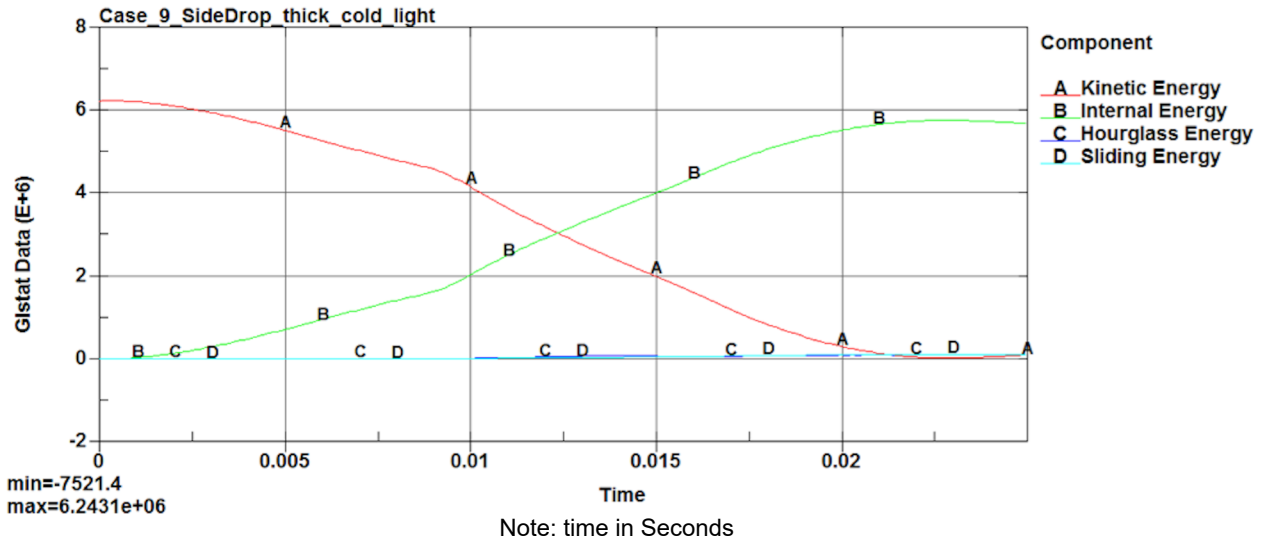


Figure 2.12.1.11-35. Case 9 Impact Energy Plot

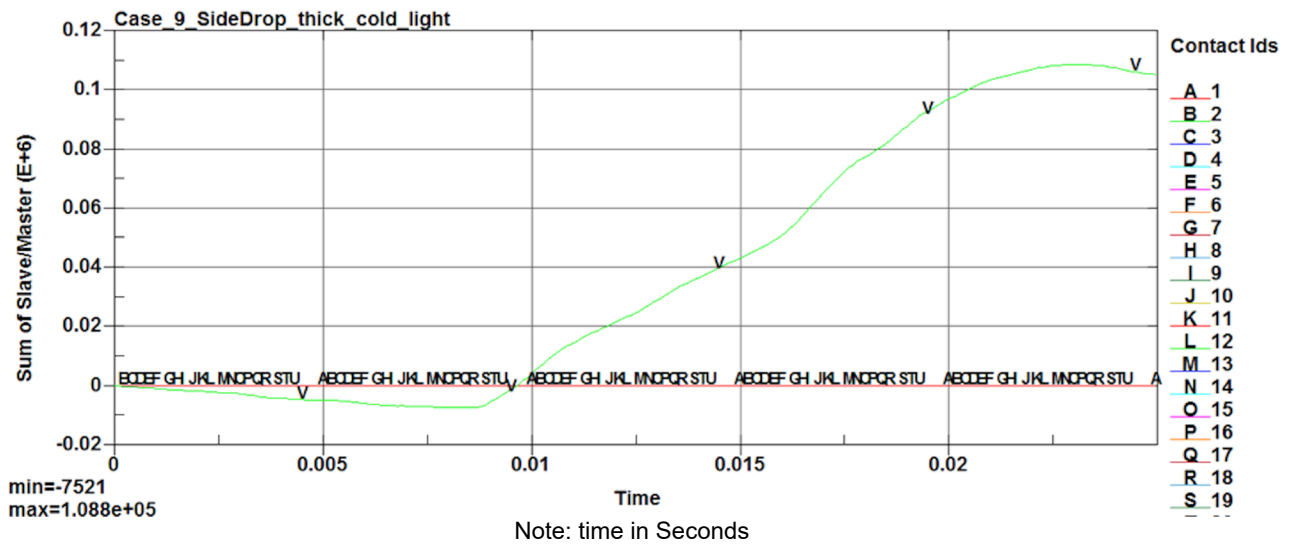


Figure 2.12.1.11-36. Case 9 Interface Sliding Energy Time History



#### 2.12.1.11.10. Case 10 Side Drop with Thin Shell, Hot Condition and Heavy Payload

Case\_10\_SideDrop\_thin\_hot\_heavy  
Time = 0.035  
Contours of Effective Plastic Strain  
max IP. value  
min=-0.0438089, at elem# 388059  
max=0.469419, at elem# 398124

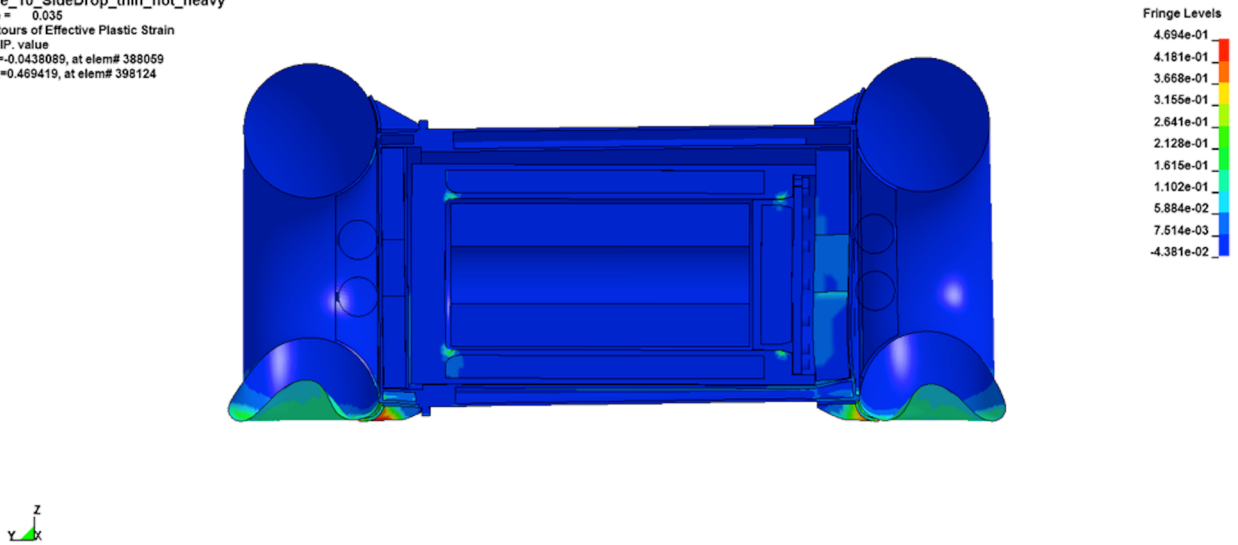


Figure 2.12.1.11-37. Case 10 Deformed Overpack Shape (Effective Plastic Strain)

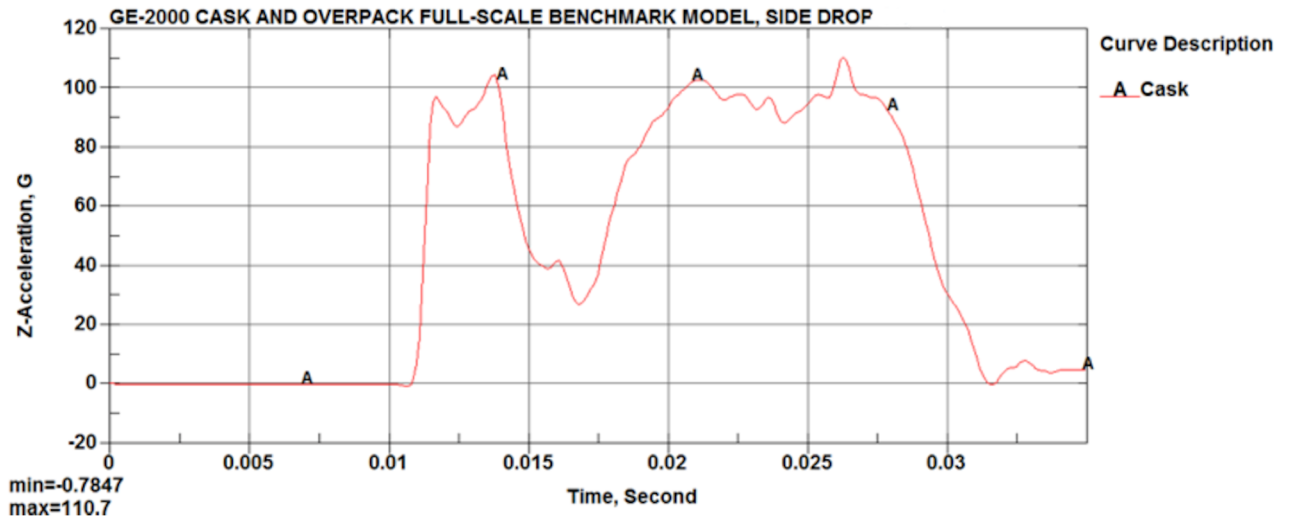


Figure 2.12.1.11-38. Case 10 Payload Acceleration Time History

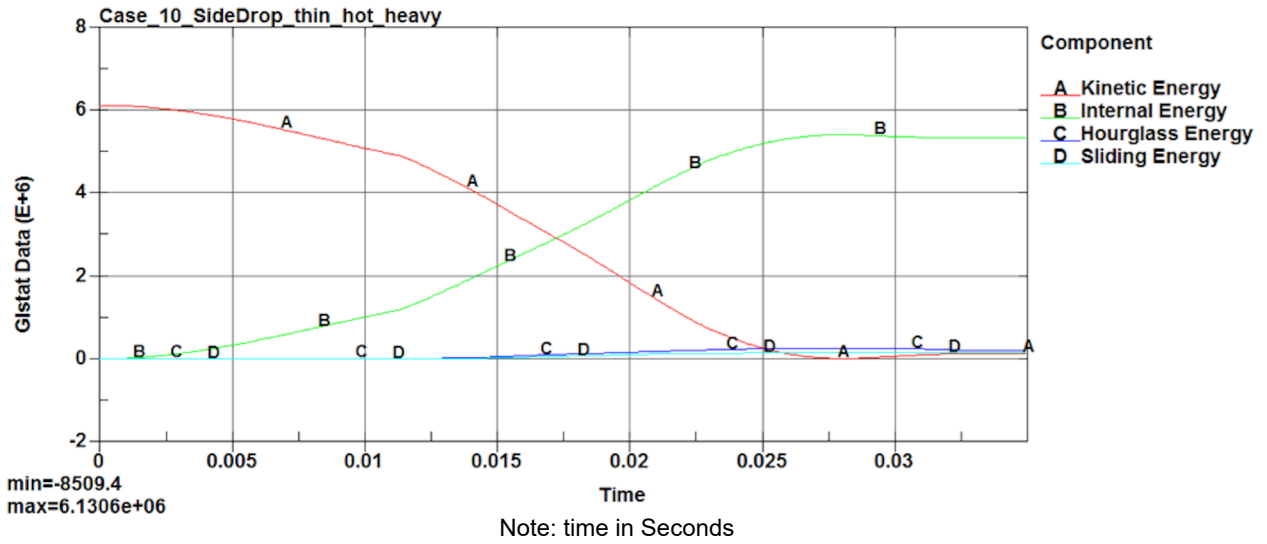


Figure 2.12.11-39. Case 10 Impact Energy Plot

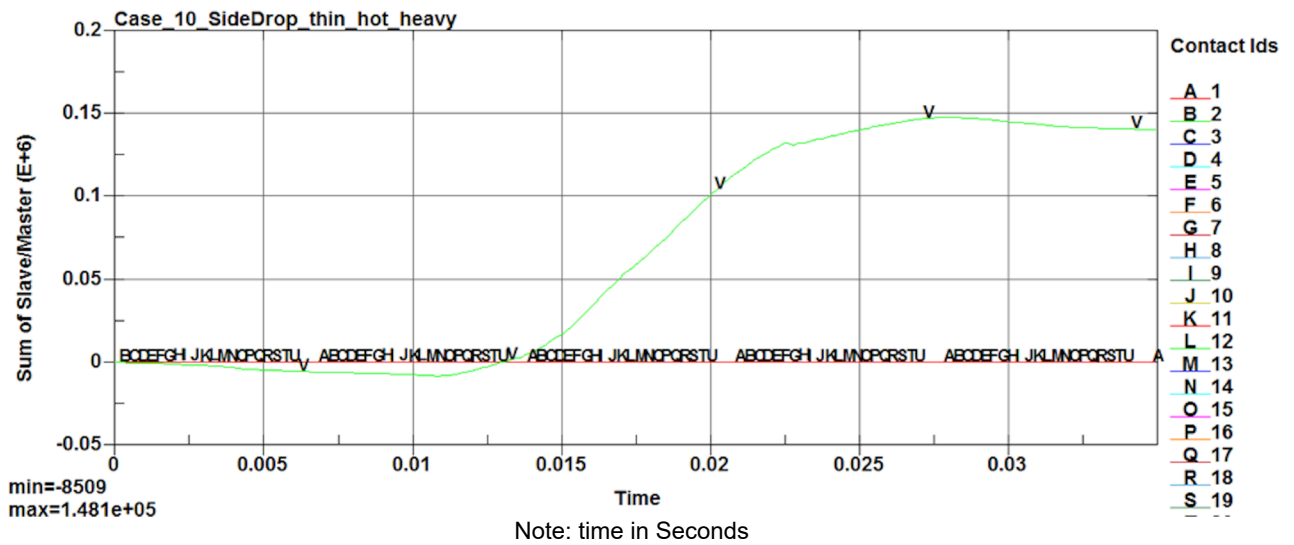


Figure 2.12.11-40. Case 10 Interface Sliding Energy Time History

### 2.12.1.11.11. Case 11 Corner Drop with Thick Shell, Cold Condition and Light Payload

Case\_11\_CornerDrop\_thick\_cold\_light  
Time = 0.045001  
Contours of Effective Plastic Strain  
max IP. value  
min=-1.38925, at elem# 388062  
max=0.395552, at elem# 296780

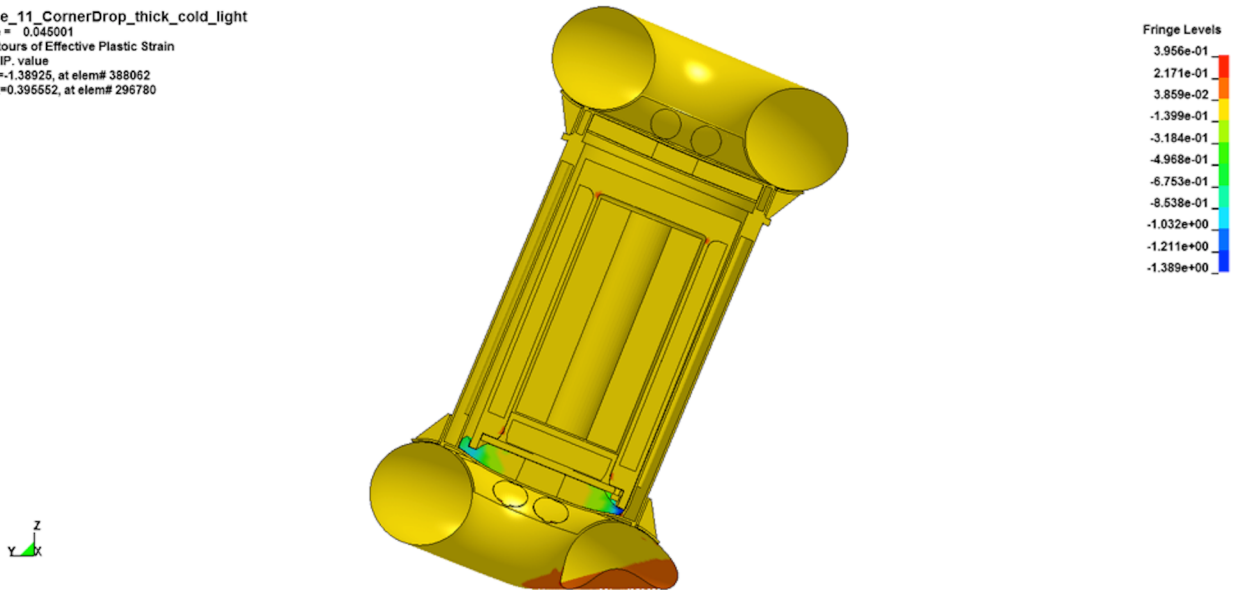


Figure 2.12.1.11-41. Case 11 Deformed Overpack Shape (Effective Plastic Strain)

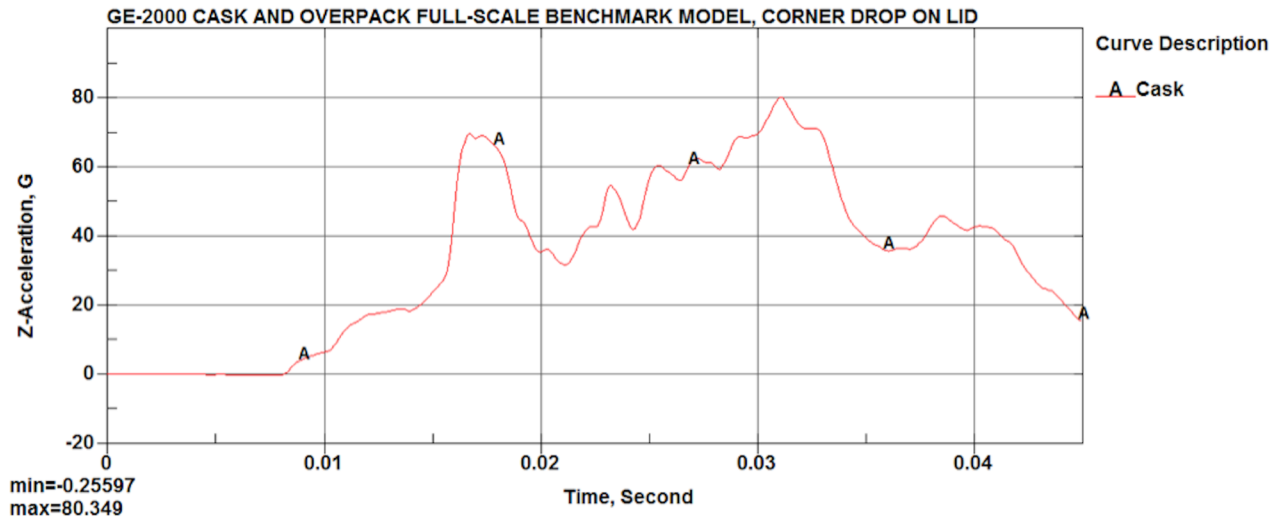


Figure 2.12.1.11-42. Case 11 Payload Acceleration Time History

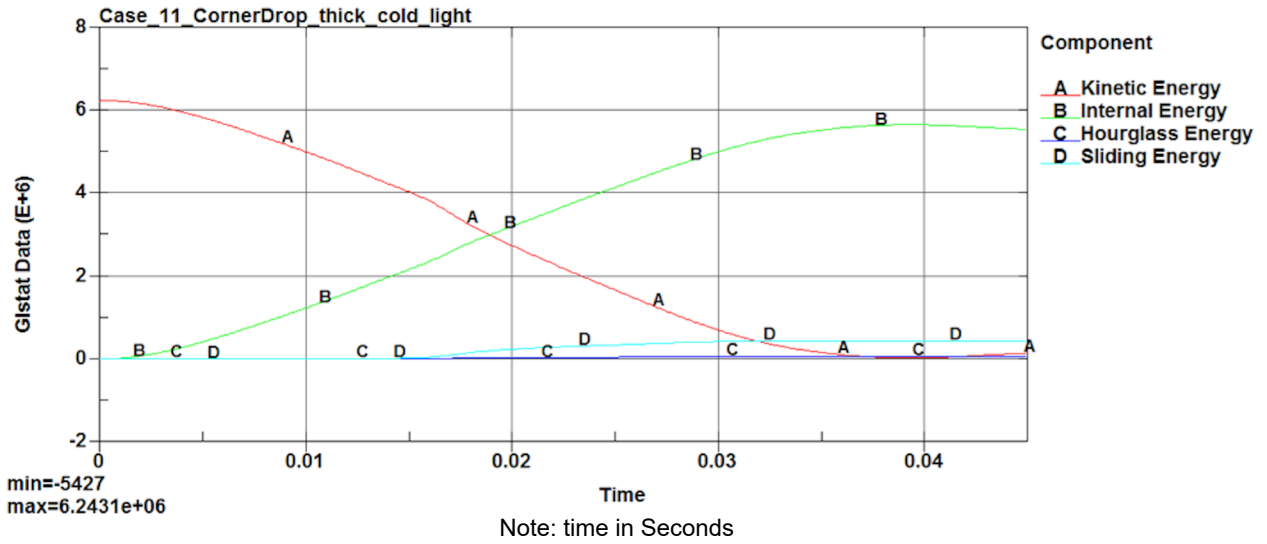


Figure 2.12.1.11-43. Case 11 Impact Energy Plot

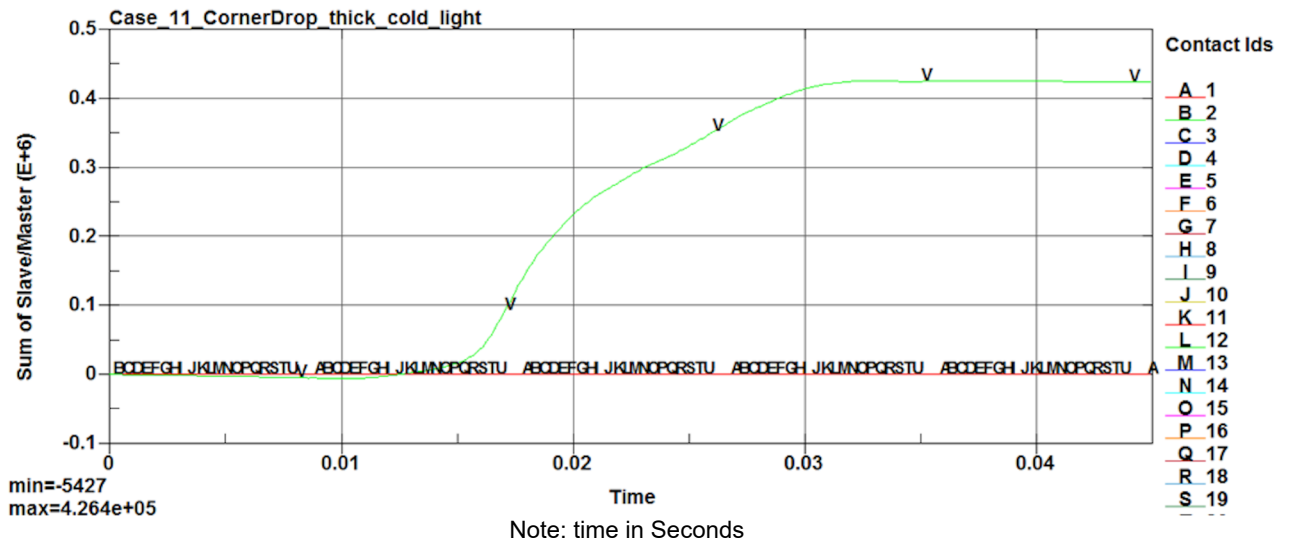


Figure 2.12.1.11-44. Case 11 Interface Sliding Energy Time History

## 2.12.1.11.12. Case 12 Corner Drop with Thin Shell, Hot Condition and Heavy Payload

Case\_12\_CornerDrop\_thin\_hot\_heavy  
Time = 0.045001  
Contours of Effective Plastic Strain  
max IP. value  
min=-1.59837, at elem# 388060  
max=0.470001, at elem# 79087

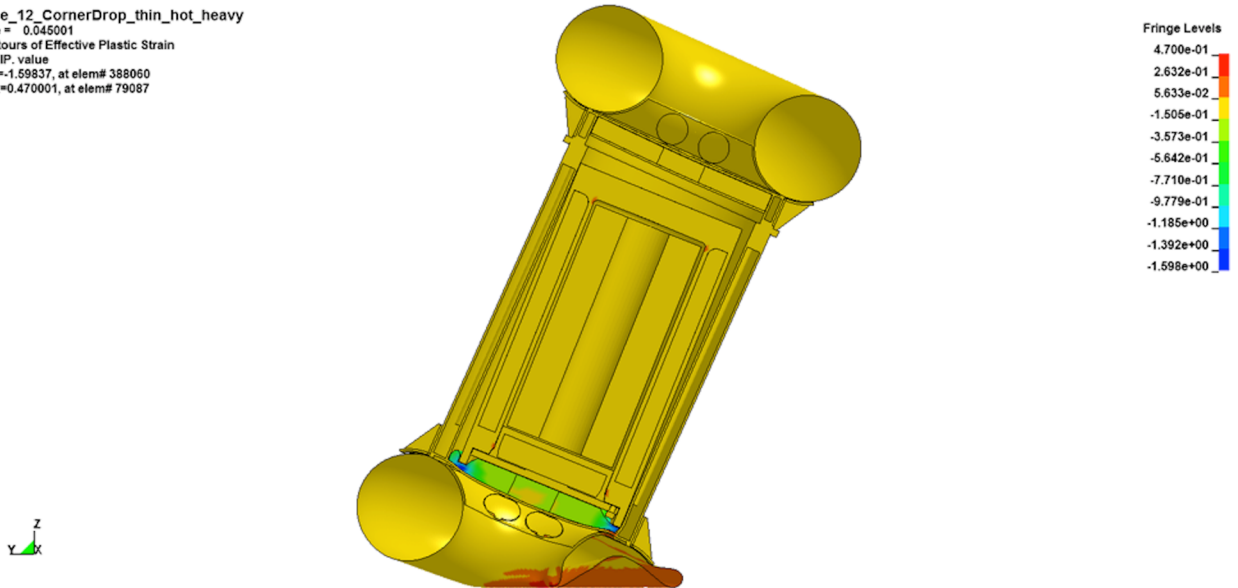


Figure 2.12.1.11-45. Case 12 Deformed Overpack Shape (Effective Plastic Strain)

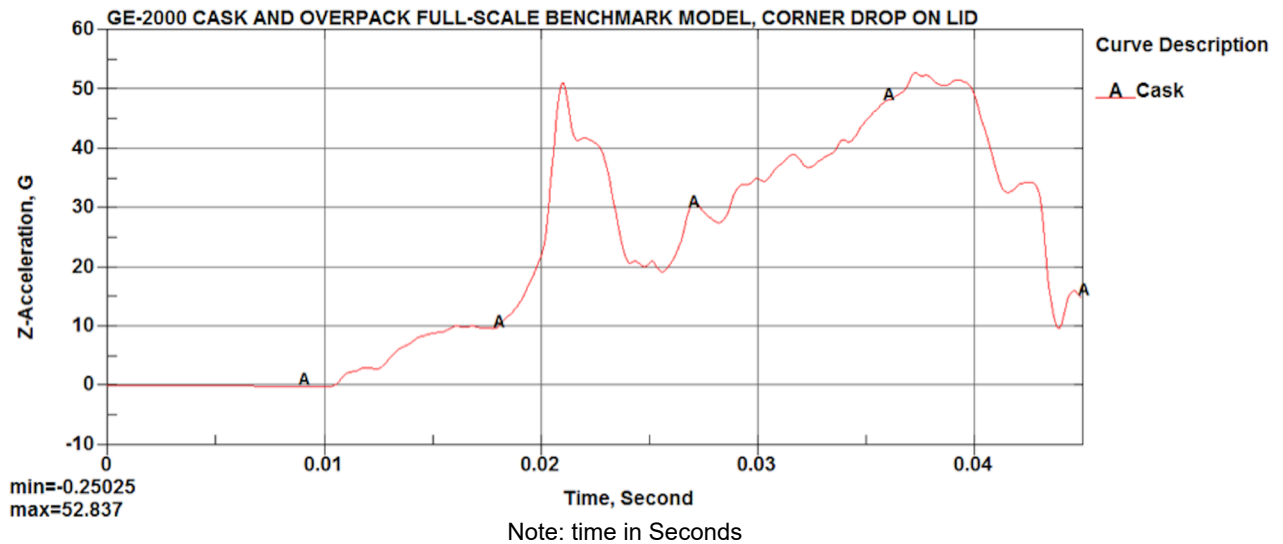


Figure 2.12.1.11-46. Case 12 Payload Acceleration Time History

NEDO-33866 Revision 6  
Non-Proprietary Information

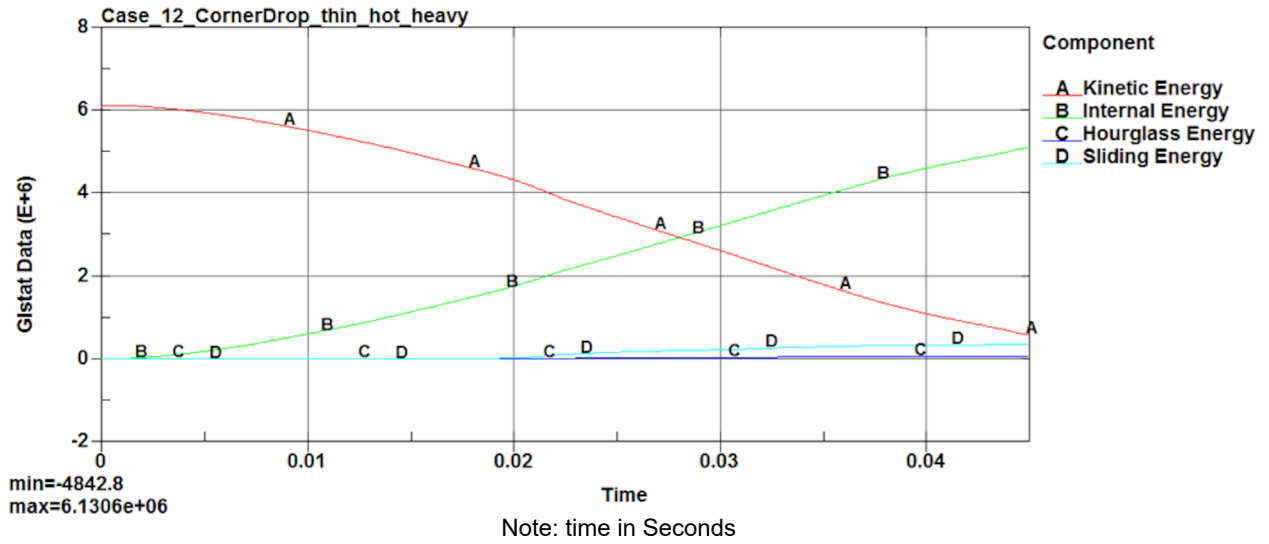


Figure 2.12.1.11-47. Case 12 Impact Energy Plot

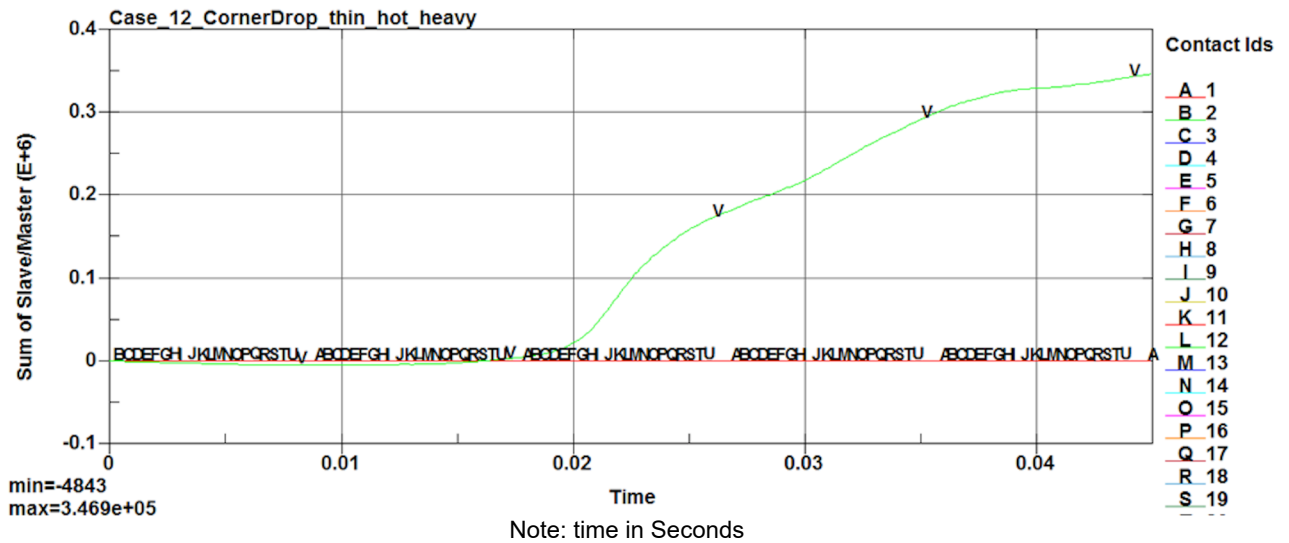


Figure 2.12.1.11-48. Case 12 Interface Sliding Energy Time History

### 2.12.1.11.13. Case 13 Slapdown Drop (5°), Thick Shell, Ambient Condition and Nominal Payload

Case\_13\_SlapDown\_Thick\_ambient\_normal  
Time = 0.035  
Contours of Effective Plastic Strain  
max IP. value  
min=-0.192596, at elem# 387736  
max=0.453218, at elem# 398568

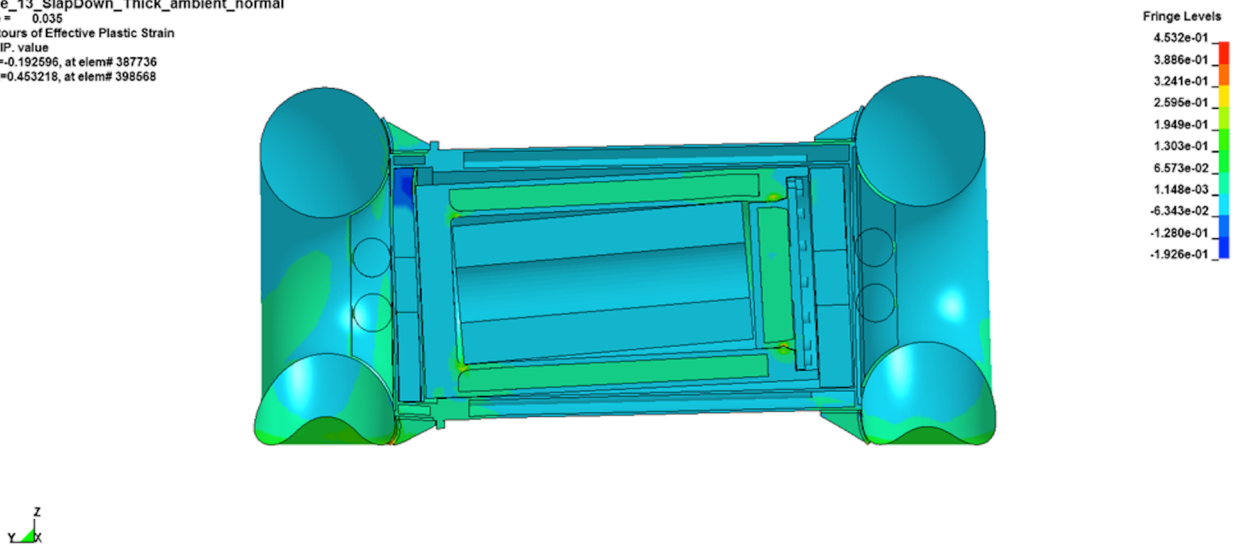


Figure 2.12.1.11-49. Case 13 Deformed Overpack Shape (Effective Plastic Strain)

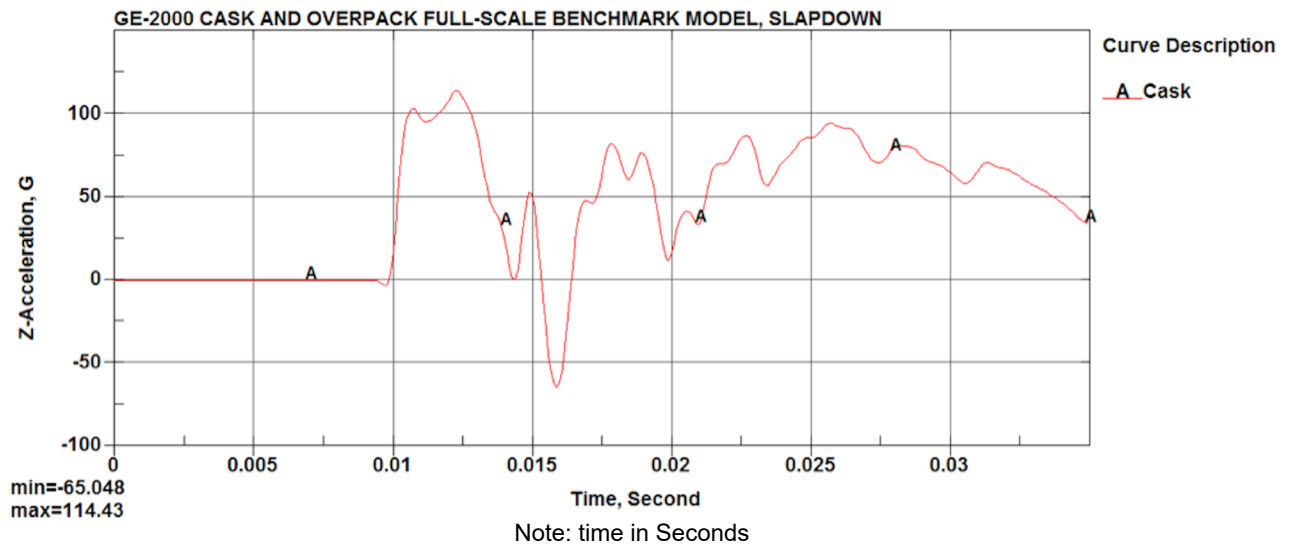


Figure 2.12.1.11-50. Case 13 Payload Acceleration Time History

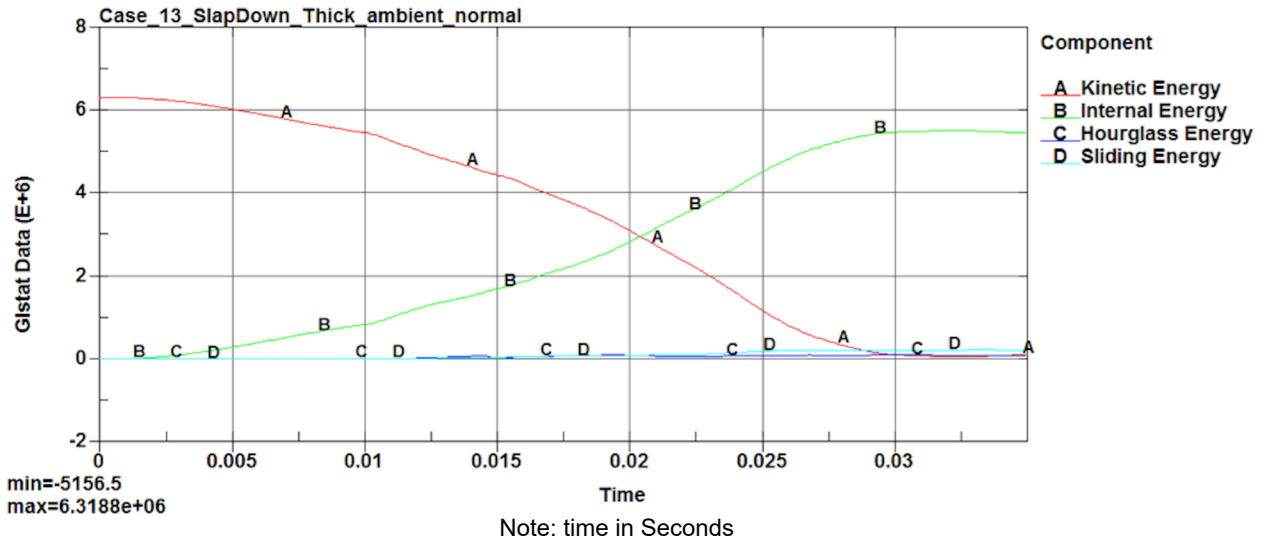


Figure 2.12.1.11-51. Case 13 Impact Energy Plot

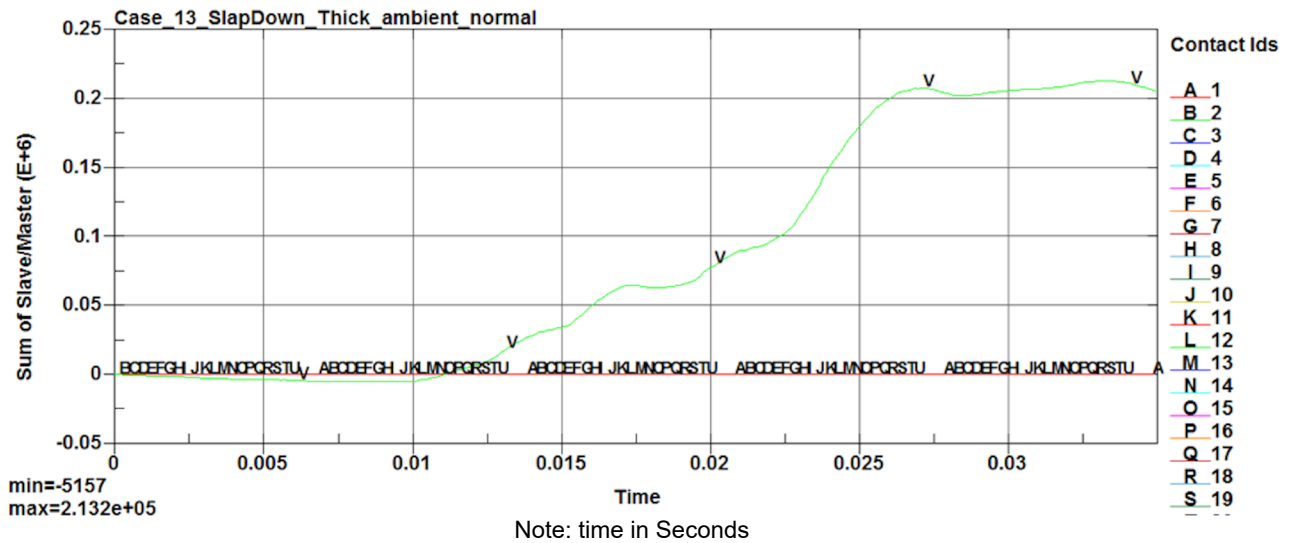


Figure 2.12.1.11-52. Case 13 Interface Sliding Energy Time History



## 2.12.1.11.14. Case 14 Slapdown Drop (10°), Thick Shell, Ambient Condition and Nominal Payload

Case\_14\_SlapDown\_thick\_ambient\_normal  
Time = 0.05  
Contours of Effective Plastic Strain  
max IP. value  
min=-0.582812, at elem# 387736  
max=0.446691, at elem# 777857

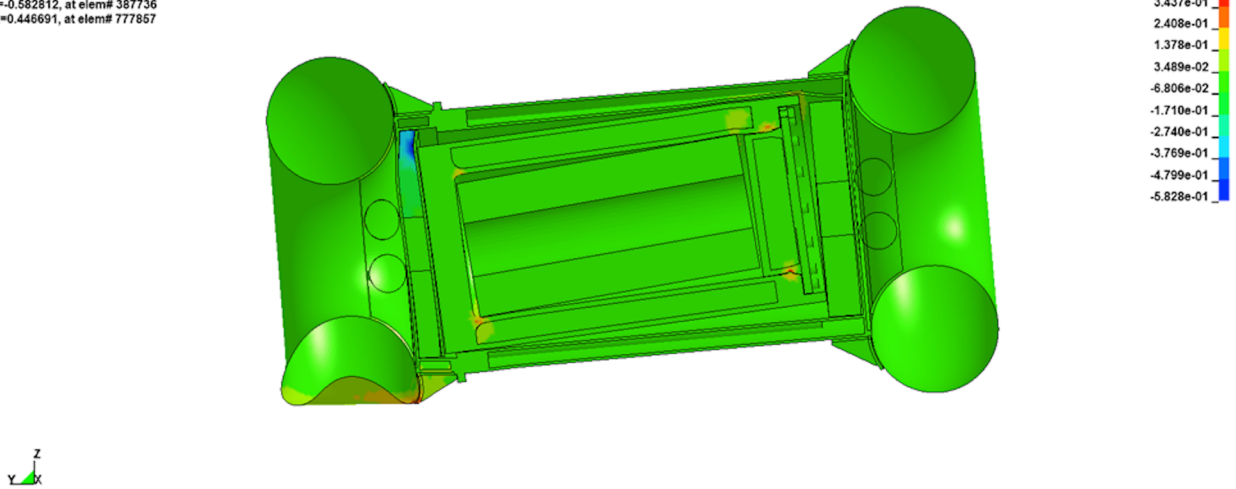


Figure 2.12.1.11-53. Case 14 Deformed Overpack Shape (Effective Plastic Strain)

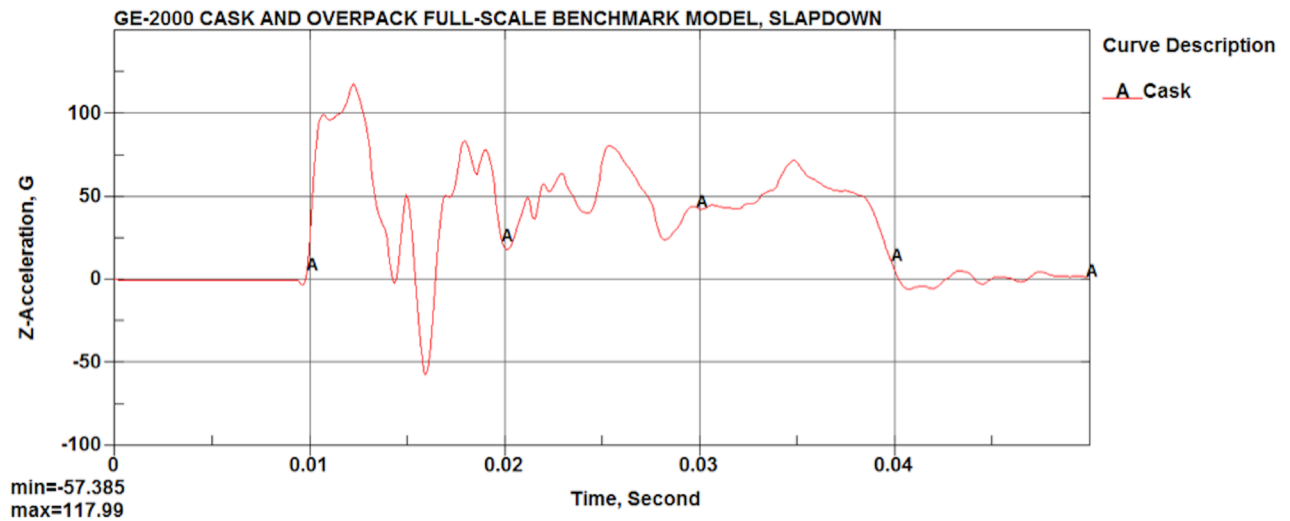


Figure 2.12.1.11-54. Case 14 Payload Acceleration Time History

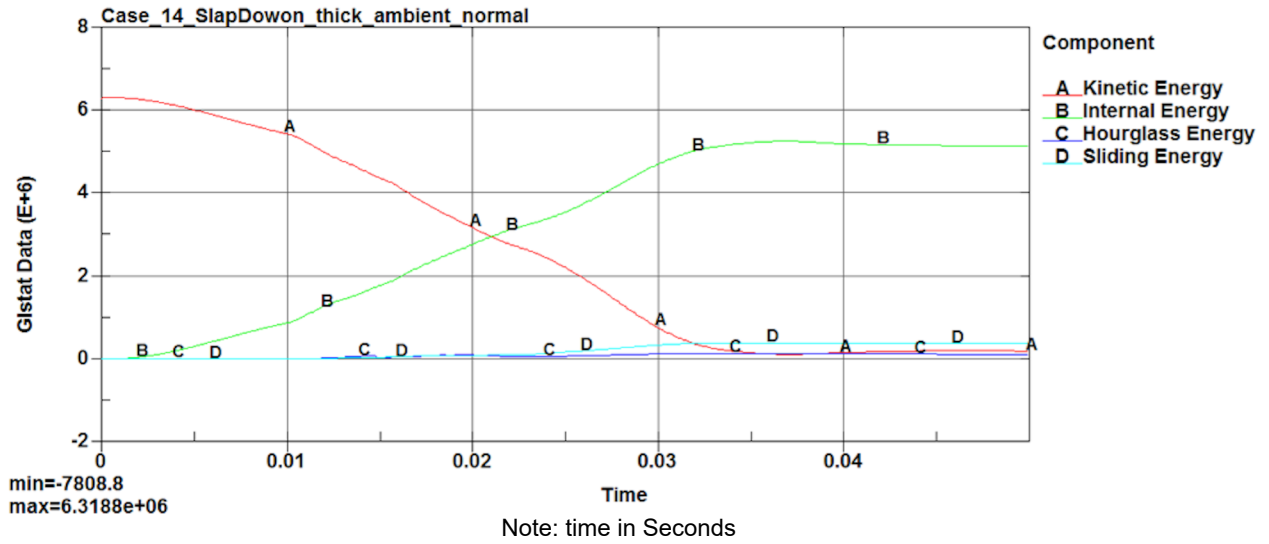


Figure 2.12.1.11-55. Case 14 Impact Energy Plot

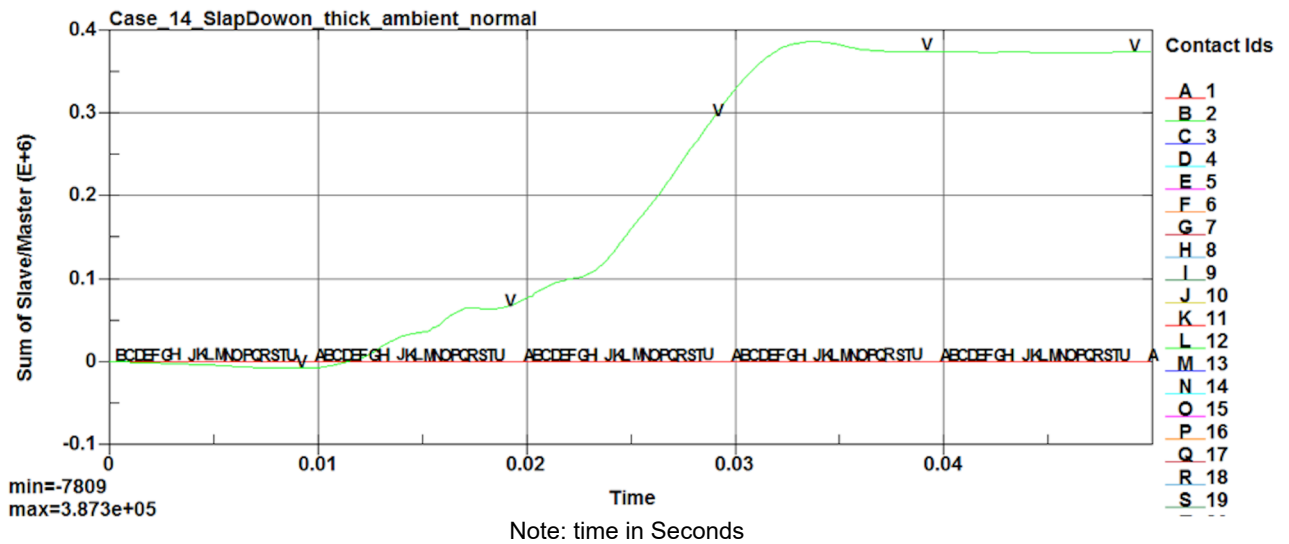
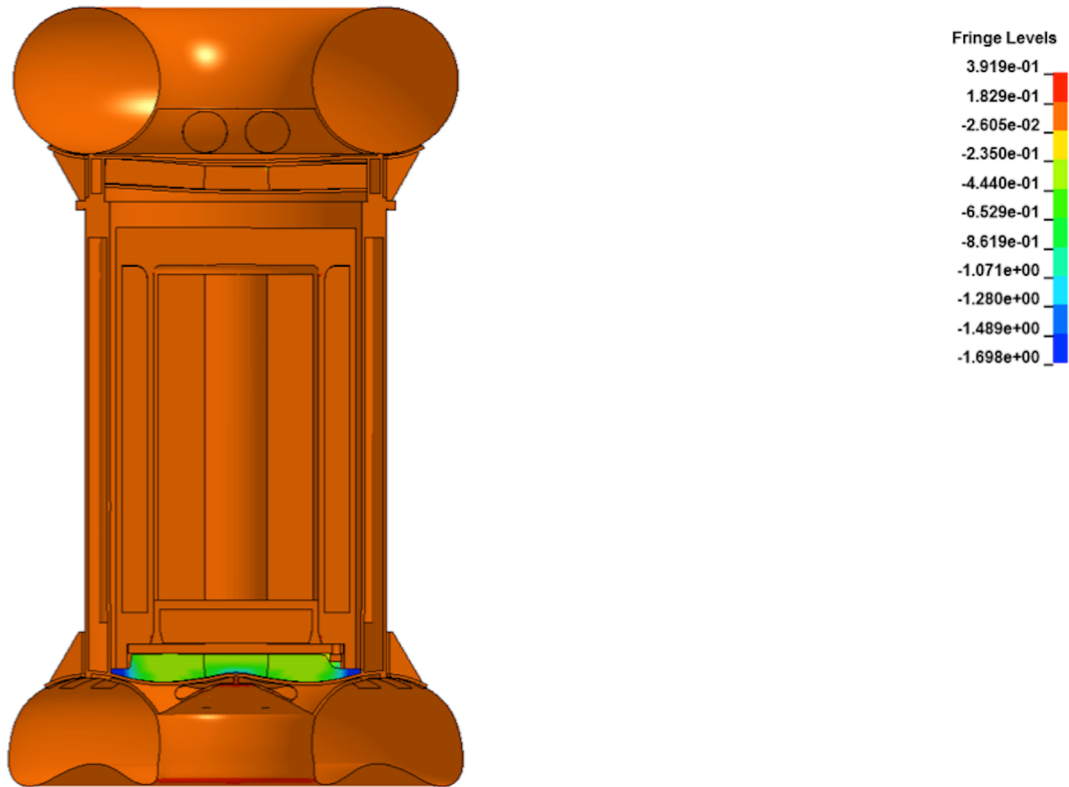
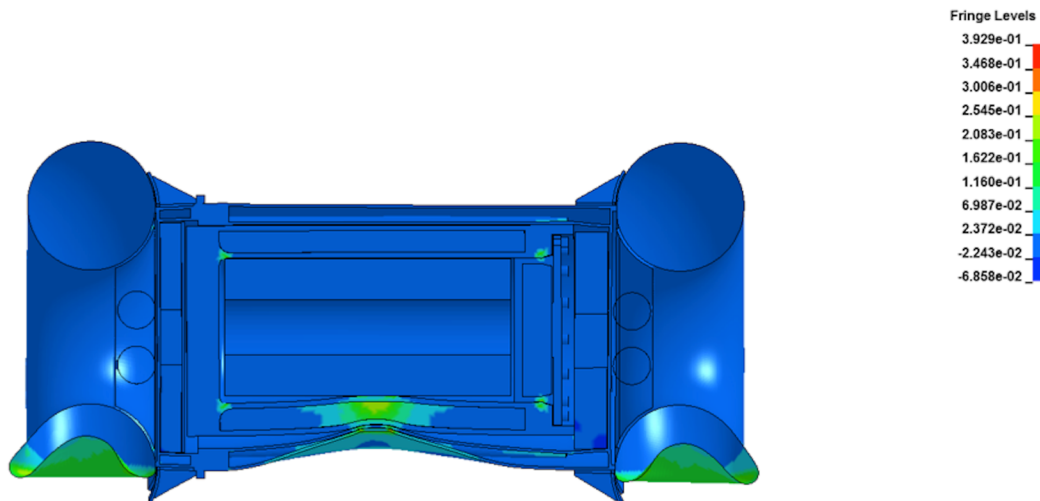


Figure 2.12.1.11-56. Case 14 Interface Sliding Energy Time History

**2.12.1.11.15. Results for 30 ft Drop Followed and 40 in Pin Puncture Drop Sequence**



**Figure 2.12.1.11-57. Strain Contour of Package after 30 ft End Drop and Pin Puncture Sequence**



**Figure 2.12.1.11-58. Strain Contour of Package after 30 ft Side Drop and Pin Puncture Sequence**

### 2.12.1.12. Summary of Impact Analysis Results

Conservative impact analyses of the Model 2000 cask during the NCT and HAC impact events were performed to evaluate the performance of impact limiter design. This report summarizes the results of structural analyses of the Model 2000 Transport Package during NCT per 10 CFR 71.71 and HAC per 10 CFR 71.73. The summary of results for the bounding drop cases are presented in Table 2.12.1-1.

The worst-case HAC accelerations occur during the cold/thick/light side drop and the hot/thin/heavy bottom end drop. For the bottom end drop, the acceleration trend showed that the accelerations dropped until the honeycomb temperature was increased to 400°F and the honeycomb fully compresses. Because the average temperature of the honeycomb is less than 350°F, the honeycomb has sufficient capacity to protect the package during hot conditions.

The results of the evaluations presented in this section show that the Model 2000 overpack provides sufficient protection of the cask and contents.

#### 2.12.1.12.1. Benchmark Tests

The peak accelerations of the benchmark analysis results from Drop Cases 1 through 3 are compared with the drop test results from Section 2.12.5 in Table 2.12.1-14.

**Table 2.12.1-14. Comparison of Benchmark Simulations and Drop Tests Acceleration**

Drop Case No.	Drop Configuration	LS-DYNA Analysis	Drop Test <sup>1</sup> Measurements	Notes
1	30-ft End Drop	130.0 g	408/4 = 102 g	Quarter-scale model
2	30-ft Side Drop	157.0 g	Not available	Instrument failure, No result
3	30-ft Corner Drop	70.9 g	156/4 = 39 g	Quarter-scale model

Note: 1. Section 2.12.5.

The comparison of ¼-scale drop test deformation results and the LS-DYNA benchmark simulation is provided in Table 2.12.1-15.

**Table 2.12.1-15. Comparison of Benchmark Simulations and Drop Tests Deformations**

Drop Case No.	Drop Configuration	LS-DYNA Analysis	Drop Test <sup>1</sup> Measurements
1	30-ft End Drop	3.5 in	2.255×4 = 9.0 in
2	30-ft Side Drop	9.4 in	3.18×4 = 12.7 in
3	30-ft Corner Drop	11.8 in	5.3×4 = 21.2 in

Note: 1. Section 2.12.5.

The comparison of measured accelerations and deformations with LS-DYNA analysis results for each drop orientation shows that the LS-DYNA model is stiffer, which results in higher accelerations.

#### 2.12.1.12.2. Shallow Angle Drops—Slap Down

Two shallow angle drop simulations are also performed. The drop configurations include nominal payload at ambient temperature with thick toroidal shell thickness ( $t=0.76$  inches) to compare with the side-drop test performed for the benchmarking test. The two shallow angles are  $5^\circ$  and  $10^\circ$  slapdown drops that are designated as Drop Cases 13 and 14. The results of shallow angle drops for the  $0^\circ$  (Drop Case 2, side drop),  $5^\circ$  (Drop Case 13) and  $10^\circ$  (Drop Case 14) conclude that the side drop (Drop Case 2) bounds the shallow angle cases with and acceleration of 157 g. Table 2.12.1-16 provides a summary of results for the shallow angle analyses.

**Table 2.12.1-16. Comparison of Shallow Angle Drop Analyses**

Drop Case No.	Shallow Angle Drop Angle	Peak Acceleration
2	$0^\circ$	157.0 g
13	$5^\circ$	115.0 g
14	$10^\circ$	118.0 g

#### 2.12.1.12.3. Pin Puncture

Besides the 30-foot drop configurations, two HAC drop configurations (side drop and end drop) are selected to perform the code-required pin puncture test, where the cask is dropped 30-feet and then followed by a drop height of 40 inches onto a rigid pin 6 inches in diameter. Evaluation of the pin puncture results shows that the maximum strain is limited to local area and will not result in the degradation of the containment boundary. As the figures show, the maximum strain is 39%. However review of results show the maximum strain is limited to local deformation of the overpack. The maximum strain in the outer shell of the cask is 31% and limited to the puncture area. Therefore, no gross deformations of the cask are predicted. Additionally, results for the combined 30-foot impact and pin puncture are used as input for the HAC thermal evaluation.

#### 2.12.1.12.4. Containment Integrity

Based on the analyses presented in the calculation, there are no gross structural deformations of the cask body or containment boundary. Therefore, the containment integrity of the cask is maintained.

### 2.12.2. Lead Slump Calculation

The following sections provide a detailed analysis for lead slump. Section 2.12.2.1 assesses the thermal expansion of the lead at the operating temperature of the lead shielding. Subsequently, in Sections 2.12.2.2 and 2.12.2.3, the shielding capability of the Model 2000 cask is evaluated for the potential of lead slump during a bottom end drop using classic methods to support the shielding analysis assumptions. Further, Sections 2.12.2.4 through 2.12.2.6 assess the thermal contraction of the lead and the lead deformation that results at the NCT extreme cold ambient temperature of  $-40^\circ\text{F}$  ( $-40^\circ\text{C}$ ).

### 2.12.2.1. Thermal Expansion of Lead Shielding at Operating Temperature

It is possible that during fabrication an air gap will develop between the lead and the outer steel shell of the cask (Reference 2-24), which could potentially result in a lead slump condition, meanwhile noting that the lead is inspected during fabrication. However, during NCT the operating temperature of the lead is taken at 500°F (260°C) (see Section 3.3.1.1) to envelope all conditions. The change in the outer radius of the lead shield due to thermal expansion is calculated as follows:

$$r_{\text{final}} = r_0 (1 + \alpha \Delta T) = 18.40 \text{ in (467.4 mm)}$$

where

$$\begin{aligned} r_0 &= 18.25 \text{ in} \\ &= \text{Outside radius of lead shield} \\ \alpha &= 1.90 \times 10^{-5} \text{ in/in/}^\circ\text{F} \\ &= \text{Coefficient of thermal expansion at } 500^\circ\text{F} \\ \Delta T &= 500^\circ\text{F} - 70^\circ\text{F} = 430^\circ\text{F} \\ &= \text{Temperature difference} \end{aligned}$$

NOTE: Coefficient of thermal expansion for lead extrapolated from data provided in Section 2.2.1.

For the outer steel shell the thermal expansion for the inside radius is:

$$r_{\text{final}} = r_i (1 + \alpha \Delta T) = 18.33 \text{ in (465.6 mm)}$$

where

$$\begin{aligned} r_i &= 18.25 \text{ in} \\ &= \text{Inside radius of steel shell} \\ \alpha &= 9.70 \times 10^{-6} \text{ in/in/}^\circ\text{F} \\ &= \text{Coefficient of thermal expansion at } 500^\circ\text{F} \\ \Delta T &= 500^\circ\text{F} - 70^\circ\text{F} = 430^\circ\text{F} \\ &= \text{Temperature difference} \end{aligned}$$

Comparing the final outside radius of the lead shield to the inner radius of the outer shell, the difference is -0.07000 inches (1.800 mm), which indicates that the lead expands more than the steel shell during NCT. Further, this demonstrates the temperature sensitivity of lead and steel at high temperatures. Relative expansion of the lead exceeds the expansion of the steel. Therefore, any existing gap that may have formed during fabrication will close, minimizing the potential for lead slump.

### 2.12.2.2. Compressive Stress in Lead Slump During Bottom End Drop

The previous section shows that the relative change in thermal expansion does not create a void. However, if the lead shield column did not bond to the mating steel shells during the fabrication process, compressive stress will develop in the column. The maximum stress occurs at the bottom of the column and progressively decreases as the elevation increases. The maximum compressive stress is

$$\sigma_{\max} = \frac{P}{A} = 3,613.6 \text{ psi}$$

where

$$\begin{aligned} P &= \text{Total load} \\ &= W \times G = 1.476 \times 10^6 \text{ lb} \\ &= \text{Weight of lead shield} \\ W &= V \times \rho = 9370.2 \text{ lb} \\ V &= \text{Volume of lead shield} \\ &= A \times h = 22870.8 \text{ in}^3 \\ A &= \text{Cross-sectional area of lead shield} \\ &= \pi(r_o^2 - r_i^2) = 408.4 \text{ in}^2 \\ r_o &= \text{Outside radius of lead shield} \\ &= 18.25 \text{ in} \\ r_i &= \text{Inside radius of lead shield} \\ &= 14.25 \text{ in} \\ h &= \text{Height of lead column} \\ &= 56 \text{ in} \\ \rho &= \text{Density of lead} \\ &= 0.4097 \text{ lb/in}^3 \\ G &= \text{End drop acceleration} \\ &= 157.5 \text{ g} \end{aligned}$$

NOTE: Value for the height of the lead column is rounded up to the nearest integer for conservatism.

Table 2.12.2-1 shows the stresses varying along the length of the lead column. The yield strength at 500°F is 189 psi. However, lead is sensitive to the strain-rate effects of the material. During the end drop, the estimated strain-rate is 12 in/in/sec (see Section 2.12.1). The yield strength varies from 823 psi at 0.002 in/in to 6,279 psi at 0.30 in/in. Therefore, during the end drop if yielding of the lead occurs it is localized to a small region near the bottom of the column.

NOTE: Yield strength of lead shielding at 500°F is extrapolated from data provided in Section 2.2.1.

### 2.12.2.3. Elastic Deformation During Bottom Impact

The elastic deformation is calculated assuming the cask lead shield column is unsupported by the steel inner and outer shells during an end drop event. The response of the lead shield is determined by multiplying the shield weight by the HAC end drop acceleration of 1,57.5 g. Therefore, an estimate of lead slump during HAC free drop conditions is (Reference 2-19):

$$y_{\max} = \frac{P}{k} = 0.075 \text{ in (1.91 mm)}$$

where

$$\begin{aligned} k &= \text{Effective stiffness of the lead shield} \\ &= \frac{A \times G}{h} = 1.98 \times 10^7 \text{ lb/in} \\ G &= \text{Bulk modulus of lead} \\ &= \frac{E}{3(1-2\nu)} = 2.72 \times 10^6 \text{ psi} \\ A &= \text{Cross-sectional area of lead shield} \\ &= \pi(r_o^2 - r_i^2) = 408.4 \text{ in}^2 \\ W &= \text{Weight of lead shield} \\ &= 9370.2 \text{ lb} \\ P &= \text{Total load} \\ &= W \times g = 1.476 \times 10^6 \text{ lb} \\ g &= \text{End drop acceleration} \\ &= 157.5 \text{ g} \\ h &= \text{Height of lead column} \\ &= 56 \text{ in} \\ E &= 1.63 \times 10^6 \text{ psi} \\ &= \text{Modulus of elasticity of lead at 500°F} \\ \nu &= \text{Poisson's ratio for lead} \\ &= 0.4 \end{aligned}$$

The calculation shows that this estimate of lead slump is small for an unsupported lead shield. With the lead fully supported by the inner and outer shells of the cask, the actual lead slump is even smaller.

**Table 2.12.2-1. Compressive Stress in Lead Shield**

Column Height from Bottom	Compressive Stress / G (psi)	Compressive Stress (psi)
55.0	0.4	64.5
50.0	2.5	387.2
45.0	4.5	709.8
40.0	6.6	1032.4
35.0	8.6	1355.1
30.0	10.7	1677.7
25.0	12.7	2000.4
20.0	14.7	2323.0



#### 2.12.2.4. Axial Thermal Expansion at NCT Extreme Cold Ambient Temperature

A small gap occurs at the top of the lead column when the cask is exposed to the extreme cold temperature of -40°F (-40°C) per the NRC requirements of 10 CFR 71.71 (c)(2). This is due to changes at the molecular level that cause the materials to contract. This reduction in the height of the lead shield is represented by the following equation:

$$h_{\text{lead}} = h_{0\text{-lead}} (1 + \alpha_{\text{lead}} \Delta T) = 55.904 \text{ in (1420.0 mm)}$$

where

$$\begin{aligned} h_{0\text{-lead}} &= \text{Initial lead shield height} \\ &= 56 \text{ in} \\ \alpha_{\text{lead}} &= \text{Lead coefficient of thermal expansion at -40°F} \\ &= 1.56\text{E-}^{05} \text{ in/in/°F} \\ \Delta T &= \text{Temperature difference} \\ &= -40°F - 70°F = -110°F \end{aligned}$$

The same calculation can be made to determine the reduction in the height of the steel shells:

$$h_{\text{steel}} = h_{0\text{-steel}} (1 + \alpha_{\text{steel}} \Delta T) = 55.95 \text{ in (1421.1 mm)}$$

where

$$\begin{aligned} h_{0\text{-steel}} &= \text{Initial steel shell height} \\ &= 56 \text{ in} \\ \alpha_{\text{steel}} &= \text{Steel coefficient of thermal expansion at -40°F} \\ &= 8.09\text{E-}^{06} \text{ in/in/°F} \\ \Delta T &= \text{Temperature difference} \\ &= -40°F - 70°F = -110°F \end{aligned}$$

#### 2.12.2.5. Radial Thermal Expansion at NCT Extreme Cold Ambient Temperature

The radial gaps that occur during exposure to NCT extreme cold conditions can also be calculated in a similar manner by taking the initial radius prior to exposure and then adding the change in radius due to thermal expansion. The outside radius of the lead shield at -40°F is:

$$r_o = r_{0\text{-outer}} (1 + \alpha_{\text{lead}} \Delta T) = 18.22 \text{ in (462.8 mm)}$$

where

$$\begin{aligned} r_{0\text{-outer}} &= \text{Initial outside radius of the lead shield} \\ &= 18.25 \text{ in (463.6 mm)} \end{aligned}$$

Accordingly, the inside radius of the lead shield at -40°F is:

$$r_i = r_{0\text{-inner}} (1 + \alpha_{\text{lead}} \Delta T) = 14.23 \text{ in (361.3 mm)}$$

where

$$\begin{aligned} r_{0\text{-inner}} &= \text{Initial inside radius of the lead shield} \\ &= 14.25 \text{ in (362 mm)} \end{aligned}$$

Now the decrease in radius is evaluated for the steel shells starting with the inside radius of the outer steel shell at -40°F:

$$R_o = R_{0\text{-outer}} (1 + \alpha_{\text{steel}} \Delta T) = 18.23 \text{ in (463.1 mm)}$$

where

$$\begin{aligned} R_{0\text{-outer}} &= \text{Initial inside radius of the outer steel shell} \\ &= 18.25 \text{ in (463.6 mm)} \end{aligned}$$

The decrease in the outside radius of the inner steel shell at -40°F is:

$$R_i = R_{0\text{-inner}} (1 + \alpha_{\text{steel}} \Delta T) = 14.24 \text{ in (361.6 mm)}$$

where

$$\begin{aligned} R_{0\text{-inner}} &= \text{Initial outside radius of the inner steel shell} \\ &= 14.25 \text{ in (362 mm)} \end{aligned}$$

#### 2.12.2.6. Lead Slump Due to Impact After NCT Extreme Cold Ambient Temperature

A small gap occurs during extreme cold exposure due to the contraction of components in relation to each other as determined by the calculations in the previous section. In order to determine the magnitude of lead slump, the reduced height of the lead column based on the net gap is calculated and then the difference between the reduced height of the lead column and the height of the annular region is taken. The volume of the lead column at the extreme cold conditions (-40°F) is:

$$\begin{aligned} V_{f\text{-lead}} &= A_{f\text{-lead}} \times h_{\text{lead}} \\ &= (407.011 \text{ in}^2 \times 55.904 \text{ in}) = 22,753.59 \text{ in}^3 (3.73\text{E}+08 \text{ mm}^3) \end{aligned}$$

where

$$\begin{aligned} A_{f\text{-lead}} &= \pi(r_o^2 - r_i^2) \\ &= \pi[(18.22 \text{ in})^2 - (14.23 \text{ in})^2] = 407.011 \text{ in}^2 (262,587.22 \text{ mm}^2) \end{aligned}$$

The cross-sectional area of the annulus between the outer and inner steel shells at -40°F is:

$$\begin{aligned} A_{\text{annulus}} &= \pi(R_o^2 - R_i^2) \\ &= \pi[(18.23 \text{ in})^2 - (14.24 \text{ in})^2] = 407.68 \text{ in}^2 (263,018.83 \text{ mm}^2) \end{aligned}$$

The reduced height of the lead column when taking into account impact after contraction of components is:

$$\begin{aligned} h_{\text{final}} &= \frac{V_f}{A_{\text{annulus}}} \\ &= \frac{22,753.59 \text{ in}^3}{407.68 \text{ in}^2} = 55.81 \text{ in (1417.57 mm)} \end{aligned}$$

Taking the difference between the reduced height of the lead shielding and the height of the annular region, the lead deformation due to impact after NCT extreme cold (-40°F) is:

$$\begin{aligned} h_{\text{slump}} &= h_{\text{steel}} - h_{\text{final}} \\ &= 55.95 \text{ in} - 55.81 \text{ in} = 0.14 \text{ in (3.56 mm)} \end{aligned}$$

### 2.12.3. Lifting and Tie-Down Analysis

#### 2.12.3.1. Model 2000 Transport Package Lifting Analysis

The purpose and scope of this analysis is to demonstrate the structural integrity of the lifting ears and lid-lifting lug on the Series 2000 shielded shipping casks.

There are two types of ear designs employed during the handling of the Model 2000 cask, standard and auxiliary (see Figure 2.12.3-1). The ear design identified as standard is used for crane and fork truck lifting, and only one pair is required for these operations. The auxiliary ear is used in crane lifting only, and two pairs or four ears are required. The user may combine the different types of ears as follows:

1. 2 Standard/2 Auxiliary
2. 4 Auxiliary
3. 2 Standard

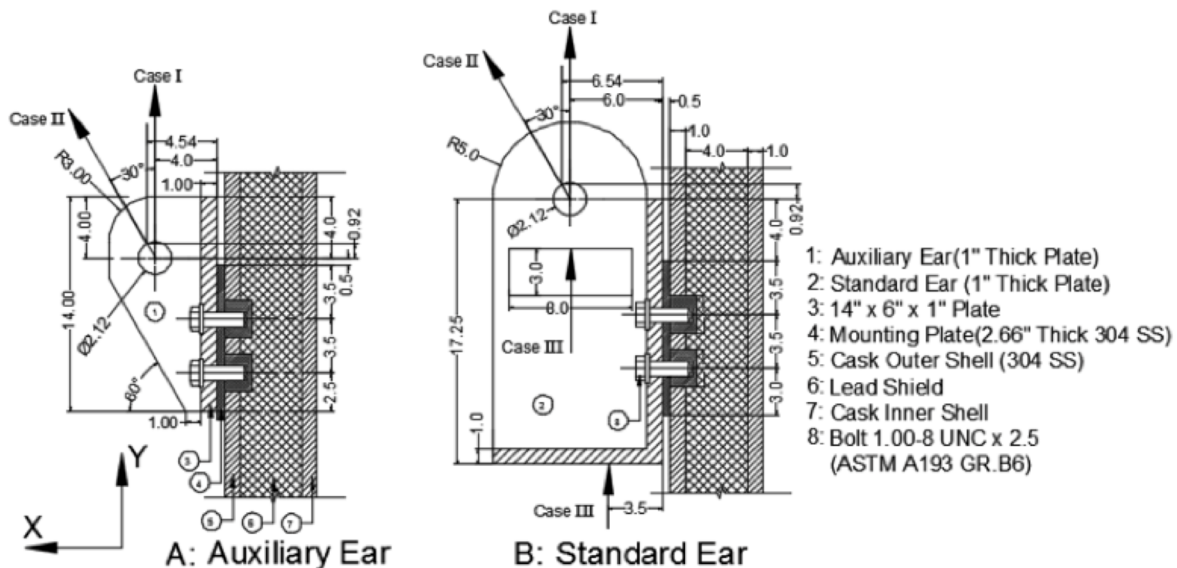


**Figure 2.12.3-1. Structural Locations for Ear Analysis**

Both ear designs (Auxiliary and Standard) are attached to the cask outer shell by means of four ASTM A193-B6 1-8 UNC-2-1/2 attaching bolts; only two bolts are shown. Also on this figure, the line of action of the different lifting forces is drawn. The different lifting forces are: Case I, straight up by crane; Case II, angular lift 30° from vertical, also by crane; and Case III, fork truck lift at two different points on the standard ear only. This analysis mainly considers Case II and I. The loading conditions are the following:

- The design rated load, W, shall be 23,630 pounds. This includes the dead weight of the cask (1 body, lid, 2 standard ears, and 2 auxiliary ears) and the cask payload including the liner.
- The two pairs of auxiliary ears (Auxiliary) are to support 3W such that the lifting cable does not make an angle of more than +30° measured from the vertical.

- The pair of standard ears (Standard) is to support 3W.
- These ears are removed from the cask during transport and are shipped separately.

Material properties are based upon 250°F for the outer cask. The 249°F temperature is the maximum temperature under normal conditions for the cask outer surface. Both types of ears, standard and auxiliary, and the cask outer shell are ASTM A240, Type 304 stainless steel. The attaching bolt material is ASTM A193-B6.

The standard ear individual load is obtained by dividing the weight of the cask and content (23,630 lbs.) by 2 (only two standard ears are used), and multiplying the resulting value by 3. The auxiliary ear load is obtained in a similar manner with the weight divided by 4 instead of 2 because 4 ears are used when this design is employed. Case III represents the fork truck loading condition on the standard ear, and it has a magnitude equal to that of Case I for the standard ear. Case III loading is not shown in Figure 2.12.3-2.

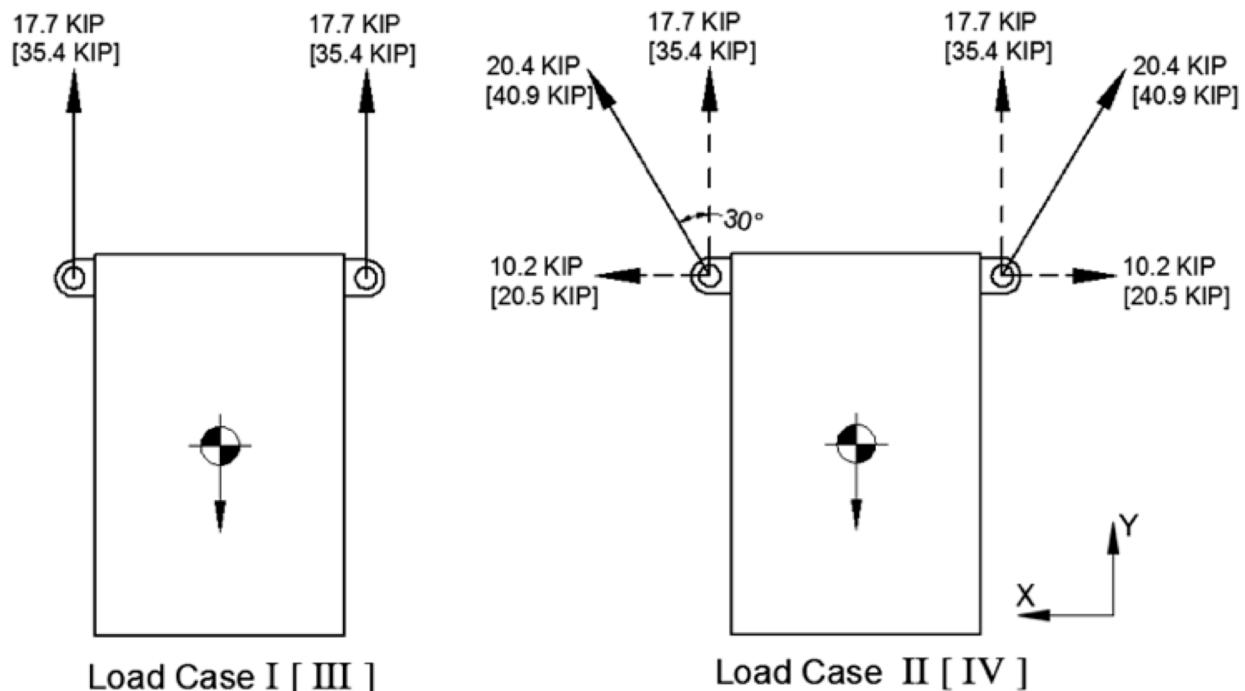


**Figure 2.12.3-2. Magnitude and Direction of Loading in Model 2000 Cask**

The following modes of failure are investigated for both ear designs:

- Shear tearout of lifting hole
- Tensile failure of ear plate
- Bearing of shackle pin on ear
- Yielding of weld joint
- Yielding of attaching bolt
- Shearing of bolt threads
- Shearing of tapped threads
- Yielding of cask outer shell

- SHEAR TEAR-OUT OF LIFTING HOLE-AUXILIARY AND STANDARD DESIGNS

Auxiliary Ear Design

For Load Case I, the shear tearout stress is computed as follows:

$$\tau = \frac{F}{A} \quad \text{Reference 2-25 page 89.}$$

where

$$F = 17.7 \text{ kip (see Figure 2.12.3-2) and}$$

$$A = \text{cross sectional area along the force line of action}$$

$$= \left(4 - \frac{2.12}{2}\right) \times 1 \quad (\text{see Figure 2.12.3-1}) = 2.94 \text{ in}^2$$

$$\tau = \frac{F}{A} = \frac{17.7}{2.94} = 6.02 \text{ ksi} < 15 \text{ ksi}$$

Standard Ear Design

For Load Case I, the shear tearout stress is:

$$\tau = \frac{F}{A} = \frac{35.4}{\left(5 - \frac{2.12}{2}\right) \times 1} = 8.98 \text{ ksi} < 15 \text{ ksi}$$

- TENSILE FAILURE OF EAR PLATE

Auxiliary Ear Design

In order to compute tensile failure for Load Case II, the internal forces that react to the lifting force are resolved into planes containing the minimum ligament cross-sectional area, as illustrated in Figure 2.12.3-3.

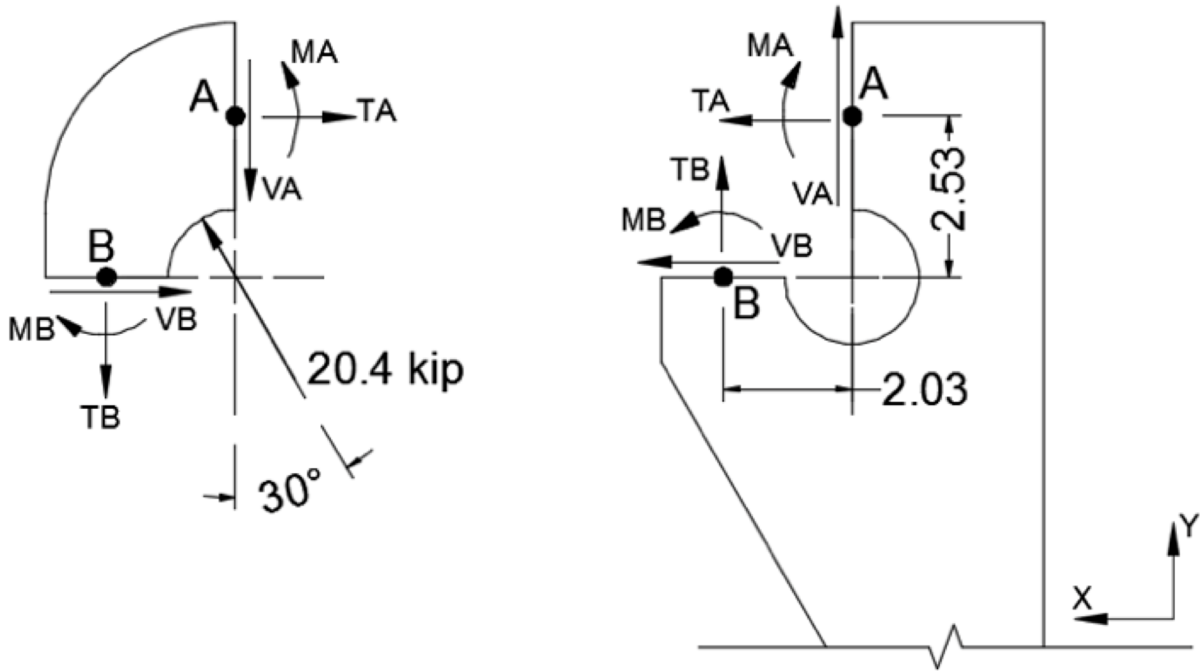


**Figure 2.12.3-3. Ear Hole Cross Section**

$$\begin{aligned} FH &= 20.4 (\sin 30^\circ) = 10.2 \text{ kip} \\ FV &= 20.4 (\cos 30^\circ) = 17.7 \text{ kip} \end{aligned}$$

Equilibrium:

$$\text{Eq. I} \quad \sum M_o = 0 = MA - MB - 2.53 TA + 2.03 TB$$

$$\text{Eq. II} \quad \sum FV = 0 = 17.7 - VA - TB$$

$$\text{Eq. III} \quad \sum FH = 0 = 10.2 - TA - VB$$

This is a statically indeterminate problem; however, by making some conservative simplifying assumptions, a solution may be obtained without resorting to indeterminate analysis methods. For the evaluation of primary stresses, we may conservatively assume  $MA = MB = 0$ . Also, on the basis of relative stiffness,  $TA > VB$ ; consequently, it may be conservatively assumed that  $TA = VB$ . Therefore, we may write the following:

From Eq. III,

$$TA = VB = \frac{10.2}{2} = 5.1 \text{ kip}$$

From Eq. I,

$$TB = \frac{2.53}{2.03} TA = 6.35 \text{ kip}$$

From Eq. II,  
$$V_A = 17.7 - T_B = 11.35 \text{ kip}$$

The principal stresses will now be calculated at point A.

From Reference 2-25, page 81, the principal stresses are calculated using:

$$\begin{aligned}\sigma_1, \sigma_2 &= \frac{\sigma}{2} \pm \sqrt{\left(\frac{\sigma}{2}\right)^2 + \tau^2} \\ \sigma &= \frac{T_A}{A} = \frac{5.1}{2.94} = 1.735 \text{ ksi} \\ \tau &= \frac{V_A}{A} = \frac{11.35}{2.94} = 3.86 \text{ ksi} \\ \sigma_1 &= \frac{1.735}{2} + \sqrt{\left(\frac{1.735}{2}\right)^2 + 3.86^2} = 4.82 < 23.7 \text{ ksi}\end{aligned}$$

### Standard Ear Design

#### Load Case I or III

Standard ear dimensions and loading are shown in Figure 2.12.3-4. The critical tensile section is at Section X-X, see Figure 2.12.3-4. The exact force distribution cannot be determined without a detailed analysis that would include all of the stiffness characteristics (e.g., a finite element analysis). However, it can be deduced that the limiting load at the critical section (i.e., point "A") will not exceed P/2. Then the tensile stress is:

$$\sigma_T = \frac{P/2}{A} = \frac{35.4/2}{1 \times 1} = 17.7 \text{ ksi} < 23.7 \text{ ksi}$$

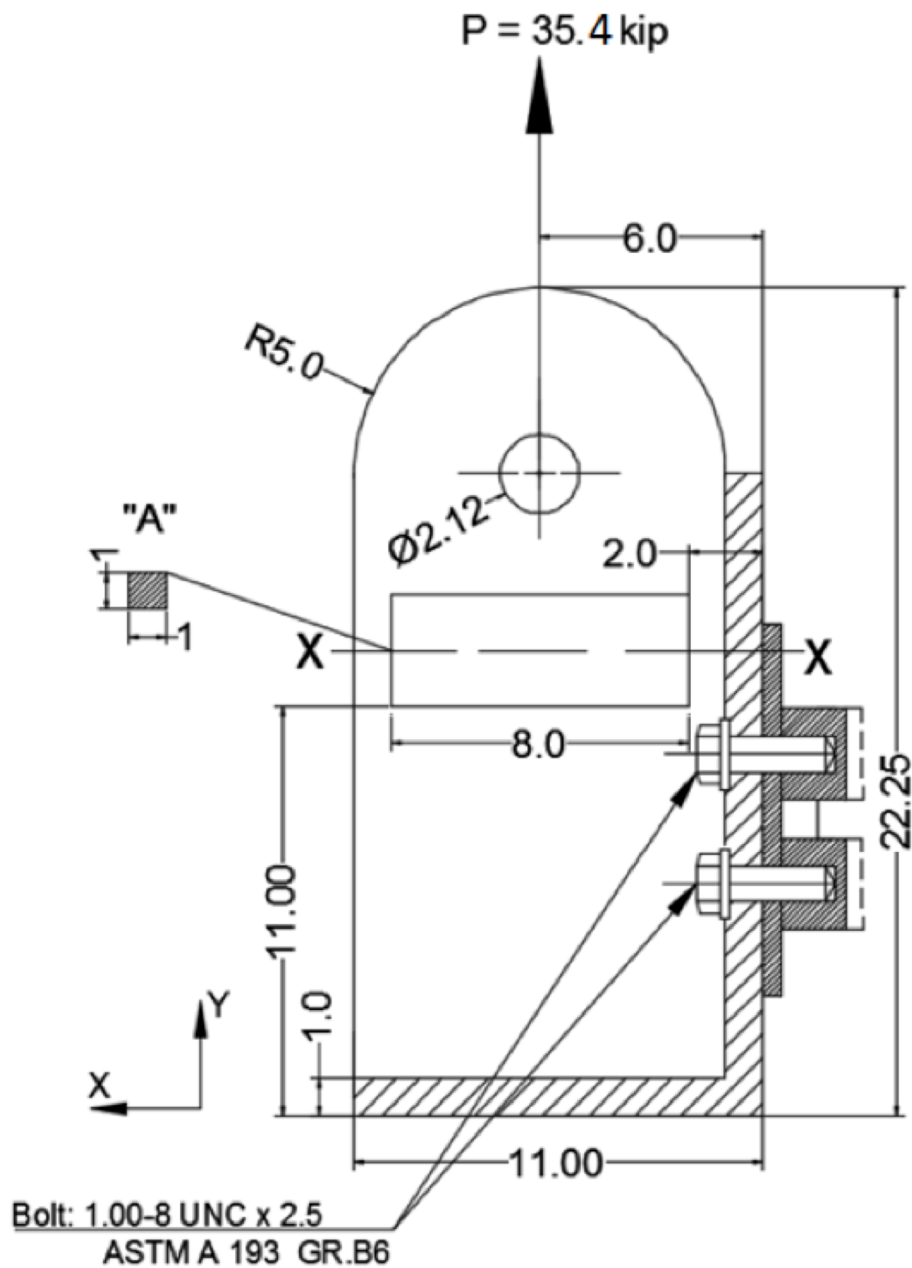


Figure 2.12.3-4. Standard Ear Load Case I or III



- BEARING OF SHACKLE PIN ON EAR

Auxiliary Ear Design

The bearing stress is computed assuming that the force is uniformly distributed over the projected contact area of the pin. This gives a stress:

$$\sigma = \frac{F}{A}$$

Where the projected area for the pin is  $A = t \times d$ . Here,  $t$  is the thickness of the ear plate (1") and  $d$  is the pin diameter (2").

$$\sigma = \frac{20.4}{1 \times 2} = 10.2 \text{ ksi} < 23.7 \text{ ksi}$$

Standard Ear Design

Case I

$$\sigma = \frac{35.4}{1 \times 2} = 17.7 \text{ ksi} < 23.7 \text{ ksi}$$

Case III

$$\sigma = \frac{35.4}{1 \times 7.5} = 4.72 \text{ ksi} < 23.7 \text{ ksi}$$

- YIELDING OF WELD JOINTS

Auxiliary Ear Design

Figure 2.12.3-5 shows a free-body diagram of the ear with the lifting force acting through the center of the hole for Load Case I and Case II. The center of gravity of the weld group and of the bottom of the bracket point A is G. The force  $F_G$  is the force of the weld group acting on the ear. Because  $F_G$  has a different line of action than the lifting force, there is also a moment  $M$ .

Load Case I

The moment  $M$  produces a bending stress in the welds. The force  $F_G$  produces shear throughout the weld. These effects are:

$$M = 17.7 \times 3 = 53.10 \text{ k-in}$$

$$F_G = 17.7 \text{ kip}$$

- WELD GEOMETRY AND CROSS SECTION PROPERTIES

Weld throat area ( $A_w$ )

$$A_w = 1.414 (0.375)(6.75 + 2.0 + 2.25) = 5.833 \text{ in}^2$$

Centroid of weld group (G)

$$\bar{Y} = \frac{\sum_1^3 (\bar{Y}_i A_i)}{\sum_1^3 A_i} = \frac{((1.125 \times 2.25 \times 0.375) + (4.75 \times 2 \times 0.375) + (10.625 \times 6.75 \times 0.375))}{(2.25 \times 0.375 + 2 \times 0.375 + 6.75 \times 0.375)} = 7.614 \text{ in}$$

Unit moment of inertia ( $I_u$ ):

$$\begin{aligned} I_u &= \sum (I_o + A_i d_i^2) \\ &= 2 \times \left\{ \left( \frac{2.25^3}{12} + 2.25 \times 6.488^2 \right) + \left( \frac{2^3}{12} + 2 \times 2.863^2 \right) + \left( \frac{6.75^3}{12} + 6.75 \times 3.012^2 \right) \right\} \\ &= 399.17 \text{ in}^3 \end{aligned}$$

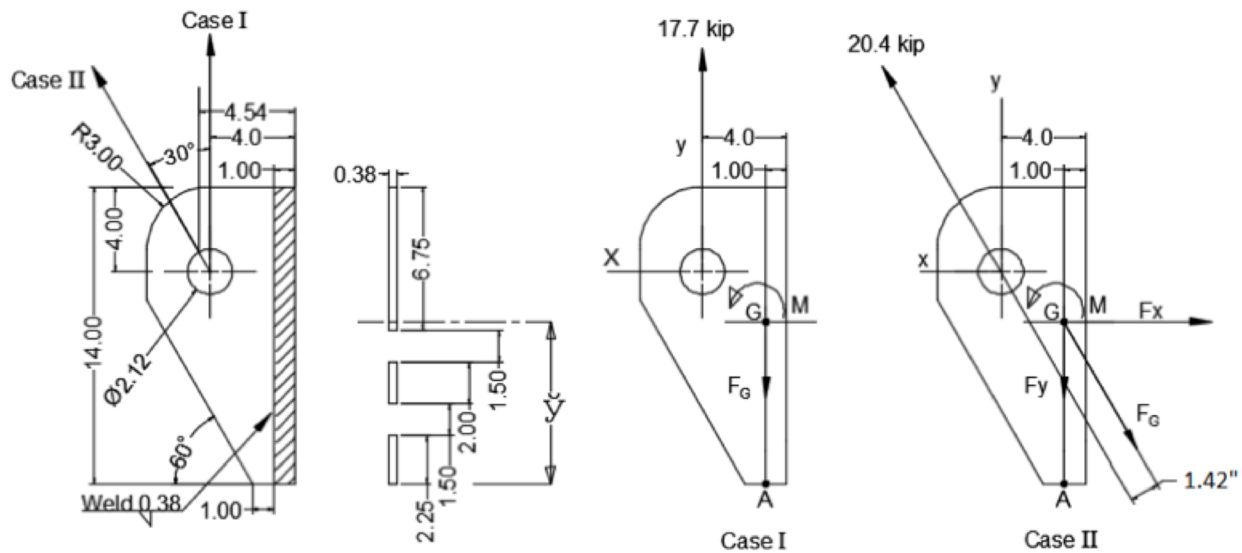


**Figure 2.12.3-5. Auxiliary Ear, Case I and Case II Weld Stresses**

Then the moment of inertia about an area through G parallel to area Z is:

$$I = 0.707 h I_u = 0.707 (0.375) (399.17) = 105.83 \text{ in}^4$$

For the weld metal the normal stress at point A:

$$\sigma_x = \frac{Mc}{I} = \frac{53.10(7.614)}{105.83} = 3.82 \text{ ksi}$$

The shear stress is:

$$\tau_{xy} = \frac{F}{A} = \frac{17.7}{5.833} = 3.03 \text{ ksi}$$

The resulting Von Mises stress in the weld metal is:

$$\sigma' = \sqrt{\sigma_x^2 + 3\tau_{xy}^2} = \sqrt{3.82^2 + 3(3.03)^2} = 6.5 \text{ ksi} < 75 \text{ ksi}$$

### CALCULATION OF STRESS IN THE PARENT METAL:

The area subject to shear is :

$$A = 0.375 (6.75 + 2.0 + 2.25) = 4.125 \text{ in}^2$$

$$\tau_{xy} = \frac{17.7}{4.125} = 4.29 \text{ ksi}$$

The section modulus of the ear at the weld interface is:

$$\frac{I}{C} = \frac{hI_u}{C} = \frac{0.375 \times 0.5 \times 399.17}{7.614} = 9.83 \text{ in}^3$$

Thus, the tensile stress at A in the parent metal is:

$$\sigma_x = \frac{M}{I/C} = \frac{53.10}{9.83} = 5.4 \text{ ksi}$$

$$\sigma' = \sqrt{\sigma_x^2 + 3\tau_{xy}^2} = \sqrt{5.4^2 + 3(4.29)^2} = 9.19 \text{ ksi} < 23.7 \text{ ksi}$$

### Load Case II

Figure 2.12.3-5 (Case II) shows a free body diagram of the ear for the Load Case II.

The moment M produces a bending stress in the welds.

The force component Fx produces tension throughout the weld.

The force component Fy produces shear throughout the weld.

These effects are:

$$M = 20.4 (1.42) = 28.97 \text{ k-in.}$$

$$F_x = 10.2 \text{ kip}$$

$$F_y = 17.7 \text{ kip}$$

$$A_w = [(2.25 + 2 + 6.75) \times 0.375 \times 0.707] \times 2 = 5.833 \text{ in}^2$$

At the point A the bending stress and tensile stress due to Fx add. For the weld metal the total normal stress is:

$$\sigma_x = \frac{F_x}{A} + \frac{M_c}{I} = \frac{10.2}{5.83} + \frac{28.97(7.614)}{105.84} = 3.83 \text{ ksi}$$

The shear stress is:

$$\tau_{xy} = \frac{F_y}{A} = \frac{17.7}{5.83} = 3.03 \text{ ksi}$$

Thus, the Von Mises stress in the weld is:

$$\sigma' = \sqrt{\sigma_x^2 + 3\tau_{xy}^2} = \sqrt{3.83^2 + 3(3.03)^2} = 6.51 \text{ ksi} < 23.7 \text{ ksi}$$

The stresses in the parent metal are:

$$A_{pm} = (2.25 + 2 + 6.75) \times 0.375 = 4.125$$

$$\tau_{xy} = \frac{F_y}{A} = \frac{17.7}{4.125} = 4.29 \text{ ksi}$$

$$\sigma_x = \frac{F_x}{A} + \frac{M}{I/C} = \frac{10.2}{4.125} + \frac{28.97}{9.83} = 5.42 \text{ ksi}$$

$$\sigma' = \sqrt{\sigma_x^2 + 3\tau_{xy}^2} = \sqrt{5.42^2 + 3(4.29)^2} = 9.2 \text{ ksi} < 23.7 \text{ ksi}$$

### Standard Ear Design

Figure 2.12.3-6 shows a detailed sketch of the standard ear design. It includes dimensions, weld lines identification diagram, and a free body diagram of the ear plate for load conditions Case I and Case II. The investigation of stress on the welds is conducted conservatively by considering only welds A and B are active, in this part the welds are analyzed for both load conditions Case I and Case II. Case III was not analyzed because the resultant force in this case acts along the same line of action as the force in Case I.

### Load case I

Figure 2.12.3-6 (Case I) shows a free body diagram of the standard ear for Load Case I.

Centroid of weld group ( $\bar{Y}$ )

$$\bar{Y} = \frac{\sum_1^2 (\bar{Y}_i A_i)}{\sum_1^2 A_i} = \frac{(2.25 \times 0.375 \times 0.19) + (15.87 \times 0.375 \times 7.935)}{2.25 \times 0.375 + 15.87 \times 0.375} = 6.97 \text{ in}$$

Unit moment of inertia ( $I_u$ ):

$$\begin{aligned} I_u &= \sum (I_o + A_i d_i^2) \\ &= 2 \times \left\{ \left( \frac{15.87^3}{12} + 15.87 \times (7.935 - 6.97)^2 \right) + (2.25 \times 6.97^2) \right\} = 914.13 \text{ in}^3 \end{aligned}$$

Then the moment of inertia about an axis through G parallel to axis Z through the weld minimum effective throat is:

$$I = 0.707 h I_u = 0.707 \times (0.375) \times 914.13 = 242.36 \text{ in}^4$$

For the weld metal the normal stress at point A:

$$\sigma_x = \frac{Mc}{I} = \frac{35.4 (5) 6.97}{242.36} = 5.09 \text{ ksi}$$

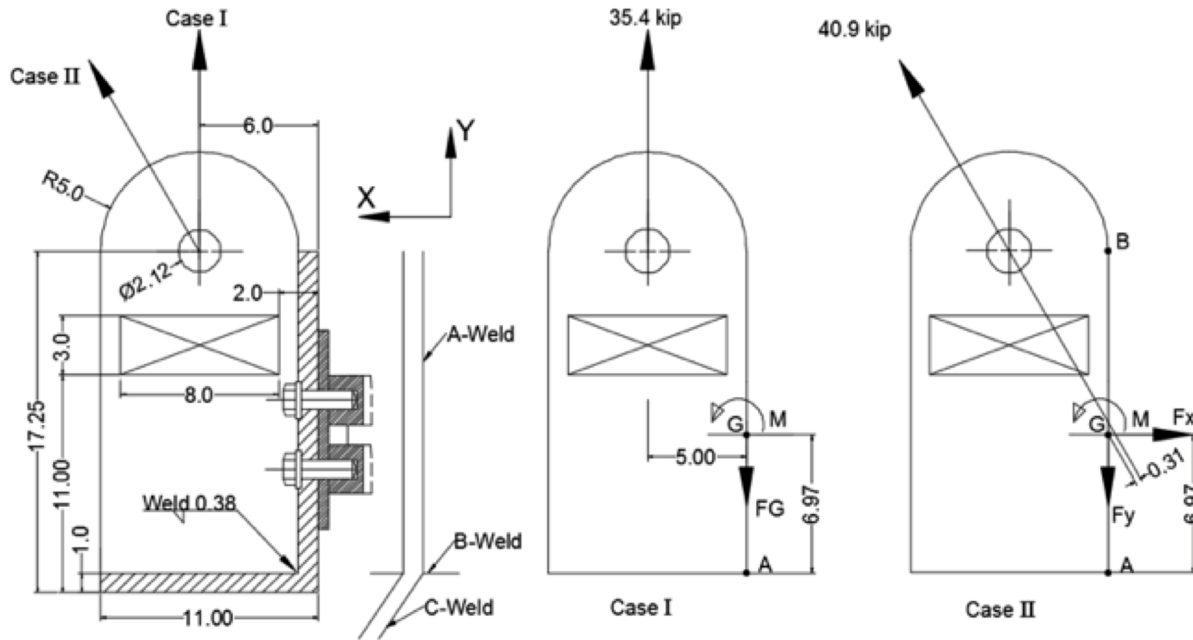


**Figure 2.12.3-6. Standard Ear, Case I and Case II Weld Stresses**

The shear stress is:

$$\tau_{xy} = \frac{F_G}{A} = \frac{35.4}{2(0.707)(2.25 \times 0.375 + 15.87 \times 0.375)} = 3.68 \text{ ksi}$$

The resulting von Mises stress in the weld metal is.

$$\sigma' = \sqrt{\sigma_x^2 + 3\tau_{xy}^2} = \sqrt{5.09^2 + 3(3.68)^2} = 8.16 \text{ ksi} < 23.7 \text{ ksi}$$

### CALCULATION OF STRESS IN THE PARENT METAL:

The area subject to shear is:

$$A = 2 \times (0.375) \times (2.25 + 15.87) = 13.59 \text{ in}^2$$

Thus, the shear stress on the parent metal is:

$$\tau_{xy} = \frac{F_G}{A} = \frac{35.4}{13.77} = 2.6 \text{ ksi} < 13.7 \text{ ksi}$$

The section modulus of the ear plate at the weld interface is:

$$\frac{I}{C} = \frac{0.38 \times 914.33}{6.97} = 49.85 \text{ in}^3$$

Thus, the tensile stress at A in the parent metal is:

$$\sigma_x = \frac{35.4 (5)}{49.85} = 3.6 \text{ ksi}$$

$$\sigma' = \sqrt{\sigma_x^2 + 3\tau_{xy}^2} = \sqrt{3.6^2 + 3(2.6)^2} = 5.77 \text{ ksi} < 23.7 \text{ ksi}$$

### Load Case II

Figure 2.12.3-6 (Case II) shows a free body diagram of the standard ear for Load Case II.

$$A = 2(0.707)(0.375)(2.25 + 15.87) = 9.61 \text{ in}^2$$

$$M = 40.9(0.31) = 12.68 \text{ k-in}$$

$$F_x = 20.5 \text{ kip}$$

$$F_y = 35.4 \text{ kip}$$

At the point B the bending stress and the tensile due to  $F_x$  add. For the weld metal the total normal stress is:

$$\sigma_x = \frac{F_x}{A} + \frac{Mc}{I} = \frac{20.5}{9.61} + \frac{12.68(16.25-6.97)}{242.36} = 2.62 \text{ ksi}$$

The shear stress is:

$$\tau_{xy} = \frac{F_y}{A} = \frac{35.4}{9.61} = 3.68 \text{ ksi}$$

Thus, the von Mises stress in the weld is:

$$\sigma' = \sqrt{\sigma_x^2 + 3\tau_{xy}^2} = \sqrt{2.62^2 + 3(3.68)^2} = 6.9 \text{ ksi} < 23.7 \text{ ksi}$$

The stresses in the parent metal are:

$$\begin{aligned}
 A &= 2 \times (0.375) \times (2.25 + 15.87) = 13.59 \text{ in}^2 \\
 T_{xy} &= \frac{35.4}{13.59} = 2.6 \text{ ksi} \\
 \sigma_x &= \frac{20.5}{13.59} + \frac{12.68}{49.85} = 1.77 \text{ ksi} \\
 \sigma' &= \sqrt{1.77^2 + 3(2.6)^2} = 4.85 \text{ ksi} < 23.7 \text{ ksi}
 \end{aligned}$$

- YIELDING OF ATTACHING BOLT AND SHEARING OF BOLT AND TAPPED THREAD

Bolt Loading Auxiliary Ear Design

For the auxiliary ear design, the external bolt force produced by the lifting condition is:

Load Case I

The moment applied to the bolts is:

$$M = 17.7(4.00) = 70.8 \text{ k-in}$$

The tensile stress  $\sigma_{tb}$  at the bottom of contact area due to the applied moment is:

$$\sigma_{tb} = \frac{Md/2}{I} = \frac{Md/2}{bd^3/12} = \frac{6M}{bd^2}$$

Where b and d are the base and height dimensions of the contact area. The tensile load on the bolt is the area  $A_{tb}$  of each fastener times  $\sigma_{tb}$ .

$$F_T = \frac{6M}{bd^2} A_{tb}$$

Where  $A_{tb}$  for the bottom row bolt is:

$$\begin{aligned}
 A_{tb} &= 3.00 \times (2.5 + 1.75) = 12.75 \text{ in}^2 \\
 F_T &= \frac{6(70.8)}{6.0 \times 9.5^2} \times 12.75 = 10.00 \text{ kip}
 \end{aligned}$$

Load Case II

The moment for this Load Case is reduced by the action of the horizontal component as follows:

$$M = 17.7 \times (4.54) - 10.2 \times (0.92 + 0.50 + 3.50 + 1.75) = 12.32 \text{ k-in. see}$$

Figure 2.12.3-1.

The tensile load on the bolt is:

$$F_T = \frac{6M}{bd^2} \times A_{tb} + \frac{F_H}{4} = \frac{6(12.32)(12.75)}{6.0(9.5)^2} + \frac{10.2}{4} = 1.74 + 2.55 = 4.29 \text{ kip}$$

Bolt Loading, Standard Ear Design

Load Case I and Case III (Slot Lift)

The moment applied to the bolt is:

$$M = 35.4(6.00) = 212.4 \text{ k-in}$$

$$A_{tb} = 3.00(3+1.75) = 14.25 \text{ in}^2$$

The tensile load  $F_t$  per bolt at the bottom row of bolts due to the applied moment is:

$$F_t = \frac{6MA_{tb}}{bd^2} = \frac{6(212.4)(14.25)}{6.0(10.0)^2} = 30.27 \text{ kip}$$

Load Case II

The moment for Load Case II is:

$$M = 35.4 (6.54) - 20.5 (0.92 + 7.75 + 3.50 + 1.75) = -53.84 \text{ k-in}$$

The tensile load  $F_t$  per bolt at the top row of bolts is:

$$A_{tb} = 3.00(3.5 + 1.75) = 15.75 \text{ in}^2$$

$$F_t = \frac{6(53.84)(15.75)}{6.0(10.0)^2} + \frac{20.5}{4} = 13.61 \text{ kip}$$

Load Case III ear base lift is not considered because the moment area is less than that of Load Case I and the load acts on the same directions as Load Case I.

Table 2.12.3-1 presents a summary of bolt loading for each of the ear designs (auxiliary and standard). Because the standard design under Load Case I, straight lift, imposes the largest tensile load on the bolt than in the other conditions, this load value (30.27 kip) is used in the analysis of the bolt.

**Table 2.12.3-1. Bolt Loading Per Ear Design and Load Case**

Ear Design	Bolt Loading (kip)			Yield Strength (ksi)	Shear Strength (ksi)
	Load Case				
	I	II	III (Slot Lift)		
Auxiliary	10	4.29	N/A	85	51
Standard	30.27	13.61	30.27	85	51



### Bolt Analysis

Bolt and thread section properties use in the analyses for both internal and external threads are evaluated for a standard 1-8 UNC x 2-1/2 in bolt as follows.

Tensile stress area ( $A_t$ ) for high strength bolt with  $\sigma_{tb} > 100\text{ksi}$ , as provided in *Machineries Handbook*, Reference 2-26, Page 1490 is:

$$A_t = \pi \left( \frac{E_{s_{min}}}{2} - \frac{0.16238}{n} \right)^2$$

where:

$$E_{s_{min}} = \text{Minimum pitch diameter} = 0.9188 \text{ inches}$$

$$n = \text{Number of threads per inch} = 8$$

$$A_t = \pi \left( \frac{0.9188}{2} - \frac{0.16238}{8} \right)^2 = 0.61 \text{ in}^2$$

Shear area of the external ( $A_s$ ) and the internal ( $A_n$ ) threads, *Machineries Handbook*, Reference 2-26, Page 1491.

$$A_s = \pi n L_e K_{n_{max}} \left[ \frac{1}{2n} + 0.57735 (E_{s_{min}} - K_{n_{max}}) \right]$$

where:

$$n = 8$$

$$L_e = \text{Length of engagement} = 1.680 \text{ inches}$$

$$K_{n_{max}} = \text{Maximum minor diameter of internal thread} = 0.8795 \text{ inches}$$

$$A_s = \pi (8)(1.680)(0.8795) \left[ \frac{1}{2(8)} + 0.57735 (0.9188 - 0.8795) \right] = 3.164 \text{ in}^2$$

$$A_n = \pi n L_e D_{s_{min}} \left[ \frac{1}{2n} + 0.57735 (D_{s_{min}} - E_{n_{max}}) \right]$$

where:

$$D_{s_{min}} = \text{Minimum major diameter of external thread} = 0.9848 \text{ inches}$$

$$E_{n_{max}} = \text{Maximum pitch diameter of internal thread} = 0.9242 \text{ inches}$$

$$A_n = \pi (8)(1.680)(0.9848) \left[ \frac{1}{2(8)} + 0.57735 (0.9848 - 0.9242) \right] = 4.05 \text{ in}^2$$

### Bolt Preload

J.E. Shigley and L.D. Mitchell (Reference 2-27) recommend the bolt preload ( $F_i$ ) be between 60% and 90% of the proof load. The proof load is equal to 85% of the yield strength ( $S_y$ ) multiplied by the tensile stress area ( $A_t$ ). For a torque of  $600 \pm 20$  ft-lbs, the corresponding preload, proof load and percent of proof load are determined as follows:

$$F_i = T/(kd)$$

$$\% \text{ proof load} = [F_i / \text{proof load}] \times 100\%$$

Where:

$$T = \text{torque} = 600 \pm 20 \text{ ft-lb} = 7,200 \pm 240 \text{ in-lb}$$

$$d = \text{bolt thread nominal diameter} = 1.0 \text{ in} \quad (\text{GEH drawings 101E8718 and 105E9520})$$

$$k = \text{torque coefficient} = 0.2 \quad (\text{Reference 2-27})$$

$$\text{proof load} = \text{proof strength} \times A_t = 43,762 \text{ lbs}$$

$$\text{proof strength} = 0.85 S_y = 72,250 \text{ psi}$$

NEDO-33866 Revision 6  
Non-Proprietary Information

$$A_t = \text{thread tensile area} = 0.6057 \text{ in}^2$$

$$S_y = \text{yield strength at room temperature} = 85,000 \text{ psi (Table 2.2-8)}$$

Table 2.12.3-2 summarizes the bolt preload, bolt proof load and % proof load for all three lifting ear bolt torque values. As indicated, maximum, nominal, and minimum torques produce loads within the recommended range of 60% to 90% of the proof load.

**Table 2.12.3-2. Lifting Ear Bolt Percent Proof Load**

Lifting Ear Bolt Torque	Torque Value (ft-lbs)	Bolt Preload (lb)	Proof Load (lb)	Percent Proof Load
Maximum	620	37,200	43,762	85%
Nominal	600	36,000		82%
Minimum	580	34,800		80%

Stresses produced by preload:

Bolt tension

$$\sigma = \frac{F_i}{A_t} = \frac{37.20}{0.606} = 61.42 \text{ ksi}$$

Bolt thread stripping

$$\tau = \frac{F_i}{A_s} = \frac{37.20}{3.164} = 11.76 \text{ ksi}$$

Tapped thread stripping

$$\tau = \frac{F_i}{A_n} = \frac{37.20}{4.054} = 9.18 \text{ ksi}$$

Minimum Bearing stress between cask and ear

$$\sigma_{ib} = \frac{(\# \text{ of bolt})(F_i)}{\text{Contact Area}} = \frac{4(34.80)}{6.0(10.0)} = 2.32 \text{ ksi}$$

The initial bearing pressure,  $\sigma_{ib}$ , previously calculated, is assumed to be uniform over the contact area. The bearing pressure should not be exceeded by tensile stress,  $\sigma_{tb}$ . Figure 2.12.3-7 shows the bearing stresses at the lifting ear contact region.

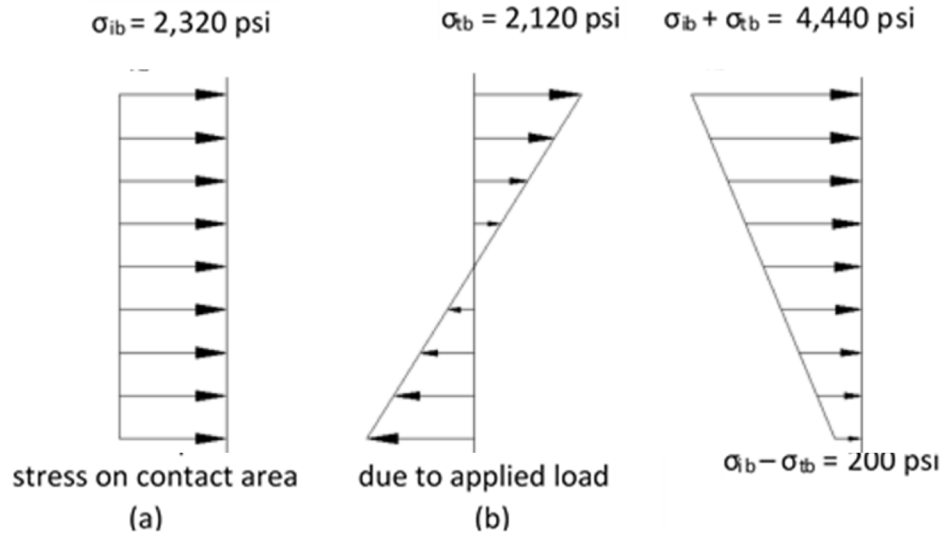


**Figure 2.12.3-7. Lifting Ear Contact Bearing Stresses**

$$\sigma_{tb} = \frac{6M}{bd^2} = \frac{6(212.4)}{6(10.0)^2} = 2.12 \text{ ksi}$$

$$\sigma_{ib} > \sigma_{tb}$$

The moment  $M$  (212.4 k-in) is produced by Load Case I or III on the standard ear design attaching bolt as previously calculated.

The nominal tensile stress,  $\sigma_t$ , in the bottom row bolts is:

$$\sigma_t = \frac{F_t}{A_t}$$

As previously calculated the tensile load for Load Case I is 30.27 kip per bolt.

$$\sigma_t = \frac{30.27}{0.606} = 49.95 \text{ ksi} < 85 \text{ ksi}$$

and the direct-shear component is:

$$\tau = \frac{35.4}{4(0.606)} = 14.6 \text{ ksi} < 51 \text{ ksi}$$

The interaction equation for the strength of a connection with bolts in combined shear and tension may be approximated by the elliptical relationship:

$$\left(\frac{\sigma_t}{\sigma_y}\right)^2 + \left(\frac{\tau}{0.6\sigma_y}\right)^2 \leq 1.0$$

$$\left(\frac{49.95}{85.0}\right)^2 + \left(\frac{14.60}{0.6(85)}\right)^2 \leq 1.0$$

$$0.43 \leq 1.0$$

Therefore, the selected bolts are adequate to carry the lifting load.

For the shearing of the bolt threads due to tensile load  $F_t$ .

$$\tau = \frac{F_t}{A_s} = \frac{30.27}{3.164} = 9.57 \text{ ksi} < 51.0 \text{ ksi}$$

For the shearing of the tapped threads due to tensile load  $F_t$ .

$$\tau = \frac{F_t}{A_n} = \frac{30.27}{4.054} = 7.47 \text{ ksi} < 51.0 \text{ ksi}$$

### Bolt Fatigue Analysis

Bolt and Load Data:

#### 1-8 UNC-2A, ASTM A193-B6

Yield Strength:	85 ksi (minimum)
Operating Temperature:	250°F
Modulus of Elasticity:	28.1 (10 <sup>6</sup> ) psi
Maximum Tensile Stress:	61.42 ksi (Preload)
Maximum Shear Stress:	14.6 ksi

(Shear neglects the reducing effect of friction between ear and cask body.)

The maximum cycle of stress is due to a combination of the preload stress, 61.42 ksi, and the shear stress (14.6 ksi) due to lifting. These give a maximum principal stress of:

$$\sigma_{\max} = \frac{61.42}{2} + \sqrt{\left(\frac{61.42}{2}\right)^2 + 14.6^2} = 64.71 \text{ ksi}$$

From ASME Section III NB 3232.3, the fatigue strength reduction factor to be used is 4.0. Because the fatigue curve (ASME Section III, Figure I-9.4 (Reference 2-18)) is based on modulus of elasticity of 30(10<sup>6</sup>) psi and the bolt has a modulus of elasticity of 28.1(10<sup>6</sup>) psi, the stress range is given by:

$$S = (64.71 \text{ ksi}) \times 4(30(10^6)/28.1(10^6)) = 276.34 \text{ ksi}$$

To select the correct fatigue curve, the stress intensity value,  $S_m$ , of 26.5 ksi is used at 250°F. Calculating the alternating stress:

$$S_a = \frac{1}{2} S = \frac{1}{2} (276.34) = 138.17 \text{ ksi}$$

Using the fatigue curve for a maximum nominal stress  $\leq 2.7 S_m$  the fatigue limit is  $\cong 530$  cycles as provided in Figure 2.12.3-8. Assuming an average of four ear lifts per usage and 12 usages per year, this gives a bolt life of:

$$\frac{530}{\left(12 \frac{\text{usages}}{\text{year}}\right) \left(4 \frac{\text{cyc.}}{\text{usage}}\right)} = 11 \text{ yrs.}$$

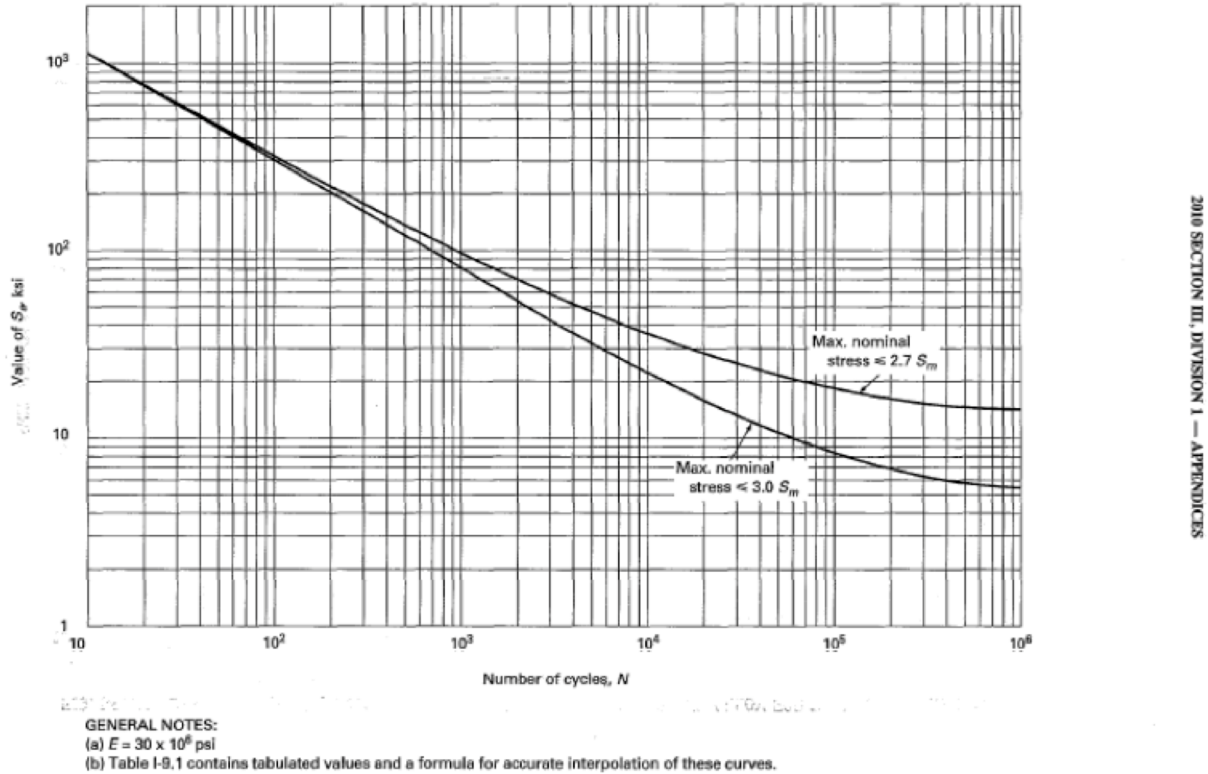


**Figure 2.12.3-8. Design Fatigue Curves For High Strength Steel Bolting Above 700°F**  
(from Reference 2-18)

- YIELDING OF CASK OUTER SHELL**

The lifting ears are mounted to the outer shell of the cask on a mounting plate embedded to the cask. The mounting plate is embedded about 1.75 inches into the cask through the outer shell and the lead shield. However, 1 inch thickness of the outer shell and the maximum vertical load of 35.4 kip (standard ear) are conservatively considered for yielding due to the lifting load.

$$\sigma_c = \frac{F_c}{A} = \frac{35.4}{7.5} = 4.72 \text{ ksi}$$

where Area ( $A$ ) = thickness of shell x width of mounting plate = 1 x 7.5 = 7.5 in<sup>2</sup>

$$\tau = \frac{F}{A_s} = \frac{35.4}{12.5} = 2.83 \text{ ksi}$$

where the shear area ( $A$ ) = 2 x (6.25 x 1) = 12.5 in<sup>2</sup>

$$\sigma_b = \frac{Mc}{I} = \frac{247.8 \times 3.125}{152.59} = 5.07 \text{ ksi}$$

where  $M = 35.4 \times 7 = 247.8$  k-in,

NEDO-33866 Revision 6  
Non-Proprietary Information

$$c = 6.25/2 = 3.125 \text{ in}$$

$$I = \frac{bh^3}{12} = \frac{7.5 \times 6.25^3}{12} = 152.59 \text{ in}^4$$

$$\sigma' = \sqrt{(4.72 + 5.07)^2 + 3 \times (2.83)^2} = 10.95 \text{ ksi}$$

- EXCESSIVE LOAD FAILURE

The lifting devices must be designed such that their failure under excessive load would not impair the ability of the package to meet other requirements of 10 CFR 71. In this section a margin of safety (MS) is determined for each of the lifting system components based on the results presented in Table 2.12.3-3.

**Table 2.12.3-3. Summary of Ear Analysis for Model 2000**

Condition	Stress Level (ksi)		Allowable (ksi) Based on Yield	MS(y) Aux./Std.	Allowable Based on Su	MS(U) Aux./Std.
	Auxiliary (Aux.)	Standard (Std.)				
Shear tearout of lift hole	6.02	8.98	14	1.33/0.56	26.18	3.35/1.92
Tensile failure of ear plate	4.82	17.7	23.7	3.92/0.34	68.6	13.23/2.88
Bearing of shackle pin on ear	10.2	17.7	23.7	1.32/0.34	68.6	5.73/2.88
Yielding of weld joint	9.2	8.16	23.7	1.58/1.9	68.6	6.46/7.41
Yielding of attaching bolt	---	61.42	85	0.38	110	0.79
Shearing of bolt thread	---	11.76	51	3.34	---	---
Shearing of tapped thread	---	9.18	14	0.53	26.18	1.85
Yielding of cask outer shell	---	10.95	23.7	1.16	68.6	5.26

Note:

Bolt and bolt thread stress levels are documented in Table 2.12.3-3 for standard ear because maximum bolt loading is documented during slot lift (Case III) of the standard ear (see Table 2.12.3-1).

The margins of safety MS(y) with respect to yield is calculated as follows:

$$MS(\text{yield}) = \frac{\text{Allowable based on yield strength}}{\text{Stress level}} - 1$$

The ear and cask shell material is ASTM 240 type 304 stainless steel. The margins of safety with respect to ultimate failure MS(U) are:

For shear tear-out of lifting hole

$$\text{Shear Strengths} = \frac{\sigma_{\text{ult}}}{2(1+\mu)} = \frac{68.6}{2(1.31)} = 26.18 \text{ ksi}$$

$$\tau = 8.98 \text{ ksi (Standard Ear, Load Case I)}$$

$$MS(U) = \frac{26.18}{8.98} - 1 = 1.92$$

NEDO-33866 Revision 6  
Non-Proprietary Information

For tensile failure of ear plate

$$\sigma_T = 17.7 \text{ ksi (Standard Ear, Load Case III)}$$

$$MS(U) = \frac{68.6}{17.7} - 1 = 2.88$$

For yielding of weld joints

$$\sigma' = 9.2 \text{ ksi (Auxiliary Ear, Load Case II)}$$

$$MS(U) = \frac{68.6}{9.2} - 1 = 6.46$$

For bolts

$$P_{ult} = 110 \times 0.606 = 66.66 \text{ kip}$$

$$F_t = 61.42(0.606) = 37.22 \text{ kip}$$

$$MS(U) = \frac{66.66}{37.22} - 1 = 0.79$$

For yielding of cask outer shell

$$\sigma' = 10.95 \text{ ksi}$$

$$MS(U) = \frac{68.6}{10.95} - 1 = 5.26$$

A review of the above margin of safety indicates that, under excessive loading, the ear attaching bolts will fail before the ear plates, ear welds or cask shell. Failure of the bolts assures that the ability of the package to meet any other regulatory requirements is not impaired.

- MODEL 2000 LID LIFTING LUG ANALYSIS

The lifting lug is covered during transport. It is shown by analysis that this lifting device complies with requirements of 10 CFR 71.45(a). The lifting lug is able to support three times the weight of the lid without yielding.

The weakest part of the lifting lug is the fillet weld, which attaches the stainless steel loop to the cask lid. Using the maximum shear stress theory the weld is determined to have a factor of safety of 1.76 when analyzed for lifting 3 times the weight of the lid.

The lifting lug is analyzed by considering the rigid frame shown in Figure 2.12.3-9. The analytical model has the same height and distance between the supports as the lifting lug.

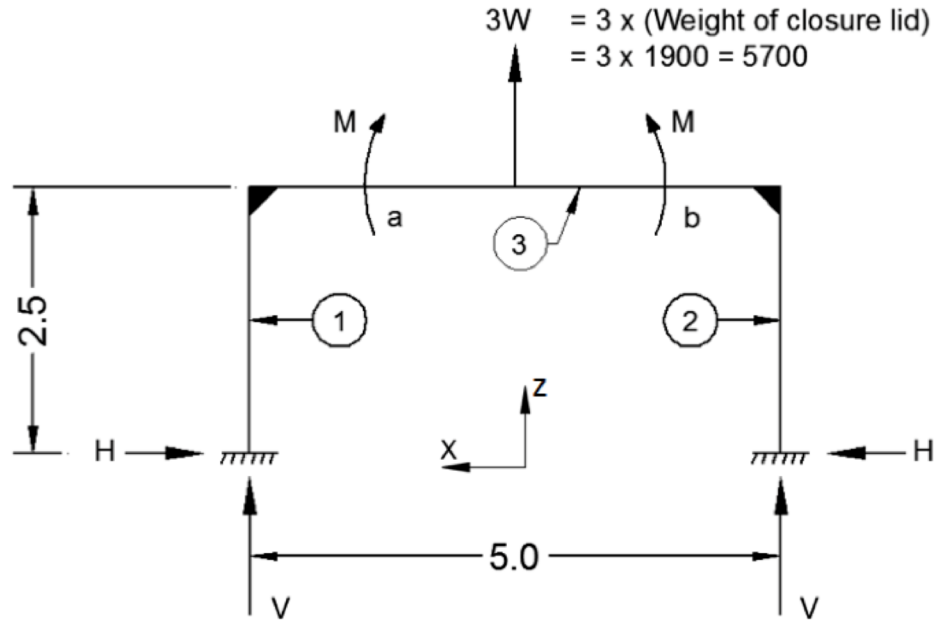


**Figure 2.12.3-9. Analytical Model of Lifting Lug**

The statically indeterminate forces and moments are obtained by solving the following set of equations from Reference 2-29.

$$\frac{-1/3HL^3_1}{I_1} + \frac{1/2M_1L^2_1}{I_1} = \frac{1/3HL^3_2}{I_2} - \frac{1/2M_2L^2_2}{I_2}$$

$$\frac{-1/2HL^2_1}{I_1} + \frac{M_1L_1}{I_1} = \frac{-1/3M_1L_3}{I_3} + \frac{1/6W(bL_3 - \frac{b^3}{L_3})}{I_3} - \frac{1/6M_2L_3}{I_3}$$

$$\frac{-1/2HL^2_2}{I_2} + \frac{M_2L_2}{I_2} = \frac{1/3M_2L_3}{I_3} + \frac{1/6M_1L_3}{I_3} - \frac{1/6W[2bL_3 + (\frac{b^3}{L_3}) - 3b^2]}{I_3}$$

And by symmetry:

$$M_1 = M_2 = M$$

$$H_1 = H_2 = H$$

$$V_1 = V_2 = V = 2,850 \text{ lb.}$$

Also,

$$L_1 = L_2 = 2.5$$

$$L_3 = 5.0$$

$$I_1 = I_2 = I_3$$

$$a = b = 2.5$$



Using substitution and solving the above equations simultaneously gives:

$$\begin{aligned} V &= 2,850 \text{ lb} \\ H &= 2,671 \text{ lb} \\ M &= 4,452 \text{ lb-in} \end{aligned}$$

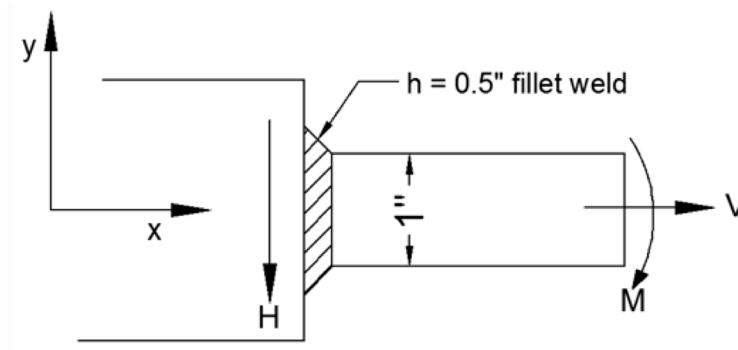


**Figure 2.12.3-10. Loading on the Weld Area**

The loading in the weld area is shown in Figure 2.12.3-10. The moment  $M$  produces a bending stress,  $\sigma_m$ , in the weld. This stress is assumed to act normal to the throat area (see Reference 2-27, P. 427).

The unit moment of inertia of the welds is from Reference 2-27, P. 429, given by:

$$I_u = \pi r^3$$

But the moment of inertia based on the weld throat is:

$$I = 0.707h\pi r^3$$

The normal stress in the weld is therefore given by:

$$\sigma = \frac{MC}{I} = \frac{MC}{0.707h\pi r^3}$$

The maximum stress occurs at the outer fibers where:

$$C = r$$

$$Z = 2\pi r$$

The maximum stress is therefore given by:

$$\sigma_m = \pm \frac{M}{0.707h\pi r^2}$$

From Reference 2-27, Equation (9.3), p. 417, the stress in the weld due to the force  $V$  is given by:

$$\tau_v = \frac{V}{0.707hZ}$$

Similarly, from Reference 2-27, Equation (a), p. 427, the stress in the weld due to the force  $H$  is given by:

$$\tau_H = \frac{H}{0.707hZ}$$

Figure 2.12.3-11 shows the stresses acting on the weld at the point where the bending moment is a maximum.

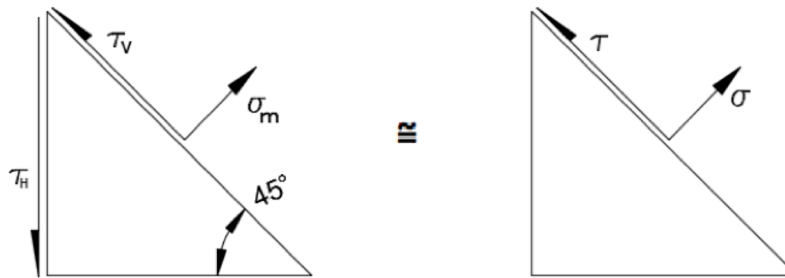


**Figure 2.12.3-11. Stresses Acting on the Weld**

$$\sigma = \sigma_m = \frac{4452}{0.707 \times 0.5 \times \pi \times (0.5)^2} = 16,035.3 \text{ psi}$$

$$\begin{aligned} \tau &= \tau_V - \tau_H \cos 45^\circ \\ &= \frac{2,850}{0.707 \times 0.5 \times 2 \times \pi \times 0.5} - \frac{2,671}{0.707 \times 0.5 \times 2 \times \pi \times 0.5} \times 0.707 \\ \tau &= 2,566 - 1,700 = 866 \text{ psi} \end{aligned}$$

From Reference 2-27, p.31, the principal stresses are found using:

$$\sigma_1, \sigma_2 = \frac{\sigma}{2} \pm \sqrt{\left(\frac{\sigma}{2}\right)^2 + \tau^2}$$

$$\tau_{\max} = \pm \sqrt{\left(\frac{\sigma}{2}\right)^2 + \tau^2}$$

Substituting for  $\sigma$  and  $\tau$  yields

$$\begin{aligned} \sigma_1, \sigma_2 &= \frac{16,035.3}{2} \pm \sqrt{\left(\frac{16,035.3}{2}\right)^2 + 866^2} \\ &= 8,017.7 \pm 8064.3 \\ \sigma_1 &= 16,082 \text{ psi} \\ \sigma_2 &= -46.6 \text{ psi} \\ \tau_{\max} &= \pm 8064.3 \text{ psi} \end{aligned}$$

The maximum shear stress is applied to determine the likelihood of failure or safety.

$$\text{Allowable} = \tau_{\text{allowable}} = 0.6 S_y$$

Where  $S_y$  denotes the yield strength.

The yield strength of stainless steel Type 304 is 23.7 ksi.

Substituting into equation (32)

$$\text{Allowable Stress} = 0.6 \times 23.7 = 14.22 \text{ ksi}$$

$$\tau_{\max} = 8.06 \text{ ksi} \leq 14.22 \text{ ksi}$$

Therefore, the factor of safety is given by

$$\text{FS} = \frac{14.22}{8.06} = 1.76 \text{ (this is for lifting 3W)}$$

#### **2.12.3.2. Tie-Down Analysis**

The purpose and scope of this analysis is to demonstrate the structural integrity of the tie-down rib. The Model 2000 Transport Package is shipped normally by truck. Figure 2.12.3-12 shows the overall plan for tying the package to the vehicle. Eight wire ropes or chains tie the package to the vehicle: four connect to the upper tie-down ribs of the overpack, and the other four connect to the overpack base tie-down ribs. In addition, the base of the package is wedged to the truck bed to prevent sliding. Evaluation of the tie-down loading on the tie-down rib adjacent area consisted of the following:

- 1) Identification of the maximum tie-down member tension force due to loading.
- 2) Evaluation of the effect of the above force on the tie-down rib.

Classical hand calculation is used to identify the maximum tie-down member tension forces due to the combined loads. The results of this analysis were added to establish the maximum load. Table 2.12.3-3 gives a summary of each rope tie-down tension load for each force component and the total force. The maximum tie-down wire tension force is estimated to be 148.62 kips. This maximum load is then applied to the tie-down rib to determine the structural integrity of the tie-down rib by analyzing the following modes of failure:

- Shear tear-out of tie-down rib hole
- Bearing of shackle pin on ear
- Yielding of weld joints and parent metal

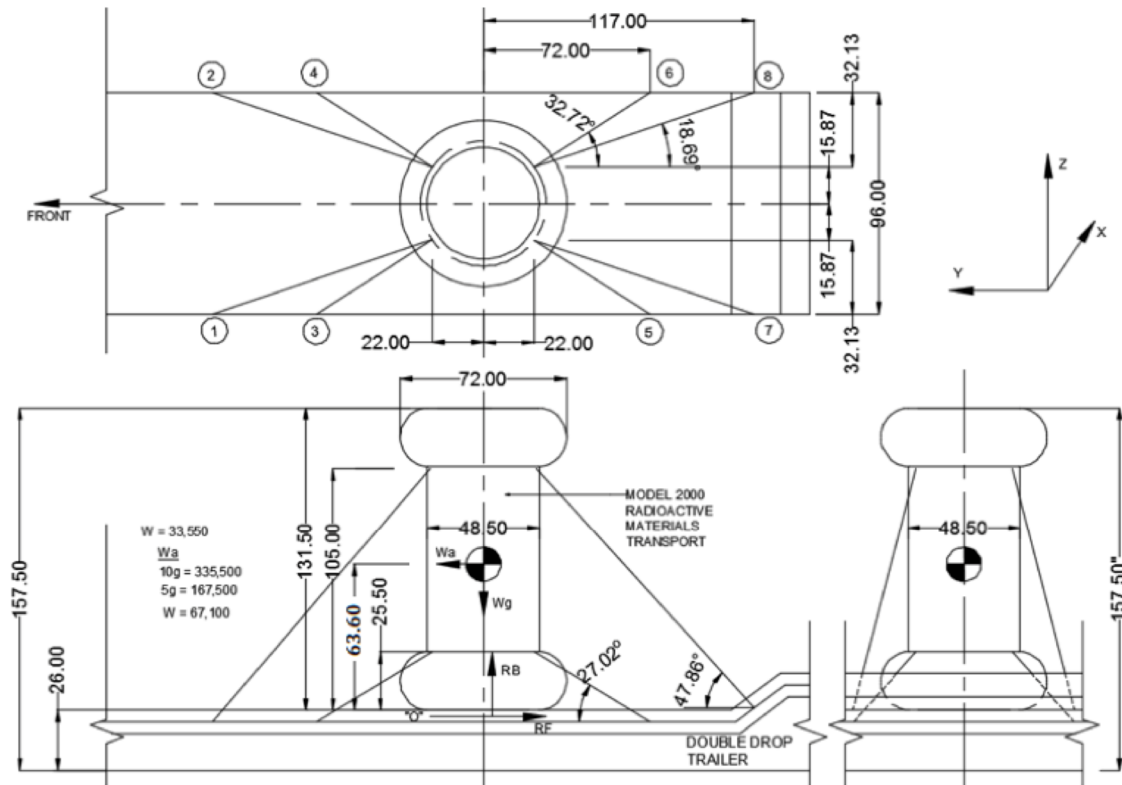


**Figure 2.12.3-12. Tie-Down of Transport Package to Vehicle**

- TIE-DOWN MEMBER TENSION FORCES**

The package (wt. = 33,550 lb) is subject to accelerations of 10g longitudinal, 5g transverse, and 2g vertical (up) Per IAEA's "Package stowage and retention" regulations. These accelerations result in the following forces acting on the C.G. of the cask:

$$F_{\text{long}} = 33,550(10) = 335,500 \text{ lbf}$$

$$F_{\text{trans}} = 33,550(5) = 167,750 \text{ lbf}$$

$$F_{\text{vert}} = 33,550(2) = 67,100 \text{ lbf}$$

In this calculation, each load is independently applied to the package and the tensile load on members for each case is calculated. The tensile loads are then added to calculate the maximum tension load on members.

**10g Longitudinal**

Because the base of the package is chocked, the 10g acceleration will cause it to rotate about point "o" counterclockwise (-x direction). This rotation will cause Ropes 1, 2, 3 and 4 to go slack and tension Ropes 5, 6, 7 and 8. From Figure 2.12.3-13.

$$F_7 = F_8$$

$$F_5 = F_6$$

NEDO-33866 Revision 6  
Non-Proprietary Information

The component forces for these ropes are:

$$\begin{aligned}
 F_{5y} &= F_{6y} = F_6 \cos 23.2^\circ \cos 32.7^\circ &= 0.774 F_6 \\
 F_{5z} &= F_{6z} = F_6 \sin 23.2^\circ &= 0.394 F_6 \\
 F_{7y} &= F_{8y} = F_8 \cos 46.3^\circ \cos 18.69^\circ &= 0.654 F_8 \\
 F_{7z} &= F_{8z} = F_8 \sin 46.3^\circ &= 0.723 F_8
 \end{aligned}$$

The reaction forces from chocking and friction ( $R_F$ ) and bearing on the package base ( $R_B$ ) are:

$$\begin{aligned}
 R_F &= F_{5y} + F_{6y} + F_{7y} + F_{8y} - W_a \\
 R_B &= F_{5z} + F_{6z} + F_{7z} + F_{8z} + W_g \quad (\text{assuming } F_1 = F_2 = F_3 = F_4 = 0)
 \end{aligned}$$

The center of gravity is 63.60 inches.

$$\begin{aligned}
 \Sigma M_{ox} &= 0 = -W_a 63.60 + W_g 24.25 - R_B 24.25 + (F_{5y} + F_{6y}) 25.5 + (F_{7y} + F_{8y}) \\
 &\quad 105.0 + (F_{5z} + F_{6z} + F_{7z} + F_{8z}) 46.25 \\
 \Sigma M_{ox} &= -W_a 63.60 + W_g 24.25 - (F_{5z} + F_{6z} + F_{7z} + F_{8z} + W_g) 24.25 + \dots \\
 &\quad \dots (F_{5y} + F_{6y}) 25.5 + (F_{7y} + F_{8y}) 105.0 + (F_{5z} + F_{6z} + F_{7z} + F_{8z}) 46.25 \\
 &= -W_a 63.60 - [2 \times 0.394 F_6 + 2 \times 0.723 F_8] 24.25 + 2 \times 0.774 F_6 (25.5) + \dots \\
 &\quad \dots 2 \times 0.654 F_8 (105.0) + [2 \times 0.394 F_6 + 2 \times 0.723 F_8] 46.25 \\
 &= -W_a 63.60 - 19.1 F_6 - 35.1 F_8 + 39.5 F_6 + 137.3 F_8 + 36.4 F_6 + 66.9 F_8 \\
 &= -W_a 63.60 + (-19.1 + 39.5 + 36.4) F_6 + (-35.1 + 137.3 + 66.9) F_8 \\
 &= -(63.60) W_a + (56.8) F_6 + (169.1) F_8 \\
 \Rightarrow 2.134 (10^7) &= (56.8) F_6 + (169.1) F_8
 \end{aligned}$$

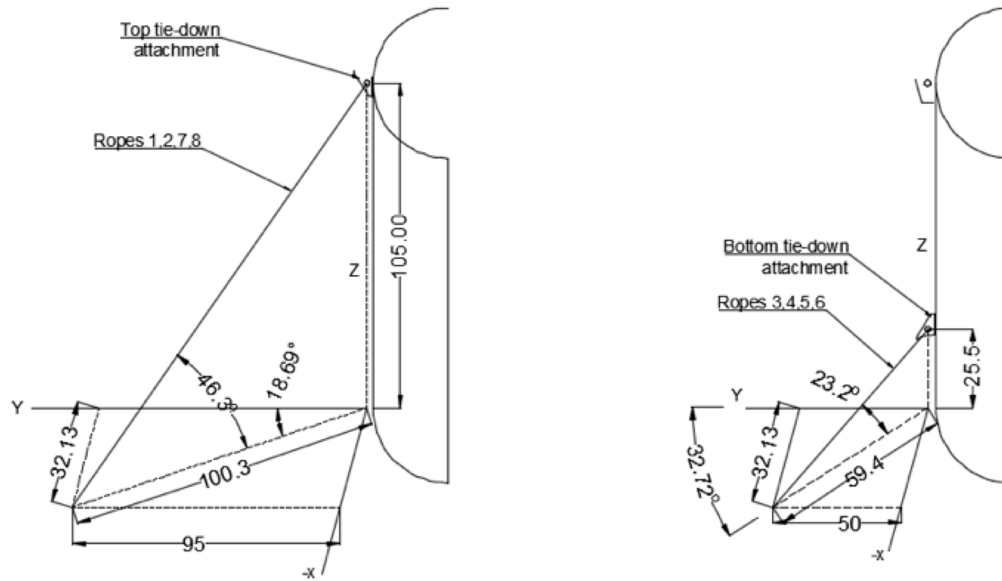


**Figure 2.12.3-13. Tie-Down Wire Ropes**

This cannot be solved for F6 and F8 so an additional equation relating F6 and F8 is required. By making certain assumptions, this equation can be obtained from consideration of the force and deflection (or extension) characteristics of the different length wire ropes. Figure 2.12.3-14 shows the extension of the ropes at small angle rotation. Assuming the ropes initially have no tension, the ratio of loads due to stretching of the ropes is:

$$\frac{F_7}{F_5} = \frac{\frac{\delta_7 EA}{L_7}}{\frac{\delta_5 EA}{L_5}}$$

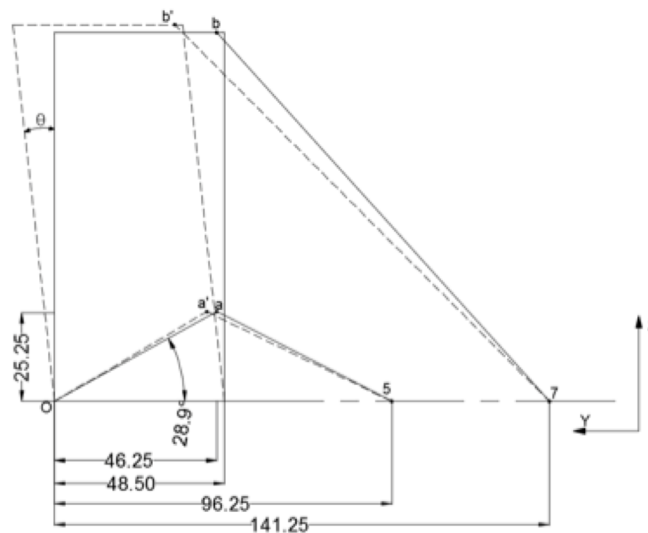


**Figure 2.12.3-14. Wire Rope Extension at Small Angle (θ) Rotation**

Because both ropes are of the same size and material,

$$\frac{F_7}{F_5} = \frac{\delta_7 L_5}{\delta_5 L_7}$$

For a rotation of  $\theta^\circ$  about point “O”, line 5 would be extended as follows

$$\delta_5 Z L_{5f} - L_{5i}$$

$L_{5f}$  is the final length of rope 5 as shown in Figure 2.12.3-15.

$$L_{5i} = \sqrt{59.4^2 + 25.5^2} = 64.6 \text{ in}$$

$$\overline{oa'} = \overline{oa} = \sqrt{46.25^2 + 25.5^2} = 52.8 \text{ in}$$

Change in “a” in y direction is:

$$\overline{aa'_y} = 52.8[\cos 28.9^\circ - \cos(28.9 + \theta)]$$

Change in “a” in z direction is:

$$\overline{aa'_z}$$

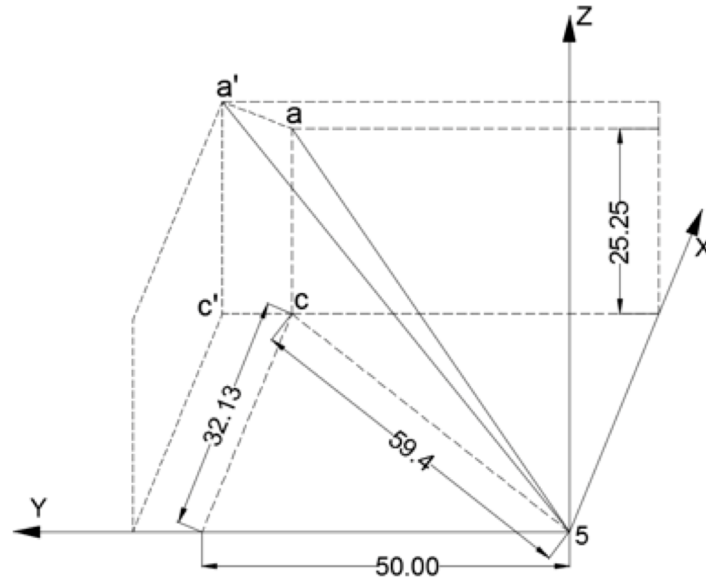


**Figure 2.12.3-15. Final Length of Rope 5**

$$L_{5f} = \sqrt{(25.5 + 52.8[\sin(28.9^\circ + \theta) - \sin 28.9^\circ])^2 + \dots + (32.13^2 + (50.0 + 52.8[\cos 28.9^\circ - \cos(28.9^\circ + \theta)])^2)}$$

To evaluate the effect of small rotations,  $L_{5f}$  will be evaluated for  $\theta = 0.1^\circ$ ,  $\theta = 1^\circ$  and  $\theta = 10^\circ$ .

NEDO-33866 Revision 6  
Non-Proprietary Information

$$\begin{aligned} L_{5f_{.1^\circ}} &= \sqrt{\frac{(25.5 + 52.8[\sin(29.0^\circ) - \sin 28.9^\circ])^2 + \dots}{32.13^2 + (50.0 + 52.8[\cos 28.9^\circ - \cos(29.0^\circ)])^2}} \\ &= \sqrt{654.4 + 3,536.8} = 64.7 \text{ in} \end{aligned}$$

$$\begin{aligned} L_{5f_{1^\circ}} &= \sqrt{\frac{(25.5 + 52.8[\sin(29.9^\circ) - \sin 28.9^\circ])^2 + \dots}{32.13^2 + (50.0 + 52.8[\cos 28.9^\circ - \cos(29.9^\circ)])^2}} \\ &= \sqrt{691.8 + 3,577.8} = 65.3 \text{ in} \end{aligned}$$

$$\begin{aligned} L_{5f_{10^\circ}} &= \sqrt{\frac{(25.5 + 52.8[\sin(38.9^\circ) - \sin 28.9^\circ])^2 + \dots}{32.13^2 + (50.0 + 52.8[\cos 28.9^\circ - \cos(38.9^\circ)])^2}} \\ &= \sqrt{1,098.2 + 4,072.0} = 71.9 \text{ in} \end{aligned}$$

A similar evaluation for line 7 yields:

$$L_{7i} = \sqrt{100.3^2 + 105^2} = 145.2 \text{ in}$$

$$\overline{ob} = \overline{ob'} = \sqrt{46.25^2 + 105^2} = 114.7 \text{ in}$$

Change in “b” in y direction is:

$$\overline{bb'_y} = 114.7[\cos 66.2^\circ - \cos(66.2 + \theta)]$$

Change in “b” in z direction is:

$$\begin{aligned} \overline{bb'_z} &= 114.7 [\sin(66.2 + \theta) - \sin 66.2] \\ L_{7f} &= \sqrt{\frac{(105 + 114.7[\sin(66.2 + \theta) - \sin 66.2])^2 + \dots}{32.13^2 + (95 + 114.7[\cos 66.2 - \cos(66.2 + \theta)])^2}} \end{aligned}$$

Evaluation at  $\theta = 0.1^\circ$ ,  $\theta = 1^\circ$  and  $\theta = 10^\circ$  gives:

$$\begin{aligned} L_{7f_{.1^\circ}} &= \sqrt{\frac{(105 + 114.7[\sin 66.3 - \sin 66.2])^2 + \dots}{32.13^2 + (95 + 114.7[\cos 66.2 - \cos 66.3])^2}} \\ &= \sqrt{11041.9 + 10,092.2} = 145.4 \text{ in} \end{aligned}$$

$$L_{7f_{1^\circ}} = \sqrt{11,191.9 + 10,410.1} = 147.0 \text{ in}$$

$$L_{7f_{10^\circ}} = \sqrt{12,419.6 + 14,011.7} = 162.6 \text{ in}$$



Calculation of the ratio  $\frac{L_f}{L_i}$  for each rope at each rotation value yields:

$\theta$	Lf/Li	
	Rope 5	Rope 7
0.1°	1.002	1.001
1°	1.011	1.012
10°	1.113	1.120

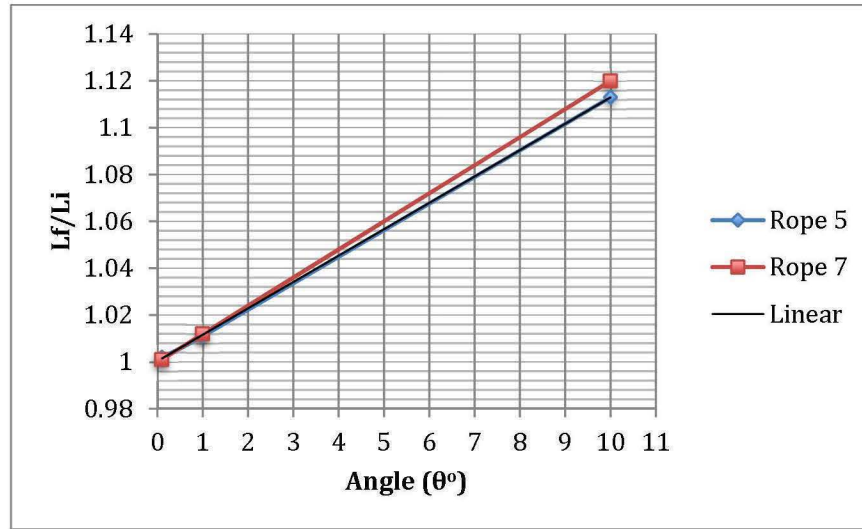


**Figure 2.12.3-16. Final to Initial Rope Length Ratio per Small Angle Rotation**

The fact that the ratios are the same for each rope and liner indicates that their derivation is correct. Their similarity and linearity would be expected from rigid body rotation.

Back to the relation between  $F_6$  and  $F_8$  (or  $F_5$  and  $F_7$ ), the ratio of loads due to stretching are for  $\delta = 0.1^\circ$ :

$$\begin{aligned}\frac{F_7}{F_5} &= \frac{\delta_7 L_5}{\delta_5 L_7} \\ \frac{F_7}{F_5} &= \frac{0.2 * 64.6}{0.1 * 145.2} = 0.8898... ** \\ L_5 &= 64.6 \\ L_7 &= 145.2 \\ \delta_5 &= L_{5f} - L_{5i} \\ &= 64.7 - 64.6 = 0.1 \\ \delta_7 &= 145.4 - 145.2 = 0.2\end{aligned}$$

For  $\theta = 10^\circ$

$$\frac{F_7}{F_5} = \frac{17.4}{7.3} = 1.061$$

Because the ropes cannot stretch 7.3 or 17.4 inches, this just shows that the ratio of forces in the ropes is fairly close at the two extremes. For the purpose of analysis, the value of 0.8898 will be used as this represents a more realistic elongation of the ropes.

$$F_7 = F_8 = 0.8898 F_5 = 0.8898 F_6$$

NEDO-33866 Revision 6  
Non-Proprietary Information

$$F_6 56.8 + (0.8898 F_6) \times 169.1 = 2.134 (10^7)$$

$$\begin{aligned} F_5 &= F_6 = 102,960.00 \\ F_7 &= F_8 = 0.8898 F_6 = 91,614.00 \\ RF &= F_5y + F_6y + F_7y + F_8y - W_a \\ &= 0.774F_5 + 0.774F_6 + 0.654F_7 + 0.654F_8 - 335,500 = -56,287 \text{ lb} \end{aligned}$$

### 5g Transverse

This time the 5g acceleration will cause the package to rotate at a point 90° clockwise from point “o”. This will cause ropes 2, 4, 6 and 8 to go slack, and tension ropes 1, 3, 5 and 7. From symmetry the following assumptions can be made with reference to Figure 2.12.3-13.

$$\begin{aligned} F_1 &= F_7 \\ F_3 &= F_5 \end{aligned}$$

The component forces for these ropes are:

$$\begin{aligned} F_{3x} &= F_{5x} = F_5 \cos 23.2^\circ \sin 32.7^\circ = 0.497 F_3 \\ F_{3z} &= F_{5z} = F_5 \sin 23.2^\circ = 0.394 F_3 \\ F_{1x} &= F_{7x} = F_7 \cos 46.3^\circ \sin 18.69^\circ = 0.221 F_1 \\ F_{1z} &= F_{7z} = F_7 \sin 46.3^\circ = 0.723 F_1 \end{aligned}$$

The reaction forces from chocking and friction (RF) and bearing on the package base (RB) are:

$$RF = F_{5x} + F_{3x} + F_{7x} + F_{1x} - W_a$$

$$RB = F_{5z} + F_{3z} + F_{7z} + F_{1z} + W_g$$

RB is calculated assuming  $F_2 = F_4 = F_6 = F_8 = 0$

$$\begin{aligned} \Sigma M_{ox} &= 0 = -W_a 63.60 + W_g 24.25 - RB 24.25 + (F_{5x} + F_{3x})25.5 + (F_{7x} + F_{1x}) \\ &\quad 105.0 + (F_{5z} + F_{3z} + F_{7z} + F_{1z}) 40.12 \end{aligned}$$

$$\begin{aligned} \Sigma M_{ox} &= -W_a 63.60 + W_g 24.25 - (F_{5z} + F_{3z} + F_{7z} + F_{1z} + W_g)24.25 + \dots \\ &\quad \dots (F_{5x} + F_{3x})25.5 + (F_{7x} + F_{1x})105.0 + (F_{5z} + F_{3z} + F_{7z} + F_{1z})40.12 \\ &= -W_a 63.60 - [2 \times 0.394F_3 + 2 \times 0.723F_1]24.25 + 2 \times 0.497F_3(25.5) + \dots \\ &\quad \dots 2 \times 0.221F_1(105.0) + [2 \times 0.394F_3 + 2 \times 0.723F_1]40.12 \\ &= -W_a 63.60 - 19.1F_3 - 35.1F_1 + 25.3F_3 + 46.41F_1 + 31.6F_3 + 58F_1 \\ &= -W_a 63.60 + (-19.1 + 25.3 + 31.6) F_3 + (-35.1 + 46.41 + 58) F_1 \\ &= - (63.60) W_a + (37.8)F_3 + (69.31)F_1 \\ &\Rightarrow 1.063 (10^7) = (37.8)F_3 + (69.3)F_1^* \end{aligned}$$

From equation\*\*  $F_5$  and  $F_7$  are related as:

$$\begin{aligned} F_7 &= 0.8898F_5 \\ &= 0.8898F_3 = F_1 \\ &\Rightarrow 1.063 (10^7) = (37.8)F_3 + (69.3)(0.8898F_3)^* \\ F_3 &= 106,874 \end{aligned}$$

NEDO-33866 Revision 6  
Non-Proprietary Information

$$\begin{aligned} F_5 &= 106,874 \\ F_1 &= 95,096 \\ F_7 &= 95,096 \end{aligned}$$

$$\begin{aligned} \text{From above: } RF &= F_{5x} + F_{3x} + F_{7x} + F_{1x} - W_a \\ &= 0.497F_5 + 0.497F_3 + 0.221F_7 + 0.221F_1 - 167,100 = -18,835 \text{ lb} \end{aligned}$$

### 2g Vertical

During the 2g vertical load all 8 members are expected to experience tension, and all vertical components of the members will react. From symmetry, the following assumptions can be made with reference to Figure 2.12.3-13.

Assumption from symmetry: For the 2g vertical load, all ropes at the bottom (3,4,5,6) experience equal load and all ropes on top (1,2,7,8) experience equal load.

$$\begin{aligned} F_{5z} &= F_{4z} = F_{3z} = F_{6z} = \sin(23.2)F_3 = 0.394 F_3 \\ F_{7z} &= F_{2z} = F_{1z} = F_{8z} = \sin(46.3)F_1 = 0.723 F_1 \end{aligned}$$

Where Fz is the vertical component of the forces on the ropes.

$$\begin{aligned} \Sigma F_z &= 0 = (F_{5z} + F_{4z} + F_{3z} + F_{6z}) + (F_{7z} + F_{2z} + F_{1z} + F_{8z}) + W_g - W_a = 0 \\ &= 4 F_{5z} + 4 F_{7z} + W_g - W_a = 0 \\ &= 4 \times 0.394 F_3 + 4 \times 0.723 F_1 + W_g - 2W_g = 0 \\ &= 1.576F_3 + 2.892F_1 - W_g = 0 \\ &= 1.576F_3 + 2.892F_1 = 33,500 \end{aligned}$$

$$\text{From above, } F_1 = 0.8898F_3.$$

$$\text{Hence } \Rightarrow \frac{1.576}{0.8898} F_1 + 2.892F_1 = 33,500$$

$$\begin{aligned} \Rightarrow 1.771F_1 + 2.892F_1 &= 33,500 \\ &= 4.663F_1 = 33,500 \end{aligned}$$

$$\begin{aligned} \Rightarrow F_1 &= 7183.93 = F_2 = F_7 = F_8 \\ \Rightarrow F_3 &= 8073.65 = F_4 = F_5 = F_6 \end{aligned}$$

**Table 2.12.3-4. Tie-Down Ropes Tension Forces**

Rope No.	10W Long. (lb)	5W Transv. (lb)	2W Vert.(lb)	Total (lbf)
1	---	95,096	7,184	95,367
2	---	---	7,184	7,184
3	---	106,874	8,074	107,179
4	---	---	8,074	8,074
5	102,960	106,874	8,074	<b>148,620<sup>max</sup></b>
6	102,960	---	8,074	103,276
7	91,614	95,096	7,184	132,242
8	91,614	---	7,184	91,895
Friction	56,287	18,835	---	---

As documented in Table 2.12.3-4, the maximum cable tension force is 148.62 kip. This load value is used in subsequent tie-down analysis of the rib.

- TIE-DOWN RIB ANALYSIS

The tie-down ribs are triangular plate two inches thick supported at the short side by a 5 inch x 6.5 inch pad that is 0.5 inch thick. This plate is rolled to conform with the toroidal shell contour. The vertical edge of the tie-down rib is welded to a stiffening ring. The tie-down rib, pad and stiffening ring are fabricated from ASTM A240, Type [[ ]] material. The toroidal shell material is ASTM A403, Type 304 stainless steel; and the overpack outer shell, where the stiffening ring attaches, is fabricated from ASTM A240, SS304.

The maximum temperature, 249°F, of the overpack bottom toroidal shell, where the tie-down ribs will be attached, is used as a reference.

Several modes of failure are investigated for the components of the tie-down rib system. These modes of failure are:

- Shear tearout of tie-down rib hole
- Bearing of shackle pin on ear
- Yielding of weld joints and parent metal

- SHEAR TEAROUT OF TIE-DOWN RIB HOLE

Figure 2.12.3-17 shows a sketch of the tie-down rib with the rope tension force line of action and lines of failure in shear.

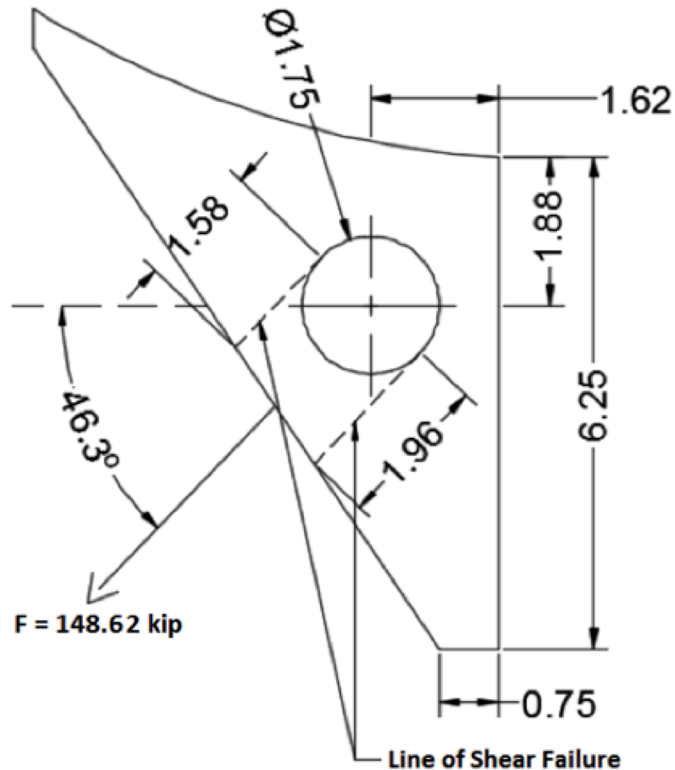


**Figure 2.12.3-17. Tie-Down Rib Hole Loading**

$$\tau = \frac{F}{A}$$

where  $A = 2 \times (1.58 + 1.96) = 7.08 \text{ in}^2$

$$\tau = \frac{148.62}{7.08} = 20.99 \text{ ksi} < 27.12 \text{ ksi}$$

- BEARING OF SHACKLE PIN ON EAR

The bearing stress is computed assuming that the force is uniformly distributed over the projected contact area of the pin's 1.75-inch diameter. This gives for the stress:

$$\sigma = \frac{F}{A} = \frac{148.62}{2.0 \times 1.75} = 42.3 \text{ ksi}$$

$$\sigma = 42.5 \text{ ksi} < 45.2 \text{ ksi}$$

- YIELDING OF WELD JOINTS AND PARENT METAL

Figure 2.12.3-18 shows the approximate weld pattern for the top tie-down rib.

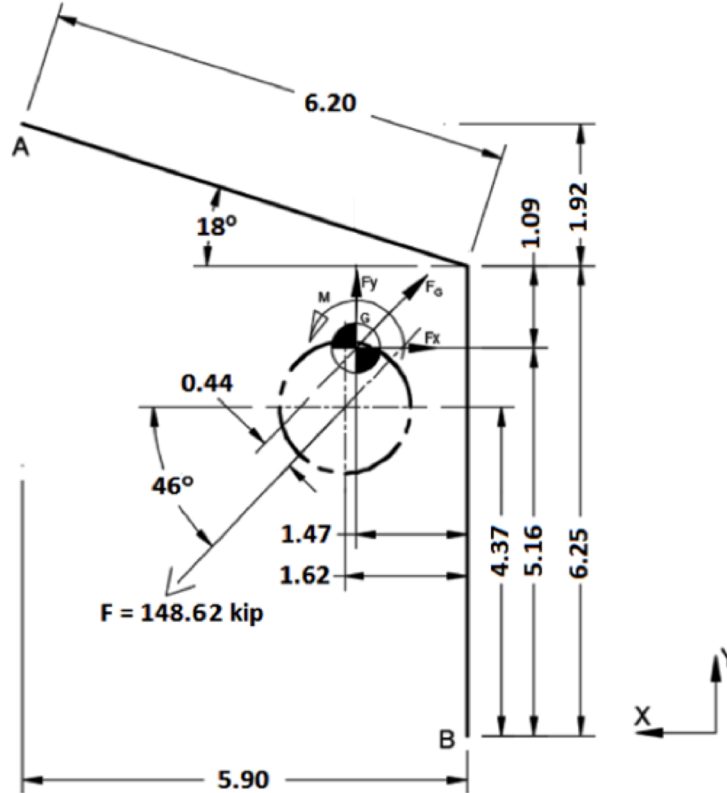


**Figure 2.12.3-18. Weld Pattern of Top Tie Down Rib**

Using the line load method (actual weld is ½ inch fillet 2 sides):

$$L = 6.2 + 6.25 = 12.45 \text{ inches}$$

$$\bar{X} = \frac{\sum \bar{X}_i L_i}{\sum L_i} = \frac{6.2 \times \left( \frac{6.2 \cos(18^\circ)}{2} \right)}{12.45} = \frac{6.2 \times 2.95}{12.45} = 1.47 \text{ in}$$

$$\bar{Y} = \frac{\sum \bar{Y}_i L_i}{\sum L_i} = \frac{6.25 \times (6.25/2) + 6.2 \times \left( 6.25 + \left( \frac{6.2 \sin(18^\circ)}{2} \right) \right)}{12.45} = 5.16 \text{ in}$$

$$\begin{aligned} I_x &= \sum (I_o + A d^2) \\ &= \frac{6.25^3}{12} + 6.25 (5.16 - (6.25/2))^2 + \frac{6.2^3 \sin^2 18^\circ}{12} + \dots \\ &\quad \dots 6.2 (6.25 + \left( \frac{6.2 \sin(18^\circ)}{2} \right) - 5.16)^2 \\ &= 74.13 \text{ in}^4/\text{in} \end{aligned}$$

$$\begin{aligned} I_y &= \frac{6.2^3 \cos^2(18^\circ)}{12} + 6.2 (2.95 - 1.47)^2 + 6.25 (1.47)^2 \\ &= 45 \text{ in}^4/\text{in} \end{aligned}$$

NEDO-33866 Revision 6  
Non-Proprietary Information

$$\therefore I_z = I_x + I_y = 119.14 \text{ in}^4/\text{in}$$

There are two welds:

$$\begin{aligned}\therefore I_z &= 119.14 \times 2 = 238.28 \text{ in}^4/\text{in} \\ \therefore M_z &= F \times r = 148.62 \times 0.44 = 65.39 \text{ k-in.}\end{aligned}$$

$$F_x = F \cos \theta = 148.62 \cos 46^\circ = 103.24 \text{ kip}$$

$$F_y = F \sin \theta = 148.62 \sin 46^\circ = 106.91 \text{ kip}$$

$\therefore @$  Point A:

$$P_x = \frac{F_x}{L} + \frac{M_{zy}}{I} = \frac{103.24}{2(12.45)} + \frac{(65.39)(6.25+1.92-5.16)}{(238.28)} = 4.97 \text{ k/in}$$

$$\begin{aligned}P_y &= \frac{F_y}{L} + \frac{M_{zx}}{I} = \frac{106.91}{(24.9)} + \frac{(65.39)(6.2 \cos(18)-1.47)}{(238.28)} = 5.51 \text{ k/in} \\ P_z &= 0\end{aligned}$$

Total line load:

$$P_T = \sqrt{P_x^2 + P_y^2 + P_z^2} = 7.42 \text{ k/in.}$$

Shear stress in the effective throat area of the weld is:

$$S_v = \frac{7.42}{0.707t} = \frac{7.42}{0.707 \times 0.5} = 20.99 \text{ ksi} < 27.12 \text{ ksi (allowable base metal)}$$

Shear stress on the weld leg

$$S_t = \frac{7.42}{0.5} = 14.84 \text{ ksi}$$

$\therefore @$  Point B:

$$P_x = \frac{103.24}{24.9} + \frac{(65.39)(5.16)}{(238.28)} = 5.56 \text{ kip}$$

$$P_y = \frac{106.9}{(24.9)} + \frac{(65.39)(1.47)}{(238.28)} = 4.7 \text{ k/in}$$

$$P_T = \sqrt{(5.56^2 + 4.7^2 + 0)} = 7.28 \text{ k/in}$$

$$S_v = \frac{7.28}{0.3535} = 20.59 \text{ ksi} < 27.12 \text{ ksi}$$

Shear stress on leg of weld:

$$S_t = \frac{7.28}{0.5} = 14.56 \text{ ksi} < 27.12 \text{ ksi}$$

The following analysis checks weld failure mode of weld attaching tie-down rib and gusset to overpack, refer to Figure 2.12.3-19.

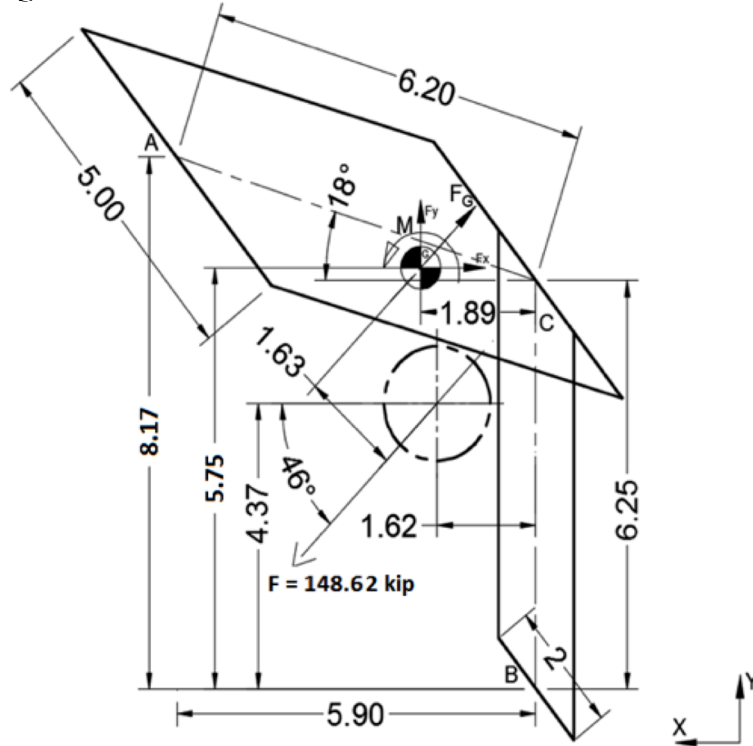


**Figure 2.12.3-19. Weld Geometry of Tie-Down Rib and Gusset to Overpack**

$$L = 5 + (6.2) \times 2 + 5 + 6.25 \times 2 = 34.9 \text{ inches}$$

$$\bar{X} = \frac{\sum \bar{X}_i L_i}{\sum L_i} = \frac{5 \times 6.2 \cos(18) + 12.4 \times \left(\frac{6.2 \cos(18)}{2}\right)}{34.9} = 1.89 \text{ in}$$

$$\bar{Y} = \frac{\sum \bar{Y}_i L_i}{\sum L_i} = \frac{5 \times (6.25 + 6.2 \sin(18)) + 12.4 \times \left(6.25 + \left(\frac{6.2 \sin(18)}{2}\right)\right) + 5 \times (6.25) + 12.5 \times \left(\frac{6.25}{2}\right)}{34.9} = 5.75 \text{ in}$$

$$\begin{aligned} I_z &= (5) \left[ (6.2 \cos(18) - 1.89)^2 + (6.2 \sin(18) + 6.25 - 5.75)^2 \right] \\ &\quad + (12.4) \left[ \left( \frac{6.2 \cos(18)}{2} - 1.89 \right)^2 + \left( 6.25 + \frac{6.2 \sin(18)}{2} - 5.75 \right)^2 \right] \\ &\quad + (5) \left[ (6.25 - 5.75)^2 + 1.89^2 \right] + (12.5) \left[ 1.89^2 + \left( \frac{6.25}{2} + (6.25 - 5.75) \right)^2 \right] + \frac{6.2^3}{12} + \frac{6.25^3}{12} \\ &= 339.77 \text{ in}^3 \end{aligned}$$

$$MZ = 148.62 \times 1.15 = 170.91 \text{ k-in.}$$

∴ @ Point A:

$$P_x = \frac{103.24}{34.9} + \frac{(170.89)(8.17 - 5.75)}{339.77} = 4.18 \frac{k}{in}$$



NEDO-33866 Revision 6  
Non-Proprietary Information

$$P_Y = \frac{106.91}{34.9} + \frac{(170.55)(5.9-1.89)}{339.77} = 5.08 \frac{k}{in}$$

$$P_Z = 0$$

∴ Total line load:

$$P_T = \sqrt{4.18^2 + 5.08^2} = 6.58 \frac{k}{in}$$

Shear stress in the effective throat area of the weld is:

$$S_V = \frac{6.58}{0.707t} = \frac{6.58}{0.707 \times 0.5} = 18.60 \text{ ksi} < 27.12 \text{ ksi (allowable base metal)}$$

For a ½ inch fillet, shear stress in the weld leg is:

$$S_V = \frac{6.58}{(0.5)} = 13.15 \text{ ksi} < 27.12 \text{ ksi}$$

∴ @ Point B:

$$P_X = \frac{103.24}{34.9} + \frac{(170.91)(5.75)}{339.77} = 5.85 \frac{k}{in}$$

$$P_Y = \frac{106.91}{34.9} + \frac{(170.91)(1.89)}{339.77} = 4.02 \frac{k}{in}$$

$$P_Z = 0$$

∴ Total line load:

$$P_T = \sqrt{5.83^2 + 4.00^2} = 7.09 \frac{k}{in}$$

Shear stress in the effective throat area of the weld is:

$$S_V = \frac{7.09}{0.707t} = 20.07 \text{ ksi} < 27.12 \text{ ksi}$$

For a ½ inch fillet, maximum shear stress on the weld is:

$$S_V = \frac{7.09}{(0.5)} = 14.19 \text{ ksi} < 27.12 \text{ ksi}$$

The lower allowable stress for welds made to the A240 material is not a problem because of the direction of the applied load. The weld takes the load in tension. At Point C:

$$P_X = \frac{103.24}{34.9} + \frac{170.91(-0.5)}{339.77} = 2.71 \frac{k}{in}$$

$$P_Y = \frac{106.9}{34.9} + \frac{170.91(1.89)}{339.77} = 4.01 \frac{k}{in}$$

Forces acting in tension against the A240 are:

$$\begin{aligned} P_T &= P_X \sin \theta + P_Y \cos \theta \\ &= 2.71 \times \sin 18^\circ + 4.01 \times \cos 18^\circ = 4.65 \frac{k}{in} \\ S_t &= \frac{4.65}{0.5} = 9.31 \text{ ksi} < 23.7 \text{ ksi} \end{aligned}$$

- EXCESSIVE LOAD FAILURE

The tie-down system must be designed such that its failure under excessive load would not impair the ability of the package to meet the requirements of 10 CFR 71. The tie-down system is attached to the overpack structure; the cask (containment vessel) resides within the overpack without attachment to its inner surface. Therefore, failure of the tie-down will not affect the performance of the cask. The results are presented in Table 2.12.3-5.

**Table 2.12.3-5. Tie-Down System Stress Analysis Results**

Condition	Stress Level (ksi)	Allowable based on Yield Strength (ksi)	MS (y)	Allowable based on Ultimate Strength (ksi)	MS (U)
Shear tear-out of hole	20.99	$0.6 \times 45.2 = 27.12$	0.29	36.95	0.76
Bearing of shackle pin	42.46	45.2	0.06	96.80	1.28
Yielding of weld joints	20.99	$0.6 \times 45.2 = 27.12$	0.29	36.95	0.76

The tie-down rib and pin materials are type [[                      ]] stainless steel.

The margins of safety (MS (y)) with respect to yield is calculated as follows:

$$MS \text{ (yield)} = \frac{\text{Allowable based on yield strength}}{\text{Stress level}} - 1$$

The margins of safety with respect to ultimate failure are:

Shear Strength:

$$\frac{\sigma_{ult}}{2(1+\mu)} = \frac{96.8}{2(1.31)} = 36.95 \text{ ksi}$$

Shear tear-out of tie-down rib hole

$$MS = \frac{36.95}{20.99} - 1 = 0.76$$

Bearing of shackle pin

$$MS = \frac{96.8}{42.46} - 1 = 1.28$$

Yielding of weld joints

$$MS = \frac{36.95}{20.99} - 1 = 0.76$$

## 2.12.4. Cask Closure Bolt Evaluation

### 2.12.4.1. Cask Lid Bolt Load Calculation

This section documents the cask lid bolt load calculations.

Cask Bolt Preload

The torque/preload relationship is defined as follows:

$$T = K \times D \times P_i \quad \text{Reference 2-14, Page 19}$$

Solving for  $P_i$  yields:

$$P_i = T / (K \times D)$$

NEDO-33866 Revision 6  
Non-Proprietary Information

where

$$\begin{aligned} K &= \text{Torque friction coefficient} \\ &= 0.15 \text{ (Reference 2-30)} \\ D &= \text{Nominal bolt diameter (in)} \\ &= 1.25 \text{ in} \\ T &= 720 \pm 30 \text{ lb-in} \end{aligned}$$

The maximum cask bolt preload is:

$$P_{i \text{ Max}} = 750 \times 12 / (0.15 \times 1.25) = 48.00 \text{ kips}$$

#### Cask Bolt Applied Load: Non-Prying

The bolt non-prying load is defined as the sum of the non-prying tensile bolt force due to temperature, non-prying tensile bolt force due to pressure, axial load for gasket seating, and axial load for gasket operation for this calculation. The non-prying tensile bolt force due to temperature and non-prying tensile bolt force due to pressure can be easily calculated utilizing the parameters and formulas specified in NUREG-6007 (Reference 2-15). The axial load for gasket varies depending on the gasket material used and gasket width, which is the focus of the following evaluation.

#### Gasket Load

The formulas for the axial loads for gasket seating and gasket operation are given in Equation (1) and Equation (2), respectively (Reference 2-15, Table 4.2, page 13).

$$F_a = \frac{\pi D_{lg} b y}{N_b} \quad (1)$$

where

$$\begin{aligned} D_{lg} &= \text{Closure lid diameter at the location of the gasket load} \\ &\quad \text{Reaction (in)} \\ &= 29.25 \text{ in} \\ b &= \text{Effective gasket surface seating width (in)} \\ y &= \text{Minimum design seating stress (psi)} \\ N_b &= \text{Total number of closure bolts} \\ &= 15 \end{aligned}$$

$$F_a = \frac{2 \pi D_{lg} b m (P_{li} - P_{lo})}{N_b} \quad (2)$$

$$\begin{aligned} m &= \text{Gasket factor for operating conditions} \\ P_{li} &= \text{Pressure inside the closure lid (psi)} \\ &= 30 \text{ psi} \\ P_{lo} &= \text{Pressure outside the closure lid (psi)} \\ &= 15 \text{ psi} \end{aligned}$$

Equations (1) and (2) use two experimentally determined constants, which are the gasket factor,  $m$ , and the minimum design seating stress,  $y$ . The gasket factor is taken into consideration for the axial load for gasket operation and is defined as the ratio of the required minimum gasket pressure to the pressure contained by the gasketed joint. Additionally, the seating stress is applied for the axial load for gasket seating and is defined as the minimum design seating stress of the gasket. Both of these constants are determined per Table E-1210-1 of the ASME Boiler and Pressure Vessel Code (B&PVC) Section III Division 1 Appendices (Reference 2-18, page 222).

Further, equation (1) and equation (2) both utilize the parameter  $b$ , which is the effective gasket or joint contact surface seating width. The effective gasket seating width is determined by first calculating the basic gasket seating width ( $b_o$ ) per Table E-1210-2 of the ASME B&PVC Section III Division 1 Appendices (Reference 2-18). From Table E-1210-2, face sketch is used for the evaluation due to the fact that this sketch is the closest to the actual geometry as Figure B-1 depicts. It can be seen that  $b_o$  is a function of the variable  $w$  for face sketch, which is based upon the contact width between the flange facing and the gasket. Following, the effective gasket seating width is determined based off of the following criteria (Reference 2-18, page 223):

$$b = b_o, \text{ when } b_o \leq \frac{1}{4} \text{ in}$$

$$b = C_b \sqrt{b_o}, \text{ when } b_o > \frac{1}{4} \text{ in}$$

where

$$C_b = \begin{aligned} &\text{effective width factor} \\ &= 0.5 \text{ for U.S Customary calculations} \\ &= 2.5 \text{ for SI calculations} \end{aligned}$$

Once the effective gasket seating width is determined, both axial loads for gasket seating and gasket operation can be calculated by use of Equation (1) and Equation (2). For the calculations of this document, the parameters presented above are determined for soft aluminum. Furthermore, the seal detail drawing shown in Figure 2.12.4-1 is used to establish the contact width between the flange facing and the gasket ( $w$ ) and is shown to be 0.872 inches (0.218 inches  $\times$  4).

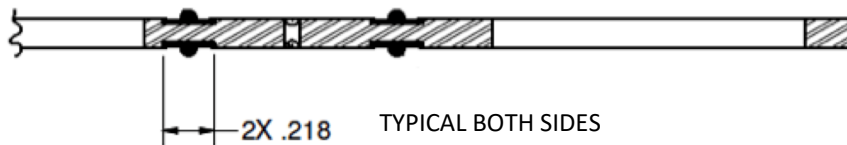


**Figure 2.12.4-1. Seal with Contact Width Dimension**

The gasket factor, minimum design seating stress, basic gasket seating width ( $b_o$ ), and effective gasket width ( $b$ ) are tabulated in Table 2.12.4-1 for the aluminum gasket material.

**Table 2.12.4-1. Input Parameters**

Material	Gasket Factor, $m$	Gasket Seating Stress, $y$ (psi)	Basic Gasket Seating Width, $b_o$ (in)	Effective Gasket Seating Width, $b$ (in)
Aluminum	4.00	8800	.109	.109

The calculation for the basic gasket seating width ( $b_o$ ) and effective gasket seating width ( $b$ ) is determined by use of face sketch per Table E-1210-2. Therefore, the effective gasket width is:

$$b_o = \frac{w}{8} = \frac{.872 \text{ in}}{8} = .109 \text{ in}$$

Because  $b_o$  is less than  $\frac{1}{4}$  in,  $b_o$  is equal to  $b$ .

With all parameters calculated, the axial loads due to gasket seating and gasket operation can be calculated.

The sections below provide a detailed analysis of the forces and moments that are subjected to the bolted joint of the Model 2000 cask during normal and accident conditions.

## 2.12.4.2. Lid Bolt Evaluation

### 2.12.4.2.1. Required Length of Engagement

For this analysis, a  $1\frac{1}{4}$ -7 UNC-2A external thread with a  $1\frac{1}{4}$ -7 UNC-2B internal thread is considered at an operating temperature of 150°F. The external thread material is ASTM A-540, Grade B22, Class 3 and the internal thread material is ASME SA-182, F304. Table 2.12.4-2 lists the required parameters needed for the analysis.

**Table 2.12.4-2. Lid Bolt Evaluation Input Parameters**

Parameter	Variable	Input	Units
Tensile Strength of External Thread at 150°F	$S_{u1}$	145*	ksi
Tensile Strength of Internal Thread at 150°F	$S_{u2}$	73	ksi
Minimum Pitch Diameter (External Thread)	$E_{s,min}$	1.1476	in
Minimum Major Diameter (External Thread)	$D_{s,min}$	1.2314	in
Maximum Pitch Diameter (Internal thread 2B)	$E_{n,max}$	1.1668	in
Maximum Major Diameter (Internal thread 2B)	$K_{n,max}$	1.123	in
Threads Per Inch	$n$	7	in
Bolt Pre-Load	$P$	82.8	kip

References:

Reference 2-30 Minimum Pitch Diameter: Table 3, Page 1827

Reference 2-30 Minimum Major Diameter: Table 3, Page 1827

Reference 2-30 Maximum Pitch Diameter (2B): Table 3, Page 1827

Reference 2-30 Maximum Minor Diameter (2B): Table 3, Page 1827

Based on these given inputs, it must be determined if the bolt will fail before the threads of either the internal or external fixtures or vice versa. To do this, the required length of engagement must be calculated and checked against the actual geometry. The length of engagement ( $L_e$ ) is calculated as follows (Reference 2-30, Page 1536),

$$L_e = \frac{2A_t}{\pi(K_{n,max})(\frac{1}{2} + .57735n[E_{s,min} - K_{n,max}])}$$

Where,

$$A_t = \text{Screw thread tensile stress area}$$

and  $A_t$  is given by the equation,

$$A_t = \pi \left[ \frac{E_{s,\min}}{2} - \frac{0.16238}{n} \right]^2$$

The length of engagement ( $L_e$ ) is for mating external and internal threads of the same strength. If the materials of the internal and external threads do not have the same strength, the relative strength ( $J$ ) must be calculated to determine if the internal thread could strip before the bolt breaks. The relative strength is calculated as follows,

$$J = \frac{A_s \times S_{ut \text{ of external thread material}}}{A_n \times S_{ut \text{ of internal thread material}}}$$

where

$$A_s = \text{Shear area of external threads}$$

$$A_n = \text{Shear area of internal threads}$$

Also, the shear area of the external and internal threads are given by,

$$A_s = \pi n L_e K_{n,\max} \left[ \frac{1}{2n} + .57735(E_{s,\min} - K_{n,\max}) \right]$$

and,

$$A_n = \pi n L_e D_{s,\min} \left[ \frac{1}{2n} + .57735(D_{s,\min} - E_{n,\max}) \right]$$

where

$$n = \text{number of threads per inch}$$

If the relative strength is calculated to be less than or equal to 1, then the length of engagement ( $L_e$ ) is sufficient to prevent stripping of the internal thread. If the relative strength is calculated to be greater than 1, then the required length of engagement is calculated by taking the product of the  $J$  factor and the length of engagement as given is:

$$Q = J L_e$$

where

$$Q = \text{Required length of engagement}$$

Once the required length of engagement is calculated, this value is checked against the actual geometry to determine if the internal threads will strip before the bolt breaks or vice versa. Table 2.12.4-3 presents the results.

**Table 2.12.4-3. Calculation of Required Length of Engagement at 150°F**

Parameter	Variable	Result	Units
Tensile stress area of bolt	$A_t$	0.952	in <sup>2</sup>
Effective length	$L_e$	0.901	in
Shear area of internal threads	$A_n$	2.652	in <sup>2</sup>
Shear area of external threads	$A_s$	1.905	in <sup>2</sup>
Relative strength of external/internal threads	J	1.427	--
Required length of engagement if $J > 1$	Q	1.285	in

Looking at the actual geometry, the engagement = 3.00 inches (lid bolt length) – 1.625 inches (flange + seal) = 1.375 inches. At 150°F, the required length of engagement is less than the engagement of the geometry. Therefore, a thread engagement of 1.375 inches will ensure that the threads of either the internal or external fixture will not strip before the bolt fails for a Class 2A bolt in 2B threads.

#### 2.12.4.2.2. Applied Load Analysis

The maximum load on the bolt to break the threaded portion is determined by taking the product of the ultimate tensile strength of the external thread and the bolt thread tensile stress area (Reference 2-30).

$$\begin{aligned}
 P_{\max} &= S_u A_t \\
 &= (145 \text{ ksi})(.952 \text{ in}^2) \\
 P_{\max} &= 138 \text{ kip}
 \end{aligned}$$

Now that the maximum load has been calculated, the minimum thread engagement,  $L_e$ , based on the applied pre-load is:

$$\begin{aligned}
 P &= \sigma A_n \\
 &= \text{bolt pre-load} \\
 &= 82.8 \text{ kip} \\
 &= \text{Tensile strength of internal thread} \\
 A_n &= \text{Internal thread shear area (Class 2A + 2B)}
 \end{aligned}$$

From Reference 2-30:

$$P = \sigma \times \pi \times n \times L_e \times D_{s,\min} \times [1/2n + .57735(D_{s,\min} - E_{n,\max})]$$

Solving for the effective length:

$$L_e = P / (\sigma \times \pi \times n \times D_{s,\min} \times [1/2n + .57735(D_{s,\min} - E_{n,\max})])$$

Solving, the minimum thread engagement is 0.3852 inches at an operating temperature of 150°F. accordingly, calculating the product of the effective length and the number of threads per inch, the minimum thread engagement to prevent internal 2B thread stripping is approximately three threads.

### 2.12.4.2.3. Bolt Stress Analysis

The cask lid of the Model 2000 cask is fastened to the cask flange by way of 15 uniformly spaced ASTM A540, Grade B-22, Class 3 socket head screws. Table 2.12.4-4 provides the input parameters that are to be used in the analysis at an operating temperature of 500°F.

**Table 2.12.4-4. Model 2000 Stress Analysis Design Input Parameter**

Parameter	Variable	Input	Units
Number of Bolts	N <sub>b</sub>	15	--
Lid Diameter at Bolt Circle	D <sub>lb</sub>	32.25	in
Lid Diameter at Gasket	D <sub>lg</sub>	29.25	in
Nominal Bolt Diameter	D <sub>b</sub>	1.25	in
Lid Diameter at Inner Edge	D <sub>li</sub>	28	in
Lid Diameter at Outer Edge	D <sub>lo</sub>	34.75	in
Equivalent Thickness of Lid	t <sub>l</sub>	7.89	in
Thickness of Lid Flange	t <sub>lf</sub>	1.5	in
Thickness of Cask Wall	t <sub>c</sub>	6	in
Bolt Length Between the Top and Bottom of Closure Lid at Bolt Circle	l <sub>b</sub>	1.5	in
Bolt Engagement Length	BEL	1.625	in
Bolt Moment of Inertia/Cir	XIB	0.018	in <sup>3</sup>
Young's Modulus for Lid	E <sub>l</sub>	25900000	psi
Young's Modulus for Cask	E <sub>c</sub>	25900000	psi
Young's Modulus for Bolt	E <sub>b</sub>	27400000*	psi
Poisson's Ratio for Lid	N <sub>ul</sub>	0.31	--
Poisson's Ration for Cask	N <sub>uc</sub>	0.31	--
Lid Thermal Expansion Coefficient	a <sub>l</sub>	9.70E-06	1/°F
Bolt Thermal Expansion Coefficient	a <sub>b</sub>	7.30E-06*	1/°F
Weight of Cask Payload	W <sub>C</sub>	5450	lb
Weight of Cask Lid	W <sub>l</sub>	1900	lb
Dynamic Load Factor	DLF	1	--
Preload Torque	Q <sub>NOM</sub>	720	lb-ft
Preload Torque Tolerance	Q <sub>TOL</sub>	30	lb-ft
Maximum Preload Torque	Q <sub>MAX</sub>	9000	lb-in
Minimum Preload Torque	Q <sub>MIN</sub>	8280	lb-in
Nut Factor for Preload Torque	K <sub>q</sub>	0.15	--
Gasket Seating Width	G <sub>b</sub>	0.109	in
Gasket Seating Stress	G <sub>y</sub>	8800	psi
Gasket Factor	G <sub>m</sub>	4	--
Wall Thermal Expansion Coefficient	a <sub>c</sub>	9.70E-06	1/°F
Basic Allowable Stress Limit	S <sub>m</sub>	7.71E+04	psi
Minimum Yield Strength	S <sub>y</sub>	115700	psi
Minimum Ultimate Strength	S <sub>u</sub>	145000	psi
Pressure Inside Closure Lid	P <sub>li</sub>	30	psi



NEDO-33866 Revision 6  
Non-Proprietary Information

Parameter	Variable	Input	Units
Pressure Outside the Closure Lid	$P_{lo}$	15	psi
Pressure Inside the Cask Wall	$P_{ci}$	30	psi
Pressure Outside the Cask Wall	$P_{co}$	15	psi
Temperature Change of the Closure Lid	$T_l$	117.5	°F
Temperature Change of the Closure Bolt	$T_b$	111.9	°F
Temperature Change of the Cask Wall	$T_c$	118.0	°F
Temperature Change of Inner Surface of Closure Lid	$T_{li}$	116.8	°F
Temperature Change for Outer Surface of Closure Lid	$T_{lo}$	118.1	°F
Maximum rigid body impact acceleration (g)	$a_i$	25**	--
Impact angle between the cask axis and the target surface	$\alpha_i$	90°	--
Maximum axial vibration acceleration (g) at the cask support	$a_{va}$	2	--
Maximum transverse vibration acceleration (g) at the cask support	$a_{vt}$	5	--
Vibration transmissibility of acceleration between the cask support and the closure lid	VTR	1	--

References:

Reference 2-31 Gasket Seating Width: Table E-1210-2

Reference 2-31 Gasket Seating Stress: Table E-1210-1

Reference 2-31 Gasket Factor: Table E-1210-1

Reference 2-15 Basic Allowable Stress Limit: Table 6.1, Page 28

Reference 2-1 Maximum Axial Vibration Acceleration (g) at the cask support

Reference 2-1 Maximum Transverse Vibration Acceleration (g) at the cask support

Reference 2-15 Vibration transmissibility of acceleration between the cask support and the closure lid

Notes:

\* Grade B21 bolt properties used because temperature dependent values could not be found for Grade B22.

\*\* Section 2.12.1, Figure 2.12.1.11-30 presents the justification for the reduced impact acceleration during the HAC end drop.

NUREG/CR-6007 (Reference 2-15) is used to accurately verify whether or not the closure bolts can effectively hold up to the various loads in both normal conditions of transport and hypothetical accident conditions. This includes forces and moments due to pressure, temperature, vibration, impact, preload, gasket, puncture, and prying. Also, NUREG/CR-6007 gives procedures for combining loads and stress limits that must be met. Loads include the axial force ( $F_a$ ), shear force ( $F_s$ ), fixed-edge closure-lid force ( $F_f$ ), fixed edge closure lid moment ( $M_f$ ), and also torsional moments ( $M_t$ ) that are created by the torque wrench in the preload and gasket seating operations. All of which are elaborated on in the following sections.

#### 2.12.4.2.4. Forces/Moments Generated By Preload

Found in Table 4.1 in NUREG/CR-6007, are the bolts loads due to use of a torque wrench. The non-prying axial bolt force per bolt is given by the equation,

$$F_a = Q / (K_q \times D_b)$$

The torsional bolt force per bolt is defined by the formula,

$$M_t = 0.5 Q$$

#### 2.12.4.2.5. Forces/Moments Generated By Gasket Loads

Per Table 4.2 in NUREG/CR-6007, are the formulas for calculating the forces and moments generated by gasket loads by utilization of a torque wrench. The axial force produced by the gasket seating operation is evaluated by use of the following equation,

$$F_a = \frac{\pi \times D_{lg} \times G_b \times G_y}{N_b}$$

and the torsional bolt moment due to the seating operation is,

$$M_t = \frac{0.5 \times \pi \times K_q \times D_b \times D_{lg} \times G_b \times G_y}{N_b}$$

Also, The non-prying tensile bolt force per bolt produced by the operating gasket seating is determined by,

$$F_a = \frac{2 \times \pi \times D_{lg} \times G_b \times G_m (P_{li} - P_{lo})}{N_b}$$

#### 2.12.4.2.6. Forces/Moments Generated By Pressure Loads

Table 4.3 in NUREG/CR-6007 is applied to determine the moments and forces that are generated due to the pressure difference between the inside and outside of the cask. The associated equation for the axial force due to pressure loads is,

$$F_a = \frac{\pi \times D_{lg}^2 \times (P_{li} - P_{lo})}{4 \times N_b}$$

where

$$\begin{aligned} P_{li} &= \text{Pressure inside the closure lid} \\ &= 30 \text{ psi} \\ P_{lo} &= \text{Pressure outside the closure lid} \\ &= 15 \text{ psi} \end{aligned}$$

The shear bolt force per bolt is then,

$$F_s = \frac{\pi \times E_t \times t_t \times (P_{li} - P_{lo}) \times D_{lb}^2}{2 \times N_b \times E_c \times t_c \times (1 - N_{ul})}$$

where

$$\begin{aligned} P_{ci} &= \text{Pressure inside the cask wall} \\ &= 30 \text{ psi} \\ P_{co} &= \text{Pressure outside the cask wall} \\ &= 15 \text{ psi} \end{aligned}$$

The fixed-edge closure-lid force generated by internal pressure is,

$$F_f = \frac{D_{lb} (P_{li} - P_{lo})}{4}$$

and the fixed-edge moment is,

$$M_f = \frac{D_{lb}^2 (P_{li} - P_{lo})}{32}$$

#### 2.12.4.2.7. Forces/Moments Generated By Temperature Loads

Table 4.4 of NUREG/CR-6007 gives the formulas for bolt forces/moments generated by thermal expansion difference between the closure lid, bolt, and wall. The axial force due to a temperature difference between the closure bolt and lid is:

$$F_a = \frac{1}{4} \times \pi \times D_b^2 \times E_b \times (\alpha_l \times T_l - \alpha_b \times T_b)$$

where

$$\begin{aligned} T_l &= \text{Temperature change of the closure lid} \\ &= 117.5^\circ\text{F} \\ T_b &= \text{Temperature change of the closure bolt} \\ &= 111.9^\circ\text{F} \end{aligned}$$

The shear force acting on each bolt is given by,

$$F_s = \frac{\pi \times E_l \times t_l \times D_{lb} \times (a_l \times T_l - a_c \times T_c)}{N_B \times (1 - N_{ul})}$$

where,

$$\begin{aligned} T_c &= \text{Temperature change of the cask wall} \\ &= 118^\circ\text{F} \end{aligned}$$

Fixed-edge force and fixed-edge moment due to temperature difference between the inner and outer surface of the closure lid is determined by use of the following equations.

$$F_f = 0 \text{ lb/bolt}$$

$$M_f = \frac{E_l \times a_l \times t_l^2 \times (T_{lo} - T_{li})}{12 \times (1 - N_{ul})}$$

where,

$$\begin{aligned} T_{lo} &= \text{Temperature change of the outer surface of the closure lid} \\ &= 118.1^\circ\text{F} \\ T_{li} &= \text{Temperature change of the inner surface of the closure lid} \\ &= 116.8^\circ\text{F} \end{aligned}$$

#### 2.12.4.2.8. Forces/Moments Generated By Impact Loads

For this evaluation, the loads created by impact are analyzed for a cask with a protected closure lid and are found via Table 4.5 in NUREG/CR-6007. As follows, the non-prying tensile bolt force per bolt due to impact is:

$$F_a = \frac{1.34 \times \sin(\alpha_i) \times DLF \times a_i \times (W_l - W_c)}{N_b}$$

Further, the shear bolt force per bolt is evaluated using,

$$F_s = \frac{\cos(\alpha_i) \times a_i \times W_l}{N_b}$$

Accordingly, the fixed-edge force and fixed-edge moment are defined by:

$$F_f = \frac{1.34 \times \sin(\alpha_i) \times DLF \times a_i \times (W_l - W_c)}{\pi \times D_{lb}}$$

and,

$$M_f = \frac{1.34 \times \sin(\alpha_i) \times DLF \times a_i \times (W_l - W_c)}{8\pi}$$

#### 2.12.4.2.9. Forces/Moments Generated By Vibration Loads

Looking at Table 4.8 in NUREG/CR-6007, the loads that are generated due to vibration are outlined. The tensile bolt force per bolt due to vibration is:

$$F_a = \frac{VTR \times a_{va} \times W_l}{N_b}$$

The shear bolt force per bolt is calculated by use of the equation,

$$F_s = \frac{VTR \times a_{vt} \times W_l}{N_b}$$

The fixed-edge force and fixed edge moment are:

$$F_f = \frac{VTR \times a_{va} \times W_l}{\pi \times D_{lb}}$$

and,

$$M_f = \frac{VTR \times a_{va} \times W_l}{8\pi}$$

#### 2.12.4.2.10. Prying Action Forces Generated by Applied Loads

Table 2.1 of NUREG/CR-6007 lays out the analysis to evaluate the axial bolt force per bolt caused by prying action of the lid is:

$$F_{ap} = \left( \frac{\pi D_{lb}}{N_b} \right) \left[ \frac{\frac{2 \times M_f}{D_{lo} - D_{lb}} - C1(B - F_f) - C2(B - P)}{C1 + C2} \right]$$

where

$$C1 = 1$$

$$C2 = \left( \frac{8}{3(D_{lo} - D_{lb})^2} \right) \left( \frac{E_l \times t_l^3}{1 - \nu_{ul}} + \frac{(D_{lo} - D_{lb}) E_{lf} \times t_{lf}^3}{D_{lb}} \right) \left( \frac{L_b}{N_b D_b^2 E_b} \right)$$

$$L_b = \text{Bolt length between the top and bottom surfaces of the closure lid at the bolt circle}$$

$$= 1.5 \text{ in}$$

$$B = F_f \text{ if } F_f > P, \text{ otherwise } B = P$$

It should be noted that the fixed-edge force and fixed-edge moment are inputs from Table 4.2, 4.3 and 4.8 for NCT and Table 4.2, 4.3 and 4.5 for HAC.

#### 2.12.4.2.11. Bending Bolt Moment Generated by Applied Loads

Located in Table 2.2 of NUREG/CR-6007 is the formula for calculating the bending bolt moment per bolt caused by the rotation or bending of the closure lid and is:

$$M_{bb} = \left( \frac{\pi D_{lb}}{N_b} \right) \left( \frac{K_b}{K_b + K_l} \right) M_f$$

where

$$K_b = \left( \frac{N_b}{L_b} \right) \left( \frac{E_b}{D_{lb}} \right) \left( \frac{D_b^4}{64} \right)$$

$$K_l = \frac{E_l t_l^3}{3 \left[ (1 - N_{ul}^2) + (1 - N_{ul})^2 \left( \frac{D_{lb}}{D_{lo}} \right) \right] D_{lb}}$$

Once again, it should be noted that the fixed-edge force and fixed-edge moment are inputs from Table 4.2, 4.3 and 4.8 for NCT and Table 4.2, 4.3 and 4.5 for HAC.

#### 2.12.4.2.12. Calculation of Total Loads and Bolt Stresses

In order to accurately combine tensile bolt forces, Table 4.9 of NUREG/CR-6007 is applied. To calculate the total non-prying axial load, the axial bolt force from Tables 4.3-4.8 is summed. The same process is used to determine the total fixed-edge force and fixed-edge moment. Further, the bolt stresses can be formulated from Table 5.1 of NUREG/CR-6007. Calculating the average bolt direct stress caused by the tensile bolt force is:

$$S_{ba} = 1.2732 F_a / D^2$$

and the average bolt shear stress is formulated as,

$$S_{bs} = 1.2732 F_s / D^2$$

The maximum bending stress and maximum shear stress are represented as,

$$S_{bb} = 10.186 M_{bb} / D^3$$

$$S_{bt} = 5.093 M_t / D^3$$

Where  $F_a$ ,  $F_s$ ,  $M_{bb}$ , and  $M_t$  all represent total values of the tensile bolt force, shear bolt force, bending bolt moment, and torsional bolt moment respectively.

#### 2.12.4.2.13. Limits on Bolt Stresses

Table 6.1 of NUREG/CR-6007 gives the acceptance criteria for normal conditions of transport. The acceptance criteria state that the average stress must be less than the allowable stress in tension. For shear, the average stress must be less than 60 percent of the allowable stress. In addition, the sum of the squares of the stress ratio for average tensile stress and stress ratio for average shear stress must be less than one. Further, the maximum stress intensity must be less than 1.35 times the allowable stress for bolts having a minimum tensile strength greater than 100 ksi and 1.5 times for bolts having a minimum tensile strength less than 100 ksi.

Looking at Table 6.3 for HAC, the average stress in tension must be less than the smaller of  $0.7S_u$  or  $S_y$  at temperature. The average stress in shear must be less than the smaller of  $0.42S_u$  or  $0.6S_y$  at temperature. Furthermore, the sum of the squares of the stress ratio for average tensile stress and stress ratio for average shear stress must be less than one.

#### 2.12.4.2.14. Analytical Results

##### *Forces and Moments*

The forces and moments that the Model 2000 Transport Package closure lid, wall, and bolt are subjected to during normal conditions of transport and hypothetical accident conditions are shown in Table 2.12.4-5 and Table 2.12.4-6, respectively.

**Table 2.12.4-5. Forces/Moments Results (NCT)**

Load Condition	Forces/Moments	Variable	Magnitude	Units
PRESSURE	Non-Prying Tensile Bolt Force	F <sub>a</sub>	671.96	lb
	Shear Bolt Force Per Bolt	F <sub>s</sub>	3113.55	lb
	Fixed-Edge Closure-Lid Force	F <sub>f</sub>	120.94	lb
	Fixed-Edge Closure-Lid Moment	M <sub>f</sub>	487.53	lb-in
TEMPERATURE	Non-Prying Tensile Bolt Force	F <sub>a</sub>	10856.79	lb
	Shear Bolt Force Per Bolt	F <sub>s</sub>	-9701.92	lb
	Fixed-Edge Closure-Lid Force	F <sub>f</sub>	0	lb
	Fixed-Edge Closure-Lid Moment	M <sub>f</sub>	2455.49	lb-in
VIBRATION	Non-Prying Tensile Bolt Force	F <sub>a</sub>	253.33	lb
	Shear Bolt Force Per Bolt	F <sub>s</sub>	633.33	lb
	Fixed-Edge Closure-Lid Force	F <sub>f</sub>	37.51	lb
	Fixed-Edge Closure-Lid Moment	M <sub>f</sub>	151.2	lb-in
PRELOAD	Non-Prying Tensile Bolt Force Per Bolt	F <sub>a</sub>	48000	lb
	Torsional Bolt Moment Per Bolt	M <sub>t</sub>	4500	lb-in
GASKET	Axial Load For Gasket Seating	F <sub>a</sub>	5876.16	lb
	Axial Load For Gasket Operation	F <sub>a</sub>	80.13	lb
	Torque Due to Gasket	M <sub>t</sub>	550.89	lb-in
PRYING	Axial Load Due to Prying	F <sub>a</sub>	-2339.42	lb
	Bending Moment Due to Prying	M <sub>bb</sub>	9.99	lb-in

**Table 2.12.4-6. Forces/Moments Results (HAC)**

Load Condition	Forces/Moments	Variable	Magnitude	Units
PRESSURE	Non-Prying Tensile Bolt Force	F <sub>a</sub>	671.96	lb
	Shear Bolt Force Per Bolt	F <sub>s</sub>	3113.55	lb
	Fixed-Edge Closure-Lid Force	F <sub>f</sub>	120.94	lb
	Fixed-Edge Closure-Lid Moment	M <sub>f</sub>	487.53	lb-in
TEMPERATURE	Non-Prying Tensile Bolt Force	F <sub>a</sub>	10856.79	lb
	Shear Bolt Force Per Bolt	F <sub>s</sub>	-9701.92	lb
	Fixed-Edge Closure-Lid Force	F <sub>f</sub>	0	lb
	Fixed-Edge Closure-Lid Moment	M <sub>f</sub>	2455.49	lb-in
IMPACT	Non-Prying Tensile Bolt Force	F <sub>a</sub>	16415.00	lb
	Shear Bolt Force Per Bolt	F <sub>s</sub>	0	lb
	Fixed-Edge Closure-Lid Force	F <sub>f</sub>	2430.26	lb
	Fixed-Edge Closure-Lid Moment	M <sub>f</sub>	9796.98	lb-in
PRELOAD	Non-Prying Tensile Bolt Force Per Bolt	F <sub>a</sub>	48000	lb
	Torsional Bolt Moment Per Bolt	M <sub>t</sub>	4500	lb-in
GASKET	Axial Load For Gasket Seating	F <sub>a</sub>	5876.16	lb
	Axial Load For Gasket Operation	F <sub>a</sub>	80.13	lb
	Torque Due to Gasket	M <sub>t</sub>	550.89	lb-in
PRYING	Axial Load Due to Prying	F <sub>a</sub>	-2149.02	lb
	Bending Moment Due to Prying	M <sub>bb</sub>	41.13	lb-in

#### 2.12.4.2.15. Total Loads and Bolt Stresses Results

Now that all of the forces and moments have been calculated for both NCT and HAC, the loads can be combined appropriately to determine the total loads. Additionally, the bolt stresses can be calculated from the total loads. The results are displayed below for NCT and HAC in Table 2.12.4-7 and Table 2.12.4-8 respectively.

**Table 2.12.4-7. Total Loads/Bolt Stresses (NCT)**

Total Loads/ Bolt Stresses	Variable	Magnitude	Units
Total Bolt Axial Load	F <sub>a</sub>	63318.83	lb
Total Bolt Shear Load	F <sub>s</sub>	-5995.04	lb
Total Bolt Bending Moment	M <sub>b</sub>	3094.22	lb-in
Total Bolt Torsional Moment	M <sub>t</sub>	4500	lb-in
Average Bolt Direct Stress	S <sub>ba</sub>	65335.10	psi
Average Bolt Shear Stress	S <sub>bs</sub>	-6144.66	psi
Maximum Bending Stress	S <sub>bb</sub>	22994.83	psi
Maximum Shear Stress	S <sub>bi</sub>	16720.98	psi
Maximum Stress Intensity	S <sub>bt</sub>	90827.37	psi

**Table 2.12.4-8. Total Loads/Bolt Stresses (HAC)**

Total Loads/ Bolt Stresses	Variable	Magnitude	Units
Total Bolt Axial Load	F <sub>a</sub>	79670.89	lb
Total Bolt Shear Load	F <sub>s</sub>	-6588.37	lb
Total Bolt Bending Moment	M <sub>b</sub>	12781.13	lb-in
Total Bolt Torsional Moment	M <sub>t</sub>	4500	lb-in
Average Bolt Direct Stress	S <sub>ba</sub>	82207.87	psi
Average Bolt Shear Stress	S <sub>bs</sub>	-6798.17	psi
Maximum Bending Stress	S <sub>bb</sub>	94983.60	psi
Total Bolt Shear Stress	S <sub>bt</sub>	16720.98	psi

#### 2.12.4.2.16. Limits on Bolt Stresses Results

Accordingly, the code evaluation is conducted using the information given in the previous subsection and the appropriate tables from NUREG/CR-6007 for both NCT and HAC. Per Table 6.1 of NUREG/CR-6007, the limits for NCT are evaluated as,

$$\begin{aligned} S_{ba} &< S_u \\ 65335.10 \text{ psi} &< 77,130 \text{ psi} \end{aligned}$$

and,

$$\begin{aligned} S_{bs} &< 0.6S_u \\ -6144.66 \text{ psi} &< 46278 \text{ psi} \end{aligned}$$

also,

$$\begin{aligned} R_t^2 + R_s^2 &< 1 \\ (0.8474)^2 + (-0.1328)^2 &< 1 \end{aligned}$$

where,

$$\begin{aligned} R_t &= \text{Stress ratio for average tensile stress} \\ R_s &= \text{Stress ratio for average shear stress} \end{aligned}$$

Per Table 6.3 of NUREG/CR-6007, the limits for HAC are evaluated as,

$$\begin{aligned} S_{ba} &< 0.7S_u \\ 82207.87 \text{ psi} &< 101500 \text{ psi} \end{aligned}$$

and,

$$\begin{aligned} S_{bs} &< 0.42S_u \\ -6798.17 \text{ psi} &< 60900 \text{ psi} \end{aligned}$$

also,

$$\begin{aligned} R_t^2 + R_s^2 &< 1 \\ (0.8099)^2 + (-0.1116)^2 &< 1 \end{aligned}$$



#### 2.12.4.2.17. Fatigue Analysis

The fatigue analysis considers vibration and operating stresses, which come from the NCT bolt stress. Included in the operating stress are the pressure, preload, gasket load, and temperature stresses. Therefore, the loads are:

$$S_{\text{Operating}} = 67487.62 \text{ psi}$$

$$S_{\text{Vibration}} = 261.40 \text{ psi}$$

Using ASME Code, Section III, NB-3232.3 (Reference 2-32, page 91), the alternating stresses can be found by the equation below,

$$S_{\text{a-Operating}} = RF \times S_{\text{Operating}} \left( \frac{E_{\text{dc}}}{E_{\text{a}}} \right)^U$$

$$S_{\text{a-Vibration}} = RF \times S_{\text{Vibration}} \left( \frac{E_{\text{dc}}}{E_{\text{a}}} \right)^U$$

where

$$RF = \text{Fatigue Strength Reduction Factor (Reference 2-32)}$$

$$E_{\text{dc}} = \text{Modulus of Elasticity on Design Fatigue Curve (Reference 2-18, Figure I-9.4, page 12)}$$

$$E_{\text{a}} = \text{Modulus of Elasticity used in the Analysis}$$

$$U = \text{Cumulative Usage Factor}$$

$$U = 1 \text{ (Reference 2-32)}$$

Applying ASME Section III, Figure I-9.4, the fatigue limit for maximum nominal stress  $\leq 2.7 S_m$  for the loads of this analysis are,

$$N_{\text{a-Operating}} = 466 \text{ Cycles}$$

$$N_{\text{a-Vibration}} = 10^{11} \text{ Cycles}$$

The above values are accurately calculated by interpolating the tabular data given in ASME Section III, Table I-9.0 (Reference 2-18, page 2). Assuming  $10^7$  cycles for vibration load and 190 transports:

$$N_{\text{Operating}} = 190 \text{ Cycles}$$

The accumulative usage is then,

$$R = \left( \frac{N_{\text{Operating}}}{N_{\text{a-Operating}}} \right) + \left( \frac{N_{\text{Vibration}}}{N_{\text{a-Vibration}}} \right)$$

Shown in Table 2.12.4-9 are the results from the analysis.

**Table 2.12.4-9. Fatigue Analysis Results**

Parameter	Variable	Value	Units
Vibration Stress	$S_{\text{vibration}}$	261.40	psi
Operating Stress	$S_{\text{operating}}$	67487.62	psi
Fatigue Strength Reduction Factor	RF	4	--
Cumulative Usage Factor	U	1	--
E given on design curve	$E_{\text{dc}}$	30000000	psi
E used in analysis	$E_{\text{a}}$	27400000	psi
Ratio of Modulus of Elasticity	$E_{\text{ratio}}$	1.09	--
Alternating Stress due to Vibration	$S_{\text{a-Vibration}}$	572.41	psi
Alternating Stress due to Operating	$S_{\text{a-Operating}}$	147783.10	psi
Number of Alt. Cycles due to Vibration	$N_{\text{a-Vibration}}$	1E+11	--
Number of Alt. Cycles due to Operating	$N_{\text{a-Operating}}$	466	--
Number of Cycles for Vibration Load	$N_{\text{Vibration}}$	1.00E+07	--
Number of Cycles for Operating Load	$N_{\text{Operating}}$	190	--
Accumulative Usage	R	0.4078	--

Because the accumulative usage is less than one, it is acceptable to have up to 190 transports before all bolts are replaced. After 190 transports, all bolts must be replaced.

#### **2.12.5. Model 2000 Scale Model Drop Test Report**

Model 2000 Drop Test Report No. 87-08-01 is provided in the following pages.



560 San Antonio Road Suite 101 Palo Alto, California 94306 (415) 494-7351

**30-FT. FREE DROP TESTS OF A  
QUARTER-SCALE MODEL 2000  
TRANSPORT PACKAGE**

**Submitted To:**

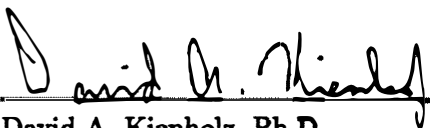
**GENERAL ELECTRIC COMPANY  
VALLECITOS NUCLEAR CENTER,  
PLEASANTON, CA**

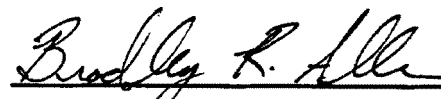
**Report No. 87-08-01  
August 1987**



---

This report describes a series of 30-foot, free drop tests performed on a 1/4-scale model of a General Electric Model 2000 Transport Package. The work was performed for General Electric Vallecitos Nuclear Center under Purchase Order No. 205-87C338.

Prepared by:   
David A. Kienholz, Ph.D.  
Principal Engineer

  
Bradley R. Allen  
Engineer

*CONTENTS* i

---

**Contents**

<b>1. Introduction and Summary</b>	<b>1</b>
<b>2. Objectives</b>	<b>1</b>
<b>3. Test Article</b>	<b>2</b>
3.1 Scaling Relations .....	6
<b>4. Instrumentation</b>	<b>8</b>
4.1 Acceleration Measurements .....	8
4.2 Force Distribution Measurements .....	11
4.3 Photography .....	13
4.4 Deformation Measurements .....	15
<b>5. Procedure</b>	<b>16</b>
<b>6. Results</b>	<b>19</b>
6.1 Head-On Drop .....	19
6.1.1 Acceleration Data and High-Speed Photography .....	19
6.1.2 Pressure- Sensing Film .....	24
6.1.3 Cask and Overpack Deformation Measurements .....	26
6.2 Side Drop .....	28
6.2.1 Acceleration Data and High-Speed Photography .....	28
6.2.2 Pressure-Sensing Film .....	35
6.2.3 Cask and Overpack Deformation Measurements .....	35
6.3 CG-Over-Corner Drop .....	35
6.3.1 Acceleration Data and High-Speed Photography .....	35
6.3.2 Pressure- Sensing Film .....	42
6.3.3 Cask and Overpack Deformation Measurements .....	42
<b>7. Summary and Conclusions</b>	<b>44</b>

**List of Figures**

1	Quarter-scale model of Model 2000 Transport Package showing accelerometer locations for drop tests .....	2
2	Model 2000 Transport Package details .....	3
3	Overpack weldments.....	4
4	Assembled package .....	5
5	Accelerometers mounted inside the cask.....	9
6	Accelerometers mounted outside the overpack.....	10
7	Accelerometer signal processing .....	11
8	Apparatus for testing response speed of pressure sensing film .....	12
9	Pressure-sensing film being applied to cask.....	14
10	Measurement of toroid profile.....	15
11	Drop test orientations.....	16
12	Package rigged for side drop .....	17
13	Head-on drop, vertical acceleration .....	20
14	Head-on drop, frames taken at 2.12 millisecond intervals .....	21
15	Overplot of cask and overpack acceleration, head-on drop.....	22
16	Toroid deformation caused by head-on drop.....	23
17	Time integral of cask vertical acceleration, head-on drop .....	24
18	Pressure-sensing film from head-on drop.....	25
19	Gage numbering for inspection of overpack top toroid.....	26
20	Side drop, vertical acceleration .....	30
21	Side drop, frames taken at 2.13 millisecond intervals .....	31
22	Overpack weldments separating after impact, side drop.....	32
23	Package after side drop .....	33
24	Time integral of cask vertical acceleration prior to cable fault, drop .....	34
25	Pressure-sensing film from side drop.....	36
26	Rigging for CG-over-corner drop.....	37
27	CG-over-corner drop vertical acceleration.....	38
28	CG-over-corner drop, frames taken at 2.16 millisecond intervals.....	39
29	Deformation of overpack produced by CG-over-corner drop.....	40
30	Time integral of cask vertical acceleration, CG-over-corner drop.....	41
31	Pressure-sensing film from CG-over-corner drop .....	43

## 1. INTRODUCTION AND SUMMARY

The General Electric Company Vallecitos Nuclear Center (GEVNC) designs and tests containers for shipping radioactive materials. These shielded containers must meet stringent safety requirements, including a 30 foot free drop onto a hard, unyielding horizontal surface. The package must withstand this drop without functional damage to the inner cask containing the radioactive payload.

CSA Engineering, Inc., was retained to perform a series of drop tests of 1/4-scale replicas of the Model 2000 transport package. Performed at the GEVNC facility on June 10, 11, and 14, 1987, the design and execution of the tests are governed by GE procurement specification 22A9367 (Rev. 2), dated June 8, 1987. This report documents the objectives, methods, results and conclusions of the tests.

Drop tests from three orientations were performed with no measurable deformation or other damage to the inner cask. Head-on and CG-over-corner drops were successfully completed with no unexpected results. Complete data on acceleration and internal load distribution were obtained for use in design verification.

An unexpected failure of the overpack bolted joint occurred when the cask was dropped on its side. The causes of the failure and requalification of the joint will be covered in a separate report.<sup>2</sup> The structural failure also caused the loss of some acceleration data. Nonetheless, a valid trace was obtained for the most important part of the impact event, including the portion during which plastic deformation of the overpack occurred and, probably, including the point of maximum vertical cask acceleration.

Subject to the above uncertainty in the side drop test, the maximum vertical accelerations recorded by sensors inside the cask for the head-on, side, and CG-over-corner drops were 408, 185, and 156 G's respectively.

## 2. OBJECTIVES

The objectives of the tests were to determine, for each of three drop orientations:

1. The damage, if any, suffered by the inner cask.
2. The vertical acceleration of the cask at impact.
3. The force distribution at impact between the inner cask and the outer protective overpack.

---

<sup>2</sup> Pomares, R. J., to be published

### 3. TEST ARTICLE

Figures 1 and 2 show the transport package in cross section with dimensions given for the 1/4-scale model. Figures 3 and 4 show the actual test article. The package is composed of two major assemblies: the inner cask and the outer protective overpack. The cask provides containment and radiation shielding for the payload. The overpack provides mechanical and thermal protection for the cask.

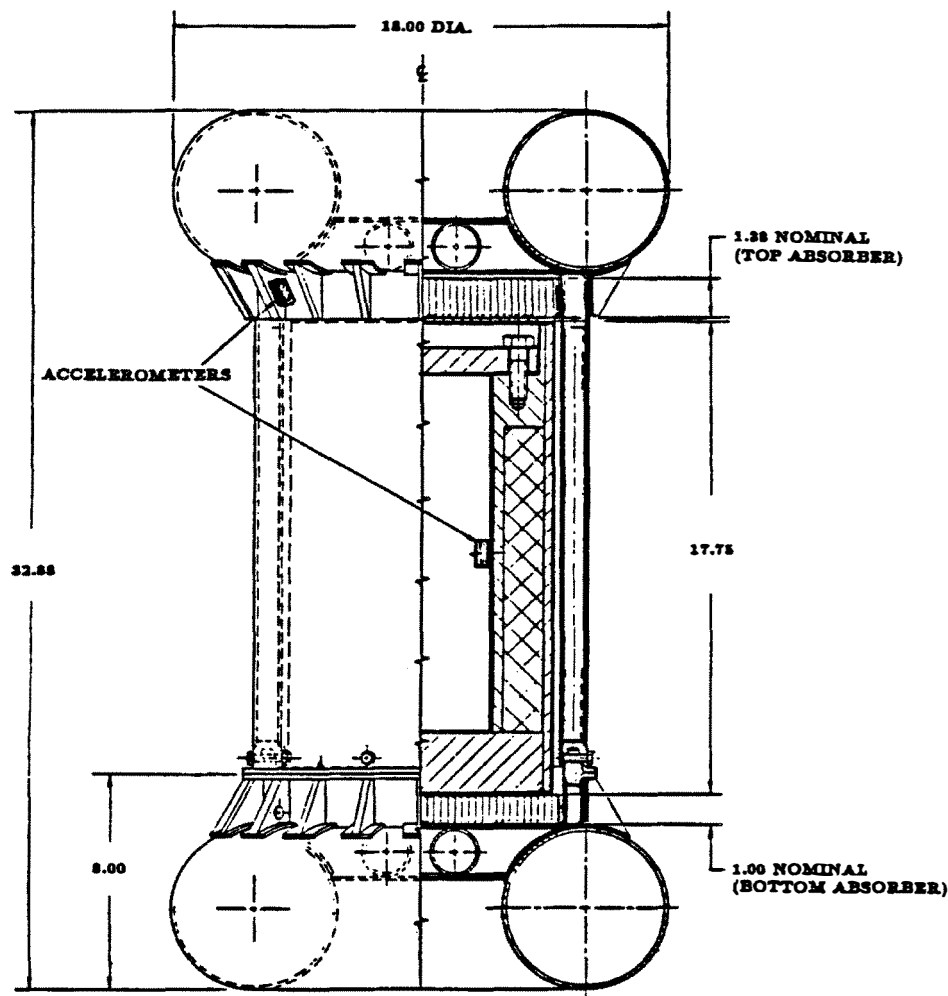
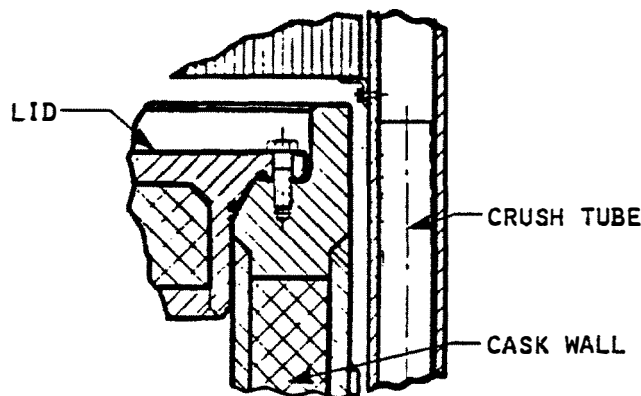


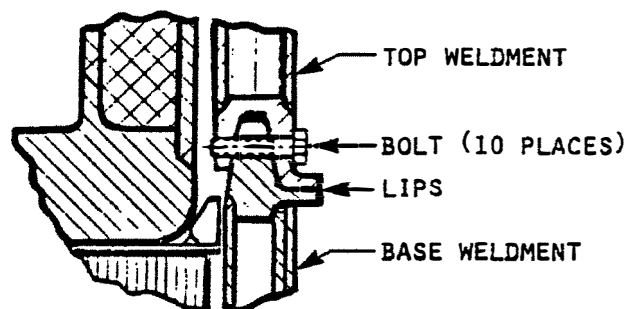
Figure 1. Quarter-scale model of Model 2000 Transport Package showing accelerometer locations for drop tests



The cask is essentially a thick-walled cylinder with a raised rim around the lid seal to protect this critical area. Of particular interest for this test are the impact-limiting features of the overpack. Constructed entirely of 304 stainless steel, it is composed of a double-walled cylindrical shell with identical toroidal shell "bumpers" at either end. Regardless of drop orientation, the initial impact will be taken by one of the toroids. They are designed to plastically deform and buckle inward at a specific load level and thus limit the acceleration of the cask. The cylindrical walls of the overpack are separated by tubular members running parallel to the cask axis. These are likewise designed to crush at a known load. Honeycomb "cushions" are provided between either end of the cask and the overpack for further impact limiting under axial acceleration.



**Lid Detail**



**Joint Detail**

Figure 2. Model 2000 Transport Package details

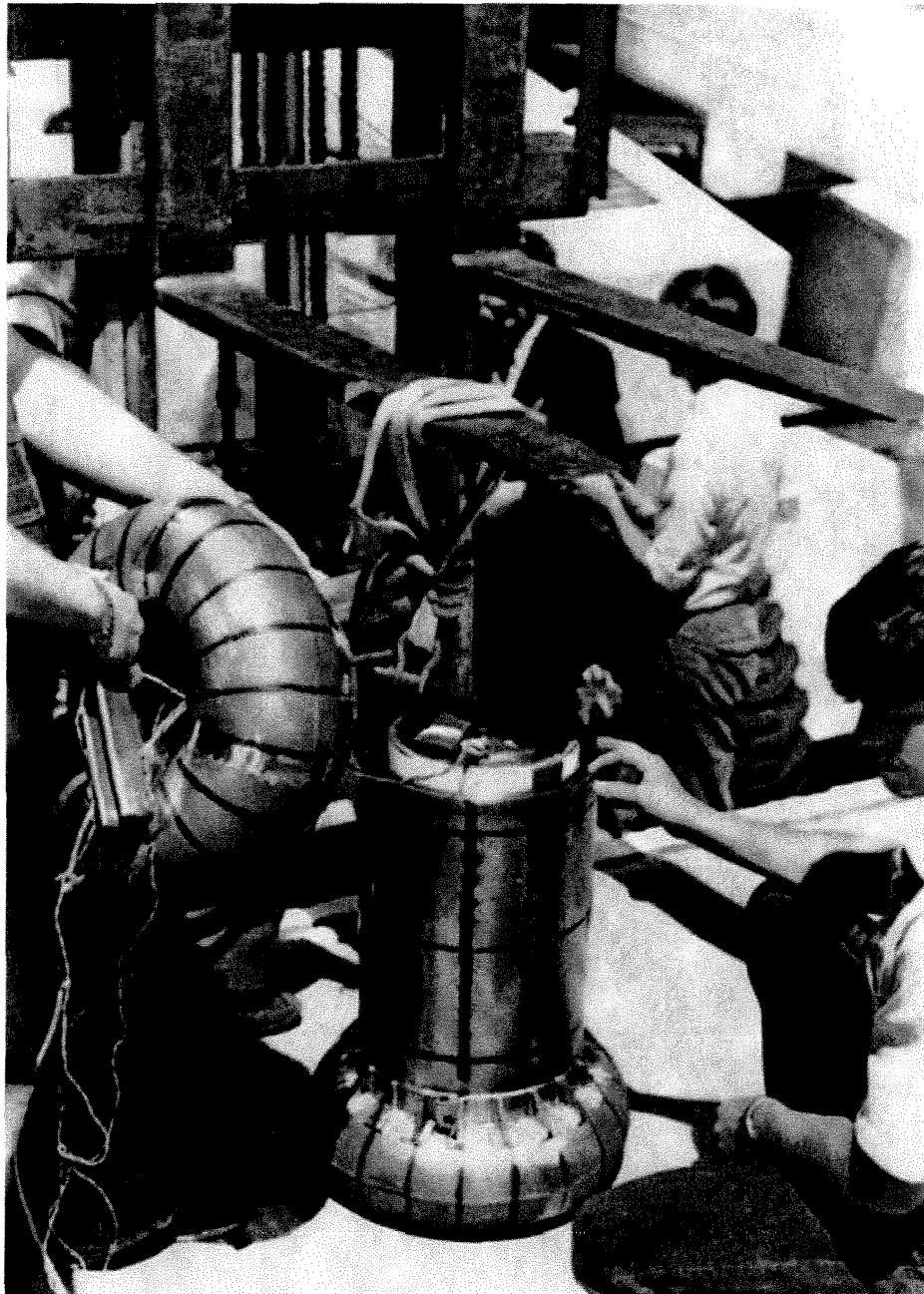


Figure 3. Overpack weldments

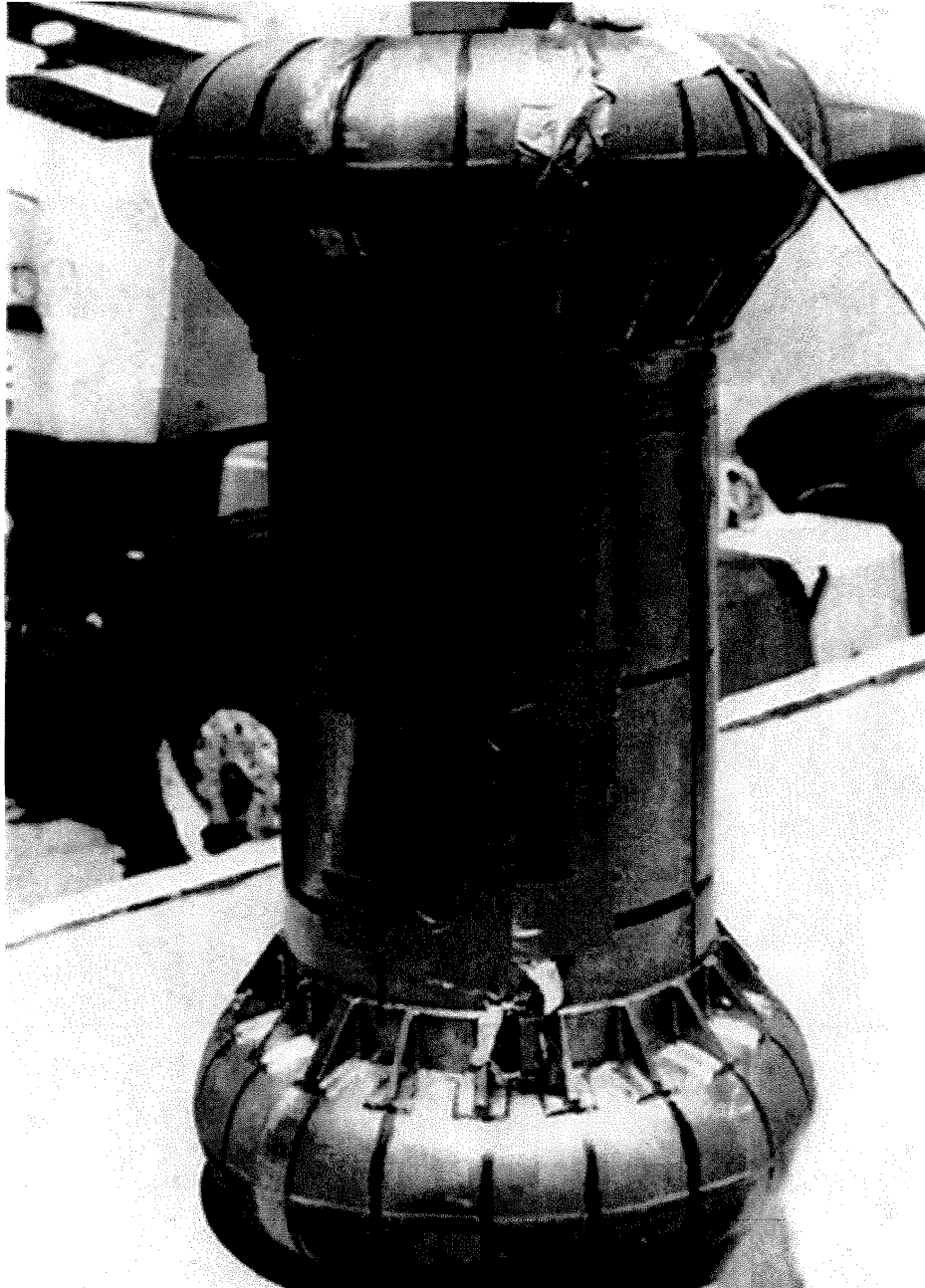


Figure 4 . Assembled package

The overpack is fabricated as two weldments bolted together at a lip joint running circumferentially around the cylinder just inboard of one toroid (see Figures 1 through 4). The smaller weldment is called the base and the larger is called the top. During normal assembly the cask is positioned, lid upwards, on the base and the top is lowered over it. The two weldments are joined at the lip seal by ten bolts, 1/4-inch in diameter for the scale model, inserted radially through the lips as shown in Figure 2.

The payload inside the cask was simulated by blocks of heavy metal, one attached to the lid and one to the floor. Weights of the package components are shown in Table 1.

Table 1: GE Model 2000 Transport Package  
Component Weights (lbm)

	Full-scale Prototype	1/4-Scale Model
Overpack	9,822	154
Cask	17,647	276
Payload (max.)	<u>5,450</u>	<u>85</u>
Total	32,919	515

One scale model cask and two scale model overpacks were fabricated for the tests. Two complete overpacks were required to insure that the initial impact in each of the three required drops occurred on an undeformed area.

### 3.1 Scaling Relations

The test article is a near-replica constructed at 1/4-scale. Table 2 shows the classical replica scaling relations for a model constructed of the same material as the full-scale prototype.

The scaling ratios of primary interest here are those for velocity, acceleration, and stress. Velocity scales independent of length. The drop height for the scale model is therefore the same as for a full-scale prototype in order to produce the correct impact velocity. Acceleration scales as  $1/\lambda$ . A measured value of  $a_{model}$  in the current model test therefore corresponds to  $a_{model}/4$  for the prototype. Neglecting strain rate effects, stress scales independent of length. Yielding or rupture of material in the model therefore implies a similar result for the prototype.

### 3.1 Scaling Relations

7

Table 2: Scaling Relations

#### Assumptions

- Monolithic structure
- Same material for model and prototype
- Length ratio (model/prototype) =  $\lambda$

Quantity	Model/Prototype Ratio	
	as function of $\lambda$	value for $\lambda = 0.25$
Length	$\lambda$	0.25
Mass or weight	$\lambda^3$	0.0156
Time	$\lambda$	0.25
Frequency	$1/\lambda$	4.00
Displacement	$\lambda$	0.25
Velocity	1	1.00
Acceleration	$1/\lambda$	4.00
Force	$\lambda^2$	0.0625
Moment	$\lambda^3$	0.0156
Stress	1	1.00
Strain	1	1.00
Stiffness	$\lambda$	0.25

## 4. Instrumentation

Several diverse types of instrumentation were utilized to sense and record the impact phenomena. These included:

1. Accelerometers with signals recorded on analog magnetic tape
2. Pressure-sensing film
3. High-speed film and videotape photography
4. Micrometers and dial gauge arrays

Details on each are given in this section.

### 4.1 Acceleration Measurements

Seven accelerometers were mounted on the package: four inside the cask and three on the outside of the overpack. Locations are shown in Figure 1. All were piezoelectric, integrated amplifier (voltage mode) devices with a time constant of 0.5 seconds or greater. A triaxial array mounted inside the cask sensed in the axial, radial, and tangential directions. An additional uniaxial sensor was mounted inside the cask sensing in a direction 29 degrees off the cask axis. Denoted as the cask oblique sensor, its purpose was to measure vertical acceleration of the cask during the CG-over-corner drop. All sensors inside the cask were miniature, general purpose accelerometers with a maximum usable range of 1000 G's. Figure 5 shows the transducers on their mounting block bonded to the inner surface of the cask.

The triaxial array outside the overpack was composed of three sensors mounted in a special machined block to sense in the axial, radial, and tangential directions. These miniature shock accelerometers have a usable range of 10,000 G's. The arrangement is shown in Figure 6.

An eighth accelerometer was mounted on the steel drop pad, several feet away from the impact point. Its output signal was to be used for a timing trigger during data processing. However it was found that using one of the package sensor signals with a small pre-trigger delay was both more reliable and more convenient. The pad accelerometer data was therefore not used.

A schematic of the accelerometer signal chain is shown in Figure 7. Signals were recorded on an instrumentation FM tape recorder for later replay and analysis. The most important signals (vertical acceleration of the cask and overpack) were recorded on two tape channels apiece with different gain settings to optimize the signal/noise ratio. One channel of each pair was ranged to

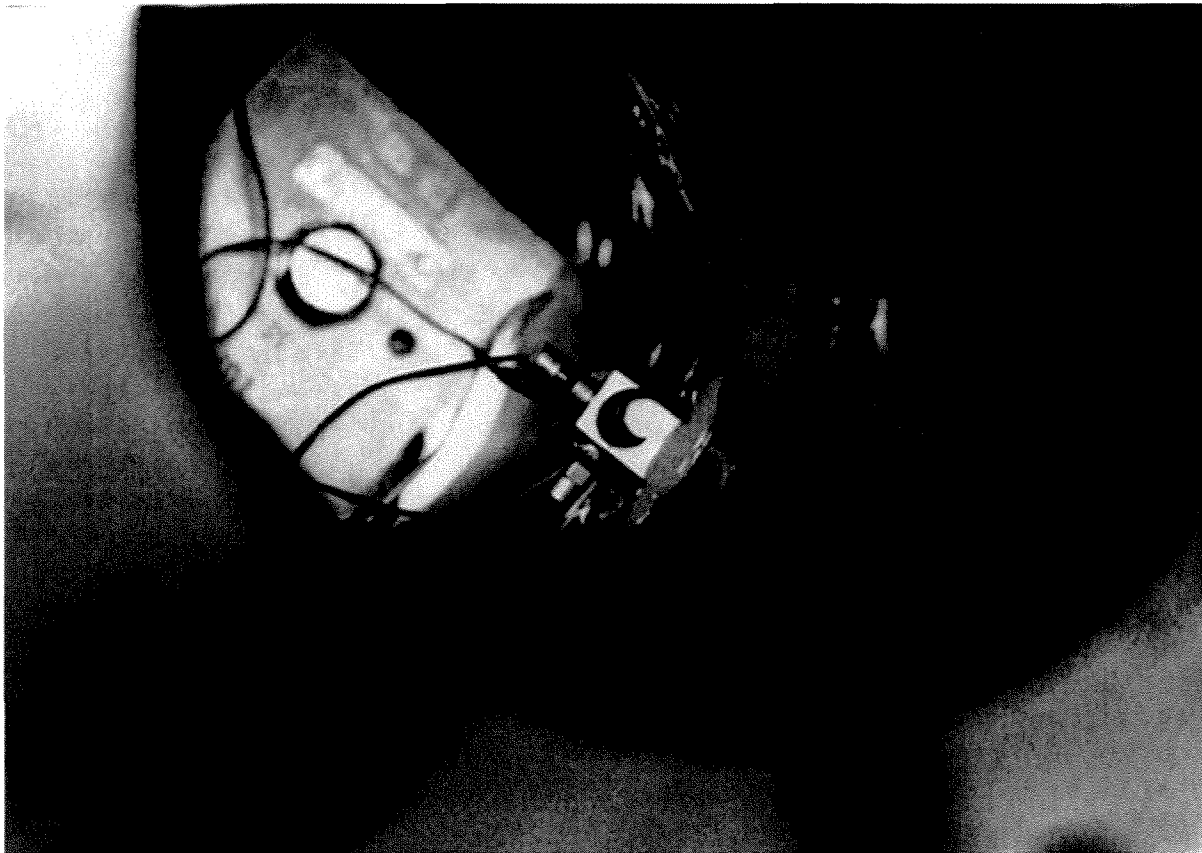


Figure 5. Accelerometers mounted inside the cask

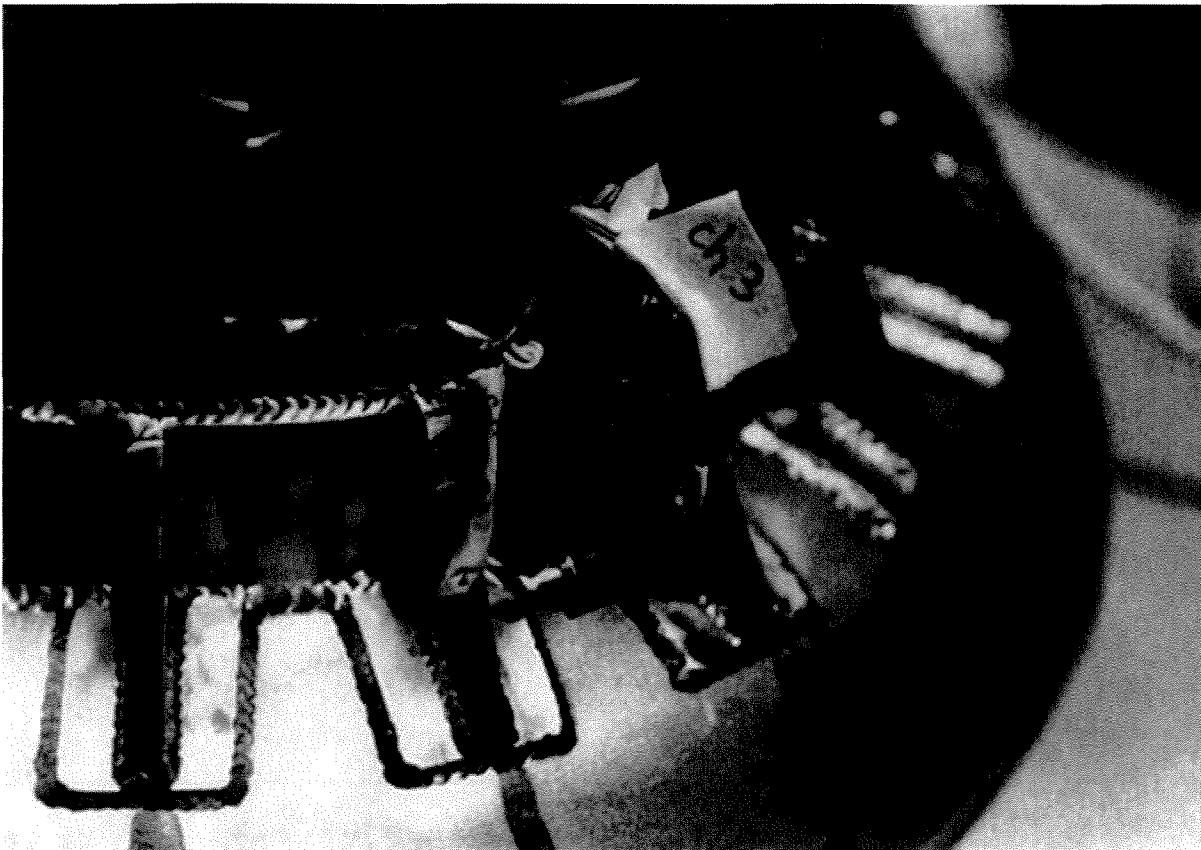


Figure 6. Accelerometers mounted outside the overpack



## 4.2 Force Distribution Measurements

11

accommodate a signal level about 3 dB above the anticipated maximum and the other was set to provide about 9 dB of headroom. On playback, the channel from each pair whose signal came closest to full-scale without exceeding it was used for analysis.

The digital signal analyzer (Figure 7) provided analog-to-digital data conversion with a maximum sampling frequency of 102.4 kHz per channel. This was effectively increased even further for certain data records by replaying the tape at a speed lower than used for recording. Data was either displayed immediately on the real time display or passed via a DMA link to the main computer for further processing.

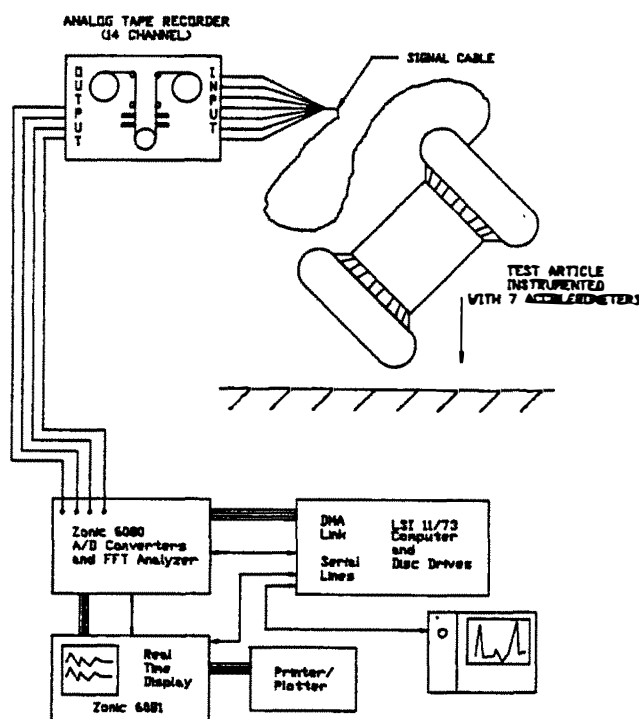


Figure 7. Accelerometer signal processing

## 4.2 Force Distribution Measurements

The distribution of force between the cask and overpack was determined by means of a pressure-sensing film on the cask exterior surface. The film undergoes a permanent color change from white to red when subjected to pressure. The color change is gradual with increasing pressure, allowing the approximate maximum pressure at any location to be determined by comparing

the exposed film to a calibrated color chart. More accurate reading is possible using a special densitometer. While somewhat subjective, the simpler comparison method was considered adequate for the present purpose.

The film provided a convenient method for determining the load distribution on the cask. It is available in several grades, each designed for a specific pressure range. The grade used for the drop test progresses from white to pink to red as the applied pressure is increased from 1000 to 3500 psi. Higher pressures have no effect, with the film simply retaining its maximum redness.

The film is normally used for static pressure measurements such as checking the flatness of mating surfaces of pipe flanges, cylinder heads, etc. Its manufacturer could not supply data on the time required for color change under sudden, impact loads. Therefore, a simple laboratory test was performed to assess its speed of response. Figure 8 shows the apparatus. Film specimens exposed at 2000 psi for a few hundred microseconds were compared to specimens exposed to the same pressure for two minutes. The specimens showed equal shades of red. It was concluded that the color change was effectively instantaneous.

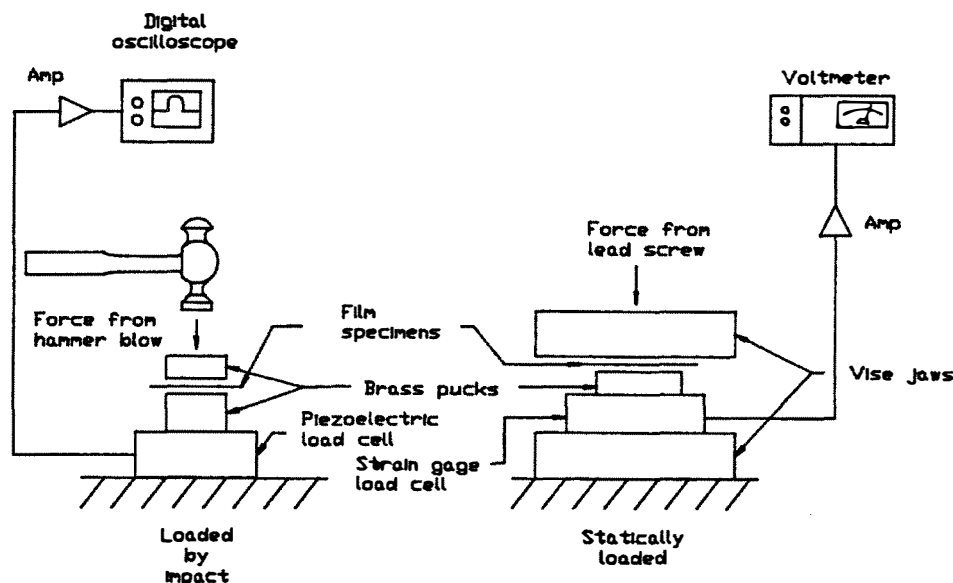


Figure 8. Apparatus for testing response speed of pressure sensing film

#### *4.3 Photography*

13

The film is composed of two separate layers, each resembling glossy paper with a total thickness is 0.008 inches. Under pressure, chemicals in the two layers react causing one layer to change color. It provides the pressure signature and the other layer is discarded.

Pieces were cut to fit the surfaces of the cask and held in place with adhesive tape as shown in Figure 9. A machined cover plate was located on the lid end of the cask to distribute the load over the entire surface of the circular honeycomb cushion. The film was placed between the cushion and the cover plate. Following each drop, the film was removed and the colored layer was annotated to become part of the permanent test record. Photographs in a later section show exposed film from each drop.

### **4.3 Photography**

High-speed films were taken of each drop using two identical cameras viewing the scene from angles 90 degrees apart. Rated speed for the cameras was 500 frames/second.

A length scale and a time scale were located in the field of view of each camera, just behind the impact point. These scales, used in film interpretation, are shown later in photographs. Length scales were simply long rulers, graduated in inches and placed vertically in the field of view of each camera. Each time scale resembled a large clock with only one hand. The hand rotated clockwise at a measured speed of 3577 RPM. The time scales allowed accurate determination of frame rates, necessary for correlating the films with acceleration traces. Frame rates for the head-on, side, and CG-over-corner drop were 471.7, 469.5, and 463.0 frames/second respectively for the camera which produced the frames shown in this report.

A standard commercial videotape camera was also used to record the tests. By providing instant replay, it allowed the orientation of the package at impact to be verified immediately following each drop. Videotape was also used to document much of the test preparation.

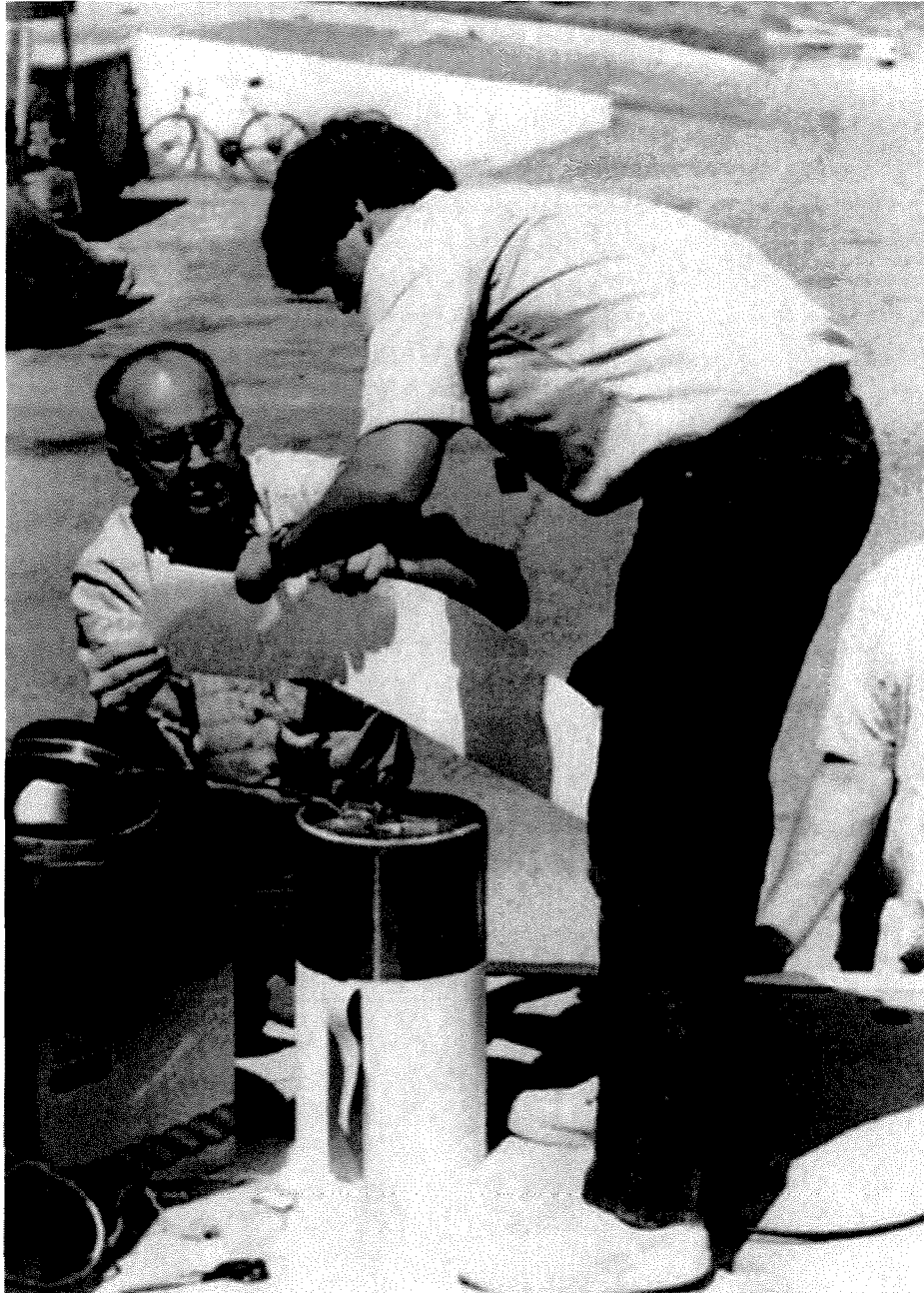


Figure 9. Pressure-sensing film being applied to cask

#### **4.4 Deformation Measurements**

Micrometer measurements of the cask diameter were made at several axial locations before and after each drop to check for plastic deformation.

Since the top of one overpack was used for two drops (side and CG-over-corner), it was necessary to carefully record the damage due to the first to insure that the effects of the two were determined separately. The fixturing for these measurements, performed before and after each drop, is shown in Figure 10. The cask was mounted between centers in a large lathe and an array of dial gages was used to determine the deformation of the toroids at a number of relocatable positions. Plaster molds were also made of the deformed sections of the toroids.

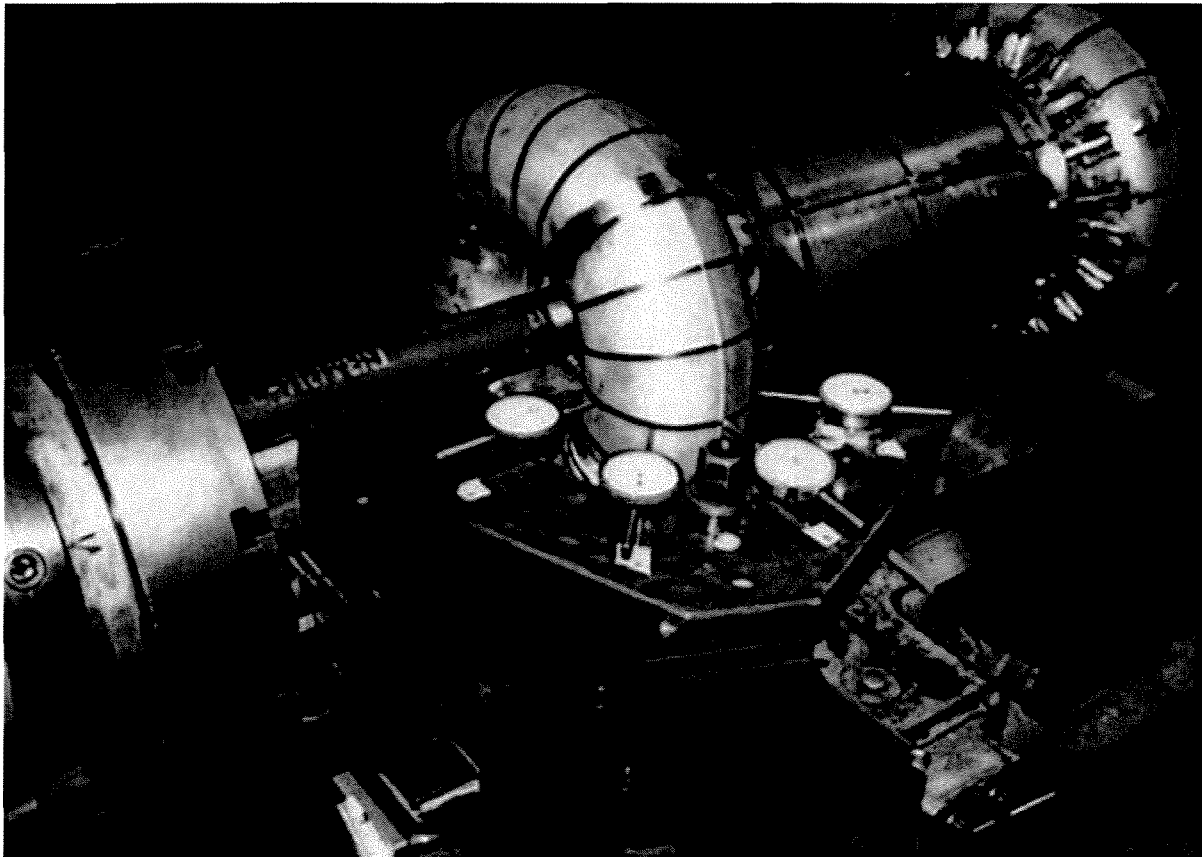


Figure 10. Measurement of toroid profile

## 5. PROCEDURE

Drop tests were performed for three different orientations of the cask. Depicted graphically in Figure 11, they are denoted in the order of performance as the head-on drop, the side drop, and the CG-over-corner drop. In the head-on and CG-over-corner drops, the cask lid and top of the overpack were oriented downwards to produce the worst-case load on the seal area of the cask.

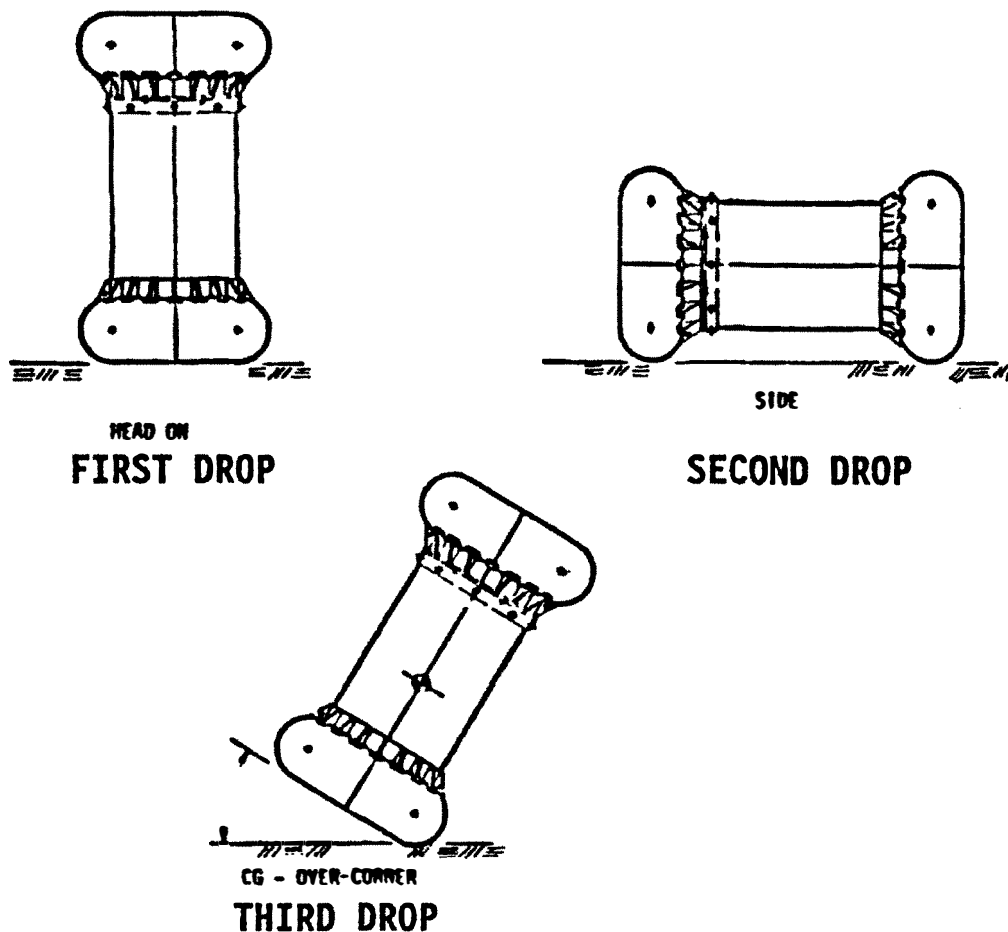


Figure 11. Drop test orientations

One cask and two complete overpack assemblies were fabricated. Overpack No. 1 was used for the head-on drop and No. 2 was used for the side drop. The CG-over-corner drop used the base of overpack No. 1 (still undamaged) and the top of overpack No. 2 with the package oriented such that the impact on the top occurred at an undamaged section.

Following the pre-drop dimensional inspection of the cask and overpack, the pressure sensing film was installed. The lateral sides and/or the lid end of the cask were covered, depending on the drop orientation. A cover plate was used between the lid end of the cask and the honeycomb cushion to distribute the load.

The cask and overpack were assembled, taking care to insure that the instrumentation cable was properly routed. The package was rigged for hoisting from the crane using an electromagnet and safety line. A magnet grip plate was secured to the overpack by a welded bracket which could be adjusted to obtain the correct orientation. Figure 12 shows the package rigged for the side drop. Special rigging was used for the CG-over-corner drop to balance the package over the contact point.

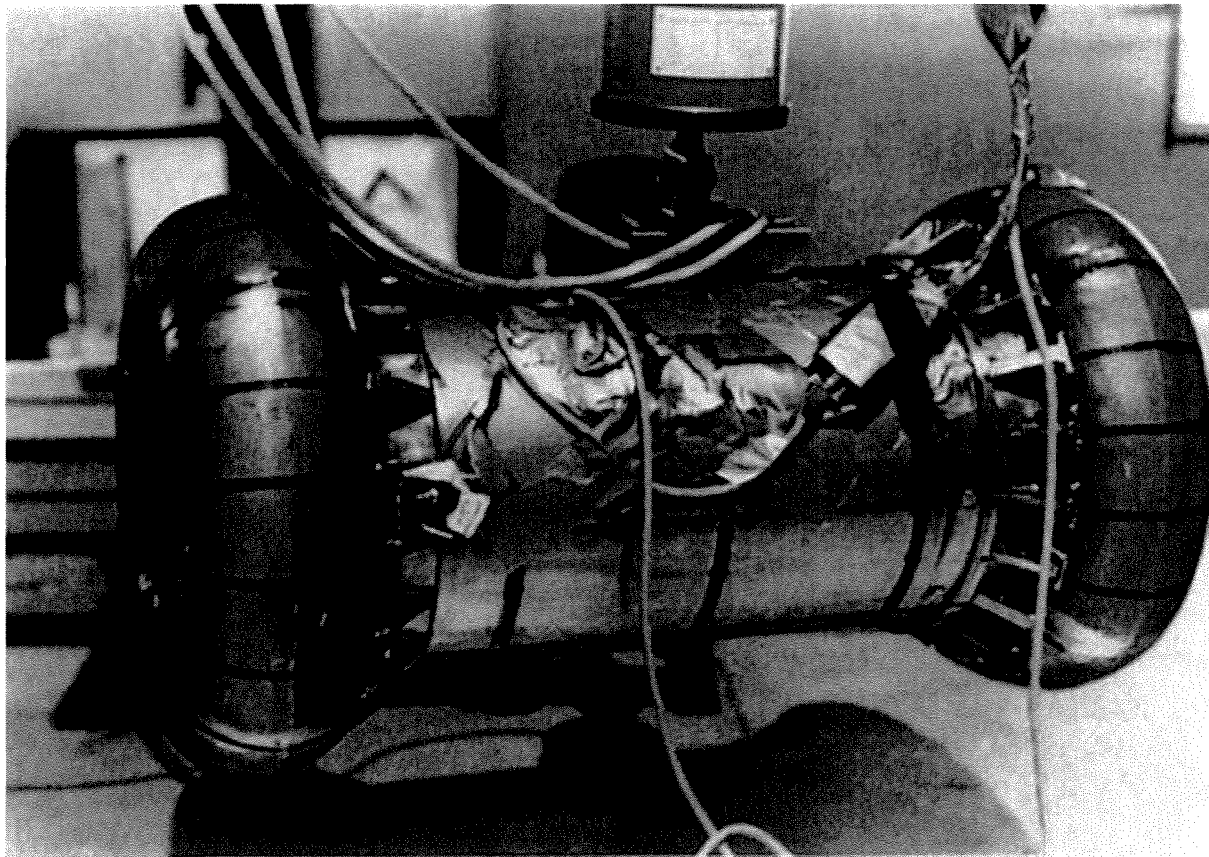


Figure 12. Package rigged for side drop

The package was hoisted by a mobile crane and the drop height was verified by a light, graduated chain hanging from the crane. The instrumentation cable was carefully routed and supported to prevent any interference with the free fall. The chain and safety line were removed just before the drop.

After a final check of all equipment, the tape recorder was started and voice-logged. The cameras were started and, after a one-second pause to allow them to reach speed, the polarity of the DC voltage to the electromagnet was reversed to release the package. Filming continued until the package came to rest.

Post-drop procedure included the following.

1. Data tapes were replayed to check signal ranging.
2. Pressure-sensing film was removed, inspected, annotated, and stored.
3. The cask and overpack were measured to determine the extent of plastic deformation.
4. Videotapes were replayed to check the package orientation at impact.

Detailed check lists were kept with each item initialed by the responsible individual after it was performed. These will become part of the final Product Quality Record.



## 6. RESULTS

Results of the drop tests are given in this section, organized by drop orientation.

### 6.1 Head-On Drop

#### 6.1.1 Acceleration Data and High-Speed Photography

Figures 13 and 14 illustrates the impact event. The traces show the time history of vertical acceleration as measured by the axial accelerometers on the overpack and cask. The photographs are from the high-speed film, taken at a rate of 471.7 frames/second (2.12 milliseconds/frame). They are numbered in order of increasing time with zero being the frame closest to initial impact. The numbered vertical lines on the plot indicate the corresponding frame. The small markers along the bottom of each plot are spaced at 2.00 millisecond intervals.

Polarity of the vertical acceleration signal is not necessarily consistent between tests having different drop orientations. The sensors were simply installed in the most convenient way that provided correct alignment. Polarity was not considered important since the sense of the net velocity change, and thus the rigid-body component of acceleration at impact, was obviously known in advance.

Interpretation of the data from the head-on drop is straightforward. The acceleration seen by each sensor is composed of two parts. Low frequency components are present, corresponding to the rigid-body deceleration that produces the net change in velocity. A large number of high frequency components (ringing) are also produced by the resonant response of the vibration modes of the package. The low frequency portion, corresponding to a smoothed version of the trace, is of primary interest since it indicates the portion of the loading relevant to the package design.

Figure 15 shows the vertical acceleration of the cask and overpack plotted on the same scale. Peak acceleration of the cask is 408 G's, much lower than the 4853 G level experienced at the overpack sensor. The impact limiters greatly reduce the acceleration experienced by the cask.

Figure 16 shows the top toroid following the head-on drop. It has buckled inwards in an almost perfect axisymmetric pattern. The package rebounded almost straight up with negligible rotation and came to rest on the impact surface. These facts indicate that the accelerating force was essentially symmetric around the cask axis. The high-speed film showed a maximum rebound height at the overpack CG of 7.6 inches. The 408 G acceleration of the cask was the highest level seen in any of the three drops. This was as expected since the head-on drop distributed the crushing load over the largest portion of the toroid surface, thus producing the highest total force.

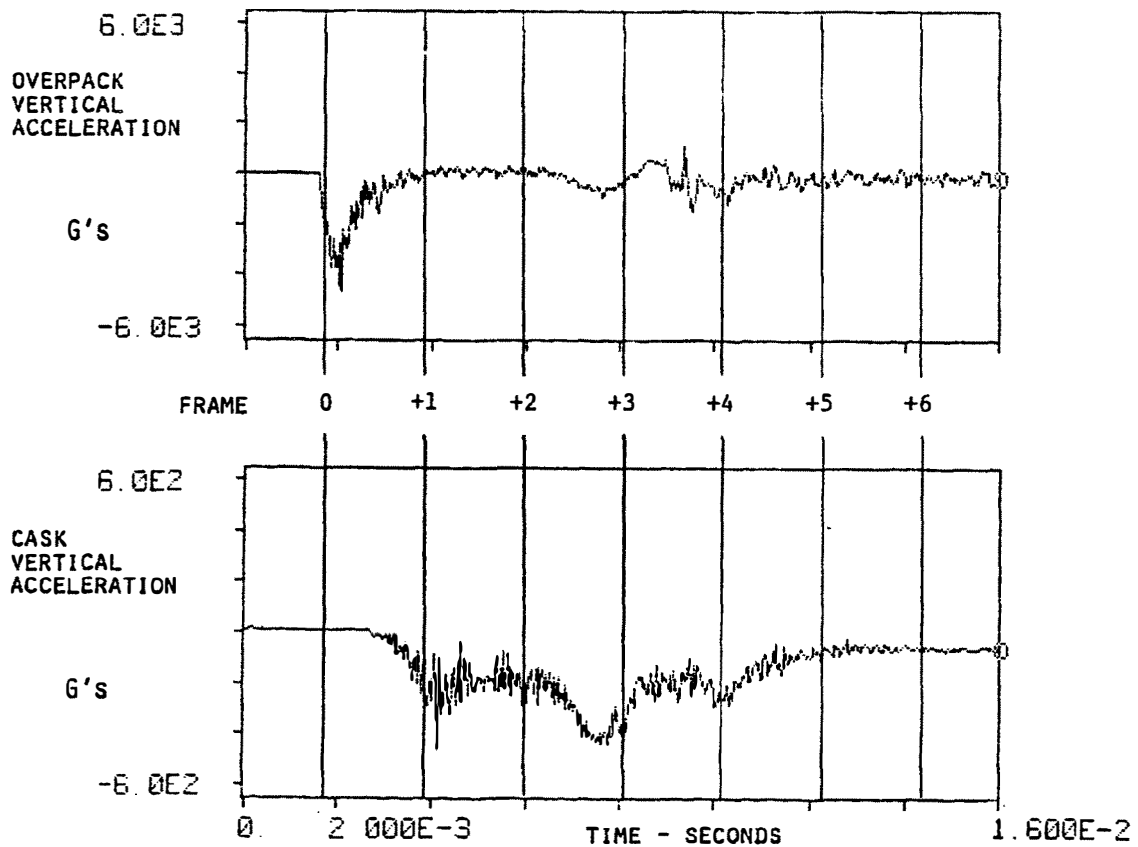


Figure 13. Head-on drop, vertical acceleration

6.1 Head-On Drop

21

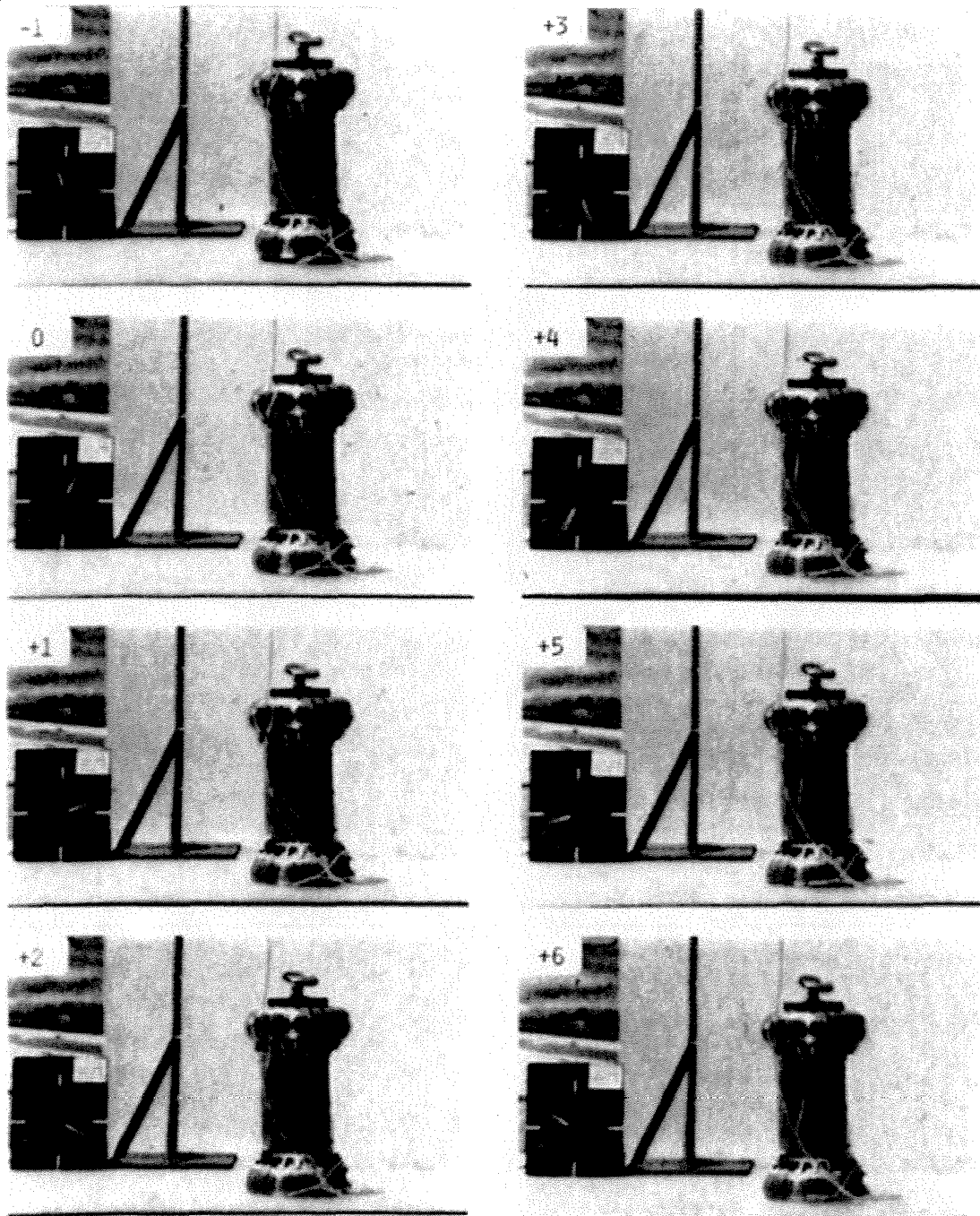


Figure 14. Head-on drop, frames taken at 2.12 millisecond intervals

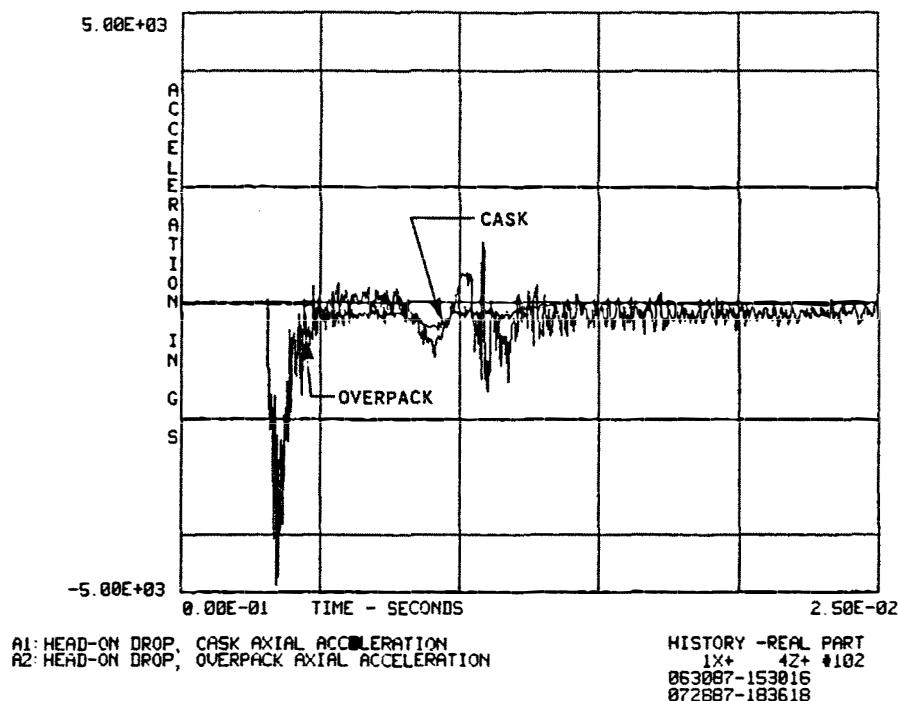


Figure 15. Overplot of cask and overpack acceleration, head-on drop

A smoothed version of the cask acceleration trace shows three distinct peaks. In Figure 13, these occur just after frame 1, just before frame 3, and just after frame 4. It is believed, based on analysis of the data from all three drops, that the first two peaks are typical of the nonlinear force-deflection characteristics of the toroid at large deformations. The momentary reduction in acceleration after the first peak probably occurs when the convex surface of the toroid is pushed through to present a concave surface over the impact area. The second, larger peak occurs as the crushing continues and this concave surface, now stiffer, is enlarged.

Figure 17 shows the time integral of the cask acceleration, computed as a forward sum over the digitized time history of Figure 15. The difference between initial and final values of the integral indicates the net velocity change. This calculation provides a check on the accuracy of the acceleration signal chain. The indicated velocity change must equal or exceed the initial impact velocity of 527 inches/second. The value of 645 inches/second indicated in Figure 17 is consistent with the observed rebound height.

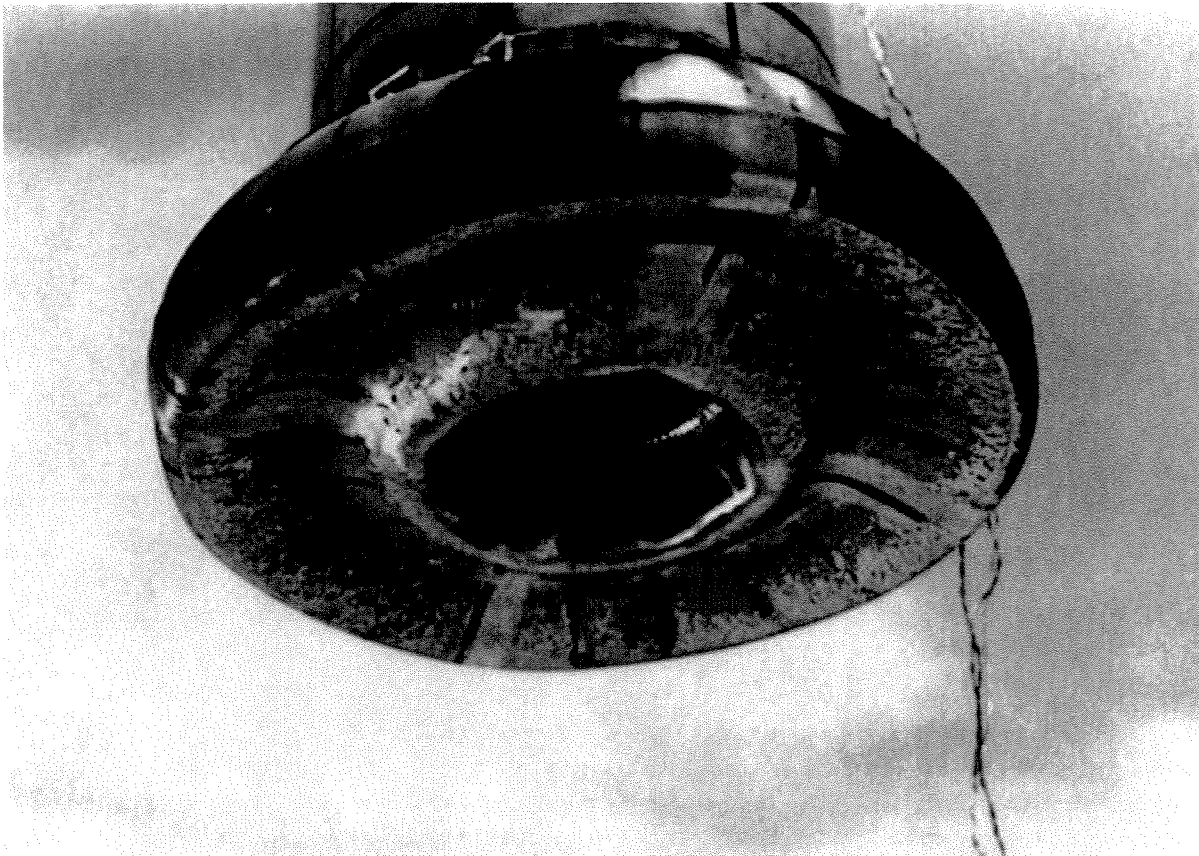


Figure 16. Toroid deformation caused by head-on drop

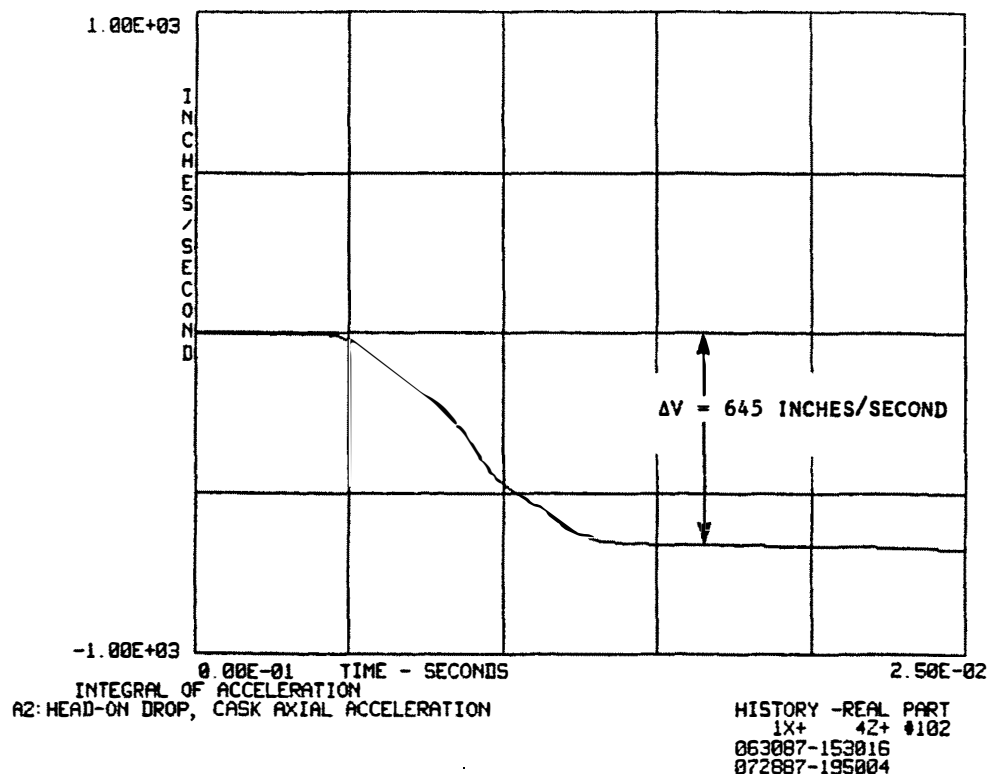


Figure 17. Time integral of cask vertical acceleration, head-on drop

### 6.1.2 Pressure-Sensing Film

Figure 18 shows the pressure sensing film after the head-on drop. The large rectangular piece, removed from the lateral sides of the cask, shows that significant pressure was applied in only a few small areas. The circular piece, removed from the cover plate on the lid end of the cask, shows an essentially axisymmetric pressure distribution. Most of the load was taken by a one-inch-wide band around the edge where the raised lip bears against the cover plate. This could occur only after the honeycomb cushion bottomed; until that point the cover plate and cushion would serve to distribute the load evenly. The film color near the rim indicates a peak pressure in excess of 3500 psi, consistent with the measured acceleration and weight of the cask.

The film color in the circular area inside the band is not quite uniform. Circular striations are visible, caused by tooling marks on the plate. This is not a defect of the film. It simply indicates the difficulty of producing a truly uniform pressure over the contact area between two hard surfaces.

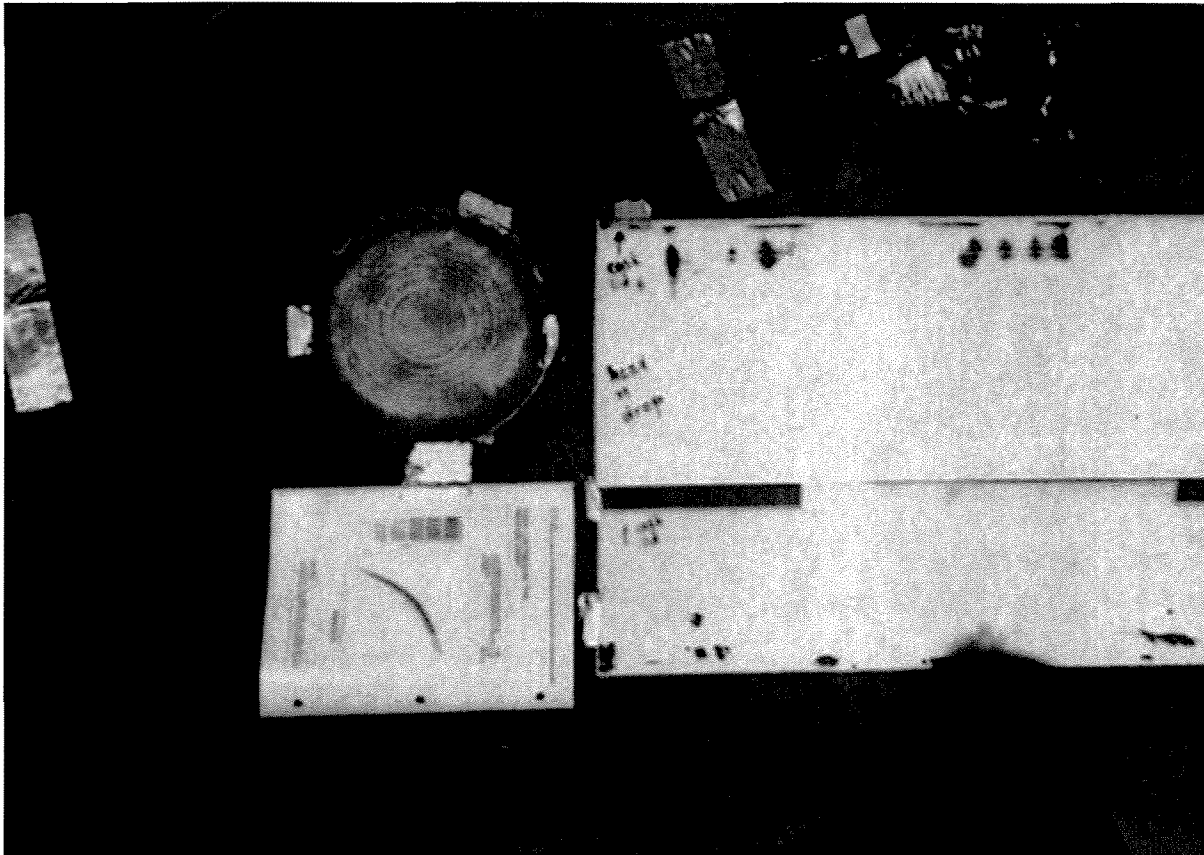


Figure 18. Pressure-sensing film from head-on drop

### 6.1.3 Cask and Overpack Deformation Measurements

Micrometer measurements were made of the cask diameter at a number of axial and azimuthal stations before and after the head-on drop. No change was found; no measurable plastic deformation of the cask had occurred.

Table 3 shows measurements of the deformed top toroid using the apparatus of Figure 10. Numbering of the dial gages is shown in Figure 19. Measurements of the toroid indicated that damage to it was localized to the impact area and was essentially axisymmetric.

The entire set of measurements made before and after the head-on drop is quite extensive and is documented in General Electric Inspection Report No. 6431, dated June 11, 1987. Data given here is excerpted from that report.

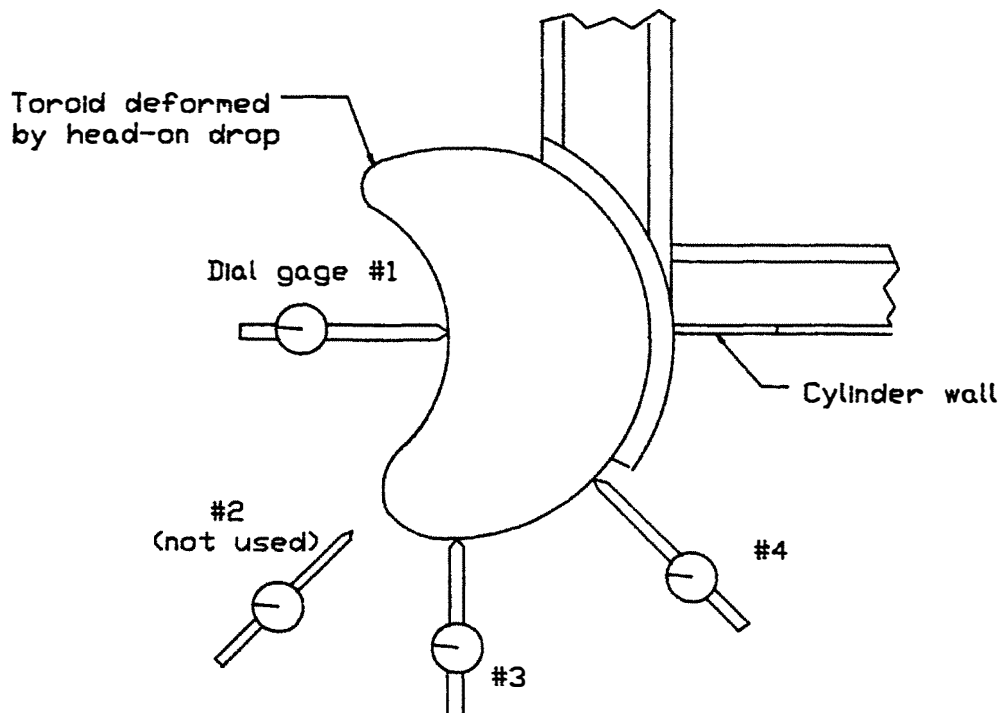


Figure 19. Gage numbering for inspection of overpack top toroid



Table 3. Deformation of top toroid due to head-on drop

Gauge Azimuth (Degrees)	1	2*	3	4
0	2.115		-0.033	-0.001
90	2.009		-0.018	0.007
180	2.393		-0.063	-0.020
270	2.501		-0.063	0.002

\*not used - deformation pattern did not produce meaningful readings  
(see Figure 19)

All reading in inches, positive values indicate inward deformation

## 6.2 Side Drop

An unexpected failure of the overpack occurred during the side drop. The bolted joint between the overpack top and base failed completely, shearing off all ten bolts and allowing the base to separate from the package. The cable carrying signals from the sensors inside the cask (routed through a hole in the overpack base) was broken almost instantaneously. As the two weldments separated, the cable connector was also pulled apart, causing loss of signal from the remaining accelerometers outside the overpack.

The causes of the overpack joint failure as well as its requalification will be discussed in a separate report.<sup>2</sup> The remainder of this subsection presents the data from the side drop test. The data suggests that, in spite of the failure, the acceleration record extends through the instant at which the peak value occurred.

### 6.2.1 Acceleration Data and High-Speed Photography

Figure 20 shows the time history of vertical acceleration as measured by the radial accelerometer inside the cask and the tangential accelerometer on the overpack. The photographs in Figure 21, taken at intervals of 2.13 milliseconds, show the critical time period between initial impact and loss of signal.

The high-speed films revealed that the package rotated slightly as it fell to strike the pad, top end first, with its axis inclined 10 degrees from the horizontal. This was probably caused either by a slight swinging of the package at the instant of release or a failure of the magnet to release uniformly over its entire surface. Implications of the contact angle for a side drop are considered in a separate report.<sup>3</sup>

Figures 20 and 21 contain much valuable information in spite of the fact that the instrumentation cable from the cask sensors was destroyed 11 milliseconds after the initial impact. Indicated on Figure 20 is the time interval during which crushing of the top toroid occurred. Following the initial impact at frame 0, the acceleration pattern shows a double peak, believed to be characteristic of the snap-through behavior of the toroid. The toroid on the overpack base strikes approximately 8 milliseconds later, after the crushing of the top toroid is complete. The second impact causes the vertical acceleration to again rise rapidly. The bolts break about 2 milliseconds later, releasing the base weldment which rotates outward and is propelled away from the package. Figure 22 shows a still photograph taken just after impact, with the base weldment in midair. Figure 23 shows the aftermath of the side drop.

---

<sup>2</sup>Ibid.

<sup>3</sup>Ibid.

*6.2 Side Drop*

29

Based on the acceleration traces and the high-speed films, the signal cable is believed to have faulted 11 milliseconds after impact, between frames +5 and +6 of the film. This coincides approximately with the point in time when the joint flange of the overpack top struck the pad. The signal went low, indicating the cable had shorted. It later went high when the conductors parted completely. There is no certain way of determining the last instant at which the acceleration signal is accurate. The point indicated on Figure 20 is based on inspection of the signal itself and the high-speed film.

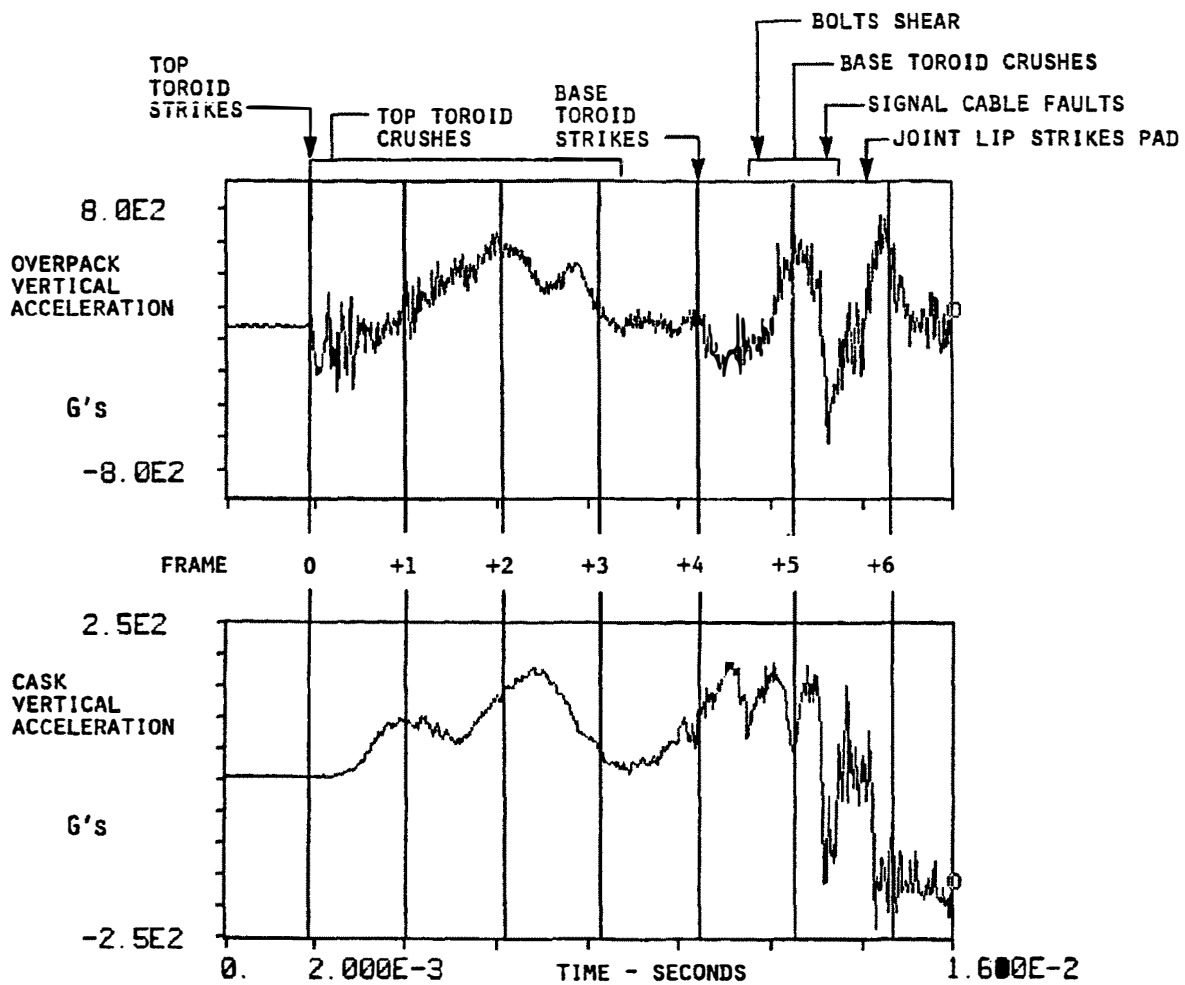


Figure 20. Side drop, vertical acceleration

6.2 Side Drop

31

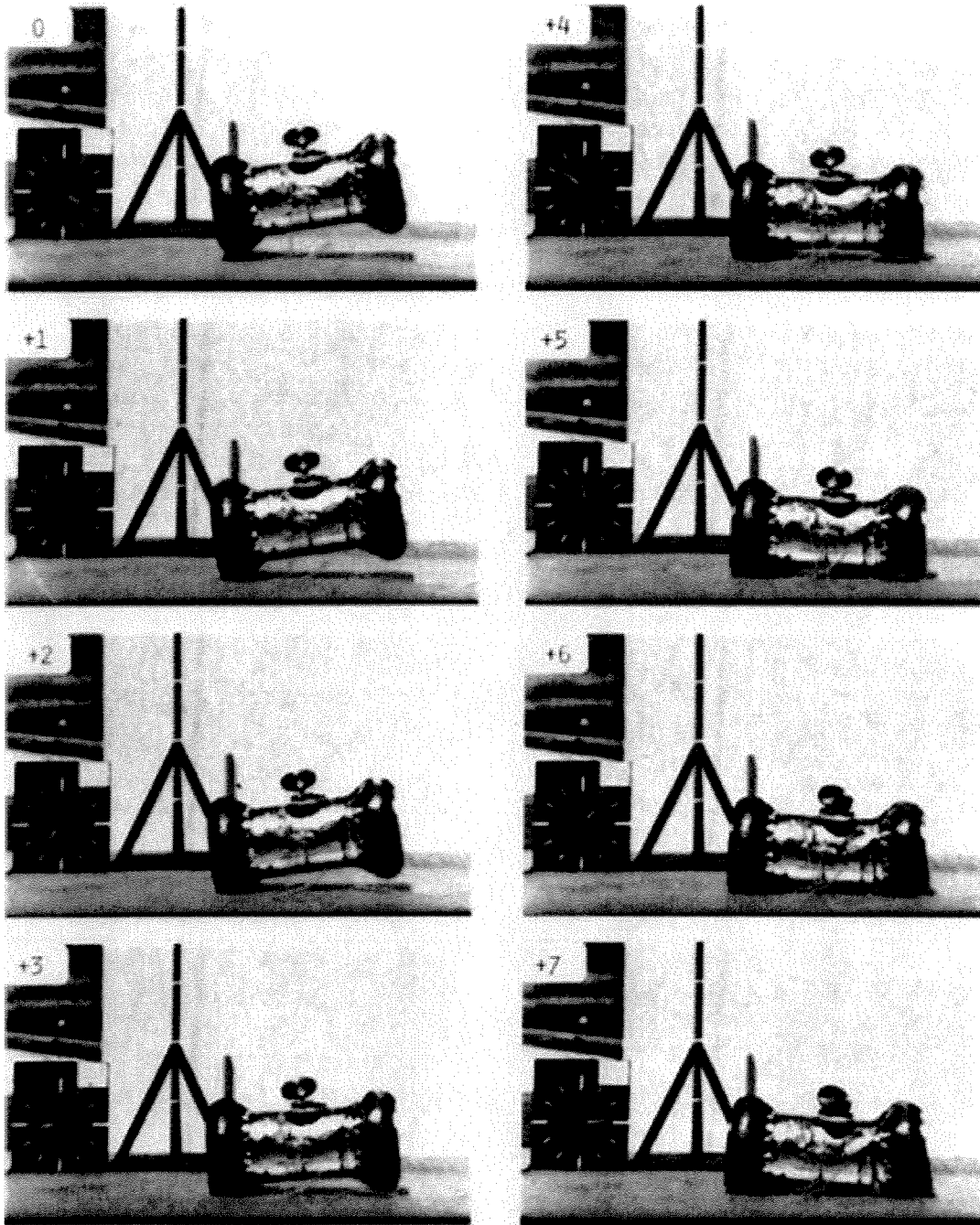


Figure 21. Side drop, frames taken at 2.13 millisecond intervals

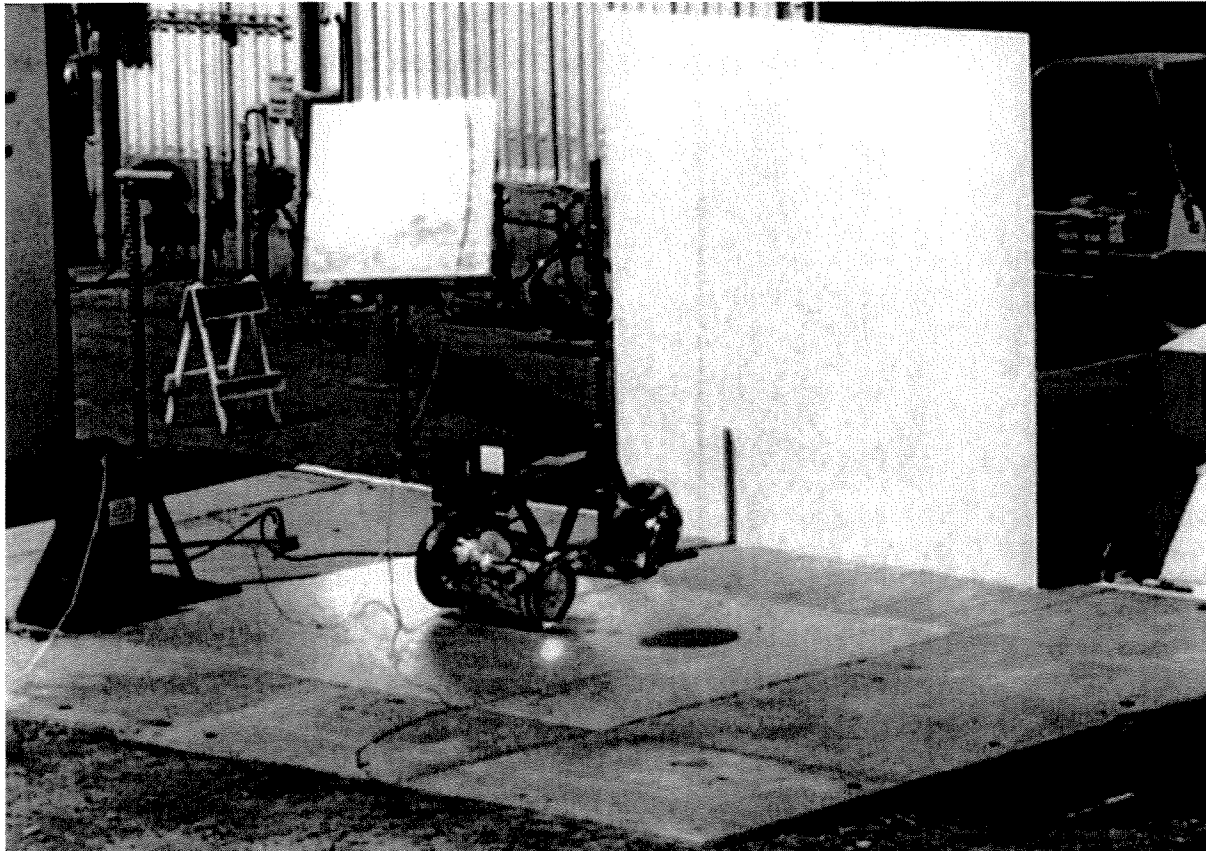


Figure 22. Overpack weldments separating after impact, side drop

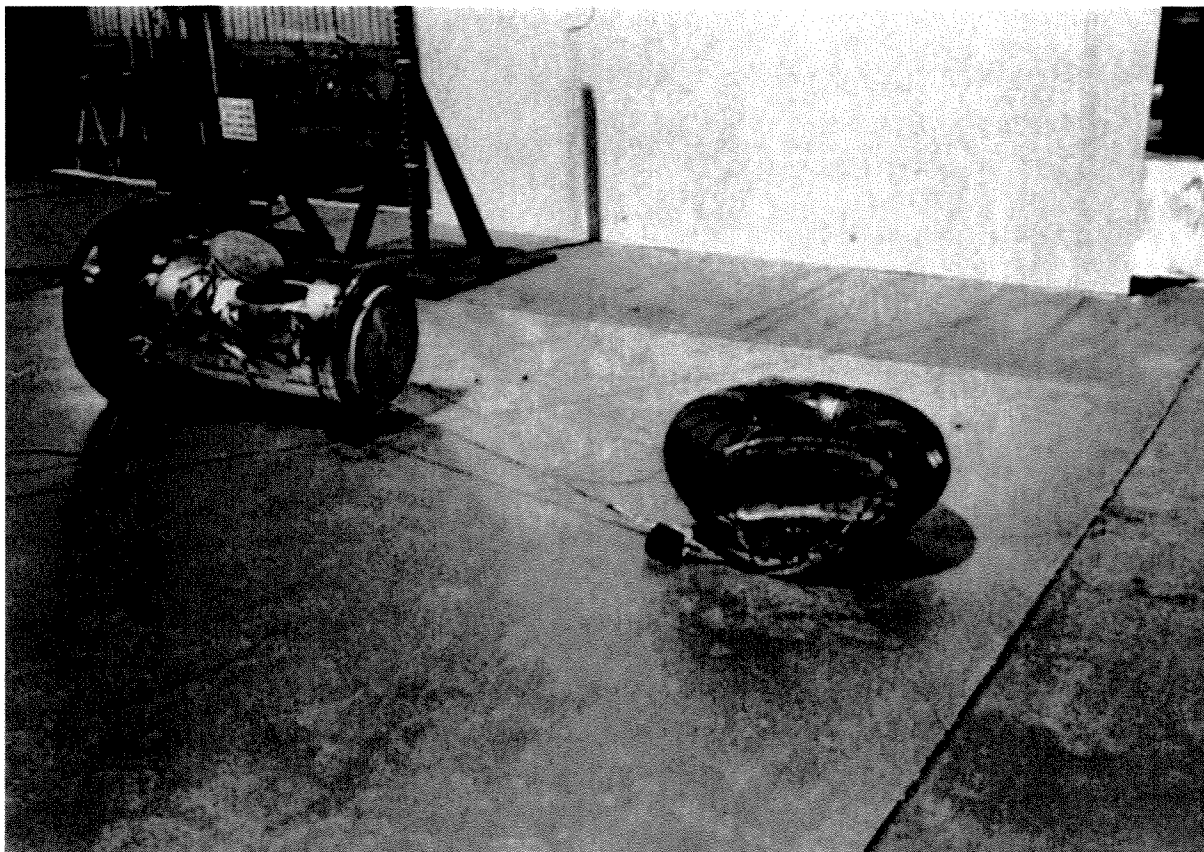


Figure 23. Package after side drop

It may be shown, however, that the important part of the impact event occurred prior to the indicated loss-of-signal point. Figure 24 shows the calculation of the net change in the cask vertical velocity between initial impact and the cable fault. The trace was zeroed from the fault point through the end of the record prior to integration. The result indicates that the cask had not come completely to rest when the signal was lost. The net velocity change up to that point was 379 inches/second. Since the impact velocity was 527 inches/second, the remaining velocity change was  $527 - 379 = 148$  inches/second. This corresponds to a free drop from 28 inches, an event unlikely to damage even an unprotected cask. Stated another way, since kinetic energy is proportional to velocity squared, the percent of the initial energy remaining when the signal was lost was only  $(148/527)^2 \times 100 = 7.9\%$  of the initial value. In effect, the impact event was essentially over before the signal was lost.

Likewise, since the toroids were extensively deformed by the side drop (Figure 23) and this deformation could only have occurred while the sensing channel was still intact, the observed maximum acceleration of 185 G's is a reasonable estimate of the maximum that would have occurred if the bolted joint had not failed.

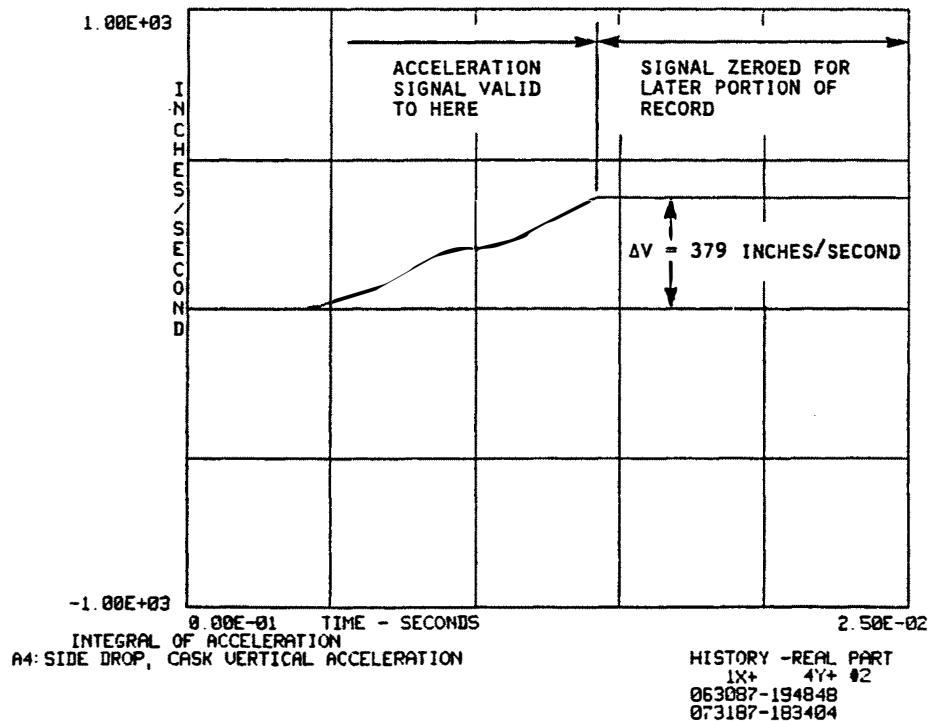


Figure 24. Time integral of cask vertical acceleration prior to cable fault, side drop



### 6.3 CG-Over-Corner Drop

35

#### 6.2.2 Pressure- Sensing Film

Figure 25 shows the pressure-sensing film after the side drop. The film was applied only to the lateral sides of the cask. It shows that the load tended to concentrate towards the ends of the cask, except for two narrow lines parallel to the cask axis. These localized areas of high pressure were caused by the crush tubes between the double walls of the overpack cylinder.

#### 6.2.3 Cask and Overpack Deformation Measurements

Micrometer measurements were made of the cask diameter at a number of axial and azimuthal stations before and after the side drop. No change was found; no measurable plastic deformation of the cask had occurred.

Extensive measurements of the overpack before and after the side drop are given in General Electric Inspection Report No. 6430, dated June 12, 1987. The radial indentation of the top toroid (which struck the ground first) was found to be 3.18 inches in depth. Damage to the base toroid was slightly greater.

### 6.3 CG-Over-Corner Drop

For the final drop, the cask was oriented as shown in Figure 26. The orientation, with the cask axis 22 degrees off the vertical, positioned the package center-of-gravity directly over the impact point on the top toroid. This was verified by balancing the cask on the contact point. The angle proved to be slightly different from the calculated value of 29 degrees used in the design of the mounting block for the cask oblique accelerometer. The resulting 7 degree misalignment of the sensing axis was not considered significant since it reduced the acceleration signal by less than 1%.

The drop was performed without incident to conclude the test series.

#### 6.3.1 Acceleration Data and High-Speed Photography

Figures 27 and 28 illustrate the impact event. The lower trace in Figure 27 shows the time history of cask acceleration in the vertical direction as sensed by the cask oblique accelerometer. The upper trace is from the overpack axial accelerometer and gives the vertical acceleration attenuated by about 7% due to the 22 degree misalignment of the sensor axis from vertical. The photographs in Figure 27 were taken at intervals of 2.16 milliseconds.

Upon striking the pad, the package rebounded in a direction roughly parallel to its axis while rotating counterclockwise (as seen in the view of Figure 28) in

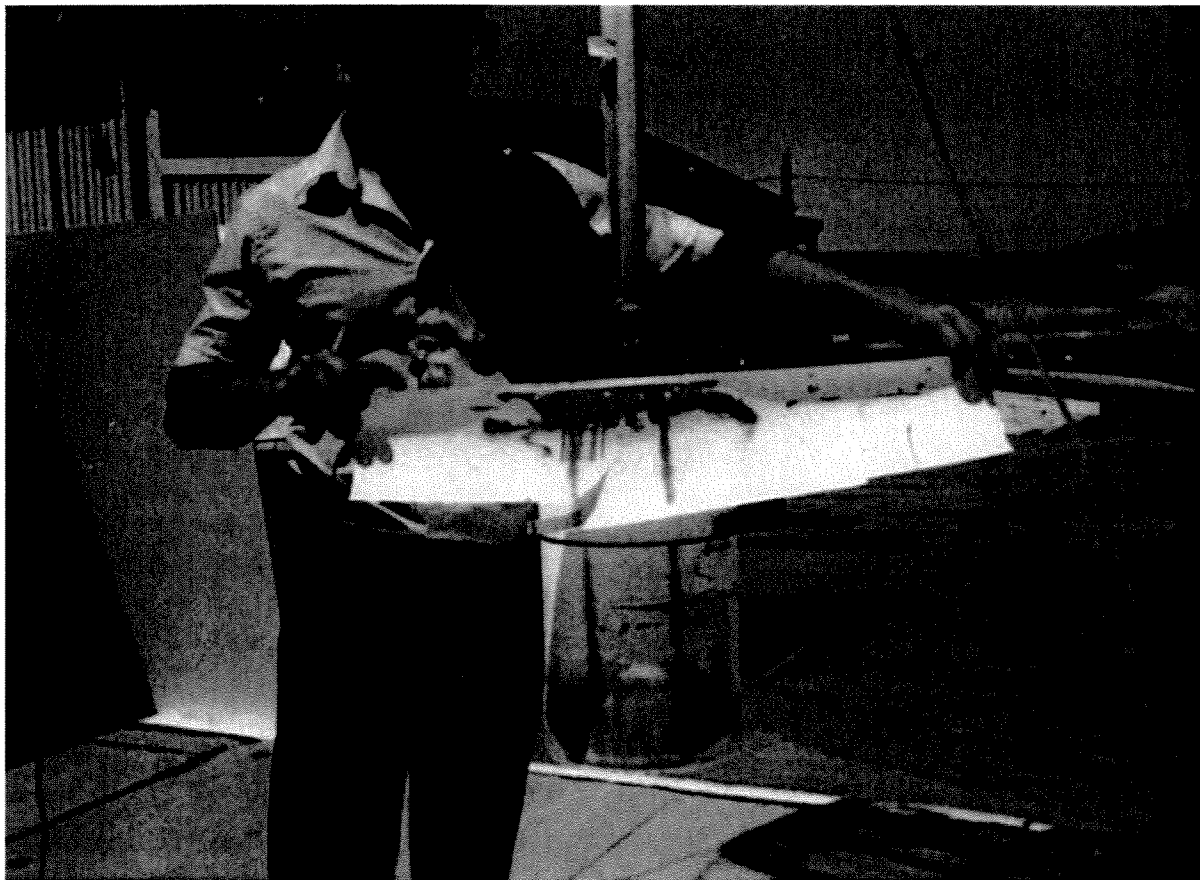


Figure 25. Pressure-sensing film from side drop

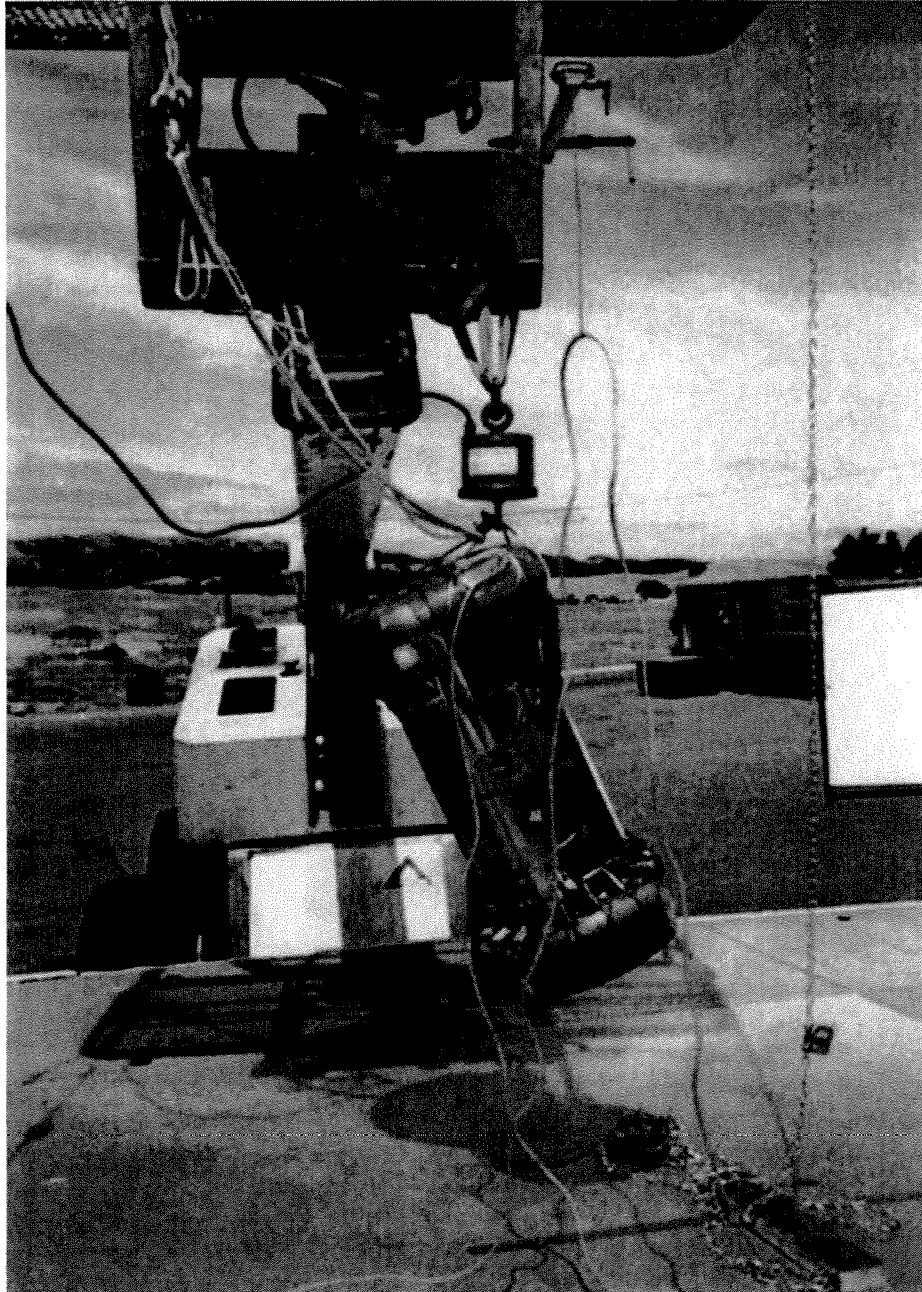


Figure 26. Rigging for CG-over-corner drop

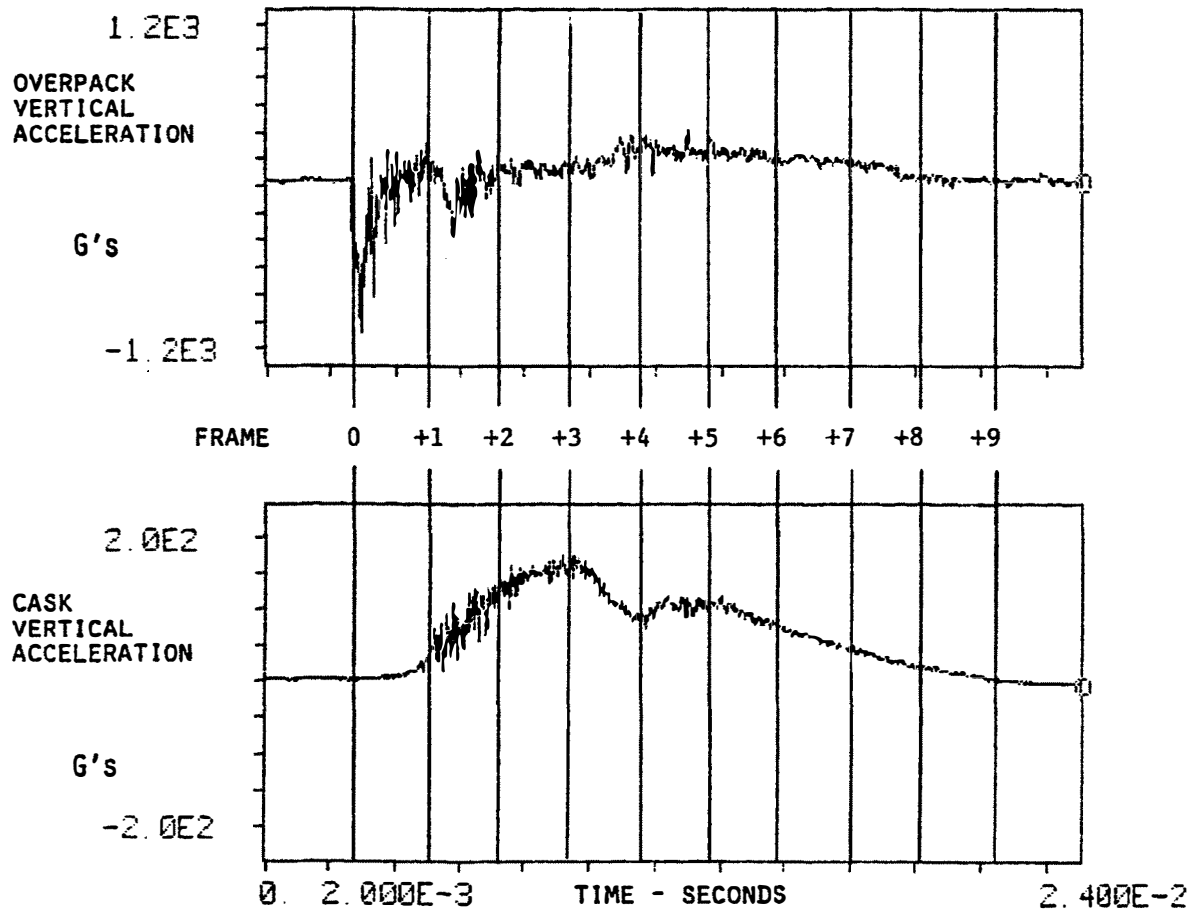


Figure 27. CG-over-corner drop, vertical acceleration

6.3 CG Over-Corner Drop

39

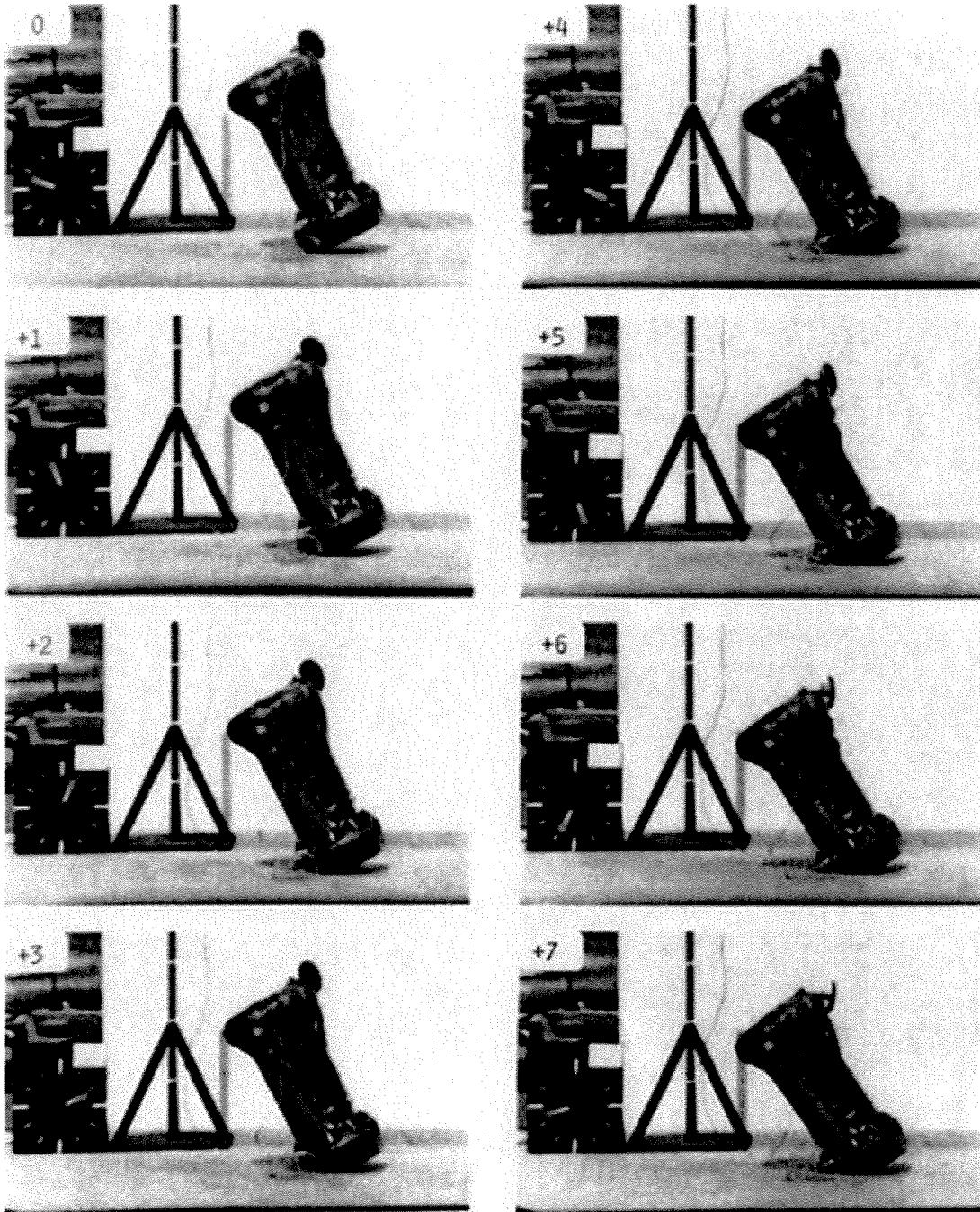


Figure 28. CG-over-corner drop, frames taken at 2.16 millisecond intervals

midair through about 250 degrees before coming to rest. The maximum rebound height and rotational velocity, determined from the high-speed films, were 4.7 inches and 15.1 radians/second. The rotational velocity produced by the impact does not mean that the CG was not aligned over the impact point. Rather, it simply implies that the deformation pattern of the toroid produced a force whose resultant did not pass through the CG. Figure 29 shows the deformation of the top toroid.

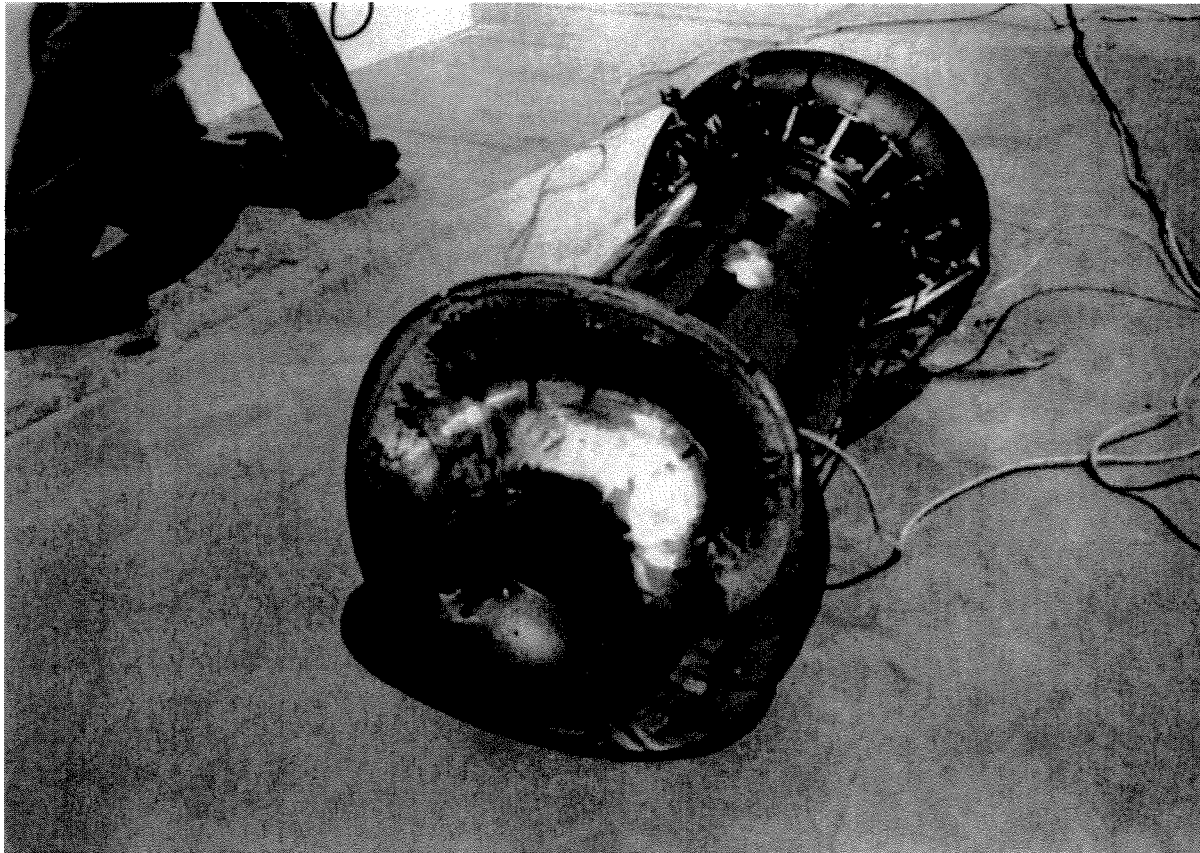


Figure 29. Deformation of overpack produced by CG-over-corner drop

### 6.3 CG-Over-Corner Drop

41

The cask acceleration transient, lasting about 18 milliseconds, was substantially longer than for either the head-on or side drop. This is related to the fact that a toroid struck on a corner produces a softer "cushion" than when struck head-on or from the side. The greater compliance produces a longer acceleration transient with a lower peak value; maximum cask acceleration was the lowest of the three tests at 156 G's. The transient showed the characteristic double peak.

Determination of the net velocity change was straightforward and is shown in Figure 30. The value of 548 inches/second, slightly greater than the impact velocity, is reasonable based on the small value of the rebound height.

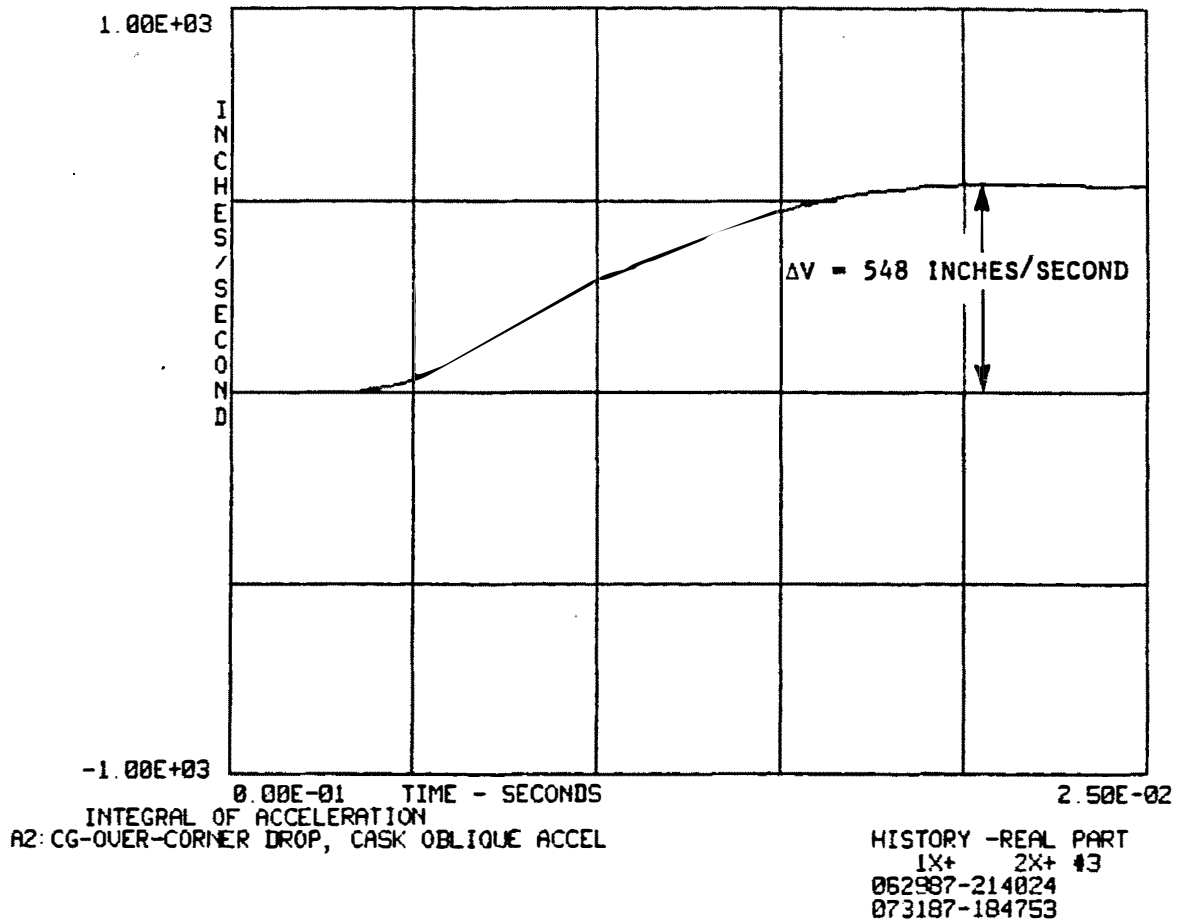


Figure 30. Time integral of cask vertical acceleration, CG-over-corner drop

### 6.3.2 Pressure-Sensing Film

Figure 31 shows the pressure sensitive film, still on the cask, following the CG-over-corner drop. The pressure over the end cover plate was fairly uniform, consistent with the fact that the honeycomb cushion did not bottom. Pressure on the lateral sides of the cask was confined to circumferential bands near the ends, particularly the lid end which was oriented downwards at impact. The pressure band extends essentially all the way around the cask although the highest pressure was seen on the downward side, as would be expected. Loading of the other side probably occurred on the second impact.

### 6.3.3 Cask and Overpack Deformation Measurements

Micrometer measurements were made of the cask diameter at a number of axial and azimuthal stations before and after the side drop. No change was found; no measurable plastic deformation of the cask had occurred.

Extensive measurements of the overpack before and after the CG-over-corner drop are given in General Electric Inspection Report No. 6432, dated June 18, 1987. Deformation, as shown in Figure 29, was significant, but was confined to the region around the impact. Maximum depth of the indenting, measured parallel to the package axis along a minor diameter of the toroid, was approximately 5.3 inches.





Figure 31. Pressure-sensing film from CG-over-corner drop

## **7. Summary and Conclusions**

Drop tests in three orientations were performed with no measurable deformation or other damage to the cask. The head-on and CG-over-corner drops were successfully completed with no unexpected results. Complete acceleration and internal load distribution data were obtained for use in design verification.

An unexpected failure of the overpack bolted joint occurred during the side drop. The causes of the failure and the requalification of the joint will be covered in a separate report. The structural failure also caused the loss of some acceleration data. Nonetheless, a valid trace was obtained for the most important part of the impact event, including the portion during which plastic deformation of the overpack occurred and, probably containing the point of maximum acceleration.

Subject to the above uncertainty in the side drop test, the maximum vertical accelerations recorded by the sensors inside the cask for the head-on, side, and CG-over-corner drops were 408, 185, and 156 G's respectively.

## 2.12.6. Fabrication Stresses

The following sections provide a detailed evaluation of the stresses that occur during the fabrication process of lead pour and also service at extreme cold temperatures between the inner stainless steel shell, lead shell, and outer stainless steel shell of the Model 2000 cask body.

### 2.12.6.1. Fabrication Stresses Due to Lead Pour

During the fabrication process, liquid lead is poured into the annulus between the inner and outer stainless steel shells of the Model 2000 cask at a temperature of ~620°F with the ambient temperature at ~70°F. Before coming into contact with the liquid lead, the stainless steel shells are at the ambient temperature. Once the liquid lead comes into contact with the stainless steel shells, the temperature difference between the two materials increases the energy in the stainless steel causing the material to expand. The dimensions of the inner and outer shells at 70°F are as follows in Table 2.12.6-1.

**Table 2.12.6-1. Dimensions of Stainless Steel Shells**

Parameter	Variable	Input	Units
Outer Diameter of Inner Shell	$d_o$	28.5	in
Inner Diameter of Inner Shell	$d_i$	26.5	in
Mean Radius Inner Shell	$R_i$	13.75	in
Outer Diameter of Outer Shell	$D_o$	38.5	in
Inner Diameter of Outer Shell	$D_i$	36.5	in
Mean Radius Outer Shell	$R_o$	18.75	in
Thickness of Inner Shell	$t_i$	1	in
Thickness of Outer Shell	$t_o$	1	in

#### 2.12.6.1.1. Thermal Expansion of Stainless Steel Shells

When the inner and outer shells are subjected to the lead temperature of 620°F, the mean radius and thickness of each shell increases and is calculated with the following equations:

$$R' = R (1 + \alpha \Delta T)$$

where

$$R = \text{Mean Radius of Shell}$$

$$\alpha = \text{Coefficient of Thermal Expansion For} \\ 304 \text{ Stainless Steel at } 620^\circ\text{F} (9.92\text{E-}06 \text{ in/in/}^\circ\text{F})$$

$$\Delta T = \text{Temperature difference } (620^\circ\text{F} - 70^\circ\text{F} = 550^\circ\text{F})$$

and

$$t' = t (1 + \alpha \Delta T)$$

where

$$t = \text{Thickness of Shell}$$

Using the above equations, the shell growth of the inner shell is:

$$\begin{aligned} R_i' &= 13.75[1 + 9.92\text{E-}06 \times 550] \\ &= 13.825 \text{ in} \\ t_i' &= 1[1 + 9.92\text{E-}06 \times 550] \\ &= 1.005 \text{ in} \end{aligned}$$

Further, the shell growth of the outer shell is:

$$\begin{aligned} R_o' &= 18.75[1 + 9.92\text{E-}06 \times 550] \\ &= 18.852 \text{ in} \\ t_o' &= 1[1 + 9.92\text{E-}06 \times 550] \\ &= 1.005 \text{ in} \end{aligned}$$

Accordingly, the dimensions at 620°F for the inner and outer radius of each shell can be calculated using the equations below. For the inner stainless steel shell:

$$\begin{aligned} r_{ii}' &= r_{ii}(1 + \alpha \Delta T) \\ &= 13.25[1 + 9.92\text{E-}06 \times 550] \\ &= 13.322 \text{ in} \end{aligned}$$

where

$$\begin{aligned} r_{ii}' &= \text{Inside radius of inner shell at } 620^\circ\text{F} \\ r_{ii} &= \text{Inside radius of inner shell at } 70^\circ\text{F} \end{aligned}$$

and

$$\begin{aligned} r_{oi}' &= r_{oi}(1 + \alpha \Delta T) \\ &= 14.25[1 + 9.92\text{E-}06 \times 550] \\ &= 14.328 \text{ in} \end{aligned}$$

where

$$\begin{aligned} r_{oi}' &= \text{Outside radius of inner shell at } 620^\circ\text{F} \\ r_{oi} &= \text{Outside radius of inner shell at } 70^\circ\text{F} \end{aligned}$$

For the outer stainless steel shell:

$$\begin{aligned} r_{io}' &= r_{io}(1 + \alpha \Delta T) \\ &= 18.251[1 + 9.92\text{E-}06 \times 550] \\ &= 18.350 \text{ in} \end{aligned}$$

where

$$\begin{aligned} r_{io}' &= \text{Inside radius of outer shell at } 620^\circ\text{F} \\ r_{io} &= \text{Inside radius of outer shell at } 70^\circ\text{F} \end{aligned}$$

and

$$\begin{aligned} r_{oo}' &= r_{oo}(1 + \alpha \Delta T) \\ &= 19.25[1 + 9.92E-06 \times 550] \\ &= 19.355 \text{ in} \end{aligned}$$

where

$$\begin{aligned} r_{oo}' &= \text{Outside radius of outer shell at } 620^{\circ}\text{F} \\ r_{oo} &= \text{Outside radius of outer shell at } 70^{\circ}\text{F} \end{aligned}$$

#### 2.12.6.1.2. Hydrostatic Pressure

In order to determine the stresses that develop in the stainless steel shells, the static pressure that develops due to the column of lead is first calculated as follows,

$$q = \rho_{\text{lead}} \times h_{\text{lead}}$$

where

$$\begin{aligned} q &= \text{Static Pressure} \\ \rho_{\text{lead}} &= \text{Density of lead (0.4097 lbf/in}^3\text{)} \\ h_{\text{lead}} &= \text{Height of lead column (56 in)} \end{aligned}$$

NOTE: Value for the density of lead is interpolated to just below the melting point (620°F). The solid lead value is conservative because the density for liquid lead at 620°F is less and would result in a lower hydrostatic pressure and therefore lower membrane stresses.

Therefore, the hydrostatic pressure is:

$$\begin{aligned} q &= 0.4097 \times 56 \\ q &= 22.943 \text{ psi} \end{aligned}$$

This hydrostatic pressure increases the outer shell radius and decreases the inner shell radius as is determined with the following equations. Decrease in inner shell mean radius due to static pressure (Reference 2-19, Table 13.8, Page 608):

$$\begin{aligned} \Delta R_i' &= \frac{-q \times (R_i')^2}{E \times t_i'} \\ &= \frac{-22.943 \times (13.825)^2}{25.2E06 \times 1.005} \\ &= -0.000173 \text{ in} \end{aligned}$$

where

$$\begin{aligned} E &= \text{Modulus of Elasticity} \\ &\text{of 304 Stainless Steel at } 620^{\circ}\text{F (25.2E06 psi)} \end{aligned}$$

Increase in outer shell mean radius due to static pressure (Reference 2-19, Table 13.8, Page 608):

$$\begin{aligned} \Delta R_o' &= \frac{q \times (R_o')^2}{E \times t_i'} \\ &= \frac{22.943 \times (18.852)^2}{25.2E06 \times 1.005} \\ &= 0.000322 \text{ in} \end{aligned}$$

### 2.12.6.1.3. Membrane Stresses

The lead column creates a radial pressure on the inner and outer shells. The stresses due to the maximum external pressure on the inner shell are (Reference 2-19, Table 13.8, Page 608):

$$\sigma_1 = 0 \text{ psi}$$

where

$$\sigma_1 = \text{Meridional Stress}$$

$$\begin{aligned}\sigma_2 &= \frac{-q \times r'_{oi}}{t'_i} \\ &= \frac{-22.943 \times 14.328}{1.005} \\ &= -326.941 \text{ psi}\end{aligned}$$

where

$$\sigma_2 = \text{Hoop Stress}$$

$$\sigma_3 = -22.943 \text{ psi}$$

where

$$\sigma_3 = \text{Radial Stress}$$

It should be noticed that the sign for the hoop stress and radial stress is negative. This is because the direction of the static pressure is acting inward instead of outward. The stresses due to the maximum internal pressure on the outer shell are (Reference 2-19, Table 13.8, Page 608):

$$\begin{aligned}\sigma_1 &= 0 \text{ psi} \\ \sigma_2 &= \frac{q \times r'_{io}}{t'_o} \\ &= \frac{22.943 \times 18.350}{1.005} \\ &= 418.713 \text{ psi} \\ \sigma_3 &= 22.943 \text{ psi}\end{aligned}$$

The allowable stress is the yield stress for the stainless steel, which is equal to 18,240 psi at 620°F. Comparing this allowable stress with the meridional, hoop and radial stresses for the inner and outer shells shows that they are all below the allowable stress and thus acceptable.

### 2.12.6.1.4. Buckling

Additional analysis is performed to see if the inner shell will buckle due to the external pressure (Reference 2-33, Equation 188, Page 220):

$$\begin{aligned}P_{cr} &= \frac{(h/R'_i) \times \sigma_{y.p.}}{1 + 4(\sigma_{y.p.}/E) \times (R'^2_i/h^2)} \\ &= \frac{(1.005/13.825) \times 18240}{1 + 4(18240/25.2E06) \times (13.825^2/1.005^2)} \\ &= 857.28 \text{ psi}\end{aligned}$$

where

$$\begin{aligned}
 E &= \text{Modulus of Elasticity} \\
 &\text{of 304 Stainless Steel at 620°F (25.2E06 psi)} \\
 P_c &= \text{Critical Pressure} \\
 h &= \text{Thickness of Wall of } [[ \quad ]] \\
 \sigma_{y.p.} &= \text{Yield Point in Compression at 620°F}
 \end{aligned}$$

As the analysis shows, the critical pressure is larger than the pressure on the inner shell. Therefore, the liquid lead has a negligible effect on the inner and outer stainless steel shells.

#### 2.12.6.2. Stresses Due to Lead Solidification and Lead Shrinkage

For this analysis, the dimensions of the unloaded solid lead shell are used as a reference point for interference fits. To do this, the loads due to the hydrostatic pressure are removed. The dimension of the inner and outer shells at 620°F are given in Table 2.12.6-2.

**Table 2.12.6-2. Dimensions of Inner and Outer Shell at 620°F**

Input Parameter	Variable	Input	Units
Inner Radius of Inner Shell at 620°F	$r_{ii}'$	13.322	in
Outer Radius of Inner Shell at 620°F	$r_{oi}'$	14.328	in
Inner Radius of Outer Shell at 620°F	$r_{io}'$	18.350	in
Outer Radius of Outer Shell at 620°F	$r_{oo}'$	19.355	in

The dimensions given in Table 2.12.6-2 are used to obtain the loaded lead dimensions of the lead shell. The inside radius of the lead shell is set equal to the outside radius of the inner steel shell and the outer radius of the lead shell is set equal to the inside radius of the outer steel shell as follows:

$$R_{i\text{-lead}} = 14.328 \text{ in}$$

$$R_{o\text{-lead}} = 18.350 \text{ in}$$

##### 2.12.6.2.1. Unloaded Lead Dimensions

To obtain the unloaded lead dimensions, a negative load is applied to the loaded dimensions. To do this, the internal and external pressures that are acting on the lead shell are first determined. For the internal pressure acting on the inner surface of the lead shell, the change in the outer radius of the lead ( $\Delta a$ ) is (Reference 2-19, Table 13.5, Page 696):

$$\begin{aligned}
 \Delta a &= \frac{qab^2(2-\nu)}{E(a^2 - b^2)} \\
 &= \frac{22.943 \times 18.350 \times 14.328^2 (2-0.4)}{1.49E06 \times (18.350^2 - 14.328^2)} \\
 &= 0.000706 \text{ in}
 \end{aligned}$$

where

$$a = \text{Outside Radius of Lead Shell}$$

NEDO-33866 Revision 6  
Non-Proprietary Information

$$\begin{aligned} b &= \text{Inside Radius of Lead Shell} \\ \nu &= \text{Poisson's Ratio for lead at 620°F (0.4)} \\ E &= \text{Modulus of Elasticity for Lead at 620°F (1.49E06 psi)} \end{aligned}$$

NOTE: Value for poisson's ratio and modulus of elasticity are that of solid lead at just below the melting point of 620°F.

The change in the inside radius of the lead ( $\Delta b$ ) is (Reference 2-19, Table 13.5, Page 696):

$$\begin{aligned} \Delta b &= qb \frac{a^2(1+\nu)+b^2(1-2\nu)}{E(a^2-b^2)} \\ &= 22.943 \times 14.328 \frac{18.350^2(1+0.4)+14.328^2(1-2 \times 0.4)}{1.49E06 \times (18.350^2-14.328^2)} \\ &= 0.000860 \text{ in} \end{aligned}$$

For the external pressure acting on the outer surface of the lead shell, the change in outer radius of the lead is:

$$\begin{aligned} \Delta a &= -qa \frac{a^2(1-2\nu)+b^2(1+\nu)}{E(a^2-b^2)} \\ &= -22.943 \times 18.350 \frac{18.350^2(1-2 \times 0.4)+14.328^2(1+0.4)}{1.49E06 \times (18.350^2-14.328^2)} \\ &= -0.000763 \text{ in} \end{aligned}$$

The change in the inside radius of the lead due to the external pressure is:

$$\begin{aligned} \Delta b &= \frac{-qba^2(2-\nu)}{E(a^2-b^2)} \\ &= \frac{-22.943 \times 14.328 \times 18.350^2(2-0.4)}{1.49E06 \times (18.350^2-14.328^2)} \\ &= -0.000904 \text{ in} \end{aligned}$$

Now that the loaded dimensions have been determined, the unloaded dimensions are determined by removing the loads. Removing the internal pressure first:

$$\begin{aligned} \Delta a &= -0.000706 \text{ in} \\ \Delta b &= -0.000860 \text{ in} \end{aligned}$$

Followed by removing the external pressure:

$$\begin{aligned} \Delta a &= 0.000763 \text{ in} \\ \Delta b &= 0.000904 \text{ in} \end{aligned}$$

Therefore the total change in the outer and inner radius of the lead with no load is:

$$\begin{aligned} \Delta a_{\text{total}} &= 0.000763 - 0.000706 \\ &= 0.000057 \text{ in} \\ \Delta b_{\text{total}} &= 0.000904 - 0.000860 \\ &= 0.000044 \text{ in} \end{aligned}$$



The dimensions of the lead at 620°F with no load is:

$$\begin{aligned} R_{i\text{-lead}} &= 14.3277480 + 0.000044 \\ &= 14.327792 \text{ in} \\ R_{o\text{-lead}} &= 18.3495720 + 0.000057 \\ &= 18.3496285 \text{ in} \end{aligned}$$

The results show that the difference between the loaded and unloaded dimensions is negligible. Using the unloaded dimensions, a check for interference is completed.

#### 2.12.6.2.2. Interference

At 70°F, stresses will accumulate between the lead and the inner stainless steel shell due to shrinkage of the materials as they cool down from the lead pour. To determine these stresses, the lead dimensions are calculated at 70°F. It is known that at 620°F the lead outer radius is 18.35 inches. Therefore, the equation shown below is used to determine the outer radius of the lead at 70°F.

$$\begin{aligned} R_{o70} &= \frac{R_{o620}}{(1+\alpha\Delta T)} \\ &= \frac{18.350}{1+24.6E-06 \times 550} \\ &= 18.105 \text{ in} \end{aligned}$$

where

$$\begin{aligned} R_{o620} &= \text{Outer Radius of Lead at 620°F} \\ R_{o70} &= \text{Outer Radius of Lead at 70°F} \\ \alpha &= \text{Coefficient of Thermal Expansion} \\ &\quad \text{for Lead at 620°F (24.6E-06 in/in/°F)} \end{aligned}$$

Accordingly, the inner radius of the lead shell at 620°F is 14.328 in and

$$\begin{aligned} R_{i70} &= \frac{R_{i620}}{1+\alpha\Delta T} \\ &= \frac{14.358}{1+24.6E-06 \times 550} \\ &= 14.137 \text{ in} \end{aligned}$$

The no-load dimensions at 70°F for all shells are displayed in Table 2.12.6-3.

**Table 2.12.6-3. Dimensions of Shells at 70°F**

Parameter		Variable	Input	Units
1	Inner Radius Inner Shell at 70°F	$r_{ii}$	13.25	in
2	Outer Radius Inner Shell at 70°F	$r_{oi}$	14.25	in
3	Inner Radius Outer Shell at 70°F	$r_{io}$	18.25	in
4	Outer Radius Outer Shell at 70°F	$r_{oo}$	19.25	in
5	Inner Radius of Lead at 70°F	$R_{i70}$	14.137	in
6	Outer Radius of Lead at 70°F	$R_{o70}$	18.105	in

The air gap between the outer shell and lead is 18.25 inches – 18.105 inches = 0.145 inches. Additionally, the interference between the inner shell and the lead is:

$$\delta = 14.25 \text{ in} - 14.137 \text{ in} = 0.113 \text{ in}$$

### 2.12.6.2.3. Interference Contact Pressure

Because there is interference between the inner shell and the lead, an interference contact pressure  $p$  arises between the two shells and is calculated with the following press fit equation (Reference 2-34, Equation 3-56, Page 110):

$$\delta = \frac{b_L p \left( \frac{C^2 + b_L^2}{C^2 - b_L^2} + \nu_L \right)}{E_L} + \frac{b_s p \left( \frac{b_s^2 + a^2}{b_s^2 - a^2} - \nu_s \right)}{E_s}$$

solving,

$$p = \frac{\delta}{\frac{b_L \left( \frac{C^2 + b_L^2}{C^2 - b_L^2} + \nu_L \right)}{E_L} + \frac{b_s \left( \frac{b_s^2 + a^2}{b_s^2 - a^2} - \nu_s \right)}{E_s}}$$

where

$\delta$	=	Interference between contact surfaces
$b_L$	=	Inner radius of lead shell
$C$	=	Outer radius of lead shell
$\nu_L$	=	Poisson's Ratio for lead at 70°F (0.4)
$E_L$	=	Modulus of Elasticity for lead at 70°F (2.42E06)
$b_s$	=	Outer radius of inner shell
$\nu_s$	=	Poisson's Ratio for 304 stainless steel at 70°F (0.31)
$a$	=	Inner radius of inner shell
$E_s$	=	Modulus of Elasticity for 304 stainless steel at 70°F

Substituting values:

$$p = \frac{0.113}{\frac{14.137 \left( \frac{18.105^2 + 14.137^2}{18.105^2 - 14.137^2} + 0.4 \right)}{2.42E06} + \frac{14.25 \left( \frac{14.25^2 + 13.25^2}{14.25^2 - 13.25^2} - 0.31 \right)}{2.83E07}}$$

$$= 3417.512 \text{ psi}$$

An interface pressure of this magnitude will cause the lead to yield.

### 2.12.6.2.4. Internal and External Loads on Lead Shell and Inner Shell

To determine a more accurate interface pressure, the maximum pressure is set equal to the pressure that corresponds to the hoop stress at which the lead yields.

#### **Loads at 70°F**

The yield strength of lead at 70°F is 620 psi and is set to the hoop stress to obtain the maximum pressure. For a thick-walled shell (Reference 2-19, Table 13.5, Page 696):

NEDO-33866 Revision 6  
Non-Proprietary Information

$$\begin{aligned}
 p &= \frac{\sigma_2(c^2 - b_L^2)}{c^2 + b_L^2} \\
 &= \frac{620(18.105^2 - 14.137^2)}{18.105^2 + 14.137^2} \\
 p &= 150.338 \text{ psi}
 \end{aligned}$$

This pressure will translate to the inner shell causing a hoop stress of (Reference 2-19, Table 13.5, Page 696):

$$\begin{aligned}
 \sigma_2 &= -\frac{p(b_s^2 + a^2)}{b_s^2 - a^2} \\
 &= -\frac{150.338(14.25^2 + 13.25^2)}{14.25^2 - 13.25^2} \\
 &= -2069.882 \text{ psi}
 \end{aligned}$$

It should be noted that any relaxation due to creep can be conservatively neglected.

**Loads at -20°F**

Now consider the HAC temperature of -20°F for the worst hoop stress on the inner shell. The coefficient of thermal expansion for the lead and stainless steel at the HAC -20°F temperature is:

$$\begin{aligned}
 \alpha_{ss-20} &= 8.17\text{E-}06 \text{ (in/in/°F)} \\
 \alpha_{L-20} &= 1.57\text{E-}05 \text{ (in/in/°F)}
 \end{aligned}$$

Then the steel and lead shell dimensions at -20°F are as follows

$$\begin{aligned}
 a &= 13.25[1 + 8.17\text{E-}06 \times -90] &= 13.240 \text{ in} \\
 b_s &= 14.25[1 + 8.17\text{E-}06 \times -90] &= 14.240 \text{ in} \\
 b_L &= 14.1365[1 + 1.57\text{E-}05 \times -90] &= 14.117 \text{ in} \\
 C &= 18.105[1 + 1.57\text{E-}05 \times -90] &= 18.079 \text{ in}
 \end{aligned}$$

This gives an interference of 0.123 in between the inner shell and the lead at -20°F. This interference will cause the lead to yield. Once again, to achieve a more accurate interface pressure, set the maximum pressure to be equal to the pressure that corresponds to the hoop stress at which the lead yields. The yield strength of lead at -20°F is 763 psi, which gives an interface pressure of (Reference 2-19, Table 13.5, Page 696):

$$\begin{aligned}
 p &= \frac{\sigma_2(c^2 - b_L^2)}{c^2 + b_L^2} \\
 &= \frac{763(18.079^2 - 14.117^2)}{18.079^2 + 14.117^2} \\
 &= 185.013 \text{ psi}
 \end{aligned}$$

This pressure will translate to the inner shell causing a hoop stress of (Reference 2-19, Table 13.5, Page 696):

$$\sigma_2 = -\frac{p(b_s^2 + a^2)}{b_s^2 - a^2}$$

$$= -\frac{185.013(14.24^2 + 13.24^2)}{14.24^2 - 13.24^2}$$

$$= -2547.290 \text{ psi}$$

### ***Loads at -40°F***

Now consider the normal conditions of transport extreme cold temperature of -40°F for the worst hoop stress on the inner steel shell. The coefficient of thermal expansion for the lead and stainless steel at the HAC -40°F temperature is:

$$\alpha_{ss-40} = 8.09\text{E-}06 \text{ (in/in/°F)}$$

$$\alpha_{L-40} = 1.56\text{E-}05 \text{ (in/in/°F)}$$

Calculating the lead and steel shell dimensions at -40°F, the following results:

$$\begin{aligned} a &= 13.25[1 + 8.09\text{E-}06 \times -110] &= 13.238 \text{ in} \\ b_s &= 14.25[1 + 8.09\text{E-}06 \times -110] &= 14.237 \text{ in} \\ b_L &= 14.1365[1 + 1.56\text{E-}05 \times -110] &= 14.112 \text{ in} \\ C &= 18.105[1 + 1.56\text{E-}05 \times -110] &= 18.074 \text{ in} \end{aligned}$$

This results in an interference fit of 0.125 in between the inner shell and lead. Accordingly, the yield strength of lead at -40°F is 795 psi, which is set to the hoop stress to obtain maximum pressure as follows (Reference 2-19, Table 13.5, Page 696):

$$\begin{aligned} p &= \frac{\sigma_2(C^2 - b_L^2)}{C^2 + b_L^2} \\ &= \frac{795(18.074^2 - 14.112^2)}{18.074^2 + 14.112^2} \\ &= 192.77 \text{ psi} \end{aligned}$$

Calculating the hoop stress in the inner shell (Reference 2-19, Table 13.5, Page 696):

$$\begin{aligned} \sigma_2 &= -\frac{p(b_s^2 + a^2)}{b_s^2 - a^2} \\ &= -\frac{192.77(14.237^2 + 13.238^2)}{14.237^2 - 13.238^2} \\ &= -2654.123 \text{ psi} \end{aligned}$$

### **2.12.6.2.5. Axial Stresses and Strains**

The previous calculations only deal with hoop stresses. Axial shrinkage of the lead will cause axial stresses to develop in the inner stainless steel and lead shells.

### ***Cooling From 620°F to -20°F***

Axial stresses and strains will occur in the inner shell from cooling down from 620°F to -20°F. The axial strain that results between the lead and stainless steel from the cooling to the extreme cold temperature of -20°F is:

$$\begin{aligned} \Sigma_{\text{strain}} &= (\alpha_{L620} - \alpha_{ss620}) \Delta T + (\alpha_{L-20} - \alpha_{ss-20}) \Delta T \\ &= (24.6\text{E-}06 - 9.92\text{E-}06)(550) + (15.7\text{E-}06 - 8.18\text{E-}06)(-90) \end{aligned}$$

NEDO-33866 Revision 6  
Non-Proprietary Information

$$= 0.0074$$

$$= 0.74\%$$

As a result of this tensile strain, the lead will yield. The yield strength for lead at -20°F is 763 psi, which will produce an effective force of:

$$\begin{aligned} P_{axial} &= S_y A \\ &= 763(\pi)(18.079^2 - 14.117^2) \\ &= 305,805 \text{ lb} \end{aligned}$$

The same force can develop a compressive axial stress in the inner steel shell from equilibrium as follows:

$$\begin{aligned} \sigma &= -\frac{P_{axial}}{A} \\ &= -\frac{305,805}{\pi(14.240^2 - 13.240^2)} \\ &= -3544.88 \text{ psi} \end{aligned}$$

***Cooling From 620°F to -40°F***

The axial strain that results between the lead and stainless steel from the cooling to the extreme cold temperature of -40°F is:

$$\begin{aligned} \Sigma_{strain} &= (\alpha_{L620} - \alpha_{SS620}) \Delta T + (\alpha_{L-40} - \alpha_{SS-40}) \Delta T \\ &= (24.6E-06 - 9.92E-06)(550) + (15.6E-06 - 8.09E-06)(-110) \\ &= 0.00725 \\ &= 0.725\% \end{aligned}$$

Once again, as a result of this tensile strain, the lead will yield. The yield strength for lead at -40°F is 795 psi, which will produce an effective force of

$$\begin{aligned} P_{axial} &= S_y A \\ &= 795(\pi)(18.074^2 - 14.112^2) \\ &= 318,437 \text{ lb} \end{aligned}$$

From equilibrium, the same force can develop a compressive axial stress in the inner steel shell as calculated below:

$$\begin{aligned} \sigma &= -\frac{P_{axial}}{A} \\ &= -\frac{318,437}{\pi(14.237^2 - 13.238^2)} \\ &= -3692.45 \text{ psi} \end{aligned}$$

### 2.12.6.3. Summary of Results

The stresses on the inner shell of the Model 2000 cask produce an axial stress of -3692.45 psi and a hoop stress of -2654.12 psi when at the low temperature of -40°F. In the case of the -20°F low temperature, an axial stress of -3544.88 psi and a hoop stress of -2547.29 psi is produced on the inner shell.

In the 620°F case, a hoop stress of -326.94 psi is produced on the inner shell and a hoop stress of 418.71 psi is produced on the outer shell. Table 2.12.6-4 below is a summary of stresses that occur in the inner and outer stainless steel shells due to lead pouring, solidification, and shrinkage.

**Table 2.12.6-4. Summary of Stresses Due to Lead Pouring, Solidification, and Shrinkage**

Temperature (°F)	Inner Shell Stress (psi)			Outer Shell Stress (psi)			Lead Yield Stress (psi)
	$\sigma_1$	$\sigma_2$	$\sigma_3$	$\sigma_1$	$\sigma_2$	$\sigma_3$	$S_y$
620	0	-326.94	-22.94	0	418.71	22.94	Liquid
70	0	-2069.88	-150.34	0	0	0	620
-20	-3544.88	-2547.29	-185.01	0	0	0	763
-40	-3692.45	-2654.12	-192.29	0	0	0	795

The results of the analysis indicate that the Model 2000 cask meets the general requirements of 10 CFR 71.43 and also the requirements of the standard review plan NUREG-1609.

## 2.13 References

- 2-1 U.S. NRC, 10 CFR 71, "Packaging and Transportation of Radioactive Material," Washington D.C.
- 2-2 U.S. NRC, Regulatory Guide 7.8, "Load Combinations for the Structural Analysis of Shipping Casks for Radioactive Material," March 1989.
- 2-3 ASME, "Boiler & Pressure Vessel Code, Section III—Subsection NF, Supports," 2010.
- 2-4 U.S. NRC, Regulatory Guide 7.11, "Fracture Toughness Criteria of Base Material for Ferritic Steel Shipping Cask Containment Vessels with a Maximum Wall Thickness of 4 Inches (0.1 m)," 7.11, June 1991.
- 2-5 U.S. NRC, "Fabrication Criteria for Shipping Containers," NUREG/CR-3854, 1985.
- 2-6 U.S. NRC, "Classification of Transportation Packaging and Dry Spent Fuel Storage System Components According to Importance to Safety," NUREG/CR-6407, February 1996.
- 2-7 ASME, "Boiler & Pressure Vessel Code (BPVC), Section II, Part D, Properties Materials," 2010.
- 2-8 American Society for Metals (ASM), "Metals Handbook Tenth Edition, Volume 2, Properties and Selection: Nonferrous Alloys and Special Purpose Materials, Uranium and Uranium Alloys," Metals Park, OH, 1990.
- 2-9 Battelle Columbus Laboratories, "The Mechanical Properties of Depleted Uranium - 2 w/o Molybdenum Alloy," BMI-2032, 1979.
- 2-10 Henry J. Rack and Gerald A. Knorovsky, "An Assessment of Stress-Strain Data Suitable for Finite-Element Elastic-Plastic Analysis of Shipping Containers," Sandia Laboratories, NUREG/CR-0481, 1978.
- 2-11 W. Hoffman, Lead and Lead Alloys, English Translation of the Second Revised German Edition ed. New York: Springer-Verlag, 1970.
- 2-12 Thomas E. Tietz, "Determination of the Mechanical Properties of a High Purity Lead and a 0.058 % Copper-Lead Alloy," Stanford Research Institute, WADC 57-695, 1958.
- 2-13 Eugene A. Avallone, Theodore Baumeister III, and Ali M. Sadegh, "Marks' Standard Handbook for Mechanical Engineers," Eleventh Edition, 2007.
- 2-14 Parker-Hannifin Corporation, "Gask-O-Seal and Integral Seal Design Handbook," 2010.
- 2-15 G. C. Mok, L. E. Fischer, and S. T. Hsu, "Stress Analysis of Closure Bolts for Shipping Casks," LLNL, NUREG/CR-6007, 1993.
- 2-16 ANSYS®, "Mechanical, Revision 14.0," November 2011.
- 2-17 U.S. NRC, "Regulatory Guide 7.6, Stress Allowables for the Design of Shipping Cask Containment Vessels," February 1977.

- 2-18 ASME, "Boiler and Pressure Vessel Code (BPVC), Section III, Division 1 - Appendices," 2010.
- 2-19 Warren C. Young, "Roark's Formulas for Stress & Strain," Seventh Edition ed. New York: McGraw Hill, 2002.
- 2-20 Livermore Software Technology Corporation, "LS-DYNA, A Program for Nonlinear Dynamic Analysis of Structure in Three Dimensions," Version 971, Ed. Livermore, CA, 03/23/2011.
- 2-21 ASME, "Boiler and Pressure Vessel Code (BPVC), Section VIII, Division 2, Alternative Rules, Annex 3.D – Strength Parameters," New York, 2008.
- 2-22 R. K. Blandford and D. K. Morton, Impact Tensile Testing of Stainless Steels at Various Temperatures, INL/EXT-08-14082. Idaho Falls, Idaho 83415: Idaho National Laboratory, March 2008.
- 2-23 Hexcel Corporation, HexWeb Honeycomb Energy Absorption System - Design Data. Southbury, CT, March 2005.
- 2-24 Oak Ridge National Laboratory, "A Guide to the Design of Shipping Casks for the Transportation of Radioactive Material, ORNL-TM-681," Oak Ridge, TN, April 1965.
- 2-25 Richard G. Budynas and J. Keith Nisbett, Shigley's Mechanical Engineering Design, 9th ed., 2011.
- 2-26 E. Oberg, F. D. Jones, H. L. Horton, and H. H. Ryffel, Machinery's Handbook, 26th ed., Christopher J. McCauley, Ed. New York, United States: Industrial Press INC., 2000.
- 2-27 J. E. Shigley and L. Mitchell, Mechanical Engineering Design, 4th ed. New York, United States: McGraw-Hill, 1965.
- 2-28 ASME, "Rules for Construction of Nuclear Facility Components," in 2010 ASME Boiler and Pressure Vessel Code, Section VIII, Division 1, ASME, Ed. New York, United States: The American Society of Mechanical Engineers, 2010.
- 2-29 R.J. Roark, Formulas for Stress and Strain, 4th ed. New York, United States: McGraw-Hill INC., 1965.
- 2-30 Erik Oberg and Franklin D. Jones, Machinery's Handbook, 29th ed. New York: Industrial press, 2012.
- 2-31 American Society of Mechanical Engineers (ASME), "Rules for Construction of Nuclear Facility Components," Article E-1000, Section III, Division I, Appendices, 2010.
- 2-32 American Society of Mechanical Engineers (ASME), "Article NB-3000," Section III, Division I, 1998.
- 2-33 Stephen P. Timoshenko, Strength of Materials, 2nd ed. New York: Van Nostrand, 1948.
- 2-34 Richard G. Budynas and J. Keith Nisbett, Shigley's Mechanical Engineering Design, 8th ed. Boston: McGraw-Hill, 2008.



### **3 THERMAL EVALUATION**

This section presents the thermal evaluation of the Model 2000 Transport Package and high performance insert (HPI) with a contents thermal loading of 1500 W and a contents thermal loading of 3000 W, both under Normal Conditions of Transport (NCT) and Hypothetical Accident Conditions (HAC) as prescribed by 10 CFR 71 (Reference 3-1). The 3000 W results are presented in Sections 3.3 and 3.4, and the 1500 W results are presented in Section 3.5.1.

The decay heat limit for shipping all contents shall be conservatively limited to 1500 W. However, a decay heat of 3000 W is evaluated as the basis for the Model 2000 Transport Package in Chapter 2.

Specifically, the following requirements of 10 CFR 71 are addressed:

- 1) General standards for all packages, 10 CFR 71.43(g)
- 2) Normal Conditions of Transport—heat, 10 CFR 71.71(c)(1)
- 3) Hypothetical Accident Conditions—thermal, 10 CFR 71.73(c)(4)

To demonstrate that the Model 2000 Transport Package, shown in Figure 3-1, meets these requirements, a three-dimensional finite element model of the package was developed and analyzed using the general-purpose finite element analysis (FEA) code ANSYS, Release 14.0 (Reference 3-2). Multiple ANSYS thermal calculations were performed simulating NCT and HAC using the finite element representation of the Model 2000 Transport Package with HPI.

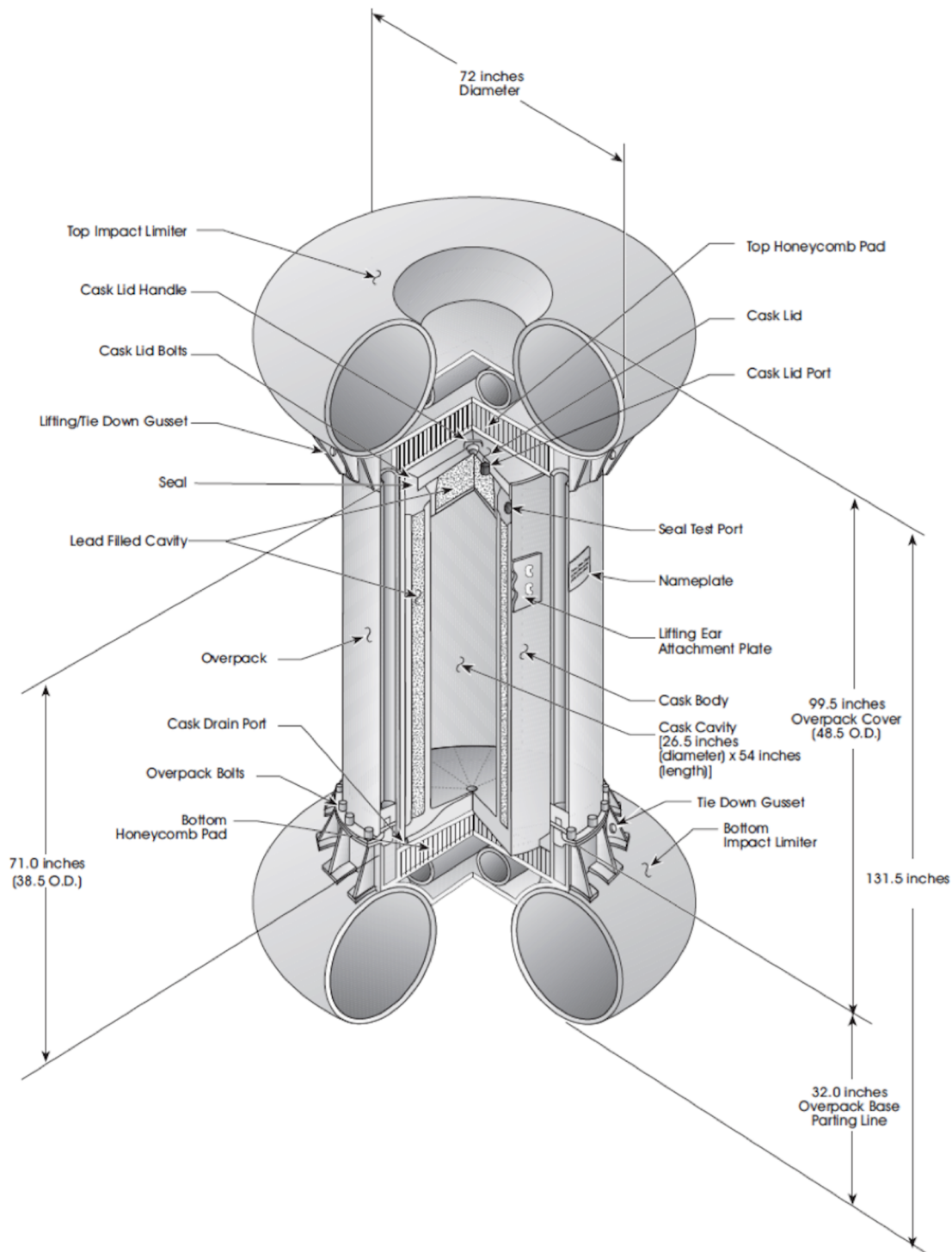


**Figure 3-1. Model 2000 Transport Package  
(High Performance Insert and Material Basket Not Shown)**

### 3.1 Description of Thermal Design

#### 3.1.1. Design Features

The Model 2000 Transport Package, described in Section 1.2, is designed with a thermally passive system. The cask is enclosed in an overpack that serves as a fire shield. The overpack is designed to reduce heat flow from the fire environment into the cask structure by the use of enclosed air spaces. It is composed of two concentric cylindrical SS304 shells approximately 83 inches long with an OD of 48.5 inches and an ID of 40.5 inches. The shells are separated radially by eight equally spaced [ ] along the length of the shells, and horizontally by two [ ] sections to provide closed air spaces. A 24-inch diameter toroidal shell is attached at both ends of the outer shell with a circular plate enclosing the inner regions of the torus. The internal shell is also closed at each end by a circular plate. All materials are SS304. The [ ]

[ ] Attached at both ends of the overpack inner surface are aluminum honeycomb pads.

The cask is designed with lead shielding on three sides and a 6-inch thick stainless steel forging at the base that functions as a heat sink that allows the heat to flow through the bottom of the package. When the cask is placed in the overpack during assembly, air gaps of 1.0-inch radially and 1.0-inch at the top separate the cask from the overpack inner surfaces.

The cask lid seal design, which includes an [ ] and metal retainer component, is based on a 1500 W content decay heat. The cask lid seal is a [ ] retainer with four Parker Compound No. [ ] rings, two concentric [ ] seals on the top and two [ ] seals on the bottom. See Chapter 4 for further discussion. The cask lid is secured to the cask body by fifteen (15) 1¼-inch diameter socket head screws.

The HPI is described in Section 1.2.1.3.

#### 3.1.2. Content's Decay Heat

The derivations of the decay heats for the different contents of the Model 2000 Transport Package are presented in Chapter 5. The decay heat for irradiated hardware and by-product, cobalt-60 isotope rod, and irradiated fuel contents is determined using watt-per-Curie conversion factors listed in Section 5.5.4 and the radionuclide inventory of the contents.

#### 3.1.3. Summary Tables of Temperatures

Thermal design criteria are specified for regions throughout the cask, cask cavity, and the outside overpack wall. The cask lid seal and port O-ring is limited to the temperature listed in Table 3.1.3-1, and this serves as the thermal criteria for the region associated with the seal area. The maximum allowable internal pressure is 30 psia, which corresponds to air of 100% humidity heated to 600°F at constant volume.

Table 3.1.3-1 presents the maximum design temperatures of the components or materials that affect structural integrity, containment, and shielding under both NCT and HAC for 3000 W of decay heat. Where available, temperature limits for the Model 2000 Transport Package

components are obtained from manufacturers' literature. Otherwise, component temperature limits are defined as the melting temperature of the material of construction.

**Table 3.1.3-1. Temperature Limits**

Component or Material	Temperature Limit (°F)
Stainless Steel Components	2546
Lead Shielding <sup>a</sup>	622
Depleted Uranium Shielding <sup>a</sup>	2071
Aluminum Honeycomb <sup>b</sup>	350
Cask Lid Seal	5 to 508 <sup>c</sup>
Cask Ports	-40 to 612 <sup>c</sup>
Accessible Surfaces of Package	< 185 <sup>d</sup>

Notes:

- a. Temperature limit is melting temperature (Reference 3-3).
- b. Maximum operating temperature (Reference 3-4).
- c. See Chapter 4 for additional discussion.
- d. Exclusive use requirement per 10 CFR 71.43(g).

### 3.1.3.1. NCT Temperature Summary

Per the requirements of 10 CFR 71.71(c)(1) (Reference 3-1), the 3000 W case is evaluated for NCT. Specifically, a steady-state thermal analysis is performed simulating exposure of the package to a 100°F ambient temperature in still air and insolation as specified in 10 CFR 71.71. The results of the analysis are presented in Section 3.3. The temperatures of several key package components are summarized and compared with their allowable temperatures in Table 3.1.3-2.

**Table 3.1.3-2. NCT Temperature Summary and Comparison with Allowable Temperatures**

Item	NCT Temperatures (°F)	Allowable Temperature (°F)
Material Basket	1,001 (max)	2,546
HPI Shielding (Depleted Uranium)	601 (max)	2,071
Cask Lid Seal	432 (max)	508 <sup>c</sup>
Cask Shielding (Lead)	449 (max)	622
Honeycomb Impact Limiters	359 (max) <sup>a</sup> / 334 (avg)	350
Cask Drain Port (Bottom)	370	612 <sup>c</sup>
Cask Test Port (Top)	426	
Cask Vent Port (Lid)	442	
Overpack Outer Surface	215	185 <sup>b</sup>

Notes:

- a. The maximum honeycomb impact limiter temperature of 359°F exceeds the allowable temperature of 350°F. However, this maximum temperature occurs in a very limited area of the impact limiter and is based on steady-state boundary conditions for the hot case, which ignores the removal of solar insolation during the night cycle. The majority of the impact limiter temperatures are below 350°F. Therefore, the average temperature of 334°F is appropriate to compare to the allowable temperature.
- b. Limit specified in 10 CFR 71.43(g), which requires the addition of a personnel barrier to satisfy this requirement. Refer to Section 7.1.4, Preparation for Transport.
- c. See Chapter 4 for additional discussion.

The Model 2000 Transport Package components remain below their allowable temperatures for NCT with insolation. Therefore, when exposed to NCT with insolation, and 1500 W decay heat, the Model 2000 Transport Package maintains containment of the contents, as neither the shielding nor the impact limiting materials exceed temperatures that would adversely affect their performance. See Chapter 4 for further details.

#### **3.1.3.2. HAC Temperature Summary**

When exposed to the HAC fire prescribed in the regulations, the Model 2000 Transport Package must maintain containment of its contents and maintain its shielding capabilities. The results of the HAC thermal evaluation are presented in Section 3.4. As shown in Table 3.1.3-3, the maximum temperatures of the different package components are below the allowable temperatures. Therefore, the HAC fire does not adversely affect the package's ability to provide containment and shielding for its contents. Note, that the maximum average fill gas temperatures in the HPI and cask are 740°F and 571°F, respectively. The maximum average combined fill gas temperature (HPI + cask) is 585°F.

**Table 3.1.3-3. HAC Maximum Temperature Summary and Comparison with Allowable Temperatures**

Item	HAC Maximum Temperature (°F)	Allowable Temperature (°F)
Material Basket	1,045	2,546
HPI Shielding (Side)	670	2,071
HPI Shielding (Top)	599	2,071
HPI Shielding (Bottom)	618	2,071
Cask Lid Seal	508	508 <sup>b</sup>
Cask Shielding (Side)	570	622
Cask Shielding (Top)	529	622
Cask Shell (Puncture Location)	782	-
Cask Shell (Opposite side to Puncture Location)	512	-
Overpack Outer Shell (Puncture Location)	1,103	-
Overpack Outer Shell (Opposite Side to Puncture Location)	1,337	-
Cask Drain Port (bottom)	612 <sup>a</sup>	612 <sup>b</sup>
Cask Test Port (top)	608 <sup>a</sup>	612 <sup>b</sup>
Cask Vent Port (lid)	520	612 <sup>b</sup>
HPI Fill Gas (Average)	740	-
Cask Fill Gas (Average)	571	-
Combined HPI and Cask Fill Gas (Average)	585	-

Notes:

- a. Temperatures for Drain Port and Test Port exceed 600°F for 21 minutes and 11 minutes, respectively. Seal acceptance testing conditions for cask lid seal and port containment components are specified in Reference 3-5.
- b. See Chapter 4 for additional discussion.

### 3.1.4. Summary Tables of Maximum Pressures

Table 3.1.4-1 shows the maximum normal operating pressure and the maximum pressure under hypothetical accident conditions.

**Table 3.1.4-1. Maximum Pressures**

Component or Material	Reference	Pressure (psia)
Maximum Design Internal Pressure	Section 2.4.3	30.0
Maximum Normal Operating Pressure	Section 3.3.2	26.8
Maximum Average Pressure under HAC	Section 3.4.3	29.0

## **3.2 Material Properties and Component Specifications**

### **3.2.1. Material Properties**

The thermal properties of the materials of construction used in the analyses for the thermal evaluation are presented in Table 3.2.1-1. When available from the open literature, temperature-dependent properties are used in the analyses. Additionally, the thermal properties of the cask fill gas (helium) and overpack gas (air) are presented in Table 3.2.1-2 (Reference 3-3).



**Table 3.2.1-1. Thermal Properties of Solid Regions in the Model 2000 Finite Element Thermal Model**

Material	Temperature (°F)	Density (lbm/in <sup>3</sup> )	Thermal Conductivity (Btu/h-in-°F)	Specific Heat (Btu/lbm-°F)	Emissivity
AISI 304 Stainless Steel <sup>a</sup>	-100	---	0.607	0.096	---
	80	0.285	0.717	0.114	0.22
	260	---	0.799	0.123	0.22
	620	---	0.953	0.133	0.24
	980	---	1.088	0.139	0.28
	1340	---	1.223	0.146	0.35
	1700	---	1.348	0.153	---
	2240	---	1.526	0.163	---
Lead <sup>a</sup>	-100	---	1.767	0.030	---
	80	0.410	1.700	0.031	---
	260	---	1.637	0.032	---
	620	---	1.512	0.034	---
Depleted Uranium <sup>a</sup>	-100	---	1.209	0.026	---
	80	0.689	1.329	0.028	---
	260	---	1.425	0.030	---
	620	---	1.637	0.035	---
	980	---	1.858	0.042	---
	1340	---	2.114	0.043	---
	1700	---	2.359	0.038	---
AISI 316 Stainless Steel <sup>a</sup>	80	0.298	0.645	0.112	0.22
	260	---	0.732	0.120	0.22
	620	---	0.881	0.131	0.24
	980	---	1.026	0.138	0.28
	1340	---	1.165	0.144	0.35
[[ ]] <sup>b</sup>	---	Same as AISI 304 or AISI 316	Same as AISI 304 or AISI 316	Same as AISI 304 or AISI 316	0.44
Aluminum Honeycomb <sup>c</sup>	-100	---	0.465	---	---
	0	---	0.608	---	---
	75	0.0046	0.715	0.208	0.20
	100	---	0.751	---	---
	200	---	0.894	---	---
	300	---	1.073	---	---

Notes:

- a. Reference 3-3, Table A.1 (density, thermal conductivity, and specific heat) and Table A.11 (emissivity).
- b. Reference 3-6.
- c. Density and thermal conductivity – Reference 3-4. Specific heat of Aluminum 2024-T6– Reference 3-3, Table A.1. Emissivity of heavily oxidized aluminum– Reference 3-7, Appendix D.

**Table 3.2.1-2. Thermal Properties of Gaseous Regions in the Finite Element Thermal Model**

Material	Temperature (°F)	Density (lbm/in <sup>3</sup> )	Thermal Conductivity (Btu/h-in-°F)	Specific Heat (Btu/lbm-°F)	Emissivity
Helium	-64	---	5.93E-3	---	---
	-28	---	6.26E-3	---	---
	8	---	6.60E-3	---	---
	44	---	6.98E-3	---	---
	80	5.871E-6	7.32E-3	1.24	---
	170	---	8.19E-3	---	---
	260	---	9.00E-3	---	---
	350	---	9.82E-3	---	---
	440	---	1.06E-2	---	---
	620	---	1.21E-2	---	---
	710	---	1.27E-2	---	---
	800	---	1.34E-2	---	---
	890	---	1.40E-2	---	---
	980	---	1.46E-2	---	---
	1160	---	1.59E-2	---	---
	1340	---	1.70E-2	---	---
Air	-100	---	8.72E-4	0.241	---
	-10	---	1.07E-3	0.240	---
	80	4.196E-5	1.27E-3	0.241	---
	170	---	1.44E-3	0.241	---
	260	---	1.63E-3	0.242	---
	350	---	1.80E-3	0.244	---
	440	---	1.96E-3	0.246	---
	530	---	2.11E-3	0.248	---
	620	---	2.26E-3	0.251	---
	710	---	2.39E-3	0.254	---
	800	---	2.52E-3	0.257	---
	890	---	2.64E-3	0.260	---
	980	---	2.76E-3	0.263	---
	1070	---	2.87E-3	0.263	---
	1160	---	2.99E-3	0.268	---
	1250	---	3.10E-3	0.270	---
	1340	---	3.21E-3	0.273	---
	1520	---	3.44E-3	0.277	---
	1700	---	3.67E-3	0.281	---

### 3.2.2. Component Specifications

The Model 2000 Transport Package component materials are primarily stainless steel, lead, and aluminum. The maximum allowable temperatures of these materials are given in Table 3.1.3-1. The temperatures resulting from normal and accident thermal conditions fall within these temperatures.

The only component material that is temperature sensitive is the [[ ]] material in the cask lid seal and port plug O-rings. The material used is [[ ]] that offers an operating temperature range adequate for 1500 W decay heat (Reference 3-8). The cask lid seal design includes an aluminum [[ ]]; temperatures resulting from normal and accident thermal conditions fall within the material limits. See Chapter 4 for additional discussion.

### 3.3 Thermal Evaluation under Normal Conditions of Transport

Thermal performance for 3000 W decay heat is analyzed for NCT (with and without insulation) by performing steady-state heat transfer analyses on a finite element representation of the package. Specifically, the general-purpose finite element code ANSYS, Release 14.0 (Reference 3-2), is used to model and analyze the Model 2000 Transport Package with a content heat load of 3000 W for NCT. Several ANSYS macros are created in order to build the model, apply boundary conditions, and perform the steady-state analyses.

Assumptions made for this evaluation are:

- The Model 2000 Transport Package is assumed to be in an upright (vertical) orientation during NCT.
- The cask and HPI are backfilled with Helium at 70°F and 14.7 psia.
- Natural convection within the package cavities is neglected.
- The contents of the HPI are assumed to generate a maximum of 3000 W that is uniformly distributed among the [[ ]].
- During NCT, the package is assumed to have an emissivity consistent with the material of construction at temperature.

As mentioned above, for the NCT analysis, a steady-state thermal analysis was performed simulating exposure of the package to a 100°F ambient temperature in still air and insulation as specified in 10 CFR 71.71. The results of the analysis are presented below. The temperatures of the key package components are summarized and compared with their allowable temperatures in Table 3.1.3-2.

NCT sensitivity studies were also performed to evaluate the thermal performance of the package using boundary conditions applied as both steady state and as constant boundary conditions solved as a transient. Because the solutions are radiation-dominated, the transient solution results in better convergence and slightly higher temperatures. To achieve steady-state conditions with the transient solver, a simulated time of 2000 hours was used. The 2000-hour duration of the transient analyses is sufficiently long enough for the temperatures within the package to reach steady-state

values, that is, the temperature of a node within the package model doesn't change from one time step to the next.

### Model Description

The general-purpose finite element code ANSYS, Release 14.0 (Reference 3-2), is used to model and analyze the Model 2000 Transport Package with a content heat load of 3000 W for NCT. Several ANSYS macros are created in order to build the model, apply boundary conditions, and perform the steady-state analyses.

The model, shown in Figure 3.3-1 through Figure 3.3-3, represents a half-symmetry of the package. A half-symmetry model is used so that damage from the HAC drop/puncture test may be incorporated using the same model.

In the model, the decay heat of the contents, applied as a heat flux to the material basket [[

]], is transferred through the solid and gaseous regions via conduction heat transfer, across gaseous regions separating solids via thermal radiation, and then rejected to the surroundings via natural convection and thermal radiation. Heat transfer via convection within the package is not considered. In addition to the decay heat of the contents, other heat sources—insolation (heat flux) and/or fire (convection/thermal radiation)—are also included as boundary conditions where appropriate.

To simulate this heat flow, a finite element model of the Model 2000 Transport Package with HPI is generated with the APDL using a combination of SOLID70, CONTA173, TARGE170, LINK34, SURF152, and SURF252 elements. Each of the element types used to model the Model 2000 Transport Package and the modes of heat transfer modeled by the various element types are discussed in the following paragraphs.

The SOLID70 elements are 3D, 8-node, single degree-of-freedom (DOF) thermal solid elements and are used to model heat flow through the solid and gaseous regions of the package via conduction heat transfer.

The CONTA173/TARGE170 pairs are 3D, 4-node, surface-to-surface contact elements that are overlaid onto area faces of the SOLID70 elements and are used to model heat flow across interfaces between contacting components or across interfaces between dissimilar meshes. The LINK34 elements are uniaxial elements with the ability to convect heat between 2 nodes; however, because thermal contact conductance has the same units as the convection heat transfer coefficient, the LINK34 elements are used to model heat flow between contacting components that either have a line-of-contact or are physically separated in the model and, therefore, do not lend themselves to the use of the CONTA173/TARG170 pairs.

The SURF152 3D thermal surface effect elements are overlaid onto area faces of the SOLID70 elements and are used to apply heat flux (fuel material basket [[ ]]) internal surfaces) and convection (overpack external surfaces) boundary conditions. For NCT, insolation (heat flux) is applied directly to area faces of the SOLID70 elements; SURF152 elements are not used to apply this heat load.

Finally, radiation exchange between solid surfaces separated by gaseous regions is modeled using the radiosity solver in conjunction with SURF252 elements. SURF252 are 3D, 4-node, radiosity surface elements that are overlaid onto area faces of the SOLID70 elements that have a radiosity boundary condition using the RSUF command, and then expanded into full 360° in order to properly calculate radiation view factors for models that only model a portion of the actual item due to symmetry.

[[

]]

**Figure 3.3-1. Finite Element Model of the Model 2000 Transport Package**

[[

]]

**Figure 3.3-2. Finite Element Model of the Model 2000 Transport Package - Air and Helium Not Shown**

[[

]]

**Figure 3.3-3. Finite Element Model of the Model 2000 Transport Package - Exploded View**



### Thermal Contact Resistance/Conductance

To simulate welded joints (e.g., the cask cavity shell welded to the cask bottom), the nodes of each mating component are merged at the weld joint. This allows heat to flow across these welded interfaces. However, for all other component interfaces, each component in the finite element model is independent and does not share nodes with its neighboring component(s). Therefore, in order to allow heat to flow through the model, each component is connected to its neighboring component using CONTA173/TARGE170 thermal contact/target elements. For components that have only a line of contact (e.g., Hertzian contact), or if the elements of contacting components are not physically modeled as being in contact, LINK34 convection 2-node elements are used to model the contact resistance.

Thermal contact resistance,  $R_{tc}$ , between mating parts results in a temperature drop across the interface between these parts (see Figure 3.3-4). Note that the surface roughness is exaggerated in the figure. The existence of a finite contact resistance is due primarily to the surface roughness of the mating parts. Other factors that affect the contact resistance are the mating materials, interfacial fluid/gas, and pressure. Theoretical methods to calculate this resistance have been developed; however, empirically derived resistances have provided better correlation with actual measured temperature drops across contact interfaces (Reference 3-3).

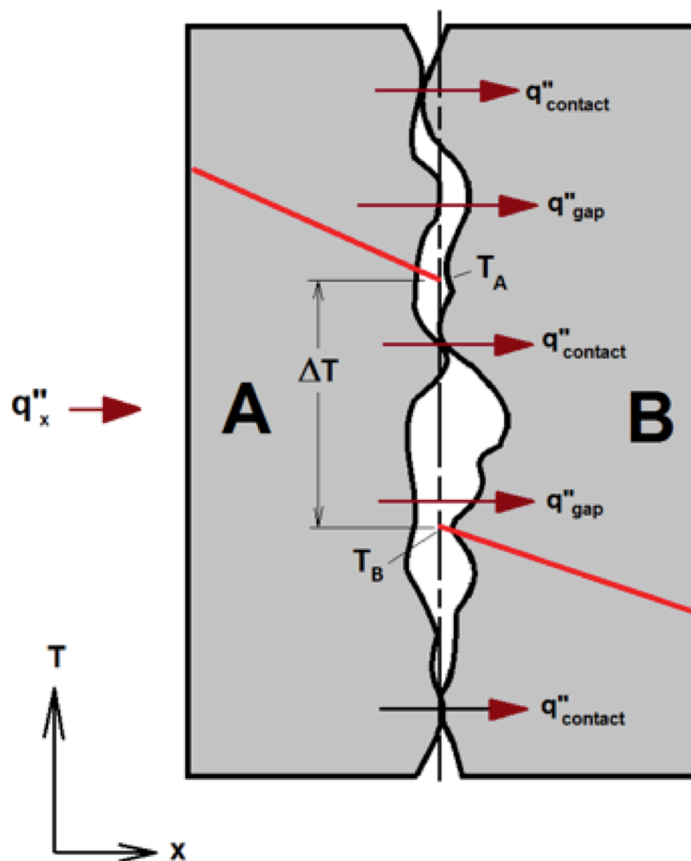


Figure 3.3-4. Heat Transfer Through the Contact Plane Between Two Solid Surfaces

The thermal resistance effect shown in Figure 3.3-4 is described by the following equation from Reference 3-3, Equation 3.20, for a unit area of interface:

$$R''_{tc} = \frac{T_A - T_B}{q''_x}$$

where  $R''_{tc}$  = thermal resistance per unit area,  
 $T_A$  = temperature of material A,  
 $T_B$  = temperature of material B, and  
 $q''_x$  = heat flux.

Thermal contact is modeled in ANSYS by specifying the thermal contact conductance (TCC) of the interface either as a real constant (for the CONTA173/TARGE170 pairs) or as a material property (LINK34). The TCC is defined as the reciprocal of the thermal contact resistance; therefore, a high TCC value implies low thermal contact resistance, and a low TCC value implies high thermal contact resistance.

While the LINK34 is a 2-node convection element, the natural convection coefficient has the same units as that of thermal contact conductance. Therefore, the LINK34 element can be used to simulate thermal contact between two nodes by substituting the TCC value for the convection coefficient.

Experimentally determined TCC values for various mating materials, surface finishes, interfacial gases, and interface pressures are shown in Table 3.3-1.

Because there are a large number of thermal contact interfaces to manage in the Model 2000 Transport Package thermal model, and because exact conditions (such as surface finish and pressure) at the interfaces are unknown, a subjective approach is taken when assigning TCC values to these interfaces in the FEA model. To this end, five contact resistance levels ranging from low to high resistance are established with an assigned TCC value based on the typical values obtained from the open literature as presented in Table 3.3-1. The five TCC values used in the analyses presented in this report are presented in Table 3.3-2. Then, each thermal contact interface in the model is assigned one of these five resistance levels (see Table 3.3-3 and Figure 3.3-5). The approach to assigning the five contact resistance levels is:

- The interfaces (when dissimilar meshes exist) between elements representing fill gases and their adjacent solid meshes are assigned “Low” resistance levels.
- Interfaces between bolted junctures are assigned “Low” or “Low/Moderate” resistance levels.
- Interfaces between shielding materials and the shells that contain them are assigned “Low/Moderate” resistance levels.
- Interfaces between loosely fitted components (e.g., the cask lid cylindrical sides and the cask top flange) are assigned “High” resistance levels.

- Interfaces between heavy objects and the component on which they rest are assigned “Low/Moderate”, “Moderate”, or “Moderate/High” resistance levels depending on how heavy the object is and how much the component on which they rest may flex under the weight.

During normal transport, the Model 2000 Transport Package is in an upright orientation with the material basket bottom contacting the HPI bottom [[ ]], the HPI bottom [[ ]] contacting the cask bottom, and the cask bottom contacting the cask support plate of the overpack. Because the inner surface of the cask bottom is dished to allow for water drainage, the entire surface of the HPI bottom [[ ]] will not be in contact with the cask bottom. Additionally, in order to maintain well-shaped elements, the outer, bottom corner of the HPI is modeled with a small offset from the cask bottom. Therefore, LINK34 elements are used to model a line of contact between the outer edge of the HPI bottom [[ ]] and cask bottom. The LINK34 elements are assigned a thermal conductance value of 15.0 Btu/h-in<sup>2</sup>-°F, and the contact area is modeled as a 2.5-inch wide annular band with an outer diameter equivalent to the outer diameter of the HPI bottom [[ ]].

**Table 3.3-1. Typical Thermal Contact Conductance Values from Open Literature**

Material (Both Surfaces)	Surface Roughness (μ in)	Interfacial Gas	Pressure (psi)	TCC (Btu/h-in <sup>2</sup> -°F)	Source
Stainless Steel	Not Specified	Vacuum	14.5	0.5 – 2.0	Reference 3-3 Table 3.1
Stainless Steel	Not Specified	Vacuum	1450	3.1 – 17.5	Reference 3-3 Table 3.1
Stainless Steel	Normal Finish	Air	14.7 – 1470	2.1 – 4.5	Reference 3-9 Table 2.3
416 Stainless Steel	30	Air	100	13.9	Reference 3-10 Table 1.2
416 Stainless Steel	100	Air	44 – 368	4.6	Reference 3-9 Table 2.3
304 Stainless Steel	45	Air	588 – 1029	2.3	Reference 3-9 Table 2.3
Carbon Steel	1000	Air	100 – 300	0.6 – 0.8	Reference 3-10 Table 1.2
Carbon Steel	63	Air	100 – 300	3.5 – 4.6	Reference 3-10 Table 1.2
Aluminum	Not Specified	Vacuum	14.5	2.4 – 8.2	Reference 3-3 Table 3.1
Aluminum	Not Specified	Vacuum	1450	30.6 – 61.2	Reference 3-3 Table 3.1

**Table 3.3-1. Typical Thermal Contact Conductance Values from Open Literature**

Material (Both Surfaces)	Surface Roughness ( $\mu$ in)	Interfacial Gas	Pressure (psi)	TCC (Btu/h-in <sup>2</sup> -°F)	Source
Aluminum	397	Air	14500	4.4	Reference 3-3 Table 3.1
Aluminum	397	Helium	14500	11.6	Reference 3-3 Table 3.1
Aluminum	Normal Finish	Air	14.7 – 1470	2.7 – 14.7	Reference 3-9 Table 2.3
Aluminum	Rough	Vacuum	Low	0.2	Reference 3-9 Table 2.3
Aluminum	120	Air	100 – 300	6.3 – 11.5	Reference 3-10 Table 1.2
Aluminum	65	Air	100 – 300	9.0 – 14.6	Reference 3-10 Table 1.2
Aluminum	100	Air	176 – 368	13.9	Reference 3-9 Table 2.3
Aluminum	10	Air	176 – 368	69.4	Reference 3-9 Table 2.3

**Table 3.3-2. TCC Values Used in the Thermal Analyses**

Thermal Contact Resistance ID	Thermal Contact Resistance Level	TCC (Btu/h-in <sup>2</sup> -°F)
1 <sup>a</sup>	Low (Perfect Contact)	1000
2	Low/Moderate	15
3	Moderate	5
4	Moderate/High	1
5	High	0.5

Note:

- a. Thermal contact resistance ID #1 is used to connect dissimilar meshes in which perfect contact is desired.

**Table 3.3-3. Thermal Contact Resistance Levels Assigned to the Modeled Contact Elements**

<b>Contact ID (Real Constant)</b>	<b>Surface 1 (CONTA173)</b>	<b>Surface 2 (TARGE170)</b>	<b>Thermal Contact Resistance ID (See Table 3.3-2)</b>
101	Cask Shield (Side)	Cask Bottom	2
102	Cask Shield (Side)	Cask Shell	2
103	Cask Shield (Side)	Cask Cavity Shell	2
104	Cask Shield (Side)	Cask Top	2
105	Cask Bottom	Cask Shell	4
106	Cask Top	Cask Shell	4
107	Cask Top	Cask Cavity Shell	4
108	Cask Shield (Lid)	Cask Lid	2
109	Cask Lid (At Bolted Interface)	Cask Top	2
110	Cask Lid (Cylindrical Sides)	Cask Top	5
112	Cask Fill Gas	Cask Bottom	1
113	Cask Fill Gas	Cask Cavity Shell	1
114	Cask Fill Gas	Cask Lid	1
115	Overpack Toroidal Stiffener (Bottom)	Overpack Toroidal Shell (Bottom)	4
116	Overpack Gusset Base (Bottom)	Overpack Toroidal Shell (Bottom)	2
117	Overpack Gusset (Bottom)	Overpack Stiffening Ring (Bottom)	2
118	Overpack Gusset & Stiffening Ring (Bottom)	Overpack Bolting Ring (Bottom)	2
119	Overpack Stiffening Ring (Bottom)	Overpack Outer Shell	4
120	Overpack Bolting Ring (Bottom)	Overpack Outer Shell	4
121	Overpack Bolting Ring (Bottom)	Overpack Inner Shell	4
122	Overpack [[            ]] (Bottom)	Overpack Bottom End Plate	5
123	Overpack [[            ]] (Bottom)	Overpack Bottom Plate	2
124	Honeycomb Impact Limiter (Bottom)	Overpack Bottom Plate	5
125	Honeycomb Impact Limiter (Bottom)	Overpack Inner Shell	5
126	Honeycomb Impact Limiter (Bottom)	Overpack Cask Support Plate	5
127	Overpack Gas	Overpack Cask Support Plate	1

**Table 3.3-3. Thermal Contact Resistance Levels Assigned to the Modeled Contact Elements**

Contact ID (Real Constant)	Surface 1 (CONTA173)	Surface 2 (TARGE170)	Thermal Contact Resistance ID (See Table 3.3-2)
128	Overpack Gas	Overpack Inner Shell	1
129	Overpack Gas	Overpack Bolting Ring (Bottom)	1
130	Overpack Bolting Ring (Bottom)	Overpack Bolting Ring (Top)	4
131	Cask Bottom Or Cask Top*	Overpack Cask Support Plate Outer Radius (OR)	3
132	Overpack Bolting Ring (Top)	Overpack Outer Shell	4
133	Overpack Bolting Ring (Top)	Overpack Inner Shell	4
134	Overpack [[ ]] (Between Shells)	Overpack	4
135 - 139	---Not Used---		
140	Overpack Stiffening Ring (Top)	Overpack Outer Shell	4
141	Overpack Gusset (Top)	Overpack Stiffening Ring (Top)	2
142	Overpack Gusset Base (Top)	Overpack Toroidal Shell (Top)	2
143	Overpack Toroidal Stiffener (Top)	Overpack Toroidal Shell (Top)	4
144	Honeycomb Impact Limiter (Top)	Overpack Top Plate	5
145	Honeycomb Impact Limiter (Top)	Overpack Inner Shell (Top)	5
146	Overpack [[ ]] (Top)	Overpack Top Plate	2
147	Overpack [[ ]] (Top)	Overpack End Plate (Top)	5
148	Overpack Gas	Overpack Bolt Ring (Top)	1
149	Overpack Gas	Overpack Inner Shell (Top)	1
150	Overpack Gas	Honeycomb Impact Limiter (Top)	1
151	Cask Fill Gas	[[ ]]	1
152	Cask Fill Gas	[[ ]]	1
153	Cask Fill Gas	HPI Horizontal Plate	1
154	---Not Used---		
155	[[ ]]		5
156			2
157			2
158			3
159			3
160			2

**Table 3.3-3. Thermal Contact Resistance Levels Assigned to the Modeled Contact Elements**

Contact ID (Real Constant)	Surface 1 (CONTA173)	Surface 2 (TARGE170)	Thermal Contact Resistance ID (See Table 3.3-2)
161			2
162			2
163			2
164			3
165			2
166			2
167		]]	2
168	HPI Fill Gas	[[	1
169	HPI Fill Gas		1
170	HPI Fill Gas	]]	1
171	---Not Used---		
172*	Material Basket [[ ]]	[[ ]]	3
173*	[[ ]]	Cask Lid or Cask Bottom	2

Note: \* Used only if the material basket, HPI, and/or cask are not centered axially in the cavities (NCT).

[[

]]

**Figure 3.3-5. Thermal Contact Pair Locations in the Finite Element Model**



## Boundary Conditions

The following boundary conditions are applied to the model to simulate NCT (steady-state analysis with the package modeled in an upright orientation):

- 1) Natural convection from the package external surfaces to the 100°F environment
- 2) Thermal radiation (emissivity,  $\epsilon$ , of package surfaces approximately 0.22 (see Table 3.2.1-1))
- 3) Solar heat flux per 10 CFR 71.71 (additional case is run without solar heat flux to address the requirements of 10 CFR 71.43(g))
- 4) Heat flux to material basket [[            ]] to simulate the content heat generation.

## Natural Convection and Thermal Radiation to the Environment

Heat is rejected from the model via natural convection and thermal radiation boundary conditions. In order to simplify the application of boundary conditions, a single convection boundary condition is applied to each external surface of the package that has a convection coefficient (h), combining natural convection ( $h_c$ ) based on the geometry of that surface and thermal radiation ( $h_r$ ) based on the emissivity of that surface. This combined, temperature-dependent convection coefficient ( $h_c + h_r$ ) is defined for each external surface and stored in an ANSYS material property definition.

The natural convection coefficient is calculated using the following from Reference 3-3, Equation 9.24:

$$h_c = \frac{Nu \times k}{L}$$

where, Nu = Nusselt number,

k = thermal conductivity of air at the film temperature, and

L = characteristic length of the surface.

The Nusselt number (Nu) is a function of surface geometry and the Rayleigh number (Ra). The Rayleigh number is, in turn, a function of surface geometry, temperature, and properties of the surrounding air and is calculated using the following equation from Reference 3-3, Equation 9.25:

$$Ra = \frac{g \beta (T_s - T_\infty) L^3}{\nu \alpha}$$

where, g = gravitational constant (386.1 in/s<sup>2</sup>),

$\beta$  =  $1/(T_f + 459.67)$ ,

$T_f$  = film temperature =  $(T_s + T_\infty)/2$ ,

$T_s$  = surface temperature,

$T_\infty$  = ambient temperature,

L = characteristic length,

$\nu$  = air kinematic viscosity at  $T_f$ , and

$\alpha$  = air thermal diffusivity at  $T_f$ .

### Horizontal Cylinder—natural convection to environment

The characteristic length,  $L$ , of a horizontal cylinder is its diameter,  $D$ . The Nusselt number for a horizontal cylinder for a wide range of Rayleigh numbers is calculated using the following equation (Reference 3-3, Equation 9.34):

$$Nu = \left\{ 0.60 + \frac{0.387 Ra^{1/6}}{[1 + (0.559/Pr)^{9/16}]^{8/27}} \right\}^2 \quad (Ra \leq 10^{12})$$

where,  $Ra$  = Rayleigh number, and  
 $Pr$  = Prandtl number.

### Horizontal Plate—natural convection environment

The characteristic length,  $L$ , of a horizontal plate is the ratio of its surface area to its perimeter (for circular plates, this is equal to  $D/4$ , where  $D$  = the plate diameter). The Nusselt number for the upper surface of a heated horizontal plate is calculated using one of the following equations (Reference 3-3, Equations 9.30 and 9.31):

$$Nu = 0.54 Ra^{1/4} \quad (10^4 \leq Ra \leq 10^7)$$

$$Nu = 0.54 Ra^{1/3} \quad (10^4 \leq Ra \leq 10^7)$$

The Nusselt number for the lower surface of a heated horizontal plate is calculated using the following equation (Reference 3-3, Equation 9.32):

$$Nu = 0.27 Ra^{1/4}$$

### Vertical Flat Plate—natural convection to environment

The characteristic length,  $L$ , of a flat plate is its length. The Nusselt number for a vertical plate over the entire range of Rayleigh numbers (laminar and turbulent) is calculated using the following equation (Reference 3-3, Equation 9.26):

$$Nu = \left\{ 0.825 + \frac{0.387 Ra^{1/6}}{[1 + (0.492/Pr)^{9/16}]^{8/27}} \right\}^2$$

For laminar flow (i.e.,  $Ra < 10^9$ ), the Nusselt number for a vertical flat plate is calculated with slightly better accuracy using the following equation (Reference 3-3, Equation 9.27):

$$Nu = 0.68 + \frac{0.670 Ra^{1/4}}{[1 + (0.492/Pr)^{9/16}]^{4/9}}$$

The thermophysical properties of air used in the calculation of the natural convection coefficients are presented in Table 3.3-4.

**Table 3.3-4. Thermophysical Properties of Dry Air  
(from Reference 3-3)**

Temperature (°F)	Density (lbm/in <sup>3</sup> )	Thermal Conductivity (Btu/h-in-°F)	Specific Heat (Btu/lbm-°F)	Viscosity (in <sup>2</sup> /h)	Thermal Diffusivity (in <sup>2</sup> /h)	Prandtl Number
-10	5.039E-5	1.074E-3	2.403E-1	6.384E+1	8.872E+1	0.720
80	4.196E-5	1.266E-3	2.405E-1	8.867E+1	1.255E+2	0.707
170	3.595E-5	1.445E-3	2.410E-1	1.167E+2	1.668E+2	0.700
260	3.147E-5	1.628E-3	2.422E-1	1.474E+2	2.137E+2	0.690
350	2.796E-5	1.796E-3	2.439E-1	1.807E+2	2.634E+2	0.686
440	2.516E-5	1.960E-3	2.460E-1	2.164E+2	3.164E+2	0.684
530	2.286E-5	2.114E-3	2.484E-1	2.543E+2	3.722E+2	0.683
620	2.097E-5	2.258E-3	2.510E-1	2.940E+2	4.291E+2	0.685
710	1.935E-5	2.393E-3	2.539E-1	3.360E+2	4.871E+2	0.690
800	1.797E-5	2.523E-3	2.568E-1	3.800E+2	5.468E+2	0.695
890	1.677E-5	2.644E-3	2.596E-1	4.261E+2	6.082E+2	0.702
980	1.573E-5	2.759E-3	2.625E-1	4.739E+2	6.696E+2	0.709
1070	1.480E-5	2.870E-3	2.651E-1	5.234E+2	7.310E+2	0.716
1160	1.397E-5	2.985E-3	2.678E-1	5.742E+2	7.979E+2	0.720
1250	1.324E-5	3.096E-3	2.702E-1	6.261E+2	8.649E+2	0.723
1340	1.258E-5	3.212E-3	2.725E-1	6.802E+2	9.374E+2	0.726
1520	1.144E-5	3.443E-3	2.768E-1	7.912E+2	1.088E+3	0.728

### **Forced Convection Correlations**

During the HAC 30-minute fire, heat is transferred from the environment to the model via forced convection and thermal radiation boundary conditions. Again, in order to simplify the application of boundary conditions, a single convection boundary condition is applied to each external surface of the package that has a convection coefficient (h) combining forced convection (hc) based on the geometry of that surface and thermal radiation (hr) based on the emissivity of that surface. This combined temperature-dependent convection coefficient (hc + hr) is defined for each external surface and stored in an ANSYS material property definition.

The forced convection coefficient is calculated using the following equation (Reference 3-3, Equation 6.5.7):

$$h_c = \frac{Nu \times k}{L}$$

where, Nu = Nusselt number,  
k = thermal conductivity of air at the film temperature, and  
L = characteristic length of the surface.

The Nusselt number (Nu) is a function the Reynolds number (Re) and the Prandtl number. The Reynolds number is, in turn, a function of surface geometry, temperature, flow velocity, and properties (density and viscosity) of the surrounding air, which is calculated using the following equation (Reference 3-3, Equation 6.45):

$$Re = \frac{VL}{\nu}$$

where, V = air free-stream velocity,  
L = characteristic length,  
 $\nu$  = air dynamic viscosity at  $T_f$ ,  
 $T_f$  = film temperature =  $(T_s + T_\infty)/2$ ,  
 $T_s$  = surface temperature, and  
 $T_\infty$  = ambient temperature.

### ***Cylinder in Cross Flow—forced convection from environment to package***

The characteristic length, L, of a cylinder is its diameter, D. The Nusselt number for a cylinder in cross flow is calculated using the following equation (Reference 3-3, Equation 7.55b):

$$Nu = C Re_D^m Pr^{1/3}$$

where,  $Re_D$  = Reynolds number, and  
Pr = Prandtl number.

The constants 'C' and 'm' in the previous equation are functions of the Reynolds number ( $Re_D$ ) and are listed in Table 3.3-5.

**Table 3.3-5. Constants 'C' and 'm' for the Nusselt Number Calculation of a Cylinder in Cross Flow (from Reference 3-3, Table 7.2)**

Re <sub>D</sub>	C	m
0.4 – 4	0.989	0.330
4 – 40	0.911	0.385
40 – 4,000	0.683	0.466
4,000 – 40,000	0.193	0.618
40,000 – 400,000	0.027	0.805

For mixed parallel flow (laminar and turbulent), the Nusselt number for a flat plate is calculated using the following equation (Reference 3-3, Equation 7.44):

$$Nu = 0.037 Re_L^{4/5} Pr^{1/3} (5 \times 10^5 < Re_L \leq 10^8)$$

where, Re<sub>L</sub> = Reynolds number.

For mixed parallel flow (laminar and turbulent), the Nusselt number for a flat plate is calculated using the following equation (Reference 3-3, Equation 7.44):

$$Nu = 0.037 Re_L^{4/5} Pr^{1/3} (5 \times 10^5 < Re_L \leq 10^8)$$

### **Thermal Radiation to Environment**

As previously discussed, the convection boundary conditions applied to the model are a combination of both natural convection and thermal radiation coefficients. The thermal radiation coefficient (hr) is calculated by linearizing the radiation. Assuming a view factor of 1.0 with the surroundings, the heat transfer rate by thermal radiation, Q<sub>rad</sub>, from a surface can be described as follows:

$$Q_{rad} = \epsilon \sigma A (T_s^4 - T_\infty^4)$$

where, ε = emissivity,

σ = Stefan-Boltzmann constant (1.19 E -11 Btu/h-in<sup>2</sup>-°F),

A = surface area,

T<sub>s</sub> = surface temperature (R), and

T<sub>∞</sub> = temperature of surroundings (R).

Due to the temperatures being raised to the 4<sup>th</sup> power in the previous equation, the heat transfer rate is nonlinear. Instead, treating the thermal radiation as a convection boundary condition and substituting hr (radiation coefficient) for hc (convection coefficient) yields the linear equation:

$$Q_{rad} = hr A (T_s - T_\infty)$$

Setting the two equations for Qrad equal to each other yields the following equation:

$$hr A(T_s - T_\infty) = \epsilon \sigma A (T_s^4 - T_\infty^4)$$

Solving for the thermal radiation coefficient (hr) yields:

$$hr = \epsilon \sigma (T_s^2 + T_\infty^2)(T_s + T_\infty)$$

### **Normal Conditions Convection Coefficients**

During normal transport, the Model 2000 Transport Package is transported in an upright orientation as depicted in Figure 1.2-3. For the purpose of calculating natural convection coefficients, the overpack top and bottom toroidal shells are approximated as horizontal cylinders ( $L = D = 24$  inches), the overpack top cover is approximated as a heated flat plate facing up ( $L = D/4 = 48$  inches/ $4 = 12$  inches), the overpack bottom end plate is approximated as a heat flat plate facing down ( $L = D/4 = 24$  inches/ $4 = 6$  inches), and the cylindrical sides of the overpack are approximated as a vertical plate ( $L = 83.5$  inches). The convection boundary conditions for NCT are shown on a cross-section of the model in Figure 3.3-6. The calculated natural convection coefficients ( $hc$ ) and radiation coefficient ( $hr$ ) for NCT (in shade and with insolation) are presented graphically in Figure 3.3-7.

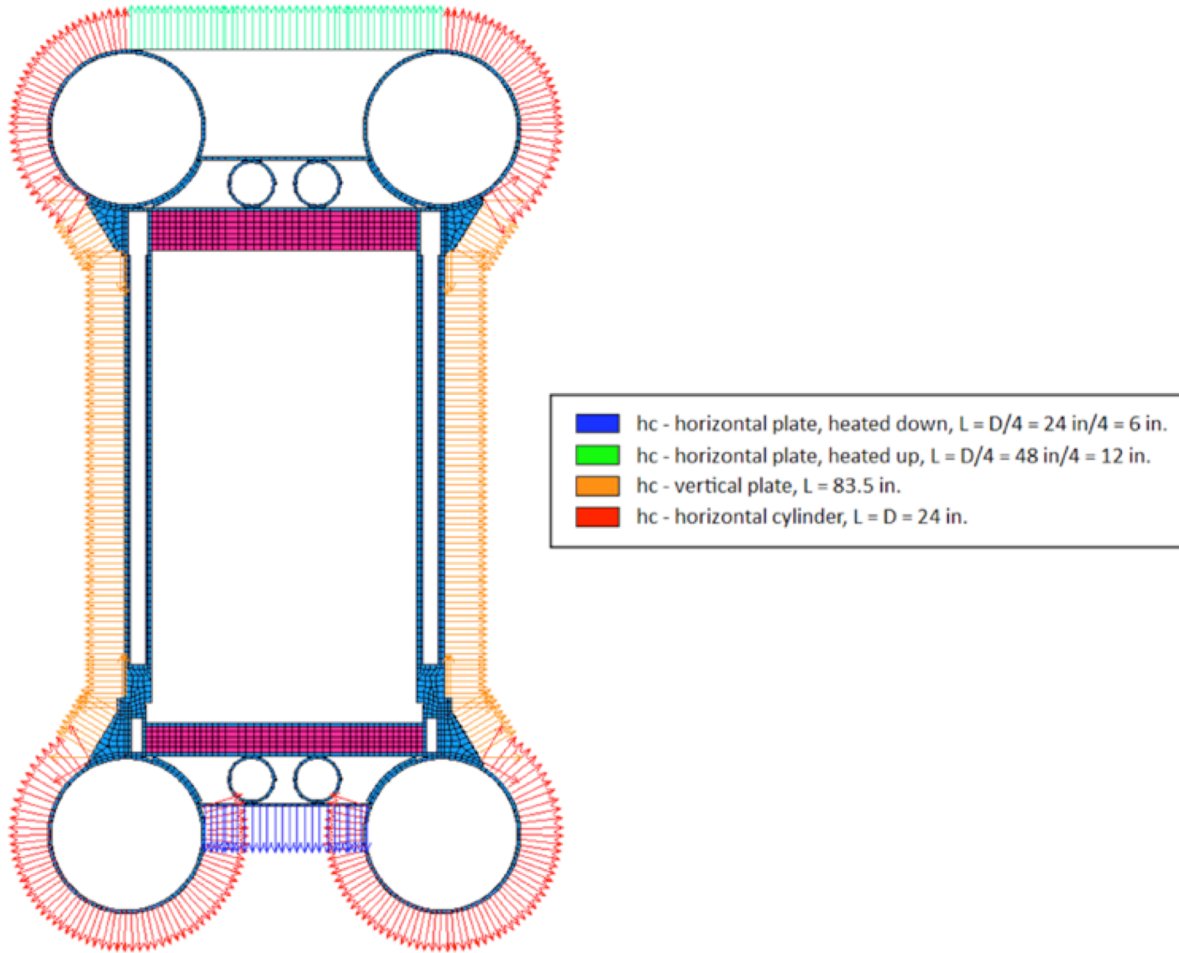


**Figure 3.3-6. Natural Convection Boundary Conditions for NCT**

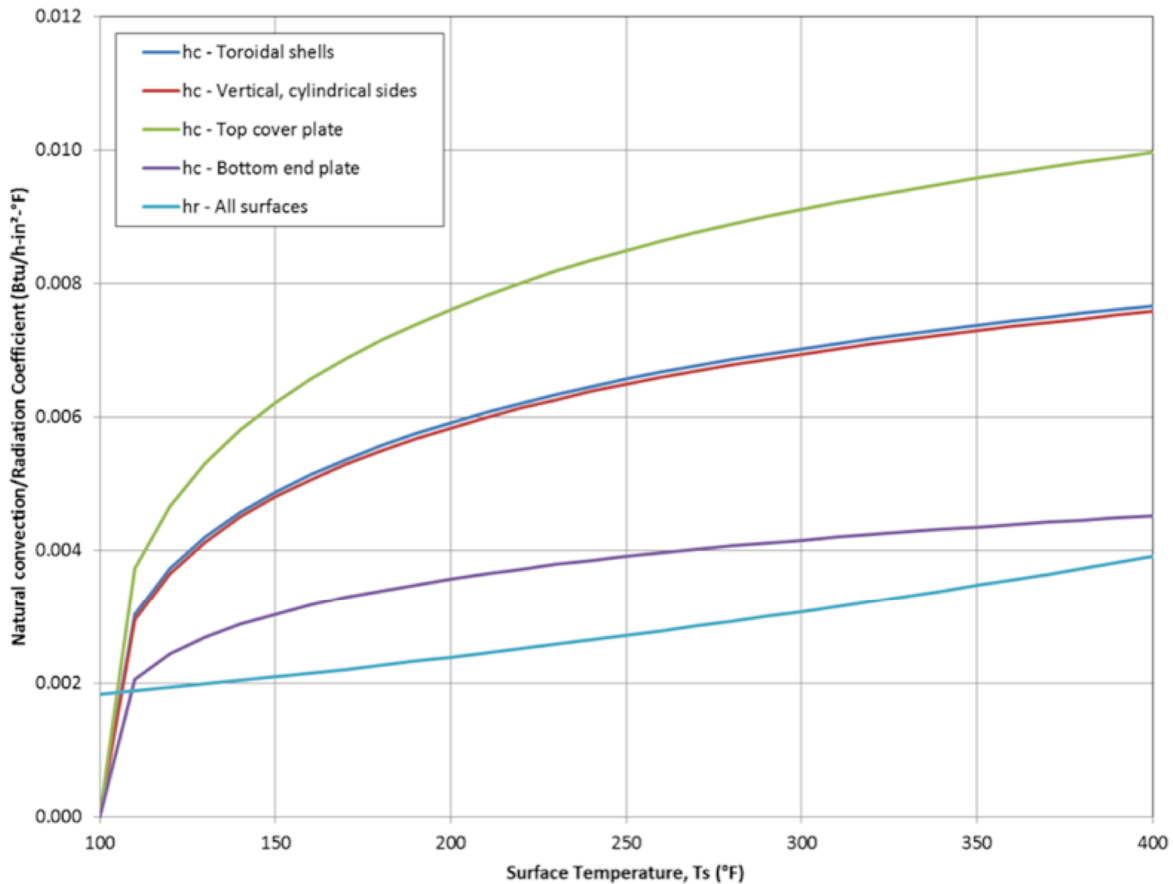


**Figure 3.3-7. Natural Convection and Thermal Radiation Coefficients for NCT**

(Note data for NCT in shade and with insolation)

### Heat Generation by Contents

In order to apply the design basis 3000 W decay heat, the HPI material basket is included in the model. The contents are not specifically modeled in the analyses. Rather, the 3000 W of decay heat is included as a heat flux applied to the material basket [[ ]] contained within the HPI.

As described in Section 1.2.1.4, the material basket has nineteen locations that are formed by twenty [[ ]] The center position does not have a full-length [[ ]], but instead two 2.0-inch long [[ ]], one fastened at either end, form the center area. In the thermal model, the 3000 W of decay heat is assumed to be evenly distributed among the nineteen [[ ]]; therefore, each [[ ]] has approximately 157.9 W applied to its inner surface as a uniformly distributed heat flux over its length [[ ]]. For the center area, the heat load is applied to the inner surface of the two shorter [[ ]] and to the external surfaces of the surrounding [[ ]] where they would contact the center [[ ]] if one existed. This results in a lower heat flux at the center due to the larger area.

SURF152 elements are overlaid onto the SOLID70 thermal solid elements of the material basket [[ ]], and the heat flux is calculated based on the area of these elements. The actual area of the



SURF152 elements (obtained using the \*GET command in ANSYS) is used to calculate the applied heat flux rather than using the area calculated from the dimensions of the [[ ]].

The heat flux,  $q''_{\text{gen}}$ , applied to the [[ ]] is:

$$[[ \text{Equation} ]]$$

where,  $A_{\text{SURF152}}$  = the area of the SURF152 elements overlaid on the inner surface of the [[ ]] (note: multiplied by 2 to account for the half-symmetry of the model).

Similarly, the heat flux applied to the center [[ ]] around the center region is:

$$[[ \text{Equation} ]]$$

where,  $A_{\text{SURF152}}$  = the area of the SURF152 elements overlaid on the inner surface of the center [[ ]] (note: multiplied by 2 to account for the half-symmetry of the model).

The actual heat flux applied to the material basket [[ ]] is shown in Figure 3.3-8.

[[

]]

**Figure 3.3-8. Contents Heat Flux Applied to Material Basket** [[ ]]

### 3.3.1. Heat and Cold

#### 3.3.1.1. Hot Case

##### 3.3.1.1.1. NCT Solar Heat Flux (Insolation)

Per the requirements of the regulations for NCT, the Model 2000 Transport Package is exposed to an ambient temperature of 100°F and insolation according to 10 CFR 71.71. The solar heat fluxes specified in 10 CFR 71.71 are per 12-hour period. This 12-hour period represents a 12-hour long “day” in a 24-hour day/night cycle. Because the solar heat flux is constant, the insolation value should be time averaged over 24 hours in order to maintain the proper total heat flux to the package over the full day/night cycle. Therefore, to simulate a day-night cycle, these heat fluxes are time-averaged over a 24-hour period as follows:

Flat surfaces (other than transported horizontally base)

$$q'' = \frac{800 \text{ cal/cm}^2}{24 \text{ h}} \left( \frac{4.1868 \text{ J}}{\text{cal}} \right) \left( \frac{100 \text{ cm}}{\text{m}} \right)^2 \left( \frac{1 \text{ h}}{3600 \text{ s}} \right) \left( \frac{1 \text{ W}}{1 \text{ J/s}} \right) \left( \frac{0.3171 \frac{\text{Btu}}{\text{h} \cdot \text{ft}^2}}{1 \text{ W/m}^2} \right) \left( \frac{1 \text{ ft}^2}{144 \text{ in}^2} \right)$$

$$= 0.854 \frac{Btu}{h \cdot in^2}$$

Curved surfaces

$$\begin{aligned} q'' &= \frac{400 \text{ cal/cm}^2}{24 \text{ h}} \left( \frac{4.1868 \text{ J}}{\text{cal}} \right) \left( \frac{100 \text{ cm}}{\text{m}} \right)^2 \left( \frac{1 \text{ h}}{3600 \text{ s}} \right) \left( \frac{1 \text{ W}}{1 \text{ J/s}} \right) \left( \frac{0.3171 \frac{Btu}{h \cdot ft^2}}{1 \text{ W/m}^2} \right) \left( \frac{1 \text{ ft}^2}{144 \text{ in}^2} \right) \\ &= 0.427 \frac{Btu}{h \cdot in^2} \end{aligned}$$

Flat surfaces not transported horizontally

$$\begin{aligned} q'' &= \frac{200 \text{ cal/cm}^2}{24 \text{ h}} \left( \frac{4.1868 \text{ J}}{\text{cal}} \right) \left( \frac{100 \text{ cm}}{\text{m}} \right)^2 \left( \frac{1 \text{ h}}{3600 \text{ s}} \right) \left( \frac{1 \text{ W}}{1 \text{ J/s}} \right) \left( \frac{0.3171 \frac{Btu}{h \cdot ft^2}}{1 \text{ W/m}^2} \right) \left( \frac{1 \text{ ft}^2}{144 \text{ in}^2} \right) \\ &= 0.214 \frac{Btu}{h \cdot in^2} \end{aligned}$$

During normal transport, the Model 2000 Transport Package is oriented in an upright position. As such, for the case with insolation, a heat flux of 0.854 Btu/h-in<sup>2</sup> is applied to the top cover plate, and a heat flux of 0.427 Btu/h-in<sup>2</sup> is applied to the toroidal shells and overpack sides as shown in Figure 3.3.1-1.

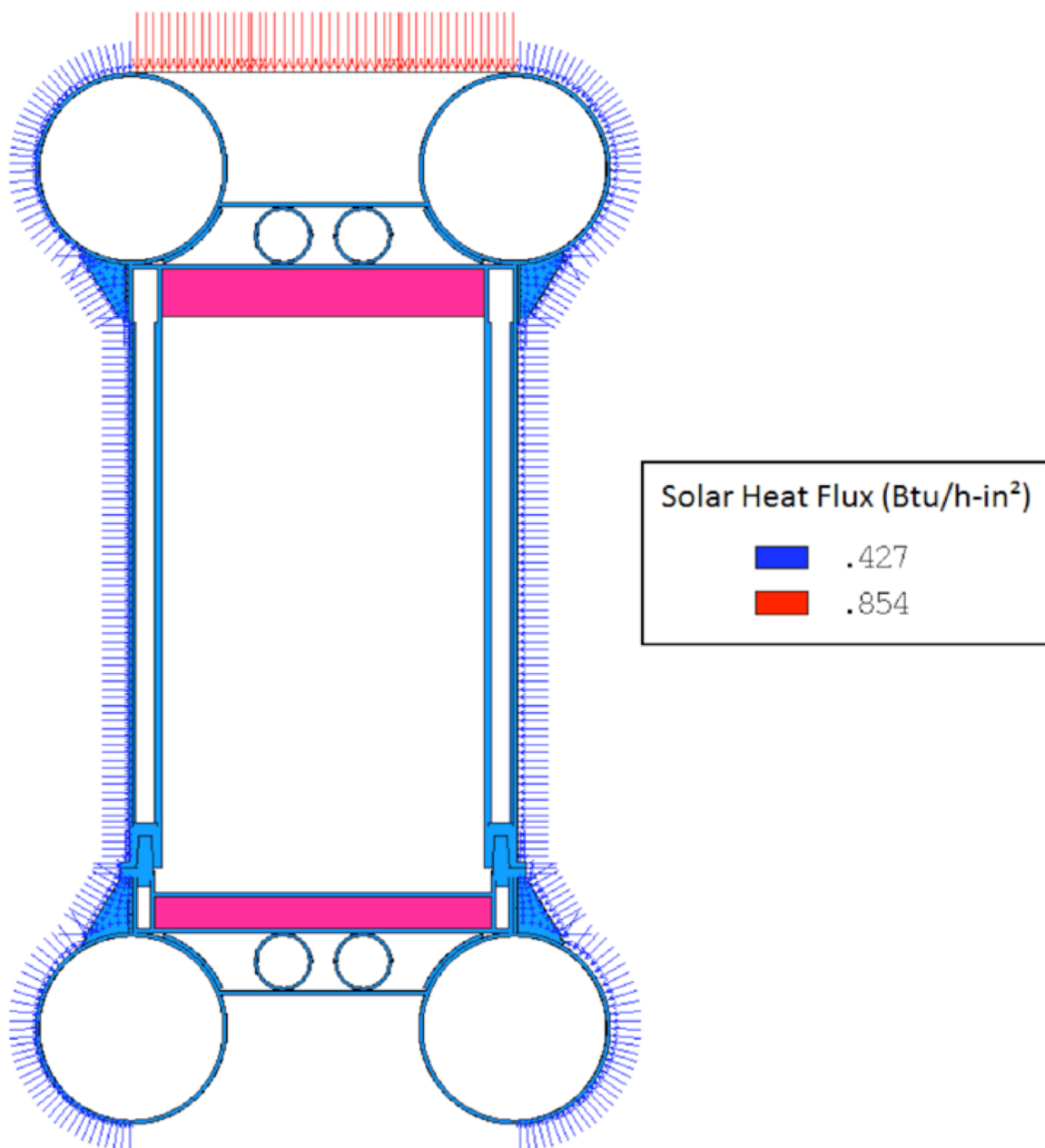


**Figure 3.3.1-1. Solar Heat Flux Boundary Conditions for NCT**

### 3.3.1.1.2. Detailed NCT Results

The results of the steady-state thermal analyses are presented in tabular format in Table 3.3.1-1 and graphically (temperature contours) in Figure 3.3.1-2. The 3000 W thermal analysis demonstrates that the Model 2000 Transport Package components remain below their allowable temperatures for NCT with insolation. There is no change in material conditions that would affect structural, shielding, or impact-limiting performance. Further, the package will maintain containment of the contents.

**Table 3.3.1-1. Temperature Results, NCT (in Shade and with Insolation)**

Component	100°F Ambient Temperature, in Shade, (°F)			100°F Ambient Temperature, with Insolation (°F)		
	Max	Min	Avg	Max	Min	Avg
Material Basket	989	465	801	1,001	490	815
HPI	581	360	---	604	388	---
HPI shielding (top)	517	506	513	539	529	535
HPI shielding (sides)	581	435	544	601	460	565
HPI shielding (bottom)	477	427	451	501	452	475
Cask (bottom, shells, top, lid)	430	309	---	455	338	---
Cask shielding (lid)	424	408	414	449	433	440
Cask shielding (sides)	405	341	385	431	370	412
Cask lid seal	406	383	---	432	409	---
Cask drain port (bottom)	342	309	---	370	338	---
Cask test port (top)	400	383	---	426	409	---
Cask vent port (lid)	416	410	---	442	435	---
Overpack base	335	159	---	364	184	---
Overpack cover	272	108	---	308	174	---
Overpack toroidal shell (top)	159	110	125	207	165	179
Overpack toroidal shell (bottom)	215	114	139	249	136	176
Overpack honeycomb impact limiter (top)	220	205	215	263	249	258
Overpack honeycomb impact limiter (bottom)	330	275	304	359	305	334
HPI fill gas	971	460	672	983	485	689
Cask fill gas	574	346	462	594	374	486
HPI and Cask fill gas, combined	971	346	481	983	374	505

[[

]]

**Figure 3.3.1-2. Steady-State Temperature Distribution—NCT**

#### **3.3.1.1.3. Maximum Surface Temperature Results**

The Model 2000 Transport Package is also evaluated to the requirements of 10 CFR 71.43(g) (Reference 3-1), which requires that no accessible surface of the package exceed 185°F in an exclusive use shipment when exposed to a 100°F ambient temperature in still air and shade. As shown in Figure 3.3.1-3, the overpack in the region of the bolting ring exceeds the allowable temperature of 185°F. Therefore, a personnel barrier not part of the packaging will be used to block access to this region when readied for transport.

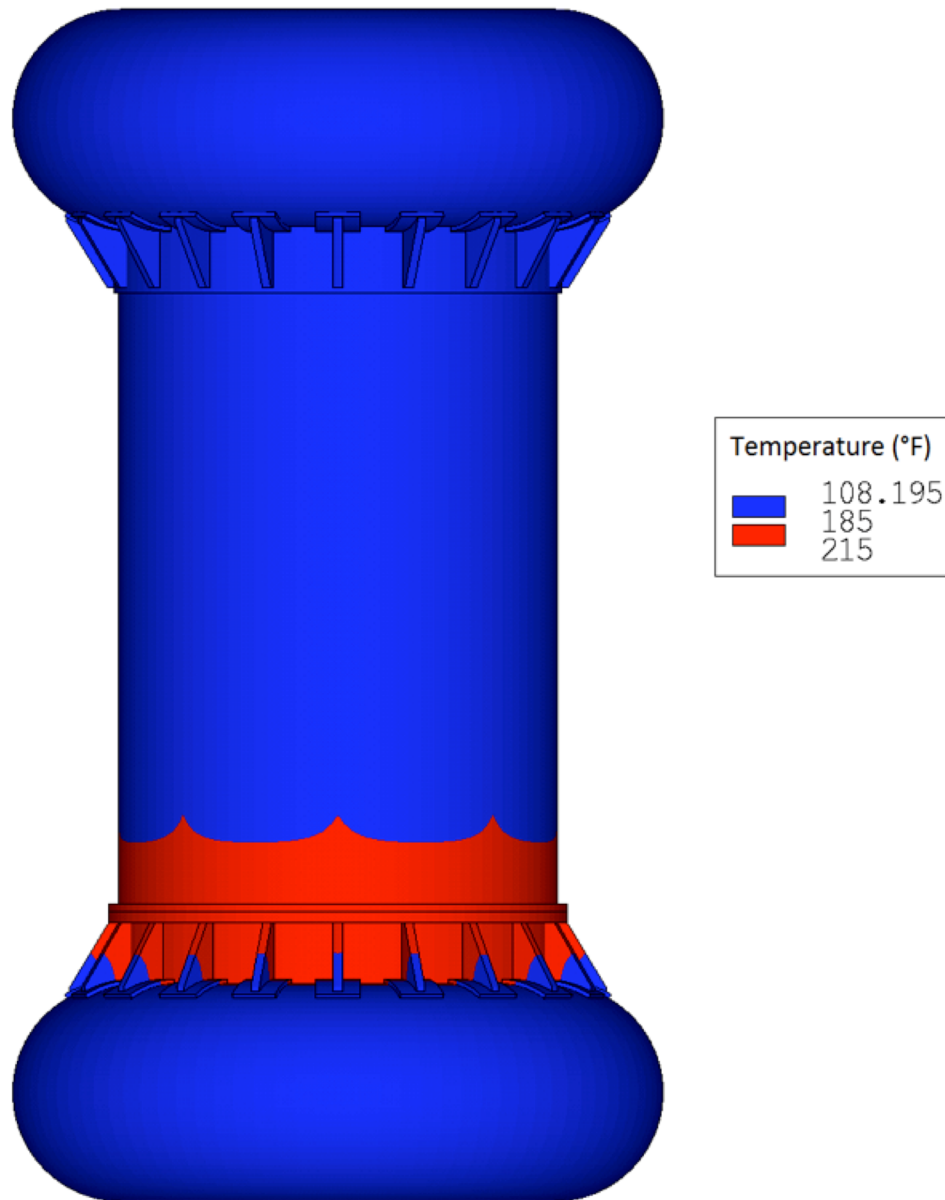


**Figure 3.3.1-3. Overpack Steady-State Temperatures, 100°F Ambient Temperature**

(Note: Assumes ambient temperature in shade)

#### **3.3.1.1.4. NCT Thermal Contact Resistance Sensitivity Study**

The presented thermal analyses have thermal contact resistance modeled between contacting components that have a mixture of low (perfect contact) to high resistance levels as discussed above. In order to assess the effect that using the mixed thermal resistance levels have on package temperatures, the analyses for NCT (with insulation) is repeated with all of the thermal resistance levels set to “low” (i.e., perfect contact). The results of this analysis is compared with the results from Table 3.3.1-1, and presented in Table 3.3.1-2.

**Table 3.3.1-2. Comparison of Mixed and Perfect Thermal Contact for NCT with Insolation**

Item	100°F Ambient temperature, with insolation, mixed thermal contact resistance <sup>1</sup> (°F)			100°F Ambient temperature, with insolation, perfect contact (°F)		
	Max	Min	Avg	Max	Min	Avg
Material Basket	1,001	490	815	998	482	811
HPI	604	388	---	598	379	---
HPI shielding (top)	539	529	535	534	523	530
HPI shielding (sides)	601	460	565	596	452	559
HPI shielding (bottom)	501	452	475	494	444	468
Cask (bottom, shells, top, lid)	455	338	---	450	327	---
Cask shielding (lid)	449	433	440	443	428	434
Cask shielding (sides)	431	370	412	426	361	407
Cask lid seal	432	409	---	428	405	---
Cask drain port (bottom)	370	338	---	362	327	---
Cask test port (top)	426	409	---	422	405	---
Cask vent port (lid)	442	435	---	436	430	---
Overpack base	364	184	---	356	184	---
Overpack cover	308	174	---	305	174	---
Overpack toroidal shell (top)	207	165	179	206	165	179
Overpack toroidal shell (bottom)	249	136	176	250	136	177
Overpack honeycomb impact limiter (top)	263	249	258	259	243	254
Overpack honeycomb impact limiter (bottom)	359	305	334	355	298	329
HPI fill gas	983	485	689	979	477	684
Cask fill gas	594	374	486	589	366	480
HPI and Cask fill gas, combined	983	374	505	979	366	499

Note:

1. In general, the package temperatures are lower when modeling the thermal contact as perfect as opposed to the mixed thermal contact levels. This is because the mixed thermal contact resistances impede the flow of the heat generated by the contents from getting out of the package where it is rejected to the surroundings.

### 3.3.1.2. Cold Case

For the cold case, the thermal model is modified to calculate package temperatures for exposure to an ambient temperature of -40°F in the shade. Various content heat loads are considered, and the results are presented in Table 3.3.1-3. The cask lid seal and cask ports maintain temperatures above their minimum allowable temperatures presented in Table 3.1.3-1. It can be noted in this table that the minimum temperature at the cask lid seal and port O-rings is 21°F with an internal wattage of only 500 W.



**Table 3.3.1-3. Model 2000 Transport Package Temperatures for Exposure to -40°F in Shade**

Item	Temperature (°F)											
	Q <sub>contents</sub> = 500 W			Q <sub>contents</sub> = 1,000 W			Q <sub>contents</sub> = 2,000 W			Q <sub>contents</sub> = 3,000 W		
	Max	Min	Avg	Max	Min	Avg	Max	Min	Avg	Max	Min	Avg
Material Basket	259	66	195	460	150	357	745	283	588	954	387	756
HPI	104	36	---	216	96	---	391	193	---	523	269	---
HPI shielding (top)	84	81	83	182	176	179	334	325	331	451	439	446
HPI shielding (sides)	103	59	91	214	136	194	388	259	355	520	355	478
HPI shielding (bottom)	69	57	63	155	132	143	291	252	271	400	346	372
Cask (bottom, shells, top, lid)	55	21	---	132	69	---	256	147	---	354	209	---
Cask shielding (lid)	54	51	52	129	123	126	251	239	244	347	330	337
Cask shielding (sides)	49	31	42	120	87	108	235	177	215	325	249	300
Cask lid seal	50	45	---	122	113	---	237	221	---	328	304	---
Cask drain port (bottom)	31	21	---	88	69	---	178	147	---	250	209	---
Cask test port (top)	48	45	---	119	113	---	232	221	---	321	304	---
Cask vent port (lid)	52	51	---	127	124	---	246	241	---	339	332	---
Overpack base	30	-22	---	84	-9	---	171	11	---	240	27	---
Overpack cover	-2	-38	---	32	-37	---	96	-36	---	155	-34	---
Overpack toroid (top)	-28	-37	-34	-17	-36	-30	4	-34	-22	24	-32	-14
Overpack toroid (bottom)	-6	-36	-28	19	-34	-21	60	-31	-8	94	-29	2
Overpack honeycomb (top)	-16	-19	-17	7	0	4	50	38	46	93	75	87
Overpack honeycomb (bottom)	29	10	20	82	49	67	167	113	143	235	165	204
HPI fill gas	255	65	147	453	148	281	732	279	476	935	382	619
Cask fill gas	101	32	66	212	89	150	383	180	283	513	253	387
HPI + Cask fill gas, combined	255	32	74	453	89	162	732	180	301	935	253	408

### 3.3.2. Maximum Normal Operating Pressure

#### 3.3.2.1. NCT Pressure Evaluation

During NCT, the average temperature of the cask fill gas (including the gas within the HPI) is 505°F. Using the ideal gas law, the cask internal pressure from gas expansion is:

$$\frac{P_1}{T_1} = \frac{P_2}{T_2}$$

$$P_2 = 14.7 \text{ psia} \times \left( \frac{505+460}{70+460} \right) = 26.8 \text{ psia} < 30 \text{ psia}$$

where,

$$\begin{aligned} P_1 &= 14.7 \text{ psia} && \text{initial fill gas pressure,} \\ T_1 &= 70^\circ\text{F} && \text{initial fill gas temperature, and} \\ T_2 &= 505^\circ\text{F} && \text{average gas volume temperature during NCT.} \end{aligned}$$

The cask internal pressure during NCT is less than the design pressure of 30 psia. Therefore, no further evaluation is required.

### 3.4 Thermal Evaluation under Hypothetical Accident Conditions

The thermal performance of the Model 2000 Transport Package is analyzed for HAC by performing a transient heat transfer analysis on a finite element representation of the package. The model represents the Model 2000 Transport Package with damage consistent with a 30-foot side drop and 40-inch drop onto a 6-inch pin. Again, the general-purpose finite element code ANSYS, Release 14.0, is used to analyze the Model 2000 Transport Package with a content heat load of 3000 W for HAC. Several ANSYS macros are created in order to build the model, modify nodal locations to simulate damage, apply boundary conditions, and perform the transient analysis. Many of the macros used to evaluate the package for NCT are used to evaluate it for HAC.

Assumptions made for this evaluation are:

- The package is assumed to be in a horizontal orientation during the HAC fire because the package is modeled with damage consistent with a side drop.
- The cask and HPI are backfilled with Helium at 70°F and 14.7 psia.
- Natural convection within the package cavities is neglected.
- The contents of the HPI are assumed to generate a maximum of 3000 W that is uniformly distributed among the [[ ]] and is consistent with the isotope rod design where the Co-60 source is uniformly distributed along the length of each [[ ]]
- For HAC, the package is assumed to be exposed to the NCT prior to and following the 30-minute fire.
- During pre-fire/post-fire HAC, the package is assumed to have an emissivity consistent with the material of construction at temperature. However, during the HAC fire, the

package is assumed to have an emissivity value of 0.9. Post-fire, the package is assumed to have an emissivity value of 0.8.

### ***Boundary Conditions***

The following boundary conditions are applied to the model to simulate HAC (with the package modeled in a horizontal orientation):

#### Pre-fire (steady-state analysis)

- Heat flux to material basket [[                    ]] to simulate the content heat generation
- Natural convection from the package external surfaces to the 100°F environment
- Thermal radiation (emissivity,  $\epsilon$ , of package surfaces approximately 0.22 (see Table 3.2.1-1))
- Solar heat flux per 10 CFR 71.71

#### Thirty minute fire (transient analysis)

- Heat flux to material basket [[                    ]] to simulate the content heat generation
- Forced convection from the 1475°F environment to the package external surfaces
- Thermal radiation exchange between the fire and the package surfaces ( $\epsilon = 0.9$ )

#### Post-fire cool-down (transient analysis)

- Heat flux to material basket [[                    ]] to simulate the content heat generation
- Natural convection from the package external surfaces to the 100°F environment
- Thermal radiation ( $\epsilon = 0.8$ , which is consistent with a heavily oxidized steel surface)
- Solar heat flux per 10 CFR 71.71

### **3.4.1. Initial Conditions**

When evaluating the package for the HAC 30-minute fire, the package must include damage from a 30-foot drop onto an unyielding surface and a 40-inch drop onto a 6-inch diameter pin (Reference 3-1). The structural evaluation of the Model 2000 Transport Package considers several drop orientations for HAC; however the side-drop orientation is chosen as the worst-case from a thermal standpoint. The reason for this is due primarily to the damage to the overpack side from the 40-inch drop onto the 6-inch diameter pin. The drop onto the pin causes the overpack outer and inner shells to come in contact—thus, creating a path for the heat from the fire to more easily reach the cask (and cask shielding). Although the damage from the drop onto the pin is not modeled in the deformed geometry (Figure 3.4.1-1), its effect is included by using LINK34 elements to model the contact of the two shells.

[[

]]

**Figure 3.4.1-1. Three-Dimensional Finite Element Model of the Model 2000  
(Half Symmetry)**

(Note: damage consistent with that sustained from a 30-foot drop and 40-inch drop onto a 6-inch pin—elements representing air and helium not shown for clarity.)

#### **3.4.1.1. Additional Thermal Contact for the Hypothetical Accident Condition**

Because the Model 2000 Transport Package is assumed to be in a horizontal orientation during the HAC fire and cool-down, additional thermal contact modeling is required. The components are not physically shifted to be in contact (e.g., the sides of the cask shell contacting the overpack inner shell). Therefore, the CONTA173/TARGE170 pairs will not be appropriate to use to model the thermal contact that will be present when the package is oriented horizontally. To model the contact present when the package is on its side, LINK34 convection elements are incorporated into the model. Although these are convection elements, they can be used to model thermal contact because the thermal contact conductance has the same units as the convection coefficient used by these elements.

When oriented on its side, the contact between the material basket [[  
]], between the HPI [[  
]] and cask cavity shell, and between the cask shell and overpack [[  
]] are modeled with a “Low/Moderate” thermal contact resistance (thermal contact conductance of 15.0 Btu/h-in<sup>2</sup>-°F) and 2° of contact as shown in Figure 3.4.1-2. Additionally, the puncture damage is simulated by adding LINK34 elements (20° contact area) between the overpack inner and outer shells as shown in Figure 3.4.1-2. The “Low/Moderate” thermal contact resistance is chosen for these contact elements in order to maximize the heat from the contents and the HAC fire into the cask shield at the puncture location.

#### **3.4.1.2. Hypothetical Accident Conditions Convection Coefficients**

For HAC, the Model 2000 is modeled with damage simulating a side drop from 30 feet onto an unyielding surface followed by a drop from 40 inches onto a 6-inch diameter pin. The HAC thermal analysis simulates exposure of the model to a 30-minute fire following this side drop/puncture; therefore, the package is assumed to be on its side when exposed to the fire. For the purpose of calculating natural convection (pre-fire and post-fire) and forced convection (fire)

coefficients, the overpack sides are approximated as a horizontal cylinder ( $L = D = 48.5$  inches), the overpack toroidal shells are approximated as horizontal cylinders ( $L = D = 24$  inches), and the overpack top and bottom end plates are approximated as vertical flat plates ( $L = D = 24$  inches). The convection boundary conditions for HAC are shown on a cross-section of the model in Figure 3.4.1-3. The calculated natural and forced convection coefficients ( $h_c$ ) and radiation coefficients for HAC (pre-fire, fire, and post-fire cool-down) are presented graphically in Figure 3.4.1-4.

[[

]]

**Figure 3.4.1-2. LINK34 Incorporated to Simulate HAC Side Contact and Puncture Damage**

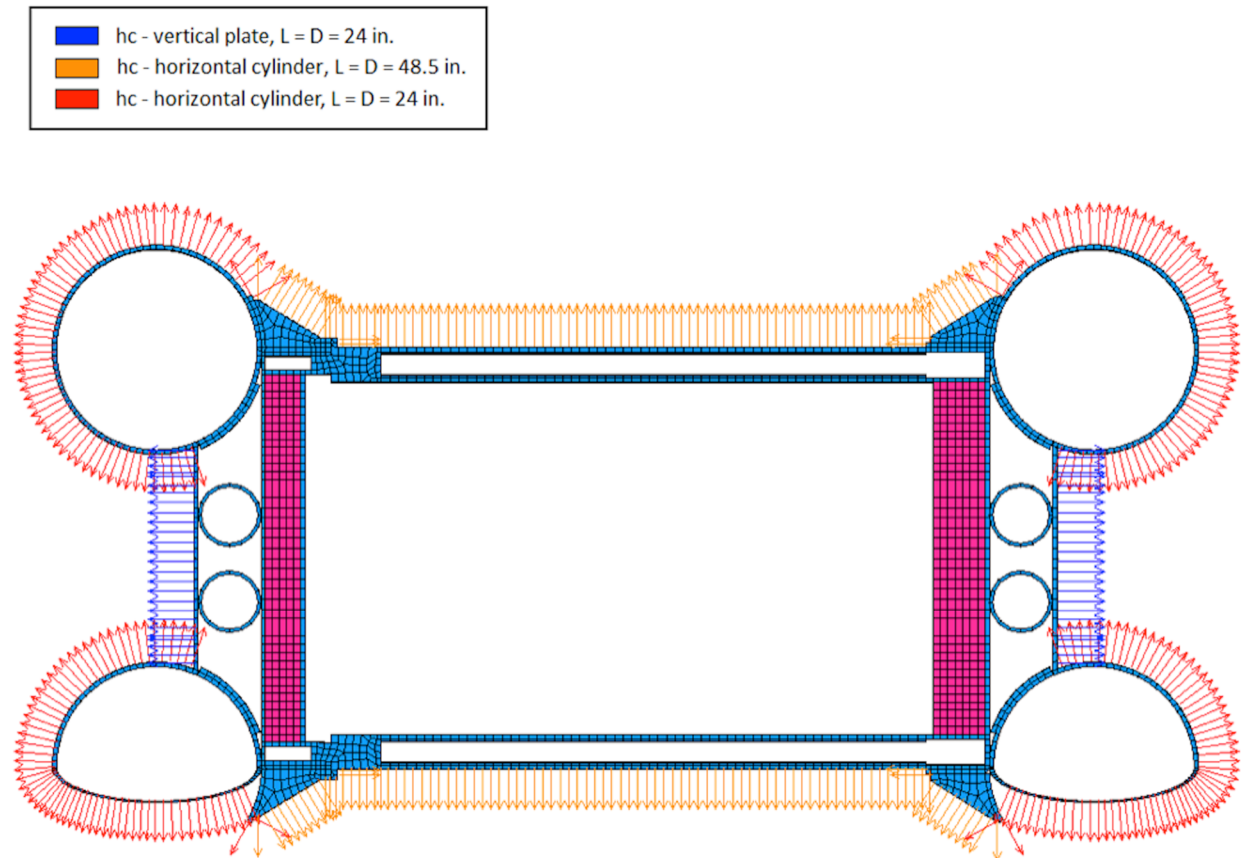


**Figure 3.4.1-3. Natural Convection Boundary Conditions for HAC**

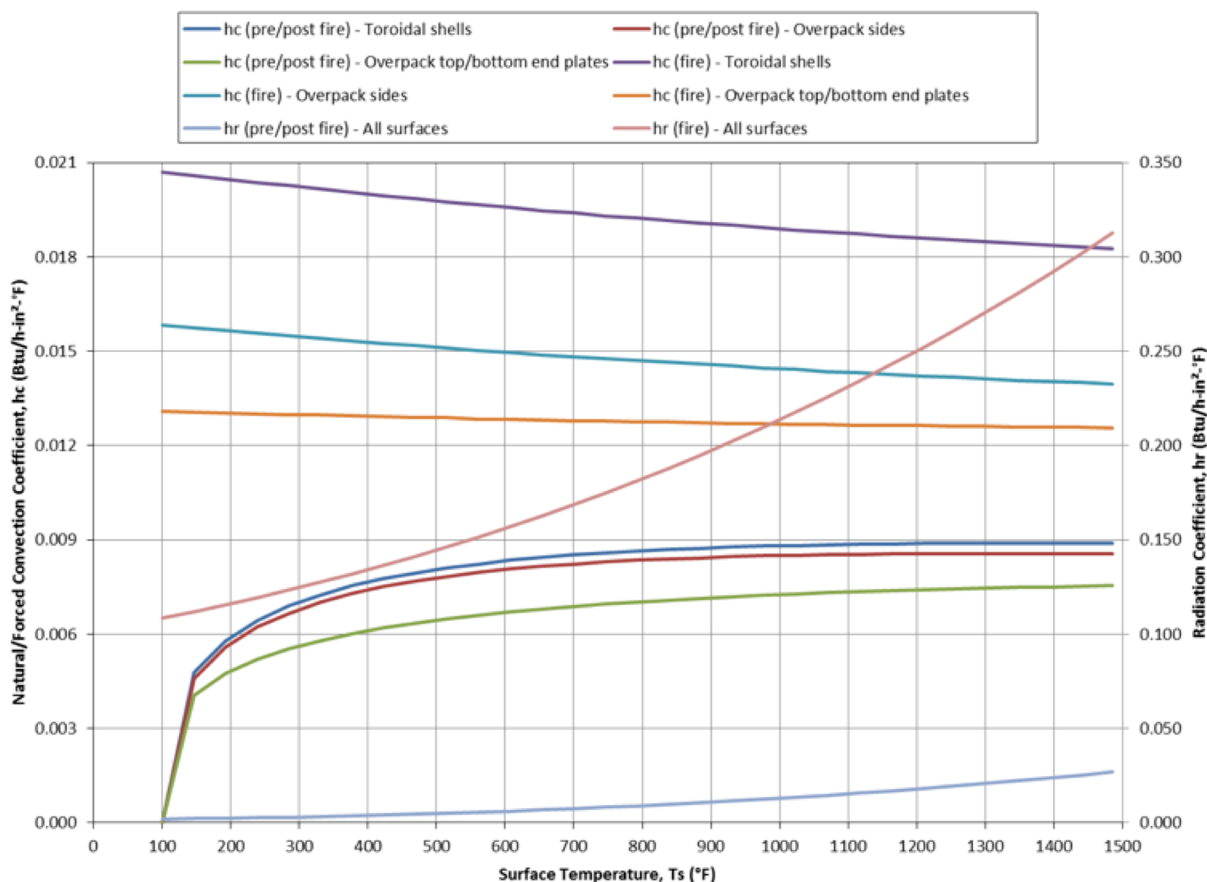


**Figure 3.4.1-4. Natural/Forced Convection and Thermal Radiation Coefficients for HAC**

(Note: Coefficients are for HAC Pre-Fire, Fire, and Post-Fire)

### 3.4.2. Fire Test Conditions

#### 3.4.2.1. HAC Solar Heat Flux (Insolation)

Previous versions of 10 CFR 71.73 (i.e., prior to ~1997), stated that insolation need not be considered before, during, or after the 30-minute hypothetical accident fire. However, the current regulations do not specifically address whether insolation should be included prior to, during, or after the HAC fire. The HAC thermal analysis presented in this report does not include insolation during the HAC fire; however, insolation is applied to the package surfaces during steady-state conditions prior to the fire and during the transient post-fire cool-down. Because the side drop and side puncture damage is simulated for the HAC thermal evaluation, the Model 2000 Transport Package is assumed to be in a horizontal orientation. Therefore, prior to the fire and during the post-fire cool-down, a heat flux of 0.427 Btu/h-in<sup>2</sup> is applied to the toroidal shells and overpack sides, and a heat flux of 0.214 Btu/h-in<sup>2</sup> is applied to the overpack top and bottom end plates as shown in Figure 3.4.2-1.

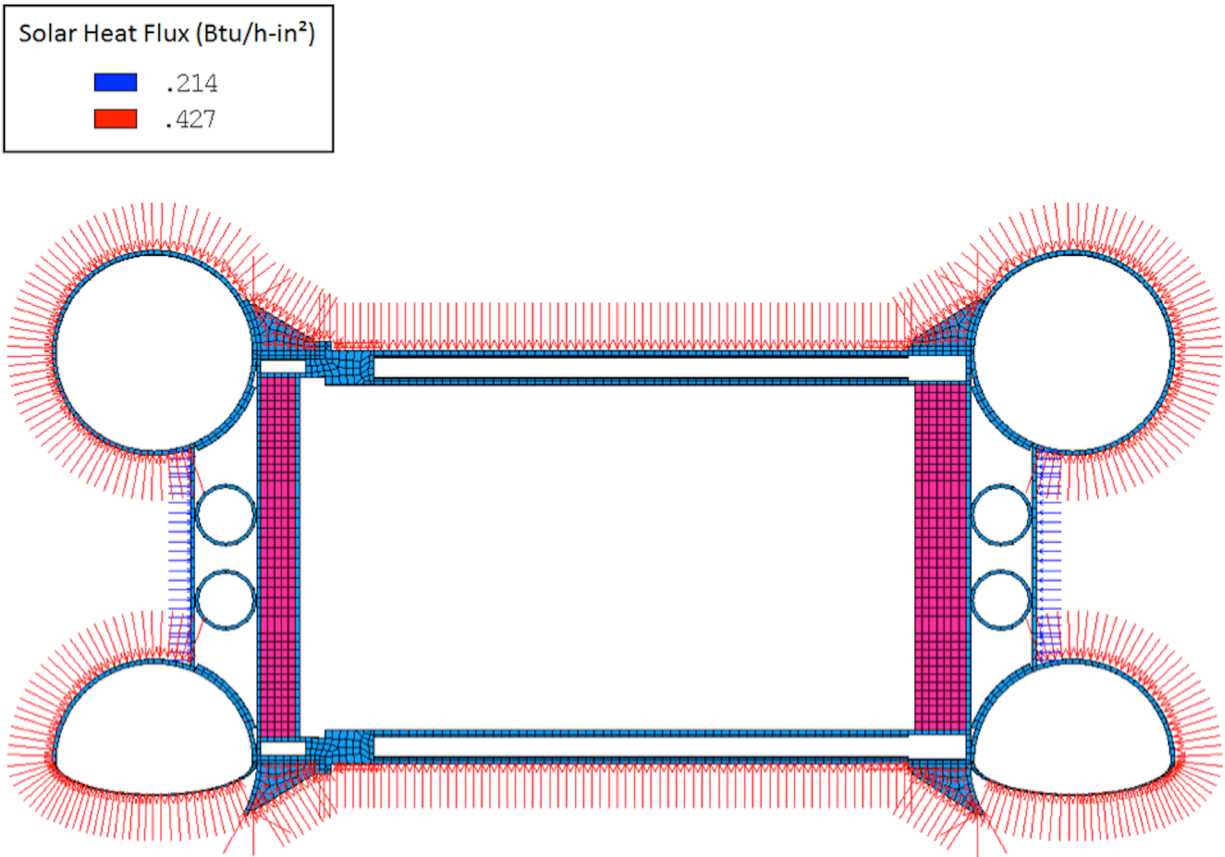


**Figure 3.4.2-1. Solar Heat Flux Boundary Conditions for HAC (Post-Fire Cool-Down)**

### **3.4.3. Maximum Temperatures and Pressure**

When exposed to the HAC fire prescribed in 10 CFR 71.73(c)(4) (Reference 3-1), the Model 2000 Transport Package must maintain containment of its contents and maintain its shielding capabilities. The results of the HAC thermal evaluation are presented in Table 3.4.3-1. Comparing with Table 3.1.3-1, it can be seen that the maximum temperatures of the different components are below the allowable temperatures. Therefore, the HAC fire will not adversely affect the package's ability to provide containment and shielding for its contents.

#### **3.4.3.1. HAC Temperature Results**

A transient thermal analysis was performed on the model. This transient analysis simulates exposure of the Model 2000 Transport Package to a 30-minute hypothetical accident fire followed by a 36-hour cool-down period in which the package is exposed to a 100°F ambient temperature and insolation (solar heat flux). The 36-hour cool-down period is of sufficient length to allow the package temperatures to reach their peak values. The results of the transient HAC thermal analysis are presented in Table 3.4.3-1.



**Table 3.4.3-1. Temperature Results, Hypothetical Accident Conditions**

Item	Peak Temperature (°F)	Time at Which Peak Temperature Occurs (Hours)
Material Basket	1045	13.0
HPI shielding (side)	670	11.0
HPI shielding (top)	599	9.0
HPI shielding (bottom)	618	11.0
Cask lid seal	508	6.2
Cask shielding (side)	570	0.6
Cask shielding (top)	529	7.1
Cask shell, puncture location	782	0.5
Cask shell, opposite side to puncture location	512	4.0
Overpack outer shell, puncture location	1,103	0.5
Overpack outer shell, opposite side to puncture location	1,337	0.5
Cask drain port (bottom)	612 <sup>a</sup>	0.8
Cask test port (top)	608 <sup>b</sup>	0.6
Cask vent port (lid)	520	7.1
HPI fill gas (average)	740	11.0
Cask fill gas (average)	571	7.1
HPI and Cask fill gas, combined (average)	585	8.0

Notes: a. The cask bottom port exceeds 600°F for approximately 0.34 hours during the HAC transient analysis.

b. The cask top port exceeds 600°F for approximately 0.17 hours during the HAC transient analysis.

Additionally, temperature-history plots of several package components are presented in Figure 3.4.3-1 through Figure 3.4.3-4 (Note: the steady-state starting temperatures are shown between time = -5 and 0 hours in these figures). As shown in these figures, the cool-down period of 36 hours is sufficient to allow all package temperatures to achieve their peak values. Finally, the temperature contours of the Model 2000 Transport Package with HPI for hypothetical accident conditions are shown in Figure 3.4.3-5.

NEDO-33866 Revision 6  
Non-Proprietary Information

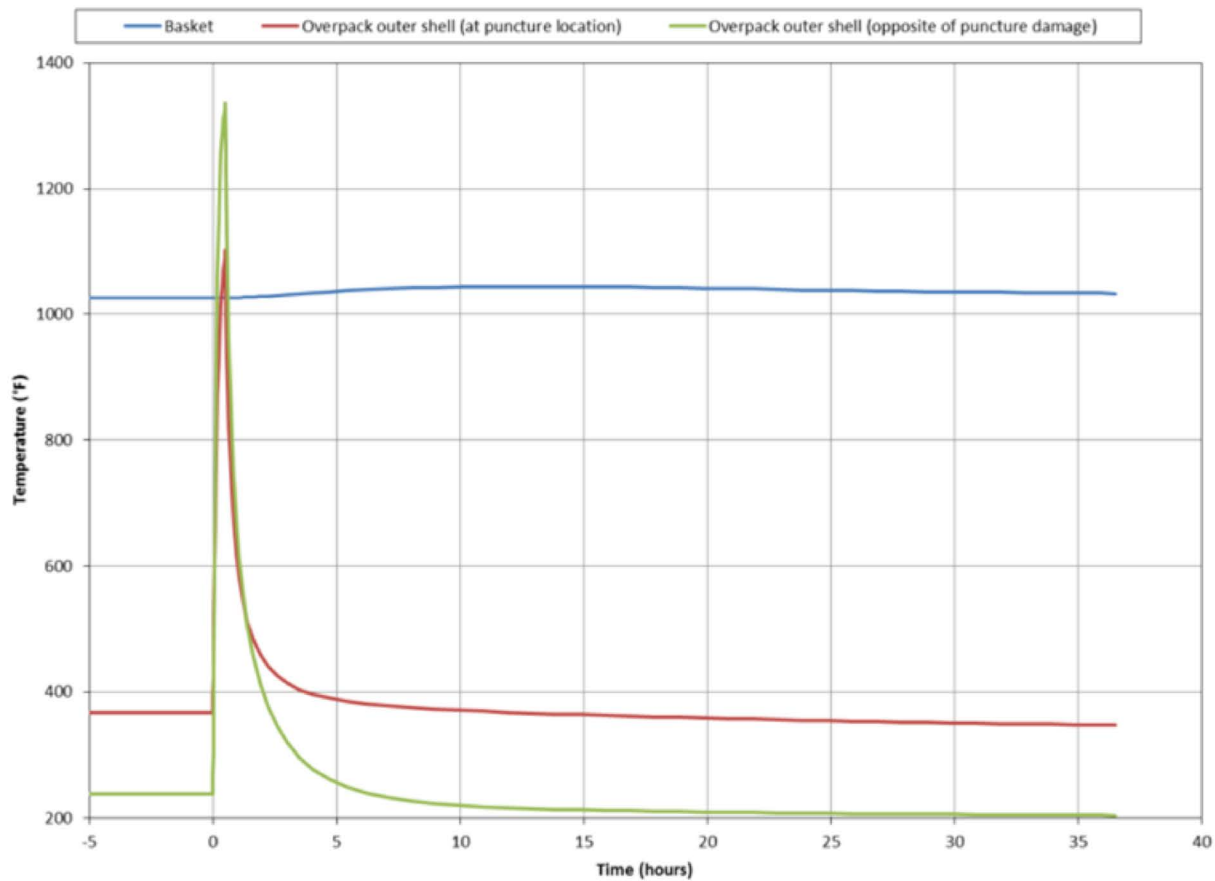


**Figure 3.4.3-1. Temperature-History of the Material Basket and Overpack for HAC**

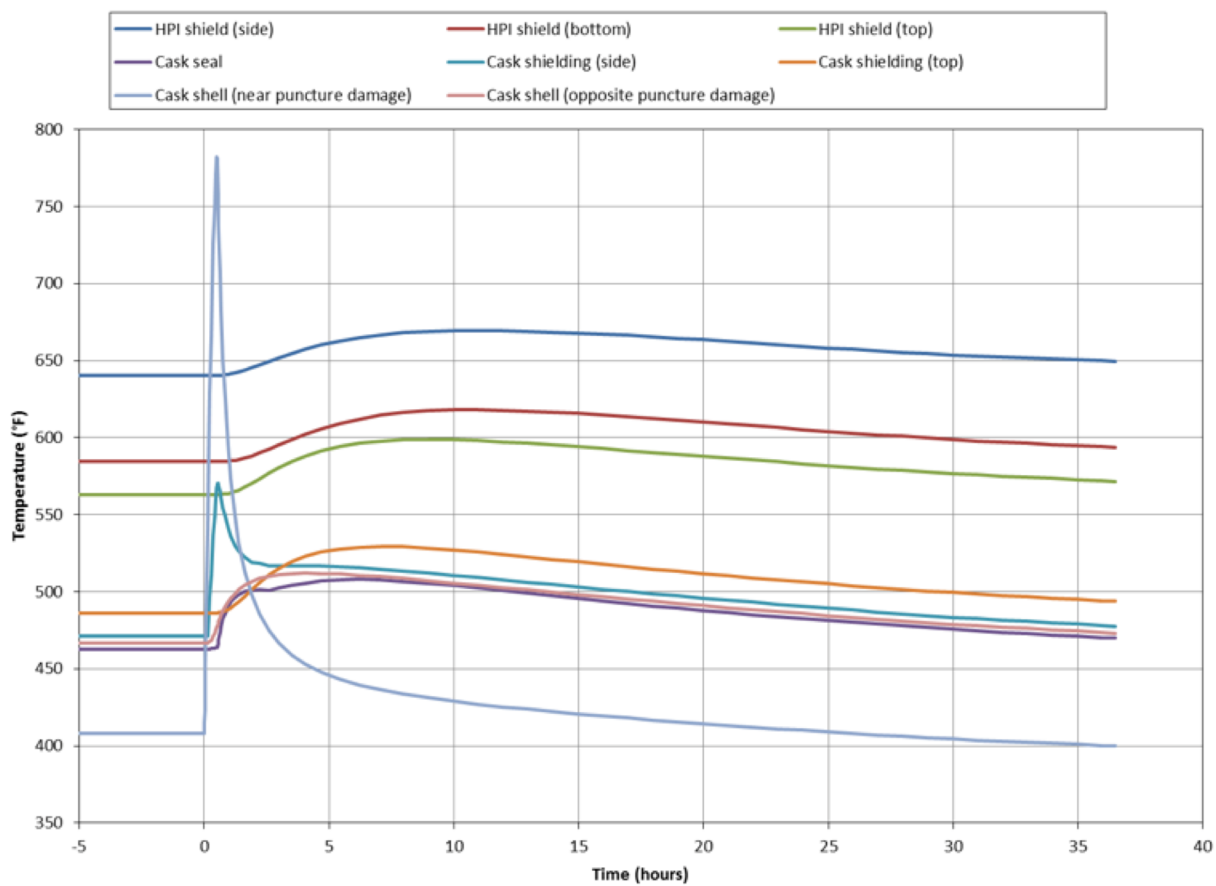
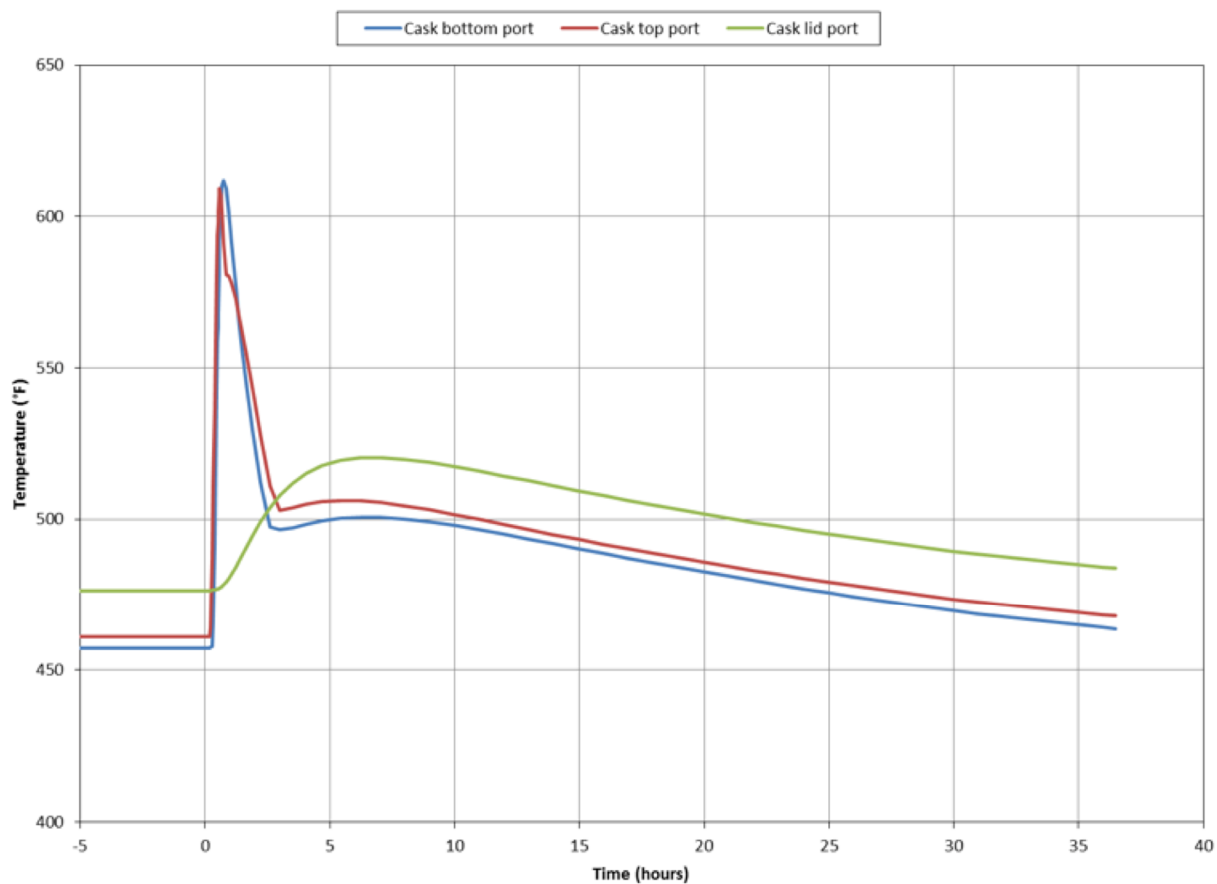
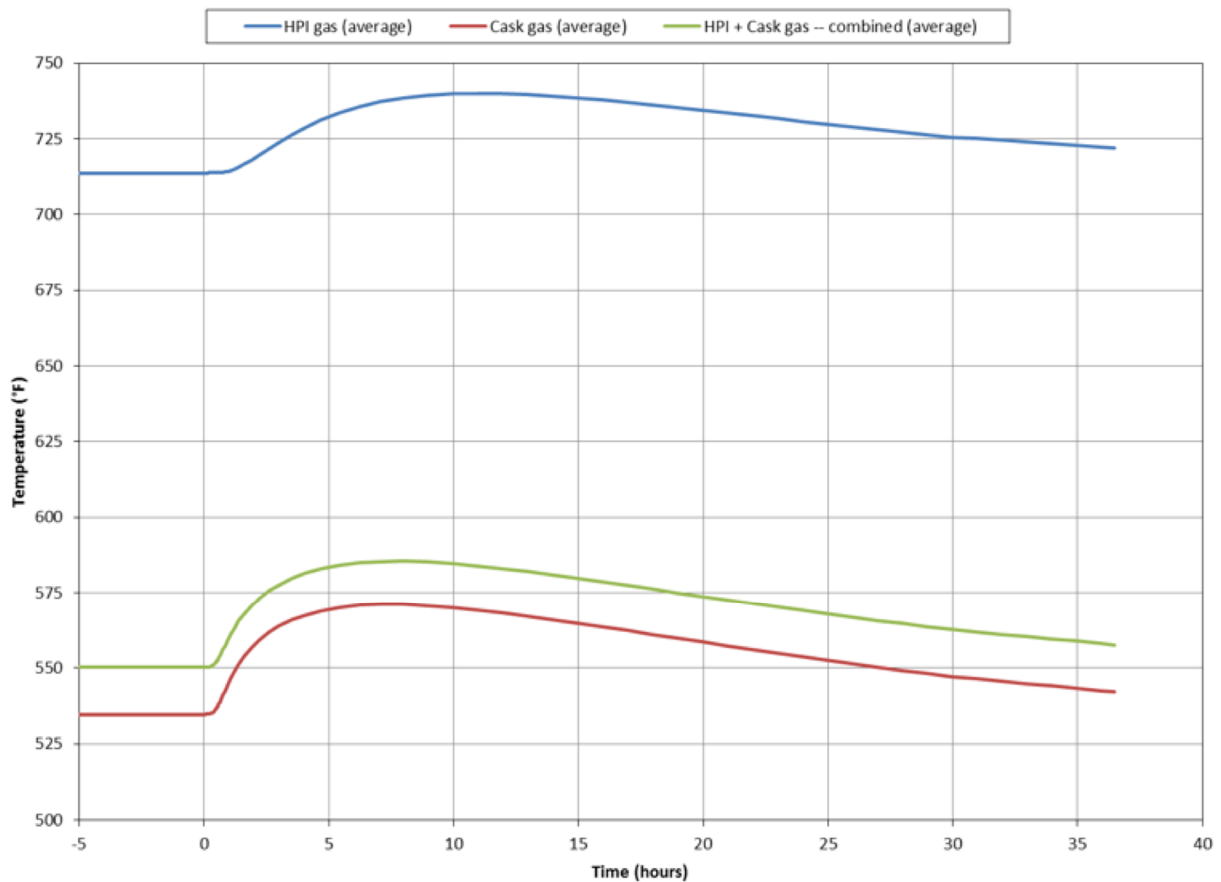


Figure 3.4.3-2. Temperature-History of the HPI and Cask for HAC



**Figure 3.4.3-3. Temperature-History of the Cask Ports for HAC**



**Figure 3.4.3-4. Temperature-History of the HPI and Cask Fill Gases**  
(Note: Volumetric Average Temperature)

[[

]]

**Figure 3.4.3-5. Temperature Contours During HAC 30-Minute Fire and Cool-Down**

### HAC Thermal Contact Resistance Sensitivity Study

Similar to the NCT thermal conductivity resistance sensitivity study, to assess the effect that using the mixed thermal resistance levels have on package temperatures, the analyses for HAC is repeated with all of the thermal resistance levels set to “low” (i.e., perfect contact). The results of this analysis is compared with the results from Table 3.4.3-1, and presented in Table 3.4.3-2.

**Table 3.4.3-2. Comparison of Mixed and Perfect Thermal Contact for HAC**

Item	Peak temperature (°F)	
	Mixed Thermal Contact Resistance	Perfect Thermal Contact
Material basket	1,045	1,043
HPI shielding (side)	670	668
HPI shielding (top)	599	596
HPI shielding (bottom)	618	617
Cask lid seal	508	506
Cask shielding (side)	570	576
Cask shielding (top)	529	527
Cask shell, puncture location	782	795
Cask shell, opposite side to puncture location	512	511
Cask drain port (bottom)	612 <sup>a</sup>	655 <sup>c</sup>
Cask test port (top)	609 <sup>b</sup>	613 <sup>d</sup>
Cask vent port (lid)	520	518
Overpack outer shell, puncture location	1,103	1,094
Overpack outer shell, opposite side to puncture location	1,337	1,336
HPI fill gas (average)	740	738
Cask fill gas (average)	571	569
HPI and cask fill gases, combined (average)	585	584

- Notes:
- a. The cask bottom port exceeds 600°F for approximately 0.34 hours during the HAC transient analysis.
  - b. The cask top port exceeds 600°F for approximately 0.17 hours during the HAC transient analysis.
  - c. The cask bottom port exceeds 600°F for approximately 0.69 hours during the HAC transient analysis.
  - d. The cask top port exceeds 600°F for approximately 0.20 hours during the HAC transient analysis.

The same conclusion that was made for NCT thermal contact resistance can be made for HAC in that, in general, the package temperatures are lower when modeling the thermal contact as perfect as opposed to the mixed thermal contact levels. However, the cask drain port (bottom) and the cask test port (top) have peak temperatures that are higher when modeling the thermal contact as perfect. This is due to their proximity to the modeled puncture damage, which allows the heat from the fire to more readily enter the package.

It should be noted that the significant increase in the maximum temperature at the bottom port (drain port) for the perfect contact case is due to the perfect contact between the bottom plug of the HPI and the bottom of the cask cavity. This perfect contact causes a significant increase in the heat driven out the bottom of the cask from the internal heat load. However, it should be considered that perfect contact between the HPI bottom plug and the bottom of the cask is an unrealistic

scenario. For drainage purposes, there is a slight dish in the bottom of the Model 2000 cask cavity that will provide a significant separation between the HPI bottom plug and the bottom of the cask. This separation, shown in Figure 3.4.3-6, will cause the temperature for the cask drain port (bottom) to be more accurately calculated with mixed thermal resistance.

[[

]]

**Figure 3.4.3-6. Gap Between HPI Bottom Plug and Cask Cavity Bottom (INCH)**

#### **3.4.3.2. HAC Maximum Pressure Calculation**

During HAC, the average temperature of the cask fill gas (including the gas within the HPI) peaks at 585°F 11 hours after the end of the 30-minute fire. Using the ideal gas law, the cask internal pressure from gas expansion is:

$$\frac{P_1}{T_1} = \frac{P_2}{T_2}$$
$$P_2 = 14.7 \text{ psia} \times \left( \frac{585+460}{70+460} \right) = 29.0 \text{ psia} < 30 \text{ psia}$$

where,

$P_1$	=	14.7 psia	initial fill gas pressure,
$T_1$	=	70°F	initial fill gas temperature, and
$T_2$	=	585°F	average gas volume temperature during HAC.

The cask internal pressure during HAC is less than the design pressure of 30 psia. Therefore, no further evaluation is required.

#### **3.4.4. Maximum Thermal Stresses**

Section 2.7.4.3 discusses thermal stresses.

#### **3.4.5. Accident Conditions for Fissile Material Packages for Air Transport**

The Model 2000 Transport Package will not be transported by air.



### **3.5 Appendix**

#### **3.5.1. Model 2000 Transport Package with HPI and No Material Basket**

This section evaluates the Model 2000 Transport Package with the HPI and no material basket, 1500 W, for both NCT and HAC using a subset of the finite element model described in the main text of this document. The evaluation presented in this section concludes that the temperatures and pressures generated in the Model 2000 Transport Package by 1500 W of decay heat results in package temperatures and pressures which are bounded by the 3000 W results.

##### **3.5.1.1. Thermal Model with HPI and No Material Basket 1500 Watt Decay Heat**

The model (see Figure 3.5.1-1) consists of the Overpack (with trapped air), cask, HPI, and cask fill gas. The contents are assumed to generate 1500 W of heat that is uniformly distributed on the internal surfaces of the HPI.

[[

]]

**Figure 3.5.1-1. 3D FEA Model of the Model 2000 Transport Package with HPI and No Material Basket (Half Symmetry) - Elements Representing Air and Helium Not Shown for Clarity**

$$q''_{\text{gen}} = \frac{Q}{A_{\text{SURF152}}} = \frac{1500 \text{ W} \left( \frac{3.4123 \text{ Btu/h}}{\text{W}} \right)}{2 \times 816.846194 \text{ in}^2} = 3.133 \frac{\text{Btu}}{\text{h-in}^2}$$

where

$A_{\text{SURF152}}$  = the area of the SURF152 elements overlaid on the inner surface of the HPI (multiplied by 2 to account for the half-symmetry of the model).

The package is exposed to NCT and HAC using boundary conditions as described in the main text of this document. Additionally, the package is modeled with damage consistent with a side drop for HAC as described in the main text of this document. For HAC, the package is assumed to be

exposed to a 100°F ambient temperature with insolation prior to and following the 1,475°F fire, and is assumed to be exposed to a -20°F ambient temperature in shade prior to and following the 1,475°F fire.

### 3.5.1.2. NCT Temperature Results

The NCT thermal analysis results are presented in Table 3.5.1-1 (NCT, 100°F ambient temperature) and Table 3.5.1-2 (NCT cold conditions, -40°F and -20°F ambient temperatures). Table 3.5.1-3 provides a comparison of the component temperature and allowable. As the table shows, the cask lid seal and port temperatures are within the allowable limits for the [[

]] seal material and port testing as specified in Chapter 4.

Additionally, the steady-state temperature contours for NCT (100°F ambient temperature) are shown in Figure 3.5.1-2. As evident from Figure 3.5.1-3, no accessible surface of the package is greater than or equal to 185°F (maximum is less than 175°F) when exposed to a 100°F ambient temperature in shade.

**Table 3.5.1-1. Model 2000 Transport Package with HPI (No Material Basket)  
Temperature Results, NCT (100°F Ambient Temperature in Shade and with Insolation)**

Item	100°F Ambient Temperature, in Shade (°F)			100°F Ambient Temperature, with Insolation (°F)		
	Max	Min	Avg	Max	Min	Avg
HPI	390	254	---	420	289	---
HPI shielding (top)	356	346	352	388	378	383
HPI shielding (sides)	389	300	367	419	334	398
HPI shielding (bottom)	313	294	306	346	328	340
Cask (bottom, shells, top, lid)	296	223	---	331	261	---
Cask shielding (lid)	292	283	287	327	318	322
Cask shielding (sides)	280	242	267	316	279	303
Cask lid seal	282	269	---	317	305	---
Cask drain port (bottom)	243	223	---	279	261	---
Cask test port (top)	278	269	---	314	305	---
Cask vent port (lid)	288	284	---	323	319	---
Overpack base	239	136	---	275	158	---
Overpack cover	193	105	---	237	171	---
Overpack toroidal shell (top)	131	106	114	185	163	171
Overpack toroidal shell (bottom)	168	109	124	212	130	164
Overpack honeycomb impact limiter (top)	163	155	161	213	205	210
Overpack honeycomb impact limiter (bottom)	236	202	220	272	241	258
Cask fill gas	385	245	316	415	281	349

**Table 3.5.1-2. Model 2000 Transport Package with HPI (No Material Basket)  
Temperature Results, -40°F & -20°F Ambient Temperatures in Shade**

Item	-40°F Ambient Temperature, in Shade (°F)			-20°F Ambient Temperature, in Shade (°F)		
	Max	Min	Avg	Max	Min	Avg
HPI	305	147	---	317	162	---
HPI shielding (top)	268	258	263	280	270	276
HPI shielding (sides)	304	201	279	316	215	291
HPI shielding (bottom)	216	195	208	230	209	222
Cask (bottom, shells, top, lid)	199	110	---	213	126	---
Cask shielding (lid)	195	185	189	208	199	203
Cask shielding (sides)	182	134	164	195	150	179
Cask lid seal	183	171	---	197	184	---
Cask drain port (bottom)	135	110	---	150	126	---
Cask test port (top)	179	171	---	193	184	---
Cask vent port (lid)	190	187	---	204	200	---
Overpack base	130	1	---	145	21	---
Overpack cover	64	-36	---	83	-16	---
Overpack toroidal shell (top)	-7	-35	-26	13	-15	-6
Overpack toroidal shell (bottom)	41	-33	-14	59	-12	6
Overpack honeycomb impact limiter (top)	29	19	25	48	39	45
Overpack honeycomb impact limiter (bottom)	127	82	107	142	100	123
Cask fill gas	301	137	221	312	152	234

**Table 3.5.1-3. NCT Temperature Summary and Comparison with Allowable Temperatures**

Item	NCT Temperatures (°F)	Allowable Temperature (°F)
HPI Shielding (Depleted Uranium)	419 (max)	2071
Cask lid seal	317 (max)	400 <sup>b</sup>
Cask Shielding (Lead)	327 (max)	622
Honeycomb Impact Limiters	272	350
Cask Drain Port (Bottom)	279	612 <sup>a</sup>
Cask Test Port (Top)	314	
Cask Vent Port (Lid)	323	
Overpack Outer Surface	175	185

Notes: See Table 3.1.3-1 for allowable temperature referencing;

<sup>a</sup> Temperature limit applies to the port plug containment boundary

<sup>b</sup> See Section 4

[[

]]

**Figure 3.5.1-2. Package Temperature Contours for NCT with 100°F Ambient Temperature in Shade and with Insolation**

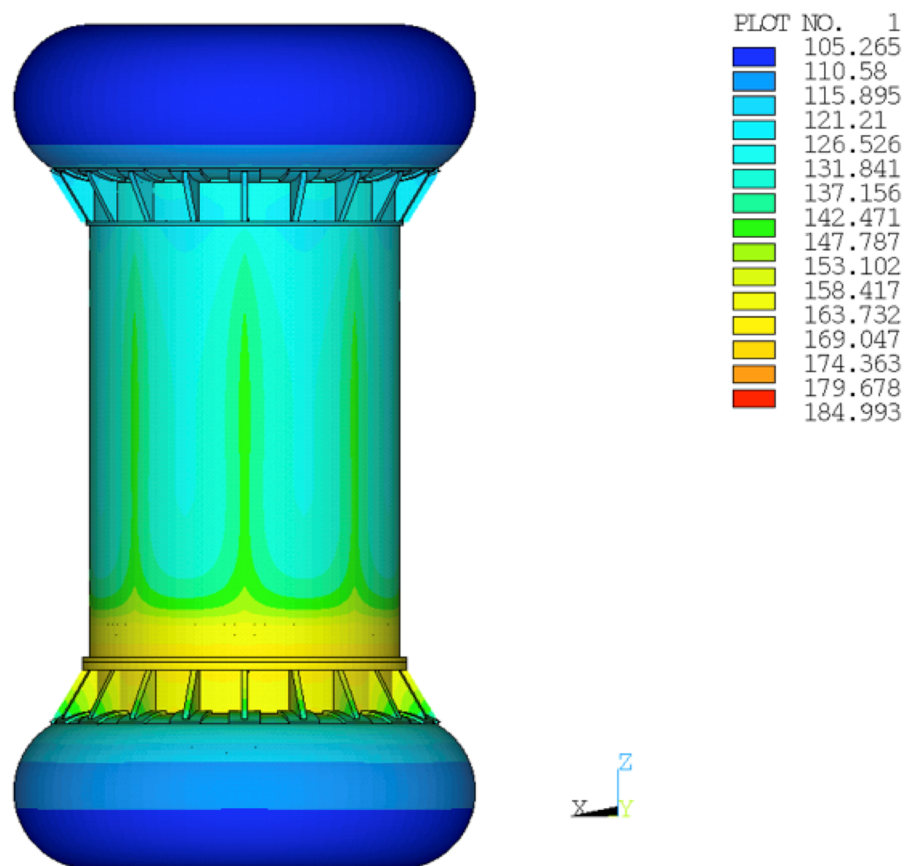


**Figure 3.5.1-3. Package Exterior Surface Temperature Contours for NCT with 100°F Ambient Temperature in Shade**

### 3.5.1.3. HAC Temperature Results

The HAC thermal analysis results are presented in Table 3.5.1-4. The table presents the temperature results for both hot and cold pre/post fire conditions. Table 3.5.1-5 provides a comparison of the component temperature and allowable. As the table shows, the cask lid seal and port temperatures are within the allowable limits for the [[ ]] seal material as specified in Chapter 4.

**Table 3.5.1-4. Model 2000 Transport Package with HPI (No Material Basket)  
Temperature Results, HAC**

Item	Fire with 100°F and Insolation Pre/Post Fire		Fire with -20°F and Shade Pre/Post Fire	
	Peak Temp. (°F)	Time at Which Peak Temp. Occurs (hours)	Peak Temp. (°F)	Time at Which Peak Temp. Occurs (hours)
HPI shielding (side)	482	12.3	389	16.5
HPI shielding (top)	439	10.3	338	13.5
HPI shielding (bottom)	446	12.3	348	15.5
Cask lid seal	389	2.2	275	10.5
Cask shielding (side)	456	0.6	344	0.6
Cask shielding (top)	396	8.3	287	10.5
Cask shell, puncture location	704	0.5	621	0.5
Cask shell, opposite side to puncture location	385	5.6	273	8.5
Overpack outer shell, puncture location	1,063	0.5	1,017	0.5
Overpack outer shell, opposite side to puncture location	1,330	0.5	1,314	0.5
Cask drain port (bottom)	537	0.8	435	0.8
Cask test port (top)	515	0.6	406	0.6
Cask vent port (lid)	392	8.3	283	10.5
Cask fill gas (average)	421	9.3	319	12.5

**Table 3.5.1-5. HAC Temperature Summary and Comparison with Allowable Temperatures**

Item	HAC Temperatures (°F)	Allowable Temperature (°F)
HPI Shielding (Depleted Uranium)	482 (max)	2071
Cask lid seal	389 (max)	400 ([[ ]]) <sup>a</sup>
Cask Shielding (Lead)	456 (max)	622
Cask Drain Port (Bottom)	537	612 <sup>a</sup>
Cask Test Port (Top)	515	
Cask Vent Port (Lid)	392	

Notes: See Table 3.1.3-1 for allowable temperature referencing;

<sup>a</sup> See Chapter 4

#### **3.5.1.4. Thermal Contact Resistance Study**

The thermal contact resistance levels in this model are modified to simulate perfect contact, and the NCT (100°F ambient with insulation) and HAC (100°F ambient with insulation during pre-fire and post-fire) analyses are performed and compared with those that include mixed thermal contact resistances. The results of these studies are presented in Table 3.5.1-6 (NCT) and Table 3.5.1-7 (HAC). As shown in Table 3.5.1-6, the simulation with perfect thermal contact results in component temperatures being lower than their mixed thermal contact counterparts.

The simulation for HAC with perfect thermal contact results in most component temperatures being lower than their mixed thermal contact counterparts while other component temperatures are higher for the case with perfect thermal contact. The item exhibiting the greatest sensitivity in the HAC study is the cask drain port (increased temperature of 50°F). However, as discussed in Section 3.4.3.1, there is a slight dish in the bottom of the Model 2000 cask cavity that will provide a significant separation between the HPI bottom plug and the bottom of the cask. This separation, shown in Figure 3.4.3-6, will cause the temperature for the cask drain port (bottom) to be more accurately calculated with mixed thermal resistance. Therefore, a maximum temperature of 537°F is predicted for the drain port.



**Table 3.5.1-6. Model 2000 Transport Package with HPI (No Material Basket) Temperature Results, 100°F Ambient Temperature with Insolation, NCT, Thermal Contact Resistance Study**

Item	Mixed Contact Resistances (°F)			Perfect Contact (°F)		
	Max	Min	Avg	Max	Min	Avg
HPI	420	289	---	415	283	---
HPI shielding (top)	388	378	383	384	374	379
HPI shielding (sides)	419	334	398	414	327	393
HPI shielding (bottom)	346	328	340	341	322	334
Cask (bottom, shells, top, lid)	331	261	---	326	253	---
Cask shielding (lid)	327	318	322	322	314	317
Cask shielding (sides)	316	279	303	312	272	298
Cask lid seal	317	305	---	313	301	---
Cask drain port (bottom)	279	261	---	273	253	---
Cask test port (top)	314	305	---	310	301	---
Cask vent port (lid)	323	319	---	318	315	---
Overpack base	275	158	---	269	157	---
Overpack cover	237	171	---	235	170	---
Overpack toroidal shell (top)	185	163	171	184	162	170
Overpack toroidal shell (bottom)	212	130	164	208	130	164
Overpack honeycomb impact limiter (top)	213	205	210	210	202	207
Overpack honeycomb impact limiter (bottom)	272	241	258	268	236	254
Cask fill gas	415	281	349	411	275	344

**Table 3.5.1-7. Model 2000 Transport Package with HPI (No Material Basket)  
Temperature Results, 100°F Ambient with Insolation During Pre- and Post-Fire, HAC,  
Thermal Contact Resistance Study**

Item	Mixed Contact Resistances		Perfect Contact	
	Peak Temp. (°F)	Time at Which Peak Temp. Occurs (hours)	Peak Temp. (°F)	Time at Which Peak Temp. Occurs (hours)
HPI shielding (side)	482	12.3	480	12.2
HPI shielding (top)	439	10.3	438	10.2
HPI shielding (bottom)	446	12.3	446	12.2
Cask lid seal	389	2.2	389	2.2
Cask shielding (side)	456	0.6	463	0.2
Cask shielding (top)	396	8.3	395	8.2
Cask shell, puncture location	704	0.5	718	0.5
Cask shell, opposite side to puncture location	385	5.6	384	5.5
Overpack outer shell, puncture location	1,063	0.5	1,054	0.5
Overpack outer shell, opposite side to puncture loc.	1,330	0.5	1,330	0.5
Cask drain port (bottom)	537	0.8	587	0.7
Cask test port (top)	515	0.6	519	0.9
Cask vent port (lid)	392	8.3	390	7.2
Cask fill gas (average)	421	9.3	420	9.2

### **3.6 References**

- 3-1 U.S. NRC, 10 CFR 71, "Packaging and Transportation of Radioactive Material," Washington D.C.
- 3-2 ANSYS®, "Mechanical, Revision 14.0," November 2011.
- 3-3 Incropera, Frank P., and DeWitt, David P., "Fundamentals of Heat and Mass Transfer," Fifth Edition, John Wiley & Sons, Inc., New York, 2002.
- 3-4 Hexcel Corporation, "HexWeb Honeycomb Attributes and Properties," 2016.
- 3-5 GE Hitachi Nuclear Energy, "Model 2000 Cask Containment Boundary Testing," Test Specification 003N1962, Revision 0 (2015), or latest revision.
- 3-6 Editors H.K Hammond III and H.L Mason, "Precision Measurement and Calibration, Selected NBS Papers on Radiometry and Photometry," Editors H.K Hammond III and H.L Mason, Ed.: National Bureau of Standards (NBS), 1971, Volume 7.
- 3-7 Robert Siegel and John R. Howell, "Thermal Radiation Heat Transfer, Third Edition," Hemisphere Publishing Corporation, New York, 1992.
- 3-8 Parker Hannifin Corporation. (2014) Parker O-Ring Handbook, 50th Anniversary Edition.
- 3-9 Lienhard IV, John H., and Lienhard V, John H., "A Heat Transfer Textbook," Fourth Edition, Phlogiston Press, Cambridge, Massachusetts, 1981.
- 3-10 Guyer, Eric C., Editor, "Handbook of Applied Thermal Design," McGraw-Hill, New York, 1989.

## **4 CONTAINMENT**

This section demonstrates the ability of the Model 2000 Transport Package to meet the containment requirements of 10 CFR 71. The containment system for the Model 2000 Transport Package consists of the cask alone. The other components (e.g., overpack, high performance insert (HPI)) are not part of the containment system. The entire containment boundary, including containment welds and base metals (as shown in Figure 4.1.3-1), are leakage rate tested for fabrication, maintenance, and periodically as defined in Chapter 8.

### **4.1 Description of Containment System**

The cask design has been evaluated to support 3000 W decay heat as stated in Section 1.2.2.1. However, for the purposes of this chapter, the allowable contents are limited to 1500 W decay heat.

#### **4.1.1. Containment Vessel**

Figure 1.2-1 shows the containment vessel (cask) for the Model 2000 Transport Package. The containment boundary for the cask is shown in Figure 4.1.3-1. The cask is constructed of a steel-clad lead cylinder with a stainless steel forging at each end. The cask lid is placed within the upper forging to protect the seal area during the accident conditions. Refer to Section 2.2 for information regarding the materials of construction of the cask.

#### **4.1.2. Closure**

The cask lid connects to the cask body by fifteen 1.25-inch diameter ASTM A540, Grade B22 or ASME SA540 socket head screws, which compress the cask lid seal. The screws are equally spaced on a 32.25-inch diameter bolt circle. Each screw is tightened to 720±30 ft-lb of torque, as shown in Section 2.12.4. The cask lid closure evaluation is presented in Section 2.4.3. The stress analysis of these screws is given in Section 2.12.4. These analyses show that positive closure is maintained during all conditions.

#### **4.1.3. Containment Penetrations**

The Model 2000 cask has three penetrations or ports. One port, located two inches from the bottom of the cask, serves as a drain for the cask cavity. This port is made by a series of offset ½-inch drilled holes through the 6-inch thick steel forging. The second penetration is located approximately in the center of the cask lid. It is made of 3/8-inch diameter tubing, shown as Item 13 - [[ ]], in the Model 2000 Transport Package Licensing Cask Drawings 101E8718 and 105E9520, respectively (see Section 1.3.1), spiraled through the lead and welded at both ends to the steel flanges that make up the lid. The combined use of these two ports provides means to eliminate water from the cask cavity collected during underwater operations. The third penetration or port is used to test the adequacy of the cask lid closure seal after each loading operation.

A ½ NPT hex socket head pipe plug followed by 1¾-12 UNC cap close each of these penetrations (see Figure 4.1.3-2). The closure of pipe plug is designed for leaktightness as defined in

ANSI N14.5-1997, Section 2.1 (Reference 4-1). Dimensions and components of the port seals are provided in the Model 2000 cask licensing drawings included in Section 1.3.1. Additional information is provided in Section 4.1.3.3.

#### **4.1.3.1. Welds**

All cask welds are [[ ]] to ensure structural and containment integrity. Each weld is liquid penetrant tested on the root and final passes. In addition, the welds are helium leak tested as required in Chapter 8.

[[

]]

**Figure 4.1.3-1. Cask Containment Boundary**

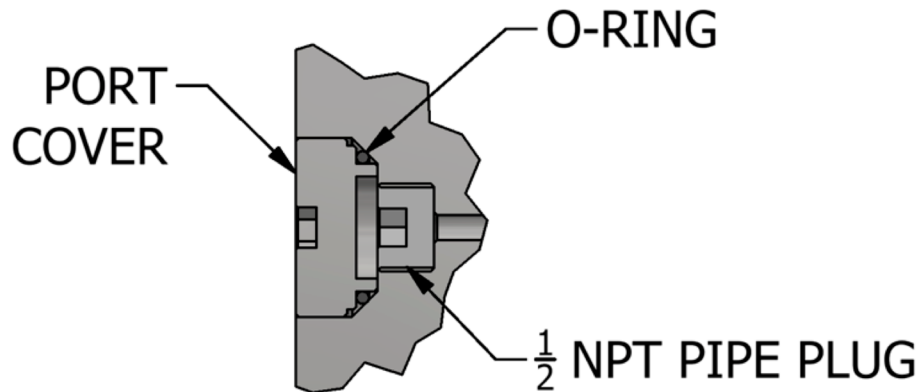


**Figure 4.1.3-2. Cask Port Configuration (Assembled View)**

#### **4.1.3.2. Cask Lid Closure Seal**

The cask lid seal (Parker Gask-O-Seal design) consists of a [[ ]] thick metal retainer with two concentric [[ ]] seals on the top and two concentric [[ ]] seals on the bottom (4 total), as seen in Figure 4.1.3-3. The surfaces of the Model 2000 cask body and the lid flanges have an electropolished finish to ensure that they are clean sealing surfaces for the [[ ]]. As the load from bolting the lid down is applied, the [[ ]] seals are compressed between the cask body flange and cask lid flange, and the seals deform to occupy the free volume in the metal retainer. A [[ ]] are used as the seal material.

[[

]]

**Figure 4.1.3-3. Cask Lid Seal Design**

#### 4.1.3.3. Cask Port Seals

The containment boundary for each port is at the respective pipe plug. As illustrated in Figure 4.1.3-1, the port O-rings and port covers are outside the containment boundary. An exploded view of these components is shown in Figure 4.1.3-4. For the cask port seals, an [[ ]] is used as the O-ring seal material. See cask licensing drawings in Section 1.3.1 for more detailed information. For details of the pipe plug installation controls, see Chapter 7.

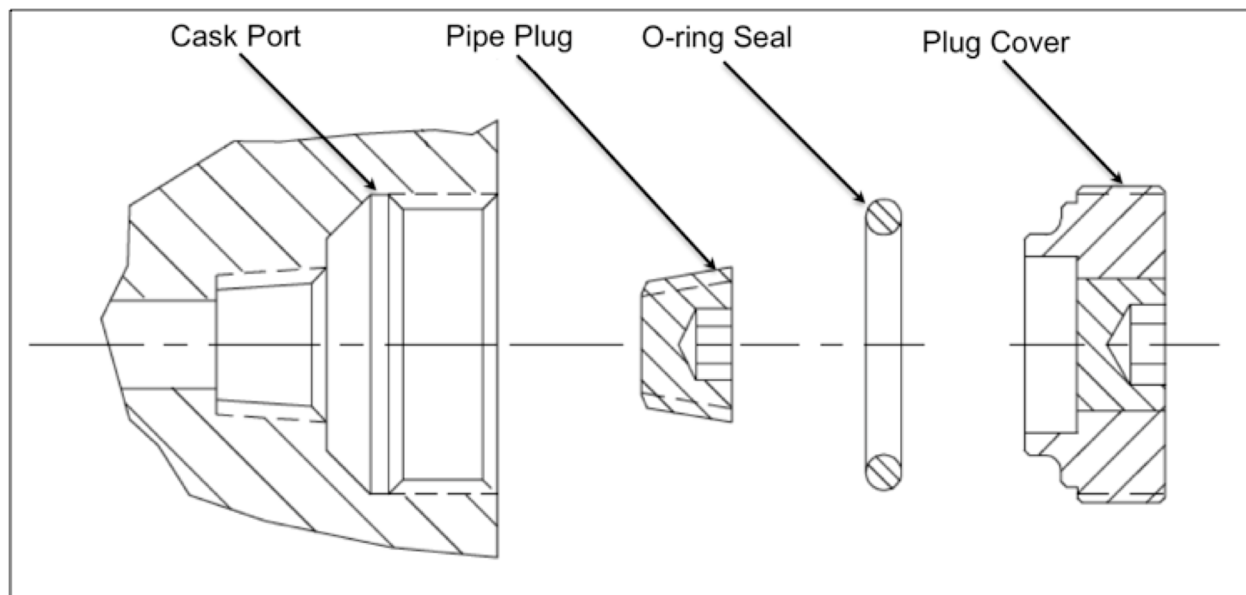


**Figure 4.1.3-4. Cask Port Configuration (Exploded View)**

## 4.2 Containment Under Normal Conditions of Transport

The Model 2000 cask containment is designed so that no release of radioactive materials will occur under the NCT, and there will not be any significant increase in external radiation or reduction in package effectiveness. This conclusion is supported by the analyses in Chapters 2 and 3 and the various component qualification tests.

The cask withstands pressures and temperatures in excess of those encountered in routine transport and normal conditions of transport. The maximum average cask fill gas temperature is determined to be 349°F in Section 3.5.1. This temperature value is based on helium occupying the entire cavity volume. The maximum pressure encountered under NCT, 22.4 psia (calculated using the formula in Section 3.3.2.1 with  $T_2=349^\circ\text{F}$ ), is bounded by the 30 psia cask design pressure. The structural evaluation presented in Chapter 2 shows low stress values throughout the cask structure, especially in the seal area under NCT. The maximum cask lid seal temperatures are bounded by the operational limit of 400°F, which is qualified for the cask seal (Reference 4-2). Additionally, cask port temperatures are bounded by the operational limit of 612°F, thus containment integrity is maintained (Reference 4-2).



### 4.3 Containment Under Hypothetical Accident Conditions

As seen in Section 3.5.1.3, the maximum average cask fill gas temperature in the cask cavity for HAC is 421°F. This temperature is based on helium occupying the entire cavity volume. The maximum pressure encountered during HAC (24.4 psia - calculated using the formula in Section 3.4.3.2 with  $T_2=421^\circ\text{F}$ ) is bounded by the 30 psia cask design pressure. Temperatures at the cask lid closure seal region and cask vent port are bounded by the 400°F design temperature of the seal material (see Table 3.5.1-5 and Reference 4-2). Temperatures at the drain port and test port exceed the seal material allowable temperature by 137°F and 115°F respectively. This is considered acceptable because: (a) the port O-rings and port covers are outside the containment boundary as illustrated in Figure 4.1.3-1, and (b) the duration of HAC maximum temperatures at these ports is short, < 1 hour per Table 3.5.1-4, resulting in minor material degradation. The analytical evaluations under HAC presented in Chapter 2 show that the stresses throughout the cask structure are below the failure criteria for the material.

### 4.4 Leakage Rate Tests for Type B Packages

The maximum temperature at the cask lid seal region is bounded by 400°F and the maximum temperature at the penetrations or port areas are bounded by 612°F. The internal pressure in the cask cavity may increase to 24.4 psia due to rise in the temperature. The Model 2000 cask is loaded dry or underwater. If loaded underwater, the cavity must be vacuum dried to remove any residual moisture.

Regardless of how the cask is loaded, a leak test is performed after it is loaded. To perform the leak test, helium is introduced into the cavity to a pressure of 15 psig. The preshipment, fabrication, periodic, and maintenance leakage rate tests are performed in accordance with ANSI N14.5 (Reference 4-1) standards. At the conclusion of the pre-shipment test, the pressure is released. Therefore it can be assumed that helium remains inside the cavity. The peak average fill gas temperature is 421°F under hypothetical accident conditions.

Full-scale acceptance testing of the cask lid closure seal [[ ]] was performed at maximum pressure at ambient temperature. Full-scale acceptance testing of the port NPT fittings was performed at maximum pressure with both maximum (612°F) and minimum (5°F) temperature predictions in accordance with ANSI N14.5 standards (Reference 4-1). The 5°F minimum test temperature bounds the lowest temperature at the port O-rings (21°F) as stated in Section 3.3.1.2. The seal material for both the cask lid seal and port O-rings [[

]] is suitable for conditions less than -40°F. The maximum internal pressure of 24.4 psia is less than the design pressure of 30 psia. Therefore, the Model 2000 Transport Package design pressure is a conservative design basis for the shipment of the 1500 W decay heat content.

#### **4.5 References**

- 4-1 American National Standards Institute (ANSI), "American National Standard for Radioactive Materials – Leakage Tests on Packages for Shipment," ANSI N14.5, 1997.
- 4-2 GE Hitachi Nuclear Energy, "Model 2000 Cask Containment Boundary Testing," Test Specification 003N1962, Revision 0 (2015), or latest revision.

## 5 SHIELDING EVALUATION

This chapter outlines the Model 2000 cask shielding analysis and demonstrates compliance with the external radiation requirements of 10 CFR 71, "Packaging and Transportation of Radioactive Material" (Reference 5-1). This shielding evaluation was performed to demonstrate that the Model 2000 Transport Package with the high performance insert (HPI) provides sufficient shielding such that the external radiation limits are satisfied under Normal Conditions of Transport (NCT) and Hypothetical Accident Conditions (HAC).

### 5.1 Description of Shielding Design

#### 5.1.1. Design Features

The Model 2000 cask is a cylindrical lead lined cask used for transporting Type B quantities of radioactive materials and solid fissile materials. For any shipments of radioactive material in the Model 2000 cask, the use of the HPI is required, and all contents must be confined inside the HPI cavity. The radiation shielding design features of the Model 2000 with the HPI are the lead and Stainless Steel (SS) in the Model 2000 cask and the depleted uranium (DU) and SS in the HPI. Narrative descriptions of the HPI, Model 2000 cask, and Model 2000 overpack are provided in Section 1.2. The radiation shielding design features of the Model 2000 with the HPI are provided in Table 5.1-1, including nominal dimensions, materials of construction, and densities of the materials that provide gamma shielding.

**Table 5.1-1. Model 2000 Transport Package Shielding Design Features**

Model 2000 Component	Part	Component	Thickness (in)	Thickness (cm)	Material of Construction	Material Density (lb/in <sup>3</sup> )	Material Density (g/cm <sup>3</sup> )
HPI	Top Plug	Inner Shell	[[		[[ ]]	0.29	8.000
		DU			DU	[[	]]
		Outer Shell			[[ ]]	0.29	8.000
	HPI Body	Inner Shell			[[ ]]	0.29	8.000
		DU			DU	[[	]]
		Outer Shell			[[	0.29	8.000
	Bottom Plug	Inner Shell			]]	0.29	8.000
		DU			DU	[[	]]
		Outer Shell		]]	[[ ]]	0.29	8.000
Cask	Cask Lid	Lid Flange	1.75	4.445	SS304	0.29	8.000
		Lead	5.37	13.64	Lead	0.41	11.34
		Inner Plate	1.50	3.810	SS304	0.29	8.000
	Cask Body (Side)	Cavity Shell	1.00	2.540	SS304	0.29	8.000
		Lead	4.00	10.16	Lead	0.41	11.34
		Cask Shell	1.00	2.540	SS304	0.29	8.000

NEDO-33866 Revision 6  
Non-Proprietary Information

Model 2000 Component	Part	Component	Thickness (in)	Thickness (cm)	Material of Construction	Material Density (lb/in <sup>3</sup> )	Material Density (g/cm <sup>3</sup> )
	Cask Body (Bottom)	Cask Bottom <sup>a</sup>	5.88	14.92	SS304	0.29	8.000
Overpack <sup>b</sup>	Overpack (Top)	Top Plate	0.50	1.270	SS304	0.29	8.000
		End Plate	0.50	1.270	SS304	0.29	8.000
	Overpack (Side)	Inner Shell	0.50	1.270	SS304	0.29	8.000
		Outer Shell	0.50	1.270	SS304	0.29	8.000
	Overpack (Bottom)	Support Plate	0.50	1.270	SS304	0.29	8.000
		Bottom Plate	0.50	1.270	SS304	0.29	8.000
		End Plate	0.50	1.270	SS304	0.29	8.000

Notes: <sup>a</sup> Due to the minimum thickness is used.

<sup>b</sup> Credit for shielding provided by the cask overpack is only taken for NCT analyses.

General: All dimensions are based on component licensing drawings in Section 1.3.1.

### 5.1.2. Summary Table of Maximum Radiation Levels

Table 5.1-2 and Table 5.1-3 present the maximum calculated NCT and HAC dose rates at the appropriate locations for exclusive use shipment of the Model 2000 Transport Package with the HPI. The calculated NCT and HAC dose rates are reported for each of the three content types described in Section 5.2, as well as the overall maximum dose rates from all contents. The 1-meter transportation index dose rate limits are not applicable as the Model 2000 cask will only be shipped as exclusive use. The Model 2000 cask will only be shipped in the upright position, thus the 2-meter and occupied position (cab) dose rates are calculated at the appropriate distances from the side of the cask. Dose rates are limited to 90% of the regulatory limit at each location to provide additional assurance that any small uncertainties in the source term or cask modeling will not result in external dose rates exceeding the respective regulatory limit.

**Table 5.1-2. Maximum NCT Dose Rates**

Contents	Radiation	Package Surface mSv/hr (mrem/hr)			2-meter mSv/hr (mrem/hr)	Cab mSv/hr (mrem/hr)
		Top	Side	Bottom	Side	Side
1	Gamma + Neutron	0.3141 (31.41)	1.8000 (180.00)	1.0677 (106.77)	0.0434 (4.34)	0.0078 (0.78)
2	Gamma	0.1026 (10.26)	1.7999 (179.99)	0.1651 (16.51)	0.0251 (2.51)	0.0044 (0.44)
3	Gamma	0.1799 (17.99)	0.8578 (85.78)	0.3832 (38.32)	0.0162 (1.62)	0.0028 (0.28)
Overall Maximum		0.3141 (31.41)	1.8000 (180.00)	1.0677 (106.77)	0.0434 (4.34)	0.0078 (0.78)
10 CFR 71.47(b) Limits		2 (200)	2 (200)	2 (200)	0.1 (10)	0.02 (2)

Contents:

- 1 – Irradiated fuel
- 2 – Irradiated hardware and byproducts
- 3 – Cobalt-60 isotope rods

**Table 5.1-3. Maximum HAC Dose Rates**

Contents	HAC	1 Meter from Package Surface mSv/hr (mrem/hr)		
	Radiation	Top	Side	Bottom
1	Gamma + Neutron	0.3342 (33.42)	0.5363 (53.63)	0.3112 (31.12)
2	Gamma	0.1335 (13.35)	0.3421 (34.21)	0.0841 (8.41)
3	Gamma	0.5843 (58.43)	1.6951 (169.51)	0.3454 (34.54)
Overall Maximum		0.5843 (58.43)	1.6951 (169.51)	0.3454(34.54)
10 CFR 71.51(a)(2) Limit		10 (1000)	10 (1000)	10 (1000)

Contents:

- 1 – Irradiated fuel
- 2 – Irradiated hardware and byproducts
- 3 – Cobalt-60 isotope rods

## 5.2 Source Specification

The allowable contents for the Model 2000 cask are: 1) irradiated fuel, 2) irradiated hardware and byproducts and 3) cobalt-60 isotope rods. The irradiated fuel contents have photon and neutron source terms for determining package external dose rates. The irradiated hardware and byproduct and cobalt-60 isotope rod contents have photon source terms for determining package external dose rates. Due to the thick layers of shielding provided by the HPI and Model 2000 cask, external dose rate contributions from charged particles (alpha and beta particles) and their secondary particles from interactions (e.g., bremsstrahlung) are negligible. The exception to the above statement is that the neutron source from alpha-n reactions in the irradiated fuel contents is considered, as explained in Section 5.5.1.

### Irradiated Fuel

The irradiated fuel content is GE BWR 10x10 fuel, which is segmented and placed into the HPI. The required parameters for the irradiated fuel that are relevant to the shielding analysis include:

1. Cooling time: Minimum of at least 120 days.
2. Length: Minimum active fuel length of at least 5.3 inches for each segment.
3. Arrangement: Confined and placed into the HPI material basket in the upright position with or without additional shoring component that ensures the fuel remain upright.
4. Initial enrichment U-235: Minimum of 1.5 wt%, maximum of 5 wt%.
5. Fuel exposure: Maximum of 72 GWd/MTU.
6. If the irradiated fuel is encapsulated (e.g., in cladding), the encapsulation material is treated as irradiated hardware and must be composed of an approved irradiated hardware material as described in the next paragraphs.

## **Irradiated Hardware and Byproducts**

The irradiated hardware and byproduct contents are irradiated components from typical reactor operation. These contents include:

1. Hardware: Irradiated components composed of metallic alloys (e.g., SS, carbon steels, FeCrAl, nickel alloys, and zirconium alloys). Examples include:
  - Bundle components: fuel cladding, water rods, spacers, and upper/lower tie plates
  - Reactor internals: jet pump components, core shroud samples
2. Irradiated Byproducts: Irradiated control rod blades with the following neutron poison materials:
  - Hafnium
  - Boron Carbide

## **Cobalt-60 Isotope Rods**

The radioactive material in the cobalt-60 isotope rod contents is in the form of pellets or cylindrical solid rods with the source(s) evenly distributed and encapsulated in normal or special form. The isotope rods are loaded into a commercial or research reactor to irradiate the cobalt source pellets. After discharge from the reactor, the isotope rods are loaded into the Model 2000 cask for transport. These [[ ]] prior to loading into the HPI. Herein for the cobalt-60 isotope rod contents, the term 'rod' refers to a full-length rod, in its form as it is irradiated in a reactor; and the term [[ ]] in its form as it is loaded and shipped in the Model 2000 Transport Package.

### **5.2.1. Gamma Source**

#### **5.2.1.1. Irradiated Fuel**

To calculate gamma source strengths, ORIGIN-ARP is used, which implements the ORIGIN-S module with the GE BWR 10x10 cross section library (ge10x10-8) distributed in the SCALE6.1 code package (Reference 5-2). With the ORIGIN-ARP methodology, a problem dependent cross section library is generated by interpolating between cross sections in the SCALE6.1 pre-generated libraries. The pre-generated GE BWR 10x10 library covers initial uranium enrichments from 1.5 to 6 wt%, with burnups from 0 to 72 GWd/MTU, and moderator densities from 0.1 to 0.9 g/cm<sup>3</sup>. Any mention of enrichment refers to the initial U-235 enrichment of the fuel. ORIGIN-ARP has been validated extensively for light water reactor spent fuel, as documented in the Oak Ridge National Lab report ORNL/TM-13584 (Reference 5-9).

The [[ ]] irradiated fuel contents is based on the radionuclide inventory generated from the irradiation and decay of various nuclides over time. The gamma source strength is dependent on the enrichment (E) band and burnup (B) band. In the ORIGIN-S source term analysis, for each initial enrichment band the minimum enrichment is considered, and for each burnup band the maximum burnup is considered. This generates a bounding source strength for each burnup-enrichment pairing. For the calculated source strength for each burnup-enrichment pairing the basis is 1 gram of U-235.

The dose rate contribution from a given fuel segment at a regulatory dose rate location is calculated by multiplying the burnup- and enrichment-dependent dose rate per gram of initial U-235 by the initial U-235 mass of that fuel segment. The total dose rate from a payload of irradiated fuel is calculated by summing the dose rate contributions from each fuel segment included in the shipment. The burnup- and enrichment-dependent dose rate per gram of initial U-235 includes contributions from both gamma rays and neutrons. Details of the parameters used for the ORIGEN-S neutron and photon irradiated fuel source term calculations are provided in Section 5.5.1.

#### **5.2.1.2. Irradiated Hardware and Byproducts**

For the irradiated hardware and byproduct contents, the gamma source strength and spectra are based on the individual radionuclides in a given shipment. Multiple ORIGEN-S irradiation calculations were used to identify the radionuclides that could be in a shipment of irradiated hardware and byproduct. Table 5.2-1 provides a list of radionuclides that may be present in irradiated hardware and byproduct contents that contribute to external dose rates. Other radionuclides which may be present in irradiated hardware and byproducts but do not emit significant gammas were excluded from Table 5.2-1. However, all radionuclides that may be present in irradiated hardware and byproducts are considered when determining the total decay heat of the payload as described in Section 5.5.4.

External dose rates are calculated individually for 1 Ci of activity with the energy spectrum from each of the listed radionuclides. The energy spectrum for each radionuclide is from the ORIGEN-S Data Library `origen.rev04.mpdkgam.data` (Reference 5-2). The dose rate contribution from a specific radionuclide at a regulatory dose rate location is calculated by multiplying the total activity for the radionuclide by its respective dose rate per curie multiplier. The total dose rate from a payload of irradiated hardware and byproduct is calculated by summing the dose rate contributions from each radionuclide included in the shipment. Details of the ORIGEN-S irradiated hardware and byproduct source term calculations and the energy spectra for each radionuclide of interest are provided in Section 5.5.2.

**Table 5.2-1. Irradiated Hardware and Byproduct Radionuclides Significant to External Dose Rates**

Radionuclides
Sc-46
Cr-51
Mn-54
Co-58
Fe-59
Co-60
Zn-65
Nb-92m
Nb-94
Zr/Nb-95
Sb-124
Sb-125
Sb-126
Cs-134
Cs-137 (Ba-137m)
Hf-175
Hf-181
Ta-182

#### 5.2.1.3. Cobalt-60 Isotope Rods

The primary gamma source in the cobalt-60 isotope rod content is from the cobalt-60 source pellets. Dose rate contributions from the small quantities of radionuclides in crud that has built up on the rods while in the reactor is negligible due to insignificant gammas emitted. The cask external dose rates are dominated by the quantity of cobalt-60 in the isotope rods, and any dose rate contributions from any radionuclides in the rod cladding can be accounted for as irradiated hardware (see Section 5.4.4.4 for further explanation). Table 5.2-2 provides the energy spectrum and gamma source strength for cobalt-60 used for dose rate calculations. The energy spectrum is from the ORIGEN-S data library `origen.rev04.mpdkgam.data` (Reference 5-2). All energy lines less than 0.1 MeV are considered negligible and are neglected from the energy spectrum. The source strength is based on the cobalt-60 activity equivalent to the thermal limit of 1500 W. The watt/curie (W/Ci) conversion factor is based on the ORIGEN-S decay library `origen.rev03.decay.data` (Reference 5-2). The values from this library and the calculation of a W/Ci conversion factor for multiple radionuclides are presented in Section 5.5.3. Using the W/Ci conversion factor presented in Section 5.5.4, the equivalent activity for 1500 W is 97,250 Ci of cobalt-60.



**Table 5.2-2. Isotope Rod Source Term (97,250 Ci Cobalt-60)**

Energy (MeV)	Relative Intensity	Source Strength (γ/sec)
0.347	7.500E-05	2.699E+11
0.826	7.600E-05	2.735E+11
1.173	9.985E-01	3.593E+15
1.333	9.998E-01	3.598E+15
2.159	1.200E-05	4.318E+10
2.506	2.000E-08	7.197E+07
<b>Total</b>	1.998E+00	7.191E+15

## **5.2.2. Neutron Source**

### **5.2.2.1. Irradiated Fuel**

The neutron source strengths for the irradiated fuel contents are calculated with the same method as the gamma source term. The ORIGEN-S source term calculations detailed in Section 5.5.1 generate both the gamma and neutron source terms for the irradiated fuel contents.

In Section 5.2.1.1 it was described how the neutron contribution is already included in the total dose rate per gram of initial U-235.

### **5.2.2.2. Irradiated Hardware and Byproducts / Cobalt-60 Isotope Rods**

There is no applicable neutron source term for the irradiated hardware and byproduct or cobalt-60 isotope rod contents.

## **5.3 Shielding Model**

### **5.3.1. Configuration of Source and Shielding**

The following subsections describe the shielding model geometry and source configuration for the dose rate calculations of each of the described content types of the Model 2000 cask.

#### **5.3.1.1. Source Distribution**

An individual source geometry is used in the shielding model for each of the Model 2000 cask contents. The source geometry for each content type is based on the respective content specifications and the source term calculation.

#### **Irradiated Fuel**

Similar to the cobalt-60 isotope rods, the NCT irradiated fuel content source geometry is modeled as a single 5.3-inch line source to represent the entire irradiated fuel content. Within this single 5.3-inch line source the entire irradiated fuel photon and neutron sources are uniformly distributed. The irradiated fuel source term specification requires that the active fuel length when loaded into the Model 2000 Transport Package must be greater than or equal to 5.3 inches. Using the minimum allowable segment length for the line source ensures a bounding dose rate calculation, as greater

distribution of the source activity (e.g., a longer line source) results in lower calculated maximum external dose rates.

The axial distribution of activity along the irradiated fuel is a function of different initial U-235 enrichment axially and variations in moderator density during irradiation. The bounding gamma and neutron source strength considered for any given segment is based on the minimum enrichment and maximum burnup in the segment. During the irradiation of the fuel, lower moderator densities results in higher source strengths (Reference 5-10). By calculating all gamma and neutron source strengths at the minimum moderator density ( $0.1 \text{ g/cm}^3$ ) available in the library, the calculated source strengths are bounding for any expected changes in axial moderator density. Thus, a single uniform line source is acceptable to represent the entire irradiated fuel content despite variations in the irradiated fuel activity profile because the source term calculation results in bounding gamma and neutron source strengths.

For the HAC shielding model source geometry, it is conservative to assume that the entire irradiated fuel content is concentrated into a single point. The source locations for the NCT model line source and the HAC model point source are in the locations shown in Figure 5.3-1. See Section 5.4.4.1 for how the external dose rates are determined for irradiated fuel.

### **Irradiated Hardware and Byproducts**

Due to the uncertainty in the form and activity distribution of irradiated hardware or byproduct contents, both the NCT and HAC shielding models conservatively assume that all the activity is concentrated into a single point. Therefore, the use of the HPI material basket is not required for irradiated hardware and byproduct shipments. However, use of the HPI material basket for shipments of irradiated hardware and byproducts is optionally allowable because the material basket 12-inch line source is bounded by the shielding results obtained from the point source model, as long as all dose rates and thermal limits are satisfied. The source locations of the point sources in the shielding models for the irradiated hardware and byproduct dose rate calculations are shown in Figure 5.3-1.

### **Cobalt-60 Isotope Rods**

For the cobalt-60 isotope rod content, the NCT source geometry is a single 12-inch line source, across which the photon source activity is distributed uniformly. There is variation in the distribution of cobalt-60 activity in the HPI cavity with a shipment of cobalt-60 isotope [[ ]] and loading of the rods into the HPI. Section 5.5.3 provides a discussion of the distribution of activity in the HPI cavity for the cobalt-60 isotope rod contents, and the basis for a 12-inch line source for NCT dose rate calculations.

For the HAC shielding model source geometry, the structural components in the cask cavity were conservatively assumed to fail. Therefore, all source activity was concentrated into a single point. The source locations for the NCT model 12-inch line source and the HAC model point source are shown in Figure 5.3-1. The 12-inch line source modeling limitation imposed during the NCT evaluations requires that the HPI material basket be present for cobalt-60 isotope rod shipments.

### 5.3.1.2. Source Locations

The sources for the dose rate calculations are modeled in the HPI cavity in the position that results in the highest dose rate for the respective regulatory dose rate location. This limiting source position changes based on the geometry of the source and the direction of interest. Figure 5.3-1 provides two depictions of the Model 2000 cask with the HPI. This figure shows the positions for any point or line sources in the HPI cavity for all dose rate calculations.

The source positions for side dose rate locations are located at the bottom corner of the HPI cavity, at the interface of the HPI body and the HPI bottom plug. This is the most restrictive location for side dose rates because in this area the [[ ]], due to the step at this interface. For the HAC side 1-meter dose rate, the calculated dose rate is higher with a point source in the bottom corner than in the top corner of the HPI cavity, despite the slump in the lead column.

The line source positions for top and bottom dose rate locations are centered in the HPI cavity so that particles emitted at any location along the line source can travel at any angle in the direction of interest, unimpeded before entering the respective plug (top or bottom). For a line source pushed to the side against the HPI body, there is a reduction in the calculated dose rates for the top and bottom.

[[

]]

**Figure 5.3-1. Point / Line Source Locations**

### 5.3.1.3. NCT Shielding Model Geometry

The NCT model geometry used for the dose rate calculations in this shielding analysis is a detailed three-dimensional model of the HPI, the Model 2000 cask, and the overpack. Table 5.3-1 provides the relevant dimensions of the shielding model including the modeled thicknesses of each material. This table along with Table 5.1-1 allow for a quick review of the most significant dimensions of the shielding model geometry. All HPI shield dimensions are at the minimum (except cavity radius which is nominal), per the respective licensing drawings, with the fabrication tolerances subtracted from the nominal values. The model dimensions for the Model 2000 cask and overpack use predominantly nominal dimensions with some areas of reduced thickness. For example, for the [[ ]], the cask bottom is considered to be flat at the minimum thickness. The majority of the material thicknesses prescribed by the Model 2000 cask and overpack licensing drawings have tolerances based on American Society for Testing and Materials (ASTM) specifications, as the component dimensions are based on ASTM SS stock plate. Per ASTM A480 (Reference 5-3), for plates up to 10 inches in thickness, the tolerance under the specified thickness is 0.01 inches. These plate thicknesses are modeled at the specified nominal plate value.

**Table 5.3-1. Relevant Shielding Model Dimensions**

Model 2000 Component	Part	Parameter	Dimension (cm)	Dimension (in)
Cask	Cask Lid	Lid Flange ( $t_{SS1}$ )	3.810	1.500
		Lead ( $t_{pb}$ )	13.64	5.370
		Inner Plate ( $t_{SS2}$ )	4.445	1.750
	Cask Side	Cavity Radius ( $r_{cavity}$ )	33.66	13.25
		Cavity Shell	2.540	1.000
		Lead ( $t_{pb}$ )	10.16	4.000
		Cask Shell ( $t_{SS2}$ )	2.540	1.000
		Lead ( $h_{pb}^c$ )	141.9	55.87
	Cask Bottom	Cask Bottom ( $t_{SS}$ )	14.94 <sup>a</sup>	5.880 <sup>a</sup>
		Cavity Height ( $h_{cavity}$ )	137.5	54.13
HPI	HPI Top Plug	Inner Shell ( $t_{SS1}$ )	[[	
		DU ( $t_{DU}$ )		
		Outer Shell ( $t_{SS2}$ )		
	HPI Body Side	Cavity Radius ( $r_{cavity}$ )		
		Inner Shell ( $t_{SS1}$ )		
		DU ( $t_{DU}$ )		
		Outer Shell ( $t_{SS2}$ )		
	HPI Bottom Plug	Inner Shell ( $t_{SS1}$ )		
		DU ( $t_{DU}$ )		
		Outer Shell ( $t_{SS2}$ )		]]
Overpack	Top	Top Plate ( $t_{SS1}$ )	1.270	0.500
		End Plate ( $t_{SS2}$ )	1.270	0.500
	Side	Inner Shell ( $t_{SS1}$ )	1.270	0.500
		Outer Shell ( $t_{SS2}$ )	1.270	0.500
	Bottom	Support Plate ( $t_{SS1}$ )	1.270	0.500
		Bottom Plate ( $t_{SS2}$ )	1.270	0.500
		End Plate ( $t_{SS3}$ )	1.270	0.500

Notes: <sup>a</sup> Cask Bottom modeled flat, with thickness equal to the 6.13" height [[ ]]  
<sup>b</sup> Minimum DU thicknesses considered with tolerance gaps explicitly modeled  
<sup>c</sup> Lead column height  
<sup>d</sup> Nominal value

There are two different NCT shielding models. One is for photon dose rate calculations and the other is for neutron dose rate calculations. For both models the geometry is the same. However, for the photon dose rate model the materials for the HPI, cask, and overpack are defined as prescribed in Section 5.3.2. For the neutron dose rate NCT model, all shielding provided by the materials of the packaging are neglected. Taking no credit for shielding of neutrons provided by the HPI, the Model 2000 cask, and the Model 2000 overpack results in bounding calculated dose rates. The dose rates calculated through void bound the dose rates calculated by crediting the shielding provided by all cask components, any additional neutrons from subcritical multiplication, and the additional (secondary) photons from neutron interactions in the cask. The NCT shielding models are shown in Figure 5.3-2. The materials for the HPI, cask, and overpack are defined as prescribed in Section 5.3.2.

[[

]]

**Figure 5.3-2. NCT Shielding Models**

The photon NCT model conservatively neglects the additional shielding provided by the HPI material basket and rod holders for irradiated fuel and the cobalt-60 isotope rod contents. Due to the use of vertical line sources, these contents must be shipped in the upright position. The HPI material basket may be used to position these contents in the upright position. The material basket is not required for shipments of irradiated hardware and byproducts because a point source was used for the shielding analysis.

#### **5.3.1.4. HAC Shielding Model Geometry**

For HAC, the shielding model only includes the HPI and the Model 2000 cask, with dimensions as prescribed in Table 5.3-1. This model conservatively assumes the removal of the overpack. The HAC model also includes the slump in the lead column of the Model 2000 cask body. In Section 2.12.2, the maximum deformation in the lead column is calculated to be 3.56 mm. This value is rounded up to 4 mm for this analysis. It is determined in Chapter 2 that the overpack provides adequate protection from HAC to the cask body. More specifically, in Section 2.12.1 it is stated that when the cask is dropped 30 feet followed by a drop of 40 inches onto a rigid pin 6 inches in diameter, no gross deformations of the cask are predicted. As with the NCT models, there are two different HAC shielding models, as show in Figure 5.3-3. These models have the same geometry but the photon model includes the materials of the HPI and the Model 2000 cask, and the neutron model neglects all materials.

[[

]]

**Figure 5.3-3. HAC Shielding Models**

#### **5.3.1.5. MCNP6 Tallies**

To calculate the particle flux at the regulatory dose rate locations of interest, multiple arrangements of cell tallies are modeled at each location. The void cells that are added to the model for particle tallying allow for dose rates to be calculated at the multiple locations of interest, without having an effect on the calculated flux. All of the tally cells are modeled as small 1 cm thick volumes, to ensure that the calculated flux is not averaged over too large of a region.

Figures 5.3-4 and 5.3-5 provide depictions of the tally cells used in the MCNP6 shielding models, with the tally cells highlighted in yellow.

[[

]]

**Figure 5.3-4. NCT MCNP6 Tallies with 10% Margin to the Regulatory Limit**



[[

]]

**Figure 5.3-5. HAC MCNP6 Tallies with 10% Margin to the Regulatory Limit**

### **5.3.2. Material Properties**

The material compositions used for photon dose rate calculations are listed in Tables 5.3-2 through 5.3-5. There is negligible difference between the two types of SS in terms of shielding effectiveness. However, both types are included for accuracy to the actual materials of construction. The densities and material compositions for both stainless steel types are from Pacific Northwest National Lab (PNNL) report PNNL-15870 Revision 1 (Reference 5-4). The densities of the lead and DU materials are based on the minimum specified densities for these materials in the respective component licensing drawings in Section 1.3.1. All materials are modeled as void for neutron dose rate calculations, so the isotopic composition of materials is not required.

**Table 5.3-2. Type 304 Stainless Steel Material Composition**

Elemental Composition	Element	ZAID	Mass Fraction
	C	6000	4.00E-04
	Si	14000	5.00E-03
	P	15000	2.30E-04
	S	16000	1.50E-04
	Cr	24000	1.90E-01
	Mn	25000	1.00E-02
	Fe	26000	7.02E-01
	Ni	28000	9.25E-02
Density (g/cm <sup>3</sup> )	8.0		

**Table 5.3-3. [[ ]] Material Composition**

Elemental Composition	Element	ZAID	Mass Fraction
	C	6000	4.10E-04
	Si	14000	5.07E-03
	P	15000	2.30E-04
	S	16000	1.50E-04
	Cr	24000	1.70E-01
	Mn	25000	1.01E-02
	Fe	26000	6.69E-01
	Ni	28000	1.20E-01
	Mo	42000	2.50E-02
Density (g/cm <sup>3</sup> )	8.0		

**Table 5.3-4. Lead Material Composition**

Elemental Composition	Element	ZAID	Mass Fraction
	Pb	82000	1.00E+00
Density (g/cm <sup>3</sup> )	11.34		

**Table 5.3-5. Depleted Uranium Material Composition**

Elemental Composition	Element	ZAID	Mass Fraction
	U	92000	1.00E+00
Density (g/cm <sup>3</sup> )	[[ ]]		

## 5.4 Shielding Evaluation

### 5.4.1. Methods

#### 5.4.1.1. Computer Codes

The shielding calculations for this analysis were completed using MCNP6 Version 1.0 (Reference 5-5) for the irradiated hardware and byproducts and cobalt-60 isotope rod contents, and MCNP6 Version 2.0 (Reference 5-11) for the irradiated fuel content. MCNP6 is a general-purpose, continuous-energy, generalized-geometry, time-dependent, coupled neutron/photon/electron Monte Carlo transport code. MCNP6 was used in the photon only transport mode to calculate external dose rates for the Model 2000 cask for each of the content types considered. Photon dose rate calculations used the MCNP6 photoatomic data library MCPLIB84, which compiles data from the ENDF/B-VI.8 data library (Reference 5-6).

The neutron models are voided and unshielded; therefore, MCNP6 is not needed. The neutron flux around a point or line source in a vacuum can be calculated analytically.

#### 5.4.1.2. MCNP6 Variance Reduction

Due to the thick layers of photon shielding provided by the Model 2000 cask and the HPI, multiple variance reduction techniques are used for the MCNP6 photon dose rate calculations. MCNP6 variance reduction parameters for weight windows, exponential transform, and source biasing were used as necessary to aid in the statistical convergence of the photon dose rate calculations.

#### 5.4.1.3. Irradiated Fuel Dose Rate Calculation

The flux,  $\phi(r, p, e)$ , at regulatory dose rate location of interest,  $r$ , is calculated for a photon or neutron particle,  $p$ . It is dependent on the spectrum  $[[$   $\phi(r, p, e)$   $]]$  and is normalized by its source strength  $[[$   $S$   $]]$ . The photon flux is calculated in MCNP6 and the neutron flux is calculated analytically using Equation 5-1 for a point source and Equation 5-2 for a line source. Note that the source strengths in these equations are normalized to one.

$$\phi(r, p, e) = \frac{1}{4\pi r^2} \quad (5-1)$$

$$\phi(r, p, e) = \frac{1}{4\pi x(l_1 + l_2)} \left[ \tan^{-1} \frac{l_1}{x} + \tan^{-1} \frac{l_2}{x} \right] \quad (5-2)$$

By applying the appropriate flux-to-dose-rate conversion factors (Section 5.4.3),  $\mathcal{R}(p, e)[[$   $\phi(r, p, e)$   $]]$  the dose rate response,  $R(r, p, e)$ , and associated standard deviation,  $\sigma_R(r, p, e)$ , are calculated following Equations 5-3 and 5-4.

$$R(r, p, e) \left[ \frac{\text{mrem}}{\text{hr}} \cdot \frac{\text{sec}}{\text{emitted } p} \right] = \phi(r, p, e) \left[ \frac{\frac{p}{\text{cm}^2}}{\text{emitted } p} \right] \cdot \mathcal{R}(p, e) \left[ \frac{\frac{\text{mrem}}{\text{hr}}}{\frac{p}{\text{cm}^2 \cdot \text{sec}}} \right] \quad (5-3)$$

$$\sigma_R(r, p, e) = R(r, p, e) \cdot \text{fsd}(r, p, e) \quad (5-4)$$

The quantity  $R_{\sigma}(r, p, e)$  accounts for the statistical uncertainty. Two standard deviations are added to the calculated dose rate response in Equation 5-5. Note that there is no statistical uncertainty associated with the neutron flux calculation because it was calculated analytically ( $\sigma_R = 0$ ).

$$R_{\sigma}(r, p, e) \left[ \frac{\text{mrem}}{\text{hr}} \cdot \frac{\text{sec}}{\text{emitted p}} \right] = (R(r, p, e) + 2 \cdot \sigma_R(r, p, e)) \left[ \frac{\text{mrem}}{\text{hr}} \cdot \frac{\text{sec}}{\text{emitted p}} \right] \quad (5-5)$$

Equation 5-6 shows that  $\dot{D}R(r, B|E)$  is the dose rate per gram of U-235 at a regulatory dose rate location of interest,  $r$ , at the specific burnup and enrichment band,  $B|E$ , and is calculated [[

]] with the ORIGEN-S calculated source strength,

[[

]] and is calculated per gram of U-235.

[[

]]

The total dose rate,  $DR(r, B|E)$ , at a given burnup and enrichment is determined by multiplying Equation 5-6 with the mass of U-235 in the irradiated fuel content at the respective burnup and enrichment,  $m(B|E)$ , as shown in Equation 5-7.

$$DR(r, B|E) \left[ \frac{\text{mrem}}{\text{hr}} \right] = \dot{D}R(r, B|E) \left[ \frac{\text{mrem}}{\text{hr}} \cdot \frac{\text{sec}}{\text{gU235}} \right] \cdot m(B|E) [\text{gU235}] \quad (5-7)$$

where

$\phi$	Calculated flux (MCNP6 or analytical)	$r$	Regulatory dose rate location/distance
$p$	Particle (neutron or gamma)	[[	]]
$x$	Perpendicular distance of $r$ from line source	$l_1, l_2$	Partial length of line source on either side of perpendicular line $x$
$R$	Calculated dose rate response	$\sigma$	Standard deviation
$\mathcal{R}$	Flux-to-dose-rate conversion factor	$R_{\sigma}$	Dose rate response with $2\sigma$ uncertainty
$fsd$	MCNP6 fractional standard deviation	$S$	Calculated source strength (ORIGEN-S)
$\dot{D}R$	Dose rate per gram U-235	$DR$	Total dose rate
$B E$	Burnup/Enrichment pairing		
$m$	Mass of U-235		

#### 5.4.1.4. Irradiated Hardware, Byproduct, and Cobalt-60 Isotope Rod Dose Rate Calculation

To calculate a dose rate response  $R(r, X)$  for an individual radionuclide  $X$ , the MCNP6 calculated photon flux  $\phi(r, X)$  is multiplied by the dose rate conversion factor  $\mathcal{R}$  as well as a per-curie multiplier and the total number of gammas per decay of the respective radionuclide  $I(X)$ .

$$R(r, X) \left[ \frac{\text{mrem}}{\text{hr}} \right] = \phi(r, X) \left[ \frac{\gamma}{\text{cm}^2} \right] \cdot 3.7 \times 10^{10} \left[ \frac{\text{decays}}{\text{sec}} \right] \cdot I(X) \left[ \frac{\text{emitted } \gamma}{\text{decay}} \right] \cdot \mathcal{R} \left[ \frac{\text{mrem}}{\text{cm}^2 \cdot \text{sec}} \right] \quad (5-8)$$

$$\sigma_R(r, X) = R(r, X) \cdot \text{fsd}(r, X) \quad (5-9)$$

To account for statistical uncertainty, the two standard deviations are added to the calculated MCNP6 dose rate per curie:

$$R_\sigma(r, X) \left[ \frac{\text{mrem}}{\text{hr}} \right] = (R(r, X) + 2 \cdot \sigma_R(r, X)) \left[ \frac{\text{mrem}}{\text{hr}} \right] \quad (5-10)$$

The total dose rate  $DR(r)$  is calculated by summing the dose rate from the activity of each radionuclide:

$$DR(r) \left[ \frac{\text{mrem}}{\text{hr}} \right] = \sum_X R_\sigma(r, X) \left[ \frac{\text{mrem}}{\text{hr}} \right] \cdot A(X) [\text{Ci}] \quad (5-11)$$

where

R	MCNP6 dose rate per curie	$\sigma$	Standard deviation
r	Regulatory dose rate location	fsd	MCNP6 fractional standard deviation
X	Radionuclide X	$R_\sigma$	Dose rate per curie with $2\sigma$ uncertainty
$\phi$	MCNP6 calculated flux	DR	Total dose rate
I	gammas/decay	A	Activity
$\mathcal{R}$	Flux-to-dose-rate conversion factor		

### 5.4.2. Input and Output Data

#### 5.4.2.1. Input Data

Input data will be submitted separately.

#### 5.4.2.2. Output Data

Output data will be submitted separately. The tally fluctuation chart and probability density function plot were studied for each MCNP6 tally to ensure proper tally bin convergence. This along with a check of the reported fsd for each tally bin and the additional statistical information reported for MCNP6 tallies ensured the reliability of all MCNP6 calculated dose rate results.

### 5.4.3. Flux-to-Dose-Rate Conversion

Consistent with NUREG-1609 Section 5.5.4.3 (Reference 5-7), the ANSI/ANS-6.1.1 1977 flux-to-dose-rate conversion factors (Reference 5-8) are used. The gamma and neutron conversion factors used are tabulated in Tables 5.4-1 and 5.4-2, respectively.

**Table 5.4-1. Gamma Flux-to-Dose-Rate Conversion Factors (ANSI/ANS-6.1.1 1977)**

<b>Gamma Energy (MeV)</b>	<b>Conversion Factor (mrem/hr)/(gammas/cm<sup>2</sup>-s)</b>
1.00E-02	3.96E-03
3.00E-02	5.82E-04
5.00E-02	2.90E-04
7.00E-02	2.58E-04
1.00E-01	2.83E-04
1.50E-01	3.79E-04
2.00E-01	5.01E-04
2.50E-01	6.31E-04
3.00E-01	7.59E-04
3.50E-01	8.78E-04
4.00E-01	9.85E-04
4.50E-01	1.08E-03
5.00E-01	1.17E-03
5.50E-01	1.27E-03
6.00E-01	1.36E-03
6.50E-01	1.44E-03
7.00E-01	1.52E-03
8.00E-01	1.68E-03
1.00E+00	1.98E-03
1.40E+00	2.51E-03
1.80E+00	2.99E-03
2.20E+00	3.42E-03
2.60E+00	3.82E-03
2.80E+00	4.01E-03
3.25E+00	4.41E-03
3.75E+00	4.83E-03
4.25E+00	5.23E-03
4.75E+00	5.60E-03
5.00E+00	5.80E-03
5.25E+00	6.01E-03
5.75E+00	6.37E-03
6.25E+00	6.74E-03
6.75E+00	7.11E-03
7.50E+00	7.66E-03
9.00E+00	8.77E-03
1.10E+01	1.03E-02
1.30E+01	1.18E-02
1.50E+01	1.33E-02

**Table 5.4-2. Neutron Flux-to-Dose-Rate Conversion Factors (ANSI/ANS-6.1.1 1977)**

Neutron Energy (MeV)	Conversion Factor (mrem/hr)/(neutrons/cm <sup>2</sup> -s)
2.50E-08	3.67E-03
1.00E-07	3.67E-03
1.00E-06	4.46E-03
1.00E-05	4.54E-03
1.00E-04	4.18E-03
1.00E-03	3.76E-03
1.00E-02	3.56E-03
1.00E-01	2.17E-02
5.00E-01	9.26E-02
1.00E+00	1.32E-01
2.50E+00	1.25E-01
5.00E+00	1.56E-01
7.00E+00	1.47E-01
1.00E+01	1.47E-01
1.40E+01	2.08E-01
2.00E+01	2.27E-01

#### 5.4.4. External Radiation Levels

The maximum external radiation levels are determined individually for each of the three content types. The limiting dose rate location for all content types is the NCT side package surface. That is, for each of the three contents, the maximum allowable quantity of material based on external radiation levels is limited by the NCT side surface dose rate. The external radiation levels resulting from each of the three content types are summarized below.

##### 5.4.4.1. Irradiated Fuel

For the irradiated fuel contents, the resulting external dose rates are calculated in two steps. First a dose rate  $\left[ \frac{\text{mrem/hr}}{\text{g U-235}} \right]$  is calculated in MCNP6 for photons and analytically for neutrons.  $\left[ \frac{\text{mrem/hr}}{\text{g U-235}} \right]$

$\left[ \frac{\text{mrem/hr}}{\text{g U-235}} \right]$  The ORIGEN-S source  $\left[ \frac{\text{mrem/hr}}{\text{g U-235}} \right]$  that leads to the maximum dose rate is always used  $\left[ \frac{\text{mrem/hr}}{\text{g U-235}} \right]$  The statistical uncertainty associated with the Monte Carlo calculation for photons is added on to the calculated dose rate response as shown in Equation 5-5. The result is a set of dose rates in mrem/hr  $\left[ \frac{\text{mrem/hr}}{\text{g U-235}} \right]$

Separately, ORIGEN-S is used to calculate the source strength  $\left[ \frac{\text{mrem/hr}}{\text{g U-235}} \right]$  per g U-235 for a given enrichment/burnup combination for photons and neutrons. The source strength is  $\left[ \frac{\text{mrem/hr}}{\text{g U-235}} \right]$  per g U-235 for every  $\left[ \frac{\text{mrem/hr}}{\text{g U-235}} \right]$  enrichment/burnup combination for photons and neutrons. The dose rates per g U-235 are calculated, as shown in Equation 5-6,  $\left[ \frac{\text{mrem/hr}}{\text{g U-235}} \right]$

$\left[ \frac{\text{mrem/hr}}{\text{g U-235}} \right]$  The dose rates per gram U-235 for all burnup-enrichment pairings, at each regulatory dose rate location are provided in Tables 5.4-3 through 5.4-10.

**Table 5.4-3. NCT Top Surface Dose Rates per g U-235 by Burnup-Enrichment Pairing**

Top Surface $\dot{D}\dot{R}$ (mrem/hr/gU235)							
Enrichment (wt% U-235)	Burnup (GWd/MTU)						
	0 < B ≤ 10	10 < B ≤ 20	20 < B ≤ 30	30 < B ≤ 40	40 < B ≤ 50	50 < B ≤ 60	60 < B ≤ 72
1.5 ≤ E < 2.0	5.936E-03	1.904E-02	5.181E-02	1.098E-01	1.963E-01	3.218E-01	5.635E-01
2.0 ≤ E < 2.5	4.159E-03	1.162E-02	3.057E-02	6.637E-02	1.218E-01	2.020E-01	3.535E-01
2.5 ≤ E < 3.0	3.187E-03	7.930E-03	1.973E-02	4.309E-02	8.069E-02	1.356E-01	2.375E-01
3.0 ≤ E < 3.5	2.580E-03	5.860E-03	1.363E-02	2.948E-02	5.593E-02	9.514E-02	1.668E-01
3.5 ≤ E < 4.0	2.170E-03	4.583E-03	9.930E-03	2.103E-02	4.012E-02	6.894E-02	1.212E-01
4.0 ≤ E < 4.5	1.872E-03	3.738E-03	7.577E-03	1.558E-02	2.964E-02	5.127E-02	9.041E-02
4.5 ≤ E ≤ 5.0	1.648E-03	3.146E-03	6.015E-03	1.193E-02	2.249E-02	3.900E-02	6.898E-02

**Table 5.4-4. NCT Side Surface Dose Rates per g U-235 by Burnup-Enrichment Pairing**

Side Surface $\dot{D}\dot{R}$ (mrem/hr/gU235)							
Enrichment (wt% U-235)	Burnup (GWd/MTU)						
	0 < B ≤ 10	10 < B ≤ 20	20 < B ≤ 30	30 < B ≤ 40	40 < B ≤ 50	50 < B ≤ 60	60 < B ≤ 72
1.5 ≤ E < 2.0	3.492E-02	1.105E-01	2.986E-01	6.312E-01	1.127E+00	1.845E+00	3.229E+00
2.0 ≤ E < 2.5	2.451E-02	6.761E-02	1.765E-01	3.817E-01	6.990E-01	1.159E+00	2.026E+00
2.5 ≤ E < 3.0	1.880E-02	4.627E-02	1.141E-01	2.480E-01	4.635E-01	7.782E-01	1.361E+00
3.0 ≤ E < 3.5	1.523E-02	3.426E-02	7.894E-02	1.699E-01	3.215E-01	5.461E-01	9.566E-01
3.5 ≤ E < 4.0	1.281E-02	2.684E-02	5.762E-02	1.213E-01	2.308E-01	3.958E-01	6.953E-01
4.0 ≤ E < 4.5	1.106E-02	2.192E-02	4.405E-02	8.999E-02	1.706E-01	2.945E-01	5.188E-01
4.5 ≤ E ≤ 5.0	9.734E-03	1.847E-02	3.502E-02	6.902E-02	1.296E-01	2.242E-01	3.959E-01

**Table 5.4-5. NCT Bottom Surface Dose Rates per g U-235 by Burnup-Enrichment Pairing**

Bottom Surface $\dot{D}\dot{R}$ (mrem/hr/gU235)							
Enrichment (wt% U-235)	Burnup (GWd/MTU)						
	0 < B ≤ 10	10 < B ≤ 20	20 < B ≤ 30	30 < B ≤ 40	40 < B ≤ 50	50 < B ≤ 60	60 < B ≤ 72
1.5 ≤ E < 2.0	1.571E-02	5.799E-02	1.684E-01	3.657E-01	6.607E-01	1.089E+00	1.916E+00
2.0 ≤ E < 2.5	1.078E-02	3.441E-02	9.802E-02	2.196E-01	4.084E-01	6.825E-01	1.200E+00
2.5 ≤ E < 3.0	8.140E-03	2.289E-02	6.227E-02	1.415E-01	2.696E-01	4.571E-01	8.051E-01
3.0 ≤ E < 3.5	6.523E-03	1.652E-02	4.230E-02	9.596E-02	1.860E-01	3.198E-01	5.647E-01
3.5 ≤ E < 4.0	5.445E-03	1.267E-02	3.029E-02	6.780E-02	1.327E-01	2.310E-01	4.096E-01
4.0 ≤ E < 4.5	4.673E-03	1.016E-02	2.272E-02	4.970E-02	9.749E-02	1.712E-01	3.049E-01
4.5 ≤ E ≤ 5.0	4.096E-03	8.428E-03	1.774E-02	3.764E-02	7.349E-02	1.297E-01	2.321E-01



**Table 5.4-6. NCT 2-meter Dose Rates per g U-235 by Burnup-Enrichment Pairing**

2 Meter $\dot{D}\dot{R}$ (mrem/hr/gU235)							
Enrichment (wt% U-235)	Burnup (GWd/MTU)						
	0< B ≤10	10< B ≤20	20< B ≤30	30< B ≤40	40< B ≤50	50< B ≤60	60< B ≤72
1.5≤ E <2.0	6.709E-04	2.407E-03	6.905E-03	1.493E-02	2.692E-02	4.433E-02	7.791E-02
2.0≤ E <2.5	4.623E-04	1.436E-03	4.029E-03	8.975E-03	1.665E-02	2.779E-02	4.883E-02
2.5≤ E <3.0	3.502E-04	9.599E-04	2.567E-03	5.791E-03	1.100E-02	1.862E-02	3.276E-02
3.0≤ E <3.5	2.812E-04	6.961E-04	1.749E-03	3.934E-03	7.595E-03	1.303E-02	2.298E-02
3.5≤ E <4.0	2.351E-04	5.357E-04	1.257E-03	2.784E-03	5.425E-03	9.420E-03	1.668E-02
4.0≤ E <4.5	2.020E-04	4.310E-04	9.457E-04	2.045E-03	3.989E-03	6.986E-03	1.242E-02
4.5≤ E ≤5.0	1.772E-04	3.587E-04	7.408E-04	1.552E-03	3.011E-03	5.297E-03	9.456E-03

**Table 5.4-7. NCT Cab Dose Rates per g U-235 by Burnup-Enrichment Pairing**

Cab $\dot{D}\dot{R}$ (mrem/hr/gU235)							
Enrichment (wt% U-235)	Burnup (GWd/MTU)						
	0< B ≤10	10< B ≤20	20< B ≤30	30< B ≤40	40< B ≤50	50< B ≤60	60< B ≤72
1.5≤ E <2.0	1.217E-04	4.328E-04	1.237E-03	2.671E-03	4.814E-03	7.926E-03	1.392E-02
2.0≤ E <2.5	8.397E-05	2.586E-04	7.224E-04	1.606E-03	2.978E-03	4.968E-03	8.727E-03
2.5≤ E <3.0	6.367E-05	1.731E-04	4.606E-04	1.037E-03	1.968E-03	3.329E-03	5.856E-03
3.0≤ E <3.5	5.116E-05	1.257E-04	3.142E-04	7.046E-04	1.359E-03	2.331E-03	4.109E-03
3.5≤ E <4.0	4.279E-05	9.687E-05	2.259E-04	4.990E-04	9.710E-04	1.685E-03	2.981E-03
4.0≤ E <4.5	3.678E-05	7.803E-05	1.702E-04	3.667E-04	7.142E-04	1.250E-03	2.220E-03
4.5≤ E ≤5.0	3.227E-05	6.500E-05	1.334E-04	2.785E-04	5.392E-04	9.478E-04	1.691E-03

**Table 5.4-8. HAC Top 1-meter Dose Rates per g U-235 by Burnup-Enrichment Pairing**

Top 1 Meter $\dot{D}\dot{R}$ (mrem/hr/gU235)							
Enrichment (wt% U-235)	Burnup (GWd/MTU)						
	0< B ≤10	10< B ≤20	20< B ≤30	30< B ≤40	40< B ≤50	50< B ≤60	60< B ≤72
1.5≤ E <2.0	1.088E-02	2.456E-02	5.239E-02	9.915E-02	1.675E-01	2.659E-01	4.544E-01
2.0≤ E <2.5	7.930E-03	1.630E-02	3.276E-02	6.182E-02	1.058E-01	1.688E-01	2.871E-01
2.5≤ E <3.0	6.235E-03	1.195E-02	2.247E-02	4.159E-02	7.155E-02	1.148E-01	1.944E-01
3.0≤ E <3.5	5.136E-03	9.355E-03	1.649E-02	2.960E-02	5.076E-02	8.171E-02	1.378E-01
3.5≤ E <4.0	4.372E-03	7.665E-03	1.274E-02	2.203E-02	3.738E-02	6.018E-02	1.012E-01
4.0≤ E <4.5	3.806E-03	6.486E-03	1.026E-02	1.705E-02	2.841E-02	4.557E-02	7.634E-02
4.5≤ E ≤5.0	3.372E-03	5.622E-03	8.546E-03	1.364E-02	2.222E-02	3.536E-02	5.897E-02

**Table 5.4-9. HAC Side 1-meter Dose Rates per g U-235 by Burnup-Enrichment Pairing**

Enrichment (wt% U-235)	Side 1 Meter $\dot{D}\dot{R}$ (mrem/hr/gU235)						
	Burnup (GWd/MTU)						
	0 < B ≤ 10	10 < B ≤ 20	20 < B ≤ 30	30 < B ≤ 40	40 < B ≤ 50	50 < B ≤ 60	60 < B ≤ 72
1.5 ≤ E < 2.0	2.325E-02	4.368E-02	7.559E-02	1.244E-01	1.933E-01	2.905E-01	4.745E-01
2.0 ≤ E < 2.5	1.719E-02	3.056E-02	5.013E-02	8.093E-02	1.255E-01	1.881E-01	3.039E-01
2.5 ≤ E < 3.0	1.364E-02	2.331E-02	3.632E-02	5.693E-02	8.755E-02	1.307E-01	2.089E-01
3.0 ≤ E < 3.5	1.130E-02	1.879E-02	2.800E-02	4.239E-02	6.421E-02	9.525E-02	1.506E-01
3.5 ≤ E < 4.0	9.659E-03	1.573E-02	2.257E-02	3.298E-02	4.896E-02	7.197E-02	1.126E-01
4.0 ≤ E < 4.5	8.433E-03	1.353E-02	1.883E-02	2.661E-02	3.857E-02	5.599E-02	8.659E-02
4.5 ≤ E ≤ 5.0	7.486E-03	1.187E-02	1.614E-02	2.211E-02	3.125E-02	4.468E-02	6.826E-02

**Table 5.4-10. HAC Bottom 1-meter Dose Rates per g U-235 by Burnup-Enrichment Pairing**

Enrichment (wt% U-235)	Bottom 1 Meter $\dot{D}\dot{R}$ (mrem/hr/gU235)						
	Burnup (GWd/MTU)						
	0 < B ≤ 10	10 < B ≤ 20	20 < B ≤ 30	30 < B ≤ 40	40 < B ≤ 50	50 < B ≤ 60	60 < B ≤ 72
1.5 ≤ E < 2.0	7.553E-03	2.050E-02	5.058E-02	1.029E-01	1.805E-01	2.928E-01	5.086E-01
2.0 ≤ E < 2.5	5.403E-03	1.298E-02	3.051E-02	6.289E-02	1.126E-01	1.845E-01	3.198E-01
2.5 ≤ E < 3.0	4.197E-03	9.155E-03	2.016E-02	4.135E-02	7.516E-02	1.244E-01	2.154E-01
3.0 ≤ E < 3.5	3.429E-03	6.954E-03	1.428E-02	2.870E-02	5.251E-02	8.767E-02	1.518E-01
3.5 ≤ E < 4.0	2.903E-03	5.564E-03	1.067E-02	2.081E-02	3.802E-02	6.387E-02	1.106E-01
4.0 ≤ E < 4.5	2.517E-03	4.622E-03	8.332E-03	1.567E-02	2.838E-02	4.779E-02	8.284E-02
4.5 ≤ E ≤ 5.0	2.223E-03	3.949E-03	6.758E-03	1.221E-02	2.177E-02	3.661E-02	6.346E-02

For a defined mass of uranium at a given burnup and initial enrichment, the resulting dose rate at any regulatory dose rate location can be calculated by multiplying the mass of initial fissile material (grams U-235) by the dose rates per gram U-235 in the corresponding table, as shown in Equation 5-7. Repeating this dose rate calculation for each loaded fuel segment, then summing the resulting dose rates calculates the total external dose rates for each regulatory dose rate location from a load of segmented irradiated fuel in the Model 2000 Transport Package. This process is completed and recorded in the Irradiated Fuel Loading Table (Section 7.5.3). The use of the Irradiated Fuel Loading Table is described in Section 5.5.5. The maximum possible dose rate for each regulatory location is shown in Table 5.4-11, based on the limiting masses of U-235 shown in Table 5.5-35. The maximum quantity of irradiated fuel is limited by the minimum of the quantity equivalent to the 1500 W thermal limit of the cask or the quantity resulting in an NCT side surface dose rate equal to 90% of the regulatory limit (180 mrem/hr) or the quantity equivalent to the criticality limit of 1750 g.

**Table 5.4-11. Maximum External Dose Rates - Irradiated Fuel**

Location	NCT Top Surface	NCT Side Surface	NCT Bottom Surface	NCT 2-meter	NCT Cab	HAC Top 1-meter	HAC Side 1-meter	HAC Bottom 1-meter
Dose Rate (mrem/hr)	31.41	180.00	106.77	4.34	0.78	33.42	53.63	31.12
Regulatory Limit (mrem/hr)	200.0	200.0	200.0	10.0	2.0	1000	1000	1000

It is recognized that fuel burnup is typically tracked by means of a core simulator that uses a nodal three-dimensional neutronics model. In such a case, fuel burnup is known at every axial node, and each node represents a certain axial height of fuel, e.g., 5.5 inches. A fuel segment loaded for shipment may span several core simulator nodes. For example, a 15-inch fuel segment may have been located in three, or even four, of the 5.5-inch computational nodes. The appropriate procedure in this instance to calculate the dose rate from the 15-inch segment is to multiply the mass of U-235 in each node by the dose rate per gram U-235 from Tables 5.4-3 through 5.4-10 that correspond to that node's initial enrichment and burnup, and then to sum the dose rates.

For example, assume that 5.5 inches of this fuel segment were located in node A, 5.5 inches in node B, and 4 inches in node C. Node A has a burnup of 21 GWd/MTU, node B 19 GWd/MTU, and node C 15 GWd/MTU. All nodes have an initial enrichment of 4.2 wt% U-235. To find the NCT side surface dose rate, the mass of node A is multiplied by 4.405E-02 mrem/hr/gU235 from Table 5.4-4, and the mass of nodes B and C is multiplied by 2.192E-02 mrem/hr/gU235 from the same table. These dose rates are then summed to determine the dose rate for the entire 15-inch segment.

- The following condition applies: If the node height of the core simulator is less than 5.3 inches, then the peak exposure over every 5.3 inches shall be conservatively used in order to be consistent with the minimum segment height assumed in the shielding evaluation.

For example, assume that it is desired to ship a six inch segment and that the burnups for each inch are known to be 28.2, 28.6, 29.0, 29.4, 29.8, and 30.2 GWd/MTU. To find the NCT side surface dose rate, the initial U-235 mass of all six nodes is multiplied by 8.999E-02 mrem/hr/gU235 from Table 5.4-4 so that the limiting exposure band ( $30 < B \leq 40$ ) is represented along the entire segment.

#### **5.4.4.2. Irradiated Hardware and Byproducts**

For the irradiated hardware and byproduct contents, the resulting external dose rates are calculated by calculating the dose rate per curie in MCNP6 for each radionuclide individually, using the source spectra listed in Tables 5.5-8 through 5.5-25. The  $2\sigma$  statistical uncertainty is added on to the calculated dose rate per curie as shown in Equation 5-10. The resulting values from these calculations for NCT and HAC are presented in Tables 5.4-12 and 5.4-13.

**Table 5.4-12. Irradiated Hardware and Byproduct Dose Rate per Curie Results - NCT**

Radionuclide	Dose Rate (mrem/hr/Ci)				
	Top Surface	Side Surface	Bottom Surface	2-meter	Cab
Co-58	1.356E-05	2.444E-04	2.169E-05	3.375E-06	5.945E-07
Co-60	4.183E-04	9.437E-03	6.237E-04	1.211E-04	2.078E-05
Cr-51	3.981E-15	1.648E-20	5.556E-20	2.125E-22	3.509E-23
Cs-134	1.584E-05	3.433E-04	2.402E-05	4.504E-06	7.780E-07
Cs-137	9.341E-10	3.713E-08	2.822E-09	4.381E-10	7.404E-11
Fe-59	1.239E-04	2.894E-03	1.853E-04	3.649E-05	6.292E-06
Hf-175	1.642E-13	1.917E-15	3.513E-16	1.167E-17	1.891E-18
Hf-181	1.968E-11	2.116E-11	3.427E-12	2.749E-13	4.721E-14
Mn-54	2.294E-07	9.856E-06	4.279E-07	1.116E-07	1.904E-08
Nb-92m	4.559E-05	8.088E-04	7.216E-05	1.128E-05	1.974E-06
Nb-94	5.561E-07	2.214E-05	9.703E-07	2.519E-07	4.293E-08
Sb-124	1.973E-03	3.462E-02	3.176E-03	4.809E-04	8.336E-05
Sb-125	1.440E-10	3.334E-09	3.261E-10	4.139E-11	7.082E-12
Sb-126	6.649E-06	1.526E-04	1.009E-05	1.955E-06	3.399E-07
Sc-46	4.123E-05	1.111E-03	6.179E-05	1.353E-05	2.327E-06
Ta-182	1.343E-04	3.273E-03	1.997E-04	4.080E-05	6.989E-06
Zn-65	2.023E-05	5.398E-04	3.014E-05	6.581E-06	1.131E-06
Zr-95	5.015E-08	2.505E-06	1.181E-07	2.816E-08	4.790E-09
Nb-95	5.015E-08	2.505E-06	1.181E-07	2.816E-08	4.790E-09

**Table 5.4-13. Irradiated Hardware and Byproduct Dose Rate per Curie Results - HAC**

Radionuclide	Dose Rate (mrem/hr/Ci)		
	Top 1-meter	Side 1-meter	Bottom 1-meter
Co-58	1.795E-05	4.460E-05	1.155E-05
Co-60	6.008E-04	1.743E-03	3.552E-04
Cr-51	1.268E-13	5.043E-20	9.455E-19
Cs-134	2.252E-05	6.356E-05	1.340E-05
Cs-137	3.023E-09	9.383E-09	3.140E-09
Fe-59	1.806E-04	5.370E-04	1.071E-04
Hf-175	1.676E-12	4.820E-16	7.744E-16
Hf-181	1.493E-10	6.868E-12	5.073E-12
Mn-54	4.057E-07	2.046E-06	3.326E-07
Nb-92m	5.907E-05	1.450E-04	3.671E-05
Nb-94	9.502E-07	4.548E-06	7.240E-07
Sb-124	2.568E-03	6.144E-03	1.618E-03
Sb-125	6.258E-10	9.213E-10	4.006E-10
Sb-126	9.516E-06	2.875E-05	5.919E-06
Sc-46	6.274E-05	2.115E-04	3.852E-05
Ta-182	1.976E-04	6.138E-04	1.176E-04
Zn-65	3.066E-05	1.026E-04	1.860E-05
Zr-95	9.528E-08	5.459E-07	1.039E-07
Nb-95	9.528E-08	5.459E-07	1.039E-07

The resulting dose rate at any regulatory dose rate location can be calculated, for a cask loading of irradiated hardware or byproducts with a defined radionuclide inventory, by multiplying the activity of each radionuclide by the respective dose rate per curie for the given location and summing the dose rate contributions from each radionuclide, as shown in Equation 5-11. Repeating this dose rate calculation for each regulatory dose rate location determines the total external dose rates for the Model 2000 Transport Package. This process is completed and recorded in the Irradiated Hardware and Byproduct Loading Table. The use of the Irradiated Hardware and Byproduct Loading Table is described in Section 5.5.6.

The maximum activity of each radionuclide, individually, is limited by the minimum of either the activity equivalent to the 1500 W thermal limit of the cask or the activity resulting in an NCT side surface dose rate equal to 90% of the regulatory limit (180 mrem/hr). The maximum activity limit for each radionuclide individually is presented in Table 5.4-14. These limits are based on the dose rate per curie limits in Tables 5.4-12 and 5.4-13, and the decay heat W/Ci values in Table 5.5-29. The maximum possible dose rates for each regulatory location are summarized in Table 5.4-15. These values are calculated using the activity limits in Table 5.4.14 and the dose rate per curie values in Tables 5.4-12 and 5.4-13 for each radionuclide.

**Table 5.4-14. Maximum Activities for Irradiated Hardware and Byproduct  
Individual Radionuclides**

<b>Radionuclide</b>	<b>Activity Limit (Ci)</b>	<b>Basis<sup>a,b</sup></b>
Co-58	2.508E+05	Thermal
Co-60	1.907E+04	Dose Rate
Cr-51	6.899E+06	Thermal
Cs-134	1.472E+05	Thermal
Cs-137	3.009E+05	Thermal
Fe-59	6.219E+04	Dose Rate
Hf-175	6.369E+05	Thermal
Hf-181	3.465E+05	Thermal
Mn-54	3.011E+05	Thermal
Nb-92m	2.225E+05	Dose Rate
Nb-94	1.438E+05	Thermal
Sb-124	5.199E+03	Dose Rate
Sb-125	4.742E+05	Thermal
Sb-126	8.108E+04	Thermal
Sc-46	1.192E+05	Thermal
Ta-182	5.499E+04	Dose Rate
Zn-65	3.334E+05	Dose Rate
Zr-95	1.525E+05	Thermal
Nb-95	3.127E+05	Thermal

Notes: <sup>a</sup> Thermal – 1500 W thermal limit.

<sup>b</sup> Dose Rate – 180 mrem/hr NCT side surface dose rate limit.

**Table 5.4-15. Maximum External Dose Rates - Irradiated Hardware and Byproducts**

Location	NCT Top Surface	NCT Side Surface	NCT Bottom Surface	NCT 2-meter	NCT Cab	HAC Top 1-meter	HAC Side 1-meter	HAC Bottom 1-meter
Dose Rate (mrem/hr)	10.26	179.99	16.51	2.51	0.44	13.35	34.21	8.41
Regulatory Limit (mrem/hr)	200	200	200	10	2	1000	1000	1000

#### 5.4.4.3. Cobalt-60 Isotope Rods

For the cobalt-60 isotope rod contents, the resulting external dose rates are calculated using the dose rate per curie in MCNP6 for cobalt-60, with the cobalt-60 source energy spectrum listed in Table 5.2-2. The  $2\sigma$  statistical uncertainty is added on to the calculated dose rate per curie as shown in Equation 5-10. The resulting values from these calculations for NCT and HAC are presented in Tables 5.4-16 and 5.4-17.

**Table 5.4-16. Cobalt-60 Isotope Rod Dose Rate per Curie Results – NCT**

Radionuclide	Dose Rate (mrem/hr/Ci)				
	Top Surface	Side Surface	Bottom Surface	2-meter	Cab
Co-60	1.850E-04	8.821E-04	3.940E-04	1.664E-05	2.921E-06

**Table 5.4-17. Cobalt-60 Isotope Rod Dose Rate per Curie Results - HAC**

Radionuclide	Dose Rate (mrem/hr/Ci)		
	Top 1-meter	Side 1-meter	Bottom 1-meter
Co-60	6.008E-04	1.743E-03	3.552E-04

The resulting dose rate at any regulatory dose rate location can be calculated, for a cask loading of cobalt-60 isotope rod [[ ]], by filling out the cobalt-60 isotope rod loading table.

To determine the maximum possible dose rate at each regulatory location, the dose rate per curie values in Tables 5.4-16 and 5.4-17 are multiplied by the cobalt-60 activity equivalent to the 1500 W thermal limit (97,250 Ci). The results of this calculation are presented in Table 5.4-18.

**Table 5.4-18. Maximum External Dose Rates – Cobalt-60 Isotope Rods**

Location	NCT Top Surface	NCT Side Surface	NCT Bottom Surface	NCT 2-meter	NCT Cab	HAC Top 1-meter	HAC Side 1-meter	HAC Bottom 1-meter
Dose Rate (mrem/hr)	17.99	85.78	38.32	1.62	0.28	58.43	169.51	34.54
Regulatory Limit (mrem/hr)	200	200	200	10	2	1000	1000	1000

#### **5.4.4.4. Combined Contents**

There is the possibility of a shipment that includes combined contents. For example, some shipments of irradiated fuel will also include irradiated hardware. This is due to the possibility of being encapsulated in fuel cladding. For this reason, shipments of irradiated fuel may also include segments of irradiated bundle hardware. In order to demonstrate compliance with the 10 CFR 71 external dose rate limits for a shipment of combined content types, the external dose rate contributions from each content type are calculated separately. The total thermal and dose rates for the shipment of combined contents are calculated as the sum of the thermal and dose rate contributions from each content type. This process is completed and recorded in the Combined Contents Loading Table. The use of the Combined Contents Loading Table is described in Section 5.5.7, including an example of a hypothetical shipment with irradiated fuel and bundle hardware.

Another example is a combined content of cobalt-60 isotope rods with irradiated hardware. For this case the Cobalt-60 Isotope Rod Loading Table (in Chapter 7) is confirmed for the isotope rod contents and any radionuclide activity in the rod cladding or additional irradiated hardware shipped with the isotope rods is confirmed in the Irradiated Hardware and Byproduct Loading Table (in Chapter 7). The resulting thermal and dose rate contributions from radionuclides in the hardware and cladding are summed with the thermal and dose rate contributions from the cobalt-60 isotope rods in the Combined Contents Loading Table (in Chapter 7).

### **5.5 Appendices**

#### **5.5.1. ORIGEN-S Irradiated Fuel Source Term Calculation**

Per the recommendations for spent fuel specifications provided in NUREG/CR-6716 (Reference 5-10), the principal parameters for spent fuel source term generation are burnup, enrichment, and cooling time. To generate a bounding source term, the maximum burnup should be considered, along with the minimum enrichment and cooling time. To provide flexibility for future use of the Model 2000 cask, a wide range of enrichments and burnups are considered. The irradiated fuel source term calculation is performed for several enrichment bands and burnup bands. In the ORIGEN-S (Reference 5-2) source term analysis, for each initial enrichment band the minimum enrichment is considered, and for each burnup band the maximum burnup is considered. This generates a bounding source term for each burnup-enrichment pairing. Table 5.5-1 shows the burnup bands and Table 5.5-2 shows the initial enrichment bands for which a separate source term is calculated. The source terms are taken at a cooling time of 120 days. Any irradiated fuel contents are required to have at least 120 days of cooling time prior to shipment in the Model 2000 cask.

**Table 5.5-1. Burnup Bands and Analyzed Values**

Burnup Band (GWd/MTU)	Analyzed Burnup (GWd/MTU)
$60 < B \leq 72$	72
$50 < B \leq 60$	60
$40 < B \leq 50$	50
$30 < B \leq 40$	40
$20 < B \leq 30$	30
$10 < B \leq 20$	20
$0 < B \leq 10$	10

**Table 5.5-2. Initial Enrichment Bands and Analyzed Values**

Initial Enrichment Band (wt%)	Analyzed Initial Enrichment (wt%)
$1.5 \leq E < 2.0$	1.5
$2.0 \leq E < 2.5$	2.0
$2.5 \leq E < 3.0$	2.5
$3.0 \leq E < 3.5$	3.0
$3.5 \leq E < 4.0$	3.5
$4.0 \leq E < 4.5$	4.0
$4.5 \leq E \leq 5.0$	4.5

Table 5.5-3 lists the values used for the secondary parameters for the ORIGEN-S irradiated fuel source term calculation. While these parameters are not as significant to the irradiated fuel source term calculation as the principal parameters, they are selected to generate a bounding source term. The additional parameters include the fuel assembly type analyzed, the presence of burnable poisons, the specific power analyzed, and the moderator density considered. The values used for each parameter are selected to be appropriate, or bounding, for the irradiated fuel contents outlined in Section 5.2.

**Table 5.5-3. Secondary Source Term Calculation Parameters**

Parameter	Value
Fuel Assembly Type	GE BWR 10x10
Burnable Poison	5 wt% Gd <sub>2</sub> O <sub>3</sub> <sup>1</sup>
Specific Power	40 MW/MTU <sup>2</sup>
Moderator Density	0.1 g/cm <sup>3</sup>

Notes: <sup>1</sup> Contained in UO<sub>2</sub>-Gd<sub>2</sub>O<sub>3</sub>

<sup>2</sup> Conservative value for BWRs and consistent with the maximum value used in NUREG/CR-6716, Table 8 (Reference 5-10)

The source strengths calculated for each enrichment band are normalized to 1 gram of U-235, so that the total source strength for a shipment of segmented irradiated fuel can be calculated by multiplying the source strength for a respective burnup-enrichment pairing by the total mass of U-235.

The ORIGEN-S analysis calculates the source term using the parameters listed above, resulting in the gamma and neutron source strength values per gram of initial U-235 for each burnup-enrichment pairing using the 18-group energy structure for gammas (18GrpSCALE5) and the 44-group energy structure for neutrons (44GrpENDF5). The source strength values used include



120 days of cooling time. Extended cooling times beyond 120 days will only reduce the calculated source strengths.

An example source  $[[ \quad ]]$  is included in Table 5.5-4 for the  $4.0 \leq E < 4.5$  enrichment band and  $30 < B \leq 40$  burnup band,  $[[$

$]]$

**Table 5.5-4. Example Source  $[[ \quad ]]$**

$[[ \quad ]]$	4.0 wt% U-235, 40 GWd/MTU
	$[[ \quad ]]$
5.00E-02	1.119E+12
1.00E-01	3.550E+11
2.00E-01	4.053E+11
3.00E-01	9.168E+10
4.00E-01	6.905E+10
6.00E-01	4.700E+11
8.00E-01	1.694E+12
1.00E+00	9.553E+10
1.33E+00	3.235E+10
1.66E+00	1.476E+10
2.00E+00	1.916E+09
2.50E+00	7.715E+09
3.00E+00	2.018E+08
4.00E+00	9.983E+06
5.00E+00	5.388E+02
6.50E+00	2.160E+02
8.00E+00	4.235E+01
1.00E+01	8.985E+00

The neutron source term is from radionuclides that emit neutrons through spontaneous fission (SF) and emitted alphas that generate neutrons through alpha-n reactions in the fuel ( $\alpha$ -n). The neutron source terms are dominated by Cm-244(SF) and Cm-242(SF), with significant contributions at higher burnups from Cf-252(SF), and at lower burnups from Pu-238( $\alpha$ -n).

For each burnup-enrichment pairing, the total wattage per gram U-235 is listed in the outputs from the ORIGEN-S calculations. The total wattage results from all ORIGEN-S outputs are listed in Table 5.5-5. These values can be used to ensure that the thermal limit of the cask will not be exceeded from a load of irradiated fuel.

**Table 5.5-5. Irradiated Fuel Total Radionuclide Decay Heat (W/gU235)**

Enrichment (wt%)	Burnup (GWd/MTU)						
	0< B ≤10	10< B ≤20	20< B ≤30	30< B ≤40	40< B ≤50	50< B ≤60	60< B ≤72
1.5≤ E <2.0	1.088E+00	1.453E+00	1.728E+00	1.963E+00	2.163E+00	2.335E+00	2.512E+00
2.0≤ E <2.5	8.215E-01	1.086E+00	1.282E+00	1.452E+00	1.601E+00	1.731E+00	1.866E+00
2.5≤ E <3.0	6.604E-01	8.664E-01	1.016E+00	1.147E+00	1.264E+00	1.368E+00	1.478E+00
3.0≤ E <3.5	5.527E-01	7.210E-01	8.403E-01	9.453E-01	1.041E+00	1.128E+00	1.220E+00
3.5≤ E <4.0	4.751E-01	6.171E-01	7.160E-01	8.026E-01	8.823E-01	9.557E-01	1.036E+00
4.0≤ E <4.5	4.170E-01	5.395E-01	6.233E-01	6.963E-01	7.643E-01	8.275E-01	8.975E-01
4.5≤ E ≤5.0	3.716E-01	4.793E-01	5.518E-01	6.144E-01	6.729E-01	7.282E-01	7.902E-01

### 5.5.2. ORIGEN-S Irradiated Hardware and Byproduct Source Term Calculation

The radionuclides that are significant to the irradiated hardware and byproduct dose rate calculations, were determined with multiple ORIGEN-S (Reference 5-2) irradiation calculations. For the irradiation case there are two significant inputs; the composition of the material that is being irradiated and the neutron flux that the material is exposed to. For determining the source term, the quantity of material is irrelevant for the determination of which radionuclides are generated. A generic thermal neutron flux of  $1\text{E}+14$  n/s-cm<sup>2</sup> is assumed for the irradiation cases. For the material compositions of the irradiated hardware/byproducts, there are six materials considered. These materials along with their compositions are listed in Table 5.5-6. The materials selected include multiple SS, a nickel alloy, a zirconium alloy, as well as hafnium and boron carbide. The materials listed in parentheses in Table 5.5-6 are included as they are similar in composition to the material listed. The materials listed contain elements expected in any irradiated hardware or byproduct contents. Thus, the resulting total radionuclide inventory from the ORIGEN-S calculations is comprehensive. The basis for each ORIGEN-S input is 1 kg of the respective material being irradiated. Because elements for each material are entered into the ORIGEN-S input in grams, Table 5.5-6 lists the gram amount of each element per kilogram of the material. While an increase or decrease in the flux or a variation in the material composition entered for the irradiation case would result in a change to the relative activity of the radionuclides generated, the purpose of the ORIGEN-S source term calculations is not to determine the inventory of each radionuclide, but simply to identify which radionuclides may be present in irradiated hardware/byproduct contents. The quantity of each radionuclide that is significant to dose rate calculations must be entered into the Irradiated Hardware and Byproduct Loading Table to calculate the maximum external dose rates. The quantity of each radionuclide that is significant to the thermal calculations must also be entered into the Irradiated Hardware and Byproduct Loading Table to calculate the total thermal content.

The radionuclides calculated from the ORIGEN-S irradiation cases are listed in Table 5.5-7. This table also includes some radionuclides that may be included on the hardware or byproduct contents in the form of surface contamination, as these contents may be exposed to a reactor environment. Radionuclides in cells that are highlighted are considered significant to dose rate calculations. The selection of significant radionuclides is based on the energy of the gamma emissions and half-lives. A radionuclide is considered insignificant to dose rate calculations if it has no gamma emissions greater than 0.3 MeV, or if it has a half-life less than 3 days. All shipments of irradiated

hardware and byproducts are required to include a decay time of 30 days prior to shipment. Thus, for any radionuclide with a half-life less than 3 days, there are more than 10 half-lives of decay time prior to shipment.

Tables 5.5-8 through 5.5-25 provide the energy spectra for all radionuclides considered significant to the irradiated hardware and byproduct dose rate calculations. These radionuclide energy spectra are from the ORIGEN-S Data Library `origen.rev04.mpdkgam.data` (Reference 5-2). Any gamma lines under 0.1 MeV are neglected from the listed radionuclide spectra. Though Cs-137 does not emit any significant gammas, the gamma emission of its short-lived daughter Ba-137m is used as its representative spectrum. Also, because Nb-95 is the daughter of Zr-95, the energy spectra of the two radionuclides are combined and only one set of dose rate calculations is performed for both radionuclides. Thus, the dose rates calculated for this combined spectrum account for one decay of each radionuclide. This calculates an appropriate dose rate for Zr-95, as it accounts for the decay of its daughter Nb-95. However, this spectrum results in a conservative dose rate for Nb-95, as the calculated dose rate includes the contribution from its parent radionuclide as well. The resulting dose rates from this combined spectrum are used to calculate external dose rates for activities of both Zr-95 and Nb-95, individually.

NEDO-33866 Revision 6  
Non-Proprietary Information

**Table 5.5-6. Irradiated Hardware and Byproduct Irradiation Materials**

Material	Symbol	Element ID No.	wt %	g/kg material	# nuclides
SS304 (SS302, SS304L)	C	60000	0.0800	0.8000	10
	N	70000	0.1000	1.0000	
	Si	140000	0.7500	7.5000	
	P	150000	0.0450	0.4500	
	S	160000	0.0300	0.3000	
	Cr	240000	19.000	190.00	
	Mn	250000	2.0000	20.000	
	Fe	260000	67.495	674.95	
	Co	270000	0.0800	0.8000	
	Ni	280000	10.420	104.20	
SS CF3M (SS316)	C	60000	0.0300	0.300	8
	Si	140000	2.0000	20.000	
	Cr	240000	19.000	190.00	
	Mn	250000	1.5000	15.000	
	Fe	260000	62.970	629.70	
	Co	270000	0.0800	0.8000	
	Ni	280000	11.920	119.20	
	Mo	420000	2.5000	25.000	
SS348H	C	60000	0.0700	0.7000	11
	Si	140000	1.0000	10.000	
	P	150000	0.0450	0.4500	
	S	160000	0.0300	0.3000	
	Cr	240000	18.000	180.00	
	Mn	250000	2.0000	20.000	
	Fe	260000	64.555	645.55	
	Co	270000	0.2000	2.0000	
	Ni	280000	13.000	130.00	
	Nb	410000	1.0000	10.000	
	Ta	730000	0.1000	1.0000	
Inconel-718 (Inconel X-750)	B	50000	0.0060	0.0600	16
	C	60000	0.0800	0.8000	
	Al	130000	0.5000	5.0000	
	Si	140000	0.3500	3.5000	
	P	150000	0.0150	0.1500	
	S	160000	0.0150	0.1500	
	Ti	220000	0.9000	9.0000	
	Cr	240000	19.000	190.00	
	Mn	250000	0.3500	3.5000	
	Fe	260000	14.934	149.34	
	Co	270000	1.0000	10.000	
	Ni	280000	54.000	540.00	
	Cu	290000	0.3000	3.0000	
	Nb	410000	2.7500	27.500	
	Mo	420000	3.0500	30.500	
	Ta	730000	2.7500	27.500	

NEDO-33866 Revision 6  
Non-Proprietary Information

Material	Symbol	Element ID No.	wt %	g/kg material	# nuclides
Zircaloy-2 (Zircaloy-4)	O	80000	0.1200	1.2000	6
	Cr	240000	0.1000	1.0000	
	Fe	260000	0.2000	2.0000	
	Ni	280000	0.0800	0.8000	
	Zr	400000	97.800	978.00	
	Sn	500000	1.7000	17.000	
Boron Carbide (B <sub>4</sub> C)	B	50000	78.261	782.61	2
	C	60000	21.739	217.39	
Hafnium	Hf	720000	100.00	1000.0	1

**Table 5.5-7. Irradiated Hardware and Byproduct Radionuclides**

H-3	Co-58m	Sr-91	Tc-99 <sup>a</sup>	<b>Sb-125</b>	Lu-177m
C-14	<b>Co-60</b>	Y-89m	Tc-99m	<b>Sb-126</b>	Yb-175
Na-24	Co-60m	Y-90	Tc-101	Te-125m	Yb-177
Si-31	Co-61	Y-90m	Ru-106a	I-129 <sup>a</sup>	Ta-180
P-32	Ni-57	Y-91	In-113m	<b>Cs-134<sup>a</sup></b>	<b>Ta-182</b>
P-33	Ni-59	Y-91m	In-114	<b>Cs-137 (Ba-137m)<sup>a</sup></b>	Ta-183
S-35	Ni-63	Y-92	In-114m	La-140 <sup>a</sup>	W-181
Ca-45	Ni-65	Nb-91m	In-115m	Ba-140 <sup>a</sup>	W-183m
<b>Sc-46</b>	Fe-55	<b>Nb-92m</b>	Sn-113	Ce-144 <sup>a</sup>	W-185
Sc-47	<b>Fe-59</b>	<b>Nb-94</b>	Sn-113m	Hf-173	Re-186
Sc-48	Cu-64	<b>Nb-95</b>	Sn-117m	<b>Hf-175</b>	Np-237 <sup>a</sup>
V-49	Cu-66 <sup>a</sup>	Nb-96	Sn-119m	Hf-177m	Pu-238 <sup>a</sup>
V-52 <sup>a</sup>	<b>Zn-65</b>	Nb-95m	Sn-121	Hf-180m	Pu-239 <sup>a</sup>
<b>Cr-51</b>	Zr-89	Nb-97	Sn-121m	<b>Hf-181</b>	Pu-240 <sup>a</sup>
Cr-55 <sup>a</sup>	<b>Zr-95</b>	Nb-97m	Sn-123	Lu-173	Pu-241 <sup>a</sup>
<b>Mn-54</b>	Zr-97	Mo-93	Sn-123m	Lu-174	Am-241 <sup>a</sup>
Mn-56	Sr-87m	Mo-93m	Sn-125	Lu-174m	Cm-242 <sup>a</sup>
Co-57	Sr-89	Mo-99	Sb-122	Lu-176m	Cm-243 <sup>a</sup>
<b>Co-58</b>	Sr-90 <sup>a</sup>	Mo-101	<b>Sb-124</b>	Lu-177	Cm-244 <sup>a</sup>

Notes: <sup>a</sup> Radionuclides not calculated in ORIGEN-S calculations, but included from previous shipments. Only present in small quantities in surface contamination.

**Table 5.5-8. Sc-46 Gamma Emission Energy Spectrum**

Total Photons/Disintegration	
2.000E+00	
Energy	Intensity
0.889	1.00E+00
1.121	1.00E+00
2.010	1.30E-07

**Table 5.5-9. Cr-51 Gamma Emission Energy Spectrum**

Total Photons/Disintegration	
9.910E-02	
Energy	Intensity
0.320	9.91E-02

**Table 5.5-10. Mn-54 Gamma Emission Energy Spectrum**

Total Photons/Disintegration	
9.998E-01	
Energy	Intensity
0.511	5.600E-09
0.835	9.998E-01

**Table 5.5-11. Co-58 Gamma Emission Energy Spectrum**

Total Photons/Disintegration	
1.305E+00	
Energy	Intensity
0.511	2.98E-01
0.811	9.95E-01
0.864	6.86E-03
1.675	5.17E-03

**Table 5.5-12. Fe-59 Gamma Emission Energy Spectrum**

Total Photons/Disintegration	
1.041E+00	
Energy	Intensity
0.143	1.02E-02
0.189	9.00E-06
0.192	3.08E-02
0.335	2.70E-03
0.382	1.80E-04
1.099	5.65E-01
1.292	4.32E-01
1.482	5.90E-04

**Table 5.5-13. Co-60 Gamma Emission Energy Spectrum**

Total Photons/Disintegration	
1.998E+00	
Energy	Intensity
0.347	7.5000E-05
0.826	7.6000E-05
1.173	9.9850E-01
1.333	9.9983E-01
2.159	1.2000E-05
2.506	2.0000E-08

**Table 5.5-14. Zn-65 Gamma Emission Energy Spectrum**

Total Photons/Disintegration	
5.289E-01	
Energy	Intensity
0.511	2.84E-02
0.345	2.53E-05
0.771	2.68E-05
1.116	5.00E-01

**Table 5.5-15. Nb-92m Gamma Emission Energy Spectrum**

Total Photons/Disintegration	
1.02E+00	
Energy	Intensity
0.511	1.28E-03
0.449	1.63E-05
0.561	2.23E-05
0.913	1.78E-02
0.934	9.91E-01
1.132	5.15E-05
1.848	8.52E-03

**Table 5.5-16. Nb-94 Gamma Emission Energy Spectrum**

Total Photons/Disintegration	
1.997E+00	
Energy	Intensity
0.703	9.98E-01
0.871	9.99E-01

**Table 5.5-17. Zr/Nb-95 Gamma Emission Energy Spectrum**

Total Photons/Disintegration	
1.99E+00	
Energy	Intensity
0.204	2.80E-04
0.562	1.50E-04
0.724	4.43E-01
0.757	5.44E-01
0.766	9.98E-01

**Table 5.5-18. Sb-124 Gamma Emission Energy Spectrum**

Total Photons/Disintegration					
1.878E+00					
Energy	Intensity	Energy	Intensity	Energy	Intensity
0.148	3.91E-05	0.766	1.21E-04	1.566	1.37E-04
0.190	6.36E-05	0.775	9.39E-05	1.580	3.81E-03
0.210	5.48E-05	0.791	7.39E-03	1.622	4.09E-04
0.254	1.61E-04	0.817	7.29E-04	1.691	4.76E-01
0.292	8.70E-05	0.857	2.38E-04	1.721	9.51E-04
0.336	7.43E-04	0.899	1.72E-04	1.852	6.45E-05
0.371	3.81E-04	0.968	1.88E-02	1.919	5.45E-04
0.400	1.39E-03	0.977	8.32E-04	2.016	9.49E-04
0.444	1.89E-03	1.045	1.83E-02	2.040	6.42E-04
0.469	4.99E-04	1.054	4.89E-05	2.080	2.05E-04
0.481	2.37E-04	1.087	3.78E-04	2.091	5.49E-02
0.526	1.38E-03	1.264	4.13E-04	2.099	4.57E-04
0.530	4.21E-04	1.301	3.43E-04	2.108	4.33E-04
0.572	1.90E-04	1.326	1.58E-02	2.172	2.05E-05
0.603	9.78E-01	1.355	1.04E-02	2.183	4.24E-04
0.632	1.05E-03	1.368	2.62E-02	2.284	8.02E-05
0.646	7.42E-02	1.376	4.83E-03	2.294	3.20E-04
0.662	2.93E-04	1.385	6.26E-04	2.324	2.44E-05
0.709	1.35E-02	1.437	1.22E-02	2.455	1.47E-05
0.714	2.28E-02	1.445	3.30E-03	2.682	1.65E-05
0.723	1.08E-01	1.489	6.72E-03	2.694	3.03E-05
0.736	5.57E-04	1.526	4.09E-03	2.808	1.47E-05
0.736	7.14E-04				

**Table 5.5-19. Sb-125 Gamma Emission Energy Spectrum**

Total Photons/Disintegration			
8.628E-01			
Energy	Intensity	Energy	Intensity
0.111	1.04E-05	0.408	1.84E-03
0.117	2.63E-03	0.428	2.96E-01
0.133	8.58E-06	0.444	3.06E-03
0.173	1.91E-03	0.463	1.05E-01
0.176	6.84E-02	0.490	1.36E-05
0.179	3.37E-04	0.491	4.74E-05
0.199	1.28E-04	0.497	3.20E-05
0.204	3.17E-03	0.503	3.85E-05
0.208	2.48E-03	0.539	1.39E-05
0.209	4.50E-04	0.601	1.76E-01
0.228	1.31E-03	0.607	4.98E-02
0.315	4.03E-05	0.617	5.33E-05
0.321	4.16E-03	0.636	1.12E-01
0.332	2.52E-05	0.653	2.66E-05
0.367	7.99E-05	0.671	1.79E-02
0.380	1.52E-02	0.693	4.59E-07
0.402	6.22E-05		



**Table 5.5-20. Sb-126 Gamma Emission Energy Spectrum**

Total Photons/Disintegration			
4.304E+00			
Energy	Intensity	Energy	Intensity
0.149	3.98E-03	0.667	9.96E-01
0.209	4.98E-03	0.675	3.69E-02
0.224	1.39E-02	0.695	9.96E-01
0.278	2.39E-02	0.697	2.89E-01
0.297	4.48E-02	0.721	5.38E-01
0.297	4.98E-03	0.857	1.76E-01
0.415	8.33E-01	0.954	1.20E-02
0.415	9.96E-03	0.958	4.98E-03
0.556	1.69E-02	0.990	6.77E-02
0.574	6.67E-02	1.036	9.96E-03
0.593	7.47E-02	1.061	3.98E-03
0.620	8.96E-03	1.064	8.96E-03
0.639	8.96E-03	1.213	2.39E-02
0.656	2.19E-02	1.477	2.79E-03

**Table 5.5-21. Cs-134 Gamma Emission Energy Spectrum**

Total Photons/Disintegration	
2.228E+00	
Energy	Intensity
0.243	2.72E-04
0.327	1.62E-04
0.475	1.48E-02
0.563	8.34E-02
0.569	1.54E-01
0.605	9.76E-01
0.796	8.55E-01
0.802	8.69E-02
0.847	3.00E-06
1.039	9.90E-03
1.168	1.79E-02
1.365	3.02E-02

**Table 5.5-22. Cs-137 (Ba-137m) Gamma Emission Energy Spectrum**

Total Photons/Disintegration	
8.990E-01	
Energy	Intensity
0.662	8.99E-01

**Table 5.5-23. Hf-175 Gamma Emission Energy Spectrum**

Total Photons/Disintegration	
8.683E-01	
Energy	Intensity
0.114	2.94E-03
0.161	2.27E-04
0.230	6.83E-03
0.319	1.68E-03
0.343	8.40E-01
0.353	2.28E-03
0.433	1.44E-02

**Table 5.5-24. Hf-181 Gamma Emission Energy Spectrum**

Total Photons/Disintegration	
1.466E+00	
Energy	Intensity
0.133	4.33E-01
0.136	5.85E-02
0.137	8.61E-03
0.346	1.51E-01
0.476	7.03E-03
0.482	8.05E-01
0.615	2.33E-03
0.619	2.50E-04

**Table 5.5-25. Ta-182 Gamma Emission Energy Spectrum**

Total Photons/Disintegration					
1.456E+00					
Energy	Intensity	Energy	Intensity	Energy	Intensity
0.100	1.42E-01	0.830	1.41E-04	1.189	1.65E-01
0.110	1.07E-03	0.892	5.74E-04	1.221	2.72E-01
0.114	1.87E-02	0.928	6.14E-03	1.224	2.36E-03
0.116	4.44E-03	0.960	3.50E-03	1.231	1.16E-01
0.122	2.36E-05	1.002	2.09E-02	1.257	1.51E-02
0.152	7.02E-02	1.036	6.70E-05	1.274	6.60E-03
0.156	2.67E-02	1.044	2.39E-03	1.289	1.37E-02
0.179	3.12E-02	1.113	4.45E-03	1.343	2.57E-03
0.198	1.46E-02	1.121	3.52E-01	1.374	2.22E-03
0.222	7.57E-02	1.157	7.33E-03	1.387	7.29E-04
0.229	3.64E-02	1.158	2.89E-03	1.410	3.96E-04
0.264	3.61E-02	1.181	8.74E-04	1.453	3.07E-04
0.351	1.13E-04				

### 5.5.3. Cobalt-60 Isotope Rod Activity Distribution

The cobalt-60 isotope rod shielding analysis utilizes 12-inch long line sources, which distribute the activity of the source uniformly across the line. Distribution of the cobalt-60 activity into a longer line source results in a lower external dose rate, and greater concentration of the cobalt-60 activity into a shorter line source results in a higher external dose rate. Thus, in order to demonstrate compliance with the regulatory dose rate limits for the cobalt-60 isotope rod contents, two requirements must be met. First, it must be shown that the dose rate contribution from all cobalt-60 source activity in a single shipment is less than the regulatory limit. Second, it must also be shown that the distribution of the activity in any single shipment of isotope rod [[ ]] is distributed axially, such that the uniform line source used in the shielding analysis is bounding of the actual axial distribution of activity.

For the cobalt-60 isotope rod shielding analysis, there are two source geometries considered. The first source geometry is referred to as the ‘bounding’ source geometry, which concentrates all of the cobalt-60 activity into a single 12-inch line source that is located in the most restrictive location for dose rate calculations in the given direction (top, side, or bottom). For side dose rate calculations with the bounding source geometry, dose rates are calculated with the source at both the bottom (Case 1) and top (Case 2) of the HPI cavity to determine the bounding source location.

The second geometry, referred to as the ‘Realistic’ source geometry distributes the cobalt-60 activity into [[ ]] of the HPI material basket. This source geometry provides a more realistic radial distribution of the source, as rod [[ ]] will be distributed throughout the basket during shipment, while still condensing the source axially to 12-inches. The array of line sources for the realistic arrangement is pushed against the top of the HPI for the top dose rate calculations, and is at the bottom of the HPI for bottom and side dose rate calculations. Figure 5.5-1 shows a cross section of the HPI material basket, with locations of the line sources used in the MCNP6 model.

[[

]]

**Figure 5.5-1. HPI Material Basket with ‘Realistic’ Source Geometry Locations**

A list of all source geometries analyzed is provided in Table 5.5-26 and a depiction of each source geometry is presented in Figures 5.5-2 through 5.5-8. The ‘realistic’ dose rate calculations are only included to quantify the margin in the bounding dose rates. For the demonstration of compliance with the normal and hypothetical accident condition dose rate limits, the reported dose rates are based on the more restrictive ‘bounding’ source geometries.

**Table 5.5-26. Cobalt-60 Isotope Rod Shielding Analysis Case Summary**

NCT Dose Rate Calculation Locations	Source Arrangement	Source Arrangement Figure
Bottom Surface	Realistic	5.5-2
	Bounding	5.5-3
Top Surface	Realistic	5.5-4
	Bounding	5.5-5
Side Surface	Realistic	5.5-6
	Bounding – 1	5.5-7
	Bounding – 2	5.5-8
2-meter	Realistic	5.5-6
	Bounding – 1	5.5-7
	Bounding – 2	5.5-8
Cab	Realistic	5.5-6
	Bounding – 1	5.5-7
	Bounding – 2	5.5-8

[[

]]

**Figure 5.5-2. ‘Realistic’ Source Arrangement for Bottom Dose Rates**

[[

]]

**Figure 5.5-3. 'Bounding' Source Arrangement for Bottom Dose Rates**

[[

]]

**Figure 5.5-4. 'Realistic' Source Arrangement for Top Dose Rates**

[[

]]

**Figure 5.5-5. 'Bounding' Source Arrangement for Top Dose Rates**

[[

]]

**Figure 5.5-6. 'Realistic' Source Arrangement for Side Dose Rates**

[[

]]

**Figure 5.5-7. ‘Bounding’ Source Arrangement for Side Dose Rates – Case 1**

[[

]]

**Figure 5.5-8. ‘Bounding’ Source Arrangement for Side Dose Rates – Case 2**

Table 5.5-27 lists the peak dose rate per curie calculated at each NCT regulatory dose rate location for each source geometry included in the cobalt-60 isotope rod shielding analysis, and the overall maximum calculated dose rate for each regulatory dose rate location. All maximum calculated dose rates were calculated with the ‘bounding’ source geometries, where the activity is concentrated into a single line. Also, the line source at the bottom of the HPI cavity calculated higher side dose rates than at the top.

**Table 5.5-27. Cobalt-60 Isotope Rod Shielding Analysis NCT Dose Rate Results**

NCT Dose Rate Location	Source Arrangement	Dose Rate (mrem/hr/Ci)	Maximum Location Dose Rate (mrem/hr/Ci)
Bottom Surface	Realistic	3.555E-04	3.940E-04
	Bounding	3.940E-04	
Top Surface	Realistic	1.780E-04	1.850E-04
	Bounding	1.850E-04	
Side Surface	Realistic	4.422E-04	8.821E-04
	Bounding	8.821E-04	
	Bounding	8.168E-04	
2-meter	Realistic	1.254E-05	1.664E-05
	Bounding	1.664E-05	
	Bounding	1.348E-05	
Cab	Realistic	2.277E-06	2.921E-06
	Bounding	2.921E-06	
	Bounding	2.331E-06	

Table 5.5-28 lists the maximum calculated dose rate at each NCT regulatory dose rate location using the dose rate per curie values calculated in Table 5.5-27 and the total cobalt-60 activity resulting in the dose rate equal to the 90% of regulatory limit for the respective location. This activity is 204,000 Ci, which results in an NCT side surface dose rate of 180 mrem/hr. Although a cobalt-60 activity of 204,000 Ci is not permitted in the Model 2000 cask due to the thermal limit, this table is included to demonstrate at this activity, no regulatory dose rate limits are exceeded.

**Table 5.5-28. Cobalt-60 Isotope Rod Shielding Analysis Maximum NCT Dose Rates**

Dose Rate Location	Dose Rate per Curie (mrem/hr/Ci)	Dose Rate <sup>a</sup> (mrem/hr)
Bottom Surface	3.940E-04	80.4
Top Surface	1.850E-04	37.7
Side Surface	8.821E-04	180.0
2-meter	1.664E-05	3.4
Cab	2.921E-06	0.6

Notes: <sup>a</sup> Based on an activity of 204,000 Ci cobalt-60

In Table 5.5-28 it is demonstrated that external dose rates resulting from any cobalt-60 isotope rod activity up to 204,000 Ci are less than the regulatory dose rate limits. It still must be demonstrated that the activity in any single shipment of isotope rod [[ ]] is distributed axially, such that the uniform line source used in the shielding analysis is bounding of the actual axial



distribution of activity. The exact axial activity profile of the cobalt-60 isotope rod [[ ]] is variable due to differences in the neutron flux profiles when irradiated in a commercial or research reactor. To determine that the uniform source in the MCNP6 shielding analysis is bounding of the distribution of activity in a shipment of rod [[ ]], it should first be considered that the source geometry is a single 12-inch line source. Modeling the source in this way assumes that all cobalt-60 activity loaded into the cavity is concentrated into a single line, with a uniform distribution. With all activity in a single line at the most restrictive location of the HPI cavity, any radial distribution of activity is bounded. Thus, the only variation in the source distribution that can cause the external dose rates to increase is in one direction (axially). So, it can be demonstrated that the source distribution of the contents in an actual shipment are bounded, by determining that there is no axial location in the HPI cavity where the concentration of activity is greater than what was analyzed in the MCNP6 analysis.

With the source arrangement of a single 12-inch line, no external dose rates will exceed the regulatory limits for any activity up to 204,000 Ci. By dividing the activity of 204,000 Ci evenly across the 12-inch uniform MCNP6 source, the result is a source that is concentrated in the axial direction to an activity of 17,000 Ci in each inch of the line source. Thus, it can be demonstrated that the activity distribution in the MCNP6 shielding model bounds the total activity distribution in the HPI cavity by determining for the package contents, the total activity in any axial 1-inch increment of the HPI cavity is not greater than 17,000 Ci. If for an actual shipment, there is a total activity of less than or equal to ( $\leq$ ) 17,000 Ci in any axial 1-inch increment of the HPI cavity, there is a greater distribution of the activity in the contents than in the MCNP6 source and the MCNP6 source is bounding.

#### 5.5.4. Radionuclide Decay Heat Conversion Factors

In addition to demonstrating compliance with the regulatory dose rate requirements, filling out the Irradiated Hardware and Byproduct Loading Table also demonstrates compliance with the thermal limit of the Model 2000 cask. One characteristic of every radionuclide is a given Q-value, which is the quantity of energy emitted per decay (MeV/Decay). By assuming that all energy emitted is deposited locally in the HPI material basket or the HPI body, the radionuclide decay heat in W/Ci can be calculated. All radionuclides considered in the irradiated hardware and byproduct contents are listed in Table 5.5-7 of Section 5.5.2, regardless of their significance to dose rate calculations. The Q-values for each of these radionuclides are provided in SCALE6.1 ORIGEN-S Decay library origen.rev03.decay.data (Reference 5-2). Table 5.5-29 lists all of the irradiated hardware and byproduct radionuclides with their ORIGEN-S library identification number, Q-value, and the calculated decay heat. Radionuclide Q-values are converted to decay heat values as shown in Equation 5-12.

$$\text{Decay Heat} \left[ \frac{\text{W}}{\text{Ci}} \right] = Q \left[ \frac{\text{MeV}}{\text{disintegration}} \right] \cdot 1.60217 \cdot 10^{-13} \left[ \frac{\text{J}}{\text{MeV}} \right] \cdot 3.7 \cdot 10^{10} \left[ \frac{\text{disintegrations}}{\text{s}} \right] \left[ \frac{\text{s}}{\text{Ci}} \right] \quad (5-12)$$

**Table 5.5-29. Isotope Decay Heat Data**

Isotope	ORIGEN-S Radionuclide ID	Q-Value (MeV/Decay)	Decay Heat (W/Ci)	Isotope	ORIGEN-S Radionuclide ID	Q-Value (MeV/Decay)	Decay Heat (W/Ci)
H-3	10030	5.6900E-03	3.373E-05	Tc-101	431010	8.1600E-01	4.837E-03
C-14	60140	4.9470E-02	2.933E-04	Ru-106	441060	1.0030E-02	5.946E-05
Na-24	110240	4.6769E+00	2.772E-02	In-113m	491131	3.9159E-01	2.321E-03
Si-31	140310	5.9645E-01	3.536E-03	In-114	491140	7.7607E-01	4.601E-03
P-32	150320	6.9490E-01	4.119E-03	In-114m	491141	2.2277E-01	1.321E-03
P-33	150330	7.6430E-02	4.531E-04	In-115m	491151	3.3436E-01	1.982E-03
S-35	160350	4.8758E-02	2.890E-04	Sn-113	501130	2.9753E-02	1.764E-04
Ca-45	200450	7.6860E-02	4.556E-04	Sn-113m	501131	7.1749E-02	4.253E-04
Sc-46	210460	2.1214E+00	1.258E-02				
Sc-47	210470	2.7132E-01	1.608E-03	Sn-117m	501171	3.1563E-01	1.871E-03
Sc-48	210480	3.5737E+00	2.118E-02				
V-49	230490	4.4514E-03	2.639E-05	Sn-119m	501191	8.7589E-02	5.192E-04
V-52	230520	2.5137E+00	1.490E-02	Sn-121	501210	1.1582E-01	6.866E-04
Cr-51	240510	3.6680E-02	2.174E-04	Sn-121m	501211	3.7987E-02	2.252E-04
Cr-55	240550	1.1017E+00	6.531E-03	Sn-123	501230	5.3006E-01	3.142E-03
Mn-54	250540	8.4017E-01	4.981E-03	Sn-123m	501231	6.2147E-01	3.684E-03
Mn-56	250560	2.5226E+00	1.495E-02	Sn-125	501250	1.1357E+00	6.732E-03
Co-57	270570	1.4380E-01	8.525E-04	Sb-122	511220	1.0098E+00	5.986E-03
Co-58	270580	1.0088E+00	5.980E-03	Sb-124	511240	2.2351E+00	1.325E-02
Co-58m	270581	2.4744E-02	1.467E-04	Sb-125	511250	5.3352E-01	3.163E-03
Co-60	270600	2.6006E+00	1.542E-02	Sb-126	511260	3.1205E+00	1.850E-02
Co-60m	270601	6.3045E-02	3.737E-04	Te-125m	521251	1.4546E-01	8.623E-04
Co-61	270610	5.6391E-01	3.343E-03	I-129	531290	7.4338E-02	4.407E-04
Ni-57	280570	2.0927E+00	1.241E-02	Cs-134	551340	1.7185E+00	1.019E-02
Ni-59	280590	6.9156E-03	4.100E-05	Cs-137	551370	1.7945E-01	4.985E-03 <sup>a</sup>
Ni-63	280630	1.7425E-02	1.033E-04	Ba-137m	561371	6.6140E-01	
Ni-65	280650	1.1863E+00	7.032E-03	La-140	571400	2.8438E+00	1.686E-02
Fe-55	260550	5.8421E-03	3.463E-05	Ba-140	561400	5.0041E-01	2.966E-03
Fe-59	260590	1.3060E+00	7.742E-03	Ce-144	581440	1.1059E-01	6.556E-04
Cu-64	290640	3.1188E-01	1.849E-03	Hf-173	721730	4.4558E-01	2.641E-03
Cu-66	290660	1.1645E+00	6.903E-03	Hf-175	721750	3.9728E-01	2.355E-03
Zn-65	300650	5.8284E-01	3.455E-03	Hf-177m	721771	1.5190E+00	9.005E-03
Zr-89	400890	3.5256E-01	2.090E-03	Hf-180m	721801	1.1148E+00	6.609E-03
Zr-95	400950	8.5013E-01	9.835E-03 <sup>b</sup>	Hf-181	721810	7.3010E-01	4.328E-03
Zr-97	400970	8.6426E-01	5.123E-03	Lu-173	711730	2.3057E-01	1.367E-03
Sr-87m	380871	3.8798E-01	2.300E-03	Lu-174	711740	1.5804E-01	9.369E-04
Sr-89	380890	5.8534E-01	3.470E-03	Lu-174m	711741	1.6712E-01	9.907E-04
Sr-90	380900	1.9580E-01	1.161E-03	Lu-176m	711761	4.9032E-01	2.907E-03
Sr-91	380910	1.3485E+00	7.994E-03	Lu-177	711770	1.8133E-01	1.075E-03
Y-89m	390891	9.0902E-01	5.389E-03	Lu-177m	711771	2.4764E-01	1.468E-03
Y-90	390900	9.3302E-01	5.531E-03	Yb-175	701750	2.0070E-01	1.190E-03
Y-90m	390901	6.8000E-01	4.031E-03	Yb-177	701770	6.2579E-01	3.710E-03
Y-91	390910	6.0617E-01	3.593E-03	Ta-180	731800	1.0251E-01	6.077E-04
Y-91m	390911	5.5554E-01	3.293E-03	Ta-182	731820	1.5156E+00	8.985E-03
Y-92	390920	1.7017E+00	1.009E-02	Ta-183	731830	6.3433E-01	3.760E-03
Nb-91m	410911	1.2634E-01	7.489E-04	W-181	741810	5.1849E-02	3.074E-04
Nb-92m	410921	9.7526E-01	5.781E-03	W-183m	741831	2.9876E-01	1.771E-03
Nb-94	410940	1.7599E+00	1.043E-02	W-185	741850	1.2690E-01	7.523E-04
Nb-95	410950	8.0900E-01	4.796E-03	Re-186	751860	3.5696E-01	2.116E-03

NEDO-33866 Revision 6  
Non-Proprietary Information

Isotope	ORIGEN-S Radionuclide ID	Q-Value (MeV/Decay)	Decay Heat (W/Ci)
Nb-96	410960	2.7140E+00	1.609E-02
Nb-95m	410951	2.4933E-01	1.478E-03
Nb-97	410970	1.1330E+00	6.716E-03
Nb-97m	410971	7.4336E-01	4.407E-03
Mo-93	420930	1.6143E-02	9.570E-05
Mo-93m	420931	2.4158E+00	1.432E-02
Mo-99	420990	5.4317E-01	3.220E-03
Mo-101	421010	1.9735E+00	1.170E-02
Tc-99	430990	5.5202E-02	3.272E-04
Tc-99m	430991	1.4222E-01	8.431E-04

Isotope	ORIGEN-S Radionuclide ID	Q-Value (MeV/Decay)	Decay Heat (W/Ci)
Np-237	932370	4.9445E+00	2.931E-02
Pu-238	942380	5.5899E+00	3.314E-02
Pu-239	942390	5.2433E+00	3.108E-02
Pu-240	942400	5.2522E+00	3.114E-02
Pu-241	942410	5.3555E-03	3.175E-05
Am-241	952410	5.6280E+00	3.336E-02
Cm-242	962420	6.2153E+00	3.684E-02
Cm-243	962430	6.1779E+00	3.662E-02
Cm-244	962440	5.9011E+00	3.498E-02

Notes: <sup>a</sup> Combined decay heat for Cs-137 and Ba-137m

<sup>b</sup> Decay heat calculated using summed Q-values from Zr-95 and Nb-95.

### 5.5.5. Irradiated Fuel Loading Table

In order to demonstrate compliance with the 10 CFR 71 (Reference 5-1) regulatory dose rate limits as well as the thermal and criticality limits of the cask, the Irradiated Fuel Loading Table (Section 7.5.3) must be filled out for every shipment of irradiated fuel in the Model 2000 cask. An example irradiated fuel dose rate calculation for a hypothetical shipment consisting of three irradiated fuel rods is provided. Recall from Section 5.2 that the fuel rod cladding is treated separately as irradiated hardware. An example irradiated hardware dose rate calculation is provided in Section 5.5.6. The relevant information for each of the example fuel rods is presented in Table 5.5-30.

**Table 5.5-30 Hypothetical Irradiated Fuel Rod Shipment Information**

Rod #	Active Length (cm)	Segments (#)	Fuel Rod Radius (cm)	Total Mass (gU)	Minimum Initial Enrichment <sup>3</sup> (wt% U-235)	Total Mass (gU235)	Maximum Burnup <sup>3</sup> (GWd/MTU)
1	381.0	10	0.4380	2218 <sup>1</sup>	3.100	68.77 <sup>2</sup>	46
2	381.0	13	0.4380	2218 <sup>1</sup>	2.600	57.68 <sup>2</sup>	39
3	381.0	10	0.4380	2218 <sup>1</sup>	4.200	93.17 <sup>2</sup>	58

Notes: <sup>1</sup> Based on 10.96 g/cm<sup>3</sup> UO<sub>2</sub> density and approximation of mU/mUO<sub>2</sub> = 238/(238+2×16)

<sup>2</sup> Calculated based on initial enrichment

<sup>3</sup> Uniform initial enrichment and burnup assumed for each of the hypothetical fuel rods

An example dose rate calculation is completed for the NCT side surface location in Table 5.5-31. The total initial mass (in gU235) is from Table 5.5-30 and the side surface dose rate (in mrem/hr/gU235) for the defined example enrichment and burnup is taken from Table 5.4-4. The total dose rate from each fuel rod is calculated by multiplying the initial mass of U-235 by the dose rate per gU235.

**Table 5.5-31. Irradiated Fuel NCT Side Surface Dose Rate Calculation**

Fuel Rod #	m (gU235)	$\dot{D}R$ (mrem/hr/gU235)	DR (mrem/hr)
1	68.77	3.215E-01	22.11
2	57.68	2.480E-01	14.30
3	93.17	2.945E-01	27.44

By summing the total dose rate contribution from each fuel rod, the total dose rate at the NCT side surface locations is calculated to be 63.85 mrem/hr. By repeating this calculation for each regulatory dose rate location, it can be demonstrated that this hypothetical group of irradiated fuel rods is acceptable for shipment, as the calculated dose rates do not exceed the regulatory limits. Using the hypothetical group of irradiated fuel rods in Table 5.5-30, an example of the complete loading table filled out for these contents is provided in Table 5.5-32. For this loading table example, it is assumed that each of the fuel rods is segmented to even whole lengths, with the mass of the fuel rod being divided evenly as well. It is demonstrated in this table that the criticality, dose rate, and thermal limit is not exceeded, and the hypothetical fuel rods are acceptable for shipment.

NEDO-33866 Revision 6  
Non-Proprietary Information

**Table 5.5-32. Hypothetical Irradiated Fuel Rod Shipment Irradiated Fuel Loading Table**

Segment #	Segment Length (inches)	Initial Enrichment (wt% U-235)	Burnup (GWd/MTU)	Mass U-235 (g)	Decay Heat (W)	NCT					HAC		
						DR <sub>surf</sub>			DR <sub>2m</sub>	DR <sub>cab</sub>	DR <sub>1m</sub>		
						Top	Side	Bottom			Top	Side	Bottom
1	15	3.0 ≤ E < 3.5	40 < B ≤ 50	6 877	7 159	0 3846	2 211	1 279	0 0522	0 0093	0 3491	0 4416	0 3611
2	15	3.0 ≤ E < 3.5	40 < B ≤ 50	6 877	7 159	0 3846	2 211	1 279	0 0522	0 0093	0 3491	0 4416	0 3611
3	15	3.0 ≤ E < 3.5	40 < B ≤ 50	6 877	7 159	0 3846	2 211	1 279	0 0522	0 0093	0 3491	0 4416	0 3611
4	15	3.0 ≤ E < 3.5	40 < B ≤ 50	6 877	7 159	0 3846	2 211	1 279	0 0522	0 0093	0 3491	0 4416	0 3611
5	15	3.0 ≤ E < 3.5	40 < B ≤ 50	6 877	7 159	0 3846	2 211	1 279	0 0522	0 0093	0 3491	0 4416	0 3611
6	15	3.0 ≤ E < 3.5	40 < B ≤ 50	6 877	7 159	0 3846	2 211	1 279	0 0522	0 0093	0 3491	0 4416	0 3611
7	15	3.0 ≤ E < 3.5	40 < B ≤ 50	6 877	7 159	0 3846	2 211	1 279	0 0522	0 0093	0 3491	0 4416	0 3611
8	15	3.0 ≤ E < 3.5	40 < B ≤ 50	6 877	7 159	0 3846	2 211	1 279	0 0522	0 0093	0 3491	0 4416	0 3611
9	15	3.0 ≤ E < 3.5	40 < B ≤ 50	6 877	7 159	0 3846	2 211	1 279	0 0522	0 0093	0 3491	0 4416	0 3611
10	15	3.0 ≤ E < 3.5	40 < B ≤ 50	6 877	7 159	0 3846	2 211	1 279	0 0522	0 0093	0 3491	0 4416	0 3611
11	11	2.5 ≤ E < 3.0	30 < B ≤ 40	4 230	4 852	0 1823	1 049	0 5985	0 0245	0 0044	0 1759	0 2408	0 1749
12	11	2.5 ≤ E < 3.0	30 < B ≤ 40	4 230	4 852	0 1823	1 049	0 5985	0 0245	0 0044	0 1759	0 2408	0 1749
13	11	2.5 ≤ E < 3.0	30 < B ≤ 40	4 230	4 852	0 1823	1 049	0 5985	0 0245	0 0044	0 1759	0 2408	0 1749
14	11	2.5 ≤ E < 3.0	30 < B ≤ 40	4 230	4 852	0 1823	1 049	0 5985	0 0245	0 0044	0 1759	0 2408	0 1749
15	11	2.5 ≤ E < 3.0	30 < B ≤ 40	4 230	4 852	0 1823	1 049	0 5985	0 0245	0 0044	0 1759	0 2408	0 1749
16	11	2.5 ≤ E < 3.0	30 < B ≤ 40	4 230	4 852	0 1823	1 049	0 5985	0 0245	0 0044	0 1759	0 2408	0 1749
17	12	2.5 ≤ E < 3.0	30 < B ≤ 40	4 614	5 293	0 1988	1 144	0 6529	0 0267	0 0048	0 1919	0 2627	0 1908
18	12	2.5 ≤ E < 3.0	30 < B ≤ 40	4 614	5 293	0 1988	1 144	0 6529	0 0267	0 0048	0 1919	0 2627	0 1908
19	12	2.5 ≤ E < 3.0	30 < B ≤ 40	4 614	5 293	0 1988	1 144	0 6529	0 0267	0 0048	0 1919	0 2627	0 1908
20	12	2.5 ≤ E < 3.0	30 < B ≤ 40	4 614	5 293	0 1988	1 144	0 6529	0 0267	0 0048	0 1919	0 2627	0 1908
21	12	2.5 ≤ E < 3.0	30 < B ≤ 40	4 614	5 293	0 1988	1 144	0 6529	0 0267	0 0048	0 1919	0 2627	0 1908
22	12	2.5 ≤ E < 3.0	30 < B ≤ 40	4 614	5 293	0 1988	1 144	0 6529	0 0267	0 0048	0 1919	0 2627	0 1908
23	12	2.5 ≤ E < 3.0	30 < B ≤ 40	4 614	5 293	0 1988	1 144	0 6529	0 0267	0 0048	0 1919	0 2627	0 1908
24	15	4.0 ≤ E < 4.5	50 < B ≤ 60	9 317	7 710	0 4777	2 744	1 595	0 0651	0 0116	0 4246	0 5217	0 4453
25	15	4.0 ≤ E < 4.5	50 < B ≤ 60	9 317	7 710	0 4777	2 744	1 595	0 0651	0 0116	0 4246	0 5217	0 4453
26	15	4.0 ≤ E < 4.5	50 < B ≤ 60	9 317	7 710	0 4777	2 744	1 595	0 0651	0 0116	0 4246	0 5217	0 4453
27	15	4.0 ≤ E < 4.5	50 < B ≤ 60	9 317	7 710	0 4777	2 744	1 595	0 0651	0 0116	0 4246	0 5217	0 4453
28	15	4.0 ≤ E < 4.5	50 < B ≤ 60	9 317	7 710	0 4777	2 744	1 595	0 0651	0 0116	0 4246	0 5217	0 4453
29	15	4.0 ≤ E < 4.5	50 < B ≤ 60	9 317	7 710	0 4777	2 744	1 595	0 0651	0 0116	0 4246	0 5217	0 4453
30	15	4.0 ≤ E < 4.5	50 < B ≤ 60	9 317	7 710	0 4777	2 744	1 595	0 0651	0 0116	0 4246	0 5217	0 4453
31	15	4.0 ≤ E < 4.5	50 < B ≤ 60	9 317	7 710	0 4777	2 744	1 595	0 0651	0 0116	0 4246	0 5217	0 4453
32	15	4.0 ≤ E < 4.5	50 < B ≤ 60	9 317	7 710	0 4777	2 744	1 595	0 0651	0 0116	0 4246	0 5217	0 4453
33	15	4.0 ≤ E < 4.5	50 < B ≤ 60	9 317	7 710	0 4777	2 744	1 595	0 0651	0 0116	0 4246	0 5217	0 4453
Min?	11		Total	219.6	214.9	11.11	63.85	36.90	1.507	0.2697	10.14	12.92	10.45
Limit	5.3		Limit	1750	1500	180	180	180	9	1.8	900	900	900
Criteria Met?	YES		Criteria Met?	YES	YES	YES	YES	YES	YES	YES	YES	YES	YES

For every burnup-enrichment pairing, the total allowable mass of U-235 is restricted by either the 1750 gU235 criticality limit, the mass of U-235 corresponding to the thermal limit of 1500 W, or the maximum mass of U-235 corresponding to a dose rate of 180 mrem/hr at the NCT side surface dose location. Tables 5.5-33 and 5.5-34 list the maximum mass of U-235 for each burnup-enrichment pairing corresponding to the NCT side surface dose rate limit and the 1500 W thermal limit, respectively. Table 5.5-35 provides the overall maximum allowable mass of U-235 for each burnup-enrichment pairing in the Model 2000 cask, by listing the minimum value for each pairing between those in Table 5.5-33, Table 5.5-34, and the 1750 g U-235 criticality limit.

**Table 5.5-33. Maximum Allowable Mass (g) of U-235 Based on NCT Side Surface Dose Rate**

Enrichment (wt% U-235)	Burnup (GWd/MTU)						
	0 < B ≤ 10	10 < B ≤ 20	20 < B ≤ 30	30 < B ≤ 40	40 < B ≤ 50	50 < B ≤ 60	60 < B ≤ 72
1.5 ≤ E < 2.0	5154.80	1628.96	602.82	285.17	159.76	97.54	55.74
2.0 ≤ E < 2.5	7344.89	2662.49	1019.96	471.55	257.50	155.33	88.83
2.5 ≤ E < 3.0	9575.63	3890.57	1578.15	725.73	388.32	231.30	132.21
3.0 ≤ E < 3.5	11820.69	5254.21	2280.34	1059.68	559.96	329.61	188.16
3.5 ≤ E < 4.0	14050.91	6706.34	3123.76	1483.58	780.06	454.72	258.88
4.0 ≤ E < 4.5	16278.51	8210.98	4086.65	2000.19	1054.98	611.18	346.98
4.5 ≤ E ≤ 5.0	18492.68	9743.59	5139.57	2608.01	1389.28	803.02	454.65

**Table 5.5-34. Maximum Allowable Mass (g) of U-235 Based on Thermal Limit**

Enrichment (wt% U-235)	Burnup (GWd/MTU)						
	0 < B ≤ 10	10 < B ≤ 20	20 < B ≤ 30	30 < B ≤ 40	40 < B ≤ 50	50 < B ≤ 60	60 < B ≤ 72
1.5 ≤ E < 2.0	1378.68	1032.58	868.06	764.27	693.59	642.49	597.13
2.0 ≤ E < 2.5	1825.93	1381.85	1170.50	1033.41	937.21	866.80	803.86
2.5 ≤ E < 3.0	2271.35	1731.30	1476.38	1307.99	1186.71	1096.17	1014.61
3.0 ≤ E < 3.5	2714.11	2080.44	1785.01	1586.74	1440.92	1330.18	1229.51
3.5 ≤ E < 4.0	3156.95	2430.56	2094.97	1868.99	1700.13	1569.51	1448.28
4.0 ≤ E < 4.5	3597.12	2780.35	2406.74	2154.40	1962.71	1812.69	1671.31
4.5 ≤ E ≤ 5.0	4037.08	3129.35	2718.49	2441.23	2229.19	2059.81	1898.20

**Table 5.5-35. Overall Maximum Allowable Mass (g) of U-235 Based on All Cask Limits**

Enrichment (wt% U-235)	Burnup (GWd/MTU)						
	0 < B ≤ 10	10 < B ≤ 20	20 < B ≤ 30	30 < B ≤ 40	40 < B ≤ 50	50 < B ≤ 60	60 < B ≤ 72
1.5 ≤ E < 2.0	1378.68	1032.58	602.82	285.17	159.76	97.54	55.74
2.0 ≤ E < 2.5	1750.00	1381.85	1019.96	471.55	257.50	155.33	88.83
2.5 ≤ E < 3.0	1750.00	1731.30	1476.38	725.73	388.32	231.30	132.21
3.0 ≤ E < 3.5	1750.00	1750.00	1750.00	1059.68	559.96	329.61	188.16
3.5 ≤ E < 4.0	1750.00	1750.00	1750.00	1483.58	780.06	454.72	258.88
4.0 ≤ E < 4.5	1750.00	1750.00	1750.00	1750.00	1054.98	611.18	346.98
4.5 ≤ E ≤ 5.0	1750.00	1750.00	1750.00	1750.00	1389.28	803.02	454.65

Overall Maximum Allowable Mass (g) of U-235 Based on All Cask Limits	
Table Legend	
	limited by thermal limit 1500 W
	limited by criticality mass of U-235
	limited by 90% of regulatory dose rate limit 180 mrem/hr

### 5.5.6. Irradiated Hardware and Byproduct Loading Table

In order to demonstrate compliance with the 10 CFR 71 (Reference 5-1) regulatory dose rate limits and the thermal limit of the cask, the Irradiated Hardware and Byproduct Loading Table must be confirmed for every shipment of irradiated hardware or byproducts in the Model 2000 cask. The use of this loading table is simple: for each of the radionuclides included in a shipment, enter the radionuclide into the table, enter the activity of the radionuclide, then calculate the decay heat and dose rate contribution at each regulatory location based on the dose rate per curie and decay heat values presented in Tables 5.4-12, 5.4-13 and 5.5-29.

Tables 5.5-36 through 5.5-38 provide radionuclide inventories for three hypothetical shipments of irradiated hardware, zirconium-95, and hafnium poison rods. The irradiated hardware radionuclide inventory presented in Table 5.5-39 lists the sample activities and percent-activity of the total content for a list of radionuclides based on a previous shipment of a piece of irradiated 304 SS in the Model 2000 cask with all of the radionuclide activities scaled up to higher activities. The zirconium and hafnium poison rod radionuclide inventories in Tables 5.5-40 and 5.5-41 are hypothetical radionuclide inventories, included only to provide additional examples.

**Table 5.5-36. Example Irradiated SS304 Radionuclide Inventory**

Nuclide	Ci/sample	% Activity	Total Activity (Ci)
H-3	6.75E-06	0.00%	4.605E-05
P-32	3.49E-04	0.00%	2.381E-03
S-35	8.26E-04	0.00%	5.635E-03
Cr-51	3.73E+00	2.12%	2.545E+01
Mn-54	5.60E+00	3.18%	3.821E+01
Fe-55	5.69E+01	32.35%	3.882E+02
Fe-59	3.32E-01	0.19%	2.265E+00
Co-58	2.85E+00	1.62%	1.944E+01
Co-60	1.01E+02	57.42%	6.891E+02
Ni-59	4.14E-02	0.02%	2.825E-01
Ni-63	5.42E+00	3.08%	3.698E+01
Zn-65	1.06E-02	0.01%	7.232E-02
Nb-93m	3.25E-04	0.00%	2.217E-03
Mo-99	6.13E-14	0.00%	4.182E-13
Tc-99m	5.94E-14	0.00%	4.053E-13
Total	175.89	100.00%	1200

**Table 5.5-37. Example Zr-95 Radionuclide Inventory**

Nuclide	Total Activity (Ci)
Zr-95	80,000

**Table 5.5-38. Example Hf Poison Rod Radionuclide Inventory**

Nuclide	% Activity	Total Activity (Ci)
Hf-175	4.21%	10,650
Hf-181	90.09%	228,000
Ta-182	5.70%	14,422
Total	100.00%	253,072

Tables 5.5-39 through 5.5-41 show the respective Irradiated Hardware and Byproduct Loading Tables for each of the hypothetical shipments outlined in Tables 5.5-36 through 5.5-38. These tables show that all three hypothetical shipments of irradiated hardware and byproduct contents comply with all dose rate and thermal criteria and would be acceptable for shipment.



**Table 5.5-39. Example SS304 Irradiated Hardware and Byproduct Loading Table**

Radio-nuclide	Activity (Ci)	Decay Heat (W)	NCT					HAC		
			DR <sub>surf</sub>			DR <sub>2m</sub>	DR <sub>cab</sub>	DR <sub>1m</sub>		
			Top	Side	Bottom			Top	Side	Bottom
Cr-51	25.40	5.53E-03	1.01E-13	4.19E-19	1.41E-18	5.41E-21	8.93E-22	3.23E-12	1.28E-18	2.41E-17
Mn-54	38.20	1.90E-01	8.77E-06	3.77E-04	1.63E-05	4.26E-06	7.27E-07	1.55E-05	7.82E-05	1.27E-05
Fe-55	388.20	1.34E-02	0.00E+00	0.00E+00	0.00E+00	0.00E+00	0.00E+00	0.00E+00	0.00E+00	0.00E+00
Fe-59	2.30	1.75E-02	2.81E-04	6.56E-03	4.20E-04	8.27E-05	1.43E-05	4.09E-04	1.22E-03	2.43E-04
Co-58	19.40	1.16E-01	2.64E-04	4.75E-03	4.22E-04	6.56E-05	1.16E-05	3.49E-04	8.67E-04	2.25E-04
Co-60	689.10	1.06E+01	2.88E-01	6.50E+00	4.30E-01	8.34E-02	1.43E-02	4.14E-01	1.20E+00	2.45E-01
Ni-63	37.00	3.82E-03	0.00E+00	0.00E+00	0.00E+00	0.00E+00	0.00E+00	0.00E+00	0.00E+00	0.00E+00
<b>Total</b>	-	10.970	0.289	6.514	0.431	0.084	0.014	0.415	1.203	0.245
<b>Limit</b>	-	1500	180	180	180	9	1.8	900	900	900
<b>Criteria Met?</b>	-	YES	YES	YES	YES	YES	YES	YES	YES	YES

**Table 5.5-40. Example Zr-95 Irradiated Hardware and Byproduct Loading Table**

Radionuclide	Activity (Ci)	Decay Heat (W)	NCT					HAC		
			DR <sub>surf</sub>			DR <sub>2m</sub>	DR <sub>cab</sub>	DR <sub>1m</sub>		
			Top	Side	Bottom			Top	Side	Bottom
Zr-95	80,000	787.0	4.01E-03	2.00E-01	9.45E-03	2.25E-03	3.83E-04	7.62E-03	4.37E-02	8.31E-03
<b>Total</b>	-	787.0	4.01E-03	2.00E-01	9.45E-03	2.25E-03	3.83E-04	7.62E-03	4.37E-02	8.31E-03
<b>Limit</b>	-	1500	180	180	180	9	1.8	900	900	900
<b>Criteria Met?</b>	-	YES	YES	YES	YES	YES	YES	YES	YES	YES

**Table 5.5-41. Example Hf Poison Rod Irradiated Hardware and Byproduct Loading Table**

Radionuclide	Activity (Ci)	Decay Heat (W)	NCT					HAC		
			DR <sub>surf</sub>			DR <sub>2m</sub>	DR <sub>cab</sub>	DR <sub>1m</sub>		
			Top	Side	Bottom			Top	Side	Bottom
Hf-175	10,650	25.1	1.75E-09	2.04E-11	3.74E-12	1.24E-13	2.01E-14	1.78E-08	5.13E-12	8.25E-12
Hf-181	228,000	986.8	4.49E-06	4.82E-06	7.81E-07	6.27E-08	1.08E-08	3.40E-05	1.57E-06	1.16E-06
Ta-182	14,422	129.6	1.94E+00	4.72E+01	2.88E+00	5.90E-01	1.01E-01	2.85E+00	8.85E+00	1.70E+00
<b>Total</b>	-	1141.5	1.94	47.20	2.88	0.59	0.10	2.85	8.85	1.70
<b>Limit</b>	-	1500	180	180	180	9	1.8	900	900	900
<b>Criteria Met?</b>	-	YES	YES	YES	YES	YES	YES	YES	YES	YES

### 5.5.7. Combined Content Shipments

There is the possibility of a shipment that includes multiple content types. To demonstrate compliance with all regulatory and cask requirements, the total thermal power and dose rate contributions from each content type must be determined. Using the procedure in Section 7.5.4, compliance is demonstrated for shipments of multiple content types. For illustration purposes, a shipment of mixed content that combines both irradiated fuel and hardware and byproduct is used as an example. Both the Irradiated Fuel Loading Table and the Irradiated Hardware and Byproduct Loading Table must be filled out for the respective radioactive contents. Then using the Combined Contents Loading Table in Section 7.5.4, the dose rate and thermal power contributions for each are summed, calculating the total thermal power and external dose rates for the shipment.

An example of this process can be demonstrated by using the hypothetical shipment of fuel rods introduced in Section 5.5.5 (see Table 5.5-30) and the example irradiated SS304 radionuclide inventory in Section 5.5.6 (see Table 5.5-36). For this hypothetical shipment of irradiated fuel and hardware, the Irradiated Fuel Loading Table is filled out (see Table 5.5-32) and the Irradiated Hardware and Byproduct Loading Table (see Table 5.5-39) are filled out for the respective contents. Then by following the procedure in Section 7.5.4, the Combined Contents Loading Table is filled out for this shipment, as shown in Table 5.5-42. Based on the total thermal power and external dose rates calculated in Table 5.5-42, this hypothetical shipment of irradiated fuel and hardware is acceptable for shipment in the Model 2000 cask.

**Table 5.5-42. Example Combined Contents Loading Table**

Content	Thermal Power (W)	NCT					HAC		
		DR <sub>surf</sub>			DR <sub>2m</sub>	DR <sub>cab</sub>	DR <sub>1m</sub>		
		Top	Side	Bottom			Top	Side	Bottom
Fuel	214.9	11.11	63.85	36.90	1.507	0.2697	10.14	12.92	10.45
Hardware / Byproduct	10.97	0.289	6.514	0.431	0.084	0.014	0.415	1.203	0.245
Cobalt-60 Isotope Rods	-	-	-	-	-	-	-	-	-
Total	225.87	11.399	70.364	37.331	1.591	0.2837	10.555	14.123	10.695
Limit	1500	180	180	180	9	1.8	900	900	900
Criteria Met?	YES	YES	YES	YES	YES	YES	YES	YES	YES

For other combinations of contents, the Loading Table of each content type must be completed and the total contribution to the thermal power and dose rates must be confirmed to be below the limit. Additionally, the requirements for each content type that are defined in Section 1.2.2 must be met.

## 5.6 References

- 5-1 U.S. NRC, 10 CFR 71, "Packaging and Transportation of Radioactive Material," Washington D.C.
- 5-2 Oak Ridge National Lab, "SCALE: A Comprehensive Modeling and Simulation Suite for Nuclear Safety Analysis and Design, ORNL/TM-2005/39, Version 6, Vols. I-III," ORNL/TM-2005/39, Version 6.1, June 2011.
- 5-3 American Society for Testing and Materials, "Standard Specification for General Requirements for Flat-Rolled Stainless and Heat-Resisting Steel Plate, Sheet, and Strip," ASTM A480, 2016.
- 5-4 R.J. McConn et al., "Compendium of Material Composition Data for Radiation Transport Modeling," PNNL-15870, Revision 1, March 2011.
- 5-5 T. Goorley, et al., "Initial MCNP Release Overview - MCNP6 Version 1.0," Los Alamos National Laboratory, LA-UR-13-22934, April 2013.
- 5-6 J. Conlin et al., "Listing of Available ACE Data Tables," Los Alamos National Laboratory, LA-UR-13-21822, Revision 4, June 2014.
- 5-7 U.S. Nuclear Regulatory Commission, "Standard Review Plan for Transportation Packages for Radioactive Material," NUREG-1609, March 1999.
- 5-8 ANS 6.1.1 Working Group, M. E. Battat (Chairman), "American National Standard Neutron and Gamma-Ray Flux-to-Dose-Rate Factors," American Nuclear Society, ANSI/ANS-6.1.1-1977, March 1977
- 5-9 L. C. Leal et al., "ARP: Automatic Rapid Process for the Generation of Problem-Dependent SAS2H/ORIGEN-S Cross-Section Libraries," ORNL/TM-13584, April 1998.
- 5-10 S.M. Bowman et al., "Recommendations on Fuel Parameters for Standard Technical Specifications for Spent Fuel Storage Casks," NUREG/CR-6716, February 2001.
- 5-11 C.J. Werner, et al., "MCNP Version 6.2 Release Notes," Los Alamos National Laboratory, LA-UR-18-20808, February 2018.

## **6 CRITICALITY EVALUATION**

### **6.1 Description of Criticality Design**

#### **6.1.1. Design Features**

This section describes the design features of the Model 2000 Transport Package that are important for maintaining criticality safety.

The Model 2000 cask is a cylindrical lead lined cask used for transporting Type B quantities of radioactive materials and solid fissile materials. For the fissile contents considered in this analysis, the High Performance Insert (HPI) is required to be used along with the Model 2000 cask. The HPI consists of the insert body and two plugs for the top and bottom. Attached to the insert body is a series of [[ ] in the Model 2000 cask cavity. Shoring components such as rod holders or the material basket may be present. This analysis is generic by design to allow for the simple loading flexibility of the desired contents into the HPI, then loading of the HPI into the Model 2000 cask. Figure 1.2-1 shows the package configuration. The HPI and material basket are described in Section 1.2.1.3 and Section 1.2.1.4, respectively.

The system consists of the Model 2000 cask, HPI, and other components which ensure that the fuel rod content is shipped upright (e.g., material basket and the fuel rod tube). The term fuel rod is used throughout the context of Chapter 6 to more accurately depict the form of the approved GE BWR 10x10 irradiated fuel content and to reflect how it was modeled in the supporting criticality evaluations.

The Model 2000 cask, HPI, and material basket safety components retain the contents within a fixed geometry relative to other packages in an array. Fuel content rearrangement is limited by the HPI cavity and material basket category B safety components. The fuel pellets can be confined (e.g. encapsulated) within the fuel rod tube; however, the cladding material of the fuel rod is not credited in the criticality analysis. Components such as rod holders or the material basket may provide additional confinement but are not credited in the criticality analyses.

#### **6.1.2. Summary Table of Criticality Evaluation**

The demonstration of criticality safety meeting 10 CFR 71 (Reference 6-1) provides assurance of the safe transport of the fissile contents with the Model 2000 and the HPI under normal conditions of transport (NCT) and hypothetical accident conditions (HAC).

The contents are GE BWR 10x10 irradiated fuel elements. The configuration of the contents and packaging demonstrate the most reactive configuration for the package.

A summary of most limiting cases is provided in Table 6.1.2-1 for fuel rod content. All limiting cases meet the Upper Subcritical Limit (USL), as defined in Section 6.3.4. The fissile mass limit for fuel rods defined by the criticality safety analyses provide an input to the Irradiated Fuel Rod Loading Table as further discussed in Section 7.5.3. For the fuel rod content, data trends of results in Sections 6.4, 6.5, 6.6, and 6.9.4 show that as the fuel rod outer radius increases the overall system reactivity decreases, thus, the fuel pellet outer radius of 0.392 cm is set as the minimum fuel pellet outer radius.

NEDO-33866 Revision 6  
Non-Proprietary Information

While Sections 6.4 through 6.6 form the initial basis for the criticality analysis, additional sensitivity studies provided in Section 6.9.4 determine the limitations on the allowed content. The most reactive summary results presented in Table 6.1.2-1 are from the evaluations presented in Section 6.9.4. Table 6.1.2-2 provides justification for maintaining the administratively reduced U-235 mass limit of 1750 grams from Section 6.3.1.1.1.

Fissile material evaluations and limitations are based on fresh, unirradiated fuel (no credit is applied for burnup).

**Table 6.1.2-1. Most Reactive Fuel Rod Content Summary at 5 wt.% U-235**

Case Name	Fuel OR (cm)	Half-pitch (cm)	$k_{eff}$	$\sigma$	$k_{eff}+2\sigma$	Maximum $k_{eff}$ <sup>1</sup>	H/U-235	EALF (eV) <sup>2</sup>	U-235 Mass(g)
Single Package									
5p-r392-p070	0.392	0.7	0.91594	0.00025	0.91644	0.92560	684.27	1.08	1500
NCT, 5N Package Array									
5p-r392-p070_NCT_5N	0.392	0.7	0.91127	0.00009	0.91145	0.92056	684.27	1.11	1500
HAC, 2N Package Array									
5p-r392-p070_HAC_2N	0.392	0.7	0.91669	0.00011	0.91691	0.92608	684.27	1.07	1500

NOTES: USL is defined as 0.9370 per Section 6.3.4.

<sup>1</sup> Maximum  $k_{eff}$  includes the applied 1%  $k_{eff}$  uncertainty for pitch geometric modeling –see Section 6.9.1.

<sup>2</sup> EALF is defined as energy of average lethargy causing fission.

**Table 6.1.2-2. Most Limiting Fuel Rod Content Summary using the Administrative U-235 Mass Limit**

Case Name	Fuel OR (cm)	Half-pitch (cm)	$k_{eff}$	$\sigma$	$k_{eff}+2\sigma$	Maximum $k_{eff}$ <sup>1</sup>	H/U-235	EALF (eV)	U-235 Mass Limit (g) <sup>2</sup>
Single Package									
5p-r392-p065	0.392	0.65	0.90973	0.00030	0.91033	0.91943	586.40	1.37	1750
NCT, 5N Package Array									
5p-r392-p065_NCT_5N	0.392	0.65	0.90421	0.00012	0.90445	0.91349	586.40	1.43	1750
HAC, 2N Package Array									
5p-r392-p065_HAC_2N	0.392	0.65	0.90999	0.00014	0.91027	0.91937	586.40	1.37	1750

NOTES: USL is defined as 0.9370 per Section 6.3.4.

<sup>1</sup> Maximum  $k_{eff}$  includes the applied 1%  $k_{eff}$  uncertainty for pitch geometric modeling –see Section 6.9.1.

<sup>2</sup> An administratively reduced fissile mass limit is defined –see Section 6.3.1.1.1 for further details.

### **6.1.3. Criticality Safety Index**

The Model 2000 cask is shipped exclusive use only; a single package defines a conveyance. Therefore, per the guidance in 10 CFR 71.59 the criticality safety index is 50 for the Model 2000 cask for any fissile content.

## **6.2 Fissile Material Contents**

The purpose of this analysis is to demonstrate that the contents are subcritical for a defined U-235 mass. The criticality analysis demonstrates compliance with 10 CFR 71 of the Model 2000 Transport Package with the HPI containing irradiated GE BWR 10x10 fuel elements.

### **6.2.1. Fuel Rods**

The fuel rod contents of the package are restricted to low-enriched uranium dioxide (UO<sub>2</sub>) fuel. The fissile material in fuel pellets is assumed to be uranium initially enriched up to a maximum of 6.0 wt% U-235 with the remaining 94 wt% modeled solely as U-238. Any U-232, U-234, or U-236 is assumed to be U-238 because these uranium isotopes are not fissile, are present in small amounts, and have total neutron cross sections that tend to be greater than the total neutron cross section for U-238. The 6.0 wt% U-235 enrichment was only used for those studies presented in Sections 6.4 through 6.6. Section 6.9.4 reduced the enrichment to 5 wt% U-235 to align with the Section 6.8 benchmarking and allowed content. Additionally, no pellet dishing fraction or chamfering is modeled, which conservatively increases the number of U-235 atoms. Fissile material in the fuel rod contents is only in the form of UO<sub>2</sub>, and administratively limited to 1750 grams of U-235. The models use the theoretical density, 10.96 g/cm<sup>3</sup>, for UO<sub>2</sub>. For the fuel rod content, sensitivity analyses showed that as the fuel rod OR increases the overall system reactivity decreases. Fissile material evaluations and limitations are based on initial, unirradiated fuel, without credit for burnup.

## **6.3 General Considerations**

### **6.3.1. Model Configuration**

#### **6.3.1.1. Fissile Material Contents Model Configuration**

All fissile contents must be in solid form. Theoretical material density is conservatively evaluated for each content. Fissile material evaluations and limitation are based on initial, unirradiated fuel, without credit for burnup.

##### **6.3.1.1.1. Fuel Rods**

The fuel rod contents of the package are restricted to low-enriched UO<sub>2</sub> fuel. The fissile material in fuel pellets is assumed to be uranium initially enriched up to a maximum of 6.0 wt% U-235 with the remaining 94 wt% modeled solely as U-238. The 6.0 wt% U-235 enrichment was only used for those initial studies presented in Sections 6.4 through 6.6. Section 6.9.4 reduced the enrichment to 5 wt% U-235 to align with the Section 6.8 benchmarking and allowed content. See Section 6.3.2 for material properties.

The fuel rod was initially modeled as a long cylinder with an axial length of [[        ]] cm, which is near equivalent to the interior height of the HPI cavity (i.e., [[        ]] cm modeled) in Sections 6.4 through 6.6. Section 6.9.4 provides additional sensitivity studies varying the axial length and OR of the fuel rod. The modeled axial length bounds the requirement of minimum 5.3-inch rod length segments specified by the shielding analysis. The fuel rod OR was initially varied from 0.2 to 0.5 cm to encompass a variety of fuel designs. Smaller fuel rod OR results in a higher reactivity, see Sections 6.4, 6.5, 6.6, and 6.9.4 for results of each transport assessment. The materials of the fuel rod cladding or structural components are not modeled. Fuel pellets are assumed to be confined within cylindrical components (e.g., fuel rod holders, and/or the material basket).

The fuel rods are modeled in a hexagonal array with expanding pitch. The addition of more fuel rods through the expansion of the lattice model is evaluated to determine the optimum hydrogen-to-U-235 (H/U-235) ratio. While expansion of the lattice is a condition of HAC, it is also applied to NCT to optimize H/U-235. The fissile mass modeled in the fuel rod array is determined using a mixture of UO<sub>2</sub> and H<sub>2</sub>O. The limiting evaluations in Section 6.9.4 assessed a range of UO<sub>2</sub> masses (105 kg to 4 kg) with a U-235 enrichment of 5 wt%. A circular boundary, which equates to a quantity of U-235, is defined to limit the infinite, heterogeneous lattice to a specific array size. The circular boundary may cut rods radially, thus varying the UO<sub>2</sub> mass represented a range of U-235 mass less than 4,600 grams to 180 grams. Therefore, an administratively reduced limit of 1,750 grams of U-235 is defined. The equation below displays how the circular boundary radius is calculated for the varying hexagonal pitch sizes. Additionally, as the pitch is expanded to increase H/U-235, the confinement boundary of the HPI cavity will reduce the fissile mass within the boundary.

$$cavity\ OR = \sqrt{\#rods \frac{2\sqrt{3}P^2}{\pi}}$$

where, P is the hexagonal half-pitch

$$\#rods = M_{UO_2} / (\pi * OR_{fuel}^2 * H * \rho_{UO_2})$$

where,

H is the modeled fuel rod height in cm

M<sub>UO<sub>2</sub></sub> is the mass of UO<sub>2</sub> in grams

ρ<sub>UO<sub>2</sub></sub> is the theoretical density of UO<sub>2</sub>

Table 6.3.1-1 defines the variation of fuel outer radii and pitches evaluated for the fuel rod content; the largest pitches for the smallest rods are not modeled as the k<sub>eff</sub> trend is already shown to be decreasing. Figure 6.3.1-1 shows the fuel rod model geometry, and Figure 6.3.1-2 shows examples of how the circular boundary defines the fissile mass limit by artificially cutting into the lattices.

Structural features of the rods, shoring components such as rod holders, or the HPI material basket may provide additional confinement of the fuel lattice expansion; however, only the HPI cavity is credited for the confinement boundary. Representation of the fuel structural components as water results in an increase in reactivity due to both a decrease in neutron absorption and an increase in fuel rod lattice moderation.

**Table 6.3.1-1. Initial Fuel Rod Content Model Parameters**

Parameter	Value (cm)
Fuel pellet radius (FROR)	0.2, 0.3, 0.4, 0.5
Half-pitch	FROR[XX]+0.3, FROR[XX]+0.4, FROR[XX]+0.6, FROR[XX]+0.7, FROR[XX]+0.8, FROR[XX]+0.9, FROR[XX]+1.1, FROR[XX]+1.2, FROR[XX]+1.4, FROR[XX]+1.6, FROR[XX]+2.0

[[

**Figure 6.3.1-1. Fuel Rod Content Model Geometry**

]]

[[

**Figure 6.3.1-2. Fuel Rod Content Boundary Model Geometry (Not to Scale)**

]]

For the transport evaluations of fuel rods, the maximum fuel  $k_{\text{eff}}$  occurs when the fuel lattice is moderated with full density water. For HAC, when leakage during immersion for fuel rod loading activities is possible, moderation in the fuel lattice is assumed present. The full density moderation in the fissile region is conservatively maintained for NCT.



#### **6.3.1.2. Model 2000 and HPI Model Configuration**

The MCNP6 model geometry used for criticality safety calculations is a detailed three-dimensional model of the HPI and the Model 2000 cask. Some slight simplifications are made to the MCNP6 geometry to reduce the modeling complexity, such as [[  
]]

The design features of the Model 2000 with the HPI are provided in Section 5.3, including dimensions, materials of construction, and densities of the materials. Table 6.3.1-2 provides the relevant dimensions of the MCNP6 model including the modeled thicknesses of each material used in the geometry. Table 6.3.1-2 along with Section 5.3 allows for a quick review of the most significant dimensions of the criticality model geometry. It can be noted in Table 6.3.1-2 that all HPI dimensions are minimum, with the fabrication tolerances subtracted from the nominal values. The model dimensions for the Model 2000 cask use both nominal and minimum values where it is appropriate. For example, for the [[  
]] at the minimum thickness. However, a number of the dimensions for the cask and overpack are prescribed thicknesses for steel plate that are used for the cask shells (e.g., the 1-inch rolled cask shells). For these instances the prescribed thickness of the steel plate is used for the MCNP geometry.

**Table 6.3.1-2. Relevant MCNP Model Dimensions**

Model 2000 Component	Part	Dimension	Value (cm)	Value (in)
Cask	Cask Lid	t <sub>SS1</sub>	3.810	1.500
		t <sub>Pb</sub>	13.64	5.370
		t <sub>SS2</sub>	4.445	1.750
	Cask Side	r <sub>cavity</sub>	33.66	13.25
		t <sub>SS1</sub>	2.540	1.000
		t <sub>Pb</sub>	10.16	4.000
		t <sub>SS2</sub>	2.540	1.000
		h <sub>Pb</sub> <sup>3</sup>	141.9	55.87
	Cask Bottom	t <sub>SS</sub>	14.94 <sup>1</sup>	5.880 <sup>1</sup>
		h <sub>cavity</sub>	137.5	54.13
HPI	HPI Top Lid	t <sub>SS1</sub>	[[	
		t <sub>DU</sub>		
		t <sub>SS2</sub>		
	HPI Body Side	r <sub>cavity</sub>		
		t <sub>SS1</sub>		
		t <sub>DU</sub>		
		t <sub>SS2</sub>		
	HPI Bottom Lid	t <sub>SS1</sub>		
		t <sub>DU</sub>		
		t <sub>SS2</sub>		]]

Notes: <sup>1</sup> Cask bottom modeled flat, with thickness equal to the 6.13" height minus [[ ]].  
<sup>2</sup> Minimum depleted uranium (DU) thicknesses considered with tolerance gaps explicitly modeled.  
<sup>3</sup> Lead column height.

The package has multiple void regions, including within the confinement system. The effect of variations in the package moderation is evaluated by flooding all spaces within the package and varying the light water moderator density from 0.0 to 1.0 g/cm<sup>3</sup> (full density). Although leakage during immersion is not credible for HAC, the effect of varying package moderation for HAC was conservatively evaluated to cover normal loading and unloading activities. For NCT, the package cavities, unless otherwise noted, are dry with no additional moderation, as this is representative of this transport condition. Varying the H/U-235 ratio optimizes fissile contents, thus a full spectrum of density variation for each cavity region is not necessary to show the trend toward isolation of a package in an array.

Generally, for package arrays, moderating only the content fissile region with full density water results in the maximum neutron interaction between packages in an array and bounds any variations in the flooding sequence. The voided space in packaging cavities and between packages in an array allows for increased interaction between the packages. The inclusion of interspersed moderation in these regions would increase the isolation of packages within the array, which leads to a decreasing system reactivity approaching that of a single, isolated package. For the single package analysis, the package is fully flooded. Hence, no void regions exist within the model. This generates an increase in reflection, while decreasing particle leakage. However, as the reflection from the depleted uranium (DU) HPI shields provides the dominant increase in neutron interaction within a package, the variation of moderator density provides little additional neutron moderation

to increase the package reactivity for the package array and single package. Additionally, the single package and package array model have a 30.48 cm-thick full density water reflector blanket around the exterior. The specification of 30.48 cm (12 inches) of water reflection is selected as a practical value. SSG-26 (Reference 6-2), Section 6.8.1, specifies 20 cm of water reflection as a practical value, as an additional 10 cm of water reflection would add less than 0.5% in reactivity to an infinite slab of U-235.

Chapter 2 structural evaluations show no damage or deformation to the HPI and material basket for NCT or HAC. Model 2000 cask structural evaluations define localized damage for the HAC pin-puncture test and damage to the impact limiters during drop tests, thus, the overpack is conservatively not modeled for HAC. A drop may also allow the content to shift within the HPI cavity. The fuel rod content is defined as the length of the HPI cavity and allowed to shift within the HPI.

Figure 6.3.1-3 shows the HAC MCNP model geometry.

[[

]]

**Figure 6.3.1-3. Package Model Geometry**

#### **6.3.1.2.1. NCT Model**

For NCT, the MCNP criticality model includes the HPI and the Model 2000 cask, and conservatively neglects the overpack material and spacing to be consistent with the HAC model, even though structural evaluations show that the damage to the overpack is minimal. The materials for the HPI and cask are defined as prescribed in Section 6.3.2 in the appropriate cells of the model. The NCT 5N package array is represented by seven (7) packages in a hexagonal array as to provide maximum reflection and package neutron interaction. Figure 6.3.1-4 shows the top view of the MCNP model, NCT array. For cases where the fissile content size is limited such that it does not occupy the full HPI cavity radius, the contents are positioned within the HPI cavity toward the centroid of the group of packages, see Figure 6.3.1-5 for example of fuel rod case limited by mass.

Light water moderation is used within the fissile material matrix for each content, optimizing the H/U-235 ratio. No leakage of water is evaluated in the various cavity regions of the packaging, for the evaluation of undamaged packages under NCT (per 10 CFR 71.55(d)). The Model 2000 cask cavity region is void and the HPI cavity region is flooded; this NCT configuration is evaluated for conservatism, and does not imply in-leakage of water during transportation. Full density moderation is maintained between the packages, as  $k_{eff}$  results for the single package and package array (NCT and HAC) are very close indicating the shield materials of the HPI and cask provide strong reflection thus neutronically isolating each package within the array.

[[

]]

**Figure 6.3.1-4. Package Array NCT, 5N Model Geometry**

[[

]]

**Figure 6.3.1-5. Package Array NCT, 5N Model Geometry, Content Positioning**

**6.3.1.2.2. HAC Model**

For HAC, the MCNP6 criticality model is the same as the shielding model, and only includes the HPI and the Model 2000 cask, neglecting the material and spacing of the overpack. This model conservatively assumes the complete destruction and removal of the overpack. Additionally, to be consistent with shielding analysis, the HAC model includes the lead slump from which the maximum deformation in the lead column is calculated to be 3.56 mm, which is conservatively rounded up to 4 mm (Section 2.12.2). Figure 6.3.1-6 shows the MCNP model for the HAC array. For cases where the fissile content size is limited such that it does not occupy the full HPI cavity radius, the contents are positioned within the HPI cavity toward the center package. See Figure 6.3.1-7 for an example of a case limited by fissile mass.

Light water moderation is used within the fissile material matrix for each content, optimizing the H/U-235 ratio. Moderation caused by in-leakage is limited to moderators no more effective than water from sources external to the package. Per 10 CFR 71.59(a)(2), the HAC, 2N assessment evaluates the sensitivity of hydrogenous moderation by evaluating water in-leakage into all void spaces of the package cavity regions, including those within the containment system. The moderation space is defined as all available space within the packaging cavities, not including any space occupied by the structural and shielding material design. The moderation density is varied from 0 to 1.0 g/cm<sup>3</sup> for the HPI cavity region and the Model 2000 cask region. A full spectrum of density variation for each cavity region is not necessary to show the trend toward isolation of the package in an array. The fissile material matrix region is maintained as fully flooded with full density water for both contents.

[[

]]

**Figure 6.3.1-6. Package Array HAC, 2N Model Geometry**

[[

]]

**Figure 6.3.1-7. Package Array HAC, 2N Model Geometry, Content Positioning**

### **6.3.2. Material Properties**

The material compositions used in the criticality safety analyses are listed in Table 6.3.2-1 through Table 6.3.2-5. The structural components of the Model 2000 cask are constructed of Type 304 stainless steel. The nuclear properties relevant to criticality safety for 304 stainless steel are in Table 6.3.2-1. Type [[ ]] stainless steel comprises the structural components of the HPI. The nuclear properties relevant to criticality safety for [[ ]] stainless steel are in Table 6.3.2-2. It can be noted that there is negligible difference between the two types of stainless steel in terms of absorption properties. Both types are only included for accuracy of the actual materials of construction. Any slight change in the elemental composition of these steels does not result in any significant increase in calculated reactivity. The densities and material compositions for both stainless steel types are from Pacific Northwest National Lab report PNNL-15870 (Reference 6-3). The shielding material of the Model 2000 cask is solely comprised of lead. The

nuclear properties relevant to criticality safety for lead are in Table 6.3.2-3. The shielding material of the HPI is solely comprised of DU. The nuclear properties relevant to criticality safety for DU are in Table 6.3.2-4. The densities of the lead and DU materials are based on the minimum specified densities for these materials in the respective component licensing drawings in Section 1.3.1. Isotopic masses are from SCALE6.1 Manual, Table M8.2.1 (Reference 6-4). For the modeling of water moderation, the  $S(\alpha,\beta)$  thermal kernel treatment for hydrogen in the water is applied. The collision kinematics data includes thermal kinematics kernels to describe thermal scattering in moderating materials such as hydrogen in water. Table 6.3.2-5 defines the fissile material properties.

**Table 6.3.2-1. Nuclear Properties of Type 304 Stainless Steel**

Element	Isotope	ZAID	Mass Fraction
C	C-12	6012	3.9537E-04
	C-13	6013	4.6337E-06
Si	Si-28	14028	4.5933E-03
	Si-29	14029	2.4168E-04
	Si-30	14030	1.6499E-04
P	P-31	15031	2.3000E-04
S	S-32	16032	1.4207E-04
	S-33	16033	1.1568E-06
	S-34	16034	6.7534E-06
	S-36	16036	1.6825E-08
Cr	Cr-50	24050	7.9300E-03
	Cr-52	24052	1.5903E-01
	Cr-53	24053	1.8380E-02
	Cr-54	24054	4.6614E-03
Mn	Mn-55	25055	1.0000E-02
Fe	Fe-54	26054	3.9617E-02
	Fe-56	26056	6.4490E-01
	Fe-57	26057	1.5160E-02
	Fe-58	26058	2.0529E-03
Ni	Ni-58	28058	6.2158E-02
	Ni-60	28060	2.4768E-02
	Ni-61	28061	1.0946E-03
	Ni-62	28062	3.5472E-03
	Ni-64	28064	9.3254E-04
Density (g/cm <sup>3</sup> )	8.00		

**Table 6.3.2-2. Nuclear Properties of [[**

**]]**

Element	Isotope	ZAID	Mass Fraction
C	C-12	6012	4.0525E-04
	C-13	6013	4.7496E-06
Si	Si-28	14028	4.6576E-03
	Si-29	14029	2.4507E-04
	Si-30	14030	1.6730E-04
P	P-31	15031	2.3000E-04
S	S-32	16032	1.4207E-04
	S-33	16033	1.1568E-06
	S-34	16034	6.7534E-06
	S-36	16036	1.6825E-08
Cr	Cr-50	24050	7.0953E-03
	Cr-52	24052	1.4229E-01
	Cr-53	24053	1.6445E-02
	Cr-54	24054	4.1707E-03
Mn	Mn-55	25055	1.0140E-02
Fe	Fe-54	26054	3.7769E-02
	Fe-56	26056	6.1482E-01
	Fe-57	26057	1.4453E-02
	Fe-58	26058	1.9571E-03
Ni	Ni-58	28058	8.0637E-02
	Ni-60	28060	3.2131E-02
	Ni-61	28061	1.4200E-03
	Ni-62	28062	4.6018E-03
	Ni-64	28064	1.2098E-03
Mo	Mo-92	42092	3.5374E-03
	Mo-94	42094	2.2586E-03
	Mo-95	42095	3.9322E-03
	Mo-96	42096	4.1686E-03
	Mo-97	42097	2.4141E-03
	Mo-98	42098	6.1715E-03
	Mo-100	42100	2.5175E-03
Density (g/cm <sup>3</sup> )	8.00		



**Table 6.3.2-3. Nuclear Properties of Lead**

Element	Isotope	ZAID	Mass Fraction
Pb	Pb-204	82204	1.3781E-02
	Pb-206	82206	2.3956E-01
	Pb-207	82207	2.2074E-01
	Pb-208	82208	5.2592E-01
Density (g/cm <sup>3</sup> )	11.34		

**Table 6.3.2-4. Nuclear Properties of Depleted Uranium**

Element	Isotope	ZAID	Mass Fraction
U	U-235	92235	7.0000E-03
	U-238	92238	9.9300E-01
Density (g/cm <sup>3</sup> )	[[        ]]		

**Table 6.3.2-5. Nuclear Properties of Fissile Content**

Compound	Isotope	ZAID	Mass Fraction	Density (g/cm <sup>3</sup> )
UO <sub>2</sub> , 5 wt% U-235	U-235	92235	4.4071E-02	10.96 <sup>1</sup>
	U-238	92238	8.3735E-01	
	O-16	8016	1.1857E-01	

References:

<sup>1</sup> Reference 6-4 Density, Table M8.2.4.

### 6.3.3. Computer Codes and Cross Section Libraries

The criticality safety analysis was completed using MCNP6 Version 1.0 (Reference 6-5) and 2.0 (Reference 6-6) with the continuous-energy neutron data library ENDF/B-VII.1 (Reference 6-7). MCNP6 is a general-purpose, continuous-energy, generalized-geometry, time-dependent, Monte Carlo radiation-transport code designed to track many particle types over a broad range of energies. The criticality safety assessment is for low-enriched uranium fuel rods in the Model 2000 cask with the HPI. MCNP6 meets the recommendations in Section 4, Method of Analysis defined in NUREG/CR-5661 (Reference 6-8).

### 6.3.3.1. Convergence Criteria

Convergence of the cases in criticality safety analysis was verified through inspection of the Shannon entropy of the fission source distribution. In order to determine the Shannon entropy of the problem, MCNP6 divides the fissionable regions of the problem into several bins, which then tally the fission sources during the random walks of each cycle. As the number of cycles completed increases, the fission source distribution will converge to steady state. In the output, MCNP6 prints which cycle was the first cycle to have a value of Shannon entropy within one standard deviation of the average Shannon entropy of the last half of the cycles analyzed; this is the minimum acceptable source convergence. The proper determination of the source convergence requires inspection of the plot of Shannon entropy versus cycle number, from which it can be determined at which cycle number the Shannon entropy converges. At least that many cycles were discarded, and more than 100 additional cycles are run after source convergence. Additionally, to determine adequacy of  $k_{\text{eff}}$  convergence, the behavior of  $k_{\text{eff}}$  with cycle number is evaluated to ensure no upward or downward trends are present.

### 6.3.4. Demonstration of Maximum Reactivity

A system is considered acceptably subcritical if a calculated  $k_{\text{eff}}$  plus calculational uncertainties lies at or below the USL (i.e.,  $k_{\text{system}} + \Delta k_{\text{system}} \leq \text{USL}$ ). Thus, the USL is the magnitude of the sum of the biases, uncertainties, and administrative and/or statistical margins applied to a set of critical benchmarks, such that a high degree of confidence defines subcriticality of the system (Reference 6-9):

$$\text{USL} = 1 - \Delta k_m + \beta - \Delta\beta$$

where

$\Delta k_m$  is the additional margin to ensure subcriticality (0.05)

$\beta$  is the calculation bias

$\Delta\beta$  is the uncertainty in the bias

Based on a given set of critical experiments, the USL is defined as a function of key system parameters, such as EALF, fuel enrichment, or H/U-235 ratio. Because both  $\beta$  and  $\Delta\beta$  may vary with a given parameter, the USL is typically expressed as a function of the parameter, within an appropriate range of applicability derived from the parameter bounds. Table 6.8.2-1 displays the USL functions for the Model 2000 Transport Package criticality safety analysis.

The low-enriched lattice system USL function is applicable to the fuel rod content. The H/U-235 ratio from the most limiting case for the allowed content in Section 6.9.4 was used to determine the USL. As shown in Table 6.1.2-1, the limiting cases for the single package and package array have a H/U-235 value of 684.27. The value of H/U-235 is calculated based on a ratio of volume for the pitch cell and the estimated number of rods modeled (see equation below). Applying this value to the USL equation in Table 6.8.2-1, results in a rounded USL value of 0.9370 for fuel rod contents (e.g.,  $0.9473 - 1.5031\text{E-}5 \times 684.27 = 0.93701$  for  $X > 214.9$ ).

$$\frac{H}{U^{235}} \text{ Ratio} = WTF \times \frac{H_2O \text{ Density}}{UO_2 \text{ Density}} \times \frac{(1 - \text{Enr. } U^{235})MW_{U^{238}} + \text{Enr. } U^{235}MW_{U^{235}} + 2MW_{O_2}}{MW_{H_2O}} \times \frac{2}{1} \times \frac{1}{\text{Enr. } U^{235}}$$

where

$$\text{Water to Fuel Volume Ratio} = \frac{\text{Water volume in fuel rod cell} \times \# \text{rods}}{\text{Fuel volume} \times \# \text{rods}}$$

## 6.4 Single Package Evaluation

It should be noted that the following evaluations conducted with a U-235 enrichment of 6 wt% form the initial limiting configuration for the allowed content analyses presented in Section 6.9.4.

### 6.4.1. Configuration

This single model represents NCT and HAC for the single package evaluations; models are described in Section 6.3. The reference case for the single package is to fill all cavity regions that are normally void space with full density water. The fissile matrix region is moderated with full density water.

### 6.4.2. Results

Peak cases for fuel rod content are provided in Table 6.4.2-1; full results are in Section 6.9.3, Table 6.9.3-2. Figure 6.4.2-1 displays the trends for all data. Based on the most limiting case for the single package, FRLSmh\_1\_22 (OR=0.2 cm, hex, half-pitch=0.7 cm), the  $k_{\text{eff}} + 2\sigma$  equals 0.92349. Data trends show that as the fuel rod OR increase the overall system reactivity decreases, thus the minimum fuel rod OR of 0.2 cm is a limiting parameter. Section 6.3.4 defines the USL value as 0.9370 for fuel rod contents.

**Table 6.4.2-1. Fuel Rod Content, Single Package, Maximum Cases**

Case Name	Fuel OR (cm)	Half-Pitch (cm)	Estimated No. Rods Modeled	U-235 Mass (g)	$k_{\text{eff}}$	$\sigma$	$k_{\text{eff}}+2\sigma$	H/U-235	EALF (eV)
FRLSmh_1_1	0.2	0.50	[[	1766	0.85526	0.00025	0.85576	--	--
FRLSmh_1_2	0.2	0.60		1766	0.90946	0.00023	0.90992	--	--
FRLSmh_1_21	0.2	0.65		1766	0.92134	0.00022	0.92178	--	--
FRLSmh_1_22	0.2	0.70		1766	0.92307	0.00021	0.92349	570	0.31716
FRLSmh_1_23	0.2	0.75		1766	0.91659	0.00022	0.91703	--	--
FRLSmh_1_3	0.2	0.80		1757	0.89990	0.00022	0.90034	--	--
FRLSmh_1_4 <sup>a</sup>	0.2	0.90		1429	0.83653	0.00021	0.83695	--	--
FRLSmh_1_5 <sup>a</sup>	0.2	1.00	]]	1219	0.78051	0.00020	0.78091	--	--

NOTE: <sup>a</sup> Number of rods is limited by HPI cavity size, as described in Section 6.3.1.1.1.

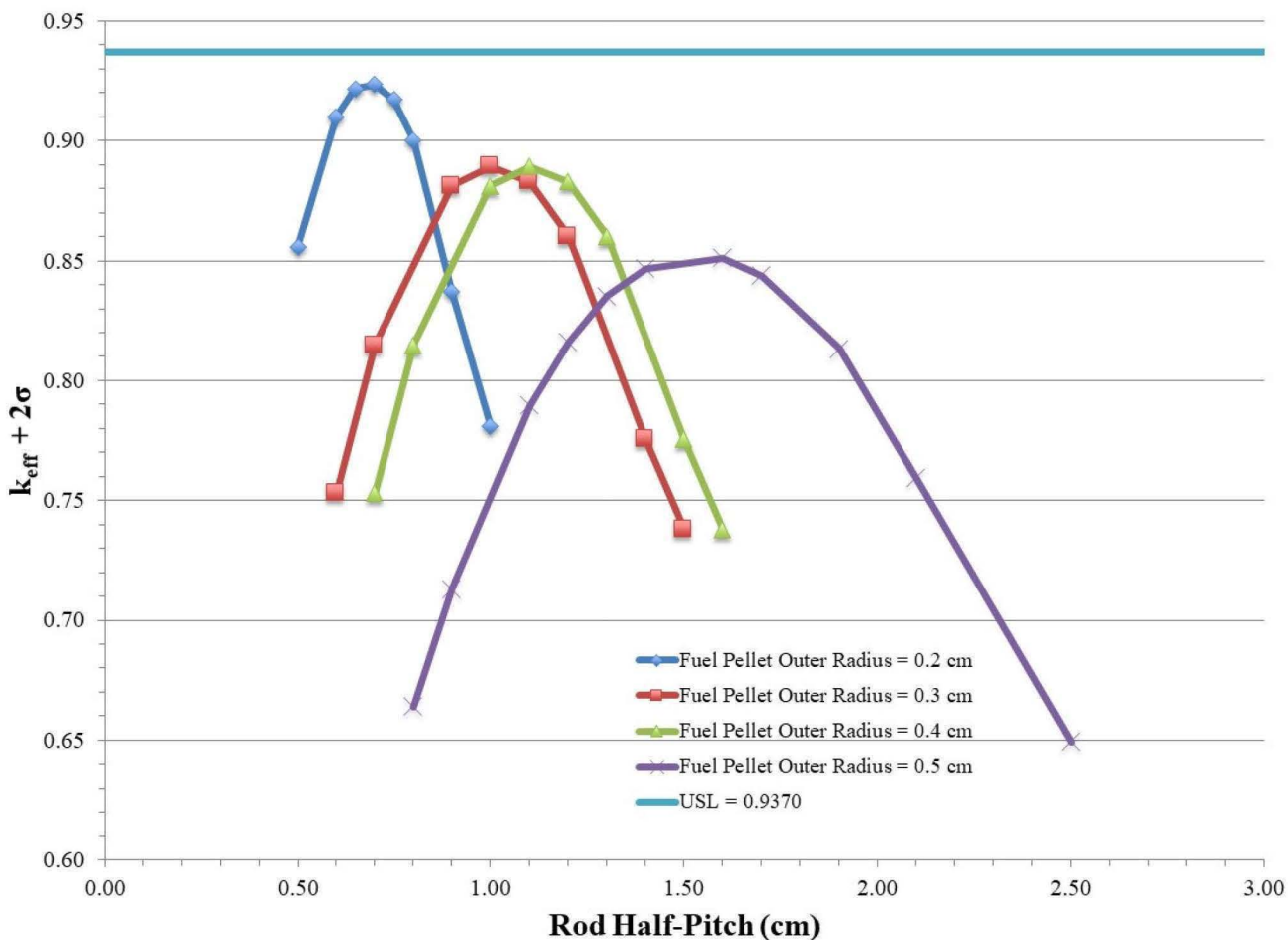


**Figure 6.4.2-1. Fuel Rod Content, Single Package, Results**

A comparison between the nominal GE BWR 10x10 fuel parameters and the fuel parameters used in the criticality evaluation is shown in Table 6.4.2-2.

**Table 6.4.2-2. Nominal vs. Analyzed Fuel Parameters for the GE2000 Criticality Analysis**

Case	Pellet Outer Diameter (cm)	Initial U-235 Enrichment Range (wt. %)	Pellet Theoretical Density
Typical GE BWR 10x10	[[ ]]	≤5.0	[[ ]]
Cases Modeled for Fuel Rod Transport	0.4-1.0	≤5.0	100%

## **6.5 Evaluation of Package Arrays Under Normal Conditions of Transport**

It should be noted that the following evaluations conducted with a U-235 enrichment of 6 wt% form the initial limiting configuration for the allowed content analyses presented in Section 6.9.4.

### **6.5.1. Configuration**

As the Model 2000 cask with HPI is shipped exclusive use, a single package defines a conveyance. Thus, the package array criticality evaluation defines the number N of packages as one. Therefore, for NCT, the package array is modeled as seven (7) packages in a hexagonal array. This evaluation demonstrates that five (5) times N packages is shown to be subcritical with the package arrangement reflected on all sides by 30.48 cm of water. The NCT package array model is described in Section 6.3.1.2.1.

The reference case for the NCT package array is to maintain void in all cavity regions that are normally void space. Full density moderation is maintained between the packages, as  $k_{eff}$  results for the single package and package array (NCT and HAC) are very similar, indicating the shield materials of the HPI and cask provide strong reflection, thus neutronically isolating each package within the array. As the reflection from the DU HPI shields provides the dominant impact on neutron interactions within a package, the variation of moderator density provides little additional neutron interaction to increase the package reactivity; see Section 6.9.2.1.2 for comparison. The confinement boundary for NCT and HAC is defined as the HPI cavity. For both contents, the fissile matrix region (HPI cavity) is moderated with full density water. The fuel rod content is described in Section 6.2.1.

### **6.5.2. Results**

Result of the HAC 2N array show that the combination of the smallest fuel rod OR and pitch variation produce the highest reactivity in the package array. Therefore, only the three smallest fuel rod OR values (0.2, 0.3, and 0.4 cm) are evaluated for the NCT 5N package array. Peak cases for NCT fuel rod content are provided in Table 6.5.2-1; full results are in Section 6.9.3, Table 6.9.3-3. Figure 6.5.2-1 displays the trends for all evaluated data. For the most limiting case for the NCT package array, FRLANmh\_1\_22 (OR=0.2 cm, hex, half-pitch=0.7 cm), the  $k_{eff} + 2\sigma$  is 0.91856. Data trends show that as the fuel rod OR increases the overall system reactivity decreases.

Section 6.3.4 defines the USL value as 0.9370 for fuel rod contents.

**Table 6.5.2-1. Fuel Rod Content, NCT 5N, Maximum Cases**

Case Name	Fuel OR (cm)	Half-pitch (cm)	Estimated No. Rods Modeled	U-235 Mass (g)	$k_{eff}$	$\sigma$	$k_{eff}+2\sigma$	H/U-235	EALF (eV)
FRLANmh_1_1	0.2	0.50	[[	1766	0.83754	0.00024	0.83802	--	--
FRLANmh_1_2	0.2	0.60		1766	0.89350	0.00023	0.89396	--	--
FRLANmh_1_21	0.2	0.65		1766	0.90893	0.00024	0.90941	--	--
FRLANmh_1_22	0.2	0.70		1766	0.91810	0.00023	0.91856	570	0.31717
FRLANmh_1_23	0.2	0.75		1766	0.91564	0.00020	0.91604	--	--
FRLANmh_1_3 <sup>a</sup>	0.2	0.80		1757	0.90089	0.00020	0.90129	--	--
FRLANmh_1_4 <sup>a</sup>	0.2	0.90		1429	0.83616	0.00020	0.83656	--	--
FRLANmh_1_5 <sup>a</sup>	0.2	1.00	]]	1219	0.77767	0.00019	0.77805	--	--

NOTE: <sup>a</sup> Number of rod is limited by HPI cavity size, as described in Section 6.3.1.1.1

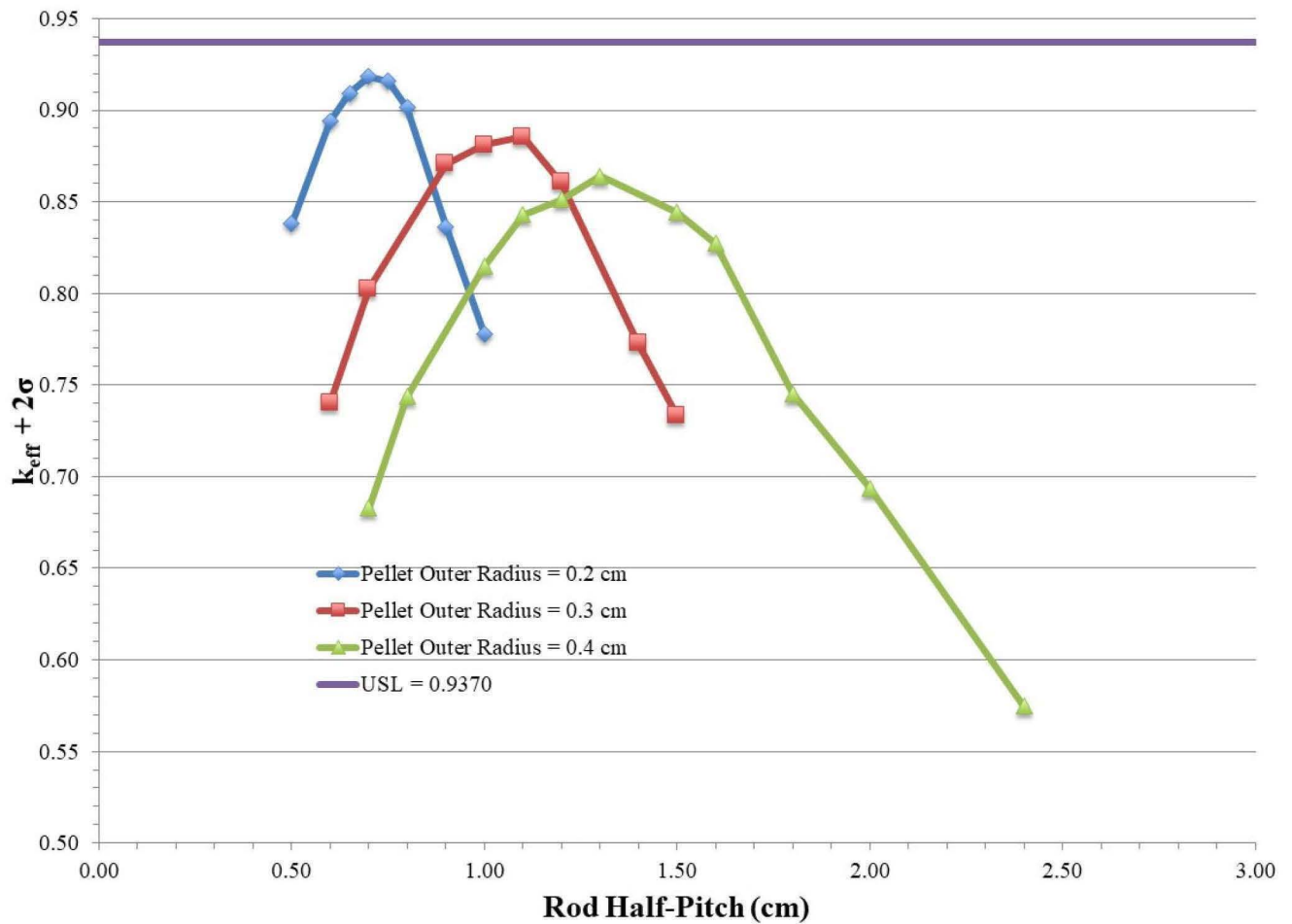


**Figure 6.5.2-1. Fuel Rod Content, NCT 5N, Results**

## 6.6 Package Arrays under Hypothetical Accident Conditions

It should be noted that the following evaluations conducted with a U-235 enrichment of 6 wt% form the initial limiting configuration for the allowed content analyses presented in Section 6.9.4.

### 6.6.1. Configuration

As the Model 2000 cask with HPI is shipped exclusive use, a single package defines a conveyance. Thus, the package array criticality evaluation defines the number N of packages as one. Therefore, for HAC, the package array is modeled as two packages side-by-side, evaluating that two times N packages is shown to be subcritical with the package arrangement reflected on all sides by 30.48 cm of water. The HAC, package array model is described in Section 6.3.1.2.2.

The reference case for the HAC package array is to fill all cavity regions that are normally void space with full density water. Full density moderation is maintained between the packages and within the packages. A parametric study assesses varied light water moderator density within the HPI and cask regions. The confinement boundary for HAC is defined as the HPI cavity. The fissile matrix region is moderated with full density water. The fuel rod content is described in Section 6.2.1.

### 6.6.2. Results

Peak cases for HAC package array, fuel rod content is provided in Table 6.6.2-1; full results are in Section 6.9.3, Table 6.9.3-4. Figure 6.6.2-1 displays the trends for all data. For the most limiting case for the HAC package array, FRLAHmh\_1\_22 (OR=0.2 cm, hex, half-pitch=0.7 cm), the  $k_{eff} + 2\sigma$  is 0.92398. Data trends show that as the fuel rod OR increases the overall system reactivity decreases.

Section 6.3.4 defines the USL value as 0.9370 for fuel rod contents.

**Table 6.6.2-1. Fuel Rod Content, HAC 2N, Maximum Cases**

Case Name	Fuel OR (cm)	Half-pitch (cm)	Estimated No. Rods Modeled	U-235 Mass (g)	$k_{eff}$	$\sigma$	$k_{eff}+2\sigma$	H/U-235	EALF (eV)
FRLAHmh_1_1	0.2	0.50	[[	1766	0.85587	0.00026	0.85639	--	--
FRLAHmh_1_2	0.2	0.60		1766	0.90895	0.00025	0.90945	--	--
FRLAHmh_1_21	0.2	0.65		1766	0.92097	0.00022	0.92141	--	--
FRLAHmh_1_22	0.2	0.70		1766	0.92350	0.00024	0.92398	570	0.31681
FRLAHmh_1_23	0.2	0.75		1766	0.91616	0.00025	0.91666	--	--
FRLAHmh_1_3 <sup>a</sup>	0.2	0.80		1757	0.89981	0.00021	0.90023	--	--
FRLAHmh_1_4 <sup>a</sup>	0.2	0.90		1429	0.83686	0.00019	0.83724	--	--
FRLAHmh_1_5 <sup>a</sup>	0.2	1.00	]]	1219	0.78005	0.00019	0.78043	--	--

NOTE: <sup>a</sup> Number of rods is limited by HPI cavity size, as described in Section 6.3.1.1.1.

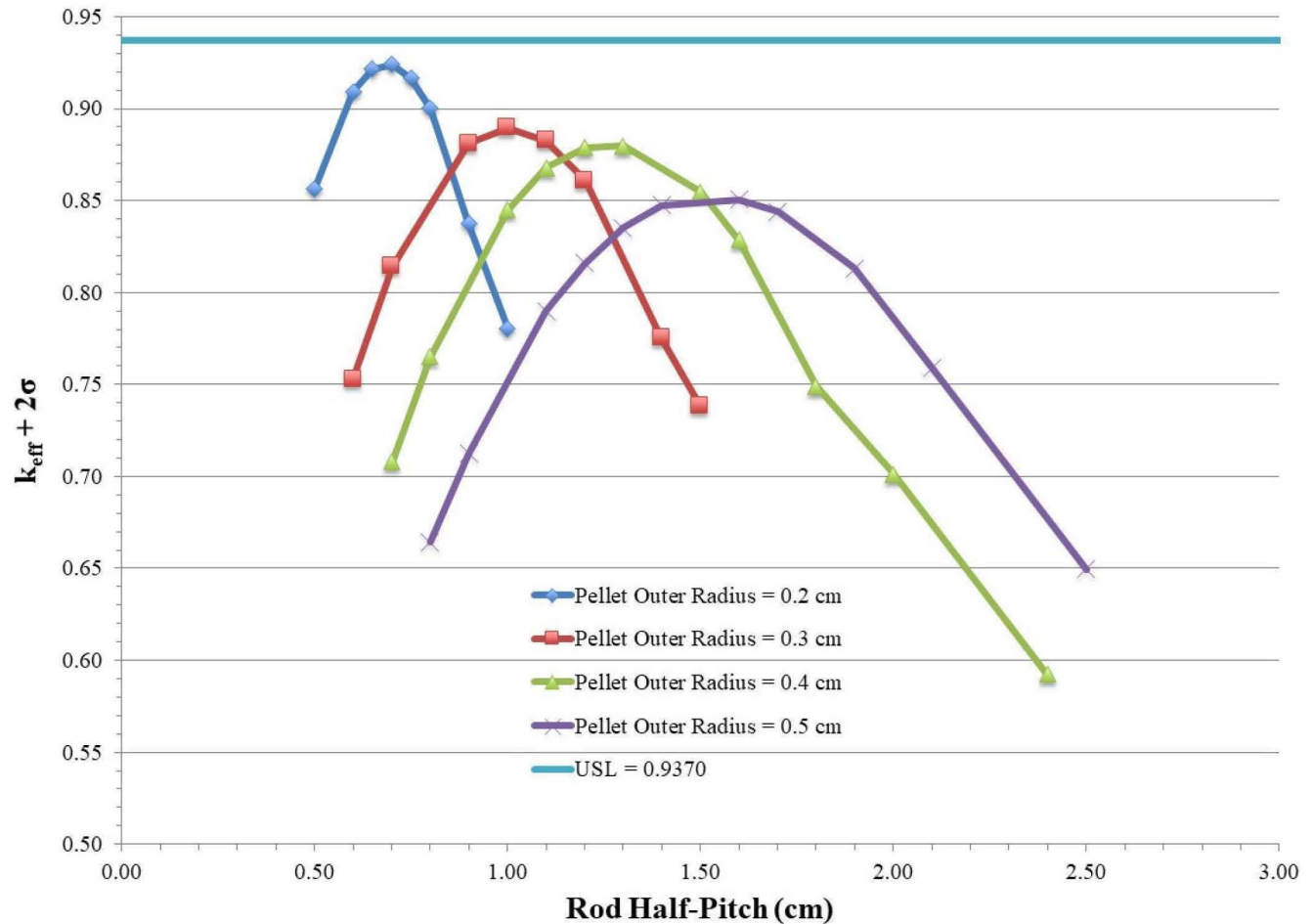


Figure 6.6.2-1. Fuel Rod Content, HAC 2N, Results

## 6.7 Fissile Material Packages for Air Transport

The Model 2000 Transport Package will not be transported by air.

## 6.8 Benchmark Evaluations

This section describes the criticality benchmarks for application of MCNP6 (Reference 6-5) with the continuous-energy neutron data library ENDF/B-VII.1 (Reference 6-7) and USLSTATS to the Model 2000 Transport Package criticality safety analysis. The application range is the criticality safety analysis of the proposed contents, consisting of high-enriched free form uranium, free form plutonium, and low-enriched uranium fuel rods in the Model 2000 cask with the HPI. It should be noted that the evaluations presented in Section 6.9.4 used MCNP6 Version 2.0 (Reference 6-6), which produce identical results as MCNP6 Version 1.0 (Reference 6-5) as documented via a direct code-to-code comparison by Los Alamos National Laboratory (Reference 6-10). Therefore, the bias and bias uncertainty as determined using MCNP6 Version 1.0 remains applicable to those  $k_{\text{eff}}$  values calculated using MCNP6 Version 2.0 in Section 6.9.4.



USLSTATS is used to generate an acceptable USL for the criticality safety analysis. The USLSTATS computer program uses two methods (i.e., (1) confidence band with administrative margin and (2) single-sided uniform width closed interval) to calculate and print USL correlations based on a set of user-supplied  $k_{eff}$  values and corresponding values of a single associated parameter X (e.g., lattice pitch, fuel enrichment, average energy group causing fission (AEG)), for a set of criticality benchmark calculations.

### **6.8.1. Applicability of Benchmark Experiments**

A total of 36 benchmark experiments were selected to develop the MCNP6 bias and bias uncertainty for the content allowed in the Model 2000 Transport Package.

The low-enriched uranium rod lattice configuration of the Model 2000 Transport Package modeled  $UO_2$  rods with 5 wt% U-235 in hexagonally pitched lattices moderated with light water. No cladding was modeled. Experiments that were chosen, had an enrichment range of 2.35 wt% through 4.306 wt% U-235. The benchmark geometries were  $UO_2$  rods in square pitched lattices submerged in light water. Reflectors consisted of steel, lead, or uranium with light water.

### **6.8.2. Bias Determination**

#### **6.8.2.1. Method**

Section 4.1 of NUREG/CR-6361 (Reference 6-9), explains two methods of determining the USL. The first method applies a statistical calculation of the bias and its uncertainty, plus an administrative margin, to a linear fit of critical experiment benchmark data, also known as Method 1: Confidence Band with Administrative Margin. In the second method, statistical techniques with a rigorous basis are applied in order to determine a combined lower confidence band plus subcritical margin, also known as Method 2: Single-Sided Uniform Width Closed Interval Approach. USLSTATS is a program that calculates USL correlations based on these methods. USLSTATS was used in this analysis in order to calculate the USL.

For this analysis, Method 1 is applied and Method 2 is used as a verification of Method 1 such that the USL function of Method 1 ( $USL_1$ ) must be less than the USL function of Method 2 ( $USL_2$ ). If the minimum margin of subcriticality,  $C^*_{s(p)} - W$ , is less than the administrative margin selected for Method 1, the administrative margin selected is sufficient, as this indicates that the administrative margin is larger than the statistical margin determined by Method 2.

### 6.8.2.2. Results

NUREG/CR-6361 states that the correlation between the trending parameter and the critical data is the primary criterion to select the parameter that will be utilized to determine the USL. The parameter with the highest correlation coefficient was used to develop the USL, which was H/U-235 for the low-enriched uranium USL function.

For the low-enriched uranium lattice Model 2000 Transport Package contents, the H/U-235 trending parameter correlation coefficient,  $|r|$ , is equivalent to 0.3900. Therefore, the USL for low-enriched uranium lattice contents is 0.9370, see Section 6.3.4 for additional details.

The results of the USLSTATS analyses are presented in Table 6.8.2-1. This table includes the USL functions, the applicable trending parameter range, the minimum margin of subcriticality ( $C^*s(p) - W$ ), which is the statistically based subcritical margin from the USL<sub>2</sub> calculation, and the correlation coefficient ( $r$ ) of the trending parameter to the critical data.

**Table 6.8.2-1. Model 2000 Transport Package Criticality Safety USL Functions**

Trending Parameter	USL Equation (Method 1)	Trending Parameter Range	$C^*s(p) - W$ (Method 2)	Correlation Coefficient ( $r$ )
H/U-235	$0.9473 - 1.5031E-5 \cdot X \quad (X > 214.9)$ $0.9441 \quad (X \leq 214.9)$	$105.5 \leq X \leq 256.3$	$9.5216E-3$	-0.3900

The administrative margin,  $\Delta k_m$ , for these analyses was 0.05, which is greater than  $C^*s(p) - W$  calculated for each trending parameter. This signifies the selected administrative margin is acceptable.

The following figures plot each trending parameter against  $k_{norm}$ . The first line plots the function  $k_c(x)$ , the line of fit to the critical data. The second line plots the function  $k_c(x) - w(x)$ , the line of fit of the critical data with a lower band of 95% confidence margin. The third line plots the function  $k_c(x) - W$ , the line of best fit of the critical data with the largest band of the 95% confidence margin from the second line,  $k_c(x) - w(x)$ , applied as a conservatism.

The USL<sub>1</sub> and USL<sub>2</sub> plots plateau at a certain constant value to not credit for positive biases in  $k_c(x) - W$ .

The USL function-defining trending parameter for low-enriched uranium lattices was H/U-235, as shown in Figure 6.8.2-1. None of the values were below the lower confidence limit,  $k_c(x) - W$ , of the calculated critical values. As the value of H/U-235 increased, the value of  $k_{norm}$  decreased. This resulted in a negative correlation between H/U-235 and  $k_{norm}$ , with a coefficient of  $r = -0.3900$ , as shown in Table 6.8.2-1. This is the strongest correlation of the three trending parameters examined for low-enriched uranium lattice systems. Therefore, H/U-235 was selected as the USL function-defining trending parameter for low-enriched uranium lattice systems.

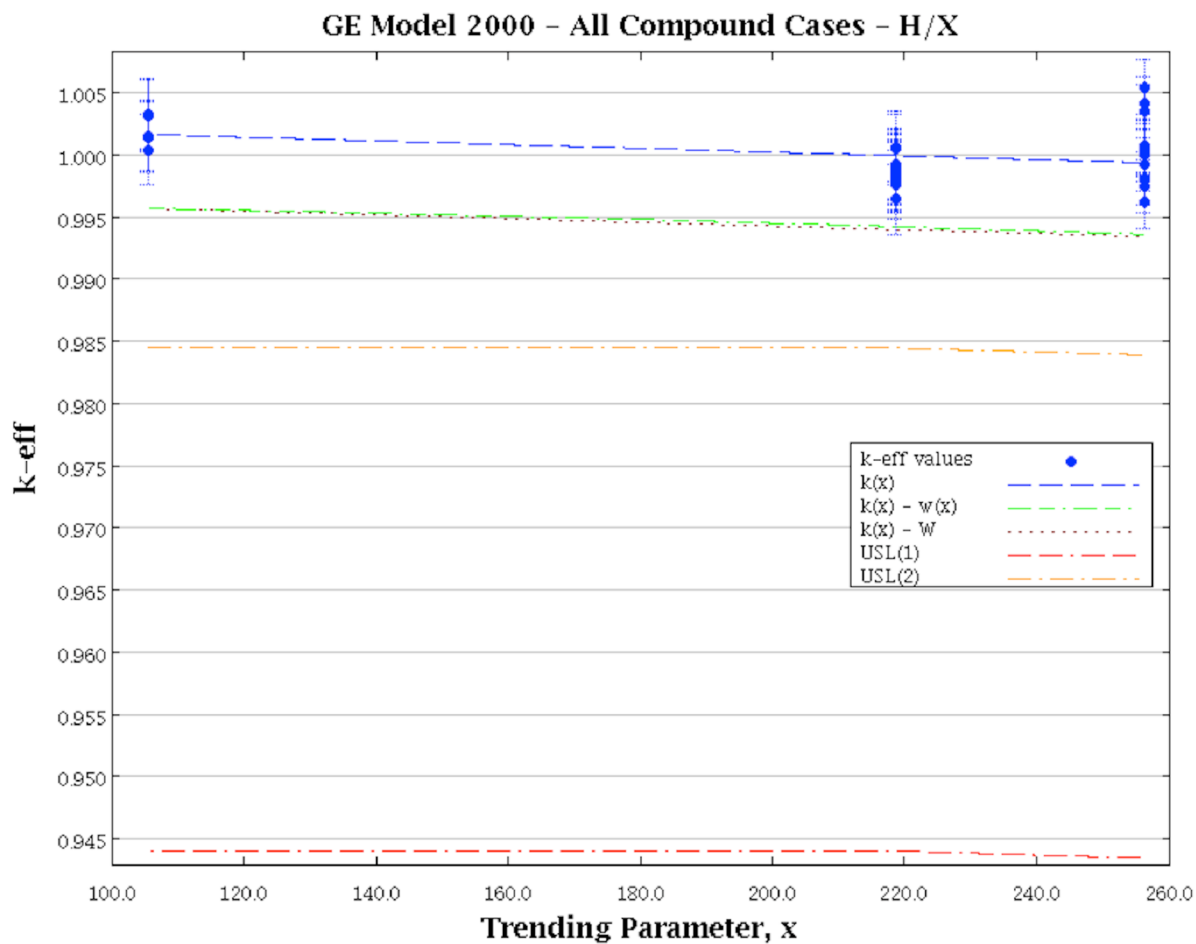


**Figure 6.8.2-1. USLSTATS Trend Plot of H/U-235 versus  $k_{\text{norm}}$  – Lattice Systems**

#### 6.8.2.2.1. Test for Normality of Benchmark Data

USLSTATS determined the benchmark experiment data to be normal. USLSTATS tests for normality using the Chi-squared method (Reference 6-11). To verify the USLSTATS result, the Shapiro-Wilk method was used as a secondary test to confirm the normality of the data. This method provided no evidence to reject the null hypothesis that the data (datum) are normal.

The Shapiro-Wilk (Reference 6-12) test is a method to verify normality that is valid for samples between 3 and 50 elements in size. It uses the null hypothesis principle to verify whether a sample of size  $n$ ,  $x_1, x_2, \dots, x_n$  came from a normally distributed population. In order for this hypothesis to be rejected, the calculated p-value of the data set must be less than the chosen alpha level of the test. For this test, the chosen alpha level is 0.05 and the null hypothesis is that the sample comes from a normally distributed population. In order to determine the p-value, the  $W$  test for normality is evaluated:

$$W = \frac{b^2}{S^2}$$

where,

$$b = \sum_{i=1}^k a_i (x_{n+1-i} - x_i)$$

$$S^2 = \sum_{i=1}^n (x_i - \bar{x})^2$$

- The values of  $x_i$  represent individual values of  $k_{\text{norm}}$  and are sorted into ascending order.
- $\bar{x}$  is the mean of the values of  $k_{\text{norm}}$ .
- $n$  is equivalent to the size of the  $k_{\text{norm}}$  sample.
- $k$  is equivalent to  $n/2$  if  $n$  is even and equivalent to  $(n-1)/2$  if  $n$  is odd.
- The values of  $a_i$  come from Table 6.8.2-2 with  $n=36$ .

If the p-value of the  $W$  test is less than the alpha level, then the null hypothesis must be rejected, which signifies the data do not come from a normally distributed population. If the p-value of the  $W$  test is greater than the alpha level, then there is no evidence to reject the null hypothesis that the data come from a normally distributed population.

Using this method, analyzing all of the critical lattice experiment  $k_{\text{norm}}$  data resulted in a  $W$  test equivalent to 0.95169. Using Table 6.8.2-3 with  $n=36$ , this value falls between p-values of 0.1 and 0.5, which correspond to  $W$  test values of 0.945 and 0.970, respectively. Linear interpolation was used to determine the p-value corresponding to a  $W$  test value of 0.95169, which was determined to be 0.2071. This p-value of 0.2071 associated with a value of  $W$  of 0.95169 is greater than the alpha level of 0.05. As a result, no evidence exists to reject the null hypothesis that the sample comes from a normally distributed population; therefore, the results of the USLSTATS test for normality are supported.

**Table 6.8.2-2. Shapiro-Wilk  $a_i$  Coefficients for the  $W$  Test (Reference 6-12)**

	<b>n = 36</b>
a1	0.4068
a2	0.2813
a3	0.2415
a4	0.2121
a5	0.1883
a6	0.1678
a7	0.1496
a8	0.1331
a9	0.1179
a10	0.1036
a11	0.0900
a12	0.0770
a13	0.0645
a14	0.0523
a15	0.0404
a16	0.0287
a17	0.0172
a18	0.0057

**Table 6.8.2-3. Shapiro-Wilk Percentage Points of the  $W$  Test (Reference 6-12)**

<b>n</b>	<b>Level [p-value]</b>								
	<b>0.01</b>	<b>0.02</b>	<b>0.05</b>	<b>0.1</b>	<b>0.5</b>	<b>0.9</b>	<b>0.95</b>	<b>0.98</b>	<b>0.99</b>
36	0.912	0.922	0.935	0.945	0.970	0.984	0.986	0.989	0.990

## 6.9 Appendices

### 6.9.1. Comparison of Modeled Fuel Rod Pitch

While the fuel rod content is limited by a mass of 1750 grams of U-235 at a maximum of 6 wt% U-235 enrichment, the modeling configuration may vary allowing for a slight variation in the H/U-235 ratio and thus affecting the system criticality. A hexagonal pitch results in tightly packed array of rods, which increases the view factor between rods in the array, while the square pitch results in a slightly higher H/U-235 ratio than a hexagonal pitch. The smallest fuel pellet OR, 0.2 cm, has shown to be the most reactive configuration for fuel rod contents. For a fuel pellet OR of 0.2 cm, the pitch comparison models a square lattice as well as a hexagonal lattice, as shown in Figure 6.9.1-1. Table 6.9.1-1 shows the results of the pitch comparison, and Figure 6.9.1-2 plots the results; full results are in Section 6.9.3, Tables 6.9.3-4 and 6.9.3-5. Table 6.9.1-1 demonstrates that the hexagonal lattice pitch bounds the square lattice pitch at optimum H/U-235 ratio. The reactivity difference between the lattice pitch geometry is minimal ( $0.92811 - 0.92398 = 0.00413$ ). However, a conservative 1.0% uncertainty is applied to  $k_{\text{eff}}$  to determine the maximum  $k_{\text{eff}} + 2\sigma$  values.

[[

]]

**Figure 6.9.1-1. Fuel Rod Content Pitch Modeling Comparison (Not to Scale)**

**Table 6.9.1-1. Fissile Mass Content, HAC 2N, Maximum Cases**

Fuel OR	Half-pitch	$k_{eff}$	$\sigma$	$k_{eff} + 2\sigma$	H/U-235	Mass U-235 (g)	$k_{eff}$	$\sigma$	$k_{eff} + 2\sigma$	H/U-235	Mass U-235 (g)
HAC 2N, square pitch							HAC 2N, hexagonal pitch				
0.2	0.50	0.88665	0.00023	0.88711	317	1821.65	0.85587	0.00026	0.85639	269	1821.65
0.2	0.60	0.92539	0.00024	0.92587	477	1821.65	0.90895	0.00025	0.90945	407	1821.65
0.2	0.65	0.92769	0.00021	0.92811	568	1821.65	0.92097	0.00022	0.92141	485	1821.65
0.2	0.7	0.91849	0.00020	0.91889	665	1821.65	0.92350	0.00024	0.92398	570	1821.65
0.2	0.75	0.89758	0.00019	0.89796	771	1821.65	0.91616	0.00025	0.91666	661	1821.65
0.2	0.8	0.86402	0.00021	0.86444	883	1644.62	0.89981	0.00021	0.90023	759	1644.62
0.2	0.9	0.79759	0.00020	0.79799	1130	1299.46	0.83686	0.00019	0.83724	972	1299.46
0.2	1.0	0.74015	0.00021	0.74057	1406	1052.56	0.78005	0.00019	0.78043	1211	1052.56

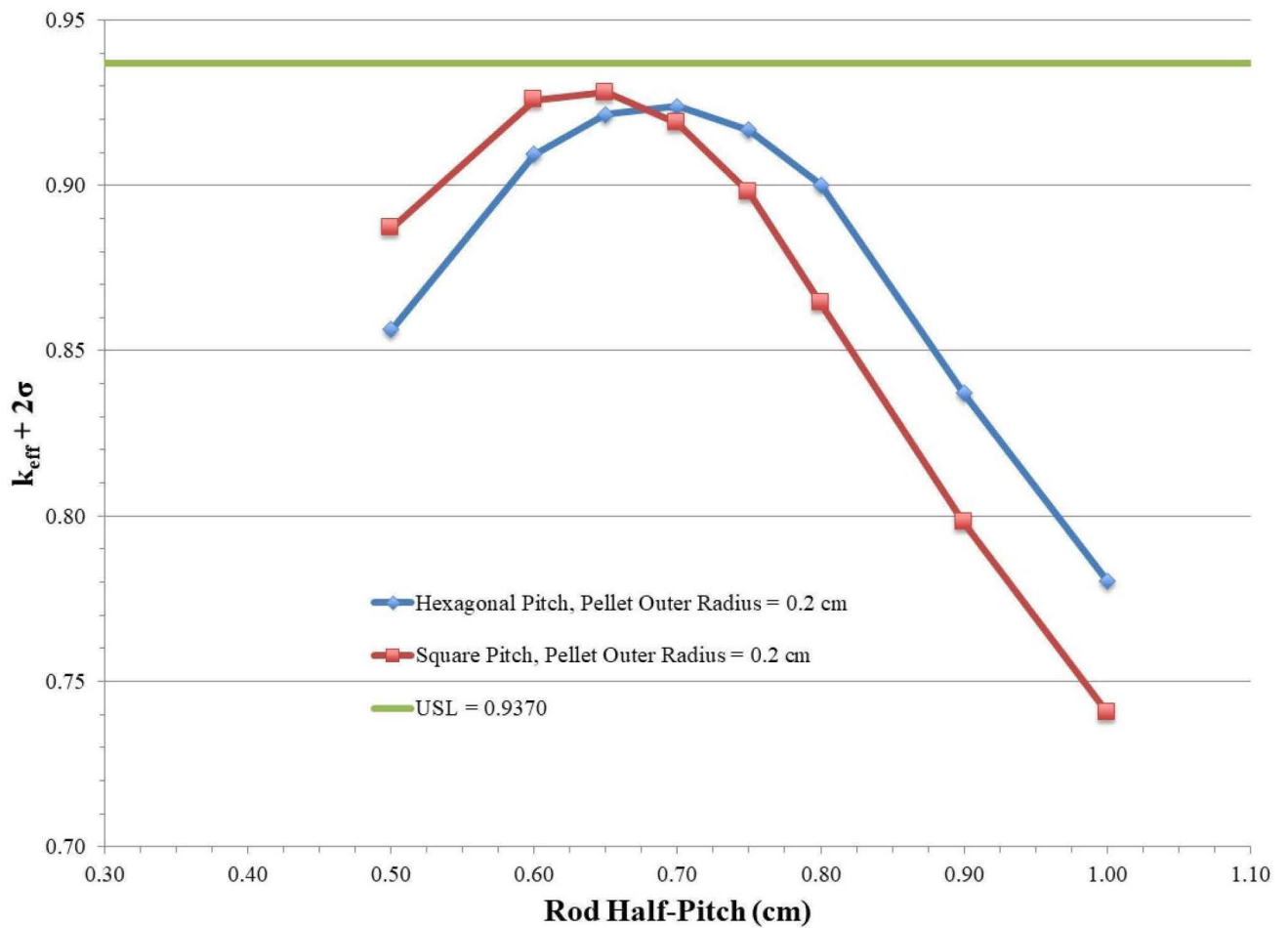


**Figure 6.9.1-2. HAC, Fuel Rod Pitch Comparison**

### 6.9.2. Benchmark Critical Experiments

Table 6.9.2-1 lists the USLSTATS input data for each critical experiment. The critical benchmark experiments were created for MCNP6 using the benchmark specifications in each critical benchmark experiment report (Reference 6-13). The values of EALF are those determined by MCNP6. The ratio H/U-235 and fuel enrichment were either reported in the critical benchmark experiment reports or were determined with hand calculations.

The values of  $k_{\text{bench}}$  and  $\sigma_{\text{bench}}$  are the reported effective multiplication factors and the  $1\sigma$  statistical error from the critical benchmark experiment reports, respectively. The values of  $k_{\text{calc}}$  and  $\sigma_{\text{calc}}$  are the effective multiplication factor and the associated Monte Carlo  $1\sigma$  determined by MCNP6, respectively. The USLSTATS input values of  $k$  and  $\sigma_{\text{sample}}$  for each critical experiment correspond to  $k_{\text{norm}}$  and  $\sigma_{\text{total}}$  in Table 6.9.2-1. The normalization of  $k$ ,  $k_{\text{norm}}$ , is calculated as  $k_{\text{calc}}$  divided by  $k_{\text{bench}}$ :

$$k_{\text{norm}} = k_{\text{calc}} / k_{\text{bench}}$$

As the benchmark uncertainty and the calculated uncertainty are independent of each other, the total uncertainty,  $\sigma_{\text{total}}$ , was determined by combining the uncertainties using the square root of the sum of the squares:

$$\sigma_{\text{total}} = (\sigma_{\text{bench}}^2 + \sigma_{\text{calc}}^2)^{1/2}$$



NEDO-33866 Revision 6  
Non-Proprietary Information

**Table 6.9.2-1. USLSTATS Input from Critical Benchmark Lattice Experiments**

Case	EALF (eV) <sup>1</sup>	H/U-235	Fissile Enrichment	M/F Ratio <sup>2</sup>	k <sub>bench</sub>	σ <sub>bench</sub>	k <sub>calc</sub>	σ <sub>calc</sub>	k <sub>norm</sub>	σ <sub>total</sub>
<i>LEU-COMP-THERM-010</i>										
1	1.2060E-01	256.3	4.306	3.882	1.0000	0.0021	1.00421	0.00041	1.00421	0.00214
2	1.1800E-01	256.3	4.306	3.882	1.0000	0.0021	1.00547	0.00043	1.00547	0.00214
3	1.1616E-01	256.3	4.306	3.882	1.0000	0.0021	1.00347	0.00044	1.00347	0.00215
4	1.1301E-01	256.3	4.306	3.882	1.0000	0.0021	0.99625	0.00041	0.99625	0.00214
5	3.5938E-01	256.3	4.306	3.882	1.0000	0.0021	0.99921	0.00039	0.99921	0.00214
6	2.6608E-01	256.3	4.306	3.882	1.0000	0.0021	1.00040	0.00045	1.00040	0.00215
7	2.1245E-01	256.3	4.306	3.882	1.0000	0.0021	1.00059	0.00038	1.00059	0.00213
8	1.8807E-01	256.3	4.306	3.882	1.0000	0.0021	0.99816	0.00041	0.99816	0.00214
9	1.2527E-01	256.3	4.306	3.882	1.0000	0.0021	0.99928	0.00045	0.99928	0.00215
10	1.2121E-01	256.3	4.306	3.882	1.0000	0.0021	1.00071	0.00044	1.00071	0.00215
11	1.1912E-01	256.3	4.306	3.882	1.0000	0.0021	1.00038	0.00043	1.00038	0.00214
12	1.1533E-01	256.3	4.306	3.882	1.0000	0.0021	1.00002	0.00043	1.00002	0.00214
13	1.1337E-01	256.3	4.306	3.882	1.0000	0.0021	0.99745	0.00043	0.99745	0.00214
20	2.9977E-01	105.5	4.306	1.597	1.0000	0.0028	1.00328	0.00045	1.00328	0.00284
21	2.9155E-01	105.5	4.306	1.597	1.0000	0.0028	1.00326	0.00046	1.00326	0.00284
22	2.7989E-01	105.5	4.306	1.597	1.0000	0.0028	1.00318	0.00044	1.00318	0.00283
23	2.7305E-01	105.5	4.306	1.597	1.0000	0.0028	1.00147	0.00047	1.00147	0.00284
24	6.0531E-01	105.5	4.306	1.597	1.0000	0.0028	1.00041	0.00042	1.00041	0.00283
25	5.5810E-01	105.5	4.306	1.597	1.0000	0.0028	1.00153	0.00045	1.00153	0.00284
26	5.1886E-01	105.5	4.306	1.597	1.0000	0.0028	1.00143	0.00042	1.00143	0.00283
27	4.8592E-01	105.5	4.306	1.597	1.0000	0.0028	1.00315	0.00045	1.00315	0.00284
<i>LEU-COMP-THERM-017</i>										
15	1.8165E-01	218.7	2.35	1.600	1.0000	0.0028	0.99830	0.00040	0.99830	0.00283
16	1.7571E-01	218.7	2.35	1.600	1.0000	0.0028	0.99839	0.00038	0.99839	0.00283
17	1.7054E-01	218.7	2.35	1.600	1.0000	0.0028	1.00044	0.00041	1.00044	0.00283
18	1.6926E-01	218.7	2.35	1.600	1.0000	0.0028	0.99894	0.00041	0.99894	0.00283
19	1.6610E-01	218.7	2.35	1.600	1.0000	0.0028	0.99882	0.00040	0.99882	0.00283
20	1.6510E-01	218.7	2.35	1.600	1.0000	0.0028	0.99878	0.00039	0.99878	0.00283
21	1.6365E-01	218.7	2.35	1.600	1.0000	0.0028	0.99811	0.00041	0.99811	0.00283
22	1.6197E-01	218.7	2.35	1.600	1.0000	0.0028	0.99761	0.00037	0.99761	0.00282
23	1.7286E-01	218.7	2.35	1.600	1.0000	0.0028	0.99927	0.00041	0.99927	0.00283
24	1.6843E-01	218.7	2.35	1.600	1.0000	0.0028	1.00066	0.00041	1.00066	0.00283
25	1.6103E-01	218.7	2.35	1.600	1.0000	0.0028	0.99879	0.00038	0.99879	0.00283
26	3.8015E-01	218.7	2.35	1.600	1.0000	0.0028	0.99647	0.00039	0.99647	0.00283
27	3.2488E-01	218.7	2.35	1.600	1.0000	0.0028	0.99816	0.00036	0.99816	0.00282
28	2.8541E-01	218.7	2.35	1.600	1.0000	0.0028	0.99897	0.00039	0.99897	0.00283
29	2.5582E-01	218.7	2.35	1.600	1.0000	0.0028	0.99916	0.00037	0.99916	0.00282

NOTES: <sup>1</sup> As calculated in MCNP6.

<sup>2</sup> M/F ratio determined through hand calculations.

NEDO-33866 Revision 6  
Non-Proprietary Information

For all the benchmark experiments, the following key input data for MCNP6 were the minimum values used in order to verify convergence of the cases:

- Neutrons per cycle: 10,000
- Number of skipped cycles: 50
- Total number of cycles: 350

This resulted in a total of 3,000,000 neutron histories analyzed per case. Convergence of the results was verified through inspection of both the Shannon entropy of the fission source distribution and the plot of  $k_{\text{eff}}$  versus cycle number for each case.

### 6.9.2.2 HAC, 2N

#### 6.9.2.1.1. Moderation

The moderator density is varied from 0 to 1.0 g/cm<sup>3</sup> within the HPI cavity region and the Model 2000 cask region. The moderation space is defined as all available space within the cavities, not including any space with lead or DU shielding. The fissile content region is maintained fully flooded with full density water for both contents. The  $k_{\text{eff}}$  result for the single package and package array (NCT and HAC) are very similar, indicating the shield materials of the HPI and cask provide strong reflection, thus neutronically isolating each package within the array. Therefore, full density water moderation between the packages is maintained to further increase reflection within the package.

#### 6.9.2.1.2. Fuel Rod Content

The moderator density is varied for the peak case of the fuel rod content results in Table 6.6.2-1, FRLAHmh\_1\_22 (OR=0.2 cm, hex, half-pitch=0.7 cm). The HPI and cask cavity moderator densities are varied independently. Peak cases for fuel rod content are provided in Table 6.9.2-2. Figure 6.9.2-1 displays the trends for all data. Based on the most limiting case, FRLAHmh\_1\_22w\_1\_9 (HPI cavity moderator density=1 g/cm<sup>3</sup>, cask cavity moderator density=0 g/cm<sup>3</sup>),  $k_{\text{eff}} + 2\sigma$  equals 0.92413, as compared to the full density flooded HAC, package array base case of  $k_{\text{eff}} + 2\sigma$  equal to 0.92398 (FRLAHmh\_1\_22w\_9\_9). The reflection from the DU HPI shields provides the dominant increase in neutron interaction within a package, while varying the water moderation within the HPI and cask cavity provides statistically similar or reduced package system reactivity. Results of the HAC package array base case (FRLAHmh\_1\_22) and the most limiting case here (FRLAHmh\_1\_22w\_1\_9) are statistically indifferent. Therefore, no additional uncertainty is added to the final, maximum  $k_{\text{eff}}$  for moderation variation.

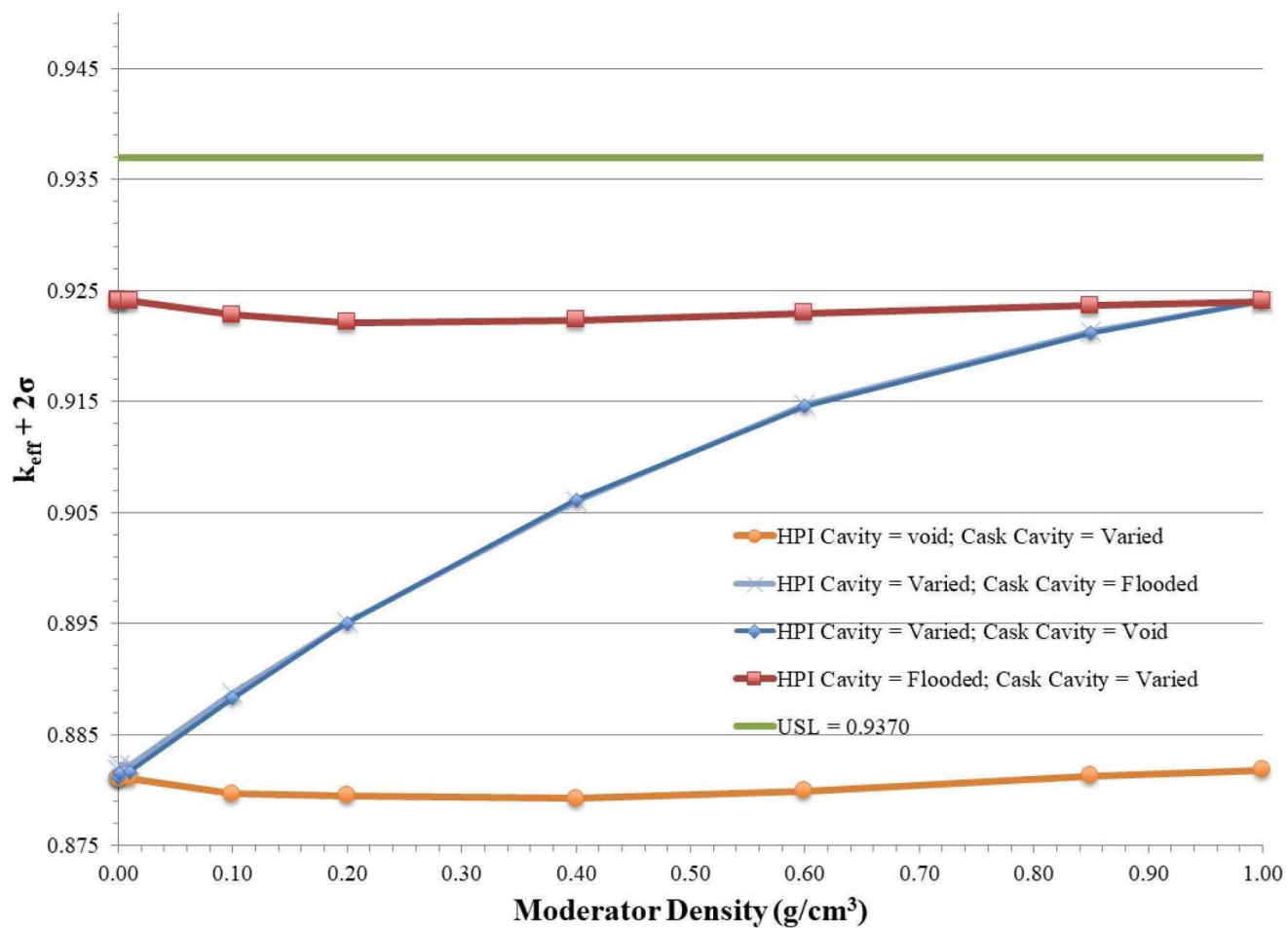


Figure 6.9.2-1. Fuel Rod Content, HAC 2N, Moderator Variation Study

NEDO-33866 Revision 6  
Non-Proprietary Information

**Table 6.9.2-2. Fuel Rod Content, HAC 2N, Moderator Variation Study**

Case Name	HPI Cavity Water Density (g/cm <sup>3</sup> )	Cask Cavity Water Density (g/cm <sup>3</sup> )	k <sub>eff</sub>	σ	k <sub>eff</sub> +2σ
Case for HPI cavity at 0 g/cc; cask cavity variation					
FRLAHmh 1 22w 1 1	0.000	0.000	0.88070	0.00023	0.88116
FRLAHmh 1 22w 2 1	0.000	0.001	0.88048	0.00024	0.88096
FRLAHmh 1 22w 3 1	0.000	0.010	0.88063	0.00024	0.88111
FRLAHmh 1 22w 4 1	0.000	0.100	0.87915	0.00025	0.87965
FRLAHmh 1 22w 5 1	0.000	0.200	0.87906	0.00023	0.87952
FRLAHmh 1 22w 6 1	0.000	0.400	0.87881	0.00023	0.87927
FRLAHmh 1 22w 7 1	0.000	0.600	0.87950	0.00023	0.87996
FRLAHmh 1 22w 8 1	0.000	0.850	0.88086	0.00021	0.88128
FRLAHmh 1 22w 9 1	0.000	1.000	0.88136	0.00024	0.88184
Case for cask cavity at 1 g/cc; HPI cavity variation					
FRLAHmh 1 22w 9 1	0.000	1.000	0.88136	0.00024	0.88184
FRLAHmh 1 22w 9 2	0.001	1.000	0.88181	0.00023	0.88227
FRLAHmh 1 22w 9 3	0.010	1.000	0.88181	0.00024	0.88229
FRLAHmh 1 22w 9 4	0.100	1.000	0.88826	0.00025	0.88876
FRLAHmh 1 22w 9 5	0.200	1.000	0.89467	0.00024	0.89515
FRLAHmh 1 22w 9 6	0.400	1.000	0.90556	0.00024	0.90604
FRLAHmh 1 22w 9 7	0.600	1.000	0.91417	0.00025	0.91467
FRLAHmh 1 22w 9 8	0.850	1.000	0.92079	0.00024	0.92127
FRLAHmh 1 22w 9 9	1.000	1.000	0.92350	0.00024	0.92398
Case for cask cavity at 0 g/cc; HPI cavity variation					
FRLAHmh 1 22w 1 1	0.000	0.000	0.88070	0.00023	0.88116
FRLAHmh 1 22w 1 2	0.001	0.000	0.88111	0.00021	0.88153
FRLAHmh 1 22w 1 3	0.010	0.000	0.88124	0.00022	0.88168
FRLAHmh 1 22w 1 4	0.100	0.000	0.88777	0.00027	0.88831
FRLAHmh 1 22w 1 5	0.200	0.000	0.89460	0.00024	0.89508
FRLAHmh 1 22w 1 6	0.400	0.000	0.90571	0.00022	0.90615
FRLAHmh 1 22w 1 7	0.600	0.000	0.91416	0.00022	0.91460
FRLAHmh 1 22w 1 8	0.850	0.000	0.92073	0.00023	0.92119
FRLAHmh 1 22w 1 9	1.000	0.000	0.92365	0.00024	0.92413
Case for HPI cavity at 1 g/cc; cask cavity variation					
FRLAHmh 1 22w 1 9	1.000	0.000	0.92365	0.00024	0.92413
FRLAHmh 1 22w 2 9	1.000	0.001	0.92353	0.00023	0.92399
FRLAHmh 1 22w 3 9	1.000	0.010	0.92357	0.00024	0.92405
FRLAHmh 1 22w 4 9	1.000	0.100	0.92238	0.00021	0.92280
FRLAHmh 1 22w 5 9	1.000	0.200	0.92162	0.00024	0.92210
FRLAHmh 1 22w 6 9	1.000	0.400	0.92185	0.00023	0.92231
FRLAHmh 1 22w 7 9	1.000	0.600	0.92253	0.00022	0.92297
FRLAHmh 1 22w 8 9	1.000	0.850	0.92320	0.00023	0.92366
FRLAHmh 1 22w 9 9	1.000	1.000	0.92350	0.00024	0.92398

### 6.9.3. MCNP Results

This section documents an explanation of the criticality analysis MCNP input/output file structure and naming convention. Representative cases are provided for review (Tables 6.9.3-1 through 6.9.3-7).

**Table 6.9.3-1. Fuel Rod Content**

Key		Description
<b>FRLA(H/N)mh_XX_YY</b>		
FRL	Fuel Rod	
A	A for package array	
H / N	H for HAC N for NCT	
mh	mh for mass limited, hexagonal pitch	
XX [1-4]	Fuel pellet radius (FROR)	0.2, 0.3, 0.4, 0.5 (centimeters)
YY [1-11] (where applicable) [21-23]	Half-pitch	FROR[XX]+0.3, FROR[XX]+0.4, FROR[XX]+0.6, FROR[XX]+0.7, FROR[XX]+0.8, FROR[XX]+0.9, FROR[XX]+1.1, FROR[XX]+1.2, FROR[XX]+1.4, FROR[XX]+1.6, FROR[XX]+2.0  For XX=1 added cases (Cases 21, 22, and 23, respectively) for FROR[XX]+0.45, FROR[XX]+0.5, FROR[XX]+0.55
<b>FRLAHm_YY</b>		
FRL	Fuel Rod	
A	A for package array	
H	H for HAC	
m	m for mass limited, square pitch	
--	Fuel pellet radius (FROR)	0.2 (centimeters)
YY [1-8]	Half-pitch	FROR[XX]+0.3, FROR[XX]+0.4, FROR[XX]+0.45, FROR[XX]+0.5, FROR[XX]+0.55, FROR[XX]+0.6, FROR[XX]+0.7, FROR[XX]+0.8
<b>FRLSmh_XX_YY</b>		
FRL	Fuel Rod	
S	S for single package	
mh	mh for mass limited, hexagonal pitch	
XX [1-9]	Fuel pellet radius (FROR)	0.2, 0.3, 0.4, 0.5 (centimeters)
YY [1-11] (where applicable) [21-23]	Half-pitch	FROR[XX]+0.3, FROR[XX]+0.4, FROR[XX]+0.6, FROR[XX]+0.7, FROR[XX]+0.8, FROR[XX]+0.9, FROR[XX]+1.1, FROR[XX]+1.2, FROR[XX]+1.4, FROR[XX]+1.6, FROR[XX]+2.0  For XX=1 added cases (Cases 21, 22, and 23, respectively) for FROR[XX]+0.45, FROR[XX]+0.5, FROR[XX]+0.55
<b>Xp-rYYY-pZZZ</b>		
X	Enrichment wt%	
p	Pellet	
r	Pellet radius	
YYY	Fuel pellet radius	0.35, 0.392, 0.4, 0.45, 0.55, 0.65 (centimeters)
p	Rod-to-Rod half pitch	
ZZZ	Half-pitch	0.4, 0.5, 0.6, 0.652, 0.7, 0.8, 0.9, 1.0, 1.1, 1.2, 1.4, 1.6, 2.0 (centimeters)

NEDO-33866 Revision 6  
Non-Proprietary Information

**Table 6.9.3-2. FRLSmh MCNP Results (Section 6.4.2)**

Input File	k <sub>eff</sub>	σ
FRLSmh_1_1_in.inp	0.85526	0.00025
FRLSmh_1_2_in.inp	0.90946	0.00023
FRLSmh_1_21.inp	0.92134	0.00022
FRLSmh_1_22.inp	0.92307	0.00021
FRLSmh_1_23.inp	0.91659	0.00022
FRLSmh_1_3_in.inp	0.89990	0.00022
FRLSmh_1_4_in.inp	0.83653	0.00021
FRLSmh_1_5_in.inp	0.78051	0.00020
FRLSmh_2_1_in.inp	0.75241	0.00022
FRLSmh_2_2_in.inp	0.81435	0.00021
FRLSmh_2_3_in.inp	0.88079	0.00024
FRLSmh_2_4_in.inp	0.88881	0.00023
FRLSmh_2_5_in.inp	0.88239	0.00021
FRLSmh_2_6_in.inp	0.85986	0.00022
FRLSmh_2_7_in.inp	0.77499	0.00021
FRLSmh_2_8_in.inp	0.73769	0.00020
FRLSmh_3_1_in.inp	0.70705	0.00026
FRLSmh_3_10_in.inp	0.70002	0.00020
FRLSmh_3_11_in.inp	0.59209	0.00017
FRLSmh_3_2_in.inp	0.76489	0.00024
FRLSmh_3_3_in.inp	0.84482	0.00024
FRLSmh_3_4_in.inp	0.86684	0.00025
FRLSmh_3_5_in.inp	0.8784	0.00021
FRLSmh_3_6_in.inp	0.87962	0.00022
FRLSmh_3_7_in.inp	0.85379	0.00021
FRLSmh_3_8_in.inp	0.82821	0.00023
FRLSmh_3_9_in.inp	0.74879	0.00020
FRLSmh_4_1_in.inp	0.66359	0.00022
FRLSmh_4_10_in.inp	0.75879	0.00020
FRLSmh_4_11_in.inp	0.64905	0.00018
FRLSmh_4_2_in.inp	0.71248	0.00026
FRLSmh_4_3_in.inp	0.78917	0.00023
FRLSmh_4_4_in.inp	0.81556	0.00026
FRLSmh_4_5_in.inp	0.83477	0.00023
FRLSmh_4_6_in.inp	0.84636	0.00025
FRLSmh_4_7_in.inp	0.85075	0.00023
FRLSmh_4_8_in.inp	0.84337	0.00024
FRLSmh_4_9_in.inp	0.81279	0.00023

NEDO-33866 Revision 6  
Non-Proprietary Information

**Table 6.9.3-3. FRLANmh MCNP Results (Section 6.5.2)**

Input File	$k_{\text{eff}}$	$\sigma$
FRLANmh_1_1_in.inp	0.83754	0.00024
FRLANmh_1_2_in.inp	0.89350	0.00023
FRLANmh_1_21.inp	0.90893	0.00024
FRLANmh_1_22.inp	0.91810	0.00023
FRLANmh_1_23.inp	0.91564	0.00020
FRLANmh_1_3_in.inp	0.90089	0.00020
FRLANmh_1_4_in.inp	0.83616	0.00020
FRLANmh_1_5_in.inp	0.77767	0.00019
FRLANmh_2_1_in.inp	0.73940	0.00030
FRLANmh_2_2_in.inp	0.80199	0.00027
FRLANmh_2_3_in.inp	0.87026	0.00026
FRLANmh_2_4_in.inp	0.88039	0.00026
FRLANmh_2_5_in.inp	0.88490	0.00023
FRLANmh_2_6_in.inp	0.86001	0.00023
FRLANmh_2_7_in.inp	0.77229	0.00019
FRLANmh_2_8_in.inp	0.73271	0.00021
FRLANmh_3_1_in.inp	0.68240	0.00025
FRLANmh_3_10_in.inp	0.69325	0.00019
FRLANmh_3_11_in.inp	0.57449	0.00018
FRLANmh_3_2_in.inp	0.74334	0.00022
FRLANmh_3_3_in.inp	0.81419	0.00025
FRLANmh_3_4_in.inp	0.84262	0.00023
FRLANmh_3_5_in.inp	0.85075	0.00025
FRLANmh_3_6_in.inp	0.86365	0.00022
FRLANmh_3_7_in.inp	0.84363	0.00024
FRLANmh_3_8_in.inp	0.82671	0.00023
FRLANmh_3_9_in.inp	0.74479	0.00022



NEDO-33866 Revision 6  
Non-Proprietary Information

**Table 6.9.3-4. FRLAHmh MCNP Results (Section 6.6.2)**

Input File	$k_{eff}$	$\sigma$
FRLAHmh_1_1_in.inp	0.85587	0.00026
FRLAHmh_1_2_in.inp	0.90895	0.00025
FRLAHmh_1_21.inp	0.92097	0.00022
FRLAHmh_1_22.inp	0.92350	0.00024
FRLAHmh_1_23.inp	0.91616	0.00025
FRLAHmh_1_3_in.inp	0.89981	0.00021
FRLAHmh_1_4_in.inp	0.83686	0.00019
FRLAHmh_1_5_in.inp	0.78005	0.00019
FRLAHmh_2_1_in.inp	0.75220	0.00025
FRLAHmh_2_2_in.inp	0.81358	0.00026
FRLAHmh_2_3_in.inp	0.88044	0.00022
FRLAHmh_2_4_in.inp	0.88897	0.00020
FRLAHmh_2_5_in.inp	0.88203	0.00022
FRLAHmh_2_6_in.inp	0.86057	0.00022
FRLAHmh_2_7_in.inp	0.77474	0.00021
FRLAHmh_2_8_in.inp	0.73764	0.00021
FRLAHmh_3_1_in.inp	0.70760	0.00023
FRLAHmh_3_10_in.inp	0.70081	0.00020
FRLAHmh_3_11_in.inp	0.59202	0.00018
FRLAHmh_3_2_in.inp	0.76450	0.00023
FRLAHmh_3_3_in.inp	0.84442	0.00023
FRLAHmh_3_4_in.inp	0.86718	0.00025
FRLAHmh_3_5_in.inp	0.87828	0.00023
FRLAHmh_3_6_in.inp	0.87916	0.00024
FRLAHmh_3_7_in.inp	0.85409	0.00022
FRLAHmh_3_8_in.inp	0.82809	0.00020
FRLAHmh_3_9_in.inp	0.74868	0.00020
FRLAHmh_4_1_in.inp	0.66372	0.00022
FRLAHmh_4_10_in.inp	0.75882	0.00021
FRLAHmh_4_11_in.inp	0.64908	0.00020
FRLAHmh_4_2_in.inp	0.71195	0.00024
FRLAHmh_4_3_in.inp	0.78927	0.00025
FRLAHmh_4_4_in.inp	0.81556	0.00024
FRLAHmh_4_5_in.inp	0.83475	0.00026
FRLAHmh_4_6_in.inp	0.84683	0.00023
FRLAHmh_4_7_in.inp	0.85022	0.00024
FRLAHmh_4_8_in.inp	0.84335	0.00023
FRLAHmh_4_9_in.inp	0.81274	0.00020

NEDO-33866 Revision 6  
Non-Proprietary Information

**Table 6.9.3-5. FRLAHm MCNP Results (Section 6.9.1)**

Input File	$k_{eff}$	$\sigma$
FRLAHm_1_1_in.inp	0.88665	0.00023
FRLAHm_1_2_in.inp	0.92539	0.00024
FRLAHm_1_3_in.inp	0.92769	0.00021
FRLAHm_1_4_in.inp	0.91849	0.00020
FRLAHm_1_5_in.inp	0.89758	0.00019
FRLAHm_1_6_in.inp	0.86402	0.00021
FRLAHm_1_7_in.inp	0.79759	0.00020
FRLAHm_1_8_in.inp	0.74015	0.00021
FRLAHm_2_1_in.inp	0.79426	0.00022
FRLAHm_2_2_in.inp	0.85183	0.00026
FRLAHm_2_3_in.inp	0.87235	0.00025
FRLAHm_2_4_in.inp	0.88724	0.00025
FRLAHm_2_5_in.inp	0.89702	0.00022
FRLAHm_2_6_in.inp	0.90125	0.00023
FRLAHm_2_7_in.inp	0.89588	0.00023
FRLAHm_2_8_in.inp	0.87092	0.00020

**Table 6.9.3-6. Limiting Fuel Pellet Radius MCNP Results (Section 6.9.4.2)**

Input File	$k_{\text{eff}}$	$\sigma$
5p-r300	0.96430	0.00027
5p-r350	0.94933	0.00026
5p-r392	0.91594	0.00025
5p-r400	0.90857	0.00028
5p-r450	0.85074	0.00011
5p-r500	0.78154	0.00030
5p-r550	0.70866	0.00025
5p-r600	0.63906	0.00023
5p-r650	0.57870	0.00021
5p-r700	0.53421	0.00018
6p-r200	0.92378	0.00022
6p-r209	0.88889	0.00026
6p-r219	0.95175	0.00016
6p-r231	0.92122	0.00023
6p-r245	0.97791	0.00018
6p-r262	0.95486	0.00028
6p-r283	0.99438	0.00027
6p-r310	0.98303	0.00025
6p-r346	0.97672	0.00030
6p-r400	0.93065	0.00014
6p-r490	0.81372	0.00026

**Table 6.9.3-7. Optimal Fuel Rod Pitch MCNP Results (Section 6.9.4.3)**

Input file	Fuel OR (cm)	Half-pitch (cm)	UO <sub>2</sub> Mass with 5 wt% U-235 (kg)	U-235 Mass (g)	k <sub>eff</sub>	σ	k <sub>eff</sub> +2σ	ΔUSL (k <sub>eff</sub> +2σ - 0.9370)
5p-r350-p040	0.350	0.40	105.5	4649	0.76018	0.00014	0.76046	-0.17654
5p-r350-p050	0.350	0.50	67.5	2975	0.89004	0.00025	0.89054	-0.04646
5p-r350-p060	0.350	0.60	46.9	2066	0.94360	0.00025	0.94410	0.00710
5p-r350-p065	0.350	0.65	39.7	1750	0.95334	0.00027	0.95388	0.01688
5p-r350-p070	0.350	0.70	34.4	1518	0.94933	0.00026	0.94985	0.01285
5p-r350-p080	0.350	0.80	26.4	1162	0.93613	0.00027	0.93667	-0.00033
5p-r350-p090	0.350	0.90	20.8	918	0.90085	0.00014	0.90113	-0.03587
5p-r350-p100	0.350	1.00	16.9	744	0.87344	0.00023	0.87390	-0.06310
5p-r350-p110	0.350	1.10	13.9	615	0.83350	0.00021	0.83392	-0.10308
5p-r350-p120	0.350	1.20	11.7	517	0.79050	0.00021	0.79092	-0.14608
5p-r350-p140	0.350	1.40	8.6	380	0.72467	0.00021	0.72509	-0.21191
5p-r350-p160	0.350	1.60	6.6	291	0.64035	0.00018	0.64071	-0.29629
5p-r350-p200	0.350	2.00	4.2	186	0.55747	0.00016	0.55779	-0.37921
5p-r392-p040	0.392	0.40	105.5	4649	0.65809	0.00025	0.65859	-0.27841
5p-r392-p050	0.392	0.50	67.5	2975	0.80860	0.00015	0.80890	-0.12810
5p-r392-p060	0.392	0.60	46.9	2066	0.88961	0.00027	0.89015	-0.04685
5p-r392-p065	0.392	0.65	39.7	1750	0.90973	0.00030	0.91033	-0.02667
5p-r392-p070	0.392	0.70	34.4	1518	0.91594	0.00025	0.91644	-0.02056
5p-r392-p080	0.392	0.80	26.4	1162	0.91849	0.00024	0.91897	-0.01803
5p-r392-p090	0.392	0.90	20.8	918	0.89728	0.00025	0.89778	-0.03922
5p-r392-p100	0.392	1.00	16.9	744	0.87657	0.00026	0.87709	-0.05991
5p-r392-p110	0.392	1.10	13.9	615	0.84334	0.00014	0.84362	-0.09338
5p-r392-p120	0.392	1.20	11.7	517	0.80540	0.00023	0.80586	-0.13114
5p-r392-p140	0.392	1.40	8.6	380	0.74548	0.00022	0.74592	-0.19108
5p-r392-p160	0.392	1.60	6.6	291	0.66147	0.00019	0.66185	-0.27515
5p-r392-p200	0.392	2.00	4.2	186	0.57527	0.00018	0.57563	-0.36137
5p-r400-p040	0.400	0.40	105.5	4649	0.64212	0.00020	0.64252	-0.29448
5p-r400-p050	0.400	0.50	67.5	2975	0.79233	0.00025	0.79283	-0.14417
5p-r400-p060	0.400	0.60	46.9	2066	0.87641	0.00027	0.87695	-0.06005
5p-r400-p065	0.400	0.65	39.7	1750	0.90021	0.00018	0.90057	-0.03643
5p-r400-p070	0.400	0.70	34.4	1518	0.90857	0.00028	0.90913	-0.02787
5p-r400-p080	0.400	0.80	26.4	1162	0.91292	0.00016	0.91324	-0.02376
5p-r400-p090	0.400	0.90	20.8	918	0.89405	0.00014	0.89433	-0.04267
5p-r400-p100	0.400	1.00	16.9	744	0.87591	0.00015	0.87621	-0.06079
5p-r400-p110	0.400	1.10	13.9	615	0.84349	0.00016	0.84381	-0.09319
5p-r400-p120	0.400	1.20	11.7	517	0.80666	0.00021	0.80708	-0.12992

NEDO-33866 Revision 6  
Non-Proprietary Information

Input file	Fuel OR (cm)	Half-pitch (cm)	UO <sub>2</sub> Mass with 5 wt% U-235 (kg)	U-235 Mass (g)	k <sub>eff</sub>	σ	k <sub>eff</sub> +2σ	ΔUSL (k <sub>eff</sub> +2σ – 0.9370)
5p-r400-p140	0.400	1.40	8.6	380	0.74811	0.00022	0.74855	-0.18845
5p-r400-p160	0.400	1.60	6.6	291	0.66462	0.00021	0.66504	-0.27196
5p-r400-p200	0.400	2.00	4.2	186	0.57807	0.00019	0.57845	-0.35855
5p-r450-p050	0.450	0.50	67.5	2975	0.68794	0.00010	0.68814	-0.24886
5p-r450-p060	0.450	0.60	46.9	2066	0.79519	0.00011	0.79541	-0.14159
5p-r450-p065	0.450	0.65	39.7	1750	0.83069	0.00010	0.83089	-0.10611
5p-r450-p070	0.450	0.70	34.4	1518	0.85074	0.00011	0.85096	-0.08604
5p-r450-p080	0.450	0.80	26.4	1162	0.87207	0.00011	0.87229	-0.06471
5p-r450-p090	0.450	0.90	20.8	918	0.86905	0.00011	0.86927	-0.06773
5p-r450-p100	0.450	0.00	16.9	744	0.85940	0.00011	0.85962	-0.07738
5p-r450-p110	0.450	1.10	13.9	615	0.83648	0.00010	0.83668	-0.10032
5p-r450-p120	0.450	1.20	11.7	517	0.80687	0.00011	0.80709	-0.12991
5p-r450-p140	0.450	1.40	8.6	380	0.75590	0.00010	0.75610	-0.18090
5p-r450-p160	0.450	1.60	6.6	291	0.67707	0.00009	0.67725	-0.25975
5p-r450-p200	0.450	2.00	4.2	186	0.59144	0.00008	0.59160	-0.34540
5p-r550-p060	0.550	0.60	46.9	2066	0.62707	0.00022	0.62751	-0.30949
5p-r550-p065	0.550	0.65	39.7	1750	0.67324	0.00022	0.67368	-0.26332
5p-r550-p070	0.550	0.70	34.4	1518	0.70866	0.00025	0.70916	-0.22784
5p-r550-p080	0.550	0.80	26.4	1162	0.75918	0.00025	0.75968	-0.17732
5p-r550-p090	0.550	0.90	20.8	918	0.78359	0.00026	0.78411	-0.15289
5p-r550-p100	0.550	1.00	16.9	744	0.79202	0.00015	0.79232	-0.14468
5p-r550-p110	0.550	1.10	13.9	615	0.78706	0.00026	0.78758	-0.14942
5p-r550-p120	0.550	1.20	11.7	517	0.77313	0.00014	0.77341	-0.16359
5p-r550-p140	0.550	1.40	8.6	380	0.73852	0.00024	0.73900	-0.19800
5p-r550-p160	0.550	1.60	6.6	291	0.67533	0.00013	0.67559	-0.26141
5p-r550-p200	0.550	2.00	4.2	186	0.59986	0.00021	0.60028	-0.33672
5p-r650-p070	0.650	0.70	34.4	1518	0.57870	0.00021	0.57912	-0.35788
5p-r650-p080	0.650	0.80	26.4	1162	0.63785	0.00021	0.63827	-0.29873
5p-r650-p090	0.650	0.90	20.8	918	0.67916	0.00026	0.67968	-0.25732
5p-r650-p100	0.650	1.00	16.9	744	0.70393	0.00024	0.70441	-0.23259
5p-r650-p110	0.650	1.10	13.9	615	0.71191	0.00024	0.71239	-0.22461
5p-r650-p120	0.650	1.20	11.7	517	0.71243	0.00023	0.71289	-0.22411
5p-r650-p140	0.650	1.40	8.6	380	0.69509	0.00024	0.69557	-0.24143
5p-r650-p160	0.650	1.60	6.6	291	0.65053	0.00023	0.65099	-0.28601
5p-r650-p200	0.650	2.00	4.2	186	0.58790	0.00022	0.58834	-0.34866

#### **6.9.4. Bounding Fuel Rod Parameters for Approved Content**

This section documents the most limiting (bounding) fuel rod configurations for justification of the allowed content (GE BWR 10x10 fuel rods with a maximum U-235 enrichment of 5 wt% with a U-235 mass limit of 1750 g).

##### **6.9.4.1. Method Overview**

Starting with the most limiting fuel rod configuration from Sections 6.4 through 6.6 (FRLSmh\_1\_22), the fuel pellet height and diameter were varied while holding the system H/U-235 ratio constant (same U-235 mass). The U-235 enrichment was then reduced to 5 wt% and a new optimal fuel rod-to-rod pitch was determined. The evaluations in the subsections below were assessed using MCNP6 Version 2.0 (Reference 6-6).

The fissile mass modeled in the fuel rod array used a range of UO<sub>2</sub> masses (105 kg to 4 kg) with a U-235 enrichment of 5 wt% at various rod diameters (heights) and rod-to-rod pitches. This is approximately 4,600 grams to 180 grams of U-235.

##### **6.9.4.2. Limiting Fuel Pellet Radius**

Starting with the most limiting fuel rod configuration from Sections 6.4 through 6.6 (FRLSmh\_1\_22), the fuel pellet height and diameter were varied while holding the system H/U-235 ratio constant (same U-235 mass). Both the fuel rod-to-rod pitch (half-pitch of 0.7 cm), total rods number of rods, and U-235 enrichment (6 wt%) were the same from the limiting HAC single package case.

As shown in Figure 6.9.4-1, certain fuel column heights/radii combinations will exceed the 0.9370 USL with U-235 enrichments at 6 wt%. Therefore, a similar study was repeated using a U-235 enrichment of 5 wt% to determine potential pellet heights/radii that would be below the USL. Figure 6.9.4-2 shows the results of the fuel column heights/radii study with a U-235 enrichment of 5 wt%.

The results of these studies are in Section 6.9.3, Table 6.9.3-6.

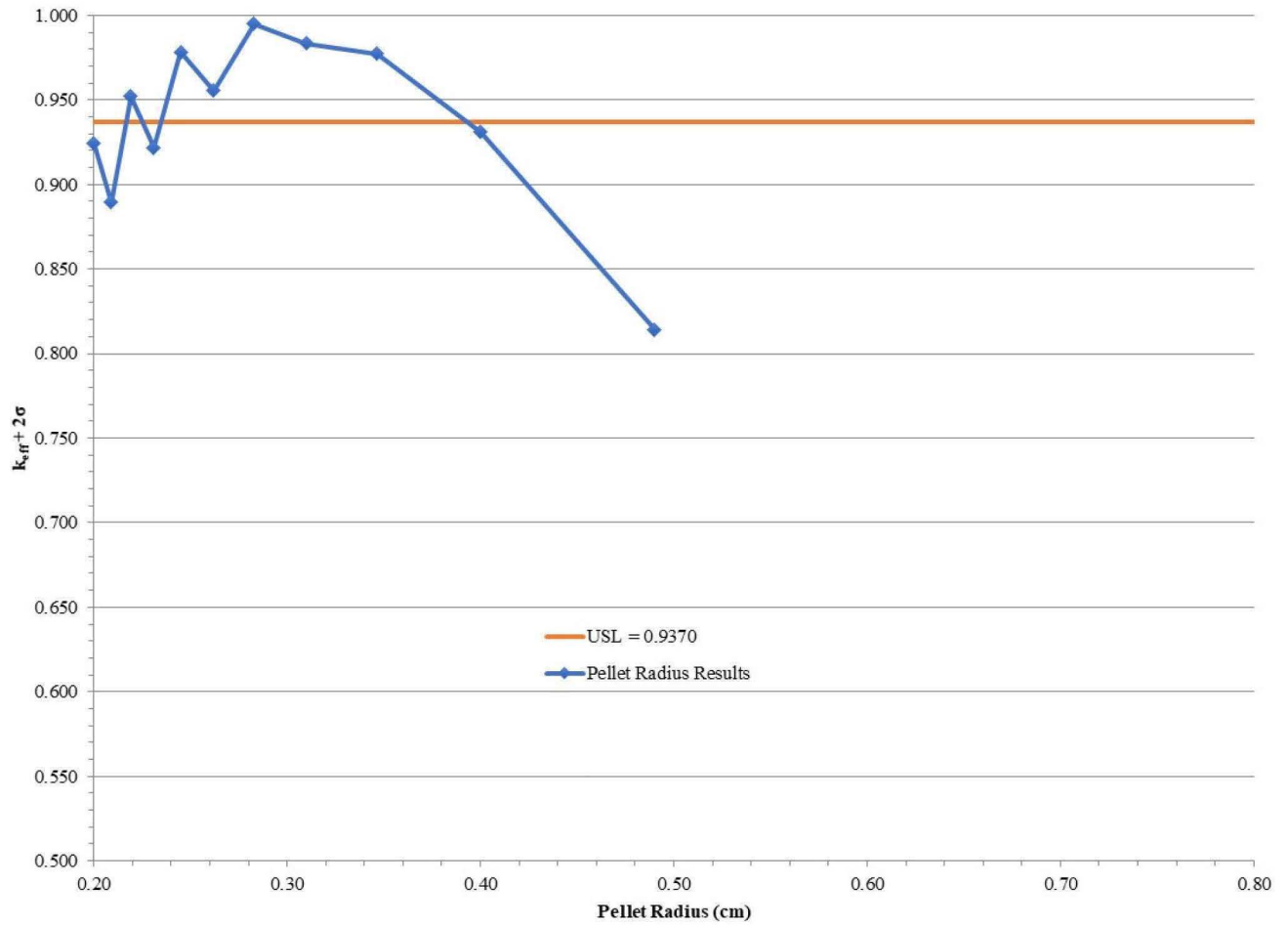


**Figure 6.9.4-1. Fuel Column Evaluation at same H/U-235 Ratio (6 wt% U-235)**

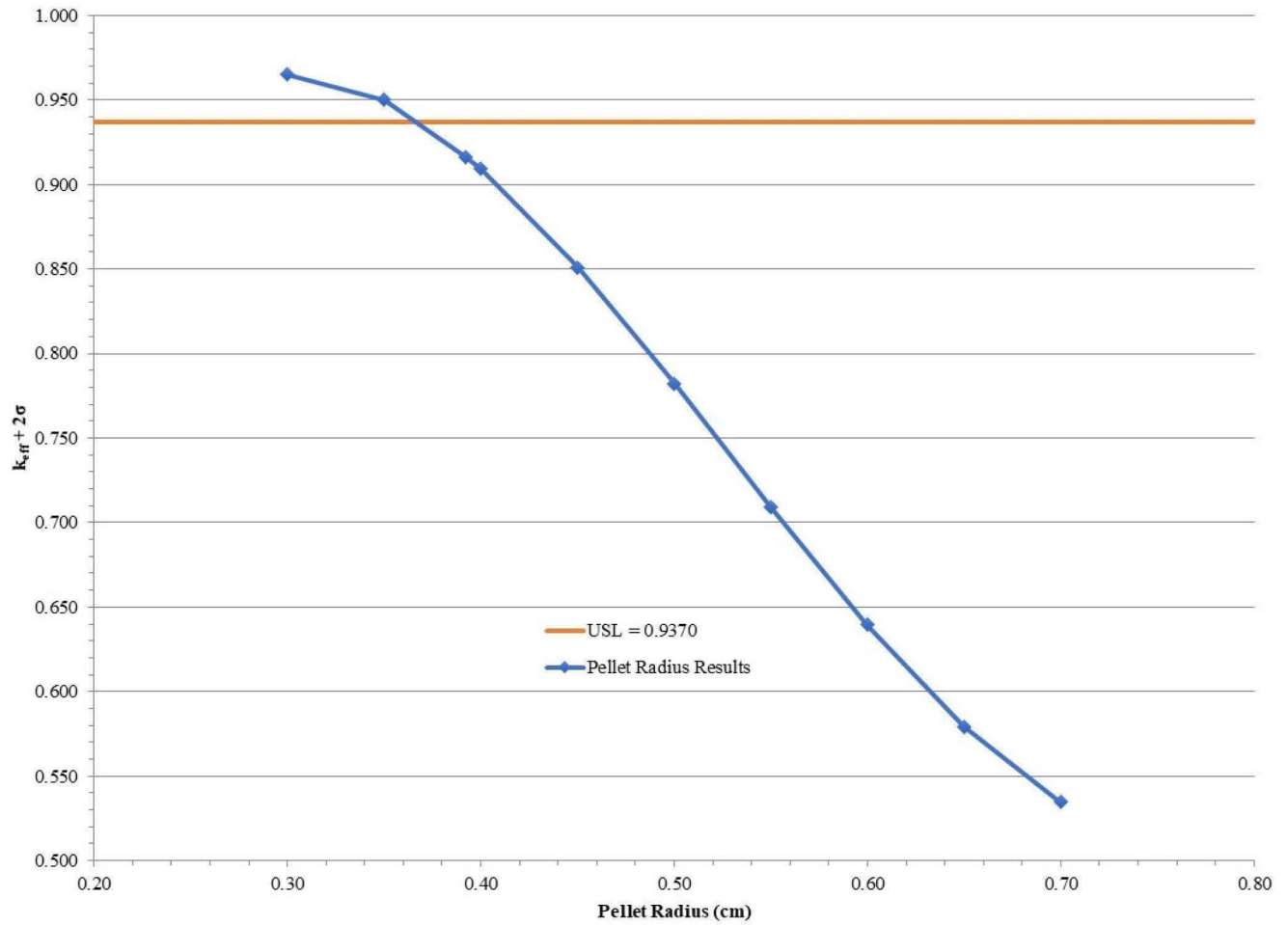


**Figure 6.9.4-2. Fuel Column Height/Radius Evaluation at 5 wt% U-235**



### 6.9.4.3. Optimal Fuel Rod Pitch

To confirm that the fuel column heights/radii would remain below the 0.9370 USL, a rod-to-rod pitch study was conducted (i.e. determine optimal system H/U-235 ratio for a given fuel column). This evaluation covered a large range of UO<sub>2</sub> masses (105 kg – 4 kg) with a U-235 enrichment of 5 wt%; see Table 6.9.3-7. Note that the 1750 U-235 mass limit correlates to a rod-to-rod half-pitch of approximately 0.65 cm and remains below the USL for the allowed fuel rod content.

Figure 6.9.4-3 provides a summary of this study. The results of these studies are in Section 6.9.3, Table 6.9.3-7.

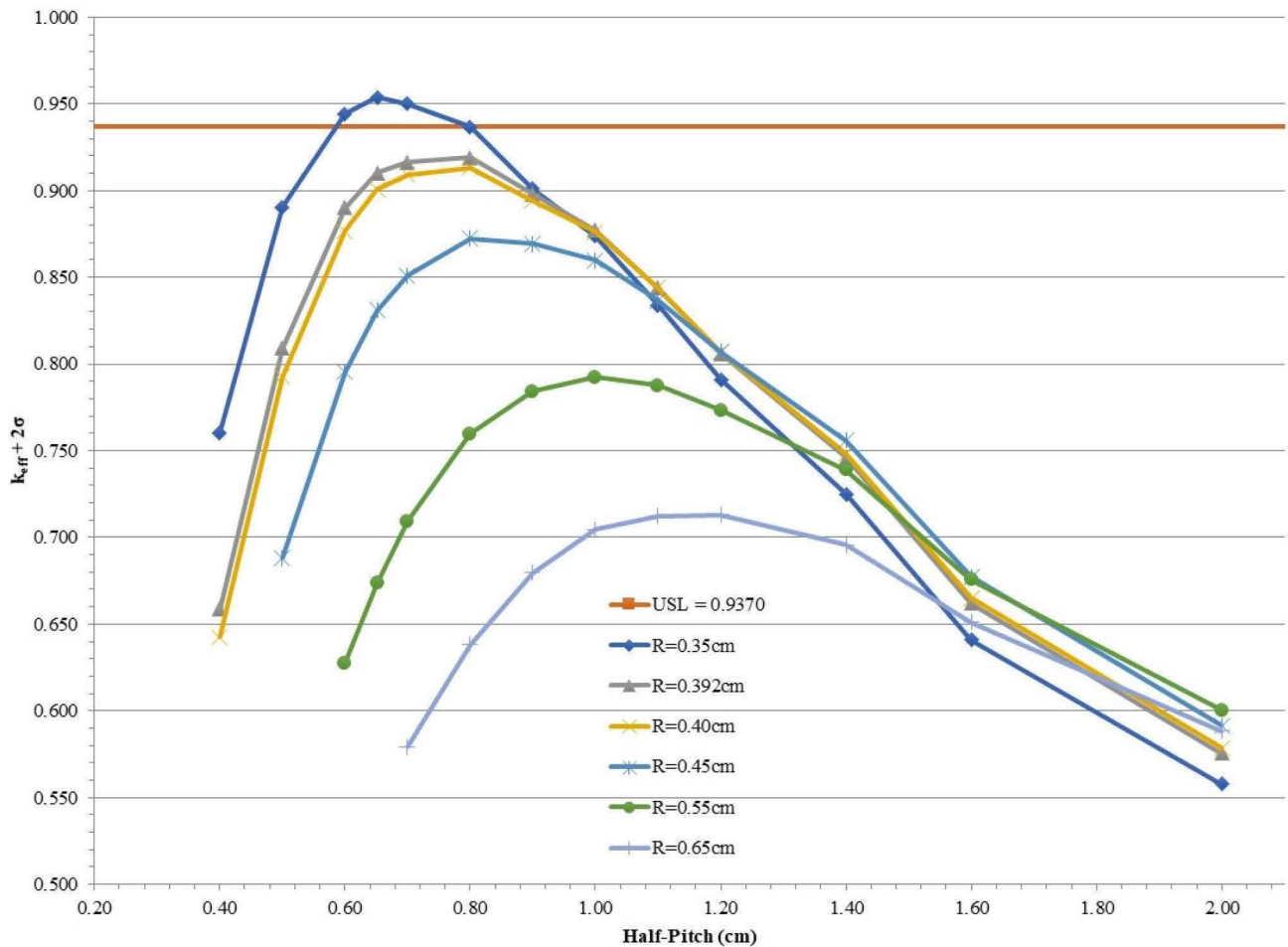


Figure 6.9.4-3. Optimal Fuel Rod Pitch Evaluation at 5 wt% U-235

#### 6.9.4.4. Conclusions

Based on the studies presented in Section 6.9.4, the following limitations apply to irradiated fuel rods to maintain criticality safety:

- a) Fuel rod pellet OD:  $\geq 0.784$  cm (0.392 cm radius).
- b) U-235 enrichment:  $\leq 5$  wt%
- c) U-235 mass:  $\leq 1750$  g

The Section 6.9.4 analysis used the single HAC model to determine the most limiting fuel rod configuration with 5 wt% U-235. Therefore, both the 2N HAC and 5N NCT arrays were assessed to confirm that the results would meet the USL. Table 6.1.2-1 provides the bounding fuel rod content results for the single HAC, 5N NCT array, and 2N HAC array. Table 6.1.2-2 provides the results of the most limiting fuel rod content when applying the U-235 administrative mass limit of 1750 grams. Note that both Tables 6.1.2-1 and 6.1.2-2 apply the 1%  $k_{eff}$  uncertainty for pitch geometric modeling as described in Section 6.9.1.

## 6.10 References

- 6-1 U.S. NRC, "Code of Federal Regulations, Packaging and Transport of Radioactive Material," 10 CFR 71, April 2016.
- 6-2 International Atomic Energy Agency, "Advisory Material for the IAEA Regulations for the Safe Transport of Radioactive Material (2012 Edition)," SSG-26 2012.
- 6-3 R.J. McConn et al., "Compendium of Material Composition Data for Radiation Transport Modeling," PNNL-15870, Revision 1, March 2011.
- 6-4 "SCALE: A Comprehensive Modeling and Simulation Suite for Nuclear Safety Analysis and Design," ORNL/TM-2005/39, Version 6.1, June 2011. Available from Radiation Safety Information Computational Center at Oak Ridge National Laboratory as CCC-785.
- 6-5 T. Goorley et al., "Initial MCNP 6 Release Overview - MCNP6 Version 1.0," Los Alamos National Laboratory, LA-UR-13-22934, April 2013.
- 6-6 "MCNP Version 6.2 Release Notes," Los Alamos National Laboratory, LA-UR-18-20808.
- 6-7 J. Conlin et al., "Listing of Available ACE Data Tables," Los Alamos National Laboratory, LA-UR-13-21822, Revision 4, June 2014.
- 6-8 H. R., Parks, C. V. Dyer, "Recommendations for Preparing the Criticality Safety Evaluation of Transportation Packages," Oak Ridge National Laboratory, NUREG/CR-5661, 1997.
- 6-9 J. J. Lichtenwalter, S. M. Bowman, M. D. DeHart, and C. M. Hopper, "Criticality Benchmark Guide for Light-Water-Reactor Fuel in Transportation and Storage Packages, NUREG/CR-6361, ORNL/TM-13211," Oak Ridge National Laboratory, 1997.
- 6-10 "Verification of MCNP6.2 for Nuclear Criticality Safety Applications," Los Alamos National Laboratory, LA-UR-17-24406, June 2017.
- 6-11 J.R. Taylor, "An Introduction to Error Analysis," page 268-271, 2<sup>nd</sup> Edition, University Science Book, 1997.
- 6-12 S.S. Shapiro and M.B. Wilk, "An Analysis of Variance Test of Normality (Complete Samples)," General Electric Co. and Bell Telephone Laboratories, Biometrika, Vol. 52, No. 3/4, 1965.
- 6-13 Organization for Economic Cooperation and Development - Nuclear Energy Agency (OECD-NEA), "International Handbook of Evaluated Criticality Safety Benchmark Experiments, NEA/NSC/DOC(95)03," 2014.

## **7 OPERATING PROCEDURES**

Instructions for use of the Model 2000 Transport Package are summarized below, beginning with Section 7.1. Note that the instructions below are limited to operating and regulatory requirements. The instructions for detailed use are implemented administratively via site specific procedures. A pre-shipment engineering evaluation is implemented to ensure that the packaging, with its proposed contents, satisfies the applicable requirements of the package's license, certificate, or equivalent authorization. This evaluation includes, but is not limited to, the review of:

- Proposed contents' isotopic composition, quantities, and decay heat
- Proposed contents' form, weight, and geometry
- Shielding requirements
- Structural requirements
- Thermal requirements
- Shipping hardware (e.g., material basket and shoring devices)
- Compliance with the respective content requirements listed in Section 7.5.

Note any damage or unusual conditions to GEH. If functionality of the part is impaired, do not repair or replace without authorization from GEH.

As discussed in Section 1.2.4, additional shoring may be added, as necessary, to ensure the [[  
]] between the bottom of the cask lid and the top of the HPI does not exceed 0.25 inches.

### **7.1 Package Loading**

- Use respective loading tables and guidance provided in Section 7.5 to ensure compliance with the authorized contents.
- The HPI material basket is required for shipping the Co-60 isotope rods and/or irradiated fuel.

#### **7.1.1. Preparation for Loading**

##### **7.1.1.1. Packaging Receipt and Inspection**

##### **7.1.1.2. Removal of the Packaging from the Transport Vehicle**

##### **7.1.1.3. Preparing to Load the Cask**

- a. Torque the lifting ear screws to 600±20 ft-lb.

#### **7.1.2. Loading of Contents**

##### **7.1.2.1. Cobalt-60 Isotope Rods**

This content type must be shipped according to the requirements in Section 7.5.2 or Section 7.5.4.

##### **7.1.2.2. Irradiated Hardware and Byproducts**

This content type must be shipped according to the requirements in Section 7.5.1 or Section 7.5.4.

#### **7.1.2.3. Irradiated Fuel**

This content type must be shipped according to the requirements in Section 7.5.3 or Section 7.5.4.

### **7.1.3. Closing the Cask and Performing Leakage Tests**

#### **7.1.3.1. Removing the Cask from the Loading Area**

- a. Decontaminate the cask exterior surfaces to a level consistent with 49 CFR 173.443 and 10 CFR 71.87.

#### **7.1.3.2. Securing the Cask Lid**

- a. Torque the lid bolts to 720±30 ft-lb in a crisscross pattern to ensure equal compression of the seal.

#### **7.1.3.3. Assembly Verification Pre-Shipment Leakage Testing**

- a. Perform leakage testing of the cask lid closure seal and vent port and drain port threaded pipe plugs in accordance with a procedure developed by an American Society for Nondestructive Testing (ASNT) Level III examiner.

### **7.1.4. Preparation for Transport**

#### **7.1.4.1. Preparing the Cask for Transport**

- a. Torque overpack screws to 100±5 ft-lb (dry) in 15 places (typ).
- b. The Model 2000 Transport Package does not have any parts or devices that would need to be rendered inoperable pursuant to 10 CFR 71.87(h).
- c. Perform the radiological survey of the package and transport vehicle consistent with 10 CFR 71.47, 71.87 and 49 CFR 173.441, 173.443.
- d. Measure and document the temperature of the overpack paying particular attention to the area around the bolting ring. If any temperature reading exceeds 185°F, install the protective personnel barrier around the package, in accordance with 10 CFR 71.43.
- e. Apply the security seal to the overpack.

## **7.2 Package Unloading**

Operations at the unloading facility are largely the reverse of loading operations. The unloading facility shall be supplied with detailed operating procedures to cover all activities as required by 10 CFR 71.89.

### **7.2.1. Receipt of Package from Carrier**

#### **7.2.1.1. Package Receipt and Inspection**

Repeat Step 7.1.1.1 and perform a radiological survey in accordance with the requirements of 10 CFR 20.205 or equivalent agreement state regulations.

#### **7.2.1.2. Removal of the Package from the Transport Vehicle**

#### **7.2.1.3. Preparing To Unload Contents**

- a. Torque the cask ear to 600±20 ft-lb.

#### **7.2.2. Removal of Contents**

##### **7.2.2.1. Co-60 Isotope Rods**

##### **7.2.2.2. Unloading Irradiated Hardware**

##### **7.2.2.3. Installing the Cask Closure Lid**

##### **7.2.2.4. Removing the Cask from the Unloading Area**

##### **7.2.2.5. Securing the Cask Lid**

- a. Repeat Section 7.1.3.2.

### **7.3 Preparation of Empty Packaging for Transport**

#### **7.3.1. Cask Cavity Inspection**

- a. Decontaminate the cavity to the limits of 49 CFR 173.428 if the cask is shipped as an empty container as defined in the regulation.

#### **7.3.2. Installation of the Cask Closure Lid**

- a. Install the head bolts and torque to 720±30 ft-lb in a crisscross pattern to ensure equal compression of the seal.

#### **7.3.3. Assembly Verification Leakage Testing**

Leakage testing is not required to be performed on the empty container. As an option, leakage testing may be performed on an empty container prior to shipment for loading operations at a user facility, to assure a new seal performs as required.

#### **7.3.4. Preparing the Empty Cask for Transport**

Decontaminate the external surfaces of the cask to a level consistent with 49 CFR 173.427, "Empty Radioactive Materials Packaging".

### **7.4 Other Operations**

There are no provisions required for any special operational controls (e.g., route, weather, mode, shipping time restrictions).

## 7.5 Appendix

The offeror is responsible for completing the loading table(s) in Sections 7.5.1 through 7.5.4 as necessary, as part of their pre-shipment evaluation review and approval process/system in advance of releasing the shipment in question.

### 7.5.1. Irradiated Hardware and Byproduct Loading Table

This section is included in order to provide clear instructions for using the Irradiated Hardware and Byproduct Loading Table. Figure 7.5.1-1 shows the Irradiated Hardware and Byproduct Loading Table with cells labeled for clear instruction for data entry. The Irradiated Hardware and Byproduct Loading Table shall be confirmed prior to any shipment of this content type.

It can be noted in this figure that:

- Column 1 is included to record each radionuclide in the Irradiated hardware or byproducts in a single shipment (with activity >1 Ci).
- Column 2 is included to record the activity of each radionuclide listed.
- Column 3 is included to demonstrate compliance with the thermal limits of the cask.
- Columns 4-11 are included to demonstrate compliance with regulatory dose rate limits for each location.
- Row A is filled out individually for each radionuclide in the shipment.
- Row B provides a summed total for each column.
- Row C provides the respective regulatory/cask limit for each column.
- Row D states whether the proposed shipment meets the respective regulatory/cask requirement. Cells in this row should be filled with either 'YES' or 'NO'. Once the Irradiated Hardware and Byproduct Loading Table is filled out entirely, if all cells in Row D say 'YES', the shipment complies with all necessary activity, thermal, and dose rate criteria.
- Row E is included to record the personnel who filled out the loading table.

			Column										
			1	2	3	4	5	6	7	8	9	10	11
A →	Radionuclide	Activity (Ci)	Thermal Power (W)	NCT					HAC				
				DR <sub>surf</sub>			DR <sub>2m</sub>	DR <sub>cab</sub>	DR <sub>1m</sub>				
				Top	Side	Bottom			Top	Side	Bottom		
	A1	A2	A3	A4	A5	A6	A7	A8	A9	A10	A11		
Row		⋮			⋮				⋮				
		⋮			⋮				⋮				
B →	Total	-	B3	B4	B5	B6	B7	B8	B9	B10	B11		
C →	Limit	-	C3	180	180	180	9	1.8	900	900	900		
D →	Criteria Met?	-	D3	D4	D5	D6	D7	D8	D9	D10	D11		
E →						Filled out by: E1							

**Figure 7.5.1-1. Irradiated Hardware and Byproduct Loading Table**

The Irradiated Hardware and Byproduct Table is filled out using the following procedure. Cell labels are from Figure 7.5.1-1.

1. Enter the thermal limit of 1500 W for the shipment in Cell C3.
2. Starting in Cell A1 enter the first radionuclide into the loading table. This column should simply list the radionuclide name or abbreviation (e.g., enter either ‘Cobalt-60’ or ‘Co-60’).
  - Only radionuclides (alpha, beta, and gamma emitters) with activity greater than 1 Ci must be entered into the loading table. Any neutron emitting radionuclides are limited to trace amounts, strictly from surface contamination of the hardware or byproducts are permitted for shipment. A list of radionuclides for consideration to include in the loading plan is provided in, but not limited to, Table 5.5-29.
  - Any radionuclide with all gamma emissions less than 0.3 MeV or a half-life less than 3 days is irrelevant to dose rate calculations, but should be entered in the table for thermal contributions. If the radionuclide is not included in Table 5.5-29, the thermal power multiplier can be calculated using Equation 5-12 and the Q-value for the radionuclide in the SCALE6.1 ORIGEN decay library origen.rev03.decay.data (Reference 7-1).
  - Any contents including radionuclides with an activity greater than 1 Ci that are not listed in Table 5.5-29, that also have gamma emissions greater than 0.3 MeV and a half-life greater than 3 days are not allowable for shipment.
3. In Cell A2 enter the activity in curies of the respective radionuclide.
4. In Cell A3, enter the thermal power for the radionuclide (in W). This value is calculated by multiplying the activity of the radionuclide (in Cell A2) by the thermal power multiplier of the radionuclide listed in Table 5.5-29.



NEDO-33866 Revision 6  
Non-Proprietary Information

5. In Cells A4 through A11, enter the dose rate contribution for the respective radionuclide (in mrem/hr) for the dose rate location of the appropriate column. This value is calculated by multiplying the activity of the radionuclide (in Cell A2) by the dose rate multiplier of the radionuclide for the respective dose rate location. Dose rate multipliers for all radionuclides that are significant to the shielding analysis are provided in Table 5.4-12 for NCT dose rates and Table 5.4-13 for HAC dose rates. Irradiated hardware and byproduct radionuclides listed in Table 5.5-7, but not in Table 5.4-12 or Table 5.4-13, are not relevant to dose rate calculations, thus cells A4 through A11 may be filled with a '0' for those radionuclides.
6. Repeat Steps 2 through 5 in the next row, filling in Columns 1 through 11, for every radionuclide that is included in the irradiated contents.
7. With the top portion of the loading table filled out, in Cell B3, sum the thermal power contributions from all radionuclides entered in Column 3 of the top portion of the loading table.
8. For Cells B4 - B11, sum the dose rate contributions from all radionuclides entered in the top portion of the loading table, for each column (e.g., for Cell B4 sum Column 4, for Cell B5, sum Column 5).
9. For Cells D3 through D11, if the respective value in Row B is less than or equal to the value in Row C, enter 'Yes', if the value in Row B is greater than the value in Row C enter 'No'.
10. If all cells in Row D say 'Yes', the proposed load of irradiated contents meet all thermal and dose rate criteria and are acceptable for shipment. If any cells in Row D say 'No', a limit has been exceeded and the proposed load of irradiated contents is not acceptable for shipment.
11. Upon completion of the Irradiated Hardware and Byproduct Table, the name of the personnel responsible for filling out the table is entered in Cell E1.

Filled out by: \_\_\_\_\_

### **7.5.2. Verification of Compliance for Cobalt-60 Isotope Rods**

Compliance with the cask thermal and regulatory dose rate limits for the cobalt-60 isotope rod contents is demonstrated through a check of the peak activity limit across any rod and using the Cobalt-60 Isotope Rod Loading Table. The Cobalt-60 Isotope Rod Loading Table shall be confirmed prior to any shipment of this content type. It is determined that a batch of cobalt-60 isotope rods is acceptable for shipment in the Model 2000 Transport Package using the following procedure:

1. Verify that the peak cobalt-60 activity in any axial 1-inch increment in the HPI cavity is less than or equal to ( $\leq$ ) 17,000 Ci.
2. Enter 1500W for the thermal power limit into the 'Limit' row of the Cobalt-60 Isotope Rod Loading Table.
3. Enter the total cobalt-60 activity of the cobalt-60 isotope rod contents (in Ci).
4. Enter the thermal power for the cobalt-60 isotope rod contents (in W). This value is calculated by multiplying the activity of the isotope rods by the thermal power multiplier for cobalt-60 from Table 5.5-29.
5. In Cells A4 through A11, enter the dose rate contribution for the cobalt-60 isotope rod contents (in mrem/hr) for the dose rate location of the appropriate column. This value is calculated by multiplying the total activity of the isotope rods by the dose rate multiplier for the respective dose rate location. The dose rate multipliers for each dose rate location are provided in Table 5.4-16 for NCT dose rates and Table 5.4-17 for HAC dose rates.
6. Upon completion of the Cobalt-60 Isotope Rod Loading Table, the name of the personnel responsible for filling out the table is entered into the appropriate cell.
7. If the maximum dose rate is less than or equal to the dose rate limit, enter 'Yes' in the 'Criteria Met?' row, otherwise enter 'No'.
8. If all cells in the 'Criteria Met?' row of the Cobalt-60 Isotope Rod Loading Table say 'Yes', the cobalt-60 isotope rod contents meet all regulatory/cask criteria.
9. Use Section 7.5.1 to determine if there is any significant radionuclide activity in the cobalt-60 isotope rod cladding in the shipment. If the use of Section 7.5.1 determines that there is significant radionuclide activity in the cobalt-60 isotope rod cladding, then fill out the Combined Contents Loading Table per the instructions in Section 7.5.4.
10. If the cobalt-60 isotope rod is being shipped with irradiated hardware, then fill out the Combined Contents Loading Table per the instructions in Section 7.5.4.

NEDO-33866 Revision 6  
Non-Proprietary Information

Model 2000 Cobalt-60 Isotope Rod Loading Table

Content	Activity (Ci)	Thermal Power (W)	NCT (mrem/hr)					HAC (mrem/hr)			
			DR <sub>surface</sub>			DR <sub>2m</sub>	DR <sub>cab</sub>	DR <sub>1m</sub>			
			Top	Side	Bottom			Top	Side	Bottom	
Cobalt-60 Isotope Rod											
Limit	-	1500	180	180	180	9	1.8	900	900	900	
Criteria Met?	-										
						Filled out by:					

### 7.5.3. Irradiated Fuel

This section is included in order to provide clear instructions for using the Irradiated Fuel Loading Table. Figure 7.5.3-1 shows the Irradiated Fuel Loading Table with cells labeled for clear instruction for data entry. The Irradiated Fuel Loading Table shall be confirmed prior to any shipment of this content type. Note that Irradiated Fuel encapsulation material (e.g., cladding) must be considered as Irradiated Hardware, which is addressed in Section 7.5.1.

It can be noted in this figure that:

- Columns 1-4 are included to record information on each irradiated fuel segment that is to be sent in a single Model 2000 Transport Package.
- Column 5 is included to demonstrate compliance with the criticality limits of the cask.
- Column 6 is included to demonstrate compliance with the thermal limits of the cask.
- Columns 7-14 are included to demonstrate compliance with regulatory dose rate limits for each location.
- Row A is filled out individually for each irradiated fuel segment (as defined in Section 5.4.4.1) in the shipment.
- Row B provides a summed total for each column.
- Row C provides the respective regulatory/cask limit for each column.
- Row D states whether the proposed shipment meets the respective regulatory/cask requirement. Cells in this row should be filled with either 'YES' or 'NO'. Once the Irradiated Fuel Loading Table is filled out entirely, if all cells in Row D say 'YES', the shipment complies with all necessary criticality, thermal, and dose rate criteria.
- Row E is included to record the personnel who filled out the loading table.

NEDO-33866 Revision 6  
Non-Proprietary Information

[illegible]

**Figure 7.5.3-1. Irradiated Fuel Loading Table**

The Irradiated Fuel Loading Table is filled out using the following procedure. Cell labels are from Figure 7.5.3-1.

1. Starting in Cell A1, enter the segment number identifier for the first segment of the loading table. This number is a label for the segment and can be any unique identifying number, or start with “1”.
2. In Cell A2 enter the active fuel length of the respective irradiated fuel segment. Every segment loaded into the cask, and entered in this loading table must have an active length of at least 5.3 inches.
3. In Cell A3 enter the initial enrichment range, considering the minimum initial enrichment (in wt% U-235) for the respective segment. Depending on the minimum initial enrichment of the segment, this cell should be filled according to Table 7.5.3-1 (e.g., if the initial enrichment for the respective segment is 2.7 wt% U-235, the label ‘2.5 ≤ e < 3.0’ should be entered into cell A3).

**Table 7.5.3-1. Irradiated Fuel Loading Table Column 3 Labels**

<b>Initial Enrichment Ranges (wt% U-235)</b>
$1.5 \leq e < 2.0$
$2.0 \leq e < 2.5$
$2.5 \leq e < 3.0$
$3.0 \leq e < 3.5$
$3.5 \leq e < 4.0$
$4.0 \leq e < 4.5$
$4.5 \leq e \leq 5.0$

4. In Cell A4 enter the burnup range, considering maximum burnup (in GWd/MTU) for the respective segment. Depending on the maximum burnup of the segment, this cell should be filled according to Table 7.5.3-2 (e.g., if the burnup for the respective segment is 45 GWd/MTU, the label ' $40 < b \leq 50$ ' should be entered into cell A4).

**Table 7.5.3-2. Irradiated Fuel Loading Table Column 4 Labels**

<b>Burnup Ranges (GWd/MTU)</b>
$0 < b \leq 10$
$10 < b \leq 20$
$20 < b \leq 30$
$30 < b \leq 40$
$40 < b \leq 50$
$50 < b \leq 60$
$60 < b \leq 72$

5. In Cell A5 enter the initial mass of U-235 for the respective rod segment (in gU-235).
6. In Cell A6, enter the thermal contribution for the respective segment (in W). This value is calculated by multiplying the mass of U-235 for the rod (in Cell A5) by the respective thermal power multiplier in Table 5.5-5. The appropriate thermal power multiplier in Table 5.5-5 is determined based on the initial enrichment range (in Cell A3) and burnup range (in Cell A4) for the respective segment (e.g., if the segment's initial enrichment range is ' $2.5 \leq e < 3.0$ ' and the burnup range is ' $40 < b \leq 50$ ', the thermal power multiplier from Table 5.5-5 is  $1.264\text{E}+00$  W/gU-235).
7. In Cells A7 through A14, enter the dose rate contribution for the respective segment (in mrem/hr) for the dose rate location in the appropriate column. This value is calculated by multiplying the mass of U-235 for the rod (in Cell A5) by the dose rate multiplier for the respective dose rate location. Table 7.5.3-3 summarizes the information for filling out

Cells A7 through A14 and provides an example dose rate contribution multiplier for the example scenario of a segment with an initial enrichment range of ' $2.5 \leq e < 3.0$ ' in Cell A3 and a burnup range of ' $40 < b \leq 50$ ' in Cell A4.

**Table 7.5.3-3. Irradiated Fuel Loading Table Dose Rate Multipliers**

<b>Irradiated Fuel Loading Table Cell Label</b>	<b>Dose Rate Location</b>	<b>Multiplier Table (in Chapter 5)</b>	<b>Example Multiplier<sup>1</sup> (mrem/hr/gU-235)</b>
A7	NCT Top Surface	5.4-3	8.069E-02
A8	NCT Side Surface	5.4-4	4.635E-01
A9	NCT Bottom Surface	5.4-5	2.696E-01
A10	NCT 2-meter	5.4-6	1.100E-02
A11	NCT Cab	5.4-7	1.968E-03
A12	HAC Top 1-meter	5.4-8	7.155E-02
A13	HAC Side 1-meter	5.4-9	8.755E-02
A14	HAC Bottom 1-meter	5.4-10	7.516E-02

Note: <sup>1</sup> Multiplier based on example case of segment with initial enrichment range  $2.5 \leq e < 3.0$  and initial burnup range  $40 < b \leq 50$

8. Repeat Steps 1 through 7 in the following row, filling in Columns 1 through 14, for each segment that shall be included in the shipment.
9. When the top portion of the loading table is filled out, enter the minimum active fuel length from all the segments in Column 2 in Cell B2.
10. In Cell B5, sum the masses of U-235 from all segments entered in Column 5 of the loading table.
11. In Cell B6, sum the thermal power contributions from all segments entered in Column 6 of the loading table.
12. For Cells B7 - B14, sum the dose rate contributions from all segments entered in the loading table, for each column (e.g., for Cell B7 sum Column 7, for Cell B8, sum Column 8).
13. For Cell D2, if the value in Cell B2 is greater than or equal to the respective value in Row C, write 'YES', if not write 'NO'.
14. For Cells D5 through D14, if the respective value in Row B is less than or equal to the value in Row C, write 'YES', if not write 'NO'.
15. If all cells in Row D say 'YES', the proposed load of irradiated fuel segments meets all criticality, thermal, and dose rate criteria and is acceptable for shipment. If any cells in Row D say 'NO', a limit has been exceeded and the proposed load of irradiated fuel segments is not acceptable for shipment.



NEDO-33866 Revision 6  
Non-Proprietary Information

16. Upon completion of the Irradiated Fuel Table, the name of the personnel responsible for filling out the table is entered in Cell E1.
17. If the irradiated fuel is encapsulated (e.g., cladding), that material is treated as irradiated hardware; fill out the irradiated hardware/byproduct (Section 7.5.1) and combined loading (Section 7.5.4) tables as needed. It should be noted that irradiated hardware and irradiated fuel have different cooling time requirements.

The following page provides the Irradiated Fuel Loading Table that is to be filled out prior to any shipment of this content type.

NEDO-33866 Revision 6  
Non-Proprietary Information

## Model 2000 Irradiated Fuel Loading Table

[illegible]

#### 7.5.4. Combined Contents

The Combined Contents Loading Table shall be confirmed prior to any shipment including multiple content types. For any shipment including multiple content types, compliance with regulatory/cask limits is demonstrated using the following procedure:

1. Fill out the Irradiated Hardware and Byproduct Loading Table per instructions in Section 7.5.1, as applicable.
2. Fill out the Cobalt-60 Isotope Rod Loading Table per instructions in Section 7.5.2, as applicable.
  - 2.1 Confirm that the total activity of all cobalt-60 in the shipment is less than or equal to ( $\leq$ ) 17,000 Ci per axial inch. Sum the peak cobalt-60 Ci per axial inch value from Step 1 of Section 7.5.2 and the total cobalt-60 point source values from the Irradiated Hardware and Byproduct Loading Table.
3. Fill out the Irradiated Fuel Loading Table per instructions in Section 7.5.3, as applicable. Note that Irradiated Fuel encapsulation material (e.g., cladding) must be considered as Irradiated Hardware, which is addressed in Section 7.5.1.
4. Enter the U-235 mass, thermal power, and dose rate values from the 'Total' row of each applicable loading table from Steps 1, 2, and 3 into the respective 'Hardware/Byproduct', 'Cobalt-60 Isotope Rod,' and 'Irradiated Fuel' rows in the Combined Contents Loading Table.
5. Sum the U-235 mass, thermal power, and dose rate values from all content types in the 'Total' row of the Combined Contents Loading Table.
6. Verify that for each column the value in the 'Total' row is less than or equal to the value in the 'Limit' row. Record this verification by writing 'YES' if the criteria is met, or 'NO' if the criteria is not met.
7. If all cells in the 'Criteria Met?' row of the Irradiated Hardware and Byproduct Loading Table, the Cobalt-60 Isotope Rod Loading Table, the Irradiated Fuel Loading Table, and the Combined Contents Loading Table say 'YES', the proposed load of combined contents meets all regulatory/cask criteria and is acceptable for shipment. If any cells in any of the four Tables say 'NO', a limit has been exceeded and the proposed load of combined contents is not acceptable for shipment.
8. Upon completion of the Combined Contents Loading Table, the name of the personnel responsible for filling out the table is entered into the appropriate cell.

NEDO-33866 Revision 6  
Non-Proprietary Information

Model 2000 Combined Contents Loading Table

Content	Mass U-235 (g)	Thermal Power (W)	NCT (mrem/hr)					HAC (mrem/hr)		
			DR <sub>surf</sub>			DR <sub>2m</sub>	DR <sub>cab</sub>	DR <sub>1m</sub>		
			Top	Side	Bottom			Top	Side	Bottom
Hardware / Byproduct	-									
Cobalt-60 Isotope Rods	-									
Irradiated Fuel										
Total										
Limit	1750	1500	180	180	180	9	1.8	900	900	900
Criteria Met?										
						Filled out by:				

## **7.6 References**

- 7-1 Oak Ridge National Lab, "SCALE: A Comprehensive Modeling and Simulation Suite for Nuclear Safety Analysis and Design, ORNL/TM-2005/39, Version 6, Vols. I-III," ORNL/TM-2005/39, Version 6.1, June 2011.

## **8 ACCEPTANCE TESTS AND MAINTENANCE PROGRAM**

This chapter describes the acceptance tests and maintenance program to be used for the Model 2000 Transport Package, required by 10 CFR 71, Subpart G. The acceptance tests are prescribed to verify materials of construction, fabrication processes, and the transport package's design adequately meets the regulations, while the maintenance program outlined in this chapter assures the packaging's performance during its service life, in full compliance with this safety analysis report.

General information related to the Model 2000 Transport Package, including package design details and contents description, is presented in Chapter 1 of this safety analysis report. For package dimensions, refer to the licensing drawings provided in Section 1.3.1. Fabrication and examination of the Model 2000 Transport Package (i.e., cask and overpack), the high performance insert (HPI) assembly, and material basket assembly, conform to the requirements of ASME Section III, as delineated in Section 8.1.

Routine inspection (prior to each loading) consists of visual examination for physical damage of all surfaces and components. Periodic or annual inspection includes visual examination, penetrant inspection of welds, and replacement of damaged or worn components, as necessary.

### **8.1 Acceptance Test**

The inspection and acceptance tests are specified in the fabrication specifications and engineering drawings for the Model 2000 Transport Package and are governed by the GEH QAP (Reference 8-1). The GEH QAP has been approved by the NRC (Docket Number 71-0254) (Reference 8-2).

#### **8.1.1. Visual Inspections and Measurements**

Visual examinations of all dimensions are conducted during fabrication to ensure that the packaging is fabricated and assembled in accordance with manufacturing drawings and specifications. All dimensions and tolerances specified on the drawings are confirmed by measurement. Fabrication deviations are addressed in compliance with the GEH QAP for all components important to Safety Category A or B.

#### **8.1.2. Weld Examinations**

Visual examinations of all welds, including overpack torodial shells, are conducted during fabrication. In addition, all welds within the cask containment boundary are liquid penetration tested (root and final passes); also, the welds forming the toroidal shell are 100% radiographed. These inspections are performed to ensure no cracks, incomplete fusion, or lack of penetration, exists. Parts that do not meet the established criteria are repaired or replaced in accordance with written procedures. For Model 2000 Transport Package serial number (S/N) 2001, nondestructive examination (NDE) procedures and acceptance standards are based on the ASME Code, Section III, Subsection NG (Reference 8-3). All future fabrication will meet the requirements of the ASME Code, Section III as follows:

Cask assembly including ears (Reference 8-4):

- Materials per NB-2000, Certification NCA-3800
- Fabrication per NB-4000
- NDE per NB-5000
- Pressure testing per NB-6000

The following components of the cask assembly shall be excluded of the above requirements:

- Shielding lead and its installation
- [[                      ]]
- Seals and test port components
- Electro-polishing
- Miscellaneous equipment (e.g., name plate and its screws, honeycomb, and thread inserts)

Overpack assembly per Subsection NF (Reference 8-5):

- Materials per NF-2000
- Fabrication per NF-4000
- NDE per NF-5000

HPI and material basket Importance to Safety Category B components and welds (Reference 8-5):

- Materials per NF-2000
- Forming, fittings, and aligning per NF-4200
- Welding per NF-4400
- Qualification of Weld Procedures and Personnel per NF-4300
- Examination per NF-5000

The shielding materials of the HPI shall be excluded of the above requirements.

### **8.1.3. Structural and Pressure Tests**

The cask cavity is hydrostatically tested to ensure that it is tight, per the requirements of the ASME Boiler and Pressure Vessel Code, Section III, Subsection NB, NB-6200. The test pressure is 45 psia, 50% greater than the design pressure of 30 psia, per the requirement in 10 CFR 71.85(b).

### **8.1.4. Fabrication Leakage Tests**

The fabrication leakage rate tests are performed in accordance with ANSI N14.5-1997, “American National Standard for Radioactive Materials – Leakage Tests on Packages for Shipment” (Reference 8-6) to ensure leaktightness of the cask welds and seals as follows. All leak testing

procedures are developed by an American Society for Nondestructive Testing (ASNT) Level III examiner per ASNT requirements.

During fabrication, maintenance, and periodic inspections, the cask containment boundary is tested to demonstrate whether it is leaktight in accordance with ANSI N14.5-1997. If the cask containment boundary is not demonstrated to be leaktight, the failed component is located, repaired or replaced, and reinspected. This applies to both the cask body and lid, as well as containment boundary components such as cask lid seal or port plugs.

### **8.1.5. Component and Material Tests**

#### **8.1.5.1. Valves, Rupture Discs, and Fluid Transport Devices**

Component tests of valves, rupture discs and/or fluid transport devices are not applicable, because these parts do not exist in the Model 2000 Transport Package design.

#### **8.1.5.2. Seal Testing**

The procedure for testing the cask containment features is based on ANSI N14.5 and is conducted in accordance with the latest revision of the applicable GEH test specification. The justification for the [[ ]] retainer with four Parker Compound No. [[ ]] is as stated in Section 4.1.3. The port penetration containment boundary demonstration is documented in the test report summary, which demonstrates leak tightness for the port pipe plug with approved sealant. Test temperatures and pressures meet the HAC requirements as defined in Table 3.5.1-4.

The [[ ]] retainer with four Parker Compound No. [[ ]] is tested at room temperature. It is shown in the cold case analysis in Section 3.3.1.2, that with an internal wattage of 500 W, the minimum seal temperature at any of the seal regions is 21°F, with a minimum cask lid seal temperature of 45°F. These temperatures are clearly bounded by the minimum service temperature for [[ ]] (-70°F per Reference 1-2). The seal material is installed in a test flange and leak tested in accordance with ANSI N14.5. Seal material exceeding the allowable leak rate (leaktight per the ANSI N14.5 definition) is rejected. The test seal/flange joint used for the Parker Compound No. [[ ]] seal tests is a full-scale model in terms of flange and seal diameter with a representative cask body/lid joint fixture. The demonstration of the cask lid seal is documented in the test report summary.

#### **8.1.5.3. Honeycomb Testing**

The honeycomb energy absorber is tested in accordance with MIL-C-7438 latest revision (Reference 8-7), or equivalent. The test procedure determines the compressive properties of the honeycomb material in the direction normal to the plane of facings. The test produces a load deformation curve, and from this curve the compressive stress at proportional limit load is calculated. If the honeycomb material does not meet the required crush strength, the material is rejected.



#### **8.1.6. Shielding Tests**

The shielding material is inspected for integrity. A cobalt source placed inside the lead-shielded cask is surveyed from the outside of the cask with a gamma detection instrument. The cask outside surface is divided by radial lines 12° apart and by equally spaced circumferential lines along the vertical axis. Dose rate readings are taken over each of the 420 rectangular regions (~4 inches square); see Figure 8-1. If an area of void is detected, radiographic film is placed over this area to determine the size and location of the void. The criterion used to evaluate the effect of the void is that the dose rate may not exceed one and one-half times the mean dose rate. Any void area that does not meet the criteria shall be re-poured with lead.

The depleted uranium shielding in the HPI is cast and machined to a high precision, to the requirements of the licensing drawings. The shielding integrity of the HPI is determined during manufacturing, where voids in the depleted uranium are checked for using a visual inspection and the density is verified using the total volume and weight.

#### **8.1.7. Thermal Tests**

A thermal test is performed on the first unit built of the Model 2000 Transport Package to determine the thermal performance of the system versus what is predicted by the analysis. This test is only done for the 600 W and 2000 W cases. The 3000 W configuration testing is completed through analysis as described in Section 3. It should be noted that the cask design has been evaluated to support 3000 W decay heat as stated in Section 1.2.2.1. However, the allowable contents are limited to 1500 W decay heat.

##### **8.1.7.1. Discussion of Test Setup**

Two thermal tests are conducted, one each with a 600 W and a 2000 W heat source. The heat source is installed concentrically within the cask cavity. Thermocouples are strategically placed within the cavity and the external portions of the cask and overpack surfaces as schematically shown in Figure 8-2.

##### **8.1.7.2. Test Procedure**

The test is conducted with each of the heat sources in a controlled ambient environment to simulate normal conditions of transport. The temperature data are recorded every 30 minutes with a data acquisition system, permitting easy analysis and plotting of the results. Data are recorded until temperature remains significantly unchanged for a one-hour period.

##### **8.1.7.3. Acceptance Criteria**

The results of the thermal test are evaluated against the predicted thermal performances. If the evaluation shows a discrepancy, the analytical thermal model is corrected based on the test results and a new thermal analysis is conducted. If the new analysis results indicate deficiency in the thermal characteristics of the packaging, thermal barrier coating could be applied to the inner surface of the overpack structure as a corrective measure.

### 8.1.8. Miscellaneous Tests

No additional tests are required prior to the use of the packaging.

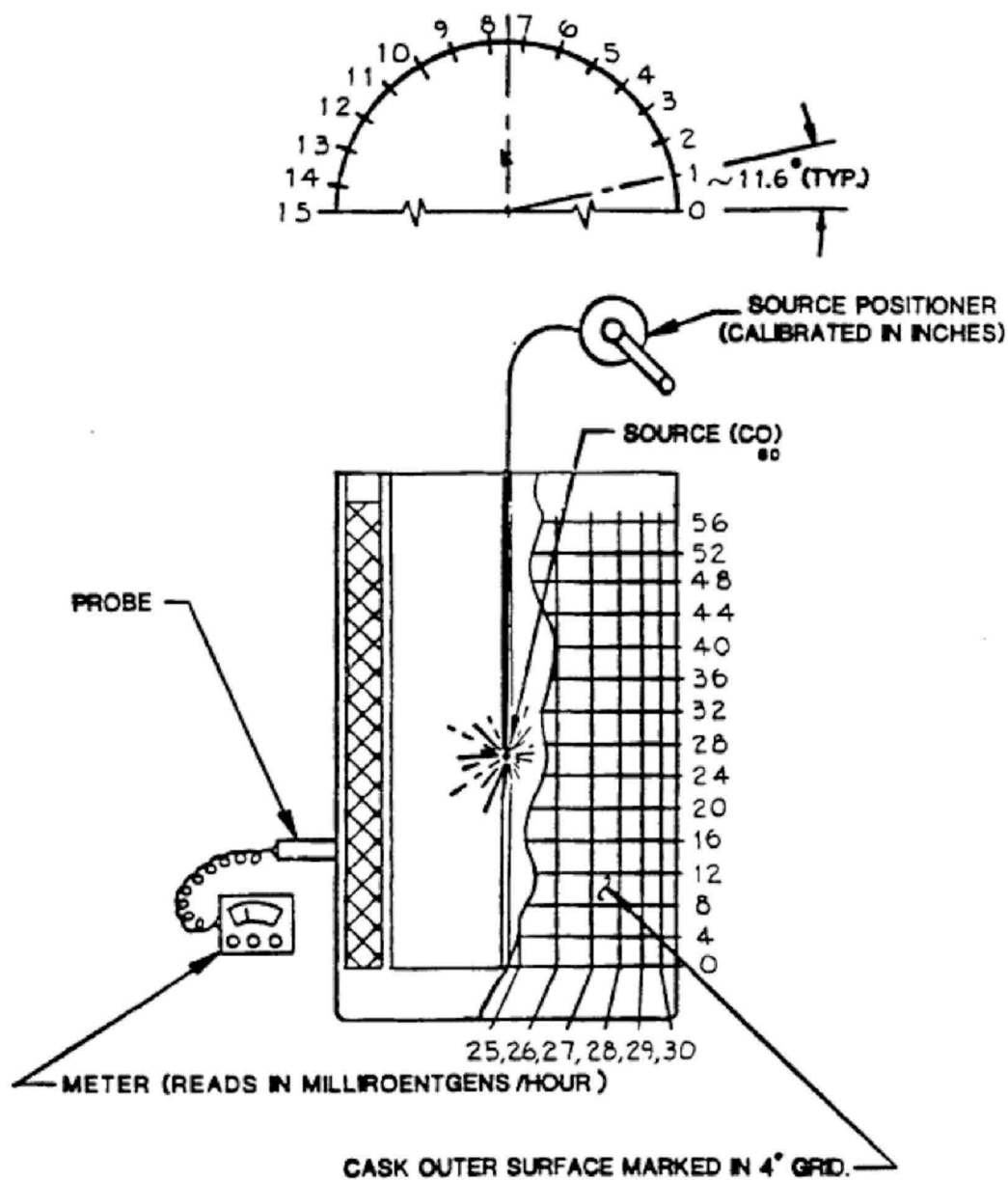


Figure 8-1. Cask Shielding Inspection Points

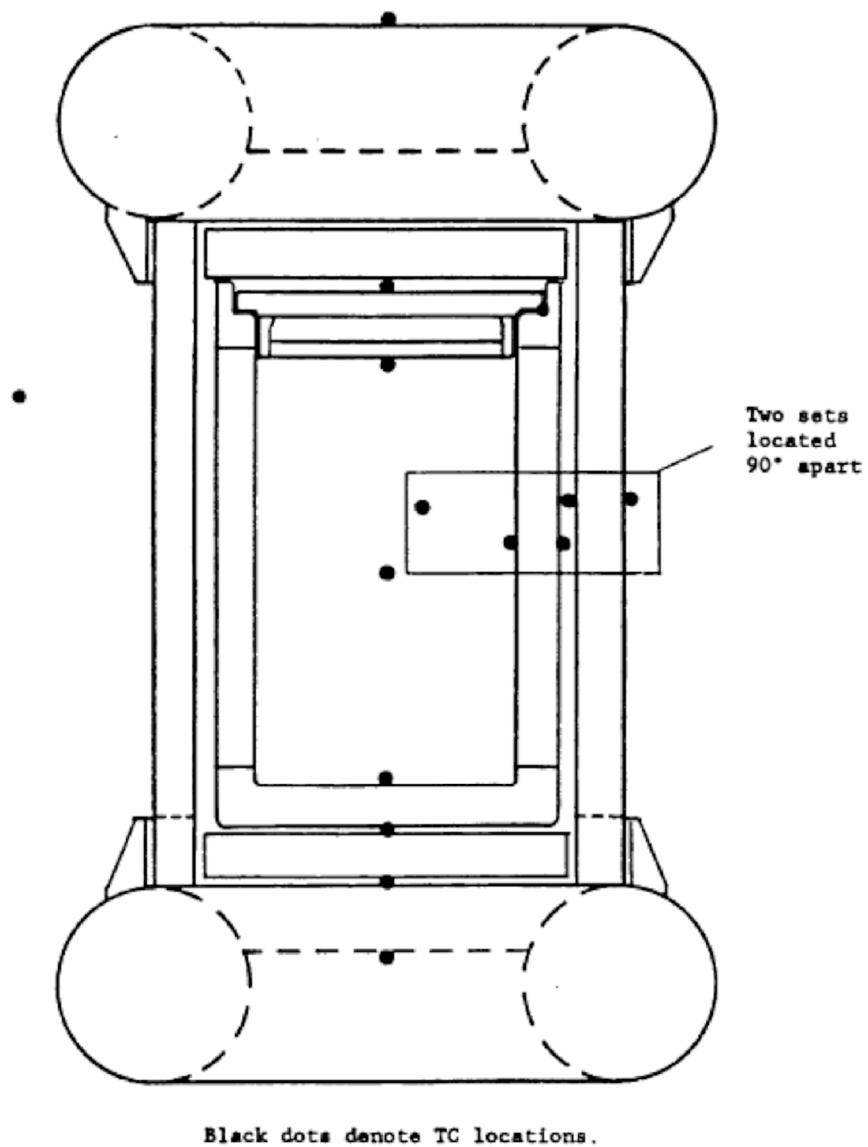


Figure 8-2. Thermocouple Locations

## **8.2 Maintenance Program**

The cask maintenance program is described in detail in the GEH operations and maintenance specification for the Model 2000 Transport Package. The specification was developed to implement the requirements established in this chapter. Operators of the Model 2000 Transport Package may develop procedures of their own within the requirements of the GEH specification to include site-specific procedures.

Routine inspections are performed prior to each assembly and prior to each shipment. These inspections include visual checks of the packaging and any support structures or devices required to properly assemble the package. It also includes visual inspection of the cask and components and pressurization of the cask cavity. This pressurization is part of the leak check procedure. Additional, more detailed inspections are also performed every twelve (12) usages or at least once within the 12-month period prior to subsequent use, whichever comes first. The cask must be leak tested to  $1 \times 10^{-7}$  ref·cm<sup>3</sup>/sec prior to its first use, after the third use, and at least once within the 12-month period prior to each shipment.

### **8.2.1. Structural and Pressure Tests**

#### **8.2.1.1. Routine Inspection**

Prior to each loading and assembly operation, the cask and lid are inspected for physical damage, especially the bolt holes, vent ports and sealing surfaces. The cask lid closure bolts, port plugs, O-rings, and lid gasket are all inspected visually and for proper dimensions and identification. In addition, the cask lid closure bolts have a 190-use limit. As part of the leak check, the cask cavity is pressurized to 15 psig with helium and tested per the pre-shipment requirements listed in Section 8.2.2.1. The overpack, HPI assembly, and HPI material basket components are inspected for visible signs of damage.

#### **8.2.1.2. Periodic Inspections**

At least once within the 12-month period prior to each shipment, the following inspections are made. Any maintenance work required is identified on a maintenance check sheet.

The overpack is inspected for:

- Signs of excessive heat or fire.
- Punctures, holes, or other surface failures.
- Crushed sides or ends indicating a drop or severe impact.
- Defects resulting from normal or abnormal wear.
- Compression or damage to the honeycomb absorber material.
- Cracks or other damage to welds.
- Proper identification and damage to the bolts.

The cask is inspected for:

- Wear, corrosion or damage to the vent and drain port plugs, caps, and O-rings.
- Damage to sealing surfaces on the cask and lid.
- Damage or cracks to welds on the cask and lid.
- Proper identification or damage to the lid and ear bolts.

### **8.2.2. Leak Tests**

The pre-shipment, periodic, and maintenance leak tests are all in accordance with ANSI N14.5 standards, with a reference air leakage rate ( $L_R$ ) criterion of leaktight per the ANSI N14.5 definition of  $1 \times 10^{-7}$  ref·cm<sup>3</sup>/sec. All leak testing procedures are developed by an ASNT Level III examiner per ASNT requirements.

#### **8.2.2.1. Pre-Shipment**

Prior to each shipment, leakage testing of the cask lid closure seal and vent and drain plugs may be performed with a helium Mass Spectrometer Leakage Detector (MSLD). The tests for the cask lid closure seal, vent port, and drain port are performed to ensure each containment boundary seal is leaktight, per the ANSI N14.5 definition ( $1 \times 10^{-7}$  ref cm<sup>3</sup>/sec).

#### **8.2.2.2. Periodic**

Prior to its first use, after the third use, and at least once within the 12-month period prior to each shipment, the cask lid closure seal and vent and drain plugs are tested to ensure each containment boundary seal is leaktight, per the ANSI N14.5 definition ( $1 \times 10^{-7}$  ref cm<sup>3</sup>/sec).

#### **8.2.2.3. Maintenance**

After any maintenance on the cask affecting a component of the containment boundary, such as a repair of a containment boundary weld, the affected component is leak tested per ANSI N14.5 standards, ensuring leaktightness ( $< 1 \times 10^{-7}$  ref·cm<sup>3</sup>/sec) of the component.

### **8.2.3. Component and Material Tests**

There are no auxiliary cooling systems or other subsystems requiring maintenance.

#### **8.2.3.1. Valves, Rupture Disks, and Gaskets on Containment Vessel**

The cask lid closure seal is used until visual and/or leak test inspections identify the seal as defective. The O-rings on the three penetration caps are replaced when visual or leak test inspections identify them as defective, or during the periodic inspection, whichever comes first.

#### **8.2.3.2. Shielding**

The shielding materials are lead and depleted uranium. The initial tests for voids during fabrication and the required radiological surveys following each loading assure shielding integrity. If the results of surveys exceed the regulatory requirements, the contents are reduced or the shipment is not initiated.

#### **8.2.4. Thermal Tests**

Thermal testing is only performed following initial fabrication of the cask.

#### **8.2.5. Miscellaneous Tests**

No additional periodic tests are required.

### **8.3 Appendix**

The only appendix information for Chapter 8 is provided in Section 8.4, References.

### **8.4 References**

- 8-1 GE Hitachi Nuclear Energy, "Quality Assurance Program Description," NEDO-11209-A, Latest NRC Approved Revision.
- 8-2 U.S. Nuclear Regulatory Commission (NRC), "Quality Assurance Program Approval Form for Proposed Amendment to Draft NEDO-11209 Revision 13, GE Hitachi Nuclear Energy Quality Assurance Program Description," Docket No. 71-0254, Revision 12, December 28, 2017, U.S. NRC ADAMS Accession Number ML17362A362.
- 8-3 American Society of Mechanical Engineers (ASME), Boiler and Pressure Vessel Code, Division I, Section III, Subsection NG, "Core Support Structures," 2010.
- 8-4 American Society of Mechanical Engineers (ASME), Boiler and Pressure Vessel Code, Division I, Section III, Subsection NB, "Class 1 Components," 2010 with addenda.
- 8-5 American Society of Mechanical Engineers (ASME), Boiler & Pressure Vessel Code, Division I, Section III, Subsection NF, "Component Supports," 2010.
- 8-6 American National Standards Institute (ANSI), "American National Standard for Radioactive Materials – Leakage Tests on Packages for Shipment," ANSI N14.5, 1997.
- 8-7 Military Specification, "Core Material, Aluminum, for Sandwich Construction," MIL-C-7438, or Equivalent.